

Electronic Thesis and Dissertation Repository

12-14-2016 12:00 AM


Synthesis of Metal-Containing Phosphines and Their Use in Coordination, Polymer, and Materials Chemistry

Amir Rabiee Kenaree
The University of Western Ontario

Supervisor
Joe B. Gilroy
The University of Western Ontario

Graduate Program in Chemistry
A thesis submitted in partial fulfillment of the requirements for the degree in Doctor of Philosophy
© Amir Rabiee Kenaree 2016

Follow this and additional works at: <https://ir.lib.uwo.ca/etd>

 Part of the [Inorganic Chemistry Commons](#), [Materials Chemistry Commons](#), and the [Polymer Chemistry Commons](#)

Recommended Citation

Rabiee Kenaree, Amir, "Synthesis of Metal-Containing Phosphines and Their Use in Coordination, Polymer, and Materials Chemistry" (2016). *Electronic Thesis and Dissertation Repository*. 4302.
<https://ir.lib.uwo.ca/etd/4302>

This Dissertation/Thesis is brought to you for free and open access by Scholarship@Western. It has been accepted for inclusion in Electronic Thesis and Dissertation Repository by an authorized administrator of Scholarship@Western. For more information, please contact wlsadmin@uwo.ca.

Abstract

This thesis describes the investigation of a novel strategy for the synthesis of metal-containing small molecules, polymers, and nanomaterials. In this context, a new family of air-stable, homo- and heterometallic primary, secondary, and tertiary phosphines were prepared via the radical-initiated hydrophosphination reaction of PH_3 with vinylferrocene and/or vinylruthenocene. The full characterization of the phosphines confirmed their targeted structures and proved that the properties of the starting metallocenes are reflected in those of the resulting phosphines.

To study the coordination behavior of this family of phosphines, primary, secondary, and tertiary ethylferrocene phosphines were reacted with Group 6 metal carbonyl adducts $[\text{M}(\text{CO})_5 \cdot \text{THF}]$; where M: Cr, Mo, and W] to generate the corresponding metal complexes. The successful coordination of all three phosphines to $\text{M}(\text{CO})_5$ and their purity were confirmed by several characterization methods, such as multinuclear NMR, FT-IR, and UV-vis absorption spectroscopy, cyclic voltammetry (CV), and elemental analysis. FT-IR spectroscopy studies revealed that ethylferrocene substituents act as electron-donating groups and that the σ donating ability of the phosphines were lower than that of PEt_3 and higher than that of PPh_3 .

To realize highly metallized polymers, two phosphorous-containing frameworks were targeted: quaternary phosphonium polyelectrolytes and tertiary phosphine polymers. The first iron-containing phosphonium monomer was synthesized by the quaternization reaction of tertiary ethylferrocene phosphine with 3-chloro-1-propanol followed by an esterification reaction with methacryloyl chloride and a salt metathesis reaction with NaOTf . In addition, four styrenic phosphonium monomers were synthesized by the quaternization reaction of 4-vinylbenzyl chloride with the tertiary ethylmetallocene phosphines (where Fe/Ru: 3/0, 2/1, 1/2, 0/3) before their counter-anion was exchanged with triflate. All five monomers were polymerized in the presence of azobisisobutyronitrile (AIBN) and carefully purified. Analysis of the polymers with methods including differential scanning calorimetry (DSC), thermogravimetric analysis (TGA), and gel permeation chromatography (GPC) confirmed their macromolecular nature. The pyrolysis of thin films of the phosphonium polymers, under an inert atmosphere, afforded highly metallized crystalline nanomaterials that were

characterized with techniques such as scanning electron microscopy (SEM) and energy-dispersive X-ray spectroscopy (EDX).

Finally, the hydrophosphination reaction of 3-buten-1-ol with a secondary ferrocene- and ruthenocene-containing phosphine followed by a *N,N'*-dicyclohexylcarbodiimide (DCC) coupling reaction with 4-vinyl benzoic acid afforded a tertiary phosphine monomer which was polymerized, in the presence of AIBN, and yielded a heterobimetallic tertiary phosphine polymer. The phosphine polymer was reacted with photogenerated $W(CO)_5 \cdot THF$ to produce the first example of a heterotrimetallic polymer. The proposed structure of the resulting polymers and their purity were confirmed by methods such as multinuclear NMR, FT-IR, and UV-vis absorption spectroscopy, CV, DSC, TGA, and GPC. The complete coordination of all phosphorous centres in the tertiary phosphine polymer to $W(CO)_5$ was confirmed by ^{31}P NMR spectroscopy and FT-IR studies, where the coordinated-tertiary phosphine polymer gave rise to three diagnostic absorption bands due to CO stretching modes from $W(CO)_5$ moieties.

Keywords

Synthesis, Ferrocene, Ruthenocene, Hydrophosphination, Stable Phosphines, Phosphonium Salts, Polyelectrolytes, Coordination Chemistry, Metal-Containing Polymers, Free-Radical Polymerization, Heterometallic Polymers, Electrochemistry, Pyrolysis, Nanomaterials

Co-Authorship Statement

The work described in this thesis contains contributions from the author as well as co-workers Dr. Brad M. Berven, Mr. Ethan R. Sauv , Mr. Tyler J. Cuthbert, Dr. Jacquelyn T. Price, Ms. Stephanie M. Barbon, Mr. Joe A. Paquette, Mr. Eric Landry, Mr. Ahmad Abu-Romeh, Dr. Anastasia Colomba, Prof. Paul J. Ragona, Prof. Elizabeth R. Gillies, Dr. Paul D. Boyle, and my supervisor Prof. Joe B. Gilroy. The contributions of each are described below.

Chapter 1 was written by the author and edited by Prof. Gilroy.

Chapter 2 describes the synthesis and characterization of metal-containing phosphines. The author was the main experimentalist. Dr. Berven conducted the preliminary hydrophosphination reaction of vinylferrocene. Mr. Cuthbert helped the author with hydrophosphination experiments. Ms. Barbon and Dr. Price performed the X-ray diffraction studies under the guidance of Dr. Boyle. The manuscript was written by the author and edited by Prof. Gilroy, Prof. Ragona, and Prof. Gillies.

Chapter 3 describes the synthesis and characterization of Group 6 metal complexes of primary, secondary, and tertiary ethylferrocenephosphines. The author was the main experimentalist. Mr. Sauv  synthesized starting materials and some of the metal complexes. Ms. Barbon performed the X-ray diffraction studies. The chapter was written by the author and edited by Prof. Joe B. Gilroy.

Chapter 4 describes the synthesis of metal-containing polymers. The author was the main experimentalist. Dr. Berven conducted the preliminary quaternization reaction of tertiary ethylferrocene phosphine. The X-ray diffraction studies were performed by Dr. Price, Dr. Colomba, and Mr. Paquette. The GPC studies were performed by Mr. Eric Landry and Mr. Ahmad Abu-Romeh (PolyAnalytik Canada). The chapter was written by the author and edited by Prof. Gilroy.

Chapter 5 describes the synthesis and characterization of a heterotrimetallic polymer. The author was the main experimentalist. The GPC studies were performed by Mr. Paquette. The chapter was written by the author and edited by Prof. Gilroy.

Chapter 6 was written by the author and edited by Prof. Gilroy.

Acknowledgments

First, I would like to give my sincere thanks to my supervisor, Prof. Joe Gilroy. He is a patient and supportive mentor who taught me how to conduct research and more importantly how to improve myself both professionally and personally.

I also would like to thank the past and present members of the Gilroy group: Joe was always ready to cheer me up when I was frustrated, Jackie and Steph were always enthusiastic to run my extremely twined crystals, Ryan was prepared to start a men's locker room/chemistry conversation, Sam introduced me to the Korean culture, and Dr. John Trant who was my walking organic synthetic library.

I am especially grateful for the support and guidance I received from Prof. Paul Ragona and his crew. Specifically, I must thank Brad, Dube, Tyler, Cam, Ryan, and Vanessa for helping me with the hydrophosphination reactions and their valuable suggestions/ideas.

This work could not be done without the excellent service I received from our technical staff who keep our facilities running. Specifically, Dr. Mathew Willans, Mr. Doug Hairsine, Dr. Paul Boyle, Ms. Aneta Borecki, Dr. Todd Simpson, and Mr. Tim Goldhawk. I am also thankful for the help I received from Ms. Darlene McDonald and Ms. Clara Fernandes.

I am thankful for what I learned from Prof. John Corrigan during the time he served on my committee. I acknowledge my current committee members, Profs. Michael Kerr, Johanna Blacquiere, John de Bruyn, and Daniel Foucher for reading my thesis and their constructive feedback.

I want to thank my parents who supported me in every step of my life and encouraged me to pursue my career in Canada. I also want to thank my lovely wife who supported me the past four years and parented our son as mom and dad, while I was working in the lab.

Table of Contents

Abstract.....	i
Co-Authorship Statement.....	iii
Acknowledgments.....	iv
Table of Contents.....	v
List of Tables.....	x
List of Figures.....	xii
List of Schemes.....	xvii
List of Appendices.....	xix
List of Abbreviations.....	xx
Chapter 1.....	1
1 Introduction.....	1
1.1 Synthesis of MCPs.....	3
1.1.1 Arene-Based MCPs.....	3
1.1.2 Alkyne-Based MCPs.....	13
1.1.3 Heteroatom-Based Ligands.....	15
1.2 Phosphorous-Based Frameworks for MCP Synthesis.....	17
1.2.1 Phosphazenes.....	17
1.2.2 Phosphinoboranes.....	18
1.2.3 Polyphosphaferrocenes.....	19
1.2.4 Phosphine Ligands.....	19
1.3 Thesis Scope.....	21
1.4 References.....	22
Chapter 2.....	33
2 Synthesis and Characterization of a Family of Air-Stable Ferrocene- and Ruthenocene-Containing Primary, Secondary, and Tertiary Phosphines.....	33

2.1	Introduction.....	33
2.2	Results and Discussion	35
2.2.1	Synthesis and NMR Spectroscopy.....	35
2.2.2	X-ray Crystallography	39
2.2.3	UV-vis Absorption Spectroscopy	40
2.2.4	Cyclic Voltammetry.....	41
2.3	Conclusion	45
2.4	Experimental Section.....	45
2.4.1	General Considerations.....	45
2.4.2	Cyclic Voltammetry.....	46
2.4.3	X-ray Crystallography	47
2.4.4	Synthetic Procedures and Characterization Data.....	49
2.5	References.....	59
	Chapter 3.....	65
3	Group 6 Metal Pentacarbonyl Complexes of Air-Stable Primary, Secondary, and Tertiary Ethylferrocenephosphines	65
3.1	Introduction.....	65
3.2	Results and Discussion	66
3.2.1	Synthesis and NMR Spectroscopy.....	66
3.2.2	X-ray Crystallography	69
3.2.3	FT-IR Spectroscopy	70
3.2.4	UV-Vis Absorption Spectroscopy and Cyclic Voltammetry.....	72
3.3	Conclusions.....	73
3.4	Experimental section.....	74
3.4.1	General Considerations.....	74
3.4.2	Cyclic Voltammetry.....	75

3.4.3	X-ray Crystallography	75
3.4.4	Representative Procedure for the Preparation of M(CO) ₅ Complexes of 3.5a–c, 3.6a–c, 3.7a–c	77
3.5	References.....	83
Chapter 4	88
4	Synthesis and Characterization of Metal-Rich Phosphonium Polyelectrolytes and Their Use as Precursors to Nanomaterials	88
4.1	Introduction.....	88
4.2	Results.....	91
4.2.1	Synthesis and Characterization of Methacrylate-Based Phosphonium Polyelectrolytes.....	91
4.2.2	Synthesis and Characterization of Styrene-Based Heterobimetallic Phosphonium Polyelectrolytes.....	96
4.3	Conclusion	104
4.4	Experimental section.....	104
4.4.1	General Considerations.....	104
4.4.2	Cyclic Voltammetry.....	105
4.4.3	X-ray Diffraction Studies.....	106
4.4.4	Gel Permeation Chromatography (GPC).....	108
4.4.5	Thermal Analysis	108
4.4.6	Pyrolysis Studies and Scanning Electron Microscopy.....	109
4.5	Notes and References.....	124
Chapter 5	132
5	An Organometallic Polymer with Three Different Metals per Repeating Unit.....	132
5.1	Introduction.....	132
5.2	Results and Discussion	133
5.2.1	Synthesis and NMR Spectroscopy.....	133
5.2.2	FT-IR Spectroscopy	136

5.2.3	UV-vis Absorption Spectroscopy and Cyclic Voltammetry.....	137
5.2.4	Gel Permeation Chromatography and Thermal Analysis	139
5.3	Conclusions.....	141
5.4	Experimental Section	142
5.4.1	General Considerations.....	142
5.4.2	Cyclic Voltammetry.....	143
5.4.3	Gel Permeation Chromatography	143
5.4.4	Thermal Analysis	143
5.5	References.....	149
Chapter 6	154
6	Conclusions and Future Work.....	154
6.1	Conclusions.....	154
6.2	Future Work	158
6.2.1	Novel MCP Designs: Based on New Stable Phosphines/ Polymerizable Groups.....	158
6.2.2	Block Copolymer Synthesis and Self-Assembly	159
6.2.3	Electron-Beam Lithography.....	160
6.2.4	Catalysis.....	161
6.3	References.....	162
Chapter 7	163
Appendices	163
Appendix 1	– Permission to Reuse Copyrighted Material.....	163
Appendix 2	– Supporting Information for Chapter 2.....	165
NMR Spectra	165
Solid-State Structures	177
Analysis of Twinning for 2.8b	180

UV-vis Absorption Spectra.....	180
Cyclic Voltammograms	183
Hydrophosphination Reaction Setup	185
Appendix 3 – Supporting Information for Chapter 3.....	186
NMR Spectra	186
Solid-State Structures.....	202
FT-IR Absorption Spectra.....	203
UV-Vis Absorption Spectra.....	208
Cyclic Voltammograms	211
Appendix 4 – Supporting Information for Chapter 4.....	215
NMR Spectra	215
UV-Vis Absorption Spectra.....	234
GPC Data	236
Cyclic Voltammograms	238
Differential Scanning Calorimetry Thermograms	241
Thermal Gravimetric Analysis.....	243
Scanning Electron Microscopy and Energy-Dispersive X-Ray Spectroscopy Results.....	244
Elemental Maps	246
Scanning Electron Microscopy and Energy-Dispersive X-ray Spectroscopy Results.....	249
Powder X-ray Diffractograms.....	253
Appendix 5 – Supporting Information for Chapter 5.....	257
NMR Spectra	257
UV-Vis Absorption Spectra.....	263
Cyclic Voltammograms	264
Curriculum Vitae.....	265

List of Tables

Table 2.1. Degradation of primary, secondary, and tertiary phosphines 2.7a–c , 2.8a–c , 2.10 , 2.11 , and 2.12 in solutions exposed to air.....	37
Table 2.2. Selected average angles (deg) and bond lengths (Å) for phosphines 2.7a–c , 2.8b , 2.8c , 2.10 , 2.11 , and 2.12	40
Table 2.3. Selected characterization data for phosphines 2.7a–c , 2.8a–c , 2.10 , 2.11 , and 2.12	44
Table 2.4. Selected X-ray diffraction data collection and refinement details for phosphines 2.7a–c , 2.8b , 2.8c , 2.10 , 2.11 , and 2.12	48
Table 3.1. Selected characterization data for complexes 3.5a–c , 3.6a–c , and 3.7a–c	68
Table 3.2. Selected bond lengths (Å) and angles (deg) for complexes 3.5c , 3.6c , and 3.7a–c	70
Table 3.3. Selected X-ray diffraction data collection and refinement details for complexes 3.5c , 3.6c , and 3.7a–c	77
Table 4.1. Characterization data for compounds 4.9 and 4.10a–c	93
Table 4.2. Selected characterization data for monomers 4.13a–d and polyelectrolytes 4.14a–d	99
Table 4.3. Thermal characterization and elemental composition data for the nanomaterials produced via the pyrolysis of polyelectrolytes 4.14a–d	102
Table 4.4. Selected X-ray diffraction data collection and refinement details for 4.8b and 4.13a	107
Table 5.1. Selected characterization data for compounds 5.6–5.10	139

Table 5.2. Selected characterization data for compounds tertiary phosphine polymer 5.8 and coordinated-tertiary phosphine polymer 5.8•W(CO)₅	141
---	-----

List of Figures

Figure 1.1. Load release of MCP-made nanocapsules upon oxidation of the metal centres. In the graphics of the nanocapsules, the poly(methyl methacrylate) phase, polyvinylferrocene phase, and pyrene molecules are represented by blue, red, and green colors, respectively.	2
Figure 1.2. A conjugated MCP used in solar cell preparation.	2
Figure 1.3. MCP types based on their connectivity.	3
Figure 1.4. Examples of half-sandwich and sandwich MCPs.	4
Figure 1.5. Examples of half-sandwich MCPs.	5
Figure 1.6. Examples of MCPs based on M-M bonds.	6
Figure 1.7. Examples of main-chain half-sandwich MCPs.	7
Figure 1.8. General structures of side- and main-chain sandwich MCPs.	8
Figure 1.9. Examples of side-chain ferrocene containing MCPs.	9
Figure 1.10. Examples of metallocene-containing polymers with metals other than Fe.	10
Figure 1.11. Examples of MCPs produced via strained-induced ROP.	12
Figure 1.12. Examples of MCPs with metals bridged by heteroatoms.	12
Figure 1.13. Examples of metallopolyyenes. ⁹⁹	13
Figure 1.14. Examples of MCPs prepared by alkyne-metal clusterization.	14
Figure 1.15. Heterobimetallic MCPs including alkyne-metal clusters.	15
Figure 1.16. Examples of macrocycle-based MCPs.	16
Figure 1.17. Example of MCPs based on acyclic ligands.	17
Figure 2.1. Examples of air-stable phosphines.	34

Figure 2.2. Examples of phosphinoferrocene compounds.....	35
Figure 2.3. ^{31}P NMR spectra of primary, secondary, and tertiary ruthenocene-containing phosphines 2.8a–c in CDCl_3	38
Figure 2.4. Solid-state structures of a) secondary phosphine 2.11 ($1 \times \text{Rc}$, $1 \times \text{Fc}$) and b) tertiary phosphine 2.12 ($2 \times \text{Rc}$, $1 \times \text{Fc}$). Thermal displacement ellipsoids are shown at 50% probability and hydrogen atoms have been omitted for clarity. For depictions of the solid-state structures of 2.7a–c , 2.8b , 2.8c , and 2.10 see Appendix 2 (Figures A2.26–A2.31).	39
Figure 2.5. UV-vis spectra of tertiary phosphines 2.7c ($3 \times \text{Fc}$; black line), 2.8c ($3 \times \text{Rc}$; red line), 2.10 ($1 \times \text{Rc}$, $2 \times \text{Fc}$; blue line), and 2.12 ($2 \times \text{Rc}$, $1 \times \text{Fc}$; green line) in THF.....	41
Figure 2.6. Cyclic voltammograms of tertiary phosphines 2.7c ($3 \times \text{Fc}$; black line), 2.8c ($3 \times \text{Rc}$; red line), 2.10 ($1 \times \text{Rc}$, $2 \times \text{Fc}$; blue line), and 2.12 ($2 \times \text{Rc}$, $1 \times \text{Fc}$; green line) recorded at 250 mV s^{-1} in 1 mM solutions of CH_2Cl_2 containing 0.1 M $[\text{n-Bu}_4\text{N}][\text{OTf}]$ as supporting electrolyte.....	43
Figure 3.1. Examples of phosphine-based ligands.....	65
Figure 3.2. $^{31}\text{P}\{^1\text{H}\}$ NMR spectra of primary, secondary, and tertiary phosphine- $\text{W}(\text{CO})_5$ complexes 3.7a (black line), 3.7b (blue line), 3.7c (red line and the inset) recorded in CDCl_3	68
Figure 3.3. Solid-state structures and partial spacefill models of primary, secondary, and tertiary phosphine- $\text{W}(\text{CO})_5$ complexes 3.7a (a,b) , 3.7b (c,d) , and 3.7c (e,f) . Thermal displacement ellipsoids are shown at 50% probability and hydrogen atoms have been omitted for clarity. Only one of the two structurally similar molecules from the asymmetric unit for 3.7a is shown.	70
Figure 3.4. FT-IR spectra (CO region) for primary, secondary, and tertiary phosphine- $\text{W}(\text{CO})_5$ complexes 3.7a (black line), 3.7b (blue line), and 3.7c (red line) recorded as thin films on KBr plates.	71

Figure 3.5. UV-Vis spectra of primary, secondary, and tertiary phosphine-W(CO) ₅ complexes 3.7a (black line), 3.7b (blue line), and 3.7c (red line) recorded in CH ₂ Cl ₂	72
Figure 3.6. Cyclic voltammograms of tertiary phosphine 3.4c (grey line) and tertiary phosphine-W(CO) ₅ complex 3.7c (red line) recorded at 250 mV s ⁻¹ for 1 mM degassed 2:1 CH ₂ Cl ₂ :CH ₃ CN solutions containing 0.1 M [n-Bu ₄ N][OTf] as supporting electrolyte.....	73
Figure 4.1. Solid-state structure of phosphonium alcohol 4.8b . Thermal displacement ellipsoids shown at 50% probability level. Hydrogen atoms and BF ₄ ⁻ counter anion have been removed for clarity. Selected bond lengths (Å) and angles (°): P1-C12 1.806(4), P1-C24 1.809(4), P1-C36 1.802(4), P1-C37 1.808(4), C11-C12 1.550(6), C23-C24 1.545(5), C35-C36 1.548(6), C37-38 1.522(6); C12-P1-C24 110.9(2), C12-P1-C36 109.1(2), C12-P1-C37 109.4(2), C24-P1-C36 110.2(2), C24-P1-C37 109.6(2), C36-P1-C37 107.6(2).	92
Figure 4.2. ¹ H NMR spectra of monomer 4.9 (black) and polyelectrolyte 4.10b (red) in CDCl ₃ . The asterisk denotes residual CHCl ₃ signals.....	93
Figure 4.3. Cyclic voltammograms of ferrocene-substituted monomer 4.9 (black) and polyelectrolyte 4.10b (red) recorded at 250 mV s ⁻¹ in 1 mM solutions of 2:1 CH ₂ Cl ₂ :CH ₃ CN containing 0.1 M [n-Bu ₄ N][OTf] as supporting electrolyte.....	94
Figure 4.4. TGA trace for polyelectrolyte 4.10b	95
Figure 4.5. (a) SEM images and (b) SEM image and elemental mapping (Si, C, P, Fe, O) for the nanostructured films produced by heating a thin film of polyelectrolyte 4.10b at 800 °C for 2 h under a flow of N ₂ gas. Representative Fe ₃ O ₄ crystallites highlighted by red circle. Scale bars = 1 μm.....	96
Figure 4.6. Solid-state structure of monomer 4.13a . Thermal displacement ellipsoids are shown at 50% probability and hydrogen atoms have been omitted for clarity. Selected bond lengths (Å): P1-C12 1.782(6), P1-C24 1.803(5), P1-C36 1.798(5), P1-C37 1.791(6), C44-C45 1.162(9). Selected bond angles (degrees): C12-P1-C24 111.7(3), C12-P1-C36 108.5(3), C12-P1-C37 110.9(3), C24-P1-C36 110.0(3), C24-P1-C37 106.2(2), and C36-P1-C37 109.6(3).	98

Figure 4.7. TGA traces for polyelectrolytes: 4.14a (3 × Fc, black), 4.14b (2 × Fc, 1 × Rc; red), 4.14c (1 × Fc, 2 × Rc; blue), and 4.14d (3 × Rc, green).....	100
Figure 4.8. SEM images of the nanomaterials prepared via the pyrolysis of films of polyelectrolytes (a) 4.14a , (b) 4.14b , (c) 4.14c , and (d) 4.14d . Scale bars = 1 μm.	101
Figure 4.9. SEM images and elemental maps (O, Ru, Fe, P, C) for the nanomaterials prepared via the pyrolysis of a film of polyelectrolyte 4.14b . Scale bar = 1 μm.	102
Figure 4.10. Powder X-ray diffractograms for the nanomaterials prepared via the pyrolysis of films of polyelectrolytes (a) 4.14a , (b) 4.14b , (c) 4.14c , and (d) 4.14d . Miller indices corresponding to Ru ₂ P are shown in panel (d).	103
Figure 5.1. ³¹ P{ ¹ H} NMR spectra of tertiary phosphine polymer 5.8 (black) and coordinated-tertiary phosphine polymer 5.8•W(CO)₅ (red) recorded in CDCl ₃	136
Figure 5.2. FT-IR spectra of tertiary phosphine polymer 5.8 (black) and coordinated-tertiary phosphine polymer 5.8•W(CO)₅ (red).....	137
Figure 5.3. Cyclic voltammograms of tertiary phosphine polymer 5.8 (black) and coordinated-tertiary phosphine polymer 5.8•W(CO)₅ (red) recorded at 250 mV s ⁻¹ in solutions of THF containing 0.1 M [n-Bu ₄ N][OTf] as supporting electrolyte.	139
Figure 5.4. GPC traces recorded for polymers 5.8•S (grey) and 5.8•W(CO)₅ (red) in THF. The limits used to estimate the molecular weights relative to monodisperse polystyrene standards are shown as black bars and the signal attributed to aggregates of 5.8•W(CO)₅ in solution is shown in the dashed box.	140
Figure 5.5. a) DSC thermograms of tertiary phosphine polymer 5.8 (black) and coordinated-tertiary phosphine polymer 5.8•W(CO)₅ (red) recorded at a scan rate of 10 °C min ⁻¹ and b) TGA data obtained for tertiary phosphine polymer 5.8 (black) and coordinated-tertiary phosphine polymer 5.8•W(CO)₅ (red).....	141
Figure 6.1. The synthesis of metal-containing phosphines from PH ₃ gas.	154
Figure 6.2. Solid-state structure and properties of W(CO) ₅ -phosphine metal complexes.	155

Figure 6.3. The production of nanomaterials from metal-containing polymers.	156
Figure 6.4. The synthesis of highly metallized nanomaterials from heterobimetallic phosphonium polyelectrolyte salts.....	157
Figure 6.5. Self-assembly and nano-patterning of metallized nanomaterials.	160
Figure 6.6. Fabrication of patterned nanomaterials by use of EBL.	160

List of Schemes

Scheme 1.1. Synthesis of ferrocene.	3
Scheme 1.2. ROMP of a Pt-containing norbornene monomer.	5
Scheme 1.3. Example of the synthesis of half-sandwich MCPs.....	6
Scheme 1.4. Synthesis and ROP of a strained half-sandwich metal containing monomer.	7
Scheme 1.5. Synthesis of ferrocenealdehyde and vinylferrocene.....	9
Scheme 1.6. Synthesis of a ferrocene-containing polyorganosilane.....	10
Scheme 1.7. Synthesis of a zirconocene tethered MCP.....	11
Scheme 1.8. Synthesis of PFSs.....	11
Scheme 1.9. Synthesis of a metallopolyyne. ¹⁰¹	13
Scheme 1.10. Example of a MCP synthesis by hydrosilylation of dialkynes.....	14
Scheme 1.11. ROP of cyclic metal-containing phosphazenes.....	18
Scheme 1.12. Example of a dehydrocoupling reaction of a phosphine-borane adduct.	18
Scheme 1.13. Example of the synthesis of a strained phospho[1]ferrocenophane.	19
Scheme 1.14. Example of ROP of a strained phospho[2]ferrocenophane.....	19
Scheme 1.15. Example of coordination of a tertiary phosphine polymer to a metal. ¹⁴³	20
Scheme 1.16. Monomer synthesis.	20
Scheme 1.17. Example of migration insertion polymerization.....	20
Scheme 2.1. The salt-elimination reaction of phosphides with alkyl halides.	33
Scheme 2.2. Hydrophosphination of olefins.....	34

Scheme 2.3. Synthesis of phosphines 2.7a–c , 2.8a–c , 2.10 , 2.11 , and 2.12 . Fc and Rc represent ferrocenyl and ruthenocenyl substituents.	36
Scheme 2.4. Summary of the known chemical oxidation behavior of ruthenocene in coordinative/non-coordinative media. L: neutral or anionic donor.	42
Scheme 2.5. Postulated reactivity pathway upon electrochemical oxidation of tertiary phosphine 2.12 ($2 \times \text{Rc}$, $1 \times \text{Fc}$). L = phosphine or OTf^- anion, E = electrochemical reaction, C = chemical reaction, and EC = electrochemical/chemical reaction.	44
Scheme 3.1. Synthesis of primary, secondary, and tertiary phosphine- $\text{M}(\text{CO})_5$ complexes 3.5a–c , 3.6a–c , and 3.7a–c . FcH = ferrocene.	67
Scheme 4.1. Synthesis of methacrylate-based phosphonium polyelectrolytes.	91
Scheme 4.2. Synthetic pathway for the preparation of polyelectrolytes 4.14a–d	97
Scheme 5.1. Suggested mechanism for the synthesis of 5.6	134
Scheme 5.2. Synthetic pathway for the preparation of heterotrimetallic polymer 5.8•W(CO)₅	135
Scheme 6.1. Synthesis of a heterotrimetallic polymer.	157
Scheme 6.2. Synthesis of rhodocenium- and cobaltocenium-based phosphines.	158
Scheme 6.3. A novel MCP design based on a hydrophosphination reaction.	159

List of Appendices

Appendix 1 – Permission to Reuse Copyrighted Material.....	163
Appendix 2 – Supporting Information for Chapter 2.....	165
Appendix 3 – Supporting Information for Chapter 3.....	186
Appendix 4 – Supporting Information for Chapter 4.....	215
Appendix 5 – Supporting Information for Chapter 5.....	257

List of Abbreviations

{ ¹ H}	proton decoupled
°	degree
°C	degrees Celsius
¹³ C	carbon thirteen
¹ H	proton
A	area
Å	angstrom
ADMET	acyclic diene metathesis
AIBN	azobisisobutyronitrile
ATR	attenuated total reflectance
ATRP	atom-transfer radical-polymerization
a.u.	arbitrary units
BHT	butylated hydroxytoluene
br	broad
Bu	butyl
<i>ca.</i>	approximately
Cb	cyclobutadienyl
CCDC	the Cambridge crystallographic data centre
CH ₃ CN	acetonitrile
cm	centimeter
cm ⁻¹	wavenumber
Cp	cyclopentadienyl
CV	cyclic voltammetry
<i>D</i>	dispersity
d	doublet
DCC	dicyclohexylcarbodiimide
dd	doublet of doublets
D.I.	deionized
DMAP	dimethylaminopyridine
DMF	dimethylformamide

DMSO	dimethylsulfoxide
DP _n	degree of polymerization
Dppf	1,1'-bis(diphenylphosphino)ferrocene
DSC	differential scanning calorimetry
E	potential
E _{1/2}	half-wave potential
EA	elemental analysis
EBL	electron-beam lithography
EDX	energy dispersive X-ray
EI	electron-impact ionization
E _{pa}	anodic peak potential
equiv.	equivalent
ESI-MS	electrospray ionization mass spectrometry
Et	ethyl
Et ₂ O	diethyl ether
Et ₃ N	triethylamine
EtOAc	ethyl acetate
EtOH	ethanol
eV	electron volts
Fc	ferrocenyl
FT-IR	Fourier transform infra-red spectroscopy
FRP	free-radical polymerization
FW	formula weight
g	gram
G3	Grubbs' third generation catalyst
gHSQCAD	gradient heteronuclear single quantum coherence spectroscopy
GPC	gel permeation chromatography
h	hours
HOMO	highest-occupied molecular orbital
Hz	hertz
<i>J</i>	NMR coupling constant
K	Kelvin

LDA	lithium diisopropylamide
LED	light emitting diode
M	molar
m	multiplet
mA	milliamps
max	maximum
MCP	metal-containing polymer
mg	milligram
MHz	megahertz
min	minute
mL	milliliter
mm	millimeter
mM	millimolar
mmol	millimole
M_n	number average molecular weight
mol	mole
mV	millivolt
MW	molecular weight
M_w	weight average molecular weight
nm	nanometer
NMR	nuclear magnetic resonance
OTf	trifluoromethanesulfonate
<i>p</i>	para
PEt ₃	triethylphosphine
PFS	polyferrocenylsilane
Ph	phenyl
PMMA	polymethylmethacrylate
POLED	polymer organic light emitting diode
ppm	parts per million
PS	polystyrene
PSC	polymer solar cell
PXRD	powder X-ray diffraction

q	quartet
R.T.	room temperature
R•	radical group
Rc	ruthenocenyl
R _f	retardation factor
RI	refractive index
RAFT	reversible addition–fragmentation chain-transfer
ROMP	ring-opening metathesis polymerization
ROP	ring-opening polymerization
RPM	rotations per minute
s	singlet
SEM	scanning electron microscopy
SOMO	singly-occupied molecular orbital
t	triplet
TEM	transmission electron microscopy
T _g	glass transition temperature
TGA	thermal gravimetric analysis
THF	tetrahydrofuran
UV	ultraviolet
UV-vis	ultraviolet-visible
V	volts
v/v	volume to volume ratio
w	weak
x	Cartesian axis
y	Cartesian axis
z	Cartesian axis
α	crystallographic lattice constant, torsional angle
β	crystallographic lattice constant, torsional angle
γ	crystallographic lattice constant, torsional angle
δ	chemical shift, partial charge
ε	molar absorptivity
θ	theta (range for crystallographic data collection)

λ	wavelength
λ_{\max}	wavelength of maximum absorption
μA	microamps
ρ	resistivity

Chapter 1

1 Introduction

Polymers are ubiquitous materials that have gained much attention in academia and industry due to their remarkable processability and durability.¹⁻² The concept that “polymers are macromolecules made by chaining small molecules together” was suggested for the first time by Staudinger in 1922 and inspired many researchers to study the polymerization of small molecules and develop numerous types of polymers that have become an indispensable part of our everyday lives.³

Most industrial polymers are composed mainly of carbon and hydrogen, are chemically inert, and are valuable only for their mechanical properties. In contrast, metallopolymers or metal-containing polymers (MCPs) are an interesting class of polymers that contain transition metal complexes in their structures.⁴⁻⁷ These metal centres add the unique properties of the corresponding crystalline inorganic compounds to the processable MCPs that have proved their utility in a variety of applications, for example as catalytic,⁸⁻⁹ magnetic,¹⁰ stimuli-responsive,¹¹⁻¹² biomedical,¹³ luminescent,¹⁴ and conductive materials.¹⁵⁻¹⁶

For instance, the Crespy and Gallei groups synthesized a poly(vinylferrocene)-*block*-poly(methyl methacrylate) copolymer, *e.g.*, **1.1**, and self-assembled it into nanocapsules with poly(vinylferrocene) patches surrounded by poly(methyl methacrylate) (Figure 1.1a). Then they encapsulated pyrene molecules in the core of the nanocapsules and demonstrated that oxidation of the ferrocene units to ferrocenium in the redox-responsive nanopatches results in swelling of the patches due to the hydrophobic to hydrophilic transition and releasing the load (Figure 1.1b).¹⁷

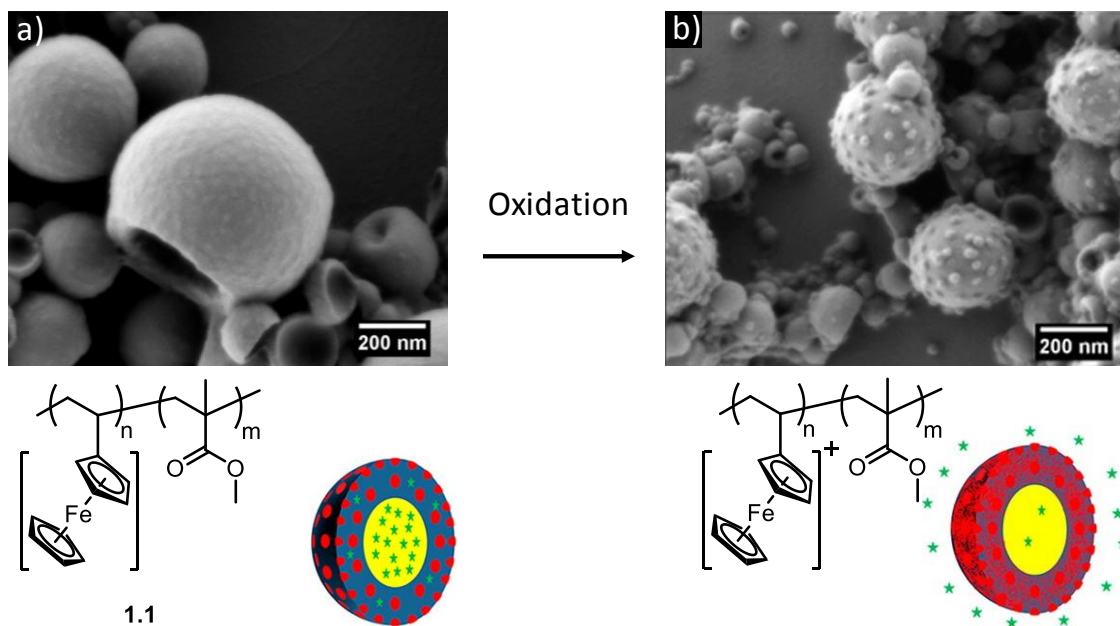


Figure 1.1. Load release of MCP-made nanocapsules upon oxidation of the metal centres. In the graphics of the nanocapsules, the poly(methyl methacrylate) phase, polyvinylferrocene phase, and pyrene molecules are represented by blue, red, and green colors, respectively.

As another example, Wong and co-workers synthesized conjugated MCPs, *e.g.*, **1.2**, and utilized them as photoactive materials for the preparation of solar cells which demonstrated relatively high power-conversion efficiencies (more examples of conjugated MCP will be described in section **1.1.2.**).¹⁸

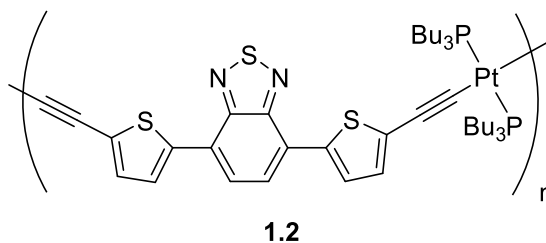


Figure 1.2. A conjugated MCP used in solar cell preparation.

Within the structure of MCPs, metal complexes can be part of the backbone or be present as pendant groups (Figure 1.3). Depending on the lability of the metal complexes, MCPs can have static (irreversibly bound metals) or dynamic (reversibly bound metals) structures.¹⁹ Since all of the targeted MCPs in this thesis have static structures, polymers with dynamic structures (*i.e.*, coordination polymers) will not be discussed here in detail.²⁰⁻

²⁴ MCPs also can be categorized based on the type of ligands used for the incorporation of metals into their structure. In the following sections, several strategies for MCP preparation will be categorized and discussed.

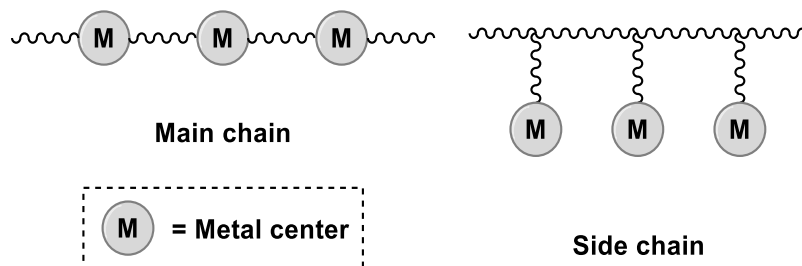


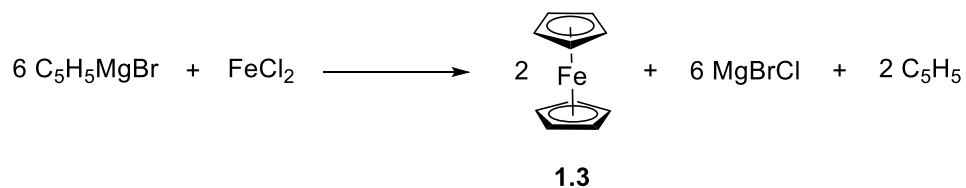
Figure 1.3. MCP types based on their connectivity.

1.1 Synthesis of MCPs

Strategies for the synthesis of MCPs are commonly based on the incorporation of organometallic species and polymerizable groups including styrene, acrylate, norbornene, and strained rings. In this regard, arene- and heteroatom-based ligands have been extensively used for the introduction of transition metals. Other common strategies include condensation polymerization reactions and metal-alkyne clusterization reactions.²⁵⁻²⁶

1.1.1 Arene-Based MCPs

Arene groups (C_nH_n) are good ligands for electron-poor metals since they can bind metals with strong haptic covalent bonds. For example ferrocene, which is comprised of two cyclopentadienyl (Cp) ligands coordinated to iron, *e.g.*, **1.3**, was the first example of an organometallic sandwich compound and was synthesized at 1951 by Kealy and Pauson (Scheme 1.1).²⁷



Scheme 1.1. Synthesis of ferrocene.

Inspired by this groundbreaking discovery, various organometallic compounds have been synthesized and utilized as metal carriers in the preparation of MCPs. Based on the number of arene ligands, these MCPs can be divided to half-sandwich, *e.g.*, **1.4**, and sandwich MCPs, *e.g.*, **1.5**.

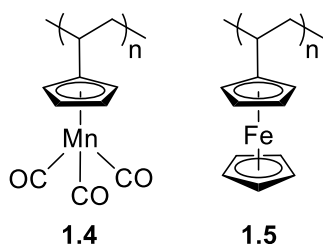


Figure 1.4. Examples of half-sandwich and sandwich MCPs.

1.1.1.1 Half-Sandwich MCPs

Half-sandwich MCPs have been prepared in main- and side-chain architectures.²⁸⁻²⁹ The side-chain MCPs mainly were generated by functionalization of arene groups in order to add a polymerizable group. Following this strategy, Pittman and co-workers synthesized the first half-sandwich MCP by free-radical polymerization (FRP) of vinylcymantrene to afford polyvinylcymantrene.³⁰ So far, different polymerizable and arene groups have been used to produce MCPs containing transition metals including Mn, Mo, Ir, W, Co, Cu, Rh, and Cr, *e.g.*, **1.6–1.10**.³⁰⁻⁴² Most of these MCPs contain metal centres complexed to Cp and carbonyl (CO) ligands but examples containing phenyl, phosphine (PEt₃), nitroxide (NO), and methyl ligands also have been reported.⁴³

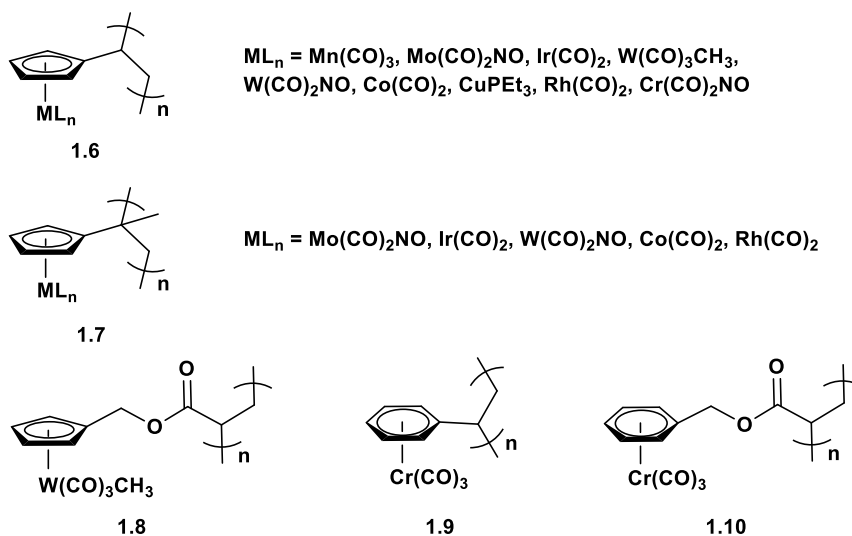
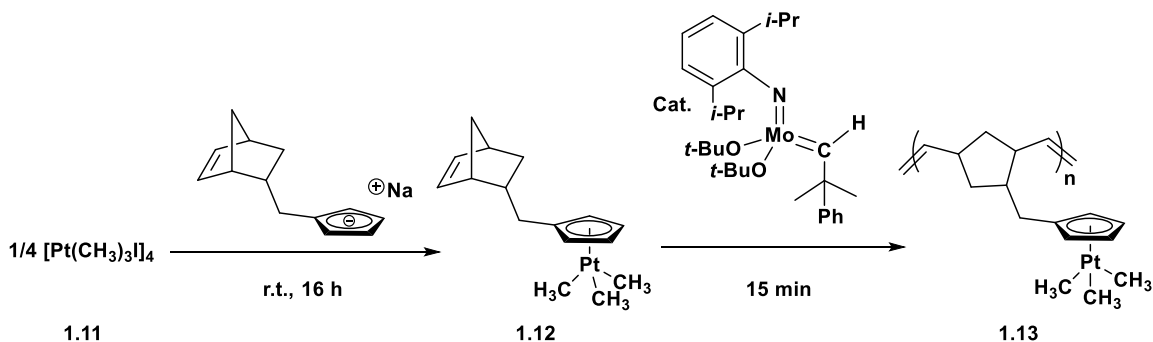


Figure 1.5. Examples of half-sandwich MCPs.

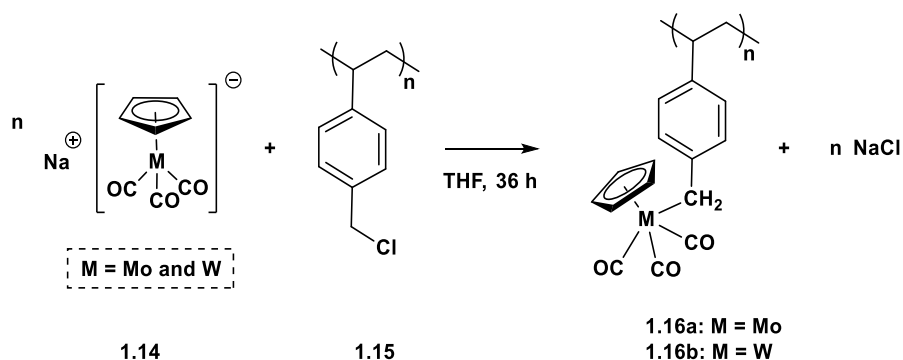
In addition, half-sandwich monomers can be prepared via the reaction of an organometallic salt with an arene ligand that carries a polymerizable group. For example, the Schrock group coordinated platinum to a pendant Cp group of a functionalized norbornene to yield a norbornene- and metal-containing monomer, *e.g.*, **1.12**, and polymerized it via ring-opening metathesis polymerization (ROMP) to produce **1.13** (Scheme 1.2).⁴⁴



Scheme 1.2. ROMP of a Pt-containing norbornene monomer.

Half-sandwich MCPs have been synthesized by several polymerization techniques, including anionic and free-radical polymerization (FRP). However, their polymerization

has not been trivial since these metal complexes often have limited stability. As an alternative, polymers such as poly(4-vinylbenzyl chloride), *e.g.*, **1.15**, can be utilized as precursors for post-polymerization functionalization reactions to produce MCPs, *e.g.*, **1.16a, b** (Scheme 1.3).⁴⁵



Scheme 1.3. Example of the synthesis of half-sandwich MCPs.

Relatively stable metal dimers which contain arene ligands and bimetallic centres, where the metals are connected via a metal-metal bond, are interesting organometallic species for the synthesis of polymers containing half-sandwich metal complexes in their backbone. In the past two decades, the Taylor group has been the main contributor to this area and they have synthesized a variety of MCPs containing M-M dimers.⁴⁶⁻⁴⁷ The metal centres are generally ligated to carbonyl and functionalized Cp or phosphine ligands that contain a polymerizable group such as alkene, alkyne, or hydroxyl. Depending on the nature of the polymerizable groups, the monomers can be polymerized using step-growth polymerization methods such as alkyne-azide cycloaddition and acylchloride-hydroxyl condensation or chain-growth polymerization methods like acyclic diene metathesis polymerization (ADMET) (Figure 1.6).⁴⁸⁻⁵⁴

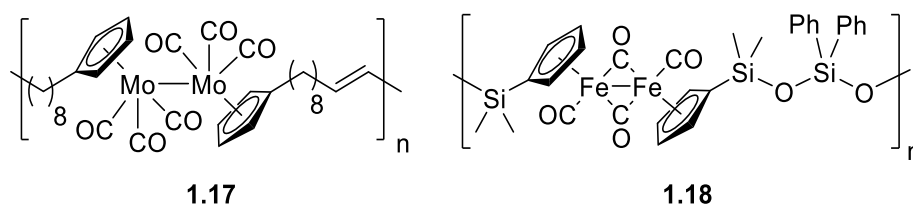
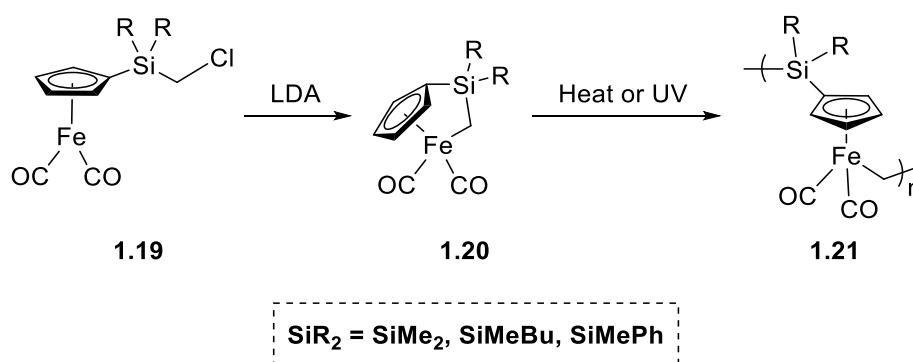


Figure 1.6. Examples of MCPs based on M-M bonds.

Ring-opening polymerization (ROP) of organometallic monomers is the most powerful technique for the synthesis of MCPs. In this regard, Pannell and co-workers have reported several cyclic monomers wherein the metal and arene group were bridged by different elements such as Si and Ge.⁵⁵⁻⁵⁷ These monomers can be synthesized by ring-closing salt elimination reactions of an organometallic salt with lithium diisopropylamide (LDA) and can undergo ROP induced by heat or UV light to yield polymers with repeating units containing metal complexes in the main chain (Scheme 1.4).⁵⁸



Scheme 1.4. Synthesis and ROP of a strained half-sandwich metal containing monomer.

MCPs with main group element bridges which contain other transition metals such as Mo, W, and Ru have also been prepared by this method (Figure 1.7).⁵⁹⁻⁶¹

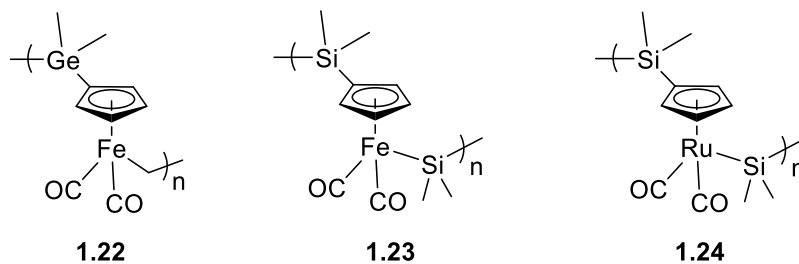


Figure 1.7. Examples of main-chain half-sandwich MCPs.

1.1.1.2 Sandwich MCPs

Sandwich compounds, and more specifically metallocenes (a family of sandwich compounds that contain two Cp ligands), are the most common organometallic compounds for MCP preparation. Ferrocene was the starting material for the synthesis of the first MCP, *i.e.*, polyvinylferrocene **1.5**, which was prepared by Aromoto and Haven.⁶² Since then, this 18-electron metallocene has been the dominant metal carrier in the field of MCPs and perhaps organometallic chemistry due to its high stability and robust redox chemistry.⁶³ This impressive stability allows for functionalization of the Cp rings of ferrocene and polymerization of ferrocene-containing monomers while the iron centre remains intact. In addition to ferrocene-containing polymers, numerous MCPs have been developed by using other metallocenes and based on their connectivity, these MCPs can be categorized into main- and side-chain sandwich MCPs (Figure 1.8).

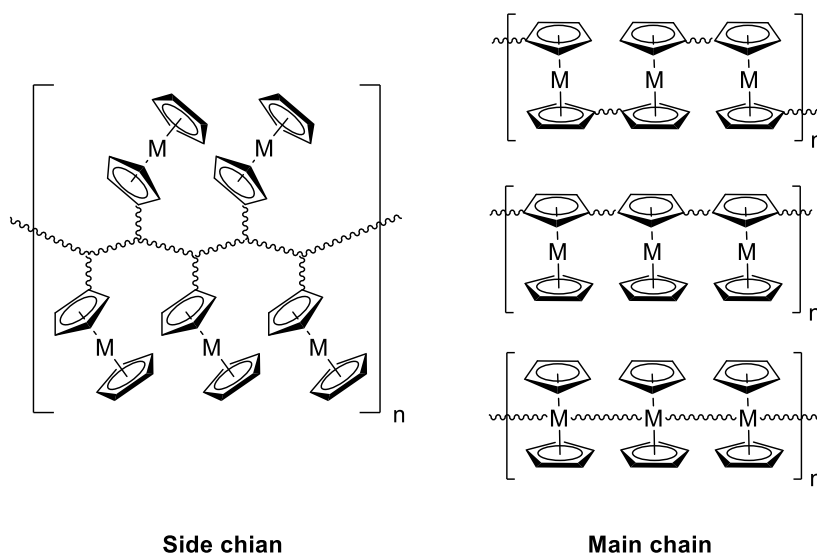
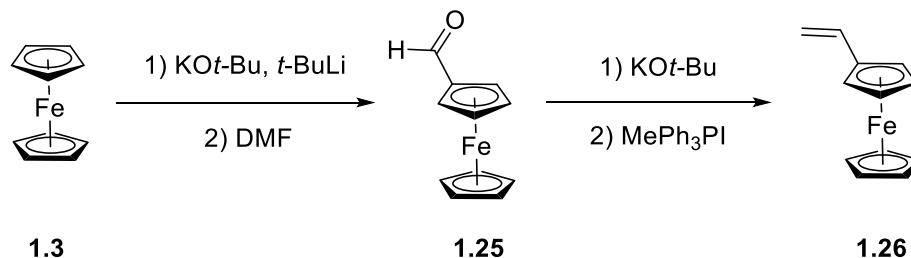


Figure 1.8. General structures of side- and main-chain sandwich MCPs.

Installation of a polymerizable group on the arene group of a sandwich compound is a well-known strategy for synthesis of side-chain sandwich MCPs. In this context, Friedel-Crafts and lithiation reactions have been extensively utilized. For example, treatment of ferrocene with potassium superbases (mixture of $\text{KO}t\text{-Bu}$ and $t\text{-BuLi}$) followed by DMF addition is a

simple and high yielding method for the preparation of ferrocenealdehyde,⁶⁴ which can be utilized as a precursor for different functional groups, including vinyl groups (Scheme 1.5).⁶⁵



Scheme 1.5. Synthesis of ferrocenealdehyde and vinylferrocene.

Upon Cp functionalization, several polymerizable groups such as acrylates, styrene, and norbornene have been installed on ferrocene and the resulting monomers were polymerized by a variety of polymerization methods including FRP, cationic, anionic, ROMP, atom-transfer radical-polymerization (ATRP), and reversible addition-fragmentation chain-transfer polymerization (RAFT) (Figure 1.9).⁶⁶⁻⁷²

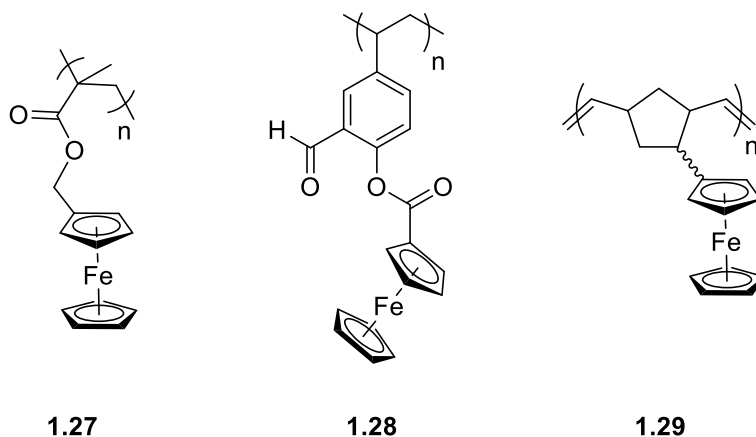
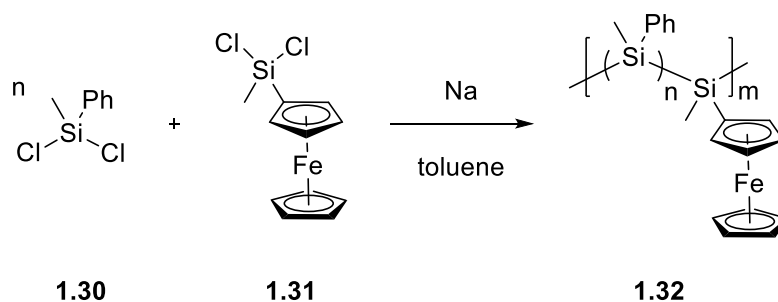


Figure 1.9. Examples of side-chain ferrocene containing MCPs.

Organosilanes, *e.g.*, **1.31**, are a family of inorganic compounds which have served as metal carriers for MCPs. For example, Pannell and Zeigler reported the preparation of MCPs by copolymerization of phenylmethyldichlorosilane **1.29**, and ferrocenylmethyldichlorosilane **1.30** (Scheme 1.6).⁷³



Scheme 1.6. Synthesis of a ferrocene-containing polyorganosilane.

In contrast to ferrocene, cobaltocene (CoCp_2) and rhodocene (RhCp_2) are 19-electron metallocenes that can be easily oxidized to form the corresponding 18-electron metallocenium cations.⁷⁴ Thus, the Tang and Astruc groups have utilized cobaltocenium and rhodocenium as metal complexes for the synthesis of several MCPs, *e.g.*, **1.33–1.35**.^{75–79} Alternatively, the Ragona group has employed cyclopentadienyl-cobalt-cyclobutadienyl CpCoCb sandwich compounds, which are stable 18-electron species, *e.g.*, **1.36**.^{80–81}

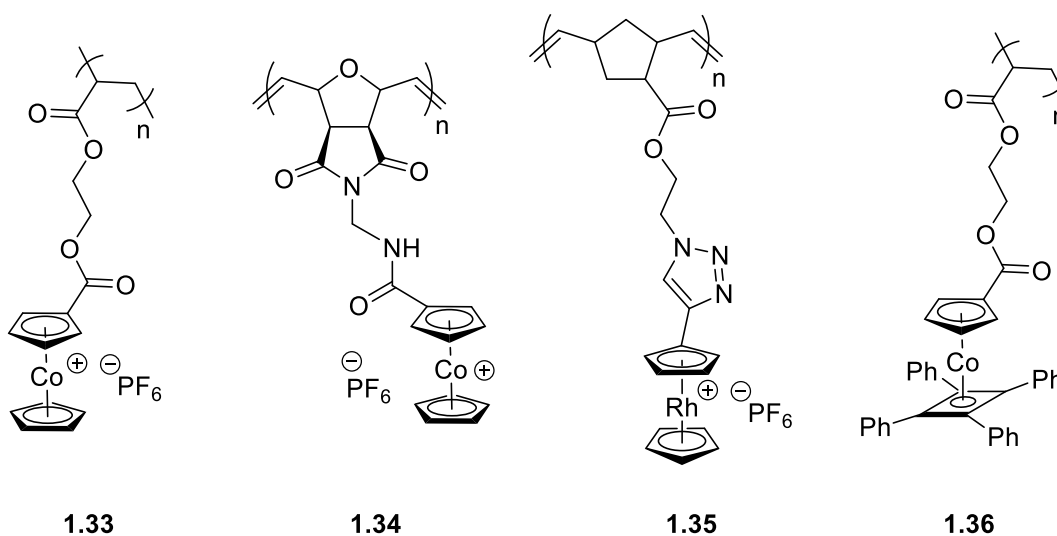
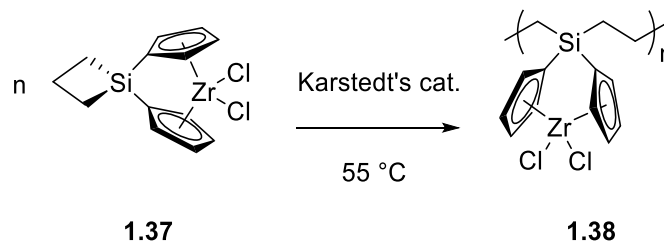


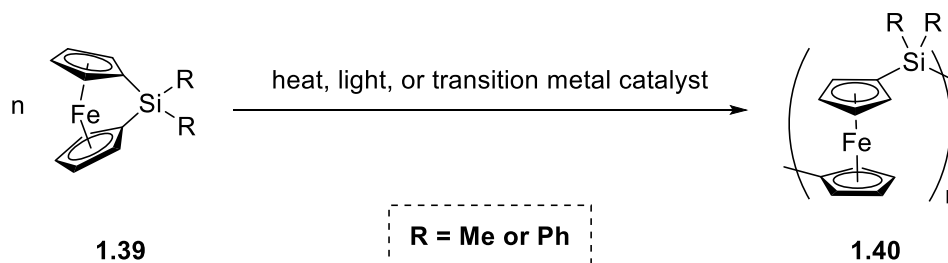
Figure 1.10. Examples of metallocene-containing polymers with metals other than Fe.

Zirconocene is another metallocene that has been incorporated into strained silacyclobutanes, *e.g.*, **1.37**, that can undergo ROP and yield zirconium-containing polymers (Scheme 1.7).⁸²



Scheme 1.7. Synthesis of a zirconocene tethered MCP.

Similar to strained silacyclobutanes, cyclic sandwich compounds with bridged Cp ligands can undergo ROP and produce MCPs with sandwich compounds in their backbones. For instance, the successful ROP of strained sila[1]ferrocenophanes by the Manners group resulted in the production of polyferrocenosilane (PFS) (Scheme 1.8).⁸³ In this method, the introduction of a bridge between the Cp ligands provides the needed strain for ROP of the cyclic monomer. This living polymerization method can be initiated by heat, light, or transition metal catalysts and affords high molecular weight polymers.⁸⁴⁻⁸⁵



Scheme 1.8. Synthesis of PFSs.

The Manners group and others including Müller, Braunschweig, Vansco, and Rehahn have developed this chemistry and extended this method to many strained monomers with different transition metals and arene groups and arene-arene bridges to prepare many types of MCPs (Figure 1.11).⁸⁶⁻⁹³

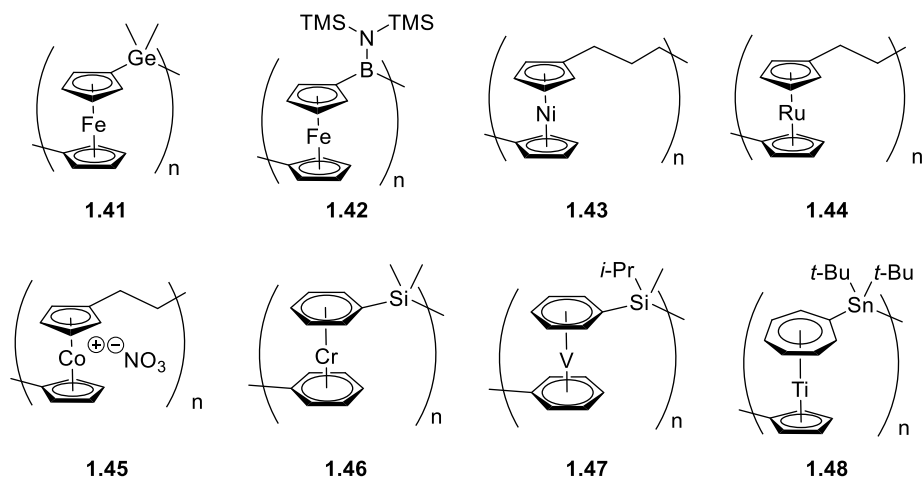


Figure 1.11. Examples of MCPs produced via strained-induced ROP.

Moreover, MCPs can be produced with metal centres bridged by heteroatom ligands. However, they are much less common and typically have been prepared by dehydrohalogenation of MCp_2X_2 salts containing Group IV (*e.g.*, Ti, Zr, Hf) metals (Figure 1.12).⁹⁴⁻⁹⁸

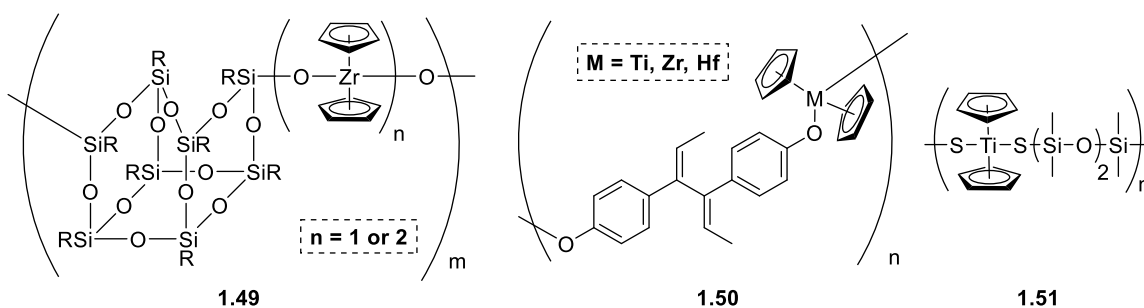
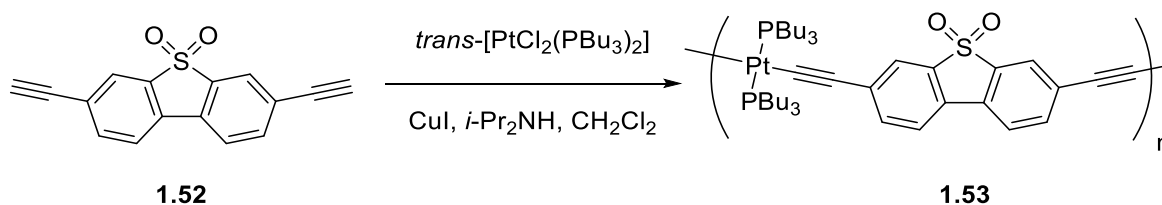


Figure 1.12. Examples of MCPs with metals bridged by heteroatoms.

1.1.2 Alkyne-Based MCPs

Terminal alkynes can go through coupling or addition reactions to link metal-containing species via step-growth polymerization. For example, metallopolyyne is a class of MCPs that have been synthesized by coupling reactions of terminal alkynes with metal salts (Scheme 1.9).⁹⁹⁻¹⁰¹



Scheme 1.9. Synthesis of a metallopolyyne.¹⁰¹

Metallopolyyne commonly contain Pt(II), Pd(II), Hg(II), and also Ni(II) metal centres and are connected by π -conjugated spacers which allows the electronic conjugation to be extended throughout the polymer backbone (Figure 13).¹⁰²⁻¹⁰⁷ As was mentioned earlier, conjugated MCPs, *e.g.*, **1.2**, can be used as flexible and lightweight conductive materials and, due to their promising properties, they have been subject of ongoing research targeting polymer solar cells (PSCs) with higher efficiencies and polymer organic light emitting diodes (POLEDs).^{18, 105, 108}

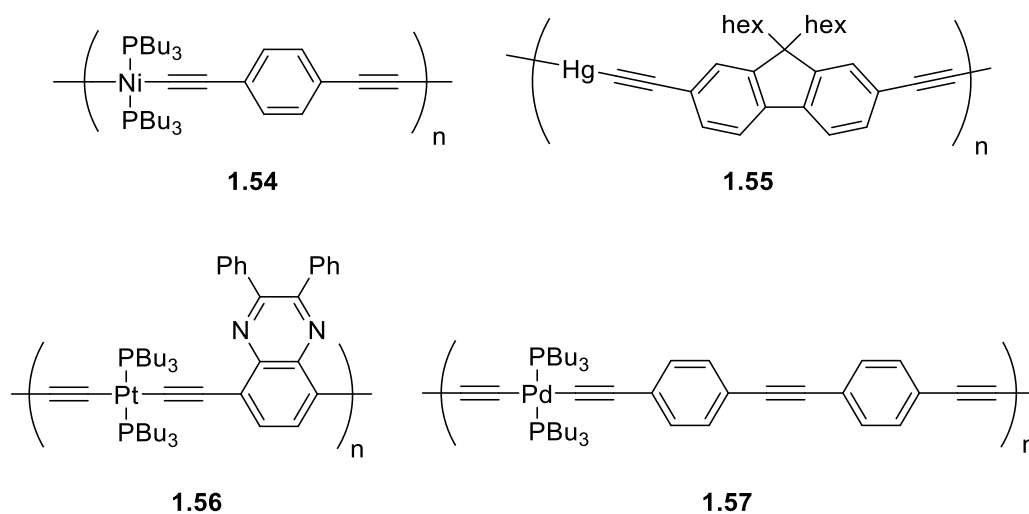
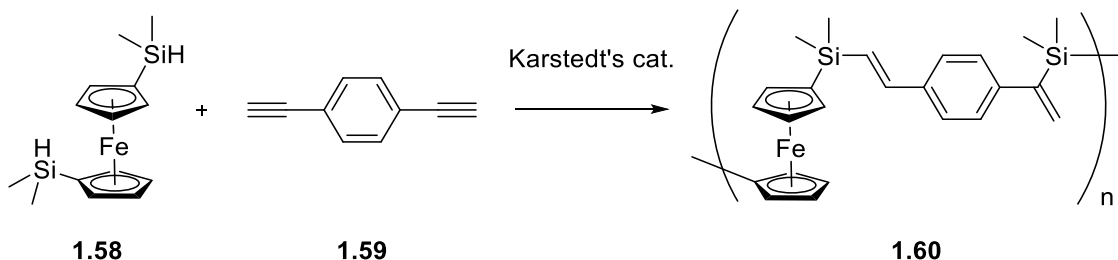


Figure 1.13. Examples of metallopolyyne.⁹⁹

The hydrosilylation reaction of dialkynes and bis(dimethylsilyl)ferrocene with Karstedt's catalyst is another way in which alkynes can be used as precursors for MCP preparation (Scheme 1.10).¹⁰⁹



Scheme 1.10. Example of a MCP synthesis by hydrosilylation of dialkynes.

In addition, alkynes with two π bonds can ligate to a metal or bridging metals to form metal clusters and serve as metal carriers for MCPs. So far, various MCPs have been prepared by polymerization of monomers containing pendant alkyne-metal clusters (Figure 1.14). Clusterization of alkynes with metals can also be performed on alkyne-containing polymers. However, as is typical for post-polymerization functionalization reactions, complete conversion of alkyne groups at the polymer stage is not trivial.¹¹⁰⁻¹¹¹

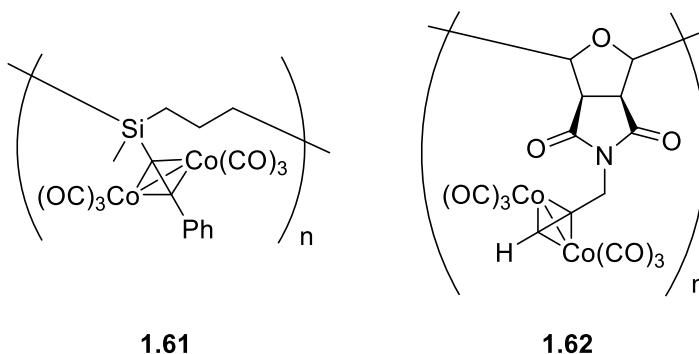


Figure 1.14. Examples of MCPs prepared by alkyne-metal clusterization.

This method can be useful for the addition of a second transition metal to an alkyne functionalized MCP in order to synthesize heterobimetallic polymers (Figure 1.15).¹¹²⁻¹¹⁶

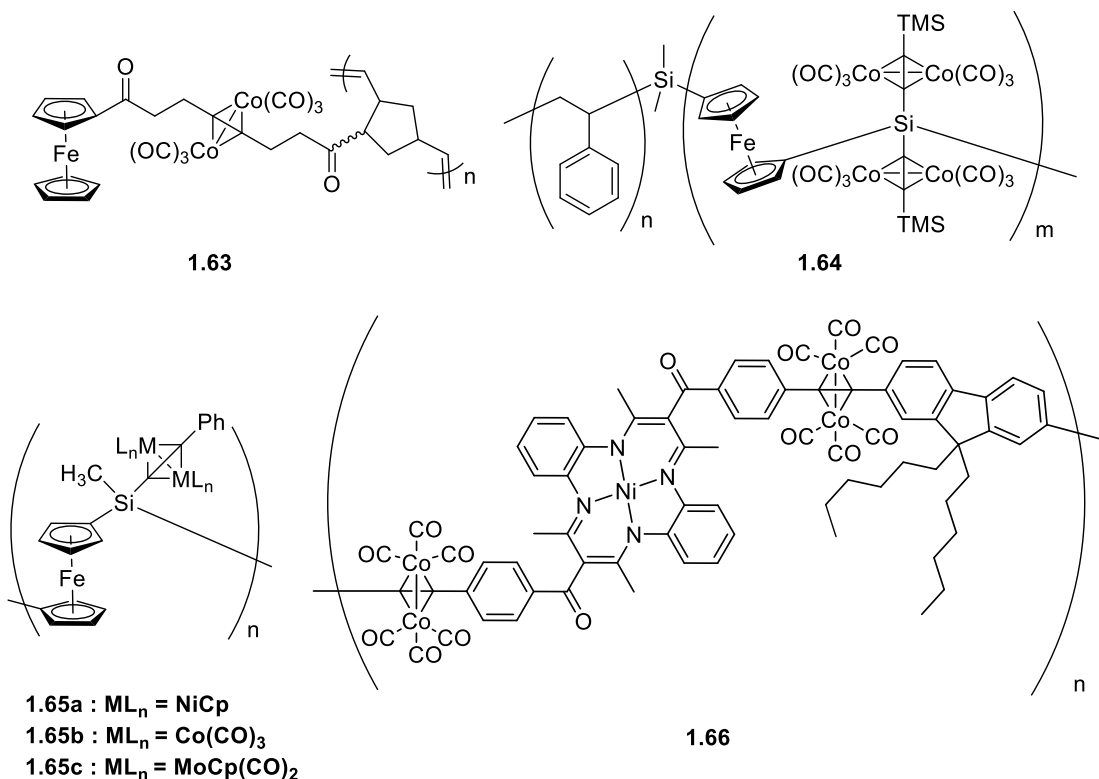


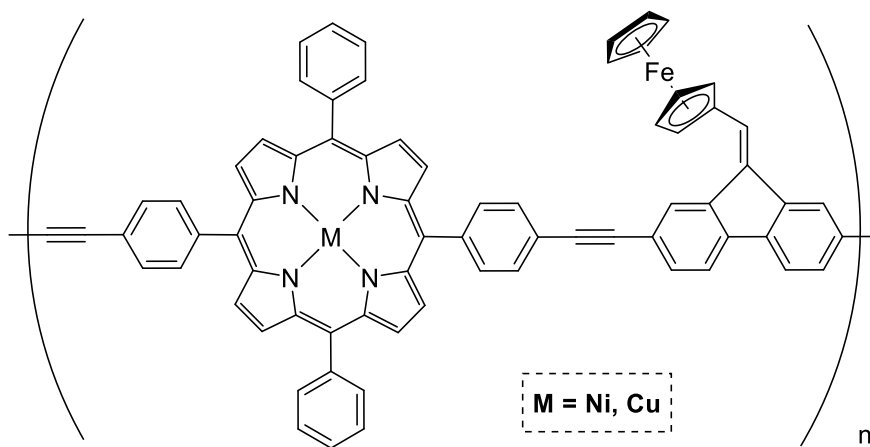
Figure 1.15. Heterobimetallic MCPs including alkyne-metal clusters.

1.1.3 Heteroatom-Based Ligands

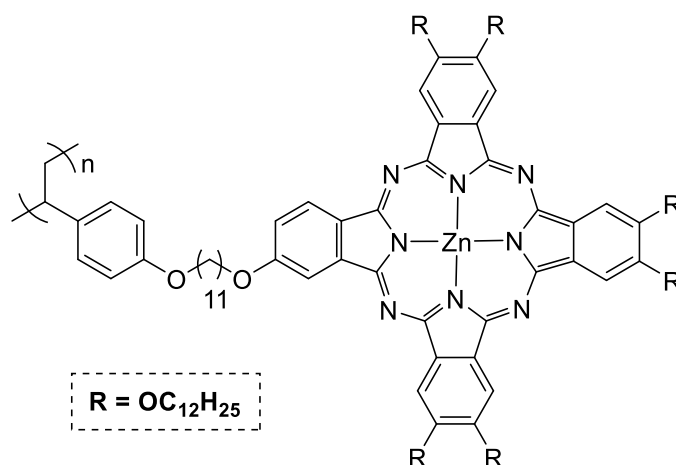
In addition to arene and alkyne groups, polydentate heteroatom-based ligands comprised of phosphorus, nitrogen, and oxygen have been used extensively as frameworks for MCP synthesis.¹¹⁷⁻¹¹⁸ The stability of these metal complexes are strongly dependent on the type of heteroatom, denticity, and rigidity/flexibility of the ligand framework.

1.1.3.1 Macrocycles

Polydentate macrocycles such as porphyrins,¹¹⁷ which have rigid structures, are excellent ligands for transition metals and have a variety of advantageous electronic properties. These macrocycle-metal complexes can serve as metal carriers for MCPs and their pocket size can be synthetically adjusted to suit metals with specific sizes. They can undergo coupling reactions and be part of the main chain, *e.g.*, **1.68**,¹¹⁹⁻¹²⁰ or be added to a polymerizable group and act as a pendant metal-containing group, *e.g.*, **1.69**.¹²¹⁻¹²⁴



1.68



1.69

Figure 1.16. Examples of macrocycle-based MCPs.

1.1.3.2 Acyclic Polydentate Ligands

Similar to macrocyclic ligands, acyclic chelating ligands produce stable complexes. Using these frameworks, many transition metal-containing polymers have been successfully synthesized. In these MCPs, the acyclic-ligand metal complexes can be part of the backbone, *e.g.*, **1.70** and **1.71**, or exist as a pendant group, *e.g.*, **1.72**.^{118, 125-127}

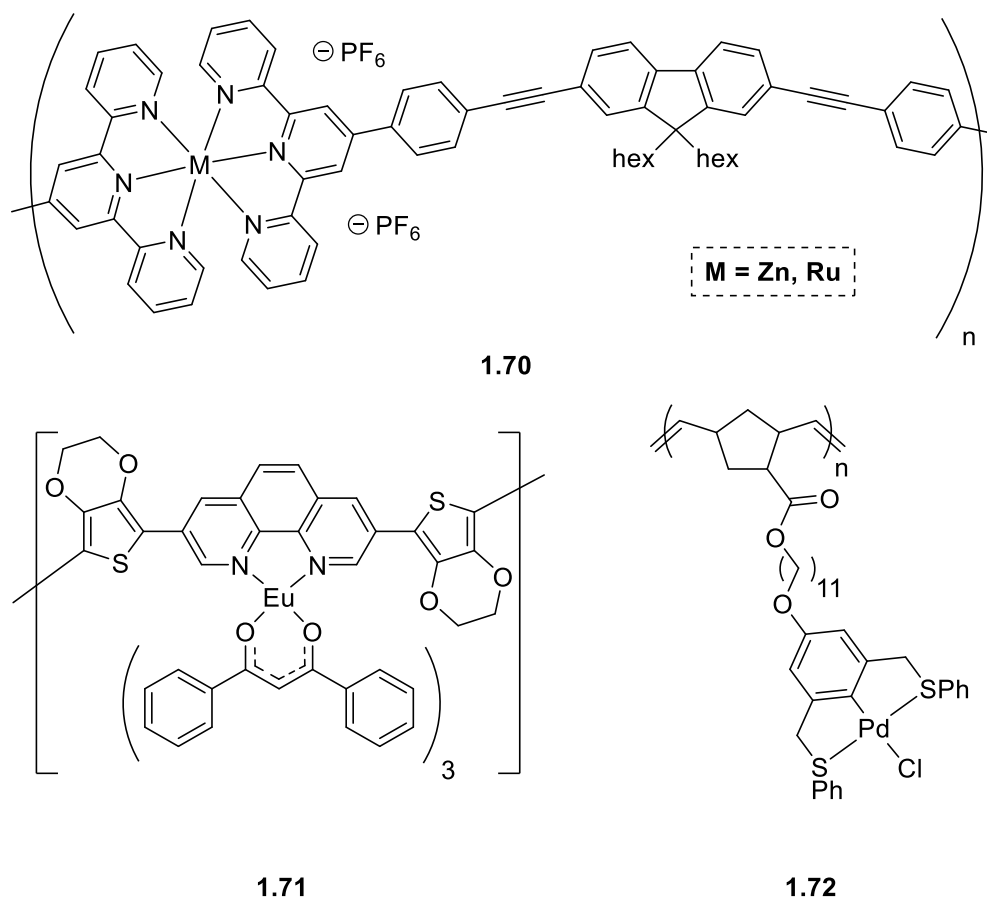


Figure 1.17. Example of MCPs based on acyclic ligands.

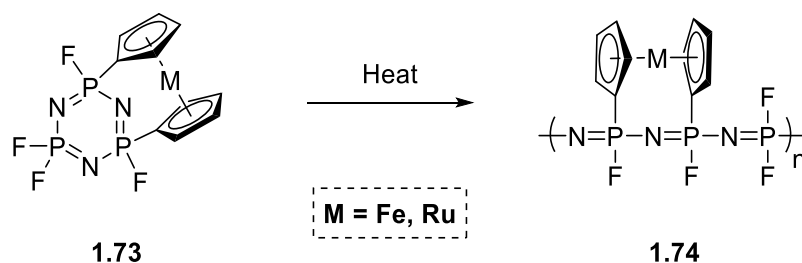
1.2 Phosphorous-Based Frameworks for MCP Synthesis

Organophosphorus compounds are one of the most extensively used ligands in coordination chemistry and can be used for the MCP synthesis. They can form P-C bonds with ligands that carry a metal or directly coordinate to metals using their lone pairs of electrons.¹²⁸

1.2.1 Phosphazenes

Phosphazenes are a family of compounds which contain P=N bonds, have high thermal stability, are flexible, and as a result they have been used as high performance elastomers and as flame retardants.¹²⁹ In the 1960s, Allcock and co-workers introduced

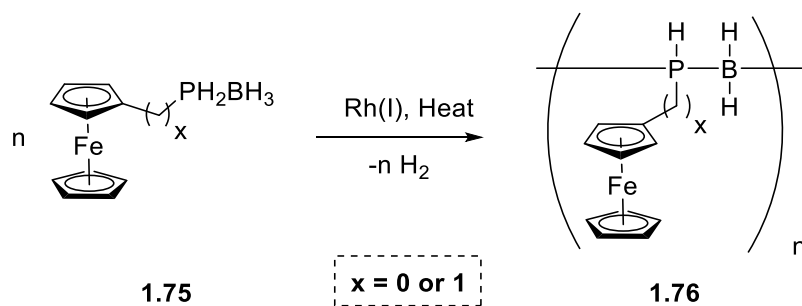
poly(dichloro)phosphazenes $(\text{NPCl}_2)_n$ that have received tremendous interest because they have an inorganic backbone and a substitutionally labile Cl attached to phosphorous that can be replaced by other groups.¹³⁰⁻¹³² Later in 80's, the Allcock group synthesized cyclic phosphazenes attached to ferrocene and ruthenocene, *i.e.*, RuCp_2 , and by ROP prepared the corresponding MCPs (Scheme 1.11).¹³³⁻¹³⁵



Scheme 1.11. ROP of cyclic metal-containing phosphazenes.

1.2.2 Phosphinoboranes

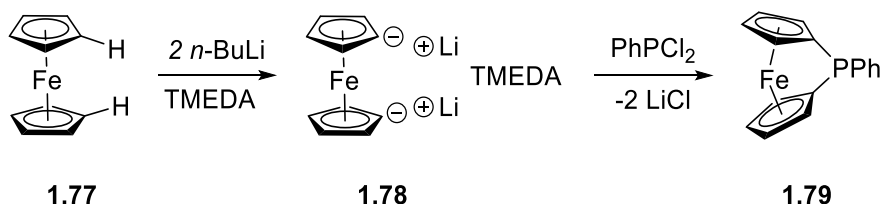
Polyphosphinoboranes are another family of polymers that have an inorganic backbone. This family was discovered in the early 50's when Burg and Wagner used heat to dehydrocouple phosphine-borane adducts in order to produce the first generation of low-melt polyphosphinoboranes.¹³⁶ However, it took about 60 years until the Hey-Hawkins group used this strategy and a Rh(I) catalyst to synthesize the first metal-containing polyphosphinoboranes (Scheme 1.12).¹³⁷⁻¹³⁸



Scheme 1.12. Example of a dehydrocoupling reaction of a phosphine-borane adduct.

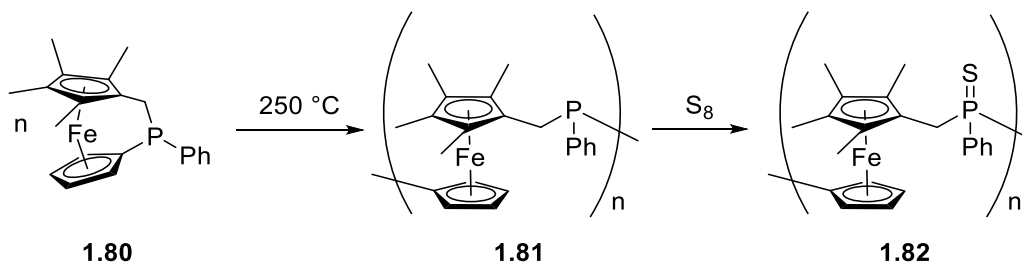
1.2.3 Polyphosphaferrocenes

Phosphaferrocenophanes are a family of strained *ansa*-ferrocenes in which the Cp rings are bridged by a phosphorous spacer. They can be synthesized by the lithiation of Cp rings of ferrocene followed by a condensation reaction with RPhPCl_2 (Scheme 1.13).¹³⁹⁻¹⁴¹



Scheme 1.13. Example of the synthesis of a strained phospha[1]ferrocenophane.

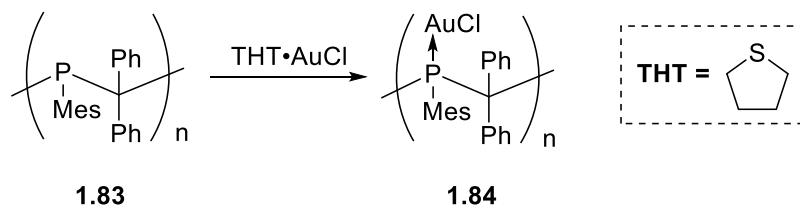
For a phosphaferrocenophane to undergo ROP, the spacer may contain one or two atoms but not more as further elongation of the bridge results in decreased ring-strain and lower reactivity.¹³⁹ As an example, Manners and co-workers reported ROP of a phosphaferroceneophane with (-PPhCH₂-) bridge **1.80**. Thermal ROP of this monomer yielded polymer **1.81**, which was sulfurized before measurement of the molecular weight by gel permeation chromatography (GPC) (Scheme 1.14).¹³⁹



Scheme 1.14. Example of ROP of a strained phospha[2]ferrocenophane.

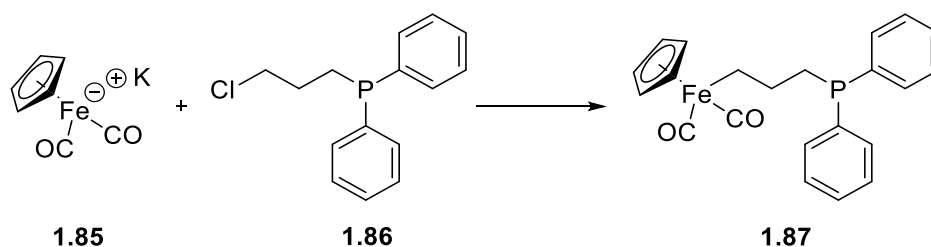
1.2.4 Phosphine Ligands

Phosphines are ubiquitous materials that have been used in various fields of chemistry. Tertiary phosphine polymers have been utilized as polyligands for the coordination of transition metals and production of MCPs. In this regard, the Gates group has reported polymerization of phosphaalkenes to gain **1.83** and later coordinated the polyphosphine to AuCl *en route* to gold nanostructures (Scheme 1.15).¹⁴²⁻¹⁴³



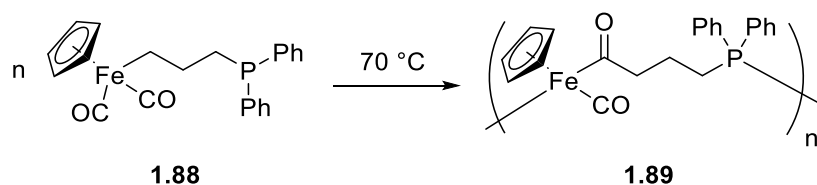
Scheme 1.15. Example of coordination of a tertiary phosphine polymer to a metal.¹⁴³

A migratory insertion is a classic organometallic reaction in which two ligands on a metal complex combine and leave an empty coordination site on the metal. Using this concept, Xiaosong Wang's group recently designed monomer **1.87**, in which the alkyl group can migrate and become a carbonyl-terminated ligand which is coordinated to iron (Scheme 1.16).



Scheme 1.16. Monomer synthesis.

The resulting vacant coordination site on the iron can be filled by ligation of a phosphine group from a second monomer which contains a metal centre that can also undergo the similar process and grow the polymer chain (Scheme 1.17).¹⁴⁴⁻¹⁴⁶



Scheme 1.17. Example of migration insertion polymerization.

1.3 Thesis Scope

The main goal of this thesis was the development of new phosphine-based frameworks for the introduction of metals into polymer scaffolds. Since the phosphines described were utilized as metal carriers for the preparation of polymers, the second chapter will describe the synthesis and characterization of a family of air-stable primary, secondary, and tertiary phosphines containing all possible combinations of ethylferrocene and ethylruthenocene substituents $[\text{PH}_{3-n}(\text{CH}_2\text{CH}_2\text{Mc})_n; n = 1-3; \text{Mc: Fc and/or Rc}]$.

In the third chapter, as an example of an application of the primary, secondary, and tertiary ethylferrocenephosphines, their coordination to Group VI transition metals and the properties of the resulting adducts $[\text{M}(\text{CO})_5\text{L}; \text{M: Cr, Mo, W}; \text{L: PH}_2(\text{CH}_2\text{CH}_2\text{Fc}), \text{PH}(\text{CH}_2\text{CH}_2\text{Fc})_2, \text{P}(\text{CH}_2\text{CH}_2\text{Fc})_3]$ will be discussed.

The fourth chapter will describe results toward the synthesis of phosphonium polyelectrolytes that were prepared by quaternization of the tertiary phosphines $[\text{P}(\text{CH}_2\text{CH}_2\text{Mc})_3; \text{Mc: Fc and/or Rc}]$ in order to install methacrylate or styrene groups which were later polymerized by using free-radical polymerization method. Pyrolysis of the phosphonium polyelectrolytes yielded metal (Fe and/or Ru) and phosphorous enriched crystalline nanomaterials with Fe/Ru ratios dictated by the phosphonium polyelectrolyte structures.

Tertiary phosphine polymers are a valuable subclass of polymers because phosphorus centres can act as ligands/nucleophiles. In this context, the secondary phosphine $[\text{PH}(\text{CH}_2\text{CH}_2\text{Mc})_2; \text{Mc: Fc and Rc}]$, was converted to a heterobimetallic tertiary phosphine monomer containing a styrene group. Free-radical polymerization of this monomer gained a heterobimetallic polymer, which was later ligated to $\text{W}(\text{CO})_5$, to afford the first example of a heterotrimetallic polymer. The fifth chapter will report their synthesis and characterization and the sixth chapter will summarize the key results and conclusions of this thesis and provide suggestions for the future directions of this research.

1.4 References

1. Morawetz, H., History of polymer science. In *Encyclopedia of Polymer Science and Technology*, John Wiley & Sons, Inc.: 2002.
2. Abd-El-Aziz, A. S.; Strohm, E. A. *Polymer* **2012**, *53*, 4879–4921.
3. Stahl, G. A., A short history of polymer science. In *Polymer Science Overview*, American Chemical Society: 1981; Vol. 175, pp 25–44.
4. Whittell, G. R.; Manners, I. *Adv. Mater.* **2007**, *19*, 3439–3468.
5. Eloi, J.-C.; Chabanne, L.; Whittell, G. R.; Manners, I. *Mater. Today* **2008**, *11*, 28–36.
6. Caminade, A.-M. *Chem. Soc. Rev.* **2016**, *45*, 5174–5186.
7. Winter, A.; Schubert, U. S. *Chem. Soc. Rev.* **2016**, *45*, 5311–5357.
8. Astruc, D.; Chardac, F. *Chem. Rev.* **2001**, *101*, 2991–3023.
9. Buchmeiser, M. R. *Chem. Rev.* **2009**, *109*, 303–321.
10. Whittell, G. R.; Hager, M. D.; Schubert, U. S.; Manners, I. *Nat. Mater.* **2011**, *10*, 176–188.
11. McConnell, A. J.; Wood, C. S.; Neelakandan, P. P.; Nitschke, J. R. *Chem. Rev.* **2015**, *115*, 7729–7793.
12. Zhang, K. Y.; Liu, S.; Zhao, Q.; Huang, W. *Coord. Chem. Rev.* **2016**, *319*, 180–195.
13. Yan, Y.; Zhang, J.; Ren, L.; Tang, C. *Chem. Soc. Rev.* **2016**, *45*, 5232–5263.
14. Stanley, J. M.; Holliday, B. J. *Coord. Chem. Rev.* **2012**, *256*, 1520–1530.
15. Holliday, B. J.; Swager, T. M. *Chem. Commun.* **2005**, 23–36.
16. Wolf, M. O. *J. Inorg. Organomet. Polym.* **2006**, *16*, 189–199.

17. Staff, R. H.; Gallei, M.; Mazurowski, M.; Rehahn, M.; Berger, R.; Landfester, K.; Crespy, D. *ACS Nano* **2012**, *6*, 9042–9049.
18. Wong, W.-Y.; Wang, X.-Z.; He, Z.; Djurisic, A. B.; Yip, C.-T.; Cheung, K.-Y.; Wang, H.; Mak, C. S. K.; Chan, W.-K. *Nat. Mater.* **2007**, *6*, 521–527.
19. Janiak, C. *Dalton Trans.* **2003**, 2781–2804.
20. Kitagawa, S.; Kitaura, R.; Noro, S.-i. *Angew. Chem. Int. Ed.* **2004**, *43*, 2334–2375.
21. Dobrawa, R.; Würthner, F. *J. Polym. Sci., Part A: Polym. Chem.* **2005**, *43*, 4981–4995.
22. Horikoshi, R.; Mochida, T. *Eur. J. Inorg. Chem.* **2010**, *2010*, 5355–5371.
23. Horike, S.; Kitagawa, S., Design of porous coordination polymers/metal–organic frameworks: Past, present and future. In *Metal-organic frameworks*, Wiley-VCH Verlag GmbH & Co. KGaA: 2011; pp 1–21.
24. de Lange, K.; Paulusse, J. M. J.; Marcelis, A. T. M.; Zuilhof, H., Reversible Coordination Polymers. In *Ionic Interactions in Natural and Synthetic Macromolecules*, John Wiley & Sons, Inc.: 2012; pp 337–359.
25. Williams, K. A.; Boydston, A. J.; Bielawski, C. W. *Chem. Soc. Rev.* **2007**, *36*, 729–744.
26. Abd-El-Aziz, A. S.; Shipman, P. O.; Boden, B. N.; McNeil, W. S. *Prog. Polym. Sci.* **2010**, *35*, 714–836.
27. Kealy, T. J.; Pauson, P. L. *Nature* **1951**, *168*, 1039–1040.
28. Hardy, C. G.; Zhang, J.; Yan, Y.; Ren, L.; Tang, C. *Prog. Polym. Sci.* **2014**, *39*, 1742–1796.
29. Cao, K.; Murshid, N.; Wang, X. *Macromol. Rapid Commun.* **2015**, *36*, 586–596.
30. Pittman, C. U.; Lin, C.-C.; Rounsefell, T. D. *Macromolecules* **1978**, *11*, 1022–1027.

31. Pittman, C. U.; Grube, P. L. *J. Polym. Sci., Part A: Polym. Chem.* **1971**, *9*, 3175–3186.
32. Lai, J. C.; Rounsfell, T.; Pittman, C. U. *J. Polym. Sci., Part A: Polym. Chem.* **1971**, *9*, 651–662.
33. Pittman, C. U.; Grube, P. L.; Ayers, O. E.; McManus, S. P.; Rausch, M. D.; Moser, G. A. *J. Polym. Sci., Part A: Polym. Chem.* **1972**, *10*, 379–386.
34. Pittman, C. U.; Marlin, G. V. *J. Polym. Sci., Part A: Polym. Chem.* **1973**, *11*, 2753–2765.
35. Pittman, C. U.; Ayers, O. E.; McManus, S. P. *J. Macromol. Sci. Chem.* **1973**, *7*, 1563–1579.
36. Pittman, C. U.; Grube, P. L. *J. Appl. Polym. Sci.* **1974**, *18*, 2269–2278.
37. Pittman, C. U. *Macromolecules* **1974**, *7*, 396–397.
38. Evans, G. O.; Pittman, C. U.; McMillan, R.; Beach, R. T.; Jones, R. *J. Organomet. Chem.* **1974**, *67*, 295–314.
39. Mintz, E. A.; Rausch, M. D.; Edwards, B. H.; Sheats, J. E.; Rounsfell, T. D.; Pittman, C. U. *J. Organomet. Chem.* **1977**, *137*, 199–205.
40. Macomber, D. W.; Hart, W. P.; Rausch, M. D.; Priester, R. D.; Pittman, C. U. *J. Am. Chem. Soc.* **1982**, *104*, 884–886.
41. Macomber, D. W.; Rausch, M. D.; Jayaraman, T. V.; Priester, R. D.; Pittman, C. U. *J. Organomet. Chem.* **1981**, *205*, 353–364.
42. Pittman, C. U.; Marlin, G. V.; Rounsfell, T. D. *Macromolecules* **1973**, *6*, 1–8.
43. Pittman, C. U. *J. Inorg. Organomet. Polym.* **2005**, *15*, 33–55.
44. Chan, Y. N. C.; Craig, G. S. W.; Schrock, R. R.; Cohen, R. E. *Chem. Mater.* **1992**, *4*, 885–894.

45. Pittman, C. U.; Felis, R. F. *J. Organomet. Chem.* **1974**, *72*, 399–413.
46. Shultz, G. V.; Tyler, D. R. *J. Inorg. Organomet. Polym.* **2009**, *19*, 423–435.
47. Tyler, D. R. *Coord. Chem. Rev.* **2003**, *246*, 291–303.
48. Tenhaeff, S. C.; Tyler, D. R. *Organometallics* **1991**, *10*, 473–482.
49. Moran, M.; Pascual, M. C.; Cuadrado, I.; Losada, J. *Organometallics* **1993**, *12*, 811–822.
50. Lucas, N. T.; Humphrey, M. G.; Rae, A. D. *Macromolecules* **2001**, *34*, 6188–6195.
51. Chen, R.; Tyler, D. R. *Macromolecules* **2004**, *37*, 5430–5436.
52. Randles, M. D.; Lucas, N. T.; Cifuentes, M. P.; Humphrey, M. G.; Smith, M. K.; Willis, A. C.; Samoc, M. *Macromolecules* **2007**, *40*, 7807–7818.
53. Shultz, G. V.; Zemke, J. M.; Tyler, D. R. *Macromolecules* **2009**, *42*, 7644–7649.
54. Brady, S. E.; Tyler, D. R. *J. Inorg. Organomet. Polym.* **2013**, *23*, 158–166.
55. Sharma, H. K.; Pannell, K. H., Synthesis, reactivity, and ring-opening polymerization of sila-metallacyclobutanes. In *Metal-Containing and Metallosupramolecular Polymers and Materials*, American Chemical Society: 2006; Vol. 928, pp 457–471.
56. Kumar, M.; Cervantes-Lee, F.; Sharma, H. K.; Pannell, K. H. *Organometallics* **2007**, *26*, 3005–3009.
57. Apodaca, P.; Kumar, M.; Cervantes-Lee, F.; Sharma, H. K.; Pannell, K. H. *Organometallics* **2008**, *27*, 3136–3141.
58. Sharma, H. K.; Cervantes-Lee, F.; Pannell, K. H. *J. Am. Chem. Soc.* **2004**, *126*, 1326–1327.
59. Sharma, H. K.; Pannell, K. H. *Chem. Commun.* **2004**, 2556–2557.

60. Kumar, M.; Metta-Magana, A. J.; Sharma, H. K.; Pannell, K. H. *Dalton Trans.* **2010**, 39, 7125–7131.
61. Braunschweig, H.; Dellermann, T.; Dewhurst, R. D.; Mies, J.; Radacki, K.; Stellwag-Konertz, S.; Vargas, A. *Organometallics* **2014**, 33, 1536–1539.
62. Arimoto, F. S.; Haven, A. C. *J. Am. Chem. Soc.* **1955**, 77, 6295–6297.
63. Hudson, R. D. A. *J. Organomet. Chem.* **2001**, 637–639, 47–69.
64. Sanders, R.; Mueller-Westerhoff, U. T. *J. Organomet. Chem.* **1996**, 512, 219–224.
65. Rabiee Kenaree, A.; Cuthbert, T. J.; Barbon, S. M.; Boyle, P. D.; Gillies, E. R.; Ragona, P. J.; Gilroy, J. B. *Organometallics* **2015**, 34, 4272–4280.
66. Kunitake, T.; Nakashima, T.; Aso, C. *Macromol. Chem. Phys.* **1971**, 146, 79–90.
67. Pittman, C. U.; Hirao, A. *J. Polym. Sci., Part A: Polym. Chem.* **1978**, 16, 1197–1209.
68. Albagli, D.; Bazan, G.; Wrighton, M. S.; Schrock, R. R. *J. Am. Chem. Soc.* **1992**, 114, 4150–4158.
69. Albagli, D.; Bazan, G. C.; Schrock, R. R.; Wrighton, M. S. *J. Am. Chem. Soc.* **1993**, 115, 7328–7334.
70. Shi, M.; Li, A.-L.; Liang, H.; Lu, J. *Macromolecules* **2007**, 40, 1891–1896.
71. Xiao, Z.-P.; Cai, Z.-H.; Liang, H.; Lu, J. *J. Mater. Chem.* **2010**, 20, 8375–8381.
72. Pietschnig, R. *Chem. Soc. Rev.* **2016**, 45, 5216–5231.
73. Pannell, K. H.; Rozell, J. M.; Zeigler, J. M. *Macromolecules* **1988**, 21, 276–278.
74. Yan, Y.; Pageni, P.; Kabir, M. P.; Tang, C. *SYNLETT* **2016**, 27, 984–1005.
75. Ren, L.; Zhang, J.; Bai, X.; Hardy, C. G.; Shimizu, K. D.; Tang, C. *Chem. Sci.* **2012**, 3, 580–583.

76. Wei, J.; Ren, L.; Tang, C.; Su, Z. *Polym. Chem.* **2014**, *5*, 6480–6488.
77. Yan, Y.; Deaton, T. M.; Zhang, J.; He, H.; Hayat, J.; Pageni, P.; Matyjaszewski, K.; Tang, C. *Macromolecules* **2015**, *48*, 1644–1650.
78. Ciganda, R.; Gu, H.; Castel, P.; Zhao, P.; Ruiz, J.; Hernández, R.; Astruc, D. *Macromol. Rapid Commun.* **2016**, *37*, 105–111.
79. Gu, H.; Ciganda, R.; Castel, P.; Ruiz, J.; Astruc, D. *Macromolecules* **2016**, *49*, 4763–4773.
80. Hadadpour, M.; Liu, Y.; Chadha, P.; Ragogna, P. J. *Macromolecules* **2014**, *47*, 6207–6217.
81. Hadadpour, M.; Gwyther, J.; Manners, I.; Ragogna, P. J. *Chem. Mater.* **2015**, *27*, 3430–3440.
82. Peckham, T. J.; Nguyen, P.; Bourke, S. C.; Wang, Q.; Harrison, D. G.; Zoricak, P.; Russell, C.; Liable-Sands, L. M.; Rheingold, A. L.; Lough, A. J.; Manners, I. *Organometallics* **2001**, *20*, 3035–3043.
83. Foucher, D. A.; Tang, B. Z.; Manners, I. *J. Am. Chem. Soc.* **1992**, *114*, 6246–6248.
84. Russell, A. D.; Musgrave, R. A.; Stoll, L. K.; Choi, P.; Qiu, H.; Manners, I. *J. Organomet. Chem.* **2015**, *784*, 24–30.
85. Hailes, R. L. N.; Oliver, A. M.; Gwyther, J.; Whittell, G. R.; Manners, I. *Chem. Soc. Rev.* **2016**, *45*, 5358–5407.
86. Kapoor, R. N.; Crawford, G. M.; Mahmoud, J.; Dementiev, V. V.; Nguyen, M. T.; Diaz, A. F.; Pannell, K. H. *Organometallics* **1995**, *14*, 4944–4947.
87. Berenbaum, A.; Manners, I. *Dalton Trans.* **2004**, 2057–2058.
88. Ma, Y.; Dong, W.-F.; Hempenius, M. A.; Mohwald, H.; Vancso, G. J. *Nat. Mater.* **2006**, *5*, 724–729.

89. Herbert, D. E.; Mayer, U. F. J.; Manners, I. *Angew. Chem. Int. Ed.* **2007**, *46*, 5060–5081.
90. Braunschweig, H.; Adams, C. J.; Kupfer, T.; Manners, I.; Richardson, R. M.; Whittell, G. R. *Angew. Chem. Int. Ed.* **2008**, *47*, 3826–3829.
91. Mayer, U. F. J.; Gilroy, J. B.; O'Hare, D.; Manners, I. *J. Am. Chem. Soc.* **2009**, *131*, 10382–10383.
92. Tagne Kuate, A. C.; Daniliuc, C. G.; Jones, P. G.; Tamm, M. *Eur. J. Inorg. Chem.* **2012**, *2012*, 1727–1733.
93. Baljak, S.; Russell, A. D.; Binding, S. C.; Haddow, M. F.; O'Hare, D.; Manners, I. *J. Am. Chem. Soc.* **2014**, *136*, 5864–5867.
94. Lichtenhan, J. D. *Comment Inorg. Chem.* **1995**, *17*, 115–130.
95. Haddad, T. S.; Lichtenhan, J. D. *J. Inorg. Organomet. Polym.* **1995**, *5*, 237–246.
96. Nguyen, P.; Gómez-Elipse, P.; Manners, I. *Chem. Rev.* **1999**, *99*, 1515–1548.
97. Roner, M. R.; Carraher, C. E.; Shahi, K.; Ashida, Y.; Barot, G. *BMC Cancer* **2009**, *9*, 1–9.
98. Bouzat, F.; Darsy, G.; Foucaud, S.; Lucas, R. *Polym. Rev.* **2016**, *56*, 187–224.
99. Wong, W.-Y. *J. Inorg. Organomet. Polym.* **2005**, *15*, 197–219.
100. Ho, C.-L.; Wong, W.-Y. *Coord. Chem. Rev.* **2013**, *257*, 1614–1649.
101. Ho, C.-L.; Poon, S.-Y.; Lo, P.-K.; Wong, M.-S.; Wong, W.-Y. *J. Inorg. Organomet. Polym.* **2013**, *23*, 206–215.
102. Yang, M. J.; Ding, K.; Zhang, L. J.; Chen, W. G. *Synth. Met.* **1995**, *71*, 1739–1740.
103. Yang, M.; Zhang, L.; Lei, Z.; Ye, P.; Si, J.; Yang, Q.; Wang, Y. *J. Appl. Polym. Sci.* **1998**, *70*, 1165–1172.

104. Wilson, J. S.; Dhoot, A. S.; Seeley, A. J. A. B.; Khan, M. S.; Kohler, A.; Friend, R. H. *Nature* **2001**, *413*, 828–831.
105. Zhou, G. J.; Wong, W. Y.; Ye, C.; Lin, Z. *Adv. Funct. Mater.* **2007**, *17*, 963–975.
106. Silvestri, F.; Marrocchi, A.; Seri, M.; Kim, C.; Marks, T. J.; Facchetti, A.; Taticchi, A. *J. Am. Chem. Soc.* **2010**, *132*, 6108–6123.
107. Keller, J. M.; Glusac, K. D.; Danilov, E. O.; McIlroy, S.; Sreearuothai, P.; R. Cook, A.; Jiang, H.; Miller, J. R.; Schanze, K. S. *J. Am. Chem. Soc.* **2011**, *133*, 11289–11298.
108. Wong, W.-Y.; Ho, C.-L. *Acc. Chem. Res.* **2010**, *43*, 1246–1256.
109. Jain, R.; Lalancette, R. A.; Sheridan, J. B. *Organometallics* **2005**, *24*, 1458–1467.
110. Abd-El-Aziz, A. S.; Winram, D. J.; Shipman, P. O.; Bichler, L. *Macromol. Rapid Commun.* **2010**, *31*, 1992–1997.
111. Chabanne, L.; Matas, I.; Patra, S. K.; Manners, I. *Polym. Chem.* **2011**, *2*, 2651–2660.
112. Clendenning, S. B.; Han, S.; Coombs, N.; Paquet, C.; Rayat, M. S.; Grozea, D.; Brodersen, P. M.; Sodhi, R. N. S.; Yip, C. M.; Lu, Z. H.; Manners, I. *Adv. Mater.* **2004**, *16*, 291–296.
113. Cheng, A. Y.; Clendenning, S. B.; Yang, G.; Lu, Z.-H.; Yip, C. M.; Manners, I. *Chem. Commun.* **2004**, 780–781.
114. Chan, W. Y.; Clendenning, S. B.; Berenbaum, A.; Lough, A. J.; Aouba, S.; Ruda, H. E.; Manners, I. *J. Am. Chem. Soc.* **2005**, *127*, 1765–1772.
115. Greenberg, S.; Clendenning, S. B.; Liu, K.; Manners, I.; Aouba, S.; Ruda, H. E. *Macromolecules* **2005**, *38*, 2023–2026.

116. Liu, K.; Clendenning, S. B.; Friebe, L.; Chan, W. Y.; Zhu; Freeman, M. R.; Yang, G. C.; Yip, C. M.; Grozea, D.; Lu, Z.-H.; Manners, I. *Chem. Mater.* **2006**, *18*, 2591–2601.
117. Burrell, A. K.; Officer, D. L.; Plieger, P. G.; Reid, D. C. W. *Chem. Rev.* **2001**, *101*, 2751–2796.
118. Wild, A.; Schlütter, F.; Pavlov, G. M.; Friebe, C.; Festag, G.; Winter, A.; Hager, M. D.; Cimrová, V.; Schubert, U. S. *Macromol. Rapid Commun.* **2010**, *31*, 868–874.
119. Choi, M.-S.; Yamazaki, T.; Yamazaki, I.; Aida, T. *Angew. Chem. Int. Ed.* **2004**, *43*, 150–158.
120. Beletskaya, I.; Tyurin, V. S.; Tsivadze, A. Y.; Guillard, R.; Stern, C. *Chem. Rev.* **2009**, *109*, 1659–1713.
121. McKeown, N. B. *J. Mater. Chem.* **2000**, *10*, 1979–1995.
122. Imahori, H. *J. Phys. Chem. B* **2004**, *108*, 6130–6143.
123. Chan, W. K. *Coord. Chem. Rev.* **2007**, *251*, 2104–2118.
124. Dong, Q.; Qu, W.; Liang, W.; Tai, F.; Guo, K.; Leung, C.-W.; Lo, Y. H.; Wong, W.-Y. *J. Mater. Chem. C* **2016**, *4*, 5010–5018.
125. Peng, Z.; Gharavi, A. R.; Yu, L. *J. Am. Chem. Soc.* **1997**, *119*, 4622–4632.
126. Pollino, J. M.; Stubbs, L. P.; Weck, M. *J. Am. Chem. Soc.* **2004**, *126*, 563–567.
127. Chen, X.-Y.; Yang, X.; Holliday, B. J. *J. Am. Chem. Soc.* **2008**, *130*, 1546–1547.
128. Noonan, K. J. T.; Gates, D. P. *Annu. Rep. Prog. Chem., Sect. A* **2007**, *103*, 407–427.
129. Allcock, H. R. *Soft Matter* **2012**, *8*, 7521–7532.
130. Manners, I.; Riding, G. H.; Dodge, J. A.; Allcock, H. R. *J. Am. Chem. Soc.* **1989**, *111*, 3067–3069.

131. Allcock, H. R. *J. Inorg. Organomet. Polym.* **1992**, *2*, 197–211.
132. Rothmund, S.; Teasdale, I. *Chem. Soc. Rev.* **2016**, *45*, 5200–5215.
133. Allcock, H. R.; Lavin, K. D.; Riding, G. H. *Macromolecules* **1985**, *18*, 1340–1345.
134. Allcock, H. R.; Desorcie, J. L.; Riding, G. H. *Polyhedron* **1987**, *6*, 119–157.
135. Allcock, H. R.; Mang, M. N.; McDonnell, G. S.; Parvez, M. *Macromolecules* **1987**, *20*, 2060–2067.
136. Burg, A. B.; Wagner, R. I. *J. Am. Chem. Soc.* **1953**, *75*, 3872–3877.
137. Pandey, S.; Lönnecke, P.; Hey-Hawkins, E. *Inorg. Chem.* **2014**, *53*, 8242–8249.
138. Pandey, S.; Lönnecke, P.; Hey-Hawkins, E. *Eur. J. Inorg. Chem.* **2014**, *2014*, 2456–2465.
139. Resendes, R.; Nelson, J. M.; Fischer, A.; Jäkle, F.; Bartole, A.; Lough, A. J.; Manners, I. *J. Am. Chem. Soc.* **2001**, *123*, 2116–2126.
140. Cao, L.; Manners, I.; Winnik, M. A. *Macromolecules* **2001**, *34*, 3353–3360.
141. Patra, S. K.; Whittell, G. R.; Nagiah, S.; Ho, C.-L.; Wong, W.-Y.; Manners, I. *Chem. Eur. J.* **2010**, *16*, 3240–3250.
142. Tsang, C.-W.; Baharloo, B.; Riendl, D.; Yam, M.; Gates, D. P. *Angew. Chem. Int. Ed.* **2004**, *43*, 5682–5685.
143. Noonan, K. J. T.; Gillon, B. H.; Cappello, V.; Gates, D. P. *J. Am. Chem. Soc.* **2008**, *130*, 12876–12877.
144. Wang, X.; Cao, K.; Liu, Y.; Tsang, B.; Liew, S. *J. Am. Chem. Soc.* **2013**, *135*, 3399–3402.
145. Liu, J.; Cao, K.; Nayyar, B.; Tian, X.; Wang, X. *Polym. Chem.* **2014**, *5*, 6702–6709.

146. Cao, K.; Murshid, N.; Li, L.; Lopez, A.; Tam, K. C.; Wang, X. *Macromolecules* **2015**, *48*, 7968–7977.

Chapter 2

2 Synthesis and Characterization of a Family of Air-Stable Ferrocene- and Ruthenocene-Containing Primary, Secondary, and Tertiary Phosphines

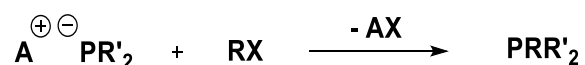
Adapted from:

1) Rabiee Kenaree, A.; Cuthbert, T.J.; Barbon, S.M.; Boyle, P.D.; Gillies, E.R.; Ragona, P.J.; Gilroy, J.B.* Synthesis and Characterization of a Family of Air-Stable Ferrocene- and Ruthenocene-Containing Primary, Secondary, and Tertiary Phosphines. *Organometallics* **2015**, *34*, 4272–4280.

2) Rabiee Kenaree, A.; Berven, B.M., Ragona, P.J.*; Gilroy, J.B.* Highly-Metallized Phosphonium Polyelectrolytes. *Chem. Commun.* **2014**, *50*, 10714–10717.

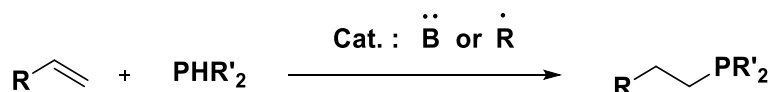
2.1 Introduction

Phosphines are common ligands in the field of coordination chemistry¹⁻⁸, and can be synthesized from various precursors such as phosphides. Phosphides are good nucleophiles and can be prepared by the metalation reactions of primary and secondary phosphines, using Li, Na, and K. They can undergo a salt-elimination coupling reaction with a variety of electrophiles, such as alkyl halides, to afford phosphines (Scheme 2.1).⁹



Scheme 2.1. The salt-elimination reaction of phosphides with alkyl halides.

The base- or radical-catalyzed hydrophosphination reaction of unsaturated hydrocarbons is another synthetic method which is widely used by industry. In this route, a radical or base breaks a P-H bond and removes the hydrogen from phosphorous. The resulting phosphine-radical or phosphide then attacks an unsaturated bond to produce a new P-C bond (Scheme 2.2).¹⁰



Scheme 2.2. Hydrophosphination of olefins.

Despite the ubiquity of phosphines in the design and synthesis of catalysts,¹¹⁻²¹ they are often overlooked in other areas, including materials science, due to the perception that they react violently when exposed to air. However, many phosphines, including primary and secondary examples, exhibit exceptional stability towards oxygen.^{22-24,25-39} Among the most common strategies for the stabilization of phosphines through synthetic variation are the incorporation of steric bulk (*e.g.*, **2.1**),^{25-26, 29} the design of molecules with relatively high energy singly occupied molecular orbitals (SOMOs) for their radical cation forms (*e.g.*, **2.2**),^{32, 35-36, 38} and the installation of heteroatoms in close proximity to phosphorus leading to localization of the highest occupied molecular orbitals (HOMOs) away from phosphorus (*e.g.*, **2.3**).^{27-28, 39}

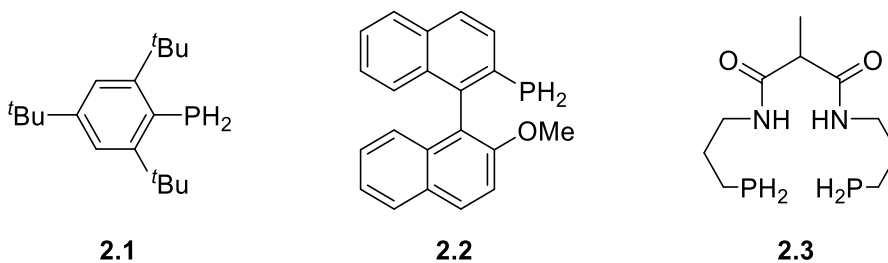


Figure 2.1. Examples of air-stable phosphines.

Phosphines bearing ferrocene substituents combine the desirable characteristics of phosphines and ferrocene, and often exhibit surprising stability towards air and moisture.³⁰

^{35, 37} Consequently, they have been utilized as rigid and potentially redox-active ligands for transition metals, *e.g.*, in Pd(dppf)Cl₂ **2.4** [dppf = 1,1'-bis(diphenylphosphino)ferrocene],^{40-43,44-48} as Lewis bases in frustrated Lewis pairs, *e.g.*, **2.5**,⁴⁹⁻⁵¹ and in the synthesis of metal-containing polymers and polymer networks, *e.g.*, **2.6**.^{37, 39, 52-53} While the properties of ferrocene-based phosphines have been widely explored, reports on ruthenocene analogs are relatively scarce throughout the literature.^{38, 54-57} Furthermore, to the best of our knowledge, phosphines bearing more than one type of metallocene have not been reported to date.

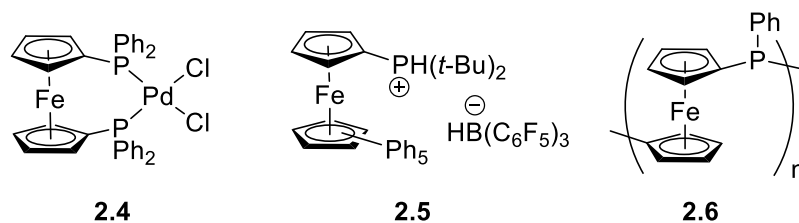


Figure 2.2. Examples of phosphinoferrrocene compounds.

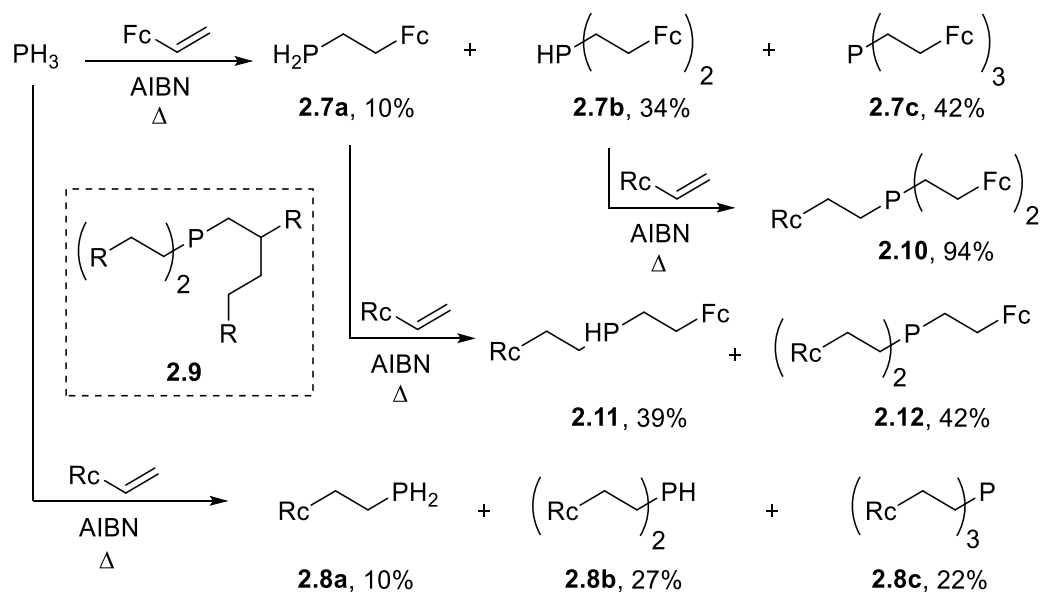
In this work, PH₃ gas was used for the radical-catalyzed hydrophosphination reactions of vinylferrocene and vinylruthenocene in order to attach metallocene units to the phosphorus through an ethylene spacer. The synthesis and characterization of a family of primary, secondary, and tertiary phosphines that include all possible combinations of ethylferrocene and ethylruthenocene substituents linked to phosphorus are described below.

2.2 Results and Discussion

2.2.1 Synthesis and NMR Spectroscopy

The ferrocene-containing phosphines **2.7a–c** and ruthenocene-containing phosphines **2.8a–c** were synthesized and purified in the same manner. For the synthesis of primary, secondary, and tertiary ferrocene-containing phosphines **2.7a–c**, vinylferrocene and phosphine gas were heated in the presence of azobisisobutyronitrile (AIBN) to produce the corresponding ferrocene-containing phosphines **2.7a–c** (Scheme 2.3). The first step of the reaction involved a large excess of PH₃ and resulted mainly in the conversion of vinylferrocene to primary phosphine **2.7a**. At this stage, the excess PH₃ was removed from the reaction flask by purging with N₂. Two additional portions of vinylferrocene and AIBN

were then added and the reaction mixture was heated to produce secondary and tertiary phosphines **2.7b** and **2.7c**. We favored a strategy that employed multiple AIBN/vinylferrocene additions in order to limit radical concentration and disfavor formation of α -addition byproducts (*i.e.*, **2.9**).⁵⁸⁻⁵⁹ As vinylferrocene and primary phosphine **2.7a** have similar polarities, their separation by column chromatography is not trivial. We therefore chose to complete the reaction sequence by charging the mixture with additional AIBN and heating at 85 °C in order to completely consume excess vinylferrocene. A typical experiment involving the synthetic strategy described above resulted in isolated yields (after column chromatography in air) of 10%, 34%, and 42% for **2.7a**, **2.7b**, and **2.7c**, respectively. Hydrophosphination reaction of vinylruthenocene with PH₃ gas resulted in lower isolated yields which were 10%, 27%, and 22% (Yields by NMR spectroscopy: 10%, 36%, and 48%) for **2.8a**, **2.8b**, and **2.8c**, respectively. Starting from primary and secondary ferrocene-containing phosphines **2.7a** and **2.7b**, mixed ferrocene- and ruthenocene-containing phosphines **2.10** (1 × Rc, 2 × Fc), **2.11** (1 × Rc, 1 × Fc), and **2.12** (2 × Rc, 1 × Fc) were synthesized using similar strategies in 94%, 39%, and 42% isolated yields (Scheme 2.3).



Scheme 2.3. Synthesis of phosphines **2.7a–c**, **2.8a–c**, **2.10**, **2.11**, and **2.12**. Fc and Rc represent ferrocenyl and ruthenocenyl substituents.

The proposed structures and bulk purity of phosphines **2.7a–c**, **2.8a–c**, **2.10**, **2.11**, and **2.12** were confirmed using ^1H , ^{13}C , and ^{31}P NMR spectroscopy, IR and UV-vis absorption spectroscopy, mass spectrometry, and elemental analysis. Primary phosphines **2.7a** and **2.8a** are soluble in a wide range of solvents including hexanes, THF, acetone, EtOH, toluene, CH_2Cl_2 , and CHCl_3 . Secondary (**2.7b**, **2.8b**, and **2.11**) and tertiary (**2.7c**, **2.8c**, **2.10**, and **2.12**) phosphines have limited solubility in hexanes and alcohols, but are soluble in THF, CH_2Cl_2 , and CHCl_3 . Each of the phosphines reported was purified by standard column chromatography techniques and are stable in air indefinitely in the solid state. In solution, each phosphine converts slowly to its corresponding phosphine oxide when exposed to air. The degradation of phosphines **2.7a–c**, **2.8a–c**, **2.10**, **2.11**, and **2.12** in solution was studied by monitoring the ^{31}P NMR spectra of 75 mM CDCl_3 solutions that were prepared in air and stored in a fume hood for 1 week with no attempt to limit air or light exposure. After 1 week, conversion to phosphine oxides ranged from 0–7.5% (Table 2.1). Within the series, primary phosphine **2.7a** ($1 \times \text{Fc}$) degraded the slowest and tertiary phosphine **2.8c** ($3 \times \text{Rc}$) degraded the quickest. In general, phosphines containing ruthenocene substituents degraded more quickly than ferrocene analogs.

Table 2.1. Degradation of primary, secondary, and tertiary phosphines **2.7a–c**, **2.8a–c**, **2.10**, **2.11**, and **2.12** in solutions exposed to air.

Compound	Percentage conversion to phosphine oxide after 1 week (168 h)
<i>Primary Phosphines</i>	
2.7a ($1 \times \text{Fc}$)	0
2.8a ($1 \times \text{Rc}$)	6.3
<i>Secondary Phosphines</i>	
2.7b ($2 \times \text{Fc}$)	1.8
2.11 ($1 \times \text{Rc}$, $1 \times \text{Fc}$)	0
2.8b ($2 \times \text{Rc}$)	2.9
<i>Tertiary Phosphines</i>	
2.7c ($3 \times \text{Fc}$)	2.9
2.10 ($1 \times \text{Rc}$, $2 \times \text{Fc}$)	0.6
2.12 ($2 \times \text{Rc}$, $1 \times \text{Fc}$)	3.8
2.8c ($3 \times \text{Rc}$)	7.5

The ^{31}P NMR spectra of primary, secondary, and tertiary ruthenocene-containing phosphines **2.8a–c** are shown in Figure 2.3, while proton-coupled and -decoupled ^{31}P NMR spectra for the remaining phosphines can be found in Appendix 2. The ^{31}P NMR resonances for the primary (**2.7a** and **2.8a**), secondary (**2.7b**, **2.8b**, and **2.11**), and tertiary (**2.7c**, **2.8c**, **2.10**, and **2.12**) phosphines appeared as triplets at approximately -137 ppm, doublets at approximately -69 ppm, and singlets at approximately -29 ppm, respectively. Coupling constants ($^1J_{\text{PH}}$) for primary and secondary phosphines were calculated to be *ca.* 200 Hz, and were consistent with the coupling constants ($^1J_{\text{HP}}$) observed in the corresponding ^1H NMR spectra (Table 2.2). The ^1H NMR spectra collected also confirmed the presence of the ethylene bridge, with peaks appearing between 1.54–1.90 ppm and 2.28–2.59 ppm in their ^1H NMR spectra. Mono-substituted metallocene units were identified by the presence of singlets for unsubstituted cyclopentadienyl (Cp) ligands and pairs of *pseudo*-triplets for each substituted Cp ligand between 4.06–4.57 ppm in their ^1H NMR spectra (Figures A2.1–A2.25).

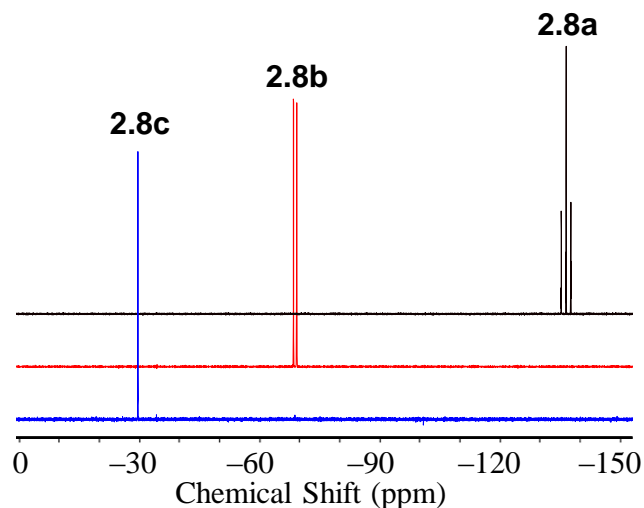


Figure 2.3. ^{31}P NMR spectra of primary, secondary, and tertiary ruthenocene-containing phosphines **2.8a–c** in CDCl_3 .

2.2.2 X-ray Crystallography

The solid-state structures of phosphines **2.7a–c**, **2.8b**, **2.8c**, **2.10**, **2.11**, and **2.12** were determined via single crystal X-ray diffraction (Figures 2.4 and A2.26–A2.31 and Tables 2.2 and 2.3). As is often observed for solid-state structures containing metallocene units, the structures exhibited elongated thermal displacement ellipsoids due to either large amplitude librations of the Cp ring about the molecular axis or a static disorder of the Cp ring over two or more orientations. Furthermore, the metal sites of the mixed-metal metallocene compounds exhibited a statistical disorder of the Fe and Ru atoms. For this reason, we have chosen to focus on the average $\text{Cp}_{\text{centroid}}\text{-Cp}_{\text{centroid}}$ and metal- $\text{Cp}_{\text{centroid}}$ distances for our discussion of the solid-state structures of the metallocene units in **2.7a–c**, **2.8b**, **2.8c**, **2.10**, **2.11**, and **2.12**. As the Rc/Fc ratio was increased, a clear trend emerged. The average $\text{M-Cp}_{\text{centroid}}$ distance increases in tertiary phosphines from 1.653(2) Å in **7c** ($3 \times \text{Fc}$), to 1.706(2) Å in **2.10** ($1 \times \text{Rc}$, $2 \times \text{Fc}$), to 1.760(2) Å in **2.12** ($2 \times \text{Rc}$, $1 \times \text{Fc}$), and 1.807(1) Å in **2.8c** ($3 \times \text{Rc}$).

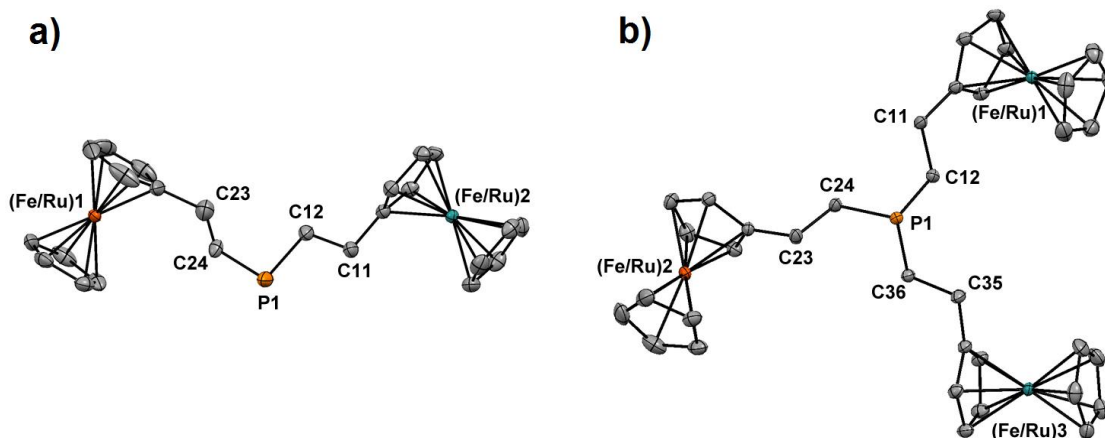


Figure 2.4. Solid-state structures of **a**) secondary phosphine **2.11** ($1 \times \text{Rc}$, $1 \times \text{Fc}$) and **b**) tertiary phosphine **2.12** ($2 \times \text{Rc}$, $1 \times \text{Fc}$). Thermal displacement ellipsoids are shown at 50% probability and hydrogen atoms have been omitted for clarity. For depictions of the solid-state structures of **2.7a–c**, **2.8b**, **2.8c**, and **2.10** see Appendix 2 (Figures A2.26–A2.31).

Each phosphine exhibits a trigonal pyramidal geometry where the average C-P-C angles are 99.03(4)° (**2.7b**), 99.68(6)° (**2.7c**), 101.2(2)° (**2.8b**), 98.67(4)° (**2.8c**), 99.66(6)° (**2.10**), 101.5(2)° (**2.11**), and 99.63(8)° (**2.12**). The average P-C bond lengths in the solid-state structures of **2.7a**, **2.7b**, **2.7c**, **2.8b**, **2.8c**, **2.10**, **2.11**, and **2.12** are 1.883(6), 1.877(7), 1.8505(12), 1.846(5) Å, 1.845(9) Å, 1.850(13) Å, 1.851(5) Å, and 1.8510(17) Å, respectively (Table 2.2).

Table 2.2. Selected average angles (deg) and bond lengths (Å) for phosphines **2.7a–c**, **2.8b**, **2.8c**, **2.10**, **2.11**, and **2.12**.

	2.7a	2.7b	2.7c	2.8b	2.8c	2.10	2.11	2.12
C-P-C	-	99.03(4)	99.68(6)	101.2(2)	98.67(4)	99.66(6)	101.5(2)	99.63(8)
P-C	1.883(6)	1.877(7)	1.8505(12)	1.846(5)	1.845(9)	1.8499(13)	1.851(5)	1.8510(17)
M-Cp _{centroid} (unsubstituted Cp)	1.660(5)	1.653(8)	1.655(2)	1.822(5)	1.810(1)	1.707(2)	1.734(3)	1.761(2)
M-Cp _{centroid} (substituted Cp)	1.665(4)	1.656(8)	1.651(2)	1.815(4)	1.803(1)	1.705(2)	1.732(4)	1.758(2)
Cp _{centroid} -Cp _{centroid}	3.325(5)	3.309(8)	3.306(2)	3.637(5)	3.613(1)	3.412(2)	3.466(4)	3.519(2)

2.2.3 UV-vis Absorption Spectroscopy

The UV-vis absorption spectra of tertiary phosphines **2.7c**, **2.8c**, **2.10**, and **2.12** in THF are shown in Figure 2.5 and the results are summarized in Table 2.2. Each phosphine gave rise to a weak absorption spectrum consistent with formally forbidden d→d electronic transitions associated with d⁸ ferrocene and/or ruthenocene moieties. Ferrocene-containing phosphines exhibited wavelengths of maximum absorption (λ_{max}) of approximately 440 nm with molar extinction coefficients proportional to the number of ferrocene units in their respective structures. However, the molar extinction coefficients (ϵ) of the absorption centered at approximately 320 nm for phosphines containing ruthenocene were not strictly proportional to the number of ruthenocenes in the structure as both ferrocene and ruthenocene absorb at *ca.* 320 nm. Nevertheless, a general trend was observed. As ferrocene groups were replaced by ruthenocene groups the intensity of the absorption peak at 440 nm decreased and the intensity of the absorption peak at 320 nm increased. Qualitatively similar trends were observed for the UV-vis absorption spectra of primary phosphines **2.7a** and **2.8a** and secondary phosphines **2.7b**, **2.8b**, and **2.11** (Figures A2.32–A2.36 and Table 2.2).

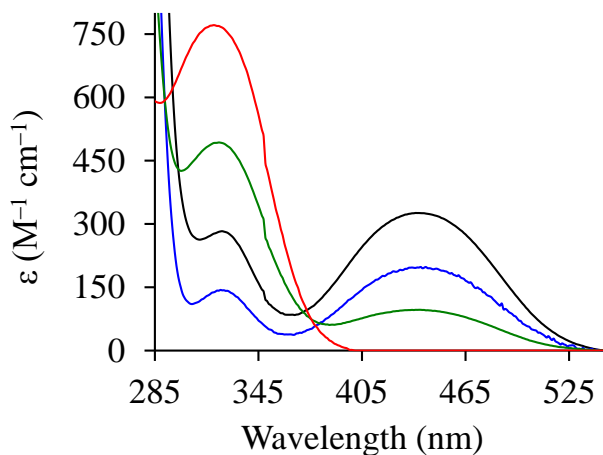
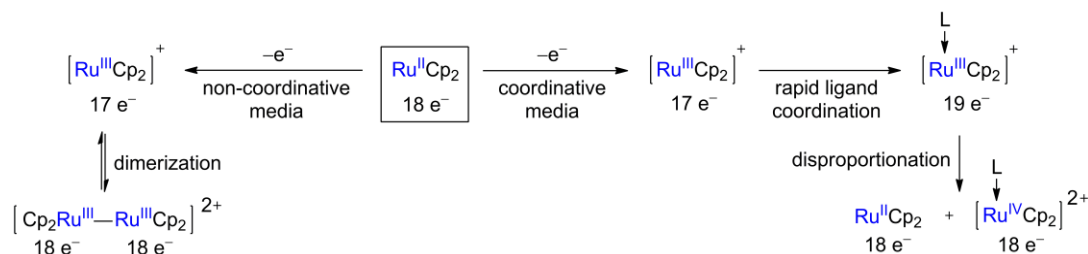


Figure 2.5. UV-vis spectra of tertiary phosphines **2.7c** ($3 \times \text{Fc}$; black line), **2.8c** ($3 \times \text{Rc}$; red line), **2.10** ($1 \times \text{Rc}$, $2 \times \text{Fc}$; blue line), and **2.12** ($2 \times \text{Rc}$, $1 \times \text{Fc}$; green line) in THF.

2.2.4 Cyclic Voltammetry

The reversible one-electron oxidation of ferrocene is well understood, so much so, that it is commonly used as an internal standard for electrochemical studies.^{60,61} Despite the structural and electronic similarities between ferrocene and ruthenocene, the electrochemical oxidation behavior of the latter has not been studied to the same extent. Most reports of the oxidation of ruthenocene indicate that it occurs as a two-electron process as 17-electron $[\text{Ru}^{\text{III}}\text{Cp}_2]^+$, formed via oxidation of 18-electron $\text{Ru}^{\text{II}}\text{Cp}_2$, is extremely Lewis acidic and readily combines with Lewis bases to form 19-electron adducts that undergo rapid disproportionation (Scheme 2.4). Previous studies have shown that $[\text{Ru}^{\text{III}}\text{Cp}_2]^+$ can scavenge mercury from electrodes,⁶²⁻⁶³ activate C-Br bonds,⁶⁴ bind to solvents such as CH_3CN ,⁶⁵ and react with dihalogens such as I_2 *en route* to the formation of Ru^{IV} complexes.⁶⁶⁻⁶⁷ However, by using $[n\text{-Bu}_4\text{N}][\text{B}(\text{PhF}_5)_4]$, a non-coordinative supporting electrolyte,⁶⁸ Geiger and co-workers have shown that the oxidation of $\text{Ru}^{\text{II}}\text{Cp}_2$ involves loss of a single electron.⁶⁹⁻⁷¹ Depending on the conditions, for example when an ethane bridge is introduced between the cyclopentadienyl substituents in dicarba[2]ruthenocenophanes, oxidation leads to formation of isolable dimers linked through a Ru-Ru bond.^{64, 72}



Scheme 2.4. Summary of the known chemical oxidation behavior of ruthenocene in coordinative/non-coordinative media. L: neutral or anionic donor.

In this study, all solvents and reagents were rigorously purified prior to electrochemical studies and CH_2Cl_2 alone was employed as the solvent to avoid the formation of ruthenocenium- CH_3CN adducts with polar solvents during the evaluation. In addition, $[\textit{n}\text{-Bu}_4\text{N}][\text{OTf}]$ was used as a supporting electrolyte since it stabilizes the oxidized phosphines and reduces plating of the analytes on the working electrode much better than the traditional supporting electrolytes (*e.g.*, $[\textit{n}\text{-Bu}_4\text{N}][\text{PF}_6]$ and $[\textit{n}\text{-Bu}_4\text{N}][\text{BF}_4]$). The number of electrons involved for each process was determined by relative comparison to the current generated during the oxidation of a stoichiometric amount of decamethylferrocene.⁷³

We began the study by collecting cyclic voltammograms of ferrocene and ruthenocene in order to establish 'baseline' behavior under the experimental conditions employed. Ferrocene yielded a reversible one-electron oxidation wave while ruthenocene underwent an irreversible two-electron oxidation with significant cathodic peak current (Figure A2.37). The cyclic voltammograms collected for tertiary phosphines **2.7c**, **2.8c**, **2.10**, and **2.12** under identical conditions are shown in Figure 2.6 and the data are summarized in Table 2.2. For each ferrocene-containing tertiary phosphine, a small, irreversible oxidation peak at *ca.* -100 mV relative to the ferrocene/ferrocenium redox couple was observed. This electrochemical feature may be due to redox reactivity and/or electrode interactions associated with the phosphorus lone pair as similar electrochemical behavior and conclusions have been reported for related phosphines.^{31, 74}

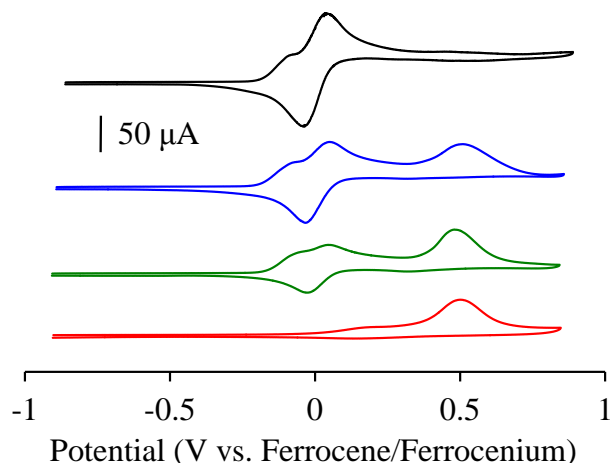
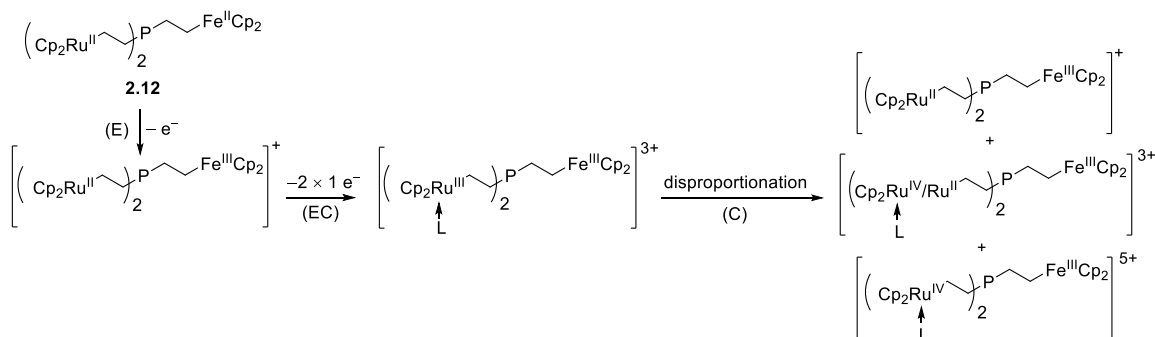


Figure 2.6. Cyclic voltammograms of tertiary phosphines **2.7c** ($3 \times \text{Fc}$; black line), **2.8c** ($3 \times \text{Rc}$; red line), **2.10** ($1 \times \text{Rc}$, $2 \times \text{Fc}$; blue line), and **2.12** ($2 \times \text{Rc}$, $1 \times \text{Fc}$; green line) recorded at 250 mV s^{-1} in 1 mM solutions of CH_2Cl_2 containing 0.1 M $[\textit{n}\text{-Bu}_4\text{N}][\text{OTf}]$ as supporting electrolyte.

Although the ferrocene moieties present in **2.7a–c**, **2.10**, **2.11**, and **2.12** underwent qualitatively reversible electrochemical oxidation ($E_{1/2,\text{Fc}} \sim 0 \text{ mV}$), irreversible oxidation events ($E_{\text{pa,Rc}} 330\text{--}550 \text{ mV}$) were observed for the ruthenocene groups in each of the ruthenocene-containing phosphines. The anodic current response did not scale linearly with the number of ruthenocene moieties present. For these compounds, we postulate that the initial formation of 17-electron ruthenocenium is rapidly followed by the formation of a 19-electron adduct. We suggest that intermolecular complexes form between phosphines in the vicinity of the working electrode and electrochemically-generated ruthenocenium compounds (e.g., $[\text{R}_3\text{P} \rightarrow \text{Ru}^{\text{III}}\text{Cp}_2]^+$). The resulting adduct can decompose or disproportionate to produce a variety of different stable 18-electron species (Scheme 2.3). At lower scan rates ($50\text{--}250 \text{ mV s}^{-1}$), decomposition of the complexes generated during the cyclic voltammetry studies (e.g., $[\text{R}_3\text{P} \rightarrow \text{Ru}^{\text{IV}}\text{Cp}_2]$) may lead to the irreversible oxidation behavior observed. When scan rates were increased ($500\text{--}1000 \text{ mV s}^{-1}$), the anodic peak current response approached the two-electrons per ruthenocene we initially expected, providing further indication that the complexes generated during the cyclic voltammetry studies are short lived. Furthermore, at high scan rates ($2000\text{--}8000 \text{ mV s}^{-1}$), reduction half-waves potentially associated with the re-formation of ruthenocene were observed (Figure A2.38). While the fate of the ruthenocene moieties is not clear, the qualitatively reversible oxidation of ferrocene in all cases implies that the

ferrocene/ferrocenium redox couple is not involved in any of the proposed disproportionation and/or decomposition pathways. This behavior was in stark contrast to that observed for the electrochemical oxidation of ruthenocene under identical conditions, where the observed oxidation wave was accompanied by a corresponding reduction wave with significant peak current.



Scheme 2.5. Postulated reactivity pathway upon electrochemical oxidation of tertiary phosphine **2.12** (2 × Rc, 1 × Fc). L = phosphine or OTf[−] anion, E = electrochemical reaction, C = chemical reaction, and EC = electrochemical/chemical reaction.

The electrochemical behavior of primary and secondary phosphines **2.7a**, **2.7b**, **2.8a**, **2.8b**, and **2.11** were found to be qualitatively similar to that described above (Figures A2.39 and A2.40 and Table 2.3). For each ferrocene-containing primary and secondary phosphine, a reversible oxidation wave with anodic/cathodic peak currents corresponding to one electron per ferrocene was observed. For each ruthenocene-containing phosphine, an irreversible oxidation wave associated with the ruthenocene moiety was observed.

Table 2.3. Selected characterization data for phosphines **2.7a–c**, **2.8a–c**, **2.10**, **2.11**, and **2.12**.

	2.7a	2.7b	2.7c	2.8a	2.8b	2.8c	2.10	2.11	2.12
M.p. (°C)	51–53	93–95	119–121	52–54	97–99	110–112	135–137	76–78	106–108
³¹ P NMR shift (δ)	−137.1	−68.8	−27.9	−137.0	−68.9	−29.4	−28.4	−68.9	−28.9
¹ J _{P-H} (Hz)	196	201	-	195	201	-	-	200	-
¹ J _{H-P} (Hz)	204	200	-	195	201	-	-	201	-
Molar absorptivity at 320 nm (M ^{−1} cm ^{−1})	75	130	280	210	480	770	375	300	495
Molar absorptivity at 440 nm (M ^{−1} cm ^{−1})	110	195	325	-	-	-	205	105	95
E _{pa, Rc} ^a (mV)	-	-	-	330	550	490	545	480	495
E _{1/2,Fc} (mV)	10	−10	10	-	-	-	10	−10	10

^aIrreversible process; anodic peak potential reported.

2.3 Conclusion

During this study, we have demonstrated that the radical-catalyzed hydrophosphination of alkenes can be used to produce primary, secondary, and tertiary ferrocene- and ruthenocene-containing phosphines. The phosphines, which degrade slowly when exposed to air in solution and are stable indefinitely in the solid state, exhibited properties consistent with the presence of ferrocene and/or ruthenocene moieties. Phosphines containing one or more ferrocenes were reversibly oxidized electrochemically (one electron per ferrocene), and absorbed visible light at a maximum of 440 nm. Analogs containing ruthenocene underwent irreversible electrochemical oxidation (two electrons per ruthenocene at high scan rates), consistent with the phosphines themselves coordinating to electrochemically generated ruthenocenium. They also showed characteristic wavelengths of maximum absorption at 320 nm. Phosphines containing both ferrocene and ruthenocene showed properties associated with both types of metallocenes, with the relative intensity of their UV-vis absorption and electrochemical responses qualitatively relating to the number of each type of metallocene present. Our future work in this area will focus on the utilization of these phosphines as metal carriers for the preparation of highly-metallized polymers and crosslinked polymer networks.

2.4 Experimental Section

2.4.1 General Considerations

Reactions and manipulations were carried out under a N₂ atmosphere using standard Schlenk techniques unless otherwise stated. Solvents were obtained from Caledon Laboratories, dried using an Innovative Technologies Inc. solvent purification system, collected under vacuum, and stored under a N₂ atmosphere over 4 Å molecular sieves. Reagents were purchased from Sigma-Aldrich or Alfa Aesar and used as received. Ferrocenecarboxaldehyde and ruthenocenecarboxaldehyde were synthesized according to literature procedures⁷⁵ and vinylruthenocene and vinylferrocene were synthesized according to modified procedures.⁷⁶ ¹H, ¹³C{¹H}, and ³¹P NMR spectra were recorded on a 600 MHz (¹H: 599.5 MHz, ¹³C: 150.8 MHz, ³¹P: 242.6 MHz) Varian INOVA instrument. ¹H NMR spectra were referenced to residual CHCl₃ (7.27 ppm) and ¹³C{¹H} NMR spectra

were referenced to CDCl_3 (77.0 ppm). ^{31}P NMR spectra were referenced internally relative to triphenyl phosphine (-6.0 ppm relative to H_3PO_4). Mass spectrometry data were recorded using a high resolution Finnigan MAT 8400 spectrometer, in positive-ion mode. UV-vis spectra were recorded using a Cary 300 Scan instrument. Infrared spectra were recorded using a PerkinElmer Spectrum Two FT-IR spectrometer with an attenuated total reflectance (ATR) attachment and a single reflection diamond. Elemental analyses (C and H) were carried out by Laboratoire d'Analyse Élémentaire de l'Université de Montréal, Montréal, QC, Canada.

CAUTION: PH_3 gas is toxic and pyrophoric

PH_3 gas must be handled carefully in a controlled environment. The use of commercially available personal and laboratory PH_3 detectors during all experiments involving PH_3 is strongly advised. Reactions should be conducted in high-pressure reactors and purged thoroughly with inert gas (*e.g.*, N_2) before they are opened inside a glove box. Excess PH_3 should be ignited as it is purged from the reaction vessel under controlled conditions. Please see Figure A2.41 for photographs of the experimental apparatus used in this study.

2.4.2 Cyclic Voltammetry

Cyclic voltammograms were collected using a Bioanalytical Systems Inc. (BASi) Epsilon potentiostat and analyzed using BASi Epsilon software. Typical electrochemical cells consisted of a three-electrode setup including a glassy carbon working electrode, platinum wire counter electrode, and silver wire *pseudo*-reference electrode. Experiments were run at variable scan rates in degassed CH_2Cl_2 solutions of the analyte (~ 1 mM) and supporting electrolyte (0.1 M [*n*- Bu_4N][OTF]) under a blanket of argon. Cyclic voltammograms were referenced against an internal standard (1 mM decamethylferrocene: -520 mV vs ferrocene/ferrocenium under identical conditions) and corrected for internal cell resistance using the BASi Epsilon software.

2.4.3 X-ray Crystallography

Single crystals of all compounds suitable for X-ray diffraction studies were grown from concentrated THF solutions of the compounds layered with hexanes, except for tertiary phosphine **2.8c**, which was grown by vapor diffusion of pentane into a concentrated CHCl_3 solution. The samples were mounted on a MiTeGen polyimide micromount with a small amount of Paratone N oil. X-ray diffraction measurements were made on a Bruker APEX-II CCD diffractometer. The unit cell dimensions were determined from a symmetry constrained fit of 9813 reflections with $6.48^\circ < 2\theta < 68.96^\circ$ for **2.8b**, 8712 reflections with $5.54^\circ < 2\theta < 46.48^\circ$ for **2.8c**, 9847 reflections with $5.88^\circ < 2\theta < 79.26^\circ$ for **2.10**, 9849 reflections with $5.50^\circ < 2\theta < 63.22^\circ$ for **2.11**, and 9420 reflections with $6.86^\circ < 2\theta < 79.66^\circ$ for **2.12**. The data collection strategy was a number of ω and ϕ scans which collected data up to 72.608° (2θ) for **2.8b**, 52.832° (2θ) for **2.8c**, 80.634° (2θ) for **2.10**, 63.400° (2θ) for **2.11**, and 87.406° (2θ) for **2.12**, respectively. The frame integration was performed using SAINT.⁷⁷ The resulting raw data were scaled and absorption corrected using a multi-scan averaging of symmetry equivalent data using SADABS,⁷⁸ except the data for **2.8b** which were processed using TWINABS.⁷⁹ The crystal of **2.8b** was non-merohedrally twinned (see supporting information for twin law). The twin fraction of the minor domain refined to a value of 0.4120(7). The structures for **2.8b**, **2.8c**, **2.10**, **2.11**, and **2.12** were solved using the SHELXT program.⁸⁰ All non-hydrogen atoms were obtained from the initial solution. The hydrogen atoms were introduced at idealized positions and were allowed to ride on the parent atom. The structural model was fit to the data using full matrix least-squares based on F^2 corrections for anomalous dispersion from the usual tabulation. The structure was refined using the SHELXL-2014 program from the SHELX program package.⁸¹ Structural disorder related to the ethylene linkers and the unsubstituted Cp ligands was modeled under unconstrained conditions. For tertiary phosphine **2.8c**, the minor component of the rotational disorder associated with two of the unsubstituted Cp ligands could not be fully resolved (see .cif file for details). For phosphines **2.10**, **2.11**, and **2.12** the occupancy of the metal sites were fixed to the stoichiometric ratios of Fe/Ru, as confirmed by elemental analysis. Graphic plots were produced using Mercury software (version 3.3). For additional collection and refinement details, see Table 2.4.

Table 2.4. Selected X-ray diffraction data collection and refinement details for phosphines **2.7a–c**, **2.8b**, **2.8c**, **2.10**, **2.11**, and **2.12**.

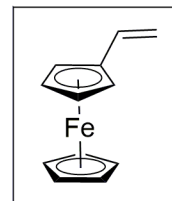
	2.7a	2.7b	2.7c	2.8b	2.8c	2.10	2.11	2.12
Chemical	C ₁₂ H ₁₅ FeP	C ₂₄ H ₂₇ Fe ₂ P	C ₃₆ H ₃₉ Fe ₃ P	C ₂₄ H ₂₇ PRu ₂	C ₁₉ H _{20.5} Cl ₃ P _{0.5}	C ₃₆ H ₃₉ Fe ₂ PRu	C ₂₄ H ₂₇ FePRu	C ₃₆ H ₃₉ FePRu ₂
FW (g mol ⁻¹)	246.07	458.13	670.2	548.56	522.29	715.41	503.29	760.63
Temp (K)	110	110	110	110	110	110	110	110
Crystal syst.	monoclinic	monoclinic	triclinic	monoclinic	monoclinic	triclinic	monoclinic	triclinic
Space group	<i>P</i> 2 ₁ / <i>c</i>	<i>P</i> 2 ₁ / <i>c</i>	<i>P</i> -1	<i>C</i> 2/ <i>c</i>	<i>P</i> 2 ₁	<i>P</i> -1	<i>C</i> 2/ <i>c</i>	<i>P</i> -1
λ (Å)	0.71073	0.71073	0.71073	0.71073	0.71073	0.71073	0.71073	0.71073
<i>a</i> (Å)	14.330(6)	5.7236(13)	11.1849(5)	29.614(4)	5.778(3)	11.190(2)	32.299(10)	11.188(2)
<i>b</i> (Å)	7.584(3)	9.910(3)	11.6315(4)	5.7191(7)	27.701(19)	11.696(4)	5.6826(12)	11.744(4)
<i>c</i> (Å)	10.513(3)	35.994(11)	11.8872(5)	25.299(3)	12.417(9)	11.888(5)	24.943(7)	11.936(4)
α (deg)	90	90	85.1800(10)	90	90	84.94(2)	90	84.99(2)
β (deg)	97.029(16)	90.579(12)	82.1170(10)	108.331(6)	100.311(17)	83.442(18)	116.23(2)	84.428(15)
γ (deg)	90	90	74.9990(10)	90	90	74.634(13)	90	74.283(10)
<i>V</i> (Å ³)	1133.9(8)	2041.6(10)	1477.77(10)	4067.4(9)	1955(2)	1487.7(8)	4107(2)	1499.4(8)
<i>Z</i>	4	4	2	8	4	2	8	2
ρ (g cm ⁻³)	1.441	1.481	1.506	1.792	1.774	1.597	1.628	1.685
μ (cm ⁻¹)	1.428	1.505	1.532	1.57	1.622	1.542	1.526	1.55
R1 [<i>I</i> > 2 σ (<i>I</i>)]	0.0398	0.052	0.0336	0.0417	0.0453	0.0353	0.0433	0.0452
ω R ² [<i>I</i> > 2 σ (<i>I</i>)]	0.1025	0.0974	0.0949	0.0993	0.0847	0.0755	0.097	0.0806
R1 (all data)	0.0709	0.0738	0.0432	0.0469	0.0625	0.0496	0.0576	0.0789
ω R ² (all data)	0.1315	0.1044	0.1018	0.1009	0.0909	0.0802	0.1035	0.0912
GOF	1.12	1.093	0.949	1.14	1.06	1.044	1.071	0.99

$$R_1 = \Sigma(|F_o| - |F_c|) / \Sigma F_o, \quad \omega R_2 = [\Sigma(\omega(F_o^2 - F_c^2)^2) / \Sigma(\omega F_o^4)]^{1/2}; \quad GOF = [\Sigma(\omega(F_o^2 - F_c^2)^2) / (\text{No. of reflns.} - \text{No. of params.})]^{1/2}.$$

2.4.4 Synthetic Procedures and Characterization Data

Preparation of Vinylferrocene

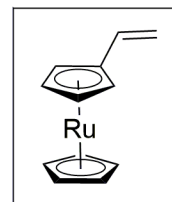
Vinylferrocene was prepared according to a modified literature procedure.⁷⁶ In a 1 L three-neck round bottom flask equipped with a dropping funnel, methyltriphenylphosphonium iodide (18.70 g, 46.03 mmol), potassium *t*-butoxide (6.00 g, 53.5 mmol) and dibenzo-18-crown-



6 (0.03 g, 0.08 mmol) were dissolved in 400 mL of dry THF and the resulting solution was stirred for 2 h at 22 °C. In a dropping funnel, ferrocenecarboxaldehyde (7.36 g, 34.4 mmol) was dissolved in 100 mL of dry THF and added dropwise to the solution. The solution was stirred for 16 h at 22 °C before it was treated with 300 mL of brine. Vinylferrocene was extracted with Et₂O (5 × 200 mL). The extracts were combined, washed with 2 × 300 mL of brine, 2 × 300 mL of deionized H₂O, and dried over MgSO₄. After gravity filtration, the solvent was removed *in vacuo* before the resulting residue was dissolved in hexanes and filtered through a silica plug (2'' × 3''). Pure vinylferrocene was isolated as an orange microcrystalline solid by removing the solvent *in vacuo*. Yield = 7.08 g, 97%. ¹H NMR (599.5 MHz, CDCl₃): δ 6.46 (d of d, ³J_{HH, cis} = 11 Hz, ³J_{HH, trans} = 18 Hz, 1H, C₅H₄CH), 5.35 (d of d, ²J_{HH, gem} = 2 Hz, ³J_{HH, trans} = 18 Hz, 1H, *trans*-CHCH₂), 5.03 (d of d, ²J_{HH, gem} = 2 Hz, ³J_{HH, cis} = 11 Hz, 1H, *cis*-CHCH₂), 4.37 (t, ³J_{HH} = 2 Hz, 2H, β-C₅H₄R), 4.22 (t, ³J_{HH} = 2 Hz, 2H, α-C₅H₄R), and 4.12 (s, 5H, C₅H₅). These data are consistent with those spectra reported previously.⁷⁶

Preparation of Vinylruthenocene

Vinylruthenocene was prepared according to a modified literature procedure.⁷⁶ In a 1 L three-neck round bottom flask equipped with a dropping funnel, methyltriphenylphosphonium iodide (18.70 g, 46.03 mmol), potassium *t*-butoxide (6.00 g, 53.5 mmol) and dibenzo-18-crown-



6 (0.03 g, 0.08 mmol) were dissolved in 400 mL of dry THF and the resulting solution was stirred for 2 h at 22 °C. In a dropping funnel, ruthenocenecarboxaldehyde (8.92 g, 34.4 mmol) was dissolved in 100 mL of dry THF and added dropwise to the solution. The solution was stirred for 16 h at 22 °C before it was treated with 300 mL of brine.

Vinylruthenocene was extracted with Et₂O (5 × 200 mL). The extracts were combined, washed with 2 × 300 mL of brine, 2 × 300 mL of deionized H₂O, and dried over MgSO₄. After gravity filtration, the solvent was removed *in vacuo* before the resulting residue was dissolved in hexanes and filtered through a silica plug (2" × 3"). Pure vinylruthenocene was isolated as a pale yellow microcrystalline solid by removing the solvent *in vacuo*. Yield = 8.52 g, 96%. ¹H NMR (599.5 MHz, CDCl₃): δ 6.34 (d of d, ³J_{HH, cis} = 11 Hz, ³J_{HH, trans} = 18 Hz, 1H, C₅H₄CH), 5.29 (d of d, ²J_{HH, gem} = 2 Hz, ³J_{HH, trans} = 18 Hz, 1H, *trans*-CHCH₂), 4.90 (d of d, ²J_{HH, gem} = 2 Hz, ³J_{HH, cis} = 11 Hz, 1H, *cis*-CHCH₂), 4.78 (t, ³J_{HH} = 2 Hz, 2H, β-C₅H₄R), 4.57 (t, ³J_{HH} = 2 Hz, 2H, α-C₅H₄R), and 4.52 (s, 5H, C₅H₅). These data are consistent with those previously reported.⁸²

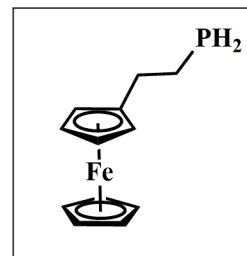
Preparation of Primary, Secondary, and Tertiary Ferrocene-Containing Phosphines **2.7a–c**

In a 300 mL autoclave, vinylferrocene (2.00 g, 9.43 mmol) and AIBN (0.06 g, 0.4 mmol) were dissolved in dry toluene (170 mL). The autoclave was degassed by N₂ purging for 10 min before it was pressurized with PH₃ gas to 80 psi. The solution was stirred for 16 h at 45 °C. Excess pressurized PH₃ gas was released in a controlled environment where it was ignited and allowed to burn. The resulting solution was then transferred to a 350 mL grease-free Schlenk flask in a glove box, which was charged with vinylferrocene (2.00 g, 9.43 mmol) and AIBN (0.06 g, 0.4 mmol) before it was stirred for 16 h at 45 °C and 8 h at 65 °C, respectively. The reaction flask was charged a second time with vinylferrocene (1.00 g, 4.71 mmol) and AIBN (0.03 g, 0.2 mmol) and stirred for 16 h at 45 °C and then 8 h at 65 °C, respectively. Vinylferrocene (0.50 g, 2.4 mmol) and AIBN (0.015 g, 0.091 mmol) were added to the reaction flask for a third time and the orange solution was stirred at 45 °C for 16 h, followed by stirring at 65 °C for 8 h and 85 °C for 2 h, respectively, before the mixture was concentrated *in vacuo*. In order to reduce decomposition of phosphines during column chromatography, Et₃N [10% (v/v) relative to dry silica] was added to the silica slurry in hexanes before the slurry was transferred to the column, which was later washed with pure hexanes (3 × volume of the column) to remove excess Et₃N. Using this column

($1.5'' \times 10''$), N_2 pressure, and a gradient solvent strategy, primary phosphine **2.7a**, secondary phosphine **2.7b**, and tertiary phosphine **2.7c** were separated (see below).

Primary Phosphine **2.7a** ($1 \times Fc$)

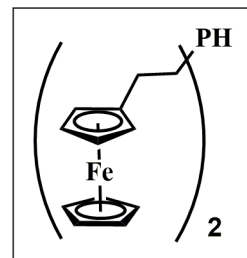
Primary phosphine **2.7a** was removed from the column using hexanes as a yellow band ($R_f = 0.21$). The solution containing **2.7a** was collected and concentrated *in vacuo* to yield **2.7a** as a yellow solid. Yield = 1.34 g, 20%. M.p.: 51–53 °C. 1H NMR (599.5 MHz, $CDCl_3$): δ 4.12 (s, 5H, C_5H_5), 4.09 (t, $^3J_{HH} = 2$ Hz, 2H, β - C_5H_4R), 4.07 (t, $^3J_{HH} = 2$ Hz, 2H, α - C_5H_4R), 2.72 (d of m, $^1J_{HP} = 204$ Hz, 2H, PH_2 , the signal is overlapped with signal at δ 2.57), 2.57 (m, 2H, $C_5H_4CH_2$, the signal is overlapped with signal at δ 2.72), 1.72 (m, 2H, CH_2PH_2).



^{31}P NMR (161.8 MHz, $CDCl_3$): δ -137.1 (t, $^1J_{PH} = 196$ Hz). Mass Spec. (EI, +ve mode): exact mass calculated for $[C_{12}H_{15}FeP]^+$: 246.0260; exact mass found: 246.0256; difference: -1.6 ppm. These data are consistent with a previous report describing the synthesis of phosphine **2.7a** by a different synthetic strategy.³⁰

Secondary Phosphine **2.7b** ($2 \times Fc$)

Secondary phosphine **2.7b** was collected by changing the elution solvent to 99:1 hexanes: Et_2O ($R_f = 0.13$). The solution containing **2.7b** was collected and concentrated *in vacuo* to yield **2.7b** as a yellow solid. Yield = 1.91 g, 31%. M.p.: 93–95 °C. 1H NMR (399.8 MHz, $CDCl_3$): δ 4.20 (s, 10H, C_5H_5), 4.18 (t, $^3J_{HH} = 2$ Hz, 4H, β - C_5H_4R), 4.16 (t, $^3J_{HH} = 2$ Hz, 4H, α - C_5H_5R), 3.25 (d of quintets, $^1J_{HP} = 200$ Hz, $^3J_{HH} = 7$ Hz, 1H, PH), 2.60 (m, 4H, $C_5H_4CH_2$), 1.87 (dm, $^2J_{HP} = 52$ Hz, 4H, CH_2PH).



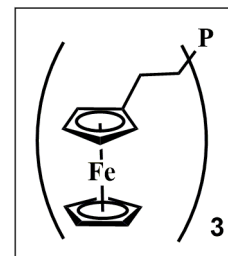
$^{13}C\{^1H\}$ NMR (100.5 MHz, $CDCl_3$): δ 89.1 (d, $^3J_{CP} = 10$ Hz, *ipso*- C_5H_4R), 68.2 (s, C_5H_5), 67.7 (d, $^5J_{CP} = 3$ Hz, β - C_5H_4R), 67.0 (d, $^4J_{CP} = 1$ Hz, α - C_5H_4R), 28.3 (d, $^2J_{CP} = 10$ Hz, $C_5H_4CH_2$), 21.7 (d, $^1J_{CP} = 11$ Hz, CH_2PH).

^{31}P NMR (161.8 MHz, $CDCl_3$): δ -68.8 (d, $^1J_{PH} = 201$ Hz). FT-IR (KBr): 815 (s), 1001 (m), 1100 (m), 1443 (w), 2254 (s), 3097 (w) cm^{-1} . UV-vis (CH_2Cl_2): λ_{max} 439 nm ($\epsilon = 232 M^{-1} cm^{-1}$). Mass Spec. (EI, +ve mode): exact mass calculated for

$[\text{C}_{24}\text{H}_{27}\text{Fe}_2\text{P}]^+$: 458.0549; exact mass found: 458.0549; difference: 0 ppm. Anal. Calcd. (%) for $\text{C}_{24}\text{H}_{27}\text{Fe}_2\text{P}$: C, 62.92; H, 5.94. Found: C, 62.88; H, 6.04.

Tertiary Phosphine **2.7c** ($3 \times \text{Fc}$)

Tertiary phosphine **2.7c** was collected by changing the elution solvent to a 9:1 mixture of hexanes: Et_2O ($R_f = 0.29$). The solution containing **2.7c** was collected and concentrated *in vacuo* to yield an orange solid. Recrystallization from 4:1 EtOAc : EtOH yielded **2.7c** as an air-stable yellow powder. Yield = 1.63 g, 27%. M.p.: 119–121 °C. ^1H NMR



(399.8 MHz, CDCl_3): δ 4.15 (s, 15H, C_5H_5), 4.13 (t, $^3J_{\text{HH}} = 2$ Hz, 6H, $\beta\text{-C}_5\text{H}_4\text{R}$), 4.11 (t, $^3J_{\text{HH}} = 2$ Hz, 6H, $\alpha\text{-C}_5\text{H}_4\text{R}$), 2.56 (m, 6H, $\text{C}_5\text{H}_4\text{CH}_2$), 1.84 (m, 6H, CH_2P). $^{13}\text{C}\{^1\text{H}\}$ NMR (150.7 MHz, CDCl_3): δ 89.3 (d, $^3J_{\text{CP}} = 11$ Hz, *ipso*- $\text{C}_5\text{H}_4\text{R}$), 68.1 (s, C_5H_5), 67.5 (s, $\beta\text{-C}_5\text{H}_4\text{R}$), 66.9 (s, $\alpha\text{-C}_5\text{H}_4\text{R}$), 28.0 (d, $^2J_{\text{CP}} = 11$ Hz, $\text{C}_5\text{H}_4\text{CH}_2$), 25.6 (d, $^1J_{\text{CP}} = 12$ Hz, CH_2P). ^{31}P NMR (161.8 MHz, CDCl_3): δ -27.9 (s). FT-IR (KBr): 808 (s), 1001 (m), 1105 (m), 1441 (w), 3097 (w) cm^{-1} . UV-vis (CH_2Cl_2): λ_{max} 440 nm ($\epsilon = 311 \text{ M}^{-1} \text{ cm}^{-1}$). Mass Spec. (EI, +ve mode): exact mass calculated for $[\text{C}_{36}\text{H}_{39}\text{Fe}_3\text{P}]^+$: 670.0838; exact mass found: 670.0822; difference: -2.4 ppm. Anal. Calcd. (%) for $\text{C}_{36}\text{H}_{39}\text{Fe}_3\text{P}$: C, 64.52; H, 5.87. Found: C, 64.63; H, 5.81.

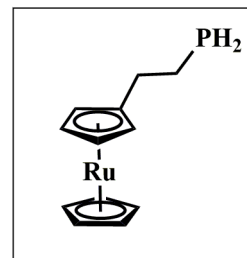
Preparation of Primary, Secondary, and Tertiary Ruthenocene-Containing Phosphines **2.8a–c**

In a 300 mL autoclave, vinylruthenocene (1.20 g, 4.66 mmol) and AIBN (0.03 g, 0.2 mmol) were dissolved in dry toluene (150 mL). The autoclave was degassed by N_2 purging for 10 min before it was pressurized with PH_3 to 80 psi. The solution was stirred for 16 h at 45 °C at which time the pressurized PH_3 gas was released in a controlled environment where it was ignited and allowed to burn. The resulting P_2O_5 was treated with H_2O to form H_3PO_4 and discarded appropriately. The resulting solution was then transferred to a 350 mL grease-free Schlenk flask, which was charged with vinylruthenocene (1.20 g, 4.66 mmol) and AIBN (0.03 g, 0.2 mmol) before it was stirred for 16 h at 45 °C then 8 h at 65 °C. Vinylruthenocene (0.72 g, 2.8 mmol) and AIBN (0.02 g, 0.1 mmol) were added to the

reaction flask for a second time and the pale yellow solution was stirred at 45 °C for 16 h, followed by stirring at 65 °C for 6 h, before AIBN (0.02 g, 0.1 mmol) was added to the reaction flask for a last time and the solution was stirred at 85 °C for 3 h before it was mixed with Celite, concentrated *in vacuo*, and transferred to the top of a silica column. In an effort to reduce the degree of decomposition of phosphines during column chromatography, Et₃N [10% (v/v) relative to dry silica] was added to the silica slurry in hexanes before the slurry was transferred to the column and later washed with pure hexanes (3 × volume of the column) to remove excess Et₃N. Using this column (1.5'' × 10'') and a gradient solvent strategy, primary phosphine **2.8a**, secondary phosphine **2.8b**, and tertiary phosphine **2.8c** were separated (see below).

Primary Phosphine **2.8a** (1 × Rc)

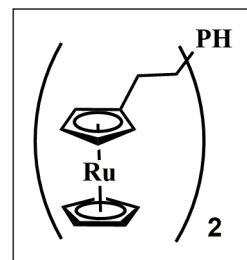
Using N₂ pressure and 95:5 hexanes: Et₂O solvent mixture as eluent, primary phosphine **2.8a** (R_f = 0.41, untreated silica TLC plate) was isolated from the column. The solution containing **2.8a** was concentrated *in vacuo* to yield a white solid. Yield = 0.35 g, 10%. M.p.: 52–54 °C. ¹H NMR (599.5 MHz, CDCl₃): δ 4.53 (s, 5H, C₅H₅),



4.52 (t, ³J_{HH} = 2 Hz, 2H, β-C₅H₄R), 4.45 (t, ³J_{HH} = 2 Hz, 2H, α-C₅H₅R), 2.72 (d of m, ¹J_{HP} = 195 Hz, 2H, PH₂), 2.40 (m, 2H, C₅H₄CH₂), 1.65 (m, 2H, CH₂PH₂). ¹³C{¹H} NMR (150.1 MHz, CDCl₃): δ 93.0 (d, ³J_{CP} = 6 Hz, *ipso*-C₅H₄R), 70.5 (s, β-C₅H₄R), 70.4 (s, C₅H₅), 69.4 (s, α-C₅H₄R), 32.8 (d, ²J_{CP} = 3 Hz, C₅H₄CH₂), 16.0 (d, ¹J_{CP} = 8 Hz, CH₂PH). ³¹P NMR (161.8 MHz, CDCl₃): δ -137.0 (t of m, ¹J_{PH} = 195 Hz). FT-IR/ATR: 3084 (w), 2916 (w), 2281 (s), 1433 (w), 1222 (w), 1099 (m), 995 (m), 806 (s) cm⁻¹. UV-vis (THF): λ_{max} 319 nm (ε = 210 M⁻¹ cm⁻¹). Mass Spec. (EI, +ve mode): exact mass calculated for [C₁₂H₁₅P¹⁰²Ru]⁺: 291.9955; exact mass found: 291.9955; difference: 0 ppm. Anal. Calcd. (%) for C₁₂H₁₅PRu: C, 49.48; H, 5.19. Found: C, 50.15; H, 5.25.

Secondary Phosphine **2.8b** (2 × Rc)

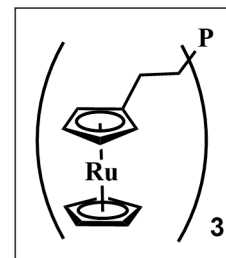
After removal of primary phosphine **2.8a**, secondary phosphine **2.8b** was isolated from the column by changing the elution solvent to 4:1 hexanes:Et₂O ($R_f = 0.58$, untreated silica TLC plate). The solution containing **2.8b** was concentrated *in vacuo* to yield a white solid. Yield = 0.90 g, 27%. M.p.: 97–99 °C. ¹H NMR (599.5 MHz, CDCl₃):



δ 4.54 (t, ³ $J_{HH} = 2$ Hz, 4H, β -C₅H₄R), 4.53 (s, 10H, C₅H₅), 4.46 (t, ³ $J_{HH} = 2$ Hz, 4H, α -C₅H₅R), 3.16 (d of m, ¹ $J_{HP} = 201$ Hz, 1H, PH), 2.36 (m, 4H, C₅H₄CH₂), 1.72 (d of m, ² $J_{HP} = 70$ Hz, 4H, CH₂PH). ¹³C{¹H} NMR (150.1 MHz, CDCl₃): δ 93.5 (d, ³ $J_{CP} = 10$ Hz, *ipso*-C₅H₄R), 70.6 (s, β -C₅H₄R), 70.4 (s, C₅H₅), 69.4 (s, α -C₅H₄R), 28.2 (d, ¹ $J_{CP} = 12$ Hz, CH₂PH), 22.3 (d, ² $J_{CP} = 10$ Hz, C₅H₄CH₂). ³¹P NMR (161.8 MHz, CDCl₃): δ -68.9 (d of m, ¹ $J_{PH} = 201$ Hz). FT-IR/ATR: 3083(w), 2920 (w), 2252 (w), 1442 (w), 1227 (w), 1100 (m), 995 (m), 803 (s), and 667 (w) cm⁻¹. UV-vis (THF): λ_{max} 319 nm ($\epsilon = 480$ M⁻¹ cm⁻¹). Mass Spec. (EI, +ve mode): exact mass calculated for [C₂₄H₂₇P⁹⁶Ru⁹⁹Ru]⁺: 540.9986; exact mass found: 540.9975; difference: -2.03 ppm. Anal. Calcd. (%) for C₂₄H₂₇PRu₂: C, 52.55; H, 4.96. Found: C, 52.84; H, 4.95.

Tertiary Phosphine **2.8c** (3 × Rc)

After removal of secondary phosphine **2.8b**, tertiary phosphine **2.8c** was also collected from the column by changing the elution solvent to a 1:1 mixture of hexanes:Et₂O ($R_f = 0.40$, untreated silica TLC plate). The solution containing **2.8c** was concentrated *in vacuo* to yield a white solid. Yield = 0.70 g, 22%. M.p.: 110–112 °C. ¹H NMR (599.5

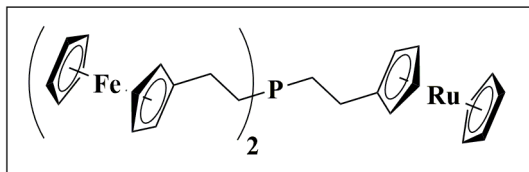


MHz, CDCl₃): δ 4.55 (t, ³ $J_{HH} = 2$ Hz, 6H, β -C₅H₄R), 4.54 (s, 15H, C₅H₅), 4.47 (t, ³ $J_{HH} = 2$ Hz, 6H, α -C₅H₅R), 2.31 (m, 6H, C₅H₄CH₂), 1.59 (m, 6H, CH₂P). ¹³C{¹H} NMR (150.1 MHz, CDCl₃): δ 93.8 (d, ³ $J_{CP} = 12$ Hz, *ipso*-C₅H₄R), 70.5 (s, β -C₅H₄R), 70.4 (s, C₅H₅), 69.4 (s, α -C₅H₄R), 28.7 (d, ² $J_{CP} = 13$ Hz, C₅H₄CH₂), 25.4 (d, ¹ $J_{CP} = 14$ Hz, CH₂P). ³¹P NMR (161.8 MHz, CDCl₃): δ -29.4 (m). FT-IR/ATR: 3101 (w), 2931 (w), 2360 (w), 2304 (w), 1409 (w), 1187 (m), 1100 (m), 1040 (m), 997 (m), 802 (s), and 683 (m) cm⁻¹. UV-vis (THF): λ_{max} 319 nm ($\epsilon = 770$ M⁻¹ cm⁻¹). Mass Spec. (EI, +ve mode): exact mass calculated

for $[\text{C}_{36}\text{H}_{39}\text{P}^{96}\text{Ru}_2^{102}\text{Ru}]^+$: 795.9985; exact mass found: 795.9998; difference: 1.63 ppm. Anal. Calcd. (%) for $\text{C}_{36}\text{H}_{39}\text{PRu}_3$: C, 53.65; H, 4.88. Found: C, 53.60; H, 4.81.

Preparation of Tertiary Phosphine **2.10** (1 × Rc, 2 × Fc)

In a 25 mL grease-free Schlenk flask, secondary phosphine **2.7b** (2.00 g, 4.37 mmol) was combined with vinylruthenocene (0.38 g, 1.5 mmol) and AIBN (0.01 g, 0.06



mmol) in 6 mL of dry THF before it was stirred for 16 h at 45 °C then 8 h at 65 °C. The reaction flask was charged a second time with vinylruthenocene (0.25 g, 0.97 mmol) and AIBN (0.008 g, 0.05 mmol) and stirred for 16 h at 45 °C then 8 h at 65 °C. Vinylruthenocene (0.16 g, 0.64 mmol) and AIBN (0.005 g, 0.03 mmol) were added to the reaction flask for a third time and the orange solution was stirred at 45 °C for 16 h, followed by stirring at 65 °C for 8 h. Vinylruthenocene (0.11 g, 0.43 mmol) and AIBN (0.003 g, 0.02 mmol) were added to the reaction flask for a fourth time and the orange solution was stirred at 45 °C for 16 h, followed by stirring at 65 °C for 8 h, and 85 °C for 2 h before it was concentrated *in vacuo*. The oily orange solid was dissolved in CH_2Cl_2 and combined with Celite before the resulting mixture was dried *in vacuo* and transferred to the top of a silica column [1.5" × 8", treated with Et_3N 10% (v/v) as described above] for subsequent purification by column chromatography using a gradient solvent strategy. Using N_2 gas and a mixture of 99:1 hexanes: Et_2O , unreacted secondary phosphine **2.7b** was removed from the column (0.38 g recovered). After removal of secondary phosphine **2.7b**, tertiary phosphine **2.10** was collected from the column by changing the elution solvent to 4:1 hexanes: Et_2O ($R_f = 0.47$, untreated silica TLC plate). The solution containing tertiary phosphine **2.10** was concentrated *in vacuo* to yield an orange solid. Yield = 2.36 g, 94%. M.p.: 135–137 °C. ^1H NMR (599.5 MHz, CDCl_3): δ 4.56 [t, $^3J_{\text{HH}} = 2$ Hz, 2H, β - $\text{C}_5\text{H}_4\text{R}(\text{Ru})$], 4.54 [s, 5H, $\text{C}_5\text{H}_5(\text{Ru})$], 4.47 [t, $^3J_{\text{HH}} = 2$ Hz, 2H, α - $\text{C}_5\text{H}_5\text{R}(\text{Ru})$], 4.13 [s, 10H, $\text{C}_5\text{H}_5(\text{Fe})$], 4.11 [t, $^3J_{\text{HH}} = 2$ Hz, 4H, β - $\text{C}_5\text{H}_4\text{R}(\text{Fe})$], 4.09 [t, $^3J_{\text{HH}} = 2$ Hz, 4H, α - $\text{C}_5\text{H}_5\text{R}(\text{Fe})$], 2.48 [m, 4H, $\text{C}_5\text{H}_4\text{CH}_2(\text{Fe})$], 2.33 [m, 2H, $\text{C}_5\text{H}_4\text{CH}_2(\text{Ru})$], 1.66 [m, 4H, $\text{CH}_2\text{P}(\text{Fe})$], 1.61 [m, 2H, $\text{CH}_2\text{P}(\text{Ru})$]. $^{13}\text{C}\{^1\text{H}\}$ NMR (150.1 MHz, CDCl_3): δ 93.9 [d, $^3J_{\text{CP}} = 13$ Hz, *ipso*-

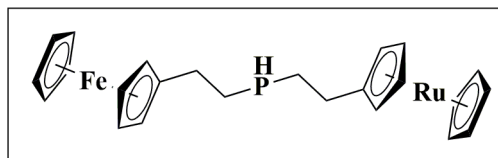
$C_5H_4R(Ru)$], 89.8 [d, $^3J_{CP} = 13$ Hz, *ipso*- $C_5H_4R(Fe)$], 70.5 [s, β - $C_5H_4R(Ru)$], 70.5 [s, $C_5H_5(Ru)$], 69.4 [s, α - $C_5H_4R(Ru)$], 68.5 [s, $C_5H_5(Fe)$], 67.8 [s, β - $C_5H_4R(Fe)$], 67.3 [s, α - $C_5H_4R(Fe)$], 28.9 [d, $^2J_{CP} = 13$ Hz, $C_5H_4CH_2(Ru)$], 28.5 [d, $^2J_{CP} = 13$ Hz, $C_5H_4CH_2(Fe)$], 26.1 [d, $^1J_{CP} = 16$ Hz, $CH_2P(Fe)$], 25.5 [d, $^1J_{CP} = 15$ Hz, $CH_2P(Ru)$]. ^{31}P NMR (161.8 MHz, $CDCl_3$): δ -28.4 (m). FT-IR/ATR: 3101 (w), 2941 (w), 2915 (w), 1440 (w), 1227 (w), 1104 (m), 1000 (m), 807 (s), and 667 (w) cm^{-1} . UV-vis (THF): λ_{max} 324 nm ($\epsilon = 375$ $M^{-1} cm^{-1}$) and 436 nm ($\epsilon = 205$ $M^{-1} cm^{-1}$). Mass Spec. (EI, +ve mode): exact mass calculated for $[C_{36}H_{39}^{56}Fe_2P^{96}Ru]^+$: 710.0564; exact mass found: 710.0557; difference: -0.98 ppm. Anal. Calcd. (%) for $C_{36}H_{39}Fe_2PRu$: C, 60.44; H, 5.49. Found: C, 60.41; H, 5.49.

Preparation of Secondary Phosphine **2.11** (1 \times Rc, 1 \times Fc) and Tertiary Phosphine **2.12** (2 \times Rc, 1 \times Fc)

In a 25 mL grease-free Schlenk flask, primary phosphine **2.7a** (1 \times Fc) (1.00 g, 4.06 mmol) was combined with vinylruthenocene (0.70 g, 2.7 mmol) and AIBN (0.02 g, 0.1 mmol) in 6 mL of dry THF before it was stirred for 16 h at 45 $^{\circ}C$, 6 h at 65 $^{\circ}C$, and 2 h at 85 $^{\circ}C$ and concentrated *in vacuo*. The oily orange solid was dissolved in CH_2Cl_2 and combined with Celite before the resulting mixture was dried *in vacuo* and transferred to the top of a silica column [1.5" \times 8", treated with Et_3N 10% (v/v) as described above] for subsequent purification by column chromatography using a gradient solvent strategy (see below).

Secondary Phosphine **2.11** (1 \times Rc, 1 \times Fc)

Using N_2 gas pressure and hexanes as eluent, unreacted primary phosphine **2.7a** (0.45g) was removed from the column before the eluent was changed to a mixture of 99:1 hexanes: Et_2O

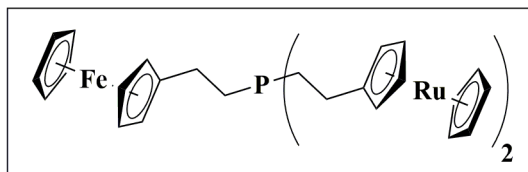


which removed secondary phosphine **2.11** from the column as a yellow band ($R_f = 0.15$, untreated silica TLC plate). The solution containing secondary phosphine **2.11** was concentrated *in vacuo* to yield an orange solid. Yield = 0.52 g, 39%. M.p.: 76–78 $^{\circ}C$. 1H NMR (599.5 MHz, $CDCl_3$): δ 4.54 [t, $^3J_{HH} = 2$ Hz, 2H, β - $C_5H_4R(Ru)$], 4.53 [s, 5H, $C_5H_5(Ru)$], 4.46 [t, $^3J_{HH} = 2$ Hz, 2H, α - $C_5H_5R(Ru)$], 4.12 [s, 5H, $C_5H_5(Fe)$], 4.08 [t, $^3J_{HH} =$

2 Hz, 2H, β -C₅H₄R(Fe)], 4.07 [t, $^3J_{\text{HH}} = 2$ Hz, 2H, α -C₅H₅R(Fe)], 3.16 (d of quintets, $^1J_{\text{HP}} = 201$ Hz, $^3J_{\text{HH}} = 7$ Hz, 1H, PH), 2.52 [m, 2H, C₅H₄CH₂(Fe)], 2.37 [m, 2H, C₅H₄CH₂(Ru)], 1.81 [m, 2H, CH₂PH(Fe)], 1.69 [m, 2H, CH₂PH(Ru)]. $^{13}\text{C}\{^1\text{H}\}$ NMR (150.1 MHz, CDCl₃): δ 93.4 [d, $^3J_{\text{CP}} = 10$ Hz, *ipso*-C₅H₄R(Ru)], 89.3 [d, $^3J_{\text{CP}} = 9$ Hz, *ipso*-C₅H₄R(Fe)], 70.5 [s, β -C₅H₄R(Ru)], 70.4 [s, C₅H₅(Ru)], 69.4 [s, α -C₅H₄R(Ru)], 68.4 [s, C₅H₅(Fe)], 67.8 [s, β -C₅H₄R(Fe)], 67.2 [s, α -C₅H₄R(Fe)], 28.4 [d, $^2J_{\text{CP}} = 10$ Hz, C₅H₄CH₂(Ru)], 28.1 [d, $^2J_{\text{CP}} = 10$ Hz, C₅H₄CH₂(Fe)], 22.3 [d, $^1J_{\text{CP}} = 10$ Hz, CH₂PH(Fe)], 21.8 [d, $^1J_{\text{CP}} = 11$ Hz, CH₂PH(Ru)]. ^{31}P NMR (161.8 MHz, CDCl₃): δ -68.9 (d of m, $^1J_{\text{PH}} = 200$ Hz). FT-IR/ATR: 3096 (w), 2915 (w), 2254 (w), 1442 (w), 1100 (w), 1000 (w), and 805 (s) cm⁻¹. UV-vis (THF): λ_{max} 324 nm ($\epsilon = 300$ M⁻¹ cm⁻¹) and 436 nm ($\epsilon = 105$ M⁻¹ cm⁻¹). Mass Spec. (EI, +ve mode): exact mass calculated for [C₂₄H₂₇⁵⁶FeP¹⁰²Ru]⁺: 504.0243; exact mass found: 504.0248; difference: 0.99 ppm. Anal. Calcd. (%) for C₂₄H₂₇FePRu: C, 57.27; H, 5.41. Found: C, 57.31; H, 5.40.

Tertiary Phosphine **2.12** (2 × Rc, 1 × Fc)

After removal of secondary phosphine **2.11**, tertiary phosphine **2.12** was collected from the column by changing the elution solvent to a mixture of 95:5 hexanes:Et₂O ($R_f = 0.46$,



untreated silica TLC plate). The solution containing tertiary phosphine **2.12** was concentrated *in vacuo* to yield a yellow solid. Yield = 0.44 g, 42%. M.p.: 106–108 °C. ^1H NMR (599.5 MHz, CDCl₃): δ 4.55 [t, $^3J_{\text{HH}} = 2$ Hz, 4H, β -C₅H₄R(Ru)], 4.54 [s, 10H, C₅H₅(Ru)], 4.47 [t, $^3J_{\text{HH}} = 4$ Hz, 4H, α -C₅H₅R(Ru)], 4.12 [s, 5H, C₅H₅(Fe)], 4.11 [t, $^3J_{\text{HH}} = 2$ Hz, 2H, β -C₅H₄R(Fe)], 4.08 [t, $^3J_{\text{HH}} = 2$ Hz, 2H, α -C₅H₅R(Fe)], 2.47 [m, 2H, C₅H₄CH₂(Fe)], 2.32 [m, 4H, C₅H₄CH₂(Ru)], 1.64 [m, 2H, CH₂P(Fe)], 1.60 [m, 4H, CH₂P(Ru)]. $^{13}\text{C}\{^1\text{H}\}$ NMR (150.1 MHz, CDCl₃): δ 93.9 [d, $^3J_{\text{CP}} = 13$ Hz, *ipso*-C₅H₄R(Ru)], 89.8 [d, $^3J_{\text{CP}} = 13$ Hz, *ipso*-C₅H₄R(Fe)], 70.5 [s, β -C₅H₄R(Ru)], 70.4 [s, C₅H₅(Ru)], 69.4 [s, α -C₅H₄R(Ru)], 68.5 [s, C₅H₅(Fe)], 67.8 [s, β -C₅H₄R(Fe)], 67.2 [s, α -C₅H₄R(Fe)], 28.8 [d, $^2J_{\text{CP}} = 14$ Hz, C₅H₄CH₂(Ru)], 28.4 [d, $^2J_{\text{CP}} = 13$ Hz, C₅H₄CH₂(Fe)], 26.0 [d, $^1J_{\text{CP}} = 15$ Hz, CH₂P(Fe)], 25.5 [d, $^1J_{\text{CP}} = 15$ Hz, CH₂P(Ru)]. ^{31}P NMR (161.8 MHz, CDCl₃): δ -28.9 (m). FT-IR/ATR: 3101 (w), 2928 (w), 1411 (w), 1229 (w), 1100 (m), 998 (m), 805 (s), and 666

(w) cm^{-1} . UV-vis (THF): λ_{max} 322 nm ($\epsilon = 495 \text{ M}^{-1} \text{ cm}^{-1}$) and 438 nm ($\epsilon = 95 \text{ M}^{-1} \text{ cm}^{-1}$). Mass Spec. (EI, +ve mode): exact mass calculated for $[\text{C}_{36}\text{H}_{39}^{56}\text{FeP}^{96}\text{Ru}^{99}\text{Ru}]^+$: 753.0274; exact mass found: 753.0274; difference: 0 ppm. Anal. Calcd. (%) for $\text{C}_{36}\text{H}_{39}\text{FePRu}_2$: C, 56.84; H, 5.17. Found: C, 56.88; H, 5.16.

2.5 References

1. Tolman, C. A. *Chem. Rev.* **1977**, *77*, 313–348.
2. Erre, G.; Enthaler, S.; Junge, K.; Gladiali, S.; Beller, M. *Coord. Chem. Rev.* **2008**, *252*, 471–491.
3. Shaughnessy, K. H. *Chem. Rev.* **2009**, *109*, 643–710.
4. Burt, J.; Levason, W.; Reid, G. *Coord. Chem. Rev.* **2014**, *260*, 65–115.
5. Chikkali, S. H.; van der Vlugt, J. I.; Reek, J. N. H. *Coord. Chem. Rev.* **2014**, *262*, 1–15.
6. Genet, J.-P.; Ayad, T.; Ratovelomanana-Vidal, V. *Chem. Rev.* **2014**, *114*, 2824–2880.
7. Stephan, D. W. *Acc. Chem. Res.* **2015**, *48*, 306–316.
8. Voituriez, A.; Marinetti, A.; Gicquel, M. *SYNLETT* **2015**, *26*, 142–166.
9. Kamer, P. C. J.; van Leeuwen, P. W. N. M. *Phosphorus(III) Ligands in Homogeneous Catalysis: Design and Synthesis*. Wiley-Blackwell: Oxford, 2012.
10. Nell, B. P.; Tyler, D. R. *Coord. Chem. Rev.* **2014**, *279*, 23–42.
11. Annen, S. P.; Bambagioni, V.; Bevilacqua, M.; Filippi, J.; Marchionni, A.; Oberhauser, W.; Schönberg, H.; Vizza, F.; Bianchini, C.; Grützmacher, H. *Angew. Chem. Int. Ed.* **2010**, *49*, 7229–7233.
12. Anderson, J. S.; Rittle, J.; Peters, J. C. *Nature* **2013**, *501*, 84–87.
13. Dobereiner, G. E.; Yuan, J.; Schrock, R. R.; Goldman, A. S.; Hackenberg, J. D. *J. Am. Chem. Soc.* **2013**, *135*, 12572–12575.
14. Kawaguchi, S.-i.; Minamida, Y.; Ohe, T.; Nomoto, A.; Sonoda, M.; Ogawa, A. *Angew. Chem. Int. Ed.* **2013**, *52*, 1748–1752.

15. Lavallo, V.; Wright, J. H.; Tham, F. S.; Quinlivan, S. *Angew. Chem. Int. Ed.* **2013**, *52*, 3172–3176.
16. Cheng, C.; Hartwig, J. F. *J. Am. Chem. Soc.* **2014**, *136*, 12064–12072.
17. Kang, P.; Zhang, S.; Meyer, T. J.; Brookhart, M. *Angew. Chem. Int. Ed.* **2014**, *53*, 8709–8713.
18. Zhang, X.-N.; Chen, G.-Q.; Tang, X.-Y.; Wei, Y.; Shi, M. *Angew. Chem. Int. Ed.* **2014**, *53*, 10768–10773.
19. Zhu, Y.; Buchwald, S. L. *J. Am. Chem. Soc.* **2014**, *136*, 4500–4503.
20. Yan, X.; Cook, T. R.; Wang, P.; Huang, F.; Stang, P. J. *Nat. Chem.* **2015**, *7*, 342–348.
21. Zhao, D.; Neubauer, T. M.; Feringa, B. L. *Nat. Commun.* **2015**, *6*.
22. Katti, K. V.; Gali, H.; Smith, C. J.; Berning, D. E. *Acc. Chem. Res.* **1999**, *32*, 9–17.
23. Brynda, M. *Coord. Chem. Rev.* **2005**, *249*, 2013–2034.
24. Fleming, J. T.; Higham, L. J. *Coord. Chem. Rev.* **2015**, *297–298*, 127–145.
25. Yoshifuji, M.; Shibayama, K.; Inamoto, N.; Matsushita, T.; Nishimoto, K. *J. Am. Chem. Soc.* **1983**, *105*, 2495–2497.
26. Ramakrishnan, G.; Jouaiti, A.; Geoffroy, M.; Bernardinelli, G. *J. Phys. Chem.* **1996**, *100*, 10861–10868.
27. Smith, C. J.; Reddy, V. S.; Karra, S. R.; Katti, K. V.; Barbour, L. J. *Inorg. Chem.* **1997**, *36*, 1786–1791.
28. Prabhu, K. R.; Pillarsetty, N.; Gali, H.; Katti, K. V. *J. Am. Chem. Soc.* **2000**, *122*, 1554–1555.
29. Twamley, B.; Hwang, C.-S.; Hardman, N. J.; Power, P. P. *J. Organomet. Chem.* **2000**, *609*, 152–160.

30. Henderson, W.; Alley, S. R. *J. Organomet. Chem.* **2002**, *656*, 120–128.
31. Downard, A. J.; Goodwin, N. J.; Henderson, W. *J. Organomet. Chem.* **2003**, *676*, 62–72.
32. Hiney, R. M.; Higham, L. J.; Müller-Bunz, H.; Gilheany, D. G. *Angew. Chem. Int. Ed.* **2006**, *45*, 7248–7251.
33. Barder, T. E.; Buchwald, S. L. *J. Am. Chem. Soc.* **2007**, *129*, 5096–5101.
34. Kalio, R.; Lönnecke, P.; Hey-Hawkins, E. *J. Organomet. Chem.* **2008**, *693*, 590–600.
35. Stewart, B.; Harriman, A.; Higham, L. J. *Organometallics* **2011**, *30*, 5338–5343.
36. Davies, L. H.; Stewart, B.; Harrington, R. W.; Clegg, W.; Higham, L. J. *Angew. Chem. Int. Ed.* **2012**, *51*, 4921–4924.
37. Rabiee Kenaree, A.; Berven, B. M.; Ragona, P. J.; Gilroy, J. B. *Chem. Commun.* **2014**, *50*, 10714–10717.
38. Asamizu, T.; Henderson, W.; Nicholson, B. K.; Hey-Hawkins, E. *Inorg. Chim. Acta* **2014**, *414*, 181–190.
39. Guterman, R.; Rabiee Kenaree, A.; Gilroy, J. B.; Gillies, E. R.; Ragona, P. J. *Chem. Mater.* **2015**, *27*, 1412–1419.
40. Colacot, T. J. *Chem. Rev.* **2003**, *103*, 3101–3118.
41. Atkinson, R. C. J.; Gibson, V. C.; Long, N. J. *Chem. Soc. Rev.* **2004**, *33*, 313–328.
42. Gómez Arrayás, R.; Adrio, J.; Carretero, J. C. *Angew. Chem. Int. Ed.* **2006**, *45*, 7674–7715.
43. Toma, Š.; Csizmadiová, J.; Mečiarová, M.; Šebesta, R. *Dalton Trans.* **2014**, *43*, 16557–16579.
44. Green, R. A.; Hartwig, J. F. *Org. Lett.* **2014**, *16*, 4388–4391.

45. Cowie, B. E.; Tsao, F. A.; Emslie, D. J. H. *Angew. Chem. Int. Ed.* **2015**, *54*, 2165–2169.
46. Gan, L.; Groy, T. L.; Tarakeshwar, P.; Mazinani, S. K. S.; Shearer, J.; Mujica, V.; Jones, A. K. *J. Am. Chem. Soc.* **2015**, *137*, 1109–1115.
47. Škoch, K.; Císařová, I.; Štěpnička, P. *Organometallics* **2015**, *34*, 1942–1956.
48. Brosmer, J. L.; Diaconescu, P. L. *Organometallics* **2015**, *34*, 2567–2572.
49. Huber, D. P.; Kehr, G.; Bergander, K.; Fröhlich, R.; Erker, G.; Tanino, S.; Ohki, Y.; Tatsumi, K. *Organometallics* **2008**, *27*, 5279–5284.
50. Ramos, A.; Lough, A. J.; Stephan, D. W. *Chem. Commun.* **2009**, 1118–1120.
51. Wang, X.; Kehr, G.; Daniliuc, C. G.; Erker, G. *J. Am. Chem. Soc.* **2014**, *136*, 3293–3303.
52. Mizuta, T.; Imamura, Y.; Miyoshi, K. *J. Am. Chem. Soc.* **2003**, *125*, 2068–2069.
53. Patra, S. K.; Whittell, G. R.; Nagiah, S.; Ho, C.-L.; Wong, W.-Y.; Manners, I. *Chem. Eur. J.* **2010**, *16*, 3240–3250.
54. Wei, B.; Li, S.; Lee, H. K.; Hor, T. S. A. *J. Organomet. Chem.* **1997**, *527*, 133–136.
55. Swartz, B. D.; Nataro, C. *Organometallics* **2005**, *24*, 2447–2451.
56. Polukeev, A. V.; Petrovskii, P. V.; Peregudov, A. S.; Ezernitskaya, M. G.; Koridze, A. A. *Organometallics* **2013**, *32*, 1000–1015.
57. Fourie, E.; van Rensburg, J. M. J.; Swarts, J. C. *J. Organomet. Chem.* **2014**, *754*, 80–87.
58. Rauhut, M. M.; Currier, H. A.; Semsel, A. M.; Wystrach, V. P. *J. Org. Chem.* **1961**, *26*, 5138–5145.
59. Obata, T.; Kobayashi, E.; Aoshima, S.; Furukawa, J. *Polym. J.* **1993**, *25*, 1039–1048.

60. Gritzner, G.; Kůta, J. *Electrochim. Acta* **1984**, *29*, 869-873.
61. Connelly, N. G.; Geiger, W. E. *Chem. Rev.* **1996**, *96*, 877–910.
62. Morrison, W. H.; Hendrickson, D. N. *Inorg. Chem.* **1972**, *11*, 2912–2917.
63. Denisovich, L. I.; Zakurin, N. V.; Bezrukova, A. A.; Gubin, S. P. *J. Organomet. Chem.* **1974**, *81*, 207–216.
64. Russell, A. D.; Gilroy, J. B.; Lam, K.; Haddow, M. F.; Harvey, J. N.; Geiger, W. E.; Manners, I. *Chem. Eur. J.* **2014**, *20*, 16216–16227.
65. Hashidzume, K.; Tobita, H.; Ogino, H. *Organometallics* **1995**, *14*, 1187–1194.
66. Sohn, Y. S.; Schlueter, A. W.; Hendrickson, D. N.; Gray, H. B. *Inorg. Chem.* **1974**, *13*, 301–304.
67. Smith, T. P.; Kwan, K. S.; Taube, H.; Bino, A.; Cohen, S. *Inorg. Chem.* **1984**, *23*, 1943–1945.
68. Geiger, W. E.; Barrière, F. *Acc. Chem. Res.* **2010**, *43*, 1030–1039.
69. Trupia, S.; Nafady, A.; Geiger, W. E. *Inorg. Chem.* **2003**, *42*, 5480–5482.
70. Swarts, J. C.; Nafady, A.; Roudebush, J. H.; Trupia, S.; Geiger, W. E. *Inorg. Chem.* **2009**, *48*, 2156–2165.
71. Erhard, M.; Lam, K.; Haddow, M.; Whittell, G. R.; Geiger, W. E.; Manners, I. *Polymer. Chem.* **2014**, *5*, 1264–1274.
72. Russell, A. D.; Gilroy, J. B.; Lam, K.; Haddow, M. F.; Harvey, J. N.; Geiger, W. E.; Manners, I. *Chem. Eur. J.* **2012**, *18*, 8000–8003.
73. Aranzaes, J. R.; Daniel, M.-C.; Astruc, D. *Can. J. Chem.* **2006**, *84*, 288–299.
74. Seibert, A. R.; Cain, M. F.; Glueck, D. S.; Nataro, C. *J. Organomet. Chem.* **2011**, *696*, 2259–2262.

75. Sanders, R.; Mueller-Westerhoff, U. T. *J. Organomet. Chem.* **1996**, *512*, 219–224.
76. Gallei, M.; Klein, R.; Rehahn, M. *Macromolecules* **2010**, *43*, 1844–1854.
77. Hudson, R. D. A. *J. Organomet. Chem.* **2001**, *637–639*, 47–69.
78. Bruker-AXS, SADABS version 2012.1, **2012**, Bruker-AXS, Madison, WI 53711, USA.
79. Shi, M.; Li, A.-L.; Liang, H.; Lu, J. *Macromolecules* **2007**, *40*, 1891–1896.
80. Sheldrick, G. *Acta Crystallogr.* **2015**, *A71*, 3–8.
81. Sheldrick, G. *Acta Crystallogr.* **2008**, *A64*, 112–122.
82. Rausch, M. D.; Siegel, A. *J. Organomet. Chem.* **1968**, *11*, 317–324.

Chapter 3

3 Group 6 Metal Pentacarbonyl Complexes of Air-Stable Primary, Secondary, and Tertiary Ethylferrocenephosphines

Adapted from:

Rabiee Kenaree, A.; Sauv , E.R.; Ragona, P.J.; Gilroy, J.B.* Group 6 Metal Pentacarbonyl Complexes of Air-Stable Primary, Secondary, and Tertiary Ethylferrocenephosphines. *Dalton Trans.* **2016**, 45, 2859–2867.

3.1 Introduction

Phosphines, including examples based on ferrocene,¹⁻⁶ are among the most widely exploited L-type ligands within the field of coordination chemistry^{7-11,12-20} as a result of their tunable steric²¹ and electronic²² properties. They have been employed extensively as ancillary and/or labile ligands in homogeneous catalysts [*e.g.*, Grubbs I **3.1**, Ni(dppp)Cl₂ **3.2**, Pd(dppf)Cl₂ **3.3**, Wilkinson's catalyst Rh(PPh₃)₃Cl, and Pd(PPh₃)₄] that rapidly facilitate polymerization,²³⁻²⁷ C-C and C-E bond formation,²⁸⁻³³ and hydrogenation reactions.³⁴⁻³⁹ While homogeneous catalysts commonly employ tertiary phosphines, relatively few examples include electron-rich primary and secondary alkyl phosphines due to their high reactivity towards air and moisture.

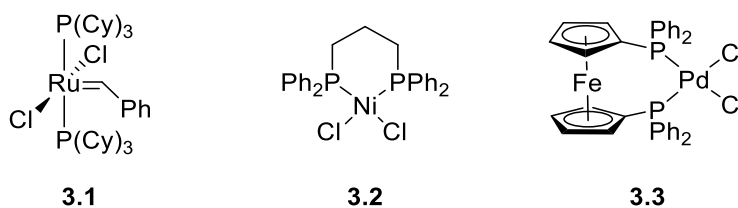


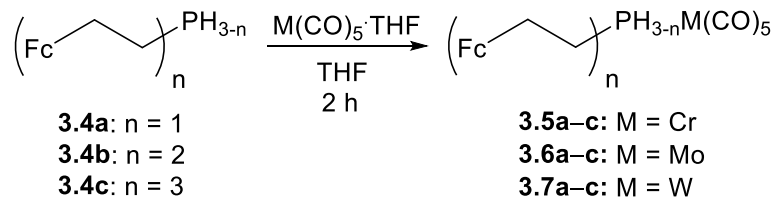
Figure 3.1. Examples of phosphine-based ligands.

Building on recent advances surrounding the design and synthesis of air-stable primary, secondary, and tertiary phosphines^{40-41,42-49} we have developed a unique series of electron-rich alkylphosphines bearing ethylferrocene and ethylruthenocene substituents (*e.g.*, **3.4a–c**).⁵⁰⁻⁵¹ These phosphines have shown utility as precursors to highly-metallized polymers⁵⁰ and polymer networks⁵² and in the phosphane-ene reaction.⁵³ They are remarkably stable towards air and moisture, redox active, and afford the ability to tune their steric properties through the sequential addition of ethylmetallocene units. Herein, we present a comprehensive study of the structure, bonding, and properties of a series of Group 6 metal pentacarbonyl (M: Cr, Mo, W) complexes of primary, secondary, and tertiary ethylferrocenephosphines in order to establish fundamental knowledge of their ligand characteristics. Specifically, these ligands may be particularly well suited for the generation of high nuclearity transition metal clusters, where the presence of ferrocene has previously led to materials with application as sensors and electrode materials.⁵⁴⁻⁵⁹

3.2 Results and Discussion

3.2.1 Synthesis and NMR Spectroscopy

Primary, secondary, and tertiary ethylferrocene phosphines **3.4a–c** were prepared according to published protocols.⁵⁰⁻⁵¹ Monosubstituted phosphine complexes of Group 6 metal pentacarbonyls [M(CO)₅, M: Cr, Mo, W] were produced by first irradiating commercially available hexacarbonyls in THF with UV light to produce the corresponding THF adducts. The THF adducts were stirred with the appropriate phosphines for 2 h, isolated, and purified via column chromatography to afford phosphine complexes **3.5a–c** (M = Cr), **3.6a–c** (M = Mo), and **3.7a–c** (M = W) in yields ranging from 78 to 90% (Scheme 3.1). The structure and purity of the reported complexes were confirmed using multinuclear NMR spectroscopy, X-ray crystallography, IR and UV-Vis absorption spectroscopy, mass spectrometry, and elemental analysis.



Scheme 3.1. Synthesis of primary, secondary, and tertiary phosphine-M(CO)₅ complexes **3.5a-c**, **3.6a-c**, and **3.7a-c**. FcH = ferrocene.

The NMR spectra of phosphine-M(CO)₅ complexes **3.5a-c**, **3.6a-c**, and **3.7a-c** were consistent with the proposed structures of the complexes, with each phosphine coordinated to a single M(CO)₅ fragment (Figures 3.1, A3.1–A3.33, and Table 3.1). The ¹H NMR spectra of the complexes confirmed the presence of ligated primary, secondary, and tertiary phosphines and gave rise to two resonances (1.97–2.26 ppm and 2.51–2.77 ppm) attributed to the ethyl linker and a singlet and pair of *pseudo*-triplets (4.04–4.26 ppm) due to the presence monosubstituted ferrocene groups. The phosphine protons were observed as complex doublets between 4.24 and 4.55 ppm for primary phosphine complexes **3.5a**, **3.6a**, and **3.7a** and between 4.52 and 4.85 for secondary phosphine complexes **3.5b**, **3.6b**, and **3.7b**.

³¹P NMR spectroscopy showed that the phosphorus atoms within the phosphine-M(CO)₅ complexes described became increasingly deshielded as the number of ethylferrocene groups was increased (*e.g.*, **3.7a**: –101.9 ppm; **3.7b**: –43.6 ppm; and **3.7c**: –6.8 ppm). A second trend emerged when we examined the effect of the transition metal on the ³¹P NMR shift. The shielding effect of the metals increased as we moved down Group 6 from Cr to W, resulting in a dramatic upfield shift of the ³¹P NMR signals (*e.g.*, **3.5a**: –47.7 ppm; **3.6a**: –80.4 ppm; and **3.7a**: –101.9 ppm). The ¹³C NMR signals observed for the CO ligands in each complex follow the same trend, with the most upfield resonances being observed for W(CO)₅ complexes and the most downfield resonances being observed for the Cr(CO)₅ complexes. Coupling to ¹⁸³W (¹J_{PW} for **3.7a**: 217 Hz; **3.7b**: 225 Hz; and **3.7c**: 233 Hz) in complexes **3.7a-c** further supports the proposed structures of the complexes and the static nature of the P-W bonds (Figures A3.27, A3.30, and A3.33). The observed trend for the P-W coupling constants is consistent with previous reports where a linear

relationship between CO stretching frequencies (E mode) and coupling constants was established (Table 3.1).⁶⁰

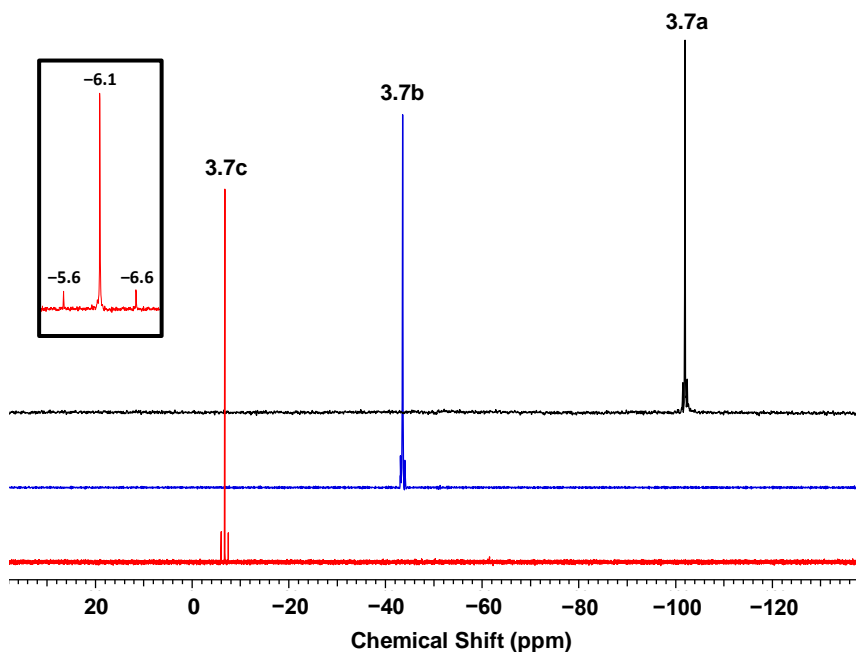


Figure 3.2. $^{31}\text{P}\{^1\text{H}\}$ NMR spectra of primary, secondary, and tertiary phosphine- $\text{W}(\text{CO})_5$ complexes **3.7a** (black line), **3.7b** (blue line), **3.7c** (red line and the inset) recorded in CDCl_3 .

Table 3.1. Selected characterization data for complexes **3.5a–c**, **3.6a–c**, and **3.7a–c**.

	3.5a	3.5b	3.5c	3.6a	3.6b	3.6c	3.7a	3.7b	3.7c
$\nu(\text{CO}) A_{1\text{cis}} (\text{cm}^{-1})$	2067	2062	2058	2075	2071	2067	2074	2070	2066
$\nu(\text{CO}) A_{1\text{trans}} (\text{cm}^{-1})$	1979	1979	1975	1993	1986	1981	1976	1978	1974
$\nu(\text{CO}) E (\text{cm}^{-1})$	1916	1916	1922	1922	1925	1929	1912	1914	1922
$^{31}\text{P} (\delta)$	-47.7	3.5	30.4	-80.4	-22.9	12.5	-101.9	-43.6	-6.8
$^1J_{\text{PH}} (\text{Hz})$	324	321	-	319	315	-	333	328	-
$^1J_{\text{PW}} (\text{Hz})$	-	-	-	-	-	-	217	225	233
$E_{1/2, \text{Fc}} (\text{mV})$	10	0	-5	10	0	-5	10	0	-5
$\lambda_{\text{max}} (\text{nm})$	437	436	439	439	436	435	441	437	436
$\epsilon (\text{M}^{-1} \text{cm}^{-1})$	130	230	350	115	250	350	120	245	335

3.2.2 X-ray Crystallography

The solid-state structures of complexes **3.5c**, **3.6c**, and **3.7a–c** were determined by single crystal X-ray diffraction and are shown in Figures 3.2, A3.34, and A3.35 and the data are summarized in Table 3.2. The structures contain many general features including a Group 6 metal in an octahedral environment, C-O bond lengths between 1.138(3) and 1.145(4) Å, and P-C bond lengths of 1.832(3)–1.842(7) Å. The P-C bond lengths observed were slightly shorter than those of free phosphines **3.4a–c** [1.843(1)–1.93(1) Å].⁵⁰

Examination of the solid-state structures of **3.7a–c** (M = W) allowed for direct comparison of the primary, secondary, and tertiary phosphine complexes. Partial space filling models, viewed down the W-P bond axis, are shown in Figure 3.2 and demonstrate the dramatic increase in relative size associated with the sequential addition of ethylferrocene substituents at phosphorus. The M-P distances are 2.492(2) Å for **3.7a**, 2.5135(10) Å for **3.7b**, and 2.5094(8) Å for **3.7c**, which provides an indication that the introduction of additional ethylferrocene substituents at phosphorus does not result in a significant enhancement in the steric interactions between the phosphine ligands and M(CO)₅ unit. A further indication that the structures of the phosphine ligands are not being altered in the complexes due to unfavorable steric interactions are the average C-P-C angles, which increased from 99.03(4)° and 99.68(6)° in free phosphines **3.4b** and **3.4c** to 104.57(19)° and 102.62(10)° in their respective W(CO)₅ complexes, **3.7b** and **3.7c**.

By comparing the solid-state structures of tertiary phosphine complexes **3.5c**, **3.6c**, and **3.7c** we assessed the influence of the different Group 6 metals on their structural metrics. The M-P bond length observed for complex **3.5c** [M = Cr, 2.3747(10) Å] was shorter than that of **3.6c** [M = Mo, 2.5121(11) Å] due to an increase in the number of electrons associated with a change from Period 4 to Period 5. Similar elongation of the M-P bond was not observed when Mo was replaced by W in **3.7c** [2.5094(8) Å] due to the lanthanoid contraction.

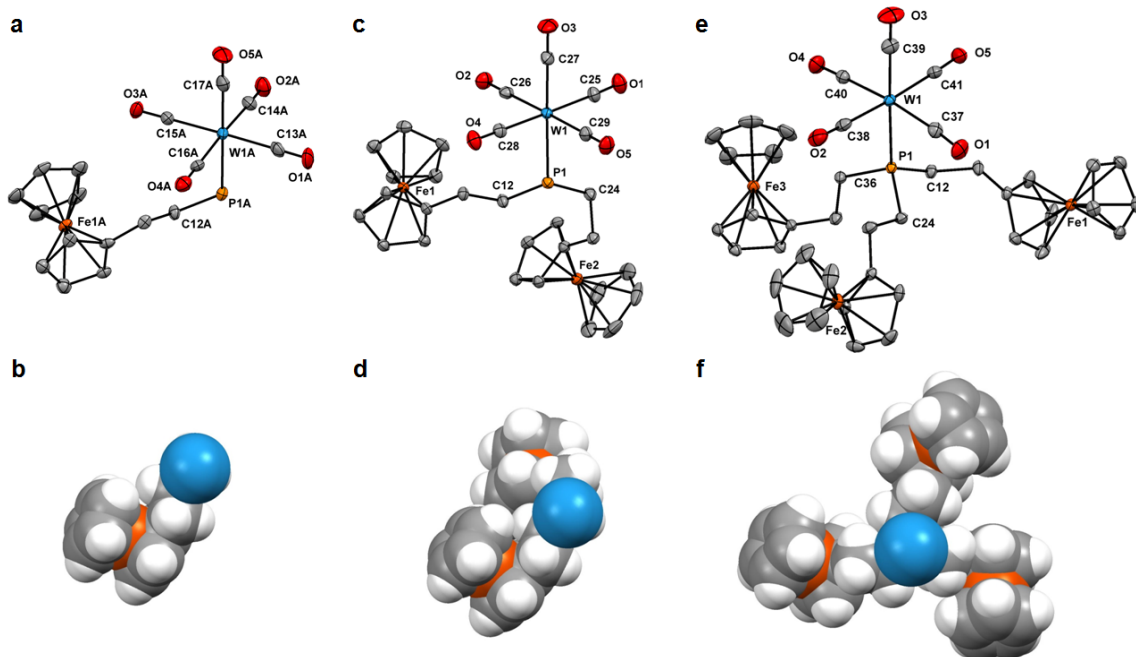


Figure 3.3. Solid-state structures and partial spacefill models of primary, secondary, and tertiary phosphine- $W(CO)_5$ complexes **3.7a** (a,b), **3.7b** (c,d), and **3.7c** (e,f). Thermal displacement ellipsoids are shown at 50% probability and hydrogen atoms have been omitted for clarity. Only one of the two structurally similar molecules from the asymmetric unit for **3.7a** is shown.

Table 3.2. Selected bond lengths (Å) and angles (deg) for complexes **3.5c**, **3.6c**, and **3.7a–c**.

	3.5c	3.6c	3.7a^a	3.7b	3.7c
<i>trans</i> M-C	1.866(4)	2.018(4)	2.012(8)	1.998(4)	2.012(2)
<i>cis</i> M-C (avg)	1.895(4)	2.041(4)	2.044(8)	2.047(5)	2.041(3)
M-C (avg)	1.890(4)	2.036(4)	2.038(8)	2.037(5)	2.035(3)
M-P	2.3747(10)	2.5121(11)	2.492(2)	2.5135(10)	2.5094(8)
<i>trans</i> C-O	1.149(4)	1.141(4)	1.145(8)	1.156(5)	1.141(3)
<i>cis</i> C-O (avg)	1.145(4)	1.144(4)	1.143(8)	1.136(6)	1.138(3)
C-O (avg)	1.145(4)	1.144(4)	1.144(8)	1.140(6)	1.138(3)
P-C (avg)	1.832(3)	1.833(3)	1.842(7)	1.832(4)	1.832(2)
C-P-C (avg)	102.28(15)	102.46(16)	-	104.57(19)	102.62(10)

^aThe asymmetric unit for **3.6a** contains two crystallographically independent molecules. Average values for the two molecules are listed.

3.2.3 FT-IR Spectroscopy

The assignment of the CO stretching frequencies [$\nu(CO)$] of monosubstituted metal carbonyl complexes $[M(CO)_5L]$ and surrounding theory was developed by Orgel and Cotton in the early 1960s.^{61–62} Based on their findings, we expected to observe three unique CO stretches (A_{1cis} , A_{1trans} , E) in the IR spectra of phosphine- $M(CO)_5$ complexes **3.5a–c**, **3.6a–c**, and **3.7a–c** (Figures 3.3, A3.36–A3.44, and Table 3.1). In general, the $\nu(CO)$ A_{1cis}

(2058–2075 cm^{-1}) and $A_{1\text{trans}}$ (1974–1993 cm^{-1}) absorptions for the complexes were shown to decrease when primary phosphine **3.4a** was replaced by secondary phosphine **3.4b** and when secondary phosphine **3.4b** was replaced by tertiary phosphine **3.4c**. This trend provides evidence that the σ donating ability of the phosphine ligands employed in this study, and thus the extent of π backbonding to CO, increased as ethylferrocene substituents were introduced at the ligand. By comparing the CO stretching frequencies [$\nu(\text{CO}) A_{1\text{trans}}$] observed for tertiary phosphine complexes **3.5c**, **3.6c**, and **3.7c** with those recorded for analogous PEt_3 ($\text{Et}_3\text{PCrCO}_5$: 1943 cm^{-1} ; $\text{Et}_3\text{PMoCO}_5$: 1944 cm^{-1} ; Et_3PWCO_5 : 1943 cm^{-1})⁶³ and PPh_3 ($\text{Ph}_3\text{PCrCO}_5$: 1989 cm^{-1} ; $\text{Ph}_3\text{PMoCO}_5$: 1990 cm^{-1} ; Ph_3PWCO_5 : 1981 cm^{-1})⁶² complexes, we conclude that the tertiary phosphine ligand employed in this study is a stronger σ donor than the phenyl-substituted analog, but a weaker σ donor than the ethyl-substituted analog. Variation of the transition metals involved provided further insight into the bonding within the series of complexes. The extent of π backbonding to the CO ligands, based on the values of $\nu(\text{CO}) A_{1\text{trans}}$ and $A_{1\text{cis}}$, followed the trend: $\text{Cr} > \text{W} > \text{Mo}$ and mirrored the trend in electronegativity for the metals involved.

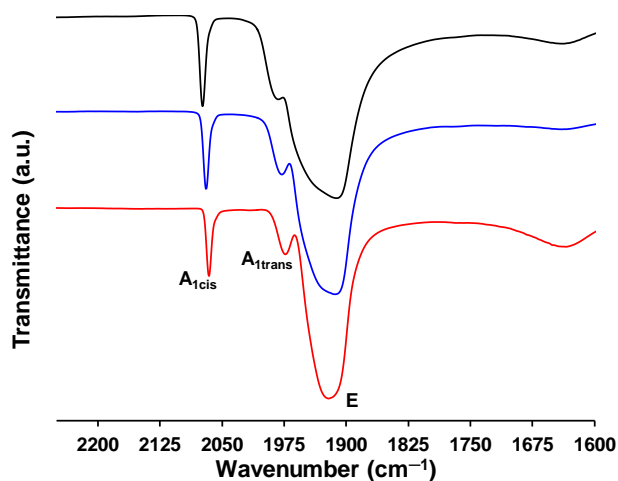


Figure 3.4. FT-IR spectra (CO region) for primary, secondary, and tertiary phosphine- $\text{W}(\text{CO})_5$ complexes **3.7a** (black line), **3.7b** (blue line), and **3.7c** (red line) recorded as thin films on KBr plates.

3.2.4 UV-Vis Absorption Spectroscopy and Cyclic Voltammetry

The UV-Vis absorption spectra and cyclic voltammograms (CVs) recorded for phosphine- $M(\text{CO})_5$ complexes **3.5a–c**, **3.6a–c**, and **3.7a–c** were consistent with the presence of electronically isolated ferrocene groups. Due to the large octahedral field splitting associated with strong field carbonyl ligands, the UV-Vis absorption spectra of phosphine- $M(\text{CO})_5$ complexes **3.5a–c**, **3.6a–c**, and **3.7a–c** in CH_2Cl_2 are comprised primarily of features associated with the ferrocene moieties (Figures 3.4, A3.45–A3.50, and Table 3.1). For each series of primary, secondary, and tertiary complexes the molar absorptivity (ϵ) at the absorption maxima ($\lambda_{\text{max}} = 435\text{--}441\text{ nm}$) associated with the formally forbidden, $d \rightarrow d$ transitions of ferrocene scaled linearly with the number of ferrocene groups present and ranged from 115 to $350\text{ M}^{-1}\text{ cm}^{-1}$.

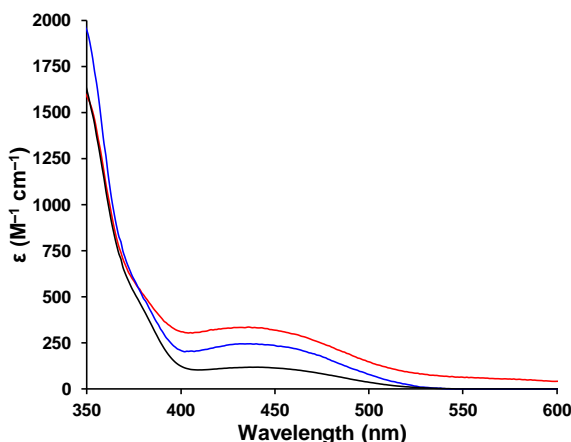


Figure 3.5. UV-Vis spectra of primary, secondary, and tertiary phosphine- $\text{W}(\text{CO})_5$ complexes **3.7a** (black line), **3.7b** (blue line), and **3.7c** (red line) recorded in CH_2Cl_2 .

The electrochemical properties of phosphine- $M(\text{CO})_5$ complexes **3.5a–c**, **3.6a–c**, and **3.7a–c** were studied by collecting CVs of 1 mM degassed 2:1 CH_2Cl_2 : CH_3CN solutions containing 0.1 M $[n\text{-Bu}_4\text{N}][\text{OTf}]$ as supporting electrolyte (Figures 3.5, A3.51–A3.58, and Table 3.1). This solvent/supporting electrolyte combination was required in order to solubilize both the ferrocene and electrogenerated ferrocenium forms of the complexes. When traditional electrolytes (*e.g.*, $[n\text{-Bu}_4\text{N}][\text{PF}_6]$) were employed in non-polar solvents such as CH_2Cl_2 , plating of the ferrocenium forms of the complexes resulted in a loss of diffusion control at the interface of the working electrode. For each complex a single

reversible oxidation wave with peak currents corresponding to one electron per ferrocene unit was observed. Significantly, the small electrochemical feature observed at *ca.* -150 mV vs. Fc/Fc⁺ in the CVs of the free phosphines (Figure 3.6), which has been previously linked to electrode adsorption relating to the phosphorus lone pair,⁵⁰⁻⁵¹ disappears upon metal coordination. Within each series the relatively electron-poor primary phosphine complexes (10 mV) were harder to oxidize than the secondary phosphine complexes which contain an additional ethylferrocene substituent (0 mV). Furthermore, the relatively electron-rich tertiary phosphine complexes were the easiest to oxidize (-5 mV). All of the complexes reported in this study were more difficult to oxidize than free phosphines **3.4a–c** under identical conditions⁵⁰ and there were no observable differences in the CVs when the transition metals were varied.

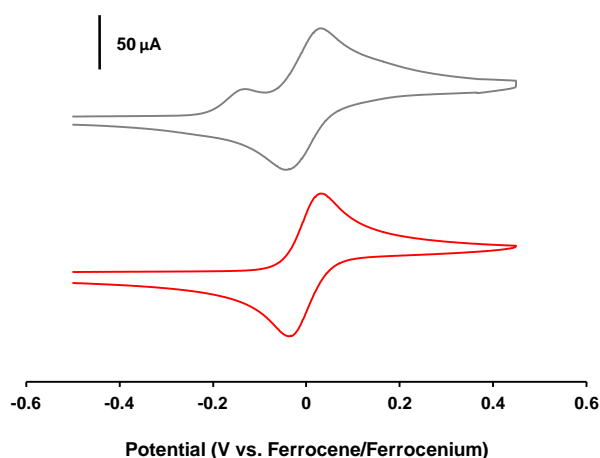


Figure 3.6. Cyclic voltammograms of tertiary phosphine **3.4c** (grey line) and tertiary phosphine- $W(CO)_5$ complex **3.7c** (red line) recorded at 250 mV s⁻¹ for 1 mM degassed $2:1$ $CH_2Cl_2:CH_3CN$ solutions containing 0.1 M $[n-Bu_4N][OTF]$ as supporting electrolyte.

3.3 Conclusions

We have reported the synthesis and characterization of a series of Group 6 $M(CO)_5$ complexes of air-stable, redox-active primary, secondary, and tertiary ethylferrocenephosphines. ³¹P NMR spectroscopic studies confirmed the phosphine units to be intact in the complexes while X-ray crystallography was used to verify the proposed structures of the complexes and demonstrated trends in M-C and M-P bond lengths that followed those of the atomic radii of the metals involved. The X-ray structures of

complexes **3.7a–c** also allowed for a qualitative assessment of the relative size of the ligands, showing that the volume occupied by the phosphine ligands increased dramatically with the sequential introduction of additional ethylferrocene substituents. Cyclic voltammetry studies confirmed that the ferrocene moieties were electronically isolated from the metals in the complexes studied, and UV-Vis absorption spectroscopy revealed properties consistent with monosubstituted ferrocenes. By monitoring the CO stretches of the complexes with IR spectroscopy, we demonstrated that the σ donating ability of the phosphine ligands increased as ethylferrocene substituents were introduced [σ donor strength: $\text{P}(\text{CH}_2\text{CH}_2\text{Fc})_3 > \text{PH}(\text{CH}_2\text{CH}_2\text{Fc})_2 > \text{PH}_2(\text{CH}_2\text{CH}_2\text{Fc})$] and that the σ donating ability of the phosphines were intermediate between those of ethyl and phenyl phosphines [σ donor strength: $\text{PEt}_3 > \text{P}(\text{CH}_2\text{CH}_2\text{Fc})_3 > \text{PPh}_3$].

Based on the fundamental knowledge of the ligand characteristics of this promising class of ethylferrocene phosphine ligands produced as a result of this work, we are hopeful that they will be employed by those working towards novel homogeneous catalysts and redox-active coordination complexes. Our future work in this area will focus on their use in the coordination chemistry of late transition metal chalcogens as we pursue large, redox-active transition metal clusters.

3.4 Experimental section

3.4.1 General Considerations

Reactions and manipulations were carried out under a N_2 atmosphere using standard glove box or Schlenk techniques unless otherwise stated. Solvents were obtained from Caledon Laboratories, dried using an Innovative Technologies Inc. solvent purification system, collected under vacuum, and stored under a N_2 atmosphere over 4 Å molecular sieves. Reagents were purchased from Sigma-Aldrich or Alfa Aesar and used as received, aside from metal carbonyls which were sublimed before use. Primary, secondary, and tertiary phosphines **3.4a–c** were synthesized according to previously reported protocols.⁵⁰⁻⁵¹ UV irradiation experiments were conducted with a medium pressure mercury lamp in a Quartz housing with reaction flasks mounted approximately 10 cm from the lamp. ^1H , $^{13}\text{C}\{^1\text{H}\}$, and ^{31}P NMR spectra were recorded on a 600 MHz (^1H : 599.5 MHz, $^{13}\text{C}\{^1\text{H}\}$: 150.8 MHz,

^{31}P : 242.6 MHz) Varian INOVA instrument. ^1H NMR spectra were referenced to residual CHCl_3 (7.27 ppm) and $^{13}\text{C}\{^1\text{H}\}$ NMR spectra were referenced to CDCl_3 (77.0 ppm). ^{31}P NMR spectra were referenced to PPh_3 , as an internal standard (-6.0 ppm relative to H_3PO_4). Mass spectrometry data were recorded in positive-ion mode using a high resolution Finnigan MAT 8400 spectrometer. UV-Vis spectra were recorded using a Cary 300 Scan instrument. Infrared spectra were recorded using a PerkinElmer Spectrum Two FT-IR spectrometer as thin films on KBr plates. Elemental analyses (C and H) were carried out by Laboratoire d'Analyse Élémentaire de l'Université de Montréal, Montréal, QC, Canada.

3.4.2 Cyclic Voltammetry

CVs were collected using a Bioanalytical Systems Inc. (BASi) Epsilon potentiostat and analyzed using BASi Epsilon software. Typical electrochemical cells consisted of a three-electrode setup including a glassy carbon working electrode, platinum wire counter electrode, and silver wire *pseudo*-reference electrode. Experiments were run at a scan rate of 250 mV s^{-1} in degassed 2:1 $\text{CH}_2\text{Cl}_2:\text{CH}_3\text{CN}$ solutions of the analyte ($\sim 1\text{ mM}$) and supporting electrolyte (0.1 M [*n*-Bu $_4$ N][OTF]) under a blanket of argon. CVs were referenced relative to a decamethylferrocene internal standard (1 mM, -520 mV relative to ferrocene/ferrocenium under identical conditions) and corrected for internal cell resistance using the BASi Epsilon software.

3.4.3 X-ray Crystallography

Single crystals of **3.5c**, **3.7b**, and **3.7c** suitable for X-ray diffraction studies were grown by slow evaporation of concentrated Et_2O solutions. Crystals of **3.6c** were grown by slow diffusion of hexanes into a concentrated THF solution and crystals of **3.7a** were grown by slow diffusion of pentane into a concentrated CHCl_3 solution. The samples were mounted on a MiTeGen polyimide micromount with a small amount of Paratone N oil. X-ray measurements for **3.6c** and **3.7a–c** were made on a Bruker ApexII CCD diffractometer. Measurements for **3.5c** were made on a Nonius KappaCCD ApexII diffractometer. The unit cell dimensions were determined from a symmetry constrained fit of 5928 reflections with $7.30^\circ < 2\theta < 121.36^\circ$ for **3.5c**, 9131 reflections with $5.58^\circ < 2\theta < 46.98^\circ$ for **3.6c**, 9155 reflections with $5.86^\circ < 2\theta < 49.02^\circ$ for **3.7a**, 9530 reflections with $7.48^\circ < 2\theta <$

64.96° for **3.7b**, and 9801 reflections with $5.58^\circ < 2\theta < 65.90^\circ$ for **3.7c**. The data collection strategy was a number of ω and ϕ scans which collected data up to 121.410° (2θ) for **3.5c**, 47.242° (2θ) for **3.6c**, 50.758° (2θ) for **3.7a**, 72.758° (2θ) for **3.7b**, and 72.824° (2θ) for **3.7c**, respectively. The frame integration was performed using SAINT.⁶⁴ The resulting raw data were scaled and absorption corrected using a multi-scan averaging of symmetry equivalent data using SADABS,⁶⁵ except the data for **3.7b** which were processed using TWINABS.⁶⁶ The twin law for **3.7b** was derived from the two orientation matrices using the GNU Octave program⁶⁷ and was determined to be:

$$\begin{array}{ccc} -0.986857 & -0.045843 & -0.154954 \\ -0.045946 & -0.839733 & 0.541052 \\ -0.154923 & 0.541061 & 0.826590 \end{array}$$

which represents a 180° rotation about $[1 \ -1 \ -1]$. The twin fraction refined to a value of 0.44883(63). The structures for **3.5c**, **3.6c**, **3.7a**, **3.7b**, and **3.7c** were solved by using a dual space methodology using the SHELXT program.⁶⁷ All non-hydrogen atoms were obtained from the initial solution. The hydrogen atoms were introduced at idealized positions and were allowed to ride on the parent atom aside for **6c** where they were treated in a mixed fashion. The structural models were fit to the data using full matrix least-squares based on F^2 . The calculated structure factors included corrections for anomalous dispersion from the usual tabulation. The structures were refined using the SHELXL-2014 program from the SHELX suite of crystallographic software.⁶⁸ For complex **3.7a**, the minor component of the rotational disorder associated with the unsubstituted Cp ligands could not be fully resolved. Graphic plots were produced using Mercury (v3.3). Structural data has been deposited in the CCDC (1423358–1423362). For additional collection and refinement details, see Table 3.3.

Table 3.3. Selected X-ray diffraction data collection and refinement details for complexes **3.5c**, **3.6c**, and **3.7a–c**.

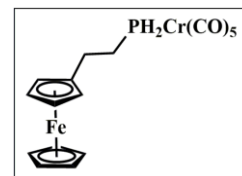
	3.5c	3.6c	3.7a	3.7b	3.7c
Chemical formula	C ₄₁ H ₃₉ CrFe ₃ O ₅ P	C ₄₁ H ₃₉ Fe ₃ MoO ₅ P	C ₁₇ H ₁₅ FeO ₅ PW	C ₂₉ H ₂₇ Fe ₂ O ₅ PW	C ₄₁ H ₃₉ Fe ₃ O ₅ PW
FW (g mol ⁻¹)	862.24	906.18	569.96	782.02	994.09
Temp (K)	110	110	110	110	110
Crystal system	monoclinic	monoclinic	monoclinic	monoclinic	monoclinic
Crystal habit	orange prism	yellow prism	yellow plate	yellow prism	orange prism
Space group	C2/c	C2/c	P2 ₁ /c	P2 ₁ /c	C2/c
λ (Å)	1.54178	0.71073	0.71073	0.71073	0.71073
a (Å)	20.142(3)	20.300(8)	20.416(7)	17.504(2)	20.307(6)
b (Å)	15.184(2)	15.312(5)	7.239(3)	12.9315(14)	15.287(5)
c (Å)	25.001(6)	25.118(10)	25.066(9)	12.708(2)	25.101(7)
α (deg)	90	90	90	90	90
β (deg)	104.581(9)	104.367(10)	97.888(15)	109.260(5)	104.391(13)
γ (deg)	90	90	90	90	90
V (Å ³)	7400(2)	7563(5)	3669(2)	2715.5(6)	7548(4)
Z	8	8	8	4	8
ρ (g cm ⁻³)	1.548	1.592	2.063	1.913	1.750
μ (cm ⁻¹)	12.369	1.538	7.166	5.377	4.254
R ₁ [I > 2σ(I)]	0.0350	0.0312	0.0379	0.0412	0.0381
ωR ₂ [I > 2σ(I)]	0.0772	0.0633	0.0631	0.0971	0.0688
R ₁ (all data)	0.0460	0.0456	0.0615	0.0684	0.0670
ωR ₂ (all data)	0.0818	0.0691	0.0686	0.1115	0.0757
GOF	1.045	1.042	1.063	1.019	1.062

$R_1 = \Sigma(|F_o| - |F_c|) / \Sigma F_o$, $\omega R_2 = [\Sigma(\omega(F_o^2 - F_c^2)^2) / \Sigma(\omega F_o^4)]^{1/2}$; GOF = $[\Sigma(\omega(F_o^2 - F_c^2)^2) / (\text{No. of reflns.} - \text{No. of params.})]^{1/2}$.

3.4.4 Representative Procedure for the Preparation of M(CO)₅ Complexes of **3.5a–c**, **3.6a–c**, **3.7a–c**.

Primary Phosphine Complex **3.5a** (M = Cr)

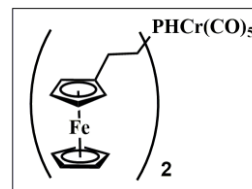
Cr(CO)₆ (0.27 g, 1.2 mmol, 5 equiv.) was dissolved in 15 mL dry THF in a sealed 1 L Pyrex flask and irradiated with UV light for 2.5 h to produce an orange solution containing Cr(CO)₅.THF. The flask was opened inside a glove box and a solution of **3.4a** (0.06 g, 0.24 mmol) in 15 mL dry THF was added dropwise over a 5 min period. The resulting solution was stirred for 2 h before the solvent was removed under reduced pressure. The reaction mixture was then combined with Et₂O (5 mL) and the mixture filtered to remove excess Cr(CO)₆. The filtrate was then mixed with Celite, concentrated *in vacuo*, and transferred to the top of a silica column (1'' × 4''). Using flash column chromatography and a gradient solvent strategy, residual Cr(CO)₆, and **3.5a** were separated. Using 4:1 hexanes: CH₂Cl₂ as eluent, **3.5a** (R_f = 0.36) was isolated from the column before Cr(CO)₆ was eluted using hexanes (R_f = 0.68). The



solution containing **3.5a** was concentrated *in vacuo* to yield an orange solid. Yield = 0.09 g, 84%. M.p.: 74–76 °C. ^1H NMR (CDCl_3): δ 4.28 (d of m, $^1J_{\text{HP}} = 324$ Hz, 2H, PH_2), 4.14 (s, 5H, C_5H_5), 4.13 (s, 2H, $\beta\text{-C}_5\text{H}_4\text{R}$), 4.11 (s, 2H, $\alpha\text{-C}_5\text{H}_4\text{R}$), 2.72 (m, 2H, $\text{C}_5\text{H}_4\text{CH}_2$), 2.04 (m, 2H, CH_2PH_2). $^{13}\text{C}\{^1\text{H}\}$ NMR (CDCl_3): δ 220.3 (d, $^2J_{\text{CP}} = 7$ Hz, *cis*-CO), 216.0 (d, $^2J_{\text{CP}} = 14$ Hz, *trans*-CO), 86.8 (d, $^3J_{\text{CP}} = 10$ Hz, *ipso*- $\text{C}_5\text{H}_4\text{R}$), 68.6 (s, C_5H_5), 68.1 (s, $\alpha\text{-C}_5\text{H}_4\text{R}$), 67.8 (s, $\beta\text{-C}_5\text{H}_4\text{R}$), 30.5 (d, $^2J_{\text{CP}} = 7$ Hz, $\text{C}_5\text{H}_4\text{CH}_2$), 23.4 (d, $^1J_{\text{CP}} = 25$ Hz, CH_2PH_2). ^{31}P NMR (CDCl_3): δ -47.7 (t of m, $^1J_{\text{PH}} = 324$ Hz). FT-IR: 2329 (w), 2067 (m), 1979 (w), 1916 (s), 1105 (w), 1090 (w), 1000 (w), 926 (w), 821 (w), 674 (m), 649 (m) cm^{-1} . UV-Vis (CH_2Cl_2): λ_{max} 437 nm ($\epsilon = 130$ $\text{M}^{-1} \text{cm}^{-1}$). Mass Spec. (EI, +ve mode): exact mass calculated for $[\text{C}_{17}\text{H}_{15}^{52}\text{Cr}^{56}\text{FeO}_5\text{P}]^+$: 437.9412; exact mass found: 437.9418; difference: +1.4 ppm. Anal. Calcd. (%) for $\text{C}_{17}\text{H}_{15}\text{CrFeO}_5\text{P}$: C, 46.60; H, 3.45. Found: C, 46.66; H, 3.47.

Secondary Phosphine Complex **3.5b** (M = Cr)

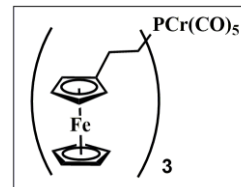
From $\text{Cr}(\text{CO})_6$ (0.24 g, 1.09 mmol, 5 equiv.) and phosphine **3.4b** (0.10 g, 0.218 mmol). Yield = 0.11 g, 80% of orange solid ($R_f = 0.23$). M.p.: 88–90 °C. ^1H NMR (CDCl_3): δ 4.52 (d of m, $^1J_{\text{HP}} = 322$ Hz, 1H, PH), 4.13 (s, 10H, C_5H_5), 4.12 (s, 4H, $\beta\text{-C}_5\text{H}_4\text{R}$), 4.11 (s,



4H, $\alpha\text{-C}_5\text{H}_4\text{R}$), 2.63 (m, 4H, $\text{C}_5\text{H}_4\text{CH}_2$), 2.09 (m, 4H, CH_2PH). $^{13}\text{C}\{^1\text{H}\}$ NMR (CDCl_3): δ 220.7 (d, $^2J_{\text{CP}} = 7$ Hz, *cis*-CO), 216.8 (d, $^2J_{\text{CP}} = 14$ Hz, *trans*-CO), 87.4 (d, $^3J_{\text{CP}} = 13$ Hz, *ipso*- $\text{C}_5\text{H}_4\text{R}$), 68.6 (s, C_5H_5), 67.8 (d, $^4J_{\text{CP}} = 16$ Hz, $\alpha\text{-C}_5\text{H}_4\text{R}$), 67.6 (s, $\beta\text{-C}_5\text{H}_4\text{R}$), 27.4 (d, $^1J_{\text{CP}} = 22$ Hz, CH_2PH), 26.6 (d, $^2J_{\text{CP}} = 2$ Hz, $\text{C}_5\text{H}_4\text{CH}_2$). ^{31}P NMR (CDCl_3): δ 3.5 (d of m, $^1J_{\text{PH}} = 321$ Hz). FT-IR: 2922 (w), 2062 (m), 1979 (w), 1916 (s), 1637 (m), 1105 (w), 999 (w), 817 (w), 676 (w), 651 (w) cm^{-1} . UV-Vis (CH_2Cl_2): λ_{max} 436 nm ($\epsilon = 230$ $\text{M}^{-1} \text{cm}^{-1}$). Mass Spec. (EI, +ve mode): exact mass calculated for $[\text{C}_{29}\text{H}_{27}^{52}\text{Cr}^{56}\text{Fe}_2\text{O}_5\text{P}]^+$: 649.9700; exact mass found: 649.9677; difference: -3.5 ppm. Anal. Calcd. (%) for $\text{C}_{29}\text{H}_{27}\text{CrFe}_2\text{O}_5\text{P}$: C, 53.57; H, 4.19. Found: C, 53.68; H, 4.24.

Tertiary Phosphine Complex **3.5c** (M = Cr)

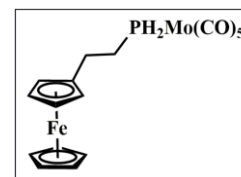
From $\text{Cr}(\text{CO})_6$ (0.25 g, 1.1 mmol, 5 equiv.) and phosphine **3.4c** (0.15 g, 0.22 mmol). Yield = 0.14 g, 78% of orange solid ($R_f = 0.14$). M.p.: 140–142 °C. ^1H NMR (CDCl_3): δ 4.18 (s, 15H, C_5H_5), 4.17 (s, 12H, $\alpha\text{-C}_5\text{H}_4\text{R}$ and $\beta\text{-C}_5\text{H}_4\text{R}$), 2.61 (m, 6H, $\text{C}_5\text{H}_4\text{CH}_2$), 2.08 (m, 6H, CH_2P).



$^{13}\text{C}\{^1\text{H}\}$ NMR (CDCl_3): δ 220.9 (d, $^2J_{\text{CP}} = 7$ Hz, *cis*-CO), 217.5 (d, $^2J_{\text{CP}} = 14$ Hz, *trans*-CO), 87.9 (d, $^3J_{\text{CP}} = 15$ Hz, *ipso*- $\text{C}_5\text{H}_4\text{R}$), 68.6 (s, C_5H_5), 67.7 (s, $\alpha\text{-C}_5\text{H}_4\text{R}$), 67.6 (s, $\beta\text{-C}_5\text{H}_4\text{R}$), 30.6 (d, $^1J_{\text{CP}} = 18$ Hz, CH_2P), 23.8 (s, $\text{C}_5\text{H}_4\text{CH}_2$). ^{31}P NMR (CDCl_3): δ 30.4 (m). FT-IR: 3092 (w), 2928 (w), 2058 (m), 1975 (w), 1922 (s), 1635 (w), 1411 (w), 1106 (w), 1000 (w), 818 (w), 755 (w), 677 (m), 655 (m) cm^{-1} . UV-Vis (CH_2Cl_2): λ_{max} 439 nm ($\epsilon = 350 \text{ M}^{-1} \text{ cm}^{-1}$). Mass Spec. (EI, +ve mode): exact mass calculated for $[\text{C}_{41}\text{H}_{39}^{52}\text{Cr}^{56}\text{Fe}_3\text{O}_5\text{P}]^+$: 861.9988; exact mass found: 861.9966; difference: -2.6 ppm. Anal. Calcd. (%) for $\text{C}_{41}\text{H}_{39}\text{CrFe}_3\text{O}_5\text{P}$: C, 57.11; H, 4.56. Found: C, 57.11; H, 4.62.

Primary Phosphine Complex **3.6a** (M = Mo)

From $\text{Mo}(\text{CO})_6$ (0.32 g, 1.2 mmol, 5 equiv.) and phosphine **3.4a** (0.06 g, 0.24 mmol). Yield = 0.09 g, 79% of orange solid ($R_f = 0.35$). M.p.: 56–58 °C. ^1H NMR (CDCl_3): δ 4.24 (d of m, $^1J_{\text{HP}} = 319$ Hz, 2H, PH_2), 4.13 (s, 5H, C_5H_5), 4.12 (*pseudo-t*, $^3J_{\text{HH}} = 2$ Hz, 2H, $\beta\text{-C}_5\text{H}_4\text{R}$), 4.11

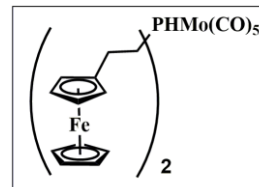


(*pseudo-t*, $^3J_{\text{HH}} = 2$ Hz, 2H, $\alpha\text{-C}_5\text{H}_4\text{R}$), 2.70 (m, 2H, $\text{C}_5\text{H}_4\text{CH}_2$), 2.02 (m, 2H, CH_2PH_2). $^{13}\text{C}\{^1\text{H}\}$ NMR (CDCl_3): δ 208.7 (d, $^2J_{\text{CP}} = 23$ Hz, *cis*-CO), 204.9 (d, $^2J_{\text{CP}} = 9$ Hz, *trans*-CO), 86.9 (d, $^3J_{\text{CP}} = 10$ Hz, *ipso*- $\text{C}_5\text{H}_4\text{R}$), 68.6 (s, C_5H_5), 68.1 (s, $\alpha\text{-C}_5\text{H}_4\text{R}$), 67.7 (s, $\beta\text{-C}_5\text{H}_4\text{R}$), 30.6 (d, $^2J_{\text{CP}} = 5$ Hz, $\text{C}_5\text{H}_4\text{CH}_2$), 23.2 (d, $^1J_{\text{CP}} = 25$ Hz, CH_2PH_2). ^{31}P NMR (CDCl_3): δ -80.4 (t of m, $^1J_{\text{PH}} = 319$ Hz). FT-IR: 3094 (w), 2917 (w), 2345 (w), 2075 (m), 1993 (w), 1922 (s), 1644 (w), 1413 (w), 1445 (w), 1105 (w), 1089 (w), 1000 (w), 925 (w), 670 (w), 607 (m) cm^{-1} . UV-Vis (CH_2Cl_2): λ_{max} 439 nm ($\epsilon = 115 \text{ M}^{-1} \text{ cm}^{-1}$). Mass Spec. (EI, +ve mode): exact mass calculated for $[\text{C}_{17}\text{H}_{15}^{56}\text{Fe}^{92}\text{MoO}_5\text{P}]^+$: 477.9076; exact mass found: 477.9056; difference: -4.2 ppm. Anal. Calcd. (%) for $\text{C}_{17}\text{H}_{15}\text{FeMoO}_5\text{P}$: C, 42.36; H, 3.14. Found: C, 42.45; H, 2.99.

Secondary Phosphine Complex **3.6b** (M = Mo)

From Mo(CO)₆ (0.29 g, 1.1 mmol, 5 equiv.) and phosphine **3.4b** (0.10 g, 0.22 mmol). Yield = 0.12 g, 81% of orange solid (R_f = 0.20).

M.p.: 64–66 °C. ¹H NMR (CDCl₃): δ 4.54 (d of m, ¹J_{HP} = 315 Hz, 1H, PH), 4.13 (s, 10H, C₅H₅), 4.11 (s, 8H, α-C₅H₄R, and β-C₅H₄R),

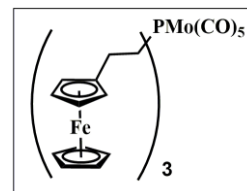


2.63 (m, 4H, C₅H₄CH₂), 2.05 (m, 4H, CH₂PH). ¹³C{¹H} NMR (CDCl₃): δ 209.2 (d, ²J_{CP} = 22 Hz, *cis*-CO), 205.7 (d, ²J_{CP} = 9 Hz, *trans*-CO), 87.5 (d, ³J_{CP} = 14 Hz, *ipso*-C₅H₄R), 68.6 (s, C₅H₅), 67.9 (d, ⁴J_{CP} = 15 Hz, α-C₅H₄R), 67.6 (s, β-C₅H₄R), 27.6 (d, ¹J_{CP} = 22 Hz, CH₂PH), 27.0 (s, C₅H₄CH₂). ³¹P NMR (CDCl₃): δ -22.9 (d of m, ¹J_{PH} = 315 Hz). FT-IR: 3094 (w), 2917 (w), 2071 (m), 1986 (w), 1925 (s), 1640 (w), 1411 (w), 1105 (w), 1000 (w), 819 (w), 608 (m) cm⁻¹. UV-Vis (CH₂Cl₂): λ_{max} 436 nm (ε = 250 M⁻¹ cm⁻¹). Mass Spec. (EI, +ve mode): exact mass calculated for [C₂₉H₂₇⁵⁶Fe₂⁹²MoO₅P]⁺: 689.9367; exact mass found: 689.9335; difference: -4.6 ppm. Anal. Calcd. (%) for C₂₉H₂₇Fe₂MoO₅P: C, 50.18; H, 3.92. Found: C, 50.25; H, 3.95.

Tertiary Phosphine Complex **3.6c** (M = Mo)

From Mo(CO)₆ (0.30 g, 1.1 mmol, 5 equiv.) and phosphine **3.4c** (0.15 g, 0.22 mmol). Yield = 0.16 g, 81% of orange solid (R_f = 0.18). M.p.:

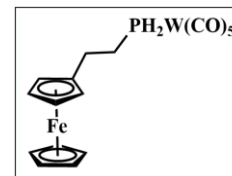
75–77 °C. ¹H NMR (CDCl₃): δ 4.20 (s, 15H, C₅H₅), 4.19 (s, 6H, β-C₅H₄R), 4.18 (s, 6H, α-C₅H₄R), 2.61 (m, 6H, C₅H₄CH₂), 2.06 (m, 6H,



CH₂P). ¹³C{¹H} NMR (CDCl₃): δ 209.4 (d, ²J_{CP} = 21 Hz, *cis*-CO), 206.3 (d, ²J_{CP} = 9 Hz, *trans*-CO), 88.0 (d, ³J_{CP} = 15 Hz, *ipso*-C₅H₄R), 68.6 (s, C₅H₅), 67.8 (s, α-C₅H₄R), 67.6 (s, β-C₅H₄R), 31.1 (d, ¹J_{CP} = 18 Hz, CH₂P), 24.3 (s, C₅H₄CH₂). ³¹P NMR (CDCl₃): δ 12.5 (m). FT-IR: 3094 (w), 2928 (w), 2067 (m), 1981 (w), 1929 (s), 1634 (w), 1411 (w), 1106 (w), 1000 (w), 818 (w), 610 (m) cm⁻¹. UV-Vis (CH₂Cl₂): λ_{max} 435 nm (ε = 350 M⁻¹ cm⁻¹). Mass Spec. (EI, +ve mode): exact mass calculated for [C₄₁H₃₉⁵⁶Fe₃⁹⁸MoO₅P]⁺: 907.9637; exact mass found: 907.9595; difference: -4.6 ppm. Anal. Calcd. (%) for C₄₁H₃₉Fe₃MoO₅P: C, 54.34; H, 4.34. Found: C, 54.40; H, 4.38.

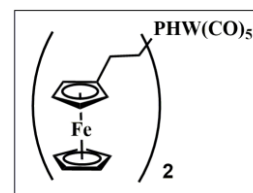
Primary Phosphine Complex **3.7a** (M = W)

From $W(CO)_6$ (0.43 g, 1.2 mmol, 5 equiv.) and phosphine **3.4a** (0.06 g, 0.24 mmol). Yield = 0.12 g, 89% of orange solid ($R_f = 0.35$). M.p.: 74–76 °C. 1H NMR ($CDCl_3$): δ 4.55 (d of m, $^1J_{HP} = 332$ Hz, 2H, PH_2), 4.14 (s, 5H, C_5H_5), 4.13 (*pseudo-t*, $^3J_{HH} = 2$ Hz, 2H, $\beta-C_5H_4R$), 4.11 (*pseudo-t*, $^3J_{HH} = 2$ Hz, 2H, $\alpha-C_5H_4R$), 2.70 (m, 2H, $C_5H_4CH_2$), 2.12 (m, 2H, CH_2PH_2). $^{13}C\{^1H\}$ NMR ($CDCl_3$): δ 198.1 (d, $^2J_{CP} = 22$ Hz, *cis*-CO), 195.5 (d, $^2J_{CP} = 7$ Hz, *trans*-CO), 86.6 (d, $^3J_{CP} = 12$ Hz, *ipso*- C_5H_4R), 68.7 (s, C_5H_5), 68.1 (s, $\alpha-C_5H_4R$), 67.8 (s, $\beta-C_5H_4R$), 30.5 (d, $^2J_{CP} = 5$ Hz, $C_5H_4CH_2$), 23.9 (d, $^1J_{CP} = 28$ Hz, CH_2PH_2). ^{31}P NMR ($CDCl_3$): δ -101.9 (t of m, 86%, $^1J_{PH} = 333$ Hz), -101.9 (t of d of m, 14%, $^1J_{PH} = 333$ Hz, $^1J_{PW} = 217$ Hz). FT-IR: 3092 (w), 2917 (w), 2345 (w), 2074 (m), 1976 (w), 1912 (s), 1638 (w), 1439 (w), 1411 (w), 1318 (w), 1105 (w), 1089 (w), 1000 (w), 926 (w), 884 (w), 821 (w), 676 (w) cm^{-1} . UV-Vis (CH_2Cl_2): λ_{max} 441 nm ($\epsilon = 120 M^{-1} cm^{-1}$). Mass Spec. (EI, +ve mode): exact mass calculated for $[C_{17}H_{15}^{56}FeO_5P^{184}W]^+$: 569.9516; exact mass found: 569.9517; difference: +0.2 ppm. Anal. Calcd. (%) for $C_{17}H_{15}FeO_5PW$: C, 35.82; H, 2.65. Found: C, 36.06; H, 2.55.



Secondary Phosphine Complex **3.7b** (M = W)

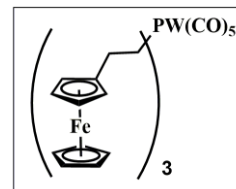
From $W(CO)_6$ (0.38 g, 1.1 mmol, 5 equiv.) and phosphine **3.4b** (0.10 g, 0.22 mmol). Yield = 0.15 g, 90% of orange solid ($R_f = 0.22$). M.p.: 84–86 °C. 1H NMR ($CDCl_3$): δ 4.85 (d of m, $^1J_{HP} = 327$ Hz, 1H, PH), 4.14 (s, 10H, C_5H_5), 4.12 (*pseudo-t*, $^3J_{HH} = 2$ Hz, 8H, $\alpha-C_5H_4R$ and $\beta-C_5H_4R$), 2.62 (m, 4H, $C_5H_4CH_2$), 2.16 (m, 4H, CH_2PH). $^{13}C\{^1H\}$ NMR ($CDCl_3$): δ 198.7 (d, $^2J_{CP} = 21$ Hz, *cis*-CO), 196.4 (d, $^2J_{CP} = 7$ Hz, *trans*-CO), 87.3 (d, $^3J_{CP} = 14$ Hz, *ipso*- C_5H_4R), 68.7 (s, C_5H_5), 67.8 (d, $^4J_{CP} = 17$ Hz, $\alpha-C_5H_4R$), 67.7 (s, $\beta-C_5H_4R$), 28.1 (d, $^1J_{CP} = 25$ Hz, CH_2PH), 27.1 (s, $C_5H_4CH_2$). ^{31}P NMR ($CDCl_3$): δ -43.6 (d of m, 86%, $^1J_{PH} = 328$ Hz), -43.6 (d of d of m, 14%, $^1J_{PH} = 328$ Hz, $^1J_{PW} = 225$ Hz). FT-IR: 3092 (w), 2917 (w), 2070 (m), 1978 (w), 1914 (s), 1640 (w), 1411 (w), 1219 (w), 1105 (w), 1000 (w), 820 (w), 772 (s), 599 (w) cm^{-1} . UV-Vis (CH_2Cl_2): λ_{max} 437 nm ($\epsilon = 245 M^{-1} cm^{-1}$). Mass Spec. (EI, +ve mode): exact mass calculated for $[C_{29}H_{27}^{56}Fe_2O_5P^{184}W]^+$: 781.9804; exact mass found:



781.9791; difference: -1.7 ppm. Anal. Calcd. (%) for $C_{29}H_{27}Fe_2O_5PW$: C, 44.54; H, 3.48. Found: C, 44.70; H, 3.44.

Tertiary Phosphine Complex **3.7c** (M = W)

From $W(CO)_6$ (0.39 g, 1.1 mmol, 5 equiv.) and phosphine **3.4c** (0.15 g, 0.22 mmol). Yield = 0.19 g, 87% of orange solid ($R_f = 0.18$). M.p.: 143–145 °C. 1H NMR ($CDCl_3$): δ 4.15 (s, 15H, C_5H_5), 4.14 (s, 12H, α - C_5H_4R and β - C_5H_4R), 2.56 (m, 6H, $C_5H_4CH_2$), 2.11 (m, 6H, CH_2P).



$^{13}C\{^1H\}$ NMR ($CDCl_3$): δ 198.8 (d, $^2J_{CP} = 21$ Hz, *cis*-CO), 197.2 (d, $^2J_{CP} = 8$ Hz, *trans*-CO), 87.8 (d, $^3J_{CP} = 15$ Hz, *ipso*- C_5H_4R), 68.6 (s, C_5H_5), 67.8 (s, α - C_5H_4R), 67.6 (s, β - C_5H_4R), 31.6 (d, $^1J_{CP} = 22$ Hz, CH_2P), 24.6 (s, $C_5H_4CH_2$). ^{31}P NMR ($CDCl_3$): δ -6.8 (m, 86%), -6.8 (d of m, 14%, $^1J_{PW} = 233$ Hz). FT-IR: 3090 (w), 2924 (w), 2066 (m), 1974 (w), 1922 (s), 1635 (w), 1411 (w), 1415 (w), 1442 (w), 1321 (w), 1230 (w), 1105 (w), 1000 (w), 820 (w), 754 (w), 601 (w) cm^{-1} . UV-Vis (CH_2Cl_2): λ_{max} 436 nm ($\epsilon = 335 M^{-1} cm^{-1}$). Mass Spec. (EI, +ve mode): exact mass calculated for $[C_{41}H_{39}^{56}Fe_3O_5P^{184}W]^+$: 994.0093; exact mass found: 994.0095; difference: +0.2 ppm. Anal. Calcd. (%) for $C_{41}H_{39}Fe_3O_5PW$: C, 49.54; H, 3.95. Found: C, 50.07; H, 4.03.

3.5 References

1. Ghent, B. L.; Sites, L. A.; Rheingold, A. L.; Nataro, C. *Organometallics* **2005**, *24*, 4788–4792.
2. Kalio, R.; Lönnecke, P.; Hey-Hawkins, E. *J. Organomet. Chem.* **2008**, *693*, 590–600.
3. Chen, C.-G.; Hou, X.-L.; Pu, L. *Org. Lett.* **2009**, *11*, 2073–2075.
4. Zirakzadeh, A.; Schuecker, R.; Gorgas, N.; Mereiter, K.; Spindler, F.; Weissensteiner, W. *Organometallics* **2012**, *31*, 4241–4250.
5. Khadka, C. B.; Najafabadi, B. K.; Hesari, M.; Workentin, M. S.; Corrigan, J. F. *Inorg. Chem.* **2013**, *52*, 6798–6805.
6. Cowie, B. E.; Tsao, F. A.; Emslie, D. J. H. *Angew. Chem. Int. Ed.* **2015**, *54*, 2165–2169.
7. Erre, G.; Enthaler, S.; Junge, K.; Gladiali, S.; Beller, M. *Coord. Chem. Rev.* **2008**, *252*, 471–491.
8. Shaughnessy, K. H. *Chem. Rev.* **2009**, *109*, 643–710.
9. *Phosphorus(III) ligands in homogeneous catalysis: Design and synthesis*. Wiley-Blackwell: Oxford, 2012.
10. Chikkali, S. H.; van der Vlugt, J. I.; Reek, J. N. H. *Coord. Chem. Rev.* **2014**, *262*, 1–15.
11. Nell, B. P.; Tyler, D. R. *Coord. Chem. Rev.* **2014**, *279*, 23–42.
12. Annen, S. P.; Bambagioni, V.; Bevilacqua, M.; Filippi, J.; Marchionni, A.; Oberhauser, W.; Schönberg, H.; Vizza, F.; Bianchini, C.; Grützmacher, H. *Angew. Chem. Int. Ed.* **2010**, *49*, 7229–7233.
13. Anderson, J. S.; Rittle, J.; Peters, J. C. *Nature* **2013**, *501*, 84–87.

14. Kang, P.; Zhang, S.; Meyer, T. J.; Brookhart, M. *Angew. Chem. Int. Ed.* **2014**, *53*, 8709–8713.
15. Horak, K. T.; Velian, A.; Day, M. W.; Agapie, T. *Chem. Commun.* **2014**, *50*, 4427–4429.
16. Johnson, B. J.; Lindeman, S. V.; Mankad, N. P. *Inorg. Chem.* **2014**, *53*, 10611–10619.
17. Tinnermann, H.; Wille, C.; Alcarazo, M. *Angew. Chem. Int. Ed.* **2014**, *53*, 8732–8736.
18. Yan, X.; Cook, T. R.; Wang, P.; Huang, F.; Stang, P. J. *Nat. Chem.* **2015**, *7*, 342–348.
19. Zhao, D.; Neubauer, T. M.; Feringa, B. L. *Nat. Commun.* **2015**, *6*.
20. Hazeland, E. L.; Chapman, A. M.; Pringle, P. G.; Sparkes, H. A. *Chem. Commun.* **2015**, *51*, 10206–10209.
21. Tolman, C. A. *Chem. Rev.* **1977**, *77*, 313–348.
22. Clarke, M. L.; Frew, J. J. R., Ligand electronic effects in homogeneous catalysis using transition metal complexes of phosphine ligands. In *Organometallic Chemistry: Volume 35*, Fairlamb, I. J. S.; Lynam, J. M., Eds. The Royal Society of Chemistry: Cambridge, 2009; pp 19–46.
23. Staubitz, A.; Soto, A. P.; Manners, I. *Angew. Chem. Int. Ed.* **2008**, *47*, 6212–6215.
24. Piedra-Aroni, E.; Ladavière, C.; Amgoune, A.; Bourissou, D. *J. Am. Chem. Soc.* **2013**, *135*, 13306–13309.
25. Nakamura, A.; Anselment, T. M. J.; Claverie, J.; Goodall, B.; Jordan, R. F.; Mecking, S.; Rieger, B.; Sen, A.; van Leeuwen, P. W. N. M.; Nozaki, K. *Acc. Chem. Res.* **2013**, *46*, 1438–1449.

26. Lee, H.-K.; Bang, K.-T.; Hess, A.; Grubbs, R. H.; Choi, T.-L. *J. Am. Chem. Soc.* **2015**, *137*, 9262–9265.
27. Bultz, E.; Ouchi, M.; Nishizawa, K.; Cunningham, M. F.; Sawamoto, M. *ACS Macro Lett.* **2015**, *4*, 628–631.
28. Dobereiner, G. E.; Yuan, J.; Schrock, R. R.; Goldman, A. S.; Hackenberg, J. D. *J. Am. Chem. Soc.* **2013**, *135*, 12572–12575.
29. Cheng, C.; Hartwig, J. F. *J. Am. Chem. Soc.* **2014**, *136*, 12064–12072.
30. Borzenko, A.; Rotta-Loria, N. L.; MacQueen, P. M.; Lavoie, C. M.; McDonald, R.; Stradiotto, M. *Angew. Chem. Int. Ed.* **2015**, *54*, 3773–3777.
31. Tollefson, E. J.; Hanna, L. E.; Jarvo, E. R. *Acc. Chem. Res.* **2015**, *48*, 2344–2353.
32. Yang, Y.; Shi, S.-L.; Niu, D.; Liu, P.; Buchwald, S. L. *Science* **2015**, *349*, 62–66.
33. Tymonko, S. A.; Smith, R. C.; Ambrosi, A.; Ober, M. H.; Wang, H.; Denmark, S. E. *J. Am. Chem. Soc.* **2015**, *137*, 6200–6218.
34. Friedfeld, M. R.; Margulieux, G. W.; Schaefer, B. A.; Chirik, P. J. *J. Am. Chem. Soc.* **2014**, *136*, 13178–13181.
35. Zell, T.; Ben-David, Y.; Milstein, D. *Angew. Chem. Int. Ed.* **2014**, *53*, 4685–4689.
36. Zirakzadeh, A.; Groß, M. A.; Wang, Y.; Mereiter, K.; Weissensteiner, W. *Organometallics* **2014**, *33*, 1945–1952.
37. Guo, C.; Sun, D.-W.; Yang, S.; Mao, S.-J.; Xu, X.-H.; Zhu, S.-F.; Zhou, Q.-L. *J. Am. Chem. Soc.* **2015**, *137*, 90–93.
38. Wesselbaum, S.; Moha, V.; Meuresch, M.; Brosinski, S.; Thenert, K. M.; Kothe, J.; vom Stein, T.; Englert, U.; Hölscher, M.; Klankermayer, J.; Leitner, W. *Chem. Sci.* **2015**, *6*, 693–704.
39. Zuo, W.; Morris, R. H. *Nat. Protoc.* **2015**, *10*, 241–257.

40. Brynda, M. *Coord. Chem. Rev.* **2005**, *249*, 2013–2034.
41. Fleming, J. T.; Higham, L. J. *Coord. Chem. Rev.* **2015**, *297–298*, 127–145.
42. Ramakrishnan, G.; Jouaiti, A.; Geoffroy, M.; Bernardinelli, G. *J. Phys. Chem.* **1996**, *100*, 10861–10868.
43. Prabhu, K. R.; Pillarsetty, N.; Gali, H.; Katti, K. V. *J. Am. Chem. Soc.* **2000**, *122*, 1554–1555.
44. Henderson, W.; Alley, S. R. *J. Organomet. Chem.* **2002**, *656*, 120–128.
45. Hiney, R. M.; Higham, L. J.; Müller-Bunz, H.; Gilheany, D. G. *Angew. Chem. Int. Ed.* **2006**, *45*, 7248–7251.
46. Barder, T. E.; Buchwald, S. L. *J. Am. Chem. Soc.* **2007**, *129*, 5096–5101.
47. Stewart, B.; Harriman, A.; Higham, L. J. *Organometallics* **2011**, *30*, 5338–5343.
48. Davies, L. H.; Stewart, B.; Harrington, R. W.; Clegg, W.; Higham, L. J. *Angew. Chem. Int. Ed.* **2012**, *51*, 4921–4924.
49. Asamizu, T.; Henderson, W.; Nicholson, B. K.; Hey-Hawkins, E. *Inorg. Chim. Acta* **2014**, *414*, 181–190.
50. Rabiee Kenaree, A.; Berven, B. M.; Ragogna, P. J.; Gilroy, J. B. *Chem. Commun.* **2014**, *50*, 10714–10717.
51. Rabiee Kenaree, A.; Cuthbert, T. J.; Barbon, S. M.; Boyle, P. D.; Gillies, E. R.; Ragogna, P. J.; Gilroy, J. B. *Organometallics* **2015**, *34*, 4272–4280.
52. Guterman, R.; Rabiee Kenaree, A.; Gilroy, J. B.; Gillies, E. R.; Ragogna, P. J. *Chem. Mater.* **2015**, *27*, 1412–1419.
53. Guterman, R.; Gillies, E. R.; Ragogna, P. J. *Dalton Trans.* **2015**, *44*, 15664–15670.
54. Labande, A.; Ruiz, J.; Astruc, D. *J. Am. Chem. Soc.* **2002**, *124*, 1782–1789.

55. Stiles, R. L.; Balasubramanian, R.; Feldberg, S. W.; Murray, R. W. *J. Am. Chem. Soc.* **2008**, *130*, 1856–1865.
56. Mahmoud, K. A.; Hrapovic, S.; Luong, J. H. T. *ACS Nano* **2008**, *2*, 1051–1057.
57. Mulrooney, R. C.; Singh, N.; Kaur, N.; Callan, J. F. *Chem. Commun.* **2009**, 686–688.
58. Aminur Rahman, M.; Ik Son, J.; Won, M.-S.; Shim, Y.-B. *Anal. Chem.* **2009**, *81*, 6604–6611.
59. Liu, Y.; Khalili Najafabadi, B.; Azizpoor Fard, M.; Corrigan, J. F. *Angew. Chem. Int. Ed.* **2015**, *54*, 4832–4835.
60. Grim, S. O.; McAllister, P. R.; Singer, R. M. *Chem. Commun.* **1969**, 38–39.
61. Orgel, L. E. *Inorg. Chem.* **1962**, *1*, 25–29.
62. Cotton, F. A.; Kraihanzel, C. S. *J. Am. Chem. Soc.* **1962**, *84*, 4432–4438.
63. Dalton, J.; Paul, I.; Smith, J. G.; Stone, F. G. A. *J. Chem. Soc. A* **1968**, 1195–1199.
64. Bruker-AXS, SAINT version 2013.8, **2013**, Bruker-AXS, Madison, WI 53711, USA.
65. Bruker-AXS, SADABS version 2012.1, **2012**, Bruker-AXS, Madison, WI 53711, USA.
66. Bruker-AXS, TWINABS version 2012.1, **2012**, Bruker-AXS, Madison, WI 53711, USA.
67. Sheldrick, G. *Acta Crystallogr.* **2015**, *A71*, 3–8.
68. Sheldrick, G. *Acta Crystallogr.* **2008**, *A64*, 112–122.

Chapter 4

4 Synthesis and Characterization of Metal-Rich Phosphonium Polyelectrolytes and Their Use as Precursors to Nanomaterials

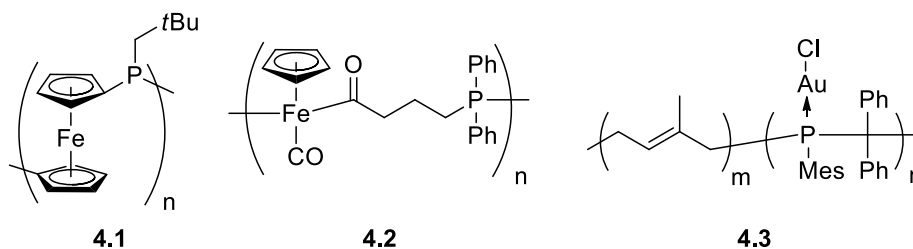
Adapted from:

- 1) Rabiee Kenaree, A.; Gilroy, J.B.* Synthesis and Characterization of Metal-Rich Phosphonium Polyelectrolytes and Their Use as Precursors to Nanomaterials. *Dalton Trans.* **2016**, *45*, 18229–18240.
- 2) Rabiee Kenaree, A.; Berven, B.M., Ragona, P.J.*; Gilroy, J.B.* Highly-Metallized Phosphonium Polyelectrolytes. *Chem. Commun.* **2014**, *50*, 10714–10717.

4.1 Introduction

Metallopolymers, which differ from coordination polymers that have dynamic structures, are an intriguing class of materials that benefit from the processability of macromolecules and functional properties of transition metals.¹⁻⁷ They have been utilized as redox-active, catalytic, emissive, biomedical, and magnetic materials⁸⁻²¹ and successfully prepared from different precursors. So far, several different synthetic strategies that exploit the chemistry of phosphorous have been introduced.²²⁻²⁶ For example, main-chain poly(ferrocenylphosphine)s (*e.g.*, **4.1**) have been produced by the ring-opening polymerization of strained [1]phosphaferrocenophanes,²⁷⁻³⁰ while a unique migration-insertion polymerization mechanism has been used to produce poly(cyclopentadienylcarbonyldiphenyl-phosphinobutanoyliron)s (*e.g.*, **4.2**).^{17, 31} Block copolymers incorporating a side-chain metallopolymer block based on poly(phosphaalkene)s (*e.g.*, **4.3**) have been realized through a sequential anionic polymerization / metal-coordination strategy before they were self-assembled into micelles with a gold core.³² Although advances towards phosphorus-containing metallopolymers

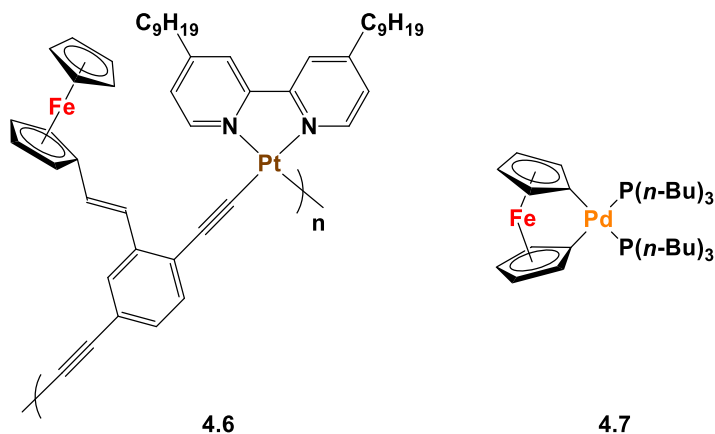
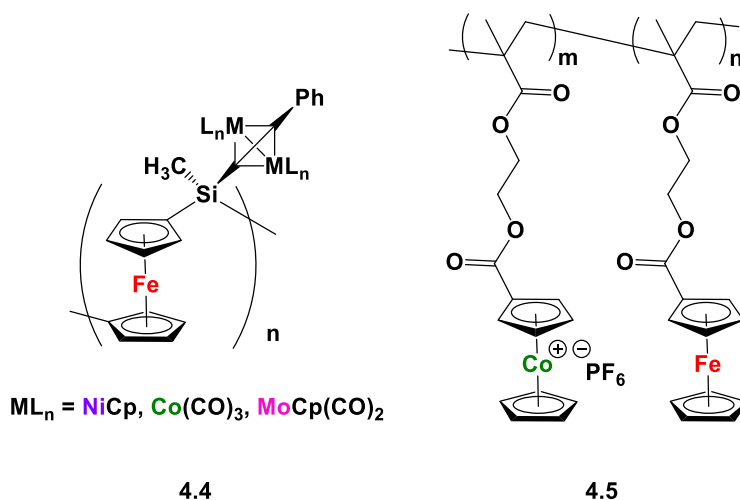
have been impressive, examples possessing more than one metal per polymer repeating unit remain elusive.



In addition to phosphorous-containing metallopolymers, examples of heterobimetallic polymers, which can take advantage of the properties of more than one type of metal, are uncommon. There are several strategies for the incorporation of more than one type of transition metal into polymer structures. For example, post-polymerization functionalization of metallopolymers can be employed for the addition of transition metals to the repeating unit of the polymer backbone.³³⁻³⁶ However, it can be a challenge to completely functionalize all of the repeating units in the polymer backbone. Manners and co-workers have used their well-established ring-opening polymerization methodology for the synthesis of polyferrocenylsilanes (PFS) to prepare monometallic acetylide-substituted PFSs, which were further reacted with $\text{Co}_2(\text{CO})_8$, $[\text{MoCp}(\text{CO})_2]_2$, and $[\text{NiCp}(\text{CO})_2]_2$ to produce heterobimetallic polymers **4.4**.³³⁻³⁵ They also showed that reactive ion etching (RIE),³³ electron-beam lithography,³⁴ and pyrolysis³⁵ can be used to convert the heterobimetallic polymers produced to the corresponding bimetallic alloy nanoparticles (NPs).

Copolymerization of more than one type of metal-containing monomer is another strategy that can yield heterobimetallic polymers, where the metal ratio can be adjusted by controlling the ratio of the repeating units.³⁷⁻⁴² Following this strategy and starting with two methacrylate-based ferrocene- and cobaltocenium-containing monomers, the Tang group recently performed a reversible addition-fragmentation chain-transfer (RAFT) polymerization and successfully synthesized heterobimetallic diblock copolymers containing cobaltocenium and ferrocene units **4.5**. By pyrolysis of the heterobimetallic copolymer under N_2/H_2 , magnetic nanomaterials comprised of $\text{Fe}_x\text{Co}_y\text{P}$ (where $x + y = 2$) were realized.⁴¹ Starting with a monomer that has more than one metal within its structure

is a strategy that affords heterobimetallic polymers with transition metal content equal to that of the monomer.⁴³⁻⁵⁰ For instance, Wong and co-workers synthesized an iron- and platinum-containing heterobimetallic polymer **4.6** and used nanoimprint lithography to generate nanopatterns. RIE converted the polymer to nanopatterned magnetic Fe/Pt NPs.⁴⁵ The Manners group has also reported the synthesis of a palladium-based [1]ferrocenophane **4.7** that was thermolized at 190 °C under vacuum to directly yield Fe/Pd alloy NPs, presumably via a heterobimetallic polymer.⁴⁷



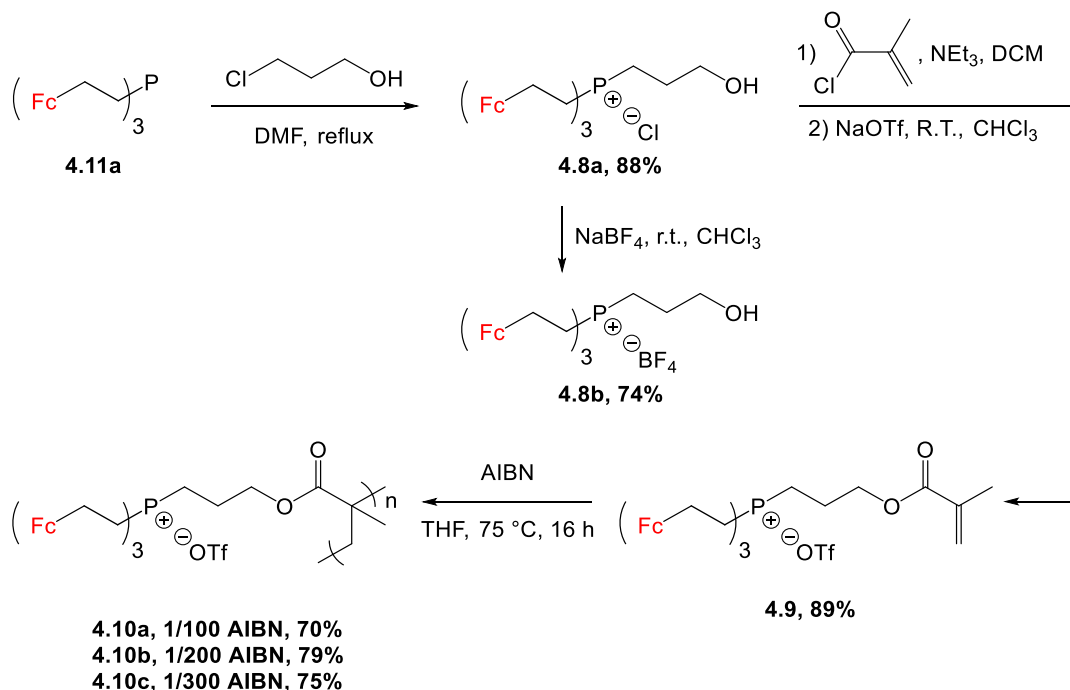
Bimetallic particles are an interesting subclass of nanomaterials that benefit from their high surface area.⁵¹⁻⁵⁹ For example, Fe/Ru heterobimetallic particles are industrially valuable materials due to their catalytic role in processes including hydrogenation,⁶⁰⁻⁶³ the water-gas shift reaction,⁶⁴ and the Fischer-Tropsch synthesis.⁶⁵⁻⁶⁶ They are conventionally prepared by techniques such as thermolysis and co-reduction of metal ions.⁶⁷⁻⁶⁸ Although,

metallopolymers can serve as precursors to metal-containing nanomaterials,⁶⁹ few reports of the generation of bimetallic nanomaterials from heterobimetallic polymers have been made. To the best of our knowledge, Fe/Ru nanomaterials have not been prepared via the degradation of heterobimetallic polymers. Herein, we describe our strategy for the synthesis of highly-metallized phosphonium polyelectrolytes bearing three metallocenes (Fe/Ru: 3/0, 2/1, 1/2, 0/3) per repeating unit, as well as conversion of these polyelectrolytes to novel nanomaterials by conducting pyrolysis experiments.

4.2 Results

4.2.1 Synthesis and Characterization of Methacrylate-Based Phosphonium Polyelectrolytes

Tertiary phosphine **4.11a** was used to produce the target phosphonium polyelectrolytes (Scheme 4.1). The quaternization of tertiary phosphine **4.11a** via reaction with 3-chloro-1-propanol led to the formation of the ferrocene-substituted phosphonium chloride salt **4.8a** as a fine yellow powder in 88% yield (Figures A4.1–A4.3).



Scheme 4.1. Synthesis of methacrylate-based phosphonium polyelectrolytes.

Ion exchange, using NaBF_4 , yielded microcrystalline phosphonium tetrafluoroborate salt **4.8b** (Figures A4.4–A4.7). The solid-state structure of **4.8b** confirmed the proposed structure and the nearly tetrahedral geometry at phosphorus (Figure 4.1, Table 4.1).

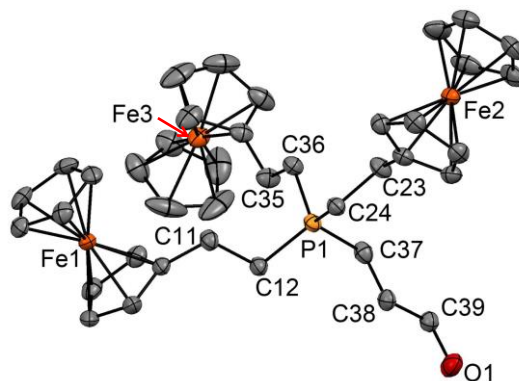


Figure 4.1. Solid-state structure of phosphonium alcohol **4.8b**. Thermal displacement ellipsoids shown at 50% probability level. Hydrogen atoms and BF_4^- counter anion have been removed for clarity. Selected bond lengths (\AA) and angles ($^\circ$): P1-C12 1.806(4), P1-C24 1.809(4), P1-C36 1.802(4), P1-C37 1.808(4), C11-C12 1.550(6), C23-C24 1.545(5), C35-C36 1.548(6), C37-C38 1.522(6); C12-P1-C24 110.9(2), C12-P1-C36 109.1(2), C12-P1-C37 109.4(2), C24-P1-C36 110.2(2), C24-P1-C37 109.6(2), C36-P1-C37 107.6(2).

Polymerizable phosphonium triflate salt **4.9** was synthesized in two steps in 89% yield (Scheme 4.1, Figures 4.2 and A4.8–A4.10). Esterification of the alcohol group in **4.8a** was accomplished by reacting it with methacryloyl chloride in the presence of NEt_3 under anhydrous conditions. The chloride counter anions were exchanged for triflate anions to overcome the tendency of the phosphonium chloride salts encountered during this study to decompose via an unidentified decomposition pathway in solution when exposed to air. Phosphonium triflate **4.9** is air- and moisture-stable and has significantly enhanced solubility in organic solvents compared to its chloride analog. The latter trait is highly desirable for further polymerization chemistry where poor solubility can be problematic.

Inspired by the work of Endo,⁷⁰⁻⁷³ Gin,⁷⁴ Long,⁷⁵⁻⁷⁷ and others,⁷⁸⁻⁷⁹ polyelectrolytes **4.10a–c** were produced via a free-radical polymerization mechanism using AIBN as a thermally-activated initiator. Three polymerization reactions were conducted by first combining monomer **4.9** and 0.01 (1.0 g monomer mL^{-1}), 0.005 (0.75 g monomer mL^{-1}), and 0.0033 (0.50 g monomer mL^{-1}) molar equivalents of AIBN in THF. Each solution was

subjected to three freeze-pump-thaw cycles, before heating at 75 °C for 17, 25, and 32 h, respectively. Polyelectrolytes **4.10a–c** were isolated in 70%, 79%, and 75% yields after purification by successive precipitation of CH₂Cl₂ solutions into benzene and pentane (Figures 4.2 and A4.11–A4.18, Table 4.2).

Table 4.1. Characterization data for compounds **4.9** and **4.10a–c**.

Compound	³¹ P NMR (δ)	ε, 434 nm (M ⁻¹ cm ⁻¹)	E _{1/2, Fe} (mV)	M _n (g mol ⁻¹)	DP _n	D
4.9	31.9	294	5	-	-	-
4.10a	31.8	322	0	118,200	46	2.74
4.10b	31.8	310	0	79,000	34	2.44
4.10c	31.9	323	0	105,700	48	2.34

¹H NMR spectroscopy confirmed the conversion of monomer **4.9** to polyelectrolytes **4.10a–c** as the signals attributed to the alkene functionality disappeared (δ 6.16 and 5.66) and new signals assigned to the saturated hydrocarbon backbone appeared (δ 3.00–0.50) in the spectrum of polyelectrolyte **4.10b** (Figure 4.2). The ¹H NMR spectra of **4.10a–c** were very broad, further supporting the proposed polyelectrolyte structures.

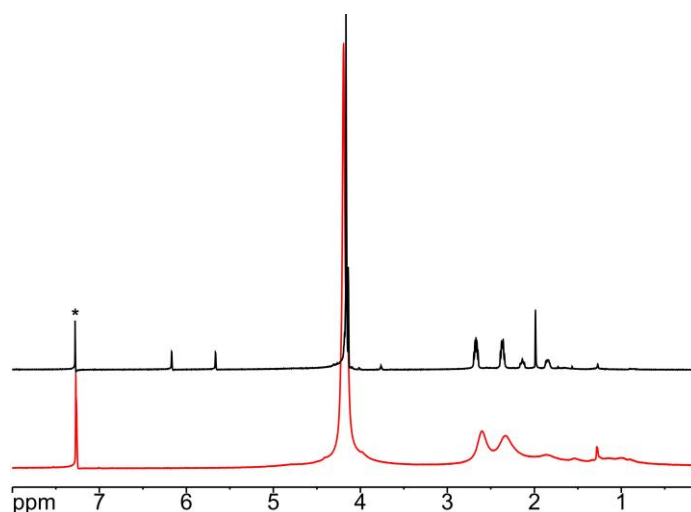


Figure 4.2. ¹H NMR spectra of monomer **4.9** (black) and polyelectrolyte **4.10b** (red) in CDCl₃. The asterisk denotes residual CHCl₃ signals.

Gel permeation chromatography experiments were used to study the molecular weight distributions of polyelectrolytes **4.10a–c**. To overcome common issues regarding strong interactions between polyelectrolytes and GPC columns and by adapting a methodology developed by the Matyjaszewski group,⁸⁰ a 60 °C DMF solution containing 0.02 M [n-Bu₄N][OTf] was used as an eluent in tandem with Teflon-treated size-exclusion columns. These studies confirmed the high molecular weight nature of **4.10a–c** (M_w = 79,000–

118,200 g mol⁻¹, $\bar{D} = 2.34\text{--}2.74$, vs. poly(methyl methacrylate) (PMMA) standards; (Tables 4.2 and A4.1 and Figure A4.42). The trends in molecular weight data were consistent with the free-radical polymerization mechanism employed, and revealed that both concentration and monomer:initiator ratio influenced the molecular weights of the polyelectrolytes isolated in an uncontrolled fashion. Each of the compounds reported in this study, including polyelectrolytes **4.10a–c**, exhibit properties consistent with the presence of ferrocene(s) in solution (Table 4.2). Their UV-vis absorption spectra exhibit maximum absorption at wavelengths (λ_{max}) of *ca.* 440 nm. Their cyclic voltammograms are comprised of reversible oxidation waves at potentials ($E_{1/2, \text{Fc}}$) between 0 and 5 mV relative to the ferrocene/ferrocenium redox couple (Figures 4.3 and A4.44–A.46). In each case, the current response observed corresponded to one electron for each ferrocene group present.

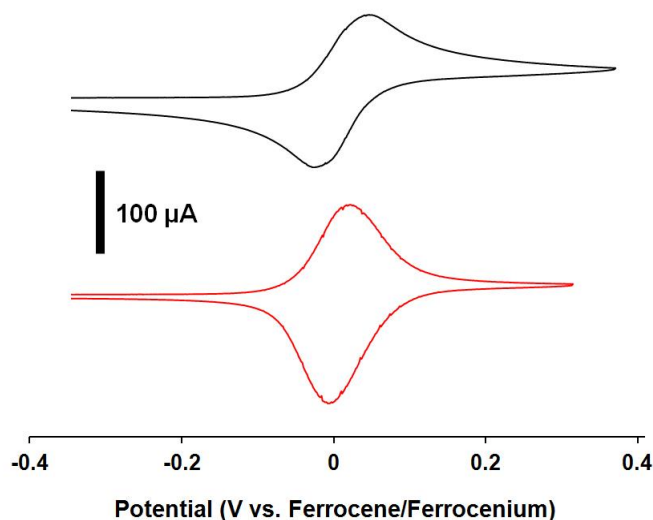


Figure 4.3. Cyclic voltammograms of ferrocene-substituted monomer **4.9** (black) and polyelectrolyte **4.10b** (red) recorded at 250 mV s⁻¹ in 1 mM solutions of 2:1 CH₂Cl₂:CH₃CN containing 0.1 M [*n*-Bu₄N][OTf] as supporting electrolyte.

Differential scanning calorimetry studies revealed glass transition temperatures of 108 °C for **4.10a–c** (Figures A4.49–A4.51). Thermal gravimetric analysis confirmed their exceptional thermal stability, as **4.10a–c** all reached 310 °C before significant mass loss was observed. After the onset of decomposition, degradation occurred in a single smooth step, before the masses plateaued above *ca.* 500 °C (Figures 4.4 and A4.53–A4.54). The high char yields of ~46% observed for polyelectrolytes **4.10a–c**, which may result from the

low volatility of the ionic compounds generated during decomposition, prompted us to conduct preliminary studies of their pyrolysis behavior.

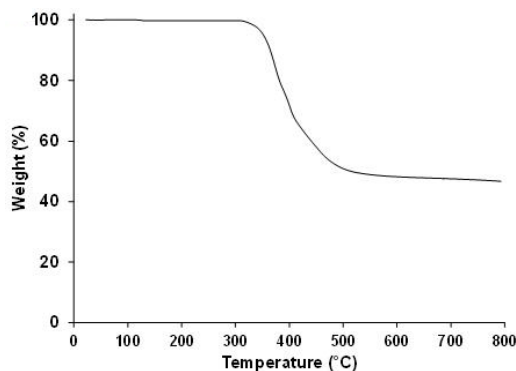


Figure 4.4. TGA trace for polyelectrolyte **4.10b**.

A thin film of polyelectrolyte **4.10b** was prepared by spin coating a 80 mg mL^{-1} 3:2 PhCl:CHCl₃ solution onto a freshly cleaned silicon wafer. The film was dried *in vacuo* for 16 h at 50 °C before it was heated to 800 °C at a rate of 10 °C min^{-1} and held at that temperature for an additional 2 h under a steady flow of nitrogen. Upon cooling to room temperature at a rate of 10 °C min^{-1} the pyrolyzed film was exposed to air and analyzed by scanning electron microscopy (SEM) (Figures 4.5 and A4.55). The resulting images and elemental mapping/analysis experiments revealed a mixture of magnetite (Fe₃O₄) crystallites and a carbon, phosphorus, and oxygen containing phase. Crucially, a significant quantity of the iron within the polyelectrolytes appears to be retained upon pyrolysis, illustrating the promise of this new class of highly-metallized polyelectrolytes as precursors to functional metal-rich ceramics and / or nanoparticles.

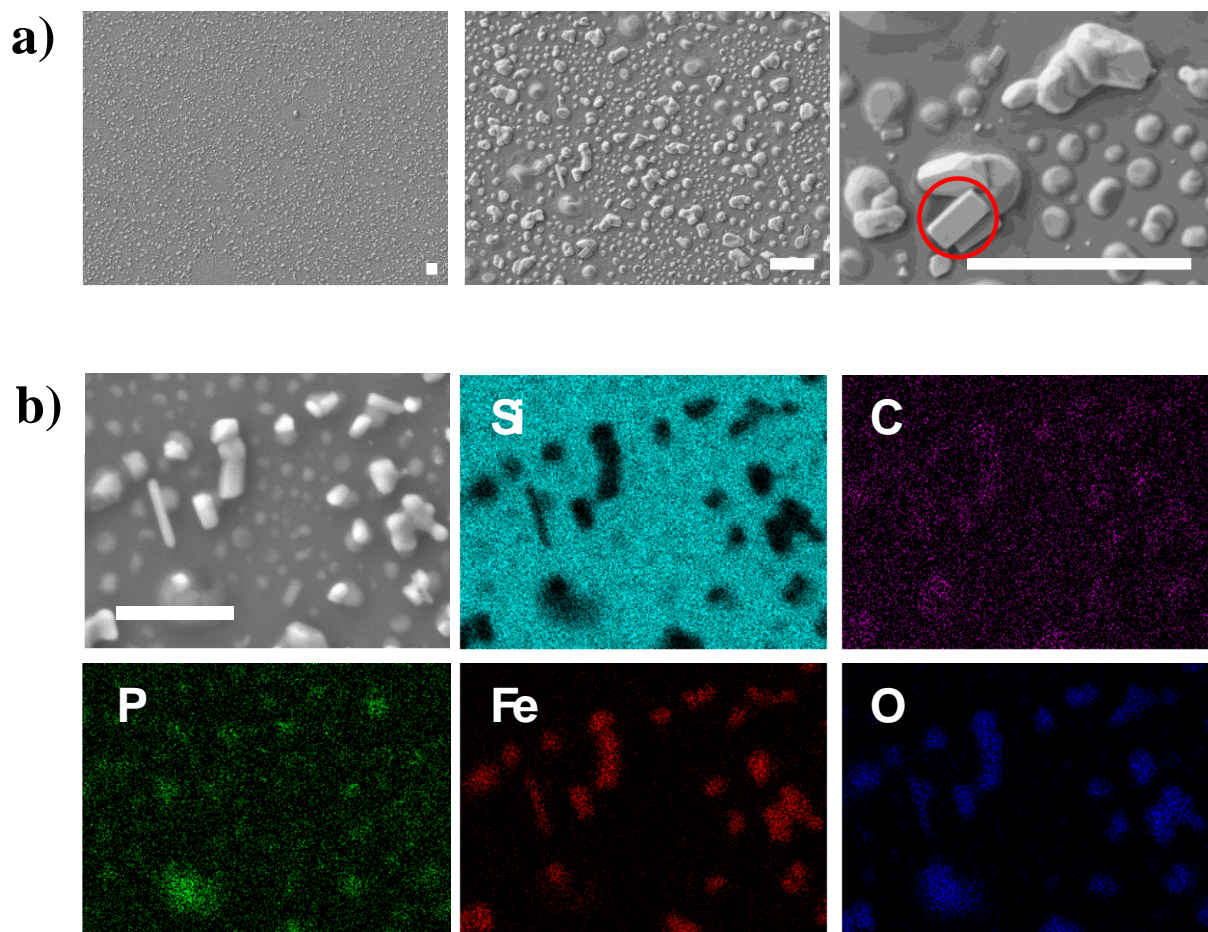
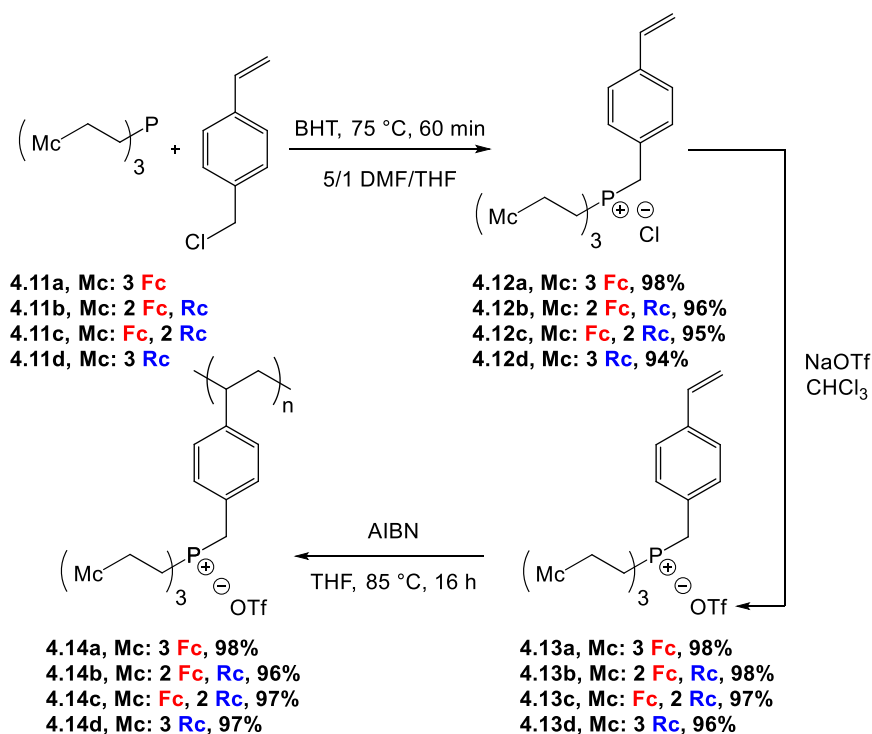


Figure 4.5. (a) SEM images and (b) SEM image and elemental mapping (Si, C, P, Fe, O) for the nanostructured films produced by heating a thin film of polyelectrolyte **4.10b** at 800 °C for 2 h under a flow of N₂ gas. Representative Fe₃O₄ crystallites highlighted by red circle. Scale bars = 1 μm.

4.2.2 Synthesis and Characterization of Styrene-Based Heterobimetallic Phosphonium Polyelectrolytes

The high efficiency of 4-vinylbenzyl chloride for the quaternization of phosphines prompted us to use it for the installation of a polymerizable group. Reaction of tertiary phosphines **4.11a–d**⁸¹ with a slight excess of 4-vinylbenzyl chloride and heating at 75 °C afforded phosphonium chloride monomers **4.12a–d** in quantitative yields (Scheme 4.2). Due to the poor solubility of the tertiary phosphines in DMF, they were initially dissolved in a minimum amount of THF and later combined with DMF, an effective solvent for the

quaternization reaction. Butylated hydroxytoluene (BHT) was added to prevent the undesired polymerization of the styrene groups during the quaternization reaction. To improve the solubility of the phosphonium salts in organic solvents and to prevent metallocene degradation,¹⁸ the chloride counter anions were once again exchanged with triflate anions to quantitatively afford monomers **4.13a–d**. The structure and purity of the monomers were confirmed using multinuclear NMR spectroscopy, IR and UV-vis absorption spectroscopy, mass spectrometry, elemental analysis, and X-ray crystallography (Figures 4.6, A4.19–A4.34, and Table 4.3).



Scheme 4.2. Synthetic pathway for the preparation of polyelectrolytes **4.14a–d**.

Phosphonium triflate monomers **4.13a–d** gave rise to a singlet in their ^{19}F NMR spectra at $\delta \sim -77$ and a singlet in their $^{31}\text{P}\{^1\text{H}\}$ NMR spectra at $\delta \sim 31.0$. Single crystals of monomer **4.13a** suitable for X-ray crystallography were grown by slow evaporation of the solvent from a THF solution (Figure 4.6 and Table 4.1). In the solid-state structure, each tetrahedral phosphonium cation was in close proximity to a triflate anion (shortest contact: P1-O2 3.958 Å). The C-P bond lengths ranged from 1.782(6) to 1.803(5) Å, and are shorter than those of the parent phosphine **4.12a** [1.843(1) to 1.855(1) Å].¹⁸ The average C-P-C angle was 109.5(3)° and the C44-C45 bond length for the vinyl group was 1.162(9) Å.

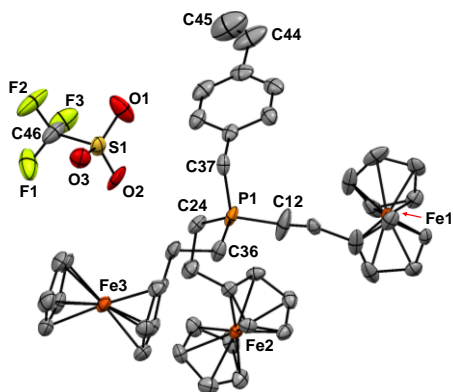


Figure 4.6. Solid-state structure of monomer **4.13a**. Thermal displacement ellipsoids are shown at 50% probability and hydrogen atoms have been omitted for clarity. Selected bond lengths (Å): P1-C12 1.782(6), P1-C24 1.803(5), P1-C36 1.798(5), P1-C37 1.791(6), C44-C45 1.162(9). Selected bond angles (degrees): C12-P1-C24 111.7(3), C12-P1-C36 108.5(3), C12-P1-C37 110.9(3), C24-P1-C36 110.0(3), C24-P1-C37 106.2(2), and C36-P1-C37 109.6(3).

Using azobisisobutyronitrile (AIBN) as an initiator, the phosphonium triflate monomers **4.13a–d** were polymerized in THF before they were precipitated into diethyl ether to yield the corresponding polyelectrolytes **4.14a–d** (Scheme 4.2). At room temperature, these polyelectrolytes gave rise to very broad ^1H , $^{31}\text{P}\{^1\text{H}\}$, and ^{19}F NMR spectra. However, upon heating to 125 °C in DMSO- d_6 the spectra sharpened (Figures A4.35–A4.38). The disappearance of the vinyl proton resonances and the observation of broad peaks associated with the unsaturated polyelectrolyte backbone (δ 0.75–2.15) in the ^1H NMR spectra of the polyelectrolytes confirmed successful polymerization. The presence of the aromatic (δ 5.75–7.50), metallocene (δ 4.00–5.00), methylene bridge (δ 3.40–4.20), and ethylene bridge (δ 2.10–3.25) proton resonances in the ^1H NMR spectra; a peak for each polyelectrolyte ($\delta \sim 31.0$) in the $^{31}\text{P}\{^1\text{H}\}$ NMR spectra; and a peak for each polyelectrolyte ($\delta \sim -77$) in the ^{19}F NMR spectra further supported the proposed structures of the polyelectrolytes.

Gel permeation chromatography (GPC) experiments were carried out to evaluate the molecular weight distributions for polyelectrolytes **4.14a–d**. The results confirmed the macromolecular nature of the polyelectrolytes **4.14a–d** (M_w : 143,450–278,100 g mol^{-1} , D : 3.16–4.10, Tables 4.3 and A4.2, and Figure A4.43).

4.2.2.1 UV-vis Absorption Spectroscopy and Cyclic Voltammetry

Similar to phosphines **4.12a–c**,⁸¹ the ferrocene units in polyelectrolytes **4.14a–d** gave rise to two absorption maxima at *ca.* 434 nm and 320 nm while the ruthenocene units exhibited a single absorption maximum at *ca.* 320 nm. The relative intensities of each peak varied with the number of ferrocene/ruthenocene units present (Table 4.3 and Figures A4.39–A4.41).

The electrochemical properties of the phosphonium triflate monomers **4.13a–d** and the corresponding polyelectrolytes **4.14a–d** were examined by cyclic voltammetry (CV) in a CH₂Cl₂/CH₃CN (2/1) solvent mixture containing 0.1 M [*n*-Bu₄N][OTf] as supporting electrolyte. Consistent with the electrochemical properties of the parent phosphines,⁸¹ the ferrocene units of the monomers and polyelectrolytes were oxidized reversibly, while the ruthenocene moieties demonstrated an irreversible oxidation wave. The observed irreversible behavior was consistent with the ability of ruthenocenium cations to rapidly engage in electrochemically-induced reactions.^{46, 82-83} Due to the presence of the cationic phosphonium centres in the monomers, the recorded $E_{1/2, \text{Fc}}$ and $E_{\text{pa, Rc}}$ values were slightly more positive than those of the parent phosphines (Table 4.3, Figures A4.47 and A4.48).⁸¹

Table 4.2. Selected characterization data for monomers **4.13a–d** and polyelectrolytes **4.14a–d**.

Compound	³¹ P NMR (δ)	ϵ , 320 nm ^b (M ⁻¹ cm ⁻¹)	ϵ , 434 nm (M ⁻¹ cm ⁻¹)	$E_{\text{pa, Rc}}$ (mV)	$E_{1/2, \text{Fc}}$ (mV)	M_n (g mol ⁻¹)	DP _n	\bar{D}
4.13a	31.2	260	320	-	10	-	-	-
4.13b	31.0	440	240	465	15	-	-	-
4.13c	30.9	730	140	510	20	-	-	-
4.13d	30.8	910	-	555	-	-	-	-
4.14a	31.1	260	330	-	20	46,900	50	3.16
4.14b	30.9	440	230	-	20	45,100	46	4.10
4.14c	30.8	620	150	410	35	69,100	67	4.02
4.14d	30.8	870	-	450	-	38,650	36	3.71

4.2.2.2 Thermal Analysis and Pyrolysis Studies

Differential scanning calorimetry studies of polyelectrolytes **4.14a–d** revealed glass transition temperatures (T_g s) between 165 and 177 °C (Figure A4.52 and Table 4.4). TGA studies demonstrated that polyelectrolytes **4.14a–d** have high thermal stability, with the onset of decomposition observed at *ca.* 310 °C and char yields ranging from 33 to 54% (Figure 4.7 and Table 4.4).

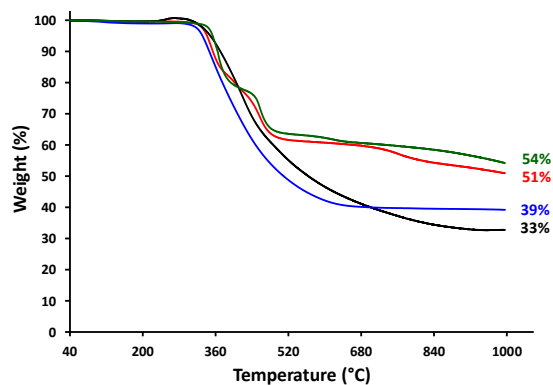


Figure 4.7. TGA traces for polyelectrolytes: **4.14a** (3 × Fc, black), **4.14b** (2 × Fc, 1 × Rc; red), **4.14c** (1 × Fc, 2 × Rc; blue), and **4.14d** (3 × Rc, green).

Based on the high char yields observed and growing interest in the catalytic and electrochemical properties of nano-structured metal phosphides,⁸⁴⁻⁸⁸ we decided to explore the preceramic behavior of polyelectrolytes **4.14a–d**. Polyelectrolyte films with approximate thickness of 6 μm (Figure A4.57) were prepared by drop casting and pyrolyzed at 1000 °C under a flow of N₂/H₂ (95/5) for 3h. Each pyrolysis experiment was repeated in triplicate, and representative SEM images and relevant data are shown in Figure 4.8 and Table 4.4. It is worth noting that we were unable to employ transmission electron microscopy (TEM) for our studies as our thorough attempts to dislodge the nanomaterials produced by pyrolysis from silicon substrates using physical scraping (razor blade), ultrasonication, and solvent rinsing were unsuccessful. However, our SEM analyses provided significant insight into the structures of the nanomaterials produced. In each case, pyrolysis of polyelectrolyte films resulted in the formation of large particles and/or continuous materials surrounded by numerous smaller particles. In the case of the nanomaterials produced from **4.14b** and **4.14c**, the multi-faceted appearance of the imaged materials hinted to the fact that they may be crystalline (*vide infra*).

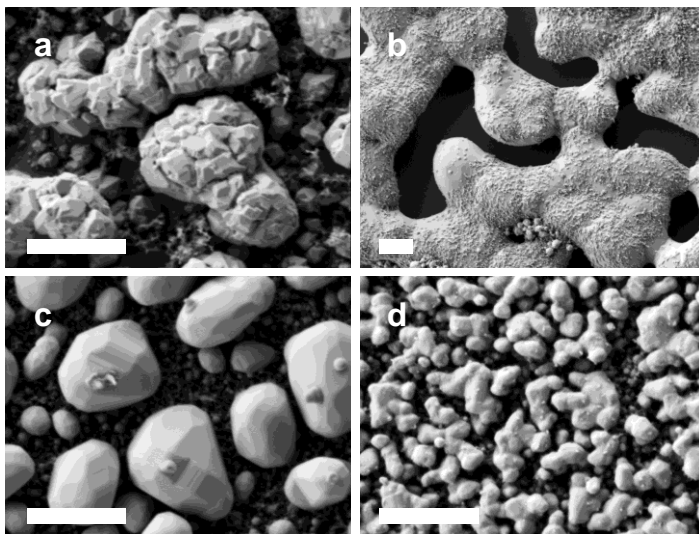


Figure 4.8. SEM images of the nanomaterials prepared via the pyrolysis of films of polyelectrolytes (a) 4.14a, (b) 4.14b, (c) 4.14c, and (d) 4.14d. Scale bars = 1 μm .

Elemental maps (EDX spectroscopy) revealed that the nanomaterials produced were comprised of C, O, P, Fe, and/or Ru and that the inorganic components were distributed throughout the nanomaterials produced (Figures 4.9, A4.58–A4.60). The presence of carbon was attributed to incomplete volatilization of the polystyrene backbone and oxidation during brief (and unavoidable) exposure of the samples to air prior to SEM analysis accounts for the presence of oxygen. Unfortunately, the elemental maps obtained provide little quantitative information about the composition of the nanomaterials produced. With this in mind, at least five different data sets were collected for regions (*ca.* 1 μm^2) of the nanomaterial surfaces densely populated with relatively large particles and/or continuous material (*'bulk'*) and with relatively small particles (*'particles'*) for each of the samples (Figures A4.61–A4.64 and Table 4.4). For each sample, the smaller particles produced were clearly embedded within a carbon-rich matrix, and the overall phosphorus/metal content was significantly lower than those observed for areas densely populated with bulk material.

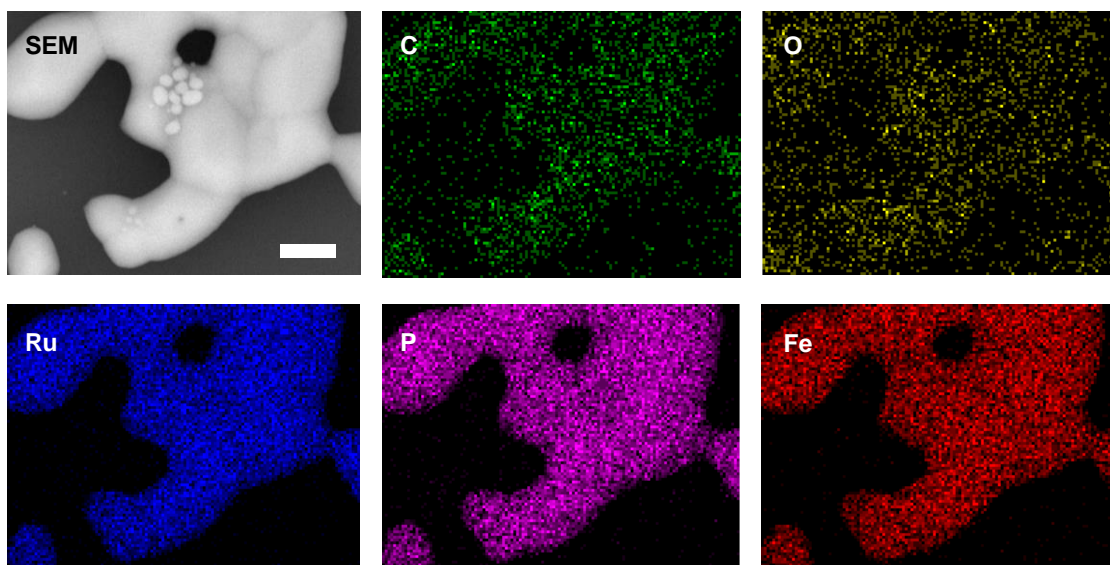


Figure 4.9. SEM images and elemental maps (O, Ru, Fe, P, C) for the nanomaterials prepared via the pyrolysis of a film of polyelectrolyte **4.14b**. Scale bar = 1 μm .

Table 4.3. Thermal characterization and elemental composition data for the nanomaterials produced via the pyrolysis of polyelectrolytes **4.14a–d**.

Polymer	T_g ($^{\circ}\text{C}$)	Onset of Decomposition ($^{\circ}\text{C}$)	Char Yield (%)	Region ^a	Atomic Ratio ^{a,b}			
					P	Fe	Ru	Fe + Ru
4.14a	177	310	33	<i>bulk</i>	1	1.9 ± 0.3	-	1.9 ± 0.3
				<i>particles</i>	1	2.1 ± 0.5	-	2.1 ± 0.5
4.14b	165	311	51	<i>bulk</i>	1	1.7 ± 0.7	1.1 ± 0.4	2.8 ± 0.8
				<i>particles</i>	1	1.5 ± 0.3	0.9 ± 0.1	2.4 ± 0.3
4.14c	173	312	39	<i>bulk</i>	1	0.5 ± 0.1	1.6 ± 0.1	2.1 ± 0.1
				<i>particles</i>	1	0.6 ± 0.3	1.8 ± 0.5	2.4 ± 0.6
4.14d	171	330	54	<i>bulk</i>	1	-	2.1 ± 0.0	2.1 ± 0.0
				<i>particles</i>	1	-	1.5 ± 0.1	1.5 ± 0.1

^aAtomic ratios determined using EDX spectroscopy for dense regions of relatively large particles (*bulk*) and less dense regions of relatively small particles (*particles*). See electronic supplementary information for additional details. ^bPhosphorus stoichiometry fixed at 1.

4.2.2.3 Powder X-ray Diffraction Studies

Powder X-ray diffraction studies of the nanomaterials produced by pyrolysis of films of polyelectrolytes **4.14a–d** are shown in Figure 4.10. In each case, the patterns produced confirmed the presence of crystalline materials. Qualitative phase identification studies were performed through careful comparison of our diffraction data with those of a PXRD

database,⁸⁹ which included data for known mono- and bimetallic phosphides (*i.e.*, M_4P , M_3P , M_2P , and MP ; where M : Fe and/or Ru), metal carbides, pure metals, etc. (Figures A4.65–A4.68). The PXRD data for the films produced from polyelectrolytes **4.14a–c** were not closely matched with those of any known phases, and were indicative of the presence of multiple crystalline phases, which prevented us from indexing the data. Conversely, the PXRD data collected for the film produced from polyelectrolyte **4.14d** was consistent with that of Ru_2P (Figure 4.10d and A4.68).

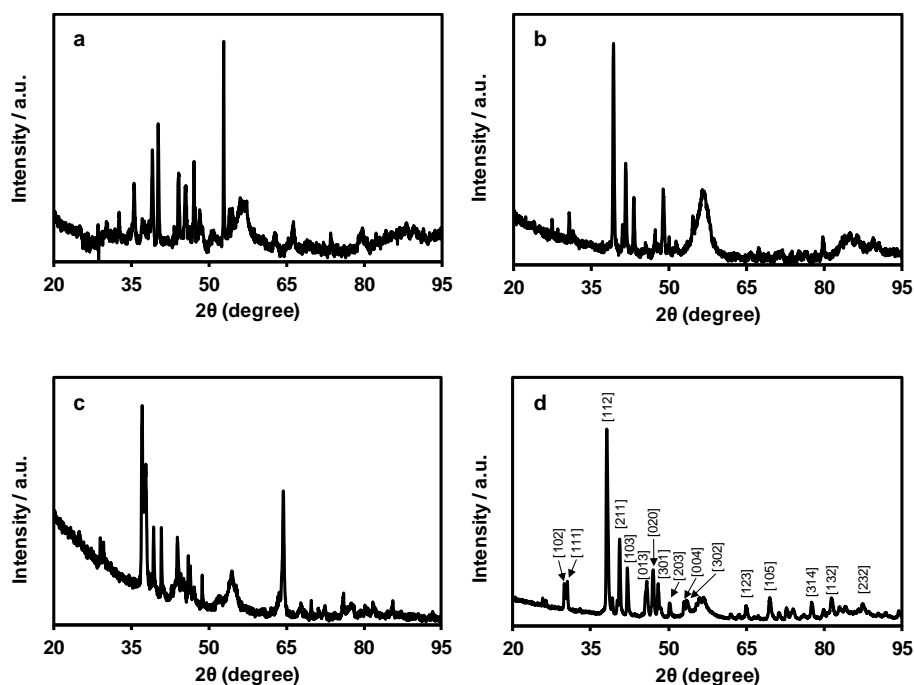


Figure 4.10. Powder X-ray diffractograms for the nanomaterials prepared via the pyrolysis of films of polyelectrolytes (a) **4.14a**, (b) **4.14b**, (c) **4.14c**, and (d) **4.14d**. Miller indices corresponding to Ru_2P are shown in panel (d).

4.2.2.4 Discussion

Considering the PXRD, EDX spectroscopy, and elemental mapping results obtained for the nanomaterials produced from pyrolyzed films of polyelectrolytes **4.14a–c**, two points become immediately obvious. First, given the large standard deviations associated with the atomic ratios determined from the EDX data collected, it is clear that phosphorus, iron, and/or ruthenium are not distributed uniformly throughout the nanomaterials produced. It is therefore probable that multiple different materials/phases have been produced. For the

heterobimetallic materials derived from **4.14b** and **4.14c**, PXRD data confirmed the absence of simple $\text{Fe}_2\text{P}/\text{Ru}_2\text{P}/\text{Fe}_3\text{P}/\text{Ru}_3\text{P}$ phases and supported this hypothesis. Second, within a single standard deviation, the average composition of the small particles and bulk materials analyzed were the same. Conversely, for the nanomaterials derived from **4.14d**, the relatively smaller standard deviations calculated point toward the uniform distribution of phosphorus and ruthenium throughout regions containing bulk material and relatively small particles. Furthermore, this was the only case where the composition of the bulk (P:Ru, 1 : 2.1 ± 0.0) and small-particle-rich (P:Ru, 1 : 1.5 ± 0.1) were statistically different. When these results are combined with the PXRD data collected and indexed for this sample, it becomes clear that the bulk phase produced from the pyrolysis of films of polyelectrolyte **4.14d** is comprised of Ru_2P .

4.3 Conclusion

In conclusion, through the use of a novel and unique approach, we have synthesized the first example of methacrylate-based phosphonium monomer in addition to a library of styrene-based phosphonium triflate monomers. By free-radical polymerization of the triflate salts, polyelectrolytes with four different stoichiometric ratios of Fe/Ru were prepared and fully characterized. Due to the presence of ferrocene/ruthenocene, these materials exhibited redox properties and gave rise to UV-vis absorption maxima consistent with the number of each metallocene present. GPC and DSC results confirmed the macromolecular nature of the polyelectrolytes and TGA studies confirmed their stability up to ~ 310 °C. Studies of the nanomaterials that resulted from the pyrolysis of polyelectrolytes using SEM showed that they can be used as precursors to crystalline nanomaterials. EDX spectroscopy and elemental mapping data indicated that the crystalline nanomaterials contained Fe, Ru, and P distributed throughout, with Fe/Ru/P ratios influenced by the polyelectrolyte structures.

4.4 Experimental section

4.4.1 General Considerations

Reactions and manipulations were carried out under a N_2 atmosphere using standard glove box or Schlenk techniques unless otherwise stated. Solvents were obtained from Caledon

Laboratories and Fischer Scientific, dried using an Innovative Technologies Inc. solvent purification system, collected under vacuum, and stored under a nitrogen atmosphere over 4 Å molecular sieves. Reagents were purchased from Sigma-Aldrich or Alfa Aesar and used as received, aside from 4-vinylbenzyl chloride which was purified according to a literature procedure and stored under N₂ at -35 °C.⁹⁰ Tertiary phosphines **4.11a–d** were synthesized according to reported protocols.⁸¹ ¹H, ¹³C{¹H}, ¹⁹F and ³¹P NMR spectra were recorded on a 600 MHz (¹H: 599.5 MHz, ¹³C{¹H}: 150.8 MHz, ¹⁹F: 563.9 MHz and ³¹P: 242.6 MHz) Varian INOVA instrument. NMR spectra were recorded on a 400 MHz (¹H: 399.8 MHz, ¹³C: 100.5 MHz, ¹⁹F: 376.4 MHz, ³¹P: 161.8 MHz) or a 600 MHz (¹H: 599.5 MHz, ¹³C{¹H}: 150.8 MHz, ³¹P: 242.6 MHz) Varian INOVA instrument, or a 400 MHz (¹H: 400.8 MHz, ¹³C{¹H}: 100.6 MHz, ³¹P: 161.9 MHz) Varian Mercury instrument. ¹H NMR spectra were referenced to residual CHCl₃ (7.27 ppm) or (CD₃)(CD₂H)SO (2.50 ppm) and ¹³C NMR spectra were referenced to CDCl₃ (77.0 ppm) or DMSO-*d*₆ (39.5 ppm). ³¹P NMR spectra were referenced to PPh₃ as an internal standard (-6.0 ppm relative to H₃PO₄). Mass spectrometry data were recorded in positive-ion mode using a Micromass/Waters Q-TOF Ultima LC-MS/MS system or Micromass LCT electrospray ionization time-of-flight mass spectrometer. UV-vis absorption spectra were recorded using a Cary 300 Scan instrument. Infrared spectra were recorded using a PerkinElmer Spectrum Two FT-IR spectrometer as thin films on KBr plates. Elemental analyses (C and H) were carried out by Laboratoire d'Analyse Élémentaire de l'Université de Montréal, Montréal, QC, Canada.

4.4.2 Cyclic Voltammetry

Cyclic voltammograms were collected using a Bioanalytical Systems Inc. (BASi) Epsilon potentiostat and analyzed using BASi Epsilon software. Typical electrochemical cells consisted of a three-electrode setup including a glassy carbon working electrode, platinum wire counter electrode, and silver wire *pseudo*-reference electrode. 1 mM degassed solutions of phosphonium salts **4.9**, **4.10a–c**, **4.13a–d**, and **4.14a–d**, combined with supporting electrolyte (0.1 M [*n*-Bu₄N][OTf]) in a CH₂Cl₂/CH₃CN (2/1) solvent mixture were prepared and run at a scan rate of 250 mV s⁻¹ under a blanket of argon. To study the electrochemical behavior of **4.14a–d**, different solvents such as THF, DMF, CH₃CN, and

CH₂Cl₂ containing 0.1 M [*n*-Bu₄N][OTf] were used to make 0.2 mM solutions of the analytes. In each case, severe plating of the oxidized forms of **4.14a–d** was observed on the glassy carbon working electrode. Therefore, a 2/1 solvent mixture of CH₂Cl₂ and CH₃CN was used as it was the least problematic combination. Degassed solutions of polyelectrolytes **4.14a–d** in a CH₂Cl₂/CH₃CN (2/1) solvent mixture were prepared by stirring the mixture overnight at 40 °C. After addition of the supporting electrolyte, the mixtures were sonicated for 20 s and filtered (Nylon membrane, 0.2 μm). Using these solutions, electrochemical studies were performed at a scan rate of 250 mV s⁻¹ under a blanket of argon. Cyclic voltammograms were referenced relative to a decamethylferrocene internal standard (1 mM, -520 mV relative to ferrocene/ferrocenium under identical conditions) and corrected for internal cell resistance using the BASi Epsilon software.

4.4.3 X-ray Diffraction Studies

Single crystals of **4.8b** were grown by vapor diffusion of pentane into a concentrated solution of the compound in CHCl₃ and single crystals of monomer **4.13a** were grown by slow evaporation of a THF solution. The samples were mounted on MiTeGen polyimide micromounts with a small amount of Paratone N oil. X-ray diffraction measurements of **4.8b** were made on a Nonius Kappa CCD diffractometer and **4.13a** were made on a Bruker Kappa Axis Apex2 diffractometer. Initial indexing indicated that the sample crystal of **4.13a** was non-merohedrally twinned. The twin law was determined to be:

$$\begin{array}{ccc} 0.99635 & 0.00646 & 0.00848 \\ 0.00835 & -1.00086 & 0.00433 \\ 0.85236 & -0.00198 & -0.99547 \end{array}$$

which represents a 179.8° rotation about [100]. The twin fraction was included in the refinement as an adjustable parameter (*vide infra*). The unit cell dimensions for **4.8b**, and **4.13a** were determined from a symmetry constrained fit of 9891 reflections with 5.14° < 2θ < 50.28°, and 5386 reflections with 6.58° < 2θ < 47.88°. The data collection strategy was a number of ω and φ scans which collected data up to 57.156 (2θ) for **4.8b** and 53.538° (2θ) for **4.13a**. The frame integration was performed using SAINT.⁹¹ The resulting raw data for **4.8b** were scaled and absorption corrected using a multi-scan averaging of

symmetry equivalent data using SADABS⁹² and the raw data for **4.13a** were scaled and absorption corrected using a multi-scan averaging of symmetry equivalent data using TWINABS.⁹³ The structure for **4.8b** was solved using the SIR92 program⁹⁴ and the structure for **4.13a** was solved by using a dual space methodology using the SHELXT program.⁹⁵ All non-hydrogen atoms were obtained from the initial solution. The hydrogen atoms were introduced at idealized positions and were allowed to ride on the parent atom. The twin fraction refined to a value of 0.465(1). The structural models were fit to the data using full matrix least-squares based on F^2 . The calculated structure factors included corrections for anomalous dispersion from the usual tabulation. The structures of **4.8b** and **4.13a** were refined using the SHELXL-2014 program from the SHELX suite of crystallographic software.⁹⁶ Graphic plots were produced using Mercury software (version 3.3). For additional collection and refinement details, see CCDC 1012823 and 1476067, Table 4.1 and Figures 4.1 and 4.6. Powder X-ray diffraction (PXRD) data for nanomaterial films deposited on silicon wafers were acquired using an Inel CPS powder diffractometer with an Inel XRG 3000 generator and Inel CPS 120 detector using a $\text{CuK}\alpha$ radiation source. For diffractograms, see Figure 4.10 and A4.65–A4.68.

Table 4.4. Selected X-ray diffraction data collection and refinement details for **4.8b** and **4.13a**.

	4.8b	4.13a
Chemical formula	$\text{C}_{39}\text{H}_{46}\text{BF}_4\text{Fe}_3\text{OP}$	$\text{C}_{46}\text{H}_{48}\text{F}_3\text{Fe}_3\text{O}_3\text{PS}$
FW (g mol^{-1})	816.1	936.42
Temp (K)	150	110
Crystal system	monoclinic	Triclinic
Space group	$P2_1/c$	$P-1$
λ (Å)	0.71073	0.71073
a (Å)	7.342(8)	12.378(6)
b (Å)	29.84(4)	12.619(5)
c (Å)	17.170(19)	14.252(7)
α (deg)	90	79.298(7)
β (deg)	106.475(19)	68.524(10)
γ (deg)	90	89.953(7)
V (Å ³)	3607(7)	2030.1(17)
Z	4	2
ρ (g cm^{-3})	1.503	1.532
μ (cm^{-1})	1.286	1.204
R_1 [$I > 2\sigma(I)$]	0.0582	0.0534
ωR_2 [$I > 2\sigma(I)$]	0.138	0.1278
R_1 (all data)	0.0869	0.0917
ωR_2 (all data)	0.1522	0.1463
GOF	1.031	1.042

$$R_1 = \Sigma(|F_o| - |F_c|) / \Sigma F_o, \omega R_2 = [\Sigma(\omega(F_o^2 - F_c^2)^2) / \Sigma(\omega F_o^4)]^{1/2}, \text{GOF} = [\Sigma(\omega(F_o^2 - F_c^2)^2) / (\text{No. of reflns.} - \text{No. of params.})]^{1/2}.$$

4.4.4 Gel Permeation Chromatography (GPC)

GPC experiments were performed by PolyAnalytik Inc. Canada (London, Ontario). Molecular weights and dispersities ($\mathcal{D} = M_w / M_n$) were obtained using a Viscotek TDA302/GPCmax gel permeation chromatograph equipped with automatic sampler, isocratic pump, injector, in-line degasser, column and detector oven (60 °C), refractive index detector, and Viscotek Inert Series Columns: 1 × Mixed Bed Low Molecular Weight (I-MBLMW, exclusion limit of 20 kg mol⁻¹ PS) and 1 × Mixed Bed High Molecular Weight (I-MBHMW, exclusion limit of 10,000 kg mol⁻¹ PS). The eluent employed was DMF (60 °C) containing 0.02 M [*n*-Bu₄N][OTf] at a flow rate of 0.7 mL min⁻¹. Samples were dissolved in the eluent (5 mg mL⁻¹), heated for 1.5 h, and filtered (Nylon membrane, 0.2 μm) before analysis. For **4.10a–c**, the conventional calibration of the refractive index detector was performed using a series of monodisperse poly(methyl methacrylate) standards (PolyAnalytik) and for **4.14a–d**, the conventional calibration of the refractive index detector was performed using a series of monodisperse polystyrene standards (PolyAnalytik). All data were processed using Viscotek's OmniSEC v4.6.2 software.

4.4.5 Thermal Analysis

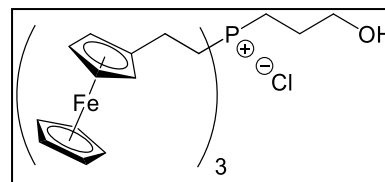
The thermal degradation studies of **4.10a–c** were performed using a TA Instruments Q600 SDT TGA instrument and the thermal degradation studies of **4.14a–d** were performed using a TA Instruments Q50 TGA instrument under an atmosphere of N₂. Samples were placed in a platinum pan and heated at a rate of 10 °C min⁻¹ under a flow of N₂ (60 mL min⁻¹). Glass transition temperatures were determined under an atmosphere of N₂ using differential scanning calorimetry (DSC) on a TA Instruments DSC Q20. The polymer samples were placed in an aluminum Tzero pan and heated (to 280 °C for **4.10a–c** and to 300 °C for **4.14a–d**) at 10 °C min⁻¹ under a flow of N₂ (50 mL min⁻¹) and cooled to 0 °C at 5 °C min⁻¹, before they underwent two more heat/cool cycles. The glass transitions were determined from the second heat/cool cycle.

4.4.6 Pyrolysis Studies and Scanning Electron Microscopy

The thin films of polyelectrolyte **4.10b** were prepared by spin coating (2000 rpm, 30 s, acceleration time < 2 s) 20 μL of a 80 mg mL^{-1} solution of polyelectrolyte **4.10b** in a 3:2 mixture of $\text{PhCl}:\text{CHCl}_3$ onto the freshly cleaned silicon wafers ($A = 1 \text{ cm}^2$) using a Laurell WS-400BZ-6NPP/LITE spin-coater and the thick films of polyelectrolytes **4.14a–d** were prepared by drop-casting 250 μL of a 20 mg mL^{-1} PhCl solution of each polyelectrolyte onto a silicon wafer ($A = 2.5 \text{ cm}^2$). The samples of **4.10b** dried in a vacuum oven at 50 $^\circ\text{C}$ for 16 h before they were heated at a rate of 10 $^\circ\text{C min}^{-1}$ to a temperature of 800 $^\circ\text{C}$ under a gentle flow of N_2 gas in a Lindberg Blue M tube furnace. The samples of **4.14a–d** were dried in air, transferred into a vacuum oven, and dried at 50 $^\circ\text{C}$ for 2 h before they were heated at a rate of 10 $^\circ\text{C min}^{-1}$ to a temperature of 1000 $^\circ\text{C}$ under a gentle flow (*ca.* 60 mL min^{-1}) of a N_2/H_2 (95/5) gas mixture in a Lindberg Blue M tube furnace. The samples of **4.10b** heated at the maximum temperature for 2 h and the samples of **4.14a–d** were heated at the maximum temperature for 3 h before the furnace was cooled to room temperature at a rate of 10 $^\circ\text{C min}^{-1}$. Polymer film thickness of **4.14a** and the surface morphologies of thermally deposited nanomaterials on silicon wafers were assessed directly using scanning electron microscopy (SEM) at 1 keV beam energy using LEO/Zeiss 1530 and LEO/Zeiss 1540XB instruments. Energy dispersive X-ray spectroscopy (EDX) experiments were performed at 10 keV beam energy on the 1540XB with the equipped Oxford X-sight X-ray detector and INCA analysis software.

Phosphonium Chloride Salt **4.8a** ($3 \times \text{Fc}$)

In a 250 mL Schlenk flask equipped with a condenser, tertiary phosphine **4.11a** (1.00 g, 1.49 mmol) and 3-chloro-1-propanol (2.00 mL, 23.4 mmol) were dissolved in 25 mL dry DMF. The solution was refluxed with

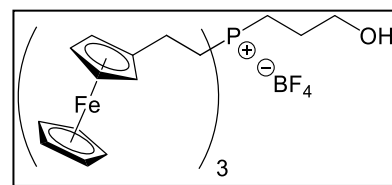


stirring for 16 h, cooled and concentrated *in vacuo*. The orange oily residue was then dissolved in about 50 mL of degassed CH_2Cl_2 , washed with $3 \times 20 \text{ mL}$ of degassed H_2O , dried over MgSO_4 , transferred to a silica plug (1'' \times 2'') for subsequent purification *in vacuo*. Unreacted tertiary phosphine **4.11a** was removed by eluting degassed CH_2Cl_2

through the plug. Phosphonium chloride salt **4.8a** remained on top of the plug while 150 mL degassed CH_2Cl_2 passed through the column before the elution solvent was changed to degassed EtOH to remove **4.8a**. The EtOH solution containing **4.8a** was collected and concentrated *in vacuo* before dissolved in a minimum amount of degassed CH_2Cl_2 , and precipitated by adding degassed hexanes. The resulting powder was filtered *in vacuo* before it was once again dissolved, precipitated, and filtered to yield **4.8a** as a yellow solid. Yield = 1.01 g, 88%. M.p. : 102–104 °C. ^1H NMR (599.4 MHz, CDCl_3): δ 5.19 (t, $^3J_{\text{HH}} = 6$ Hz, 1H, OH), 4.17 (s, 15H, C_5H_5), 4.16 (d, $^3J_{\text{HH}} = 2$ Hz, 6H, $\beta\text{-C}_5\text{H}_4\text{R}$), 4.16 (t, $^3J_{\text{HH}} = 2$ Hz, 6H, $\alpha\text{-C}_5\text{H}_4\text{R}$), 3.78 (m, 2H, CH_2OH), 2.68 (m, 6H, $\text{C}_5\text{H}_4\text{CH}_2$), 2.57 (m, 2H, $\text{PCH}_2\text{CH}_2\text{CH}_2$), 2.44 (m, 6H, $\text{C}_5\text{H}_4\text{CH}_2\text{CH}_2$), 1.92 (m, 2H, $\text{PCH}_2\text{CH}_2\text{CH}_2$). $^{13}\text{C}\{^1\text{H}\}$ NMR (150.7 MHz, CDCl_3): δ 85.5 (d, $^3J_{\text{CP}} = 12$ Hz, *ipso*- $\text{C}_5\text{H}_4\text{R}$), 68.8 (s, C_5H_5), 68.1 (d, $^5J_{\text{CP}} = 2$ Hz, $\beta\text{-C}_5\text{H}_4\text{R}$), 67.9 (d, $^4J_{\text{CP}} = 2$ Hz, $\alpha\text{-C}_5\text{H}_4\text{R}$), 60.7 (d, $^3J_{\text{CP}} = 14$ Hz, CH_2OH), 24.8 (s, $^2J_{\text{CP}} = 2$ Hz, $\text{PCH}_2\text{CH}_2\text{CH}_2$), 22.1 (s, $\text{C}_5\text{H}_4\text{CH}_2$), 21.3 (d, $^1J_{\text{CP}} = 45$ Hz, $\text{C}_5\text{H}_4\text{CH}_2\text{CH}_2$), 16.5 (d, $^1J_{\text{CP}} = 48$ Hz, $\text{PCH}_2\text{CH}_2\text{CH}_2$). ^{31}P NMR (242.7 MHz, CDCl_3): δ 32.6. FT-IR (KBr): 813 (s), 1001 (m), 1105 (m), 1411 (w), 3095 (br, w), 3267 (br, m) cm^{-1} . UV-vis (CH_2Cl_2): λ_{max} 439 nm ($\epsilon = 326 \text{ M}^{-1} \text{ cm}^{-1}$). Mass Spec. (ESI, +ve mode): exact mass calculated for $[\text{C}_{39}\text{H}_{46}\text{PFe}_3\text{O}]^+$: 729.1334; exact mass found: 729.1351; difference: +2.3 ppm. Anal. Calcd. (%) for $\text{C}_{39}\text{H}_{46}\text{PFe}_3\text{OCl}$: C, 61.25; H, 6.06. Found: C, 61.82; H, 6.31.

Preparation of Phosphonium Tetrafluoroborate Salt **4.8b**

In a 100 mL Schlenk flask, **4.8a** (0.50 g 0.65 mmol) was dissolved in 25 mL dry and degassed CHCl_3 before NaBF_4 (0.70 g, 6.2 mmol) was charged into the reaction flask. The resulting mixture was stirred at 20 °C for 16 h, gravity

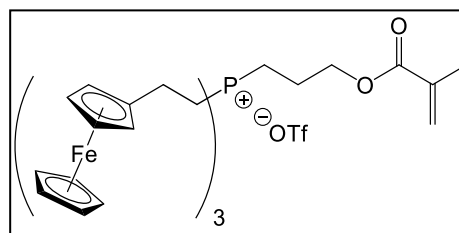


filtered to remove precipitate, washed with 3×20 mL of H_2O , dried over MgSO_4 , and gravity filtered. NaBF_4 (0.07 g, 0.06 mmol) was once again charged into a 100 mL flask containing the filtrate before the mixture was stirred for another 16 h. It was then gravity filtered to remove the precipitate, washed with 3×20 mL of H_2O , dried over MgSO_4 , and gravity filtered before it was concentrated to yield an orange solid. Recrystallization from 9:1 CH_2Cl_2 :pentane yielded **4.8b** as a yellow solid. Yield = 0.39 g, 74%. M.p. : 203–205 °C. ^1H NMR (399.8 MHz, $d_6\text{-DMSO}$): δ 4.90 (t, $^3J_{\text{HH}} = 5$ Hz, 1H, OH), 4.24 (s, 6H, $\beta\text{-$

C_5H_4R), 4.20 (s, 15H, C_5H_5), 4.15 (s, 6H, $\alpha-C_5H_4R$), 3.52 (m, 2H, CH_2OH), 2.54–2.70 (m, 12H, $C_5H_4CH_2$ and $C_5H_4CH_2CH_2$), 2.38 (m, 2H, $PCH_2CH_2CH_2$), 1.73 (m, 2H, $PCH_2CH_2CH_2$). $^{13}C\{^1H\}$ NMR (100.6 MHz, d_6 -DMSO): δ 86.9 (d, $^3J_{CP} = 17$ Hz, *ipso*- C_5H_4R), 68.5 (s, C_5H_5), 67.7 (s, $\beta-C_5H_4R$), 67.4 (s, $\alpha-C_5H_4R$), 60.4 (d, $^3J_{CP} = 16$ Hz, CH_2OH), 24.2 (s, $PCH_2CH_2CH_2$), 20.8 (s, $C_5H_4CH_2$), 18.9 (d, $^1J_{CP} = 45$ Hz, $C_5H_4CH_2CH_2$), 14.7 (d, $^1J_{CP} = 49$ Hz, $PCH_2CH_2CH_2$). ^{19}F NMR (376.4 MHz, d_6 -DMSO): δ -1483. ^{31}P NMR (162.0 MHz, d_6 -DMSO): δ 34.2 (s). FT-IR (KBr): 825 (s), 1068 (br, s), 1085 (s), 1224 (m), 1409 (br, m), 2930 (br, m), 3100 (br, w), 3437 (br, m) cm^{-1} . UV-vis (CH_2Cl_2): λ_{max} 443 nm ($\epsilon = 331 M^{-1} cm^{-1}$). Mass Spec. (ESI, +ve mode): exact mass calculated for $[C_{39}H_{46}PFe_3O]^+$: 729.1334; exact mass found: 729.1338; difference: +0.5 ppm. Anal. Calcd. (%) for $C_{39}H_{46}PFe_3OBF_4$: C, 57.40; H, 5.68. Found: C, 57.51; H, 5.76.

Preparation of Monomer **4.9**

In a 250 mL Schlenk flask, **4.8a** (0.50 g 0.65 mmol) was dissolved in dry CH_2Cl_2 (100 mL). Et_3N (1.4 mL, 10 mmol) was added to the reaction flask at room temperature. After stirring at 20 °C for 20 min, methacryloyl chloride (1.10 mL, 10.9 mmol)

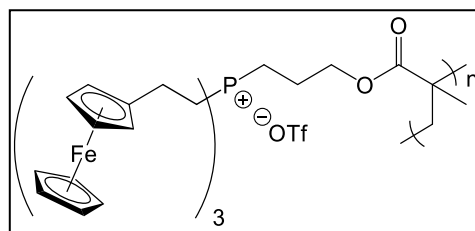


was added to the reaction flask and the resulting solution was stirred for 2 h. The reaction mixture was then stirred at 20 °C for 16 h before it was washed with 2×25 mL of saturated solution of Na_2CO_3 and 3×25 mL of H_2O , respectively, dried over $MgSO_4$, and transferred to a silica plug (1" \times 3") for subsequent purification *in vacuo*. The chloride salt remained on top of the plug while 150 mL degassed CH_2Cl_2 eluted before the solvent was changed to degassed EtOH to remove the monomer as a chloride salt. The EtOH solution containing the chloride salt was collected and concentrated *in vacuo*. The resulting residue was dissolved in 25 mL of dry and degassed $CHCl_3$ before $NaOTf$ (1.00 g, 5.70 mmol) was charged into the reaction flask. The resulting mixture was stirred at 20 °C for 16 h, gravity filtered to remove precipitate, washed with 3×20 mL of H_2O , dried over $MgSO_4$, and gravity filtered. $NaOTf$ (0.10 g, 0.57 mmol) was once again charged into a 100 mL flask containing the filtrate before the mixture was stirred for another 16 h. It was then gravity

filtered to remove the precipitate that formed, washed with 3×20 mL of H_2O , dried over MgSO_4 , and gravity filtered before it was concentrated *in vacuo*. The resulting orange residue was then dried *in vacuo* for 2 h at 35°C to remove residual solvents to afford monomer **4.9** as an orange solid. Yield = 0.54 g, 89%. M.p. : $68\text{--}70^\circ\text{C}$. ^1H NMR (599.4 MHz, CDCl_3): δ 6.16 (m, 1H, *trans*- CCH_2), 5.66 (m, 1H, *cis*- CCH_2), 4.22 (s, 15H, C_5H_5), 4.21 (s, 6H, $\beta\text{-C}_5\text{H}_4\text{R}$), 4.20 (s, 6H, $\alpha\text{-C}_5\text{H}_4\text{R}$), 4.15 (m, 2H, $\text{CH}_2\text{CH}_2\text{O}$), 2.59 (m, 6H, $\text{C}_5\text{H}_4\text{CH}_2$), 2.32 (m, 6H, $\text{C}_5\text{H}_4\text{CH}_2\text{CH}_2$), 2.10 (m, 2H, $\text{PCH}_2\text{CH}_2\text{CH}_2$), 1.98 (s, 3H, CH_3), 1.81 (m, 2H, $\text{PCH}_2\text{CH}_2\text{CH}_2$). $^{13}\text{C}\{^1\text{H}\}$ NMR (100.5 MHz, CDCl_3): δ 166.8 (s, CO), 135.7 (s, CCH_3), 126.1 (s, CCH_2), 120.8 (q, $^1J_{\text{CF}} = 321$ Hz, OTf), 85.2 (d, $^3J_{\text{CP}} = 13$ Hz, *ipso*- $\text{C}_5\text{H}_4\text{R}$), 68.8 (s, C_5H_5), 68.0 (s, $\beta\text{-C}_5\text{H}_4\text{R}$ and $\alpha\text{-C}_5\text{H}_4\text{R}$), 63.5 (d, $^3J_{\text{CP}} = 16$ Hz, $\text{CH}_2\text{CH}_2\text{O}$), 21.9 (d, $^2J_{\text{CP}} = 5$ Hz, $\text{C}_5\text{H}_4\text{CH}_2$), 21.0 (d, $^2J_{\text{CP}} = 4$ Hz, $\text{PCH}_2\text{CH}_2\text{CH}_2$), 20.6 (d, $^1J_{\text{CP}} = 46$ Hz, $\text{C}_5\text{H}_4\text{CH}_2\text{CH}_2$), 18.24 (s, CH_3), 15.8 (d, $^1J_{\text{CP}} = 48$ Hz, $\text{PCH}_2\text{CH}_2\text{CH}_2$). ^{19}F NMR (376.4 MHz, CDCl_3): δ -78.1 . ^{31}P NMR (242.7 MHz, CDCl_3): δ 31.9 (s). FT-IR (KBr): 825 (m), 1032 (s), 1163 (s), 1275 (br, s), 1645 (br, m), 1722 (br, m), 3109 (br, w), 3468 (br, s) cm^{-1} . UV-vis (CH_2Cl_2): λ_{max} 440 nm ($\epsilon = 294$ $\text{M}^{-1} \text{cm}^{-1}$). Mass Spec. (ESI, +ve mode): exact mass calculated for $[\text{C}_{44}\text{H}_{50}\text{PFe}_3\text{O}_5]^+$: 797.1597; exact mass found: 797.1598; difference: +0.1 ppm. Anal. Calcd. (%) for $\text{C}_{44}\text{H}_{50}\text{PFe}_3\text{O}_5\text{SF}_3$: C, 55.84; H, 5.32; S, 3.39. Found: C, 56.03; H, 5.49; S, 3.52.

Preparation of Polyelectrolyte **4.10a**

In a 20 mL grease-free Schlenk flask, monomer **4.9** (400 mg, 0.423 mmol) was dissolved in 400 μL of a THF solution containing AIBN (0.70 mg, 0.0042 mmol). The resulting solution was degassed using 3 freeze-pump-thaw cycles before it was stirred at

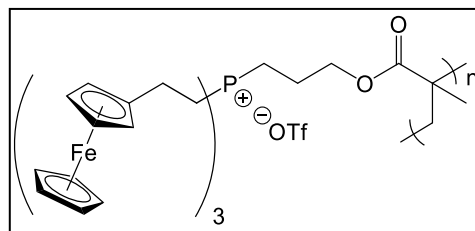


75°C for 17 h. The solution was concentrated *in vacuo* to yield a dark orange residue before it was dissolved in a minimum amount of CH_2Cl_2 , precipitated in benzene, and centrifuged for 1 min to separate the solids. The solids were collected and the precipitation process was repeated once in benzene and twice in pentane, respectively: The solid was dried *in vacuo* at 50°C for 40 h to yield polyelectrolyte **4.10a** as a yellow powder. Yield =

0.28 g, 70%. ^1H NMR (599.4 MHz, CDCl_3): δ 3.30–5.40 (broad, C_5H_5 , $\text{C}_5\text{H}_4\text{R}$ and $\text{CH}_2\text{CH}_2\text{O}$), 0.50–3.05 (broad, saturated polymer backbone CH_2 , $\text{C}_5\text{H}_4\text{CH}_2$, $\text{C}_5\text{H}_4\text{CH}_2\text{CH}_2$, $\text{PCH}_2\text{CH}_2\text{CH}_2$, CH_3 , $\text{PCH}_2\text{CH}_2\text{CH}_2$). ^{19}F NMR (376.4 MHz, CDCl_3): δ -77.2 . ^{31}P NMR (242.7 MHz, CDCl_3): δ 31.8 (s). FT-IR (KBr): 638 (m), 829 (w), 1032 (m), 1161 (m), 1265 (s), 1660 (br, w), 1734 (br, w), 2934 (br, w), 3099 (br, w) cm^{-1} . UV-vis (CH_2Cl_2): λ_{max} 437 nm ($\epsilon = 322 \text{ M}^{-1} \text{ cm}^{-1}$). Anal. Calcd. (%) for $(\text{C}_{44}\text{H}_{50}\text{PFe}_3\text{O}_5\text{SF}_3)_n$: C, 55.84; H, 5.32; S, 3.39. Found: C, 56.14; H, 5.42; S, 3.69. GPC (DMF, 0.02 M $[n\text{-Bu}_4\text{N}][\text{OTf}]$, 60 °C, conventional calibration vs. PMMA standards): $M_n = 43,100 \text{ g mol}^{-1}$, $M_w = 118,200 \text{ g mol}^{-1}$, $D = 2.74$.

Preparation of Polyelectrolyte **4.10b**

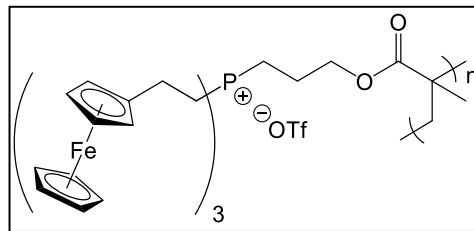
In a 20 mL grease-free Schlenk flask, monomer **4.9** (400 mg, 0.423 mmol) was dissolved in 533 μL of a THF solution containing AIBN (0.35 mg, 0.0021 mmol). The resulting solution was degassed using 3 freeze-pump-thaw cycles before it was stirred at



75 °C for 25 h. The solution was concentrated *in vacuo* to yield a dark orange residue before it was dissolved in a minimum amount of CH_2Cl_2 , precipitated in benzene, and centrifuged for 1 min to separate the solids. The solids were collocated and the precipitation process was repeated once in benzene and twice in pentane, respectively: The solid was dried *in vacuo* at 50 °C for 40 h to yield polyelectrolyte **4.10b** as a yellow powder. Yield = 0.32 g, 79%. ^1H NMR (599.4 MHz, CDCl_3): δ 3.40–5.00 (broad, C_5H_5 , $\text{C}_5\text{H}_4\text{R}$ and $\text{CH}_2\text{CH}_2\text{O}$), 0.50–3.10 (broad, saturated polymer backbone CH_2 , $\text{C}_5\text{H}_4\text{CH}_2$, $\text{C}_5\text{H}_4\text{CH}_2\text{CH}_2$, $\text{PCH}_2\text{CH}_2\text{CH}_2$, CH_3 , $\text{PCH}_2\text{CH}_2\text{CH}_2$). ^{19}F NMR (376.4 MHz, CDCl_3): δ -77.2 . ^{31}P NMR (242.7 MHz, CDCl_3): δ 31.8 (s). FT-IR (KBr): 638 (m), 827 (w), 1031 (m), 1159 (m), 1267 (s), 1656 (br, w), 1730 (br, m), 2937 (br, w), 3099 (br, w) cm^{-1} . UV-vis (CH_2Cl_2): λ_{max} 438 nm ($\epsilon = 310 \text{ M}^{-1} \text{ cm}^{-1}$). Anal. Calcd. (%) for $(\text{C}_{44}\text{H}_{50}\text{PFe}_3\text{O}_5\text{SF}_3)_n$: C, 55.84; H, 5.32; S, 3.39. Found: C, 56.96; H, 5.56; S, 3.50. GPC (DMF, 0.02 M $[n\text{-Bu}_4\text{N}][\text{OTf}]$, 60 °C, conventional calibration vs. PMMA standards): $M_n = 32,400 \text{ g mol}^{-1}$, $M_w = 79,000 \text{ g mol}^{-1}$, $D = 2.44$.

Preparation of Polyelectrolyte **4.10c**

In a 20 mL grease-free Schlenk flask, monomer **4.9** (400 mg, 0.423 mmol) was dissolved in 800 μL of a THF solution containing AIBN (0.23 mg, 0.0014 mmol). The resulting solution was degassed using 3 freeze-pump-thaw cycles before it was stirred at

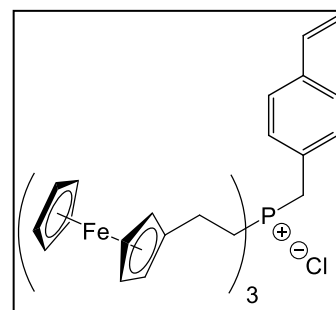


75 $^{\circ}\text{C}$ for 32 h. The solution was concentrated *in vacuo* to yield a dark orange residue before it was dissolved in a minimum amount of CH_2Cl_2 , precipitated in benzene, and centrifuged for 1 min to separate the solids. The solids were collocated and the precipitation process was repeated once in benzene and twice in pentane, respectively. The solid was dried *in vacuo* at 50 $^{\circ}\text{C}$ for 40 h to yield polyelectrolyte **4.10c** as a yellow powder. Yield = 0.30 g, 75%. ^1H NMR (599.4 MHz, CDCl_3): δ 3.50–5.50 (broad, C_5H_5 , $\text{C}_5\text{H}_4\text{R}$ and $\text{CH}_2\text{CH}_2\text{O}$), 0.50–3.20, (broad, saturated polymer backbone CH_2 , $\text{C}_5\text{H}_4\text{CH}_2$, $\text{C}_5\text{H}_4\text{CH}_2\text{CH}_2$, $\text{PCH}_2\text{CH}_2\text{CH}_2$, CH_3 , $\text{PCH}_2\text{CH}_2\text{CH}_2$). ^{19}F NMR (376.4 MHz, CDCl_3): δ -77.2. ^{31}P NMR (242.7 MHz, CDCl_3): δ 31.9 (s). FT-IR (KBr): 638 (m), 827 (w), 1032 (m), 1161 (m), 1265 (s), 1651 (br, m), 1732 (br, m), 2935 (br, w), 3101 (br, w) cm^{-1} . UV-vis (CH_2Cl_2): λ_{max} 440 nm ($\epsilon = 323 \text{ M}^{-1} \text{ cm}^{-1}$). Anal. Calcd. (%) for $(\text{C}_{44}\text{H}_{50}\text{PFe}_3\text{O}_5\text{SF}_3)_n$: C, 55.84; H, 5.32; S, 3.39. Found: C, 55.86; H, 5.54; S, 3.58. GPC (DMF, 0.02 M [*n*-Bu $_4$ N][OTf], 60 $^{\circ}\text{C}$, conventional calibration vs. PMMA standards): $M_n = 45,100 \text{ g mol}^{-1}$, $M_w = 105,700 \text{ g mol}^{-1}$, $D = 2.34$.

Representative Procedure for the Preparation of **4.12a–d**

Phosphonium Chloride Salt **4.12a** ($3 \times \text{Fc}$)

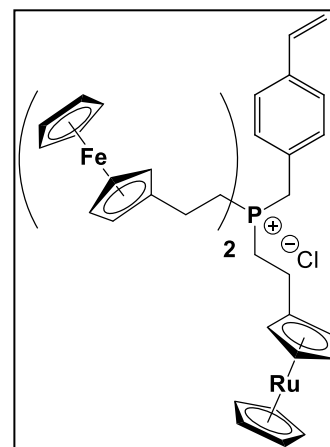
In a sealed tube, tertiary phosphine **4.11a** (1.00 g, 1.49 mmol) and 4-vinylbenzyl chloride (230 μL , 1.63 mmol, 1.1 equiv.) were combined with DMF/THF (5/1, 12 mL) before the mixture was heated with stirring for 1 h at 75 $^{\circ}\text{C}$. After cooling to room temperature, the flask was opened to air and the phosphonium chloride salt was extracted with CHCl_3 (3×40



mL), washed with H₂O (5 × 20 mL), dried over MgSO₄, and concentrated *in vacuo*. The resulting oily orange residue was then dissolved in a minimum amount of CH₂Cl₂ and precipitated into pentane. The powder produced was isolated by centrifugation before it was again dissolved, precipitated, and filtered to yield **4.12a** as an orange powder. Yield = 1.20 g, 98%. M.p. : 74–76 °C. ¹H NMR (DMSO-*d*₆): δ 7.59 (d, ³J_{HH} = 8 Hz, 2H, aryl CH), 7.46 (dd, ³J_{HH} = 8 Hz, ⁵J_{HP} = 2 Hz, 2H, aryl CH), 6.74 (dd, ³J_{HH,cis} = 11 Hz, ³J_{HH,trans} = 18 Hz, 1H, ArCH=CH₂), 5.86 (d, ³J_{HH,trans} = 18 Hz, 1H, ArCH=CH₂), 5.26 (d, ³J_{HH,cis} = 11 Hz, 1H, ArCH=CH₂), 4.17 (*pseudo-t*, ³J_{HH} = 2 Hz, 6H, β-C₅H₄R), 4.12 (s, 15H, C₅H₅), 4.10 (*pseudo-t*, ³J_{HH} = 2 Hz, 6H, α-C₅H₄R), 4.06 (d, ²J_{HP} = 15 Hz, 2H, PCH₂Ar), 2.59–2.43 (m, 12H, C₅H₄CH₂CH₂ and C₅H₄CH₂CH₂, overlaps with residual CD₃CD₂H₂SO signal). ¹³C{¹H} NMR (DMSO-*d*₆): δ 137.0 (d, J_{CP} = 3 Hz), 135.9 (d, J_{CP} = 2 Hz), 130.4 (d, J_{CP} = 6 Hz), 128.8 (d, J_{CP} = 8 Hz), 127.0 (d, J_{CP} = 3 Hz), 115.1 (s), 86.8 (d, J_{CP} = 17 Hz), 68.5 (s), 67.7 (s), 67.4 (s), 25.4 (d, J_{CP} = 43 Hz), 20.8 (d, J_{CP} = 2 Hz), 19.3 (d, J_{CP} = 44 Hz). ³¹P{¹H} NMR (DMSO-*d*₆): δ 31.1 (s). FT-IR: 3092 (w), 3009 (w), 2922 (m), 2455 (w), 1629 (w), 1511 (w), 1410 (w), 1219 (w), 1105 (m), 1000 (m), 922 (w), 820 (m), 753 (s), 660 (w) cm⁻¹. UV-vis (THF): λ_{max} 285 nm (ε = 2,620 M⁻¹ cm⁻¹), 295 nm (ε = 1,380 M⁻¹ cm⁻¹), 325 nm (ε = 290 M⁻¹ cm⁻¹), 436 nm (ε = 300 M⁻¹ cm⁻¹). Mass Spec. (ESI, +ve mode): exact mass calculated for [C₄₅H₄₈⁵⁶Fe₃P]⁺: 787.1542; exact mass found: 787.1563; difference: +2.7 ppm.

Phosphonium Chloride Salt **4.12b** (2 × Fc, 1 × Rc)

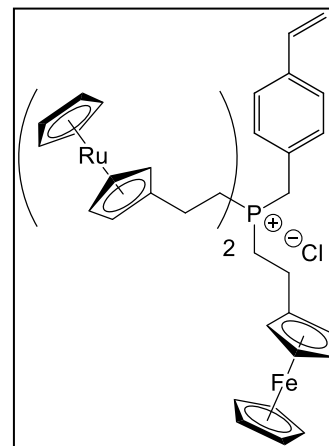
From tertiary phosphine **4.11b** (1.00 g, 1.40 mmol) and 4-vinylbenzyl chloride (217 μL, 1.54 mmol, 1.1 equiv.). Yield = 1.16 g, 96%. M.p. : 80–82 °C. ¹H NMR (DMSO-*d*₆): δ 7.62 (d, ³J_{HH} = 8 Hz, 2H, aryl CH), 7.48 (dd, ³J_{HH} = 7 Hz, ⁵J_{HP} = 2 Hz, 2H, aryl CH), 6.78 (dd, ³J_{HH,cis} = 11 Hz, ³J_{HH,trans} = 18 Hz, 1H, ArCH=CH₂), 5.90 (d, ³J_{HH,trans} = 18 Hz, 1H, ArCH=CH₂), 5.30 (d, ³J_{HH,cis} = 11 Hz, 1H, ArCH=CH₂), 4.65 [s, 2H, β-C₅H₄R(Ru)], 4.57 [s, 5H, C₅H₅(Ru)], 4.51 [s, 2H, α-C₅H₅R(Ru)], 4.21 [s, 4H, β-C₅H₄R(Fe)], 4.16 [s, 10H, C₅H₅(Fe)], 4.13 [s, 4H, α-C₅H₅R(Fe)], 4.10 (d, ²J_{HP} = 16 Hz, 2H, PCH₂Ar), 2.65–2.30 (m,



12H, C₅H₄CH₂CH₂ and C₅H₄CH₂CH₂, overlaps with residual CD₃CD₂HSO signal). ¹³C{¹H} NMR (DMSO-*d*₆): δ 137.0 (d, *J*_{CP} = 3 Hz), 135.9 (s), 130.4 (d, *J*_{CP} = 5 Hz), 128.8 (d, *J*_{CP} = 9 Hz), 126.9 (d, *J*_{CP} = 3 Hz), 115.1 (s), 91.2 (d, *J*_{CP} = 18 Hz), 86.8 (d, *J*_{CP} = 17 Hz), 70.6 (s), 70.4 (s), 69.6 (s), 68.4 (s), 67.7 (s), 67.3 (s), 25.3 (d, *J*_{CP} = 43 Hz), 20.8 (s), 20.2 (s), 20.0 (d, *J*_{CP} = 45 Hz), 19.3 (d, *J*_{CP} = 45 Hz). ³¹P{¹H} NMR (DMSO-*d*₆): δ 30.9 (s). FT-IR: 3091 (w), 3008 (w), 2922 (m), 2455 (w), 1629 (w), 1511 (w), 1410 (w), 1221 (w), 1104 (m), 999 (m), 918 (w), 811 (m), 753 (s), 661 (w) cm⁻¹. UV-vis (THF): λ_{max} 287 nm (ε = 2,170 M⁻¹ cm⁻¹), 295 nm (ε = 1,290 M⁻¹ cm⁻¹), 320 nm (ε = 420 M⁻¹ cm⁻¹), 431 nm (ε = 220 M⁻¹ cm⁻¹). Mass Spec. (ESI, +ve mode): exact mass calculated for [C₄₅H₄₈⁵⁶Fe₂P¹⁰²Ru]⁺: 833.1236; exact mass found: 833.1259; difference: +2.8 ppm.

Phosphonium Chloride Salt **4.12c** (1 × Fc, 2 × Rc)

From tertiary phosphine **4.11c** (1.00 g, 1.32 mmol) and 4-vinylbenzyl chloride (204 μL, 1.45 mmol, 1.1 equiv.). Yield = 1.14 g, 95%. M.p. : 84–86 °C. ¹H NMR (DMSO-*d*₆): δ 7.62 (d, ³*J*_{HH} = 8 Hz, 2H, aryl CH), 7.44 (dd, ³*J*_{HH} = 7 Hz, ⁵*J*_{HP} = 2 Hz, 2H, aryl CH), 6.78 (dd, ³*J*_{HH,cis} = 11 Hz, ³*J*_{HH,trans} = 18 Hz, 1H, ArCH=CH₂), 5.92 (d, ³*J*_{HH,trans} = 18 Hz, 1H, ArCH=CH₂), 5.31 (d, ³*J*_{HH,cis} = 11 Hz, 1H, ArCH=CH₂), 4.65 [s, 4H, β-C₅H₄R(Ru)], 4.56 [s, 10H, C₅H₅(Ru)], 4.52 [s, 4H, α-C₅H₅R(Ru)], 4.21 [*pseudo-t*, ³*J*_{HH} = 2 Hz, 2H, β-C₅H₄R(Fe)],

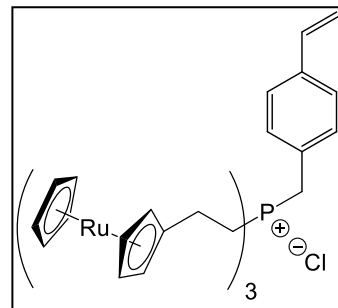


4.16 [s, 5H, C₅H₅(Fe)], 4.14 [*pseudo-t*, ³*J*_{HH} = 2 Hz, 2H, α-C₅H₅R(Fe)], 4.06 (d, ²*J*_{HP} = 16 Hz, 2H, PCH₂Ar), 2.60–2.30 (m, 12H, C₅H₄CH₂CH₂ and C₅H₄CH₂CH₂, overlaps with residual CD₃CD₂HSO signal). ¹³C{¹H} NMR (DMSO-*d*₆): δ 137.0 (d, *J*_{CP} = 5 Hz), 135.9 (s), 130.3 (d, *J*_{CP} = 5 Hz), 128.7 (d, *J*_{CP} = 9 Hz), 126.9 (d, *J*_{CP} = 3 Hz), 115.1 (s), 91.1 (d, *J*_{CP} = 17 Hz), 86.7 (d, *J*_{CP} = 17 Hz), 70.6 (s), 70.4 (s), 69.7 (s), 68.4 (s), 67.7 (s), 67.4 (s), 25.3 (d, *J*_{CP} = 43 Hz), 20.8 (s), 20.3 (d, *J*_{CP} = 3 Hz), 20.0 (d, *J*_{CP} = 44 Hz), 19.3 (d, *J*_{CP} = 45 Hz). ³¹P{¹H} NMR (DMSO-*d*₆): δ 30.8 (s). FT-IR: 3095 (w), 3010 (w), 2923 (m), 2455 (w), 1630 (w), 1511 (w), 1409 (w), 1219 (w), 1101 (m), 998 (m), 918 (w), 810 (m), 753 (s), 666 (w) cm⁻¹. UV-vis (THF): λ_{max} 287 nm (ε = 2,520 M⁻¹ cm⁻¹), 295 nm (ε = 1,600 M⁻¹ cm⁻¹), 320 nm (ε = 680 M⁻¹ cm⁻¹), 434 nm (ε = 150 M⁻¹ cm⁻¹). Mass Spec. (ESI, +ve

mode): exact mass calculated for $[\text{C}_{45}\text{H}_{48}^{56}\text{FeP}^{96}\text{Ru}^{99}\text{Ru}]^+$: 870.0978; exact mass found: 870.1002; difference: +2.8 ppm.

Phosponium Chloride Salt **4.12d** ($3 \times \text{Rc}$)

From tertiary phosphine **4.11d** (1.00 g, 1.24 mmol) and 4-vinylbenzyl chloride (192 μL , 1.36 mmol, 1.1 eq). Yield = 1.12 g, 94%. M.p. : 102–104 $^\circ\text{C}$. ^1H NMR (DMSO- d_6): δ 7.62 (d, $^3J_{\text{HH}} = 8$ Hz, 2H, aryl CH), 7.40 (dd, $^3J_{\text{HH}} = 8$ Hz, $^5J_{\text{HP}} = 2$ Hz, 2H, aryl CH), 6.77 (dd, $^3J_{\text{HH},\text{cis}} = 11$ Hz, $^3J_{\text{HH},\text{trans}} = 18$ Hz, 1H, ArCH=CH $_2$), 5.90 (d, $^3J_{\text{HH},\text{trans}} = 18$ Hz, 1H, ArCH=CH $_2$),

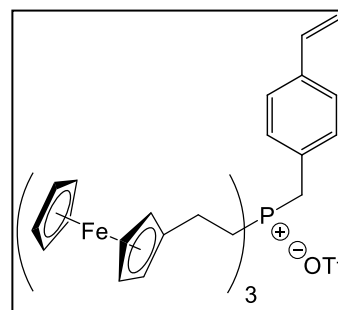


5.31 (d, $^3J_{\text{HH},\text{cis}} = 11$ Hz, 1H, ArCH=CH $_2$), 4.64 (*pseudo-t*, $^3J_{\text{HH}} = 2$ Hz, 6H, β -C $_5$ H $_4$ R), 4.55 (s, 15H, C $_5$ H $_5$), 4.51 (*pseudo-t*, $^3J_{\text{HH}} = 2$ Hz, 6H, α -C $_5$ H $_4$ R), 3.98 (d, $^2J_{\text{HP}} = 15$ Hz, 2H, PCH $_2$ Ar), 2.27–2.47 (m, 12H, C $_5$ H $_4$ CH $_2$ CH $_2$ and C $_5$ H $_4$ CH $_2$ CH $_2$). $^{13}\text{C}\{^1\text{H}\}$ NMR (DMSO- d_6): δ 137.1 (d, $J_{\text{CP}} = 3$ Hz), 135.9 (s), 130.3 (d, $J_{\text{CP}} = 5$ Hz), 128.6 (d, $J_{\text{CP}} = 9$ Hz), 127.0 (s), 115.3 (s), 91.1 (d, $J_{\text{CP}} = 18$ Hz), 70.6 (s), 70.5 (s), 69.8 (s), 25.4 (d, $J_{\text{CP}} = 44$ Hz), 20.4 (s), 20.0 (d, $J_{\text{CP}} = 45$ Hz). $^{31}\text{P}\{^1\text{H}\}$ NMR (DMSO- d_6): δ 30.8 (s). FT-IR: 3093 (w), 3010 (w), 2919 (m), 2460 (w), 1670 (w), 1511 (w), 1409 (m), 1218 (w), 1100 (m), 997 (m), 917 (w), 809 (s), 752 (s), 660 (w) cm^{-1} . UV-vis (THF): λ_{max} 287 nm ($\epsilon = 2,060 \text{ M}^{-1} \text{ cm}^{-1}$), 297 nm ($\epsilon = 1,560 \text{ M}^{-1} \text{ cm}^{-1}$), 315 nm ($\epsilon = 890 \text{ M}^{-1} \text{ cm}^{-1}$). Mass Spec. (ESI, +ve mode): exact mass calculated for $[\text{C}_{45}\text{H}_{48}^{96}\text{Ru}^{99}\text{Ru}^{100}\text{RuP}]^+$: 914.0671; exact mass found: 914.0678; difference: +0.8 ppm.

Representative Procedure for the Preparation of Phosponium Salts **4.13a–d**

Phosponium Triflate Salt **4.13a** ($3 \times \text{Fc}$)

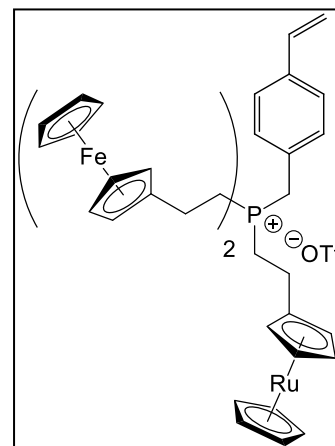
In a Schlenk flask, **4.12a** (1.00 g, 1.22 mmol) was dissolved in dry and degassed CHCl_3 (10 mL) before NaOTf (0.63 g, 3.6 mmol, 3 equiv.) was charged into the reaction flask. The resulting mixture was stirred at 20 $^\circ\text{C}$ for 16 h, gravity filtered to remove precipitate, washed with H_2O (3×10 mL), dried



over MgSO_4 , and gravity filtered. NaOTf (0.21 g, 1.2 mmol, 1 equiv.) was once again charged into a flask containing the filtrate before the contents were stirred for an additional 16 h. The reaction mixture was then gravity filtered to remove precipitate, washed with H_2O ($3 \times 10 \text{ mL}$), dried over MgSO_4 , and gravity filtered before it was concentrated *in vacuo*. The resulting orange residue was then dried *in vacuo* for 2 h at $45 \text{ }^\circ\text{C}$ to remove residual solvent to afford monomer **4.13a** as an orange solid. Yield = 1.12 g, 98%. M.p. : $66\text{--}68 \text{ }^\circ\text{C}$. ^1H NMR ($\text{DMSO-}d_6$): δ 7.61 (d, $^3J_{\text{HH}} = 8 \text{ Hz}$, 2H, aryl CH), 7.44 (dd, $^3J_{\text{HH}} = 8 \text{ Hz}$, $^5J_{\text{HP}} = 2 \text{ Hz}$, 2H, aryl CH), 6.76 (dd, $^3J_{\text{HH,cis}} = 11 \text{ Hz}$, $^3J_{\text{HH,trans}} = 18 \text{ Hz}$, 1H, $\text{ArCH}=\text{CH}_2$), 5.89 (d, $^3J_{\text{HH,trans}} = 18 \text{ Hz}$, 1H, $\text{ArCH}=\text{CH}_2$), 5.29 (d, $^3J_{\text{HH,cis}} = 11 \text{ Hz}$, 1H, $\text{ArCH}=\text{CH}_2$), 4.19 (s, 6H, $\beta\text{-C}_5\text{H}_4\text{R}$), 4.14 (s, 15H, C_5H_5), 4.13 (s, 6H, $\alpha\text{-C}_5\text{H}_4\text{R}$), 3.96 (d, $^2J_{\text{HP}} = 15 \text{ Hz}$, 2H, PCH_2Ar), 2.60–2.42 (m, 12H, $\text{C}_5\text{H}_4\text{CH}_2\text{CH}_2$ and $\text{C}_5\text{H}_4\text{CH}_2\text{CH}_2$, overlaps with residual $\text{CD}_3\text{CD}_2\text{HSO}$ signal). $^{13}\text{C}\{^1\text{H}\}$ NMR ($\text{DMSO-}d_6$): δ 137.1 (d, $J_{\text{CP}} = 5 \text{ Hz}$), 135.9 (s), 130.4 (d, $J_{\text{CP}} = 3 \text{ Hz}$), 128.6 (d, $J_{\text{CP}} = 9 \text{ Hz}$), 127.0 (s), 120.7 (q, $J_{\text{CF}} = 322 \text{ Hz}$), 115.2 (s), 86.8 (d, $J_{\text{CP}} = 18 \text{ Hz}$), 68.4 (s), 67.7 (s), 67.4 (s), 25.4 (d, $J_{\text{CP}} = 44 \text{ Hz}$), 20.8 (s), 19.2 (d, $J_{\text{CP}} = 45 \text{ Hz}$). ^{19}F NMR ($\text{DMSO-}d_6$): δ -77.6 (s). $^{31}\text{P}\{^1\text{H}\}$ NMR ($\text{DMSO-}d_6$): δ 31.2 (s). FT-IR: 3095 (w), 3010 (w), 2913 (w), 1512 (w), 1410 (w), 1262 (s), 1157 (m), 1124 (w), 1105 (w), 1030 (s), 1000 (w), 922 (w), 821 (m), 754 (m), 637 (s) cm^{-1} . UV-vis (THF): λ_{max} 285 nm ($\epsilon = 2,470 \text{ M}^{-1} \text{ cm}^{-1}$), 295 nm ($\epsilon = 1,290 \text{ M}^{-1} \text{ cm}^{-1}$), 325 nm ($\epsilon = 260 \text{ M}^{-1} \text{ cm}^{-1}$), 436 nm ($\epsilon = 320 \text{ M}^{-1} \text{ cm}^{-1}$). Mass Spec. (ESI, +ve mode): exact mass calculated for $[\text{C}_{45}\text{H}_{48}^{56}\text{Fe}_3\text{P}]^+$: 787.1542; exact mass found: 787.1564; difference: +2.7 ppm. Anal. Calcd. (%) for $\text{C}_{46}\text{H}_{48}\text{F}_3\text{Fe}_3\text{O}_3\text{PS}$: C, 59.00; H, 5.17. Found: C, 58.94; H, 5.37.

Phosphonium Triflate Salt **4.13b** ($2 \times \text{Fc}$, $1 \times \text{Rc}$)

From phosphonium chloride **4.12b** (1.00 g, 1.15 mmol) and NaOTf (0.60 g, 3.5 mmol, 3 equiv. for the first metathesis reaction and 0.20 g, 1.2 mmol, 1 equiv. for the second metathesis reaction). Yield = 1.11 g, 98%. M.p. : $68\text{--}70 \text{ }^\circ\text{C}$. ^1H NMR ($\text{DMSO-}d_6$): δ 7.64 (d, $^3J_{\text{HH}} = 8 \text{ Hz}$, 2H, aryl CH), 7.44 (d, $^3J_{\text{HH}} = 7 \text{ Hz}$, 2H, aryl CH), 6.78 (dd, $^3J_{\text{HH,cis}} = 11 \text{ Hz}$, $^3J_{\text{HH,trans}} = 18 \text{ Hz}$, 1H, $\text{ArCH}=\text{CH}_2$), 5.91 (d, $^3J_{\text{HH,trans}} = 18 \text{ Hz}$, 1H, $\text{ArCH}=\text{CH}_2$), 5.31 (d, $^3J_{\text{HH,cis}} = 11 \text{ Hz}$, 1H, $\text{ArCH}=\text{CH}_2$),

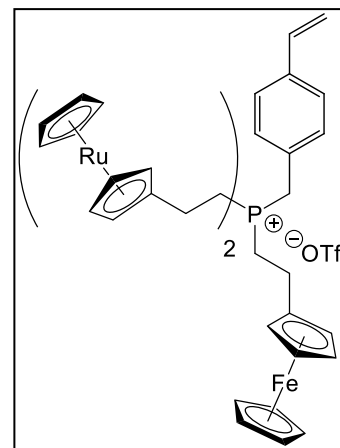


4.64 [s, 2H, β -C₅H₄R(Ru)], 4.56 [s, 5H, C₅H₅(Ru)], 4.52 [s, 2H, α -C₅H₅R(Ru)], 4.20 [s, 4H, β -C₅H₄R(Fe)], 4.15 [s, 10H, C₅H₅(Fe)], 4.14 [s, 4H, α -C₅H₅R(Fe)], 3.96 (d, $^2J_{\text{HP}} = 15$ Hz, 2H, PCH₂Ar), 2.57–2.32 (m, 12H, C₅H₄CH₂CH₂ and C₅H₄CH₂CH₂, overlaps with residual CD₃CD₂HSO signal). ¹³C{¹H} NMR (DMSO-*d*₆): δ 137.2 (d, $J_{\text{CP}} = 3$ Hz), 135.9 (s), 130.4 (d, $J_{\text{CP}} = 6$ Hz), 128.6 (d, $J_{\text{CP}} = 9$ Hz), 127.1 (d, $J_{\text{CP}} = 2$ Hz), 120.7 (q, $J_{\text{CF}} = 322$ Hz), 115.3 (d, $J_{\text{CP}} = 164$ Hz), 91.2 (d, $J_{\text{CP}} = 18$ Hz), 86.8 (d, $J_{\text{CP}} = 17$ Hz), 70.6 (s), 70.5 (s), 69.8 (s), 68.5 (s), 67.8 (s), 67.5 (s), 25.4 (d, $J_{\text{CP}} = 43$ Hz), 20.9 (s), 20.3 (s), 20.1 (d, $J_{\text{CP}} = 45$ Hz), 19.3 (d, $J_{\text{CP}} = 45$ Hz). ¹⁹F NMR (DMSO-*d*₆): δ -77.8 (s). ³¹P{¹H} NMR (DMSO-*d*₆): δ 31.0 (s). FT-IR: 3089 (w), 3011 (w), 2912 (w), 1630 (w), 1512 (w), 1410 (w), 1262 (s), 1224 (m), 1158 (m), 1104 (w), 1030 (s), 999 (w), 919 (w), 813 (m), 755 (s), 637 (s) cm⁻¹. UV-vis (THF): λ_{max} 284 nm ($\epsilon = 2,860$ M⁻¹ cm⁻¹), 295 nm ($\epsilon = 1,390$ M⁻¹ cm⁻¹), 320 nm ($\epsilon = 440$ M⁻¹ cm⁻¹), 431 nm ($\epsilon = 240$ M⁻¹ cm⁻¹). Mass Spec. (ESI, +ve mode): exact mass calculated for [C₄₅H₄₈⁵⁶Fe₂P⁹⁶Ru]⁺: 827.1268; exact mass found: 827.1274; difference: +0.7 ppm. Anal. Calcd. (%) for C₄₆H₄₈F₃Fe₂O₃PRuS: C, 56.28; H, 4.93. Found: C, 56.22; H, 5.11.

Phosphonium Triflate Salt **4.13c** (1 × Fc, 2 × Rc)

From phosphonium chloride **4.12c** (1.00 g, 1.10 mmol) and NaOTf (0.57 g, 3.3 mmol, 3 equiv. for the first metathesis reaction and 0.19 g, 1.1 mmol, 1 equiv. for the second metathesis reaction). Yield = 1.09 g, 97%. M.p. : 70–72 °C.

¹H NMR (DMSO-*d*₆): δ 7.64 (d, $^3J_{\text{HH}} = 8$ Hz, 2H, aryl CH), 7.42 (d, $^3J_{\text{HH}} = 8$ Hz, 2H, aryl CH), 6.78 (dd, $^3J_{\text{HH},\text{cis}} = 11$ Hz, $^3J_{\text{HH},\text{trans}} = 18$ Hz, 1H, ArCH=CH₂), 5.92 (d, $^3J_{\text{HH},\text{trans}} = 18$ Hz, 1H, ArCH=CH₂), 5.32 (d, $^3J_{\text{HH},\text{cis}} = 11$ Hz, 1H, ArCH=CH₂), 4.65 [s, 4H, β -C₅H₄R(Ru)], 4.56 [s, 10H, C₅H₅(Ru)], 4.52 [s,



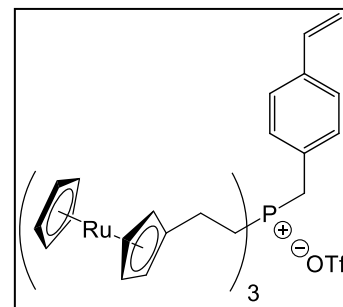
4H, α -C₅H₅R(Ru)], 4.21 [s, 2H, β -C₅H₄R(Fe)], 4.16 [s, 5H, C₅H₅(Fe)], 4.15 [s, 2H, α -C₅H₅R(Fe)], 3.96 (d, $^2J_{\text{HP}} = 15$ Hz, 2H, PCH₂Ar), 2.57–2.21 (m, 12H, C₅H₄CH₂CH₂ and C₅H₄CH₂CH₂, overlaps with residual CD₃CD₂HSO signal). ¹³C{¹H} NMR (DMSO-*d*₆): δ 137.1 (d, $J_{\text{CP}} = 3$ Hz), 135.9 (s), 130.3 (d, $J_{\text{CP}} = 5$ Hz), 128.5 (d, $J_{\text{CP}} = 8$ Hz), 127.0 (d, $J_{\text{CP}} = 2$ Hz), 115.2 (s), 91.0 (d, $J_{\text{CP}} = 18$ Hz), 86.7 (d, $J_{\text{CP}} = 17$ Hz), 70.6 (s), 70.4 (s), 69.7 (s),

68.4 (s), 67.6 (s), 67.4 (s), 25.3 (d, $J_{CP} = 44$ Hz), 20.8 (s), 20.2 (s), 19.9 (d, $J_{CP} = 45$ Hz), 19.2 (d, $J_{CP} = 45$ Hz). ^{19}F NMR (DMSO- d_6): δ -77.7 (s). $^{31}\text{P}\{^1\text{H}\}$ NMR (DMSO- d_6): δ 30.9 (s). FT-IR: 3093 (w), 3013 (w), 2911 (w), 1630 (w), 1512 (w), 1410 (w), 1262 (s), 1224 (s), 1159 (s), 1101 (m), 1030 (s), 998 (w), 918 (w), 811 (m), 756 (s), 637 (s) cm^{-1} . UV-vis (THF): λ_{max} 283 nm ($\epsilon = 3,260 \text{ M}^{-1} \text{ cm}^{-1}$), 295 nm ($\epsilon = 1,770 \text{ M}^{-1} \text{ cm}^{-1}$), 320 nm ($\epsilon = 730 \text{ M}^{-1} \text{ cm}^{-1}$), 434 nm ($\epsilon = 140 \text{ M}^{-1} \text{ cm}^{-1}$). Mass Spec. (ESI, +ve mode): exact mass calculated for $[\text{C}_{45}\text{H}_{48}^{56}\text{FeP}^{96}\text{Ru}^{99}\text{Ru}]^+$: 870.0978; exact mass found: 870.1000; difference: +2.5 ppm. Anal. Calcd. (%) for $\text{C}_{46}\text{H}_{48}\text{F}_3\text{FeO}_3\text{PRu}_2\text{S}$: C, 53.80; H, 4.71. Found: C, 53.94; H, 4.77.

Phosphonium Triflate Salt **4.13d** (3 \times Rc)

From phosphonium chloride **4.12d** (1.00 g, 1.04 mmol) and NaOTf (0.54 g, 3.1 mmol, 3 equiv. for the first metathesis reaction and 0.18 g, 1.1 mmol, 1 equiv. for the second metathesis reaction). Yield = 1.07 g, 96%. M.p. : 88–90 °C.

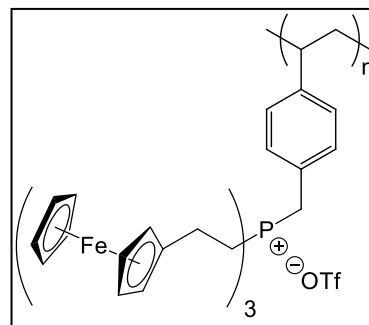
^1H NMR (DMSO- d_6): δ 7.62 (d, $^3J_{\text{HH}} = 8$ Hz, 2H, aryl CH), 7.38 (dd, $^3J_{\text{HH}} = 8$ Hz, $^5J_{\text{HP}} = 2$ Hz, 2H, aryl CH), 6.78 (dd, $^3J_{\text{HH},\text{cis}} = 11$ Hz, $^3J_{\text{HH},\text{trans}} = 18$ Hz, 1H, ArCH=CH₂), 5.92 (d, $^3J_{\text{HH},\text{trans}} = 18$ Hz, 1H, ArCH=CH₂), 5.32 (d, $^3J_{\text{HH},\text{cis}} = 11$ Hz, 1H, ArCH=CH₂), 4.64 (*pseudo-t*, $^3J_{\text{HH}} = 2$ Hz, 6H, β -C₅H₄R), 4.56 (s, 15H, C₅H₅), 4.52 (*pseudo-t*, $^3J_{\text{HH}} = 2$ Hz, 6H, α -C₅H₄R), 3.94 (d, $^2J_{\text{HP}} = 15$ Hz, 2H, PCH₂Ar), 2.49–2.25 (m, 12H, C₅H₄CH₂CH₂ and C₅H₄CH₂CH₂). $^{13}\text{C}\{^1\text{H}\}$ NMR (DMSO- d_6): δ 137.1 (s), 135.8 (s), 130.3 (s), 128.5 (d, $J_{\text{CP}} = 8$ Hz), 127.0 (s), 120.6 (q, $J_{\text{CF}} = 321$ Hz), 115.2 (s), 91.0 (d, $J_{\text{CP}} = 17$ Hz), 70.6 (s), 70.4 (s), 69.7 (s), 25.3 (d, $J_{\text{CP}} = 44$ Hz), 20.3 (s), 20.0 (d, $J_{\text{CP}} = 45$ Hz). ^{19}F NMR (DMSO- d_6): δ -77.7 (s). $^{31}\text{P}\{^1\text{H}\}$ NMR (DMSO- d_6): δ 30.8 (s). FT-IR: 3094 (w), 3013 (w), 2911 (w), 1630 (w), 1512 (w), 1409 (w), 1261 (s), 1159 (m), 1101 (w), 1030 (s), 997 (w), 917 (w), 810 (m), 755 (s), 637 (s) cm^{-1} . UV-vis (THF): λ_{max} 286 nm ($\epsilon = 1,970 \text{ M}^{-1} \text{ cm}^{-1}$), 296 nm ($\epsilon = 1,510 \text{ M}^{-1} \text{ cm}^{-1}$), 315 nm ($\epsilon = 910 \text{ M}^{-1} \text{ cm}^{-1}$). Mass Spec. (ESI, +ve mode): exact mass calculated for $[\text{C}_{45}\text{H}_{48}^{96}\text{Ru}^{99}\text{Ru}^{100}\text{RuP}]^+$: 914.0671; exact mass found: 914.0664; difference: -0.8 ppm. Anal. Calcd. (%) for $\text{C}_{46}\text{H}_{48}\text{F}_3\text{O}_3\text{PRu}_3\text{S}$: C, 51.53; H, 4.51. Found: C, 51.84; H, 4.62.



Representative Procedure for the Preparation of Polyelectrolytes 4.14a–d

Polyelectrolyte **4.14a** ($3 \times \text{Fc}$)

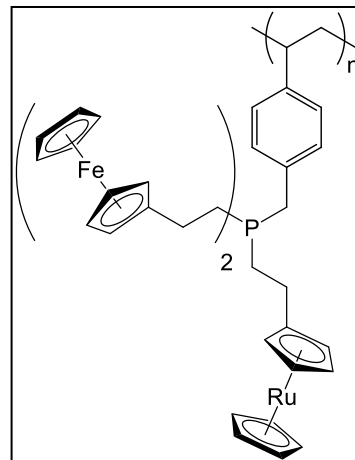
In a grease-free Schlenk flask, monomer **4.13a** (0.25 g, 0.27 mmol) was dissolved in 1.00 mL of a THF stock solution containing AIBN (0.2 mg, 0.001 mmol). The resulting solution was degassed during 3 freeze-pump-thaw cycles before the flask was sealed and the solution was stirred at 85 °C for 16 h. After cooling to room



temperature, the polymerization mixture was poured into diethyl ether and the solids were separated by centrifugation before they were collected, dissolved in a minimum amount of CH_2Cl_2 , and precipitated in Et_2O . This precipitation/centrifugation process was repeated once more in Et_2O and pentane. The polyelectrolyte **4.14a** was dried *in vacuo* at 50 °C for 16 h to yield a yellow powder. Yield = 0.25 g, 98%. ^1H NMR ($\text{DMSO-}d_6$, 125 °C): δ 6.94 (s, br, 2H, aryl CH), 6.19 (s, br, 2H, aryl CH), 4.17 (s, br, 27H, α - $\text{C}_5\text{H}_4\text{R}$, β - $\text{C}_5\text{H}_4\text{R}$, and C_5H_5), 3.77 (s, br, 2H, PCH_2Ar), 2.61 (s, br, 6H, $\text{C}_5\text{H}_4\text{CH}_2\text{CH}_2$), 2.45 (s, br, 6H, $\text{C}_5\text{H}_4\text{CH}_2\text{CH}_2$, overlaps with residual $\text{CD}_3\text{CD}_2\text{HSO}$ signal), 1.96 (s, 1H, br, ArCHCH_2), and 1.32 (s, br, 2H, ArCHCH_2). ^{19}F NMR ($\text{DMSO-}d_6$, 125 °C): δ -77.1 (s). $^{31}\text{P}\{^1\text{H}\}$ NMR ($\text{DMSO-}d_6$, 125 °C): δ 31.1 (s). FT-IR: 3094 (w), 2949 (w), 2919 (w), 1510 (w), 1410 (w), 1261 (s), 1159 (m), 1105 (w), 1030 (s), 1001 (w), 822 (m), 756 (s), 637 (s) cm^{-1} . UV-vis (THF): λ_{max} 325 nm ($\epsilon = 260 \text{ M}^{-1} \text{ cm}^{-1}$), 436 nm ($\epsilon = 330 \text{ M}^{-1} \text{ cm}^{-1}$). GPC (DMF, 0.02 M $[\text{n-Bu}_4\text{N}][\text{OTf}]$, 60 °C, conventional calibration vs. PS standards): $M_n = 46,900 \text{ g mol}^{-1}$, $M_w = 148,000 \text{ g mol}^{-1}$, $D = 3.16$.

Polyelectrolyte **4.14b** (2 × Fc, 1 × Rc)

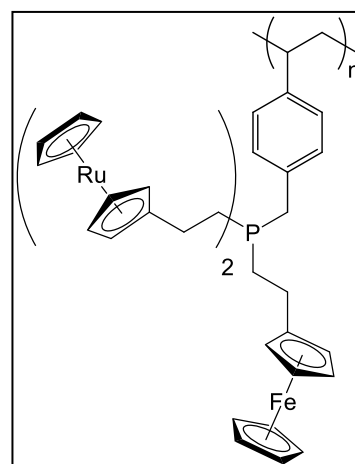
From monomer **4.13b** (0.25 g, 0.26 mmol) and AIBN (0.2 mg, 0.001 mmol). Yield = 0.24 g, 96%. ^1H NMR (DMSO- d_6 , 125 °C): δ 6.94 (s, br, 2H, aryl CH), 6.21 (s, br, 2H, aryl CH), 4.63 [s, br, 2H, β -C₅H₄R(Ru)], 4.56 [s, br, 7H, C₅H₅(Ru) and α -C₅H₅R(Ru)], 4.17 [s, br, 18H, α -C₅H₄R(Fe), β -C₅H₄R(Fe), and C₅H₅(Fe)], 3.75 (s, br, 2H, PCH₂Ar), 2.61 (s, br, 6H, C₅H₄CH₂CH₂), 2.42 (s, br, 6H, C₅H₄CH₂CH₂, overlaps with residual CD₃CD₂HSO signal), 1.96 (s, br, 1H, ArCHCH₂), and 1.34 (s, br, 2H, ArCHCH₂). ^{19}F NMR (DMSO- d_6 , 125



°C): δ -76.3 (s). $^{31}\text{P}\{^1\text{H}\}$ NMR (DMSO- d_6 , 125 °C): δ 30.9 (s). FT-IR: 3093 (w), 3013 (w), 2916 (w), 1510 (w), 1410 (w), 1260 (m), 1221 (m), 1105 (w), 1030 (s), 1000 (w), 814 (w), 772 (s), 637 (m) cm^{-1} . UV-vis (THF): λ_{max} 320 nm ($\epsilon = 440 \text{ M}^{-1} \text{ cm}^{-1}$), 431 nm ($\epsilon = 230 \text{ M}^{-1} \text{ cm}^{-1}$). GPC (DMF, 0.02 M [*n*-Bu₄N][OTf], 60 °C, conventional calibration vs. PS standards): $M_n = 45,100 \text{ g mol}^{-1}$, $M_w = 184,900 \text{ g mol}^{-1}$, $D = 4.10$.

Polyelectrolyte **4.14c** (1 × Fc, 2 × Rc)

From monomer **4.13c** (0.25 g, 0.24 mmol) and AIBN (0.2 mg, 0.001 mmol). Yield = 0.24 g, 97%. ^1H NMR (DMSO- d_6 , 125 °C): δ 6.97 (s, br, 2H, aryl CH), 6.21 (s, br, 2H, aryl CH), 4.63 [s, br, 4H, β -C₅H₄R(Ru)], 4.56 [s, br, 14H, C₅H₅(Ru) and α -C₅H₅R(Ru)], 4.17 [s, br, 9H, α -C₅H₄R(Fe), β -C₅H₄R(Fe), and C₅H₅(Fe)], 3.78 (s, br, 2H, PCH₂Ar), 2.62 (s, br, 6H, C₅H₄CH₂CH₂), 2.42 (s, br, 6H, C₅H₄CH₂CH₂, overlaps with residual CD₃CD₂HSO signal), 1.90 (s, br, 1H, ArCHCH₂), and 1.34 (s, br, 2H, ArCHCH₂). ^{19}F NMR

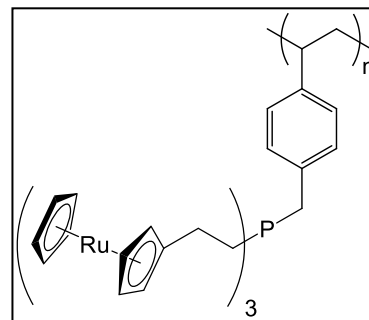


(DMSO- d_6 , 125 °C): δ -76.3 (s). $^{31}\text{P}\{^1\text{H}\}$ NMR (DMSO- d_6 , 125 °C): δ 30.8 (s). FT-IR: 3095 (w), 3014 (w), 2916 (w), 1510 (w), 1410 (w), 1260 (m), 1224 (m), 1101 (w), 1030 (s), 999 (w), 811 (m), 756 (s), 637 (s) cm^{-1} . UV-vis (THF): λ_{max} 320 nm ($\epsilon = 620 \text{ M}^{-1} \text{ cm}^{-1}$)

¹), 434 nm ($\epsilon = 150 \text{ M}^{-1} \text{ cm}^{-1}$). GPC (DMF, 0.02 M $[n\text{-Bu}_4\text{N}][\text{OTf}]$, 60 °C, conventional calibration vs. PS standards): $M_n = 69,100 \text{ g mol}^{-1}$, $M_w = 278,100 \text{ g mol}^{-1}$, $D = 4.02$.

Polyelectrolyte **4.14d** ($3 \times \text{Rc}$)

From monomer **4.13d** (0.25 g, 0.23 mmol) and AIBN (0.2 mg, 0.001 mmol). Yield = 0.24 g, 97%. ¹H NMR (DMSO-*d*₆, 125 °C): δ 6.98 (s, br, 2H, aryl CH), 6.26 (s, br, 2H, aryl CH), 4.63 (s, br, 6H, $\beta\text{-C}_5\text{H}_4\text{R}$), 4.56 (s, br, 21H, C₅H₅, and $\alpha\text{-C}_5\text{H}_5\text{R}$), 3.80 (s, br, 2H, PCH₂Ar), 2.43 (s, br, 12H, C₅H₄CH₂CH₂ and C₅H₄CH₂CH₂), 1.85 (s, br, 1H, ArCHCH₂), and 1.37 (s, br, 2H, ArCHCH₂). ¹⁹F NMR (DMSO-*d*₆, 125 °C): δ -76.5 (s). ³¹P{¹H} NMR (DMSO-*d*₆, 125 °C): δ 30.8 (s). FT-IR: 3095 (w), 3013 (w), 2914 (w), 1510 (w), 1409 (w), 1261 (s), 1224 (m), 1160 (m), 1101 (m), 1030 (s), 997 (w), 810 (m), 755 (m), and 637 (s) cm⁻¹. UV-vis (THF): λ_{max} 315 nm ($\epsilon = 870 \text{ M}^{-1} \text{ cm}^{-1}$). GPC (DMF, 0.02 M $[n\text{-Bu}_4\text{N}][\text{OTf}]$, 60 °C, conventional calibration vs. PS standards): $M_n = 38,650 \text{ g mol}^{-1}$, $M_w = 143,450 \text{ g mol}^{-1}$, $D = 3.71$.



4.5 Notes and References

1. Ho, C.-L.; Wong, W.-Y. *Coord. Chem. Rev.* **2011**, *255*, 2469–2502.
2. Whittell, G. R.; Hager, M. D.; Schubert, U. S.; Manners, I. *Nat. Mater.* **2011**, *10*, 176–188.
3. Astruc, D. *Nat. Chem.* **2012**, *4*, 255–267.
4. Friebe, C.; Hager, M. D.; Winter, A.; Schubert, U. S. *Adv. Mater.* **2012**, *24*, 332–345.
5. Hardy, C. G.; Ren, L.; Zhang, J.; Tang, C. *Isr. J. Chem.* **2012**, *52*, 230–245.
6. Bhattacharjee, H.; Müller, J. *Coord. Chem. Rev.* **2016**, *314*, 114–133.
7. Yan, Y.; Zhang, J.; Ren, L.; Tang, C. *Chem. Soc. Rev.* **2016**, *45*, 5232–5263.
8. Peckham, T. J.; Lough, A. J.; Manners, I. *Organometallics* **1999**, *18*, 1030–1040.
9. Johnson, B. F. G.; Sanderson, K. M.; Shephard, D. S.; Ozkaya, D.; Zhou, W.; Ahmed, H.; Thomas, M. D. R.; Gladden, L.; Mantle, M. *Chem. Commun.* **2000**, 1317–1318.
10. Ma, Y.; Dong, W.-F.; Hempenius, M. A.; Mohwald, H.; Julius Vancso, G. *Nat. Mater.* **2006**, *5*, 724–729.
11. Wang, X.; Guerin, G.; Wang, H.; Wang, Y.; Manners, I.; Winnik, M. A. *Science* **2007**, *317*, 644–647.
12. Ornelas, C.; Ruiz, J.; Belin, C.; Astruc, D. *J. Am. Chem. Soc.* **2009**, *131*, 590–601.
13. Zhan, H.; Lamare, S.; Ng, A.; Kenny, T.; Guernon, H.; Chan, W.-K.; Djurišić, A. B.; Harvey, P. D.; Wong, W.-Y. *Macromolecules* **2011**, *44*, 5155–5167.
14. Al-Badri, Z. M.; Maddikeri, R. R.; Zha, Y.; Thaker, H. D.; Dobriyal, P.; Shunmugam, R.; Russell, T. P.; Tew, G. N. *Nat. Commun.* **2011**, *2*, 482.
15. Ren, L.; Zhang, J.; Hardy, C. G.; Ma, S.; Tang, C. *Macromol. Rapid Commun.* **2012**, *33*, 510–516.

16. Staff, R. H.; Gallei, M.; Mazurowski, M.; Rehahn, M.; Berger, R.; Landfester, K.; Crespy, D. *ACS Nano* **2012**, *6*, 9042–9049.
17. Wang, X.; Cao, K.; Liu, Y.; Tsang, B.; Liew, S. *J. Am. Chem. Soc.* **2013**, *135*, 3399–3402.
18. Rabiee Kenaree, A.; Berven, B. M.; Ragogna, P. J.; Gilroy, J. B. *Chem. Commun.* **2014**, *50*, 10714–10717.
19. Guterman, R.; Rabiee Kenaree, A.; Gilroy, J. B.; Gillies, E. R.; Ragogna, P. J. *Chem. Mater.* **2015**, *27*, 1412–1419.
20. Zhang, J.; Yan, J.; Pageni, P.; Yan, Y.; Wirth, A.; Chen, Y.-P.; Qiao, Y.; Wang, Q.; Decho, A. W.; Tang, C. *Sci. Rep.* **2015**, *5*, 11914.
21. Hadadpour, M.; Gwyther, J.; Manners, I.; Ragogna, P. J. *Chem. Mater.* **2015**, *27*, 3430–3440.
22. Allcock, H. R.; Dodge, J. A.; Manners, I.; Riding, G. H. *J. Am. Chem. Soc.* **1991**, *113*, 9596–9603.
23. Díaz, C.; Valenzuela, M. L. *Macromolecules* **2006**, *39*, 103–111.
24. Sebastian, M.; Hissler, M.; Fave, C.; Rault-Berthelot, J.; Odin, C.; Réau, R. *Angew. Chem. Int. Ed.* **2006**, *45*, 6152–6155.
25. Ainscough, E. W.; Allcock, H. R.; Brodie, A. M.; Gordon, K. C.; Hindenlang, M. D.; Horvath, R.; Otter, C. A. *Eur. J. Inorg. Chem.* **2011**, 3691–3704.
26. Carriedo, G. A.; López, S.; Suárez-Suárez, S.; Presa-Soto, D.; Presa-Soto, A. *Eur. J. Inorg. Chem.* **2011**, 1442–1447.
27. Honeyman, C. H.; Foucher, D. A.; Dahmen, F. Y.; Rulkens, R.; Lough, A. J.; Manners, I. *Organometallics* **1995**, *14*, 5503–5512.

28. Peckham, T. J.; Massey, J. A.; Honeyman, C. H.; Manners, I. *Macromolecules* **1999**, *32*, 2830–2837.
29. Mizuta, T.; Imamura, Y.; Miyoshi, K. *J. Am. Chem. Soc.* **2003**, *125*, 2068–2069.
30. Patra, S. K.; Whittell, G. R.; Nagiah, S.; Ho, C.-L.; Wong, W.-Y.; Manners, I. *Chem. Eur. J.* **2010**, *16*, 3240–3250.
31. Cao, K.; Tsang, B.; Liu, Y.; Chelladural, D.; Power, W. P.; Wang, X. *Organometallics* **2014**, *33*, 531–539.
32. Noonan, K. J. T.; Gillon, B. H.; Cappello, V.; Gates, D. P. *J. Am. Chem. Soc.* **2008**, *130*, 12876–12877.
33. Clendenning, S. B.; Han, S.; Coombs, N.; Paquet, C.; Rayat, M. S.; Grozea, D.; Brodersen, P. M.; Sodhi, R. N. S.; Yip, C. M.; Lu, Z. H.; Manners, I. *Adv. Mater.* **2004**, *16*, 291–296.
34. Chan, W. Y.; Clendenning, S. B.; Berenbaum, A.; Lough, A. J.; Aouba, S.; Ruda, H. E.; Manners, I. *J. Am. Chem. Soc.* **2005**, *127*, 1765–1772.
35. Liu, K.; Clendenning, S. B.; Friebe, L.; Chan, W. Y.; Zhu; Freeman, M. R.; Yang, G. C.; Yip, C. M.; Grozea, D.; Lu, Z.-H.; Manners, I. *Chem. Mater.* **2006**, *18*, 2591–2601.
36. Zamora, M.; Bruña, S.; Alonso, B.; Cuadrado, I. *Macromolecules* **2011**, *44*, 7994–8007.
37. Gilroy, J. B.; Patra, S. K.; Mitchels, J. M.; Winnik, M. A.; Manners, I. *Angew. Chem. Int. Ed.* **2011**, *50*, 5851–5855.
38. Zha, Y.; Thaker, H. D.; Maddikeri, R. R.; Gido, S. P.; Tuominen, M. T.; Tew, G. N. *J. Am. Chem. Soc.* **2012**, *134*, 14534–14541.
39. Zhang, J.; Ren, L.; Hardy, C. G.; Tang, C. *Macromolecules* **2012**, *45*, 6857–6863.

40. Zhang, J.; Yan, Y.; Chance, M. W.; Chen, J.; Hayat, J.; Ma, S.; Tang, C. *Angew. Chem. Int. Ed.* **2013**, *52*, 13387–13391.
41. Zhang, J.; Yan, Y.; Chen, J.; Chance, W. M.; Hayat, J.; Gai, Z.; Tang, C. *Chem. Mater.* **2014**, *26*, 3185–3190.
42. Ciganda, R.; Gu, H.; Castel, P.; Zhao, P.; Ruiz, J.; Hernández, R.; Astruc, D. *Macromol. Rapid Commun.* **2016**, *37*, 105–111.
43. Liu, K.; Ho, C.-L.; Aouba, S.; Zhao, Y.-Q.; Lu, Z.-H.; Petrov, S.; Coombs, N.; Dube, P.; Ruda, H. E.; Wong, W.-Y.; Manners, I. *Angew. Chem. Int. Ed.* **2008**, *47*, 1255–1259.
44. Bagh, B.; Gilroy, J. B.; Staubitz, A.; Müller, J. *J. Am. Chem. Soc.* **2010**, *132*, 1794–1795.
45. Dong, Q.; Li, G.; Ho, C.-L.; Faisal, M.; Leung, C.-W.; Pong, P. W.-T.; Liu, K.; Tang, B.-Z.; Manners, I.; Wong, W.-Y. *Adv. Mater.* **2012**, *24*, 1034–1040.
46. Erhard, M.; Lam, K.; Haddow, M.; Whittell, G. R.; Geiger, W. E.; Manners, I. *Polymer. Chem.* **2014**, *5*, 1264–1274.
47. Russell, A. D.; Whittell, G. R.; Haddow, M. F.; Manners, I. *Organometallics* **2014**, *33*, 5349–5357.
48. Dong, Q.; Li, G.; Wang, H.; Wing-Tat Pong, P.; Leung, C.-W.; Manners, I.; Ho, C.-L.; Li, H.; Wong, W.-Y. *J. Mater. Chem.* **2015**, *3*, 734–741.
49. Braunschweig, H.; Damme, A.; Demeshko, S.; Dück, K.; Kramer, T.; Krummenacher, I.; Meyer, F.; Radacki, K.; Stellwag-Konertz, S.; Whittell, G. R. *J. Am. Chem. Soc.* **2015**, *137*, 1492–1500.
50. Meng, Z.; Sato, K.; Sukegawa, T.; Oyaizu, K.; Ho, C.-L.; Xiang, J.; Feng, Y.-H.; Lo, Y. H.; Nishide, H.; Wong, W.-Y. *J. Organomet. Chem.* **2016**, 51–55.
51. Rodriguez, J.; xe; A; Goodman, D. W. *Science* **1992**, *257*, 897–903.

52. Sun, S.; Murray, C. B.; Weller, D.; Folks, L.; Moser, A. *Science* **2000**, *287*, 1989–1992.
53. Astruc, D.; Lu, F.; Aranzaes, J. R. *Angew. Chem. Int. Ed.* **2005**, *44*, 7852–7872.
54. Lu, A.-H.; Salabas, E. L.; Schüth, F. *Angew. Chem. Int. Ed.* **2007**, *46*, 1222–1244.
55. Major, K. J.; De, C.; Obare, S. O. *Plasmonics* **2009**, *4*, 61–78.
56. Shylesh, S.; Schünemann, V.; Thiel, W. R. *Angew. Chem. Int. Ed.* **2010**, *49*, 3428–3459.
57. Goesmann, H.; Feldmann, C. *Angew. Chem. Int. Ed.* **2010**, *49*, 1362–1395.
58. Banin, U.; Ben-Shahar, Y.; Vinokurov, K. *Chem. Mater.* **2014**, *26*, 97–110.
59. Buchwalter, P.; Rosé, J.; Braunstein, P. *Chem. Rev.* **2015**, *115*, 28–126.
60. Li, B.; Wang, J.; Yuan, Y.; Ariga, H.; Takakusagi, S.; Asakura, K. *ACS Catal.* **2011**, *1*, 1521–1528.
61. Kelsen, V.; Meffre, A.; Fazzini, P.-F.; Lecante, P.; Chaudret, B. *ChemCatChem.* **2014**, *6*, 1714–1720.
62. Kaushik, M.; Friedman, H. M.; Bateman, M.; Moores, A. *RSC Adv.* **2015**, *5*, 53207–53210.
63. Hudson, R.; Chazelle, V.; Bateman, M.; Roy, R.; Li, C.-J.; Moores, A. *ACS Sustain. Chem. Eng.* **2015**, *3*, 814–820.
64. Du, J.-Q.; Zhang, Y.; Tian, T.; Yan, S.-C.; Wang, H.-T. *Mater. Res. Bull.* **2009**, *44*, 1347–1351.
65. Ott, G. L.; Fleisch, T.; Delgass, W. N. *J. Catal.* **1979**, *60*, 394–403.
66. Bahome, M. C.; Jewell, L. L.; Padayachy, K.; Hildebrandt, D.; Glasser, D.; Datye, A. K.; Coville, N. J. *Appl. Catal. A* **2007**, *328*, 243–251.

67. Wilcoxon, J. P.; Abrams, B. L. *Chem. Soc. Rev.* **2006**, *35*, 1162–1194.
68. Semagina, N.; Kiwi-Minsker, L. *Cat. Rev. - Sci. Eng.* **2009**, *51*, 147–217.
69. Zaheer, M.; Schmalz, T.; Motz, G.; Kempe, R. *Chem. Soc. Rev.* **2012**, *41*, 5102–5116.
70. Kanazawa, A.; Ikeda, T.; Endo, T. *J. Polym. Sci., Part A: Polym. Chem.* **1993**, *31*, 335–343.
71. Kanazawa, A.; Ikeda, T.; Endo, T. *J. Polym. Sci., Part A: Polym. Chem.* **1993**, *31*, 1467–1472.
72. Kanazawa, A.; Ikeda, T.; Endo, T. *J. Polym. Sci., Part A: Polym. Chem.* **1993**, *31*, 3003–3011.
73. Kanazawa, A.; Ikeda, T.; Endo, T. *J. Appl. Polym. Sci.* **1994**, *53*, 1237–1244.
74. Hatakeyama, E. S.; Ju, H.; Gabriel, C. J.; Lohr, J. L.; Bara, J. E.; Noble, R. D.; Freeman, B. D.; Gin, D. L. *J. Membr. Sci.* **2009**, *330*, 104–116.
75. Cheng, S.; Beyer, F. L.; Mather, B. D.; Moore, R. B.; Long, T. E. *Macromolecules* **2011**, *44*, 6509–6517.
76. Cheng, S.; Zhang, M.; Wu, T.; Hemp, S. T.; Mather, B. D.; Moore, R. B.; Long, T. E. *J. Polym. Sci., Part A: Polym. Chem.* **2012**, *50*, 166–173.
77. Hemp, S. T.; Allen, M. H., Jr.; Green, M. D.; Long, T. E. *Biomacromolecules* **2012**, *13*, 231–238.
78. Wang, R.; Lowe, A. B. *J. Polym. Sci., Part A: Polym. Chem.* **2007**, *45*, 2468–2483.
79. Noonan, K. J. T.; Hugar, K. M.; Kostalik, H. A.; Lobkovsky, E. B.; Abruna, H. D.; Coates, G. W. *J. Am. Chem. Soc.* **2012**, *134*, 18161–18164.
80. He, H.; Zhong, M.; Adzima, B.; Luebke, D.; Nulwala, H.; Matyjaszewski, K. *J. Am. Chem. Soc.* **2013**, *135*, 4227–4230.

81. Rabiee Kenaree, A.; Cuthbert, T. J.; Barbon, S. M.; Boyle, P. D.; Gillies, E. R.; Ragnogna, P. J.; Gilroy, J. B. *Organometallics* **2015**, *34*, 4272–4280.
82. Trupia, S.; Nafady, A.; Geiger, W. E. *Inorg. Chem.* **2003**, *42*, 5480–5482.
83. Swarts, J. C.; Nafady, A.; Roudebush, J. H.; Trupia, S.; Geiger, W. E. *Inorg. Chem.* **2009**, *48*, 2156–2165.
84. Teller, H.; Krichevski, O.; Gur, M.; Gedanken, A.; Schechter, A. *ACS Catalysis* **2015**, *5*, 4260–4267.
85. Shi, Y.; Zhang, B. *Chem. Soc. Rev.* **2016**, *45*, 1529–1541.
86. Berenguer, A.; Sankaranarayanan, T. M.; Gómez, G.; Moreno, I.; Coronado, J. M.; Pizarro, P.; Serrano, D. P. *Green Chem.* **2016**, *18*, 1938–1951.
87. Callejas, J. F.; Read, C. G.; Roske, C. W.; Lewis, N. S.; Schaak, R. E. *Chem. Mater.* **2016**, *28*, 6017–6044.
88. Lu, Y.; Wang, T.; Li, X.; Zhang, G.; Xue, H.; Pang, H. *RSC Adv.* **2016**, *6*, 87188–87212.
89. The PXRD patterns were compared using the ICSD database and PDF4+ software.
90. Nishikubo, T.; Iizawa, T.; Kobayashi, K.; Okawara, M. *Tetrahedron Lett.* **1981**, *22*, 3873–3874.
91. Bruker-AXS, S. v. **2013**, Bruker-AXS, Madison, WI 53711, USA.
92. Bruker-AXS, SADABS version 2012.1, **2012**, Bruker-AXS, Madison, WI 53711, USA.
93. Bruker-AXS, T. v. **2012**, Bruker-AXS, Madison, WI 53711, USA.
94. Altomare, A.; Cascarano, G.; Giacovazzo, C.; Guagliardi, A.; Burla, M. C.; Polidori, G.; Camalli, M. *J. Appl. Cryst.* **1994**, *27*, 435.

95. Sheldrick, G. M. *Acta Cryst.* **2015**, *A71*, 3–8.

96. Sheldrick, G. M. *Acta Cryst.* **2015**, *C71*, 3–8.

Chapter 5

5 An Organometallic Polymer with Three Different Metals per Repeating Unit

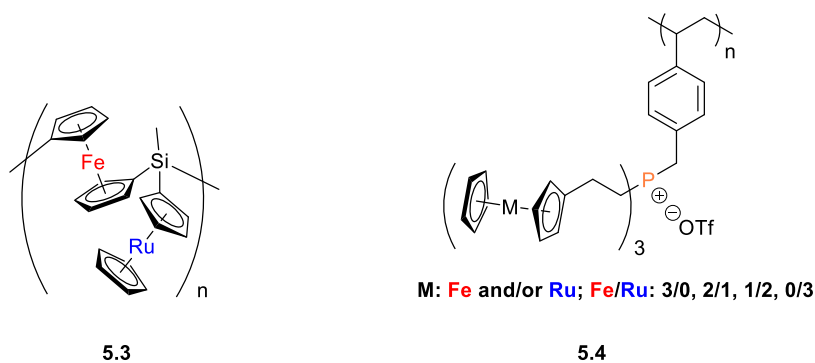
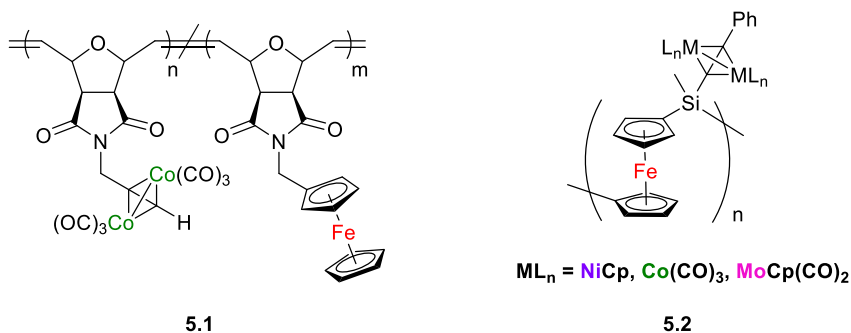
5.1 Introduction

Processable metal-containing polymers (MCPs)¹⁻¹⁰ have received great attention due to their potential applications in various fields as a result of their magnetic,¹¹⁻¹² catalytic,¹³⁻¹⁴ stimuli-responsive,¹⁵⁻¹⁶ luminescent,¹⁷ biomedical,¹⁸ and conductive materials.¹⁹⁻²⁰ Most MCPs contain a single metal, although heterobimetallic MCPs have been reported. The fact that heterobimetallic polymers can take advantage of unique properties of more than one type of transition metal has been the driving force for the investigation for new strategies for their synthesis. For example, the copolymerization of monomers that carry different transition metals is a method which can afford heterobimetallic polymers.²¹⁻³⁰ Tew and co-workers followed this strategy and synthesized cobalt-rich and iron-rich monomers and performed ring-opening metathesis polymerization (ROMP) to prepare a heterobimetallic random copolymer **5.1**.²⁵

Although gaining full conversion via post-polymerization functionalization reactions is generally a challenge, the addition of transition metals to the repeating units of homometallic polymers is a method that has also been exploited for the generation of heterometallic polymers.³¹⁻³⁷ In this regard, the Manners group utilized a strained sila[1]ferrocenophane for the synthesis of a homometallic polyferrocenylsilane (PFS)³⁸ containing alkyne groups in each repeating unit. Then, they reacted the alkyne groups with $\text{Co}_2(\text{CO})_8$, $[\text{NiCp}(\text{CO})_2]_2$, and $[\text{MoCp}(\text{CO})_2]_2$ to prepare heterobimetallic polymers **5.2**.³¹⁻³⁴

The synthesis and polymerization of heterometallic monomers is another strategy that has yielded heterometallic polymers with controlled metal content. However, examples of such monomers are rare.³⁹⁻⁴⁰ For instance, the Manners group synthesized a sila[1]ferrocenophane $[\{\text{Fe}(\eta\text{-C}_5\text{H}_4)_2\}\text{SiMe}(\eta\text{-C}_5\text{H}_4)\text{Ru}(\eta\text{-C}_5\text{H}_5)]$ and performed a photocontrolled ring-opening polymerization (ROP) to generate a monodisperse PFS with pendant ruthenocenyl groups **5.3**.

Recently, our group introduced a synthetic strategy regarding the use of metal-containing tertiary phosphines as precursors to highly metallized homometallic⁴¹⁻⁴² and heterobimetallic phosphonium polyelectrolytes with precisely controlled Fe/Ru ratios **5.4**. This methodology exploited the reactivity of P-H bonds for the installation of a polymerizable group.



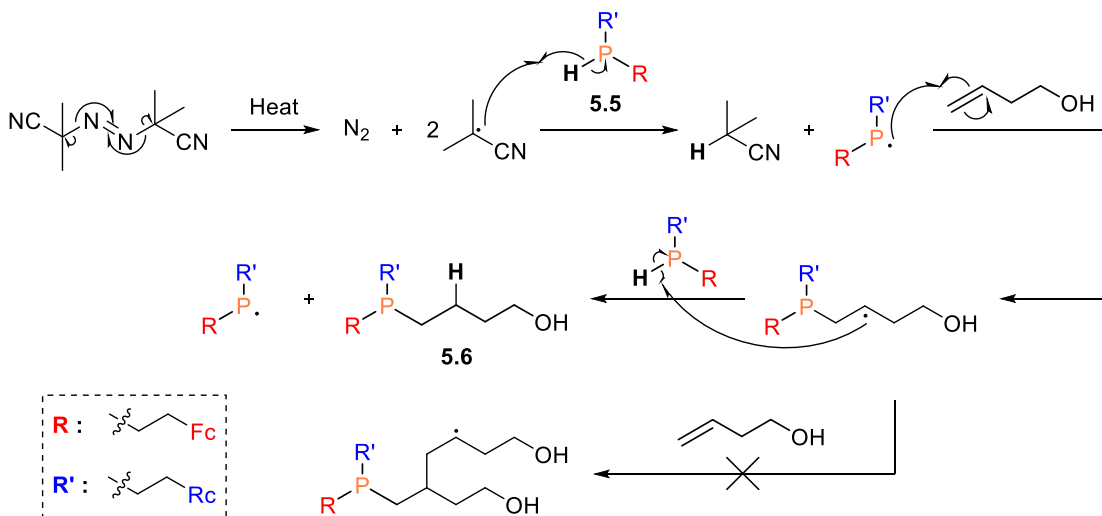
Even though, in the past few decades, the field of MCPs has witnessed great advances, to the best of our knowledge, the synthesis of a heterotrimetallic polymers has not been reported. Hence, we set out to prepare a heterobimetallic polymer based on phosphines and investigated its conversion to a heterotrimetallic polymer via a post-polymerization coordination reaction.

5.2 Results and Discussion

5.2.1 Synthesis and NMR Spectroscopy

The exceptional air-stability of secondary phosphine **5.5** prompted us to use it as a heterobimetallic precursor, which was synthesized according to a literature procedure.⁴³ In the presence of a catalytic amount of azobisisobutyronitrile (AIBN) and excess 3-buten-1-ol, **5.5** was fully converted to tertiary phosphine alcohol **5.6**, which was conveniently

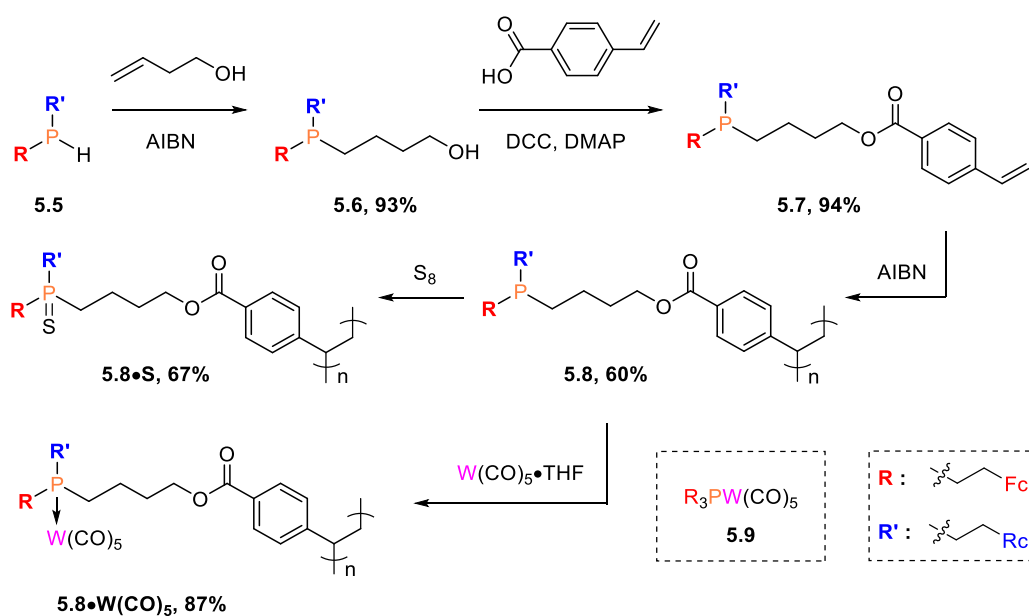
purified by column chromatography in air. The observation of tertiary phosphine alcohol **5.6** as a single product implies that the radical intermediate ($RR'PCH_2CH\cdot CH_2CH_2OH$), which was produced from the reaction of phosphine radical ($RR'P\cdot$) with 3-buten-1-ol, prefers to acquire a hydrogen radical and generate tertiary phosphine alcohol **5.6** rather than attacking another olefin to pursue oligomerization/polymerization routes (Scheme 5.1).⁴⁴⁻⁴⁵



Scheme 5.1. Suggested mechanism for the synthesis of **5.6**.

To install a styrene group, *N,N'*-dicyclohexylcarbodiimide (DCC) coupling was selected due its high efficiency and mild experimental conditions (Scheme 5.2). In the absence of external heat/light sources and under N_2 , a slight excess of 4-vinylbenzoic acid, DCC, and 4-dimethylaminopyridine (DMAP) were briefly stirred, and later combined with tertiary phosphine alcohol **5.6** to produce tertiary phosphine monomer **5.7**, which was isolated in 94% yield. The free-radical polymerization of monomer **5.7** afforded tertiary phosphine polymer **5.8**, which was simply purified by consecutive precipitation in Et_2O from THF. Contrary to tertiary phosphine sulfide polymers, GPC analysis of tertiary phosphine polymers is problematic.⁴⁶ Hence, the phosphorous centres in tertiary phosphine polymer **5.8** were sulfurized in the presence of S_8 and purified by successive precipitation in Et_2O from THF, and dried overnight at 60 °C to afford tertiary phosphine sulfide polymer **5.8•S**, which was analyzed by GPC to calculate the number average molecular weight of tertiary phosphine polymer **5.8**.

The UV light irradiation of a solution of tungsten hexacarbonyl in THF generated the $W(CO)_5 \cdot THF$ adduct, which was combined with a THF solution of tertiary phosphine polymer **5.8** in order to produce heterotrimetallic coordinated-tertiary phosphine polymer **5.8**• $W(CO)_5$ (Scheme 5.2). Characterization data gathered from methods including 1H , ^{13}C , and ^{31}P NMR spectroscopy, cyclic voltammetry, FT-IR and UV-vis absorption spectroscopy, mass spectrometry, and elemental analysis confirmed the proposed structure and purity of compounds **5.6**–**5.8**, **5.8**•**S**, and **5.8**• $W(CO)_5$ (Figures A5.1–A5.16, and Table 5.2).



Scheme 5.2. Synthetic pathway for the preparation of heterotrimetallic polymer **5.8**• $W(CO)_5$.

Complete conversion of secondary phosphine **5.5** to tertiary phosphine alcohol **5.6** was confirmed by $^{31}P\{^1H\}$ NMR spectroscopy, as the starting material peak (δ : -68.8) disappeared and a downfield-shifted singlet (δ : -28.8) for tertiary phosphine alcohol **5.6** was observed (Figures A5.3 and A5.4). The presence of the butanol substituent also confirmed by 1H NMR spectroscopy, where the butyl linker gave rise to signals which were overlapped by ethyl linker signals (δ : 3.71 – 1.39) (Figure A5.1). Tertiary phosphine monomer **5.7** appeared as a sharp singlet (δ : -29.0) in its $^{31}P\{^1H\}$ NMR spectrum and demonstrated two aromatic multiplets (δ : 8.05 – 7.42) and three diagnostic vinylic resonances (δ : 6.76 , 5.87 , and 5.39), in addition to ethyl and butyl linker and metallocene

signals (Figure A5.5, A5.7, and A5.8). Upon polymerization, the vinylic signals disappeared in the ^1H NMR spectrum of tertiary phosphine polymer **5.8** and the polymer backbone protons gave rise to two broad signals that were coincident with the aliphatic linker signals (δ : 1.80–0.85) (Figure A5.9). Furthermore, tertiary phosphine polymer **5.8** appeared as a singlet (δ : *ca.* -29.2) in the ^{31}P NMR spectrum. This shows that the phosphine centres remained intact during the synthesis and purification steps (Figure A5.10). Coordination to $\text{W}(\text{CO})_5$ deshielded the phosphorous centres and gave rise to a singlet (δ : -6.1) accompanied by two satellite peaks, which appeared due to the coupling of the phosphorous centres with ^{183}W (natural abundance of $^{183}\text{W} = 14.3\%$;⁴⁷ $^1J_{\text{PW}} = 233$ Hz) (Figure 5.1). In the ^1H NMR spectrum, coordinated-tertiary phosphine polymer **5.8**• $\text{W}(\text{CO})_5$ exhibited resonances attributed to monosubstituted ferrocene and ruthenocene (δ : 4.78–3.75), ethyl and butyl linkers (δ : 4.39–1.44), and aromatic group multiplets (δ : 8.05–5.93). The polymer backbone protons in **5.8**• $\text{W}(\text{CO})_5$ gave rise to two broad signals which were partially overlapped by aliphatic linker signals (Figure A5.13).

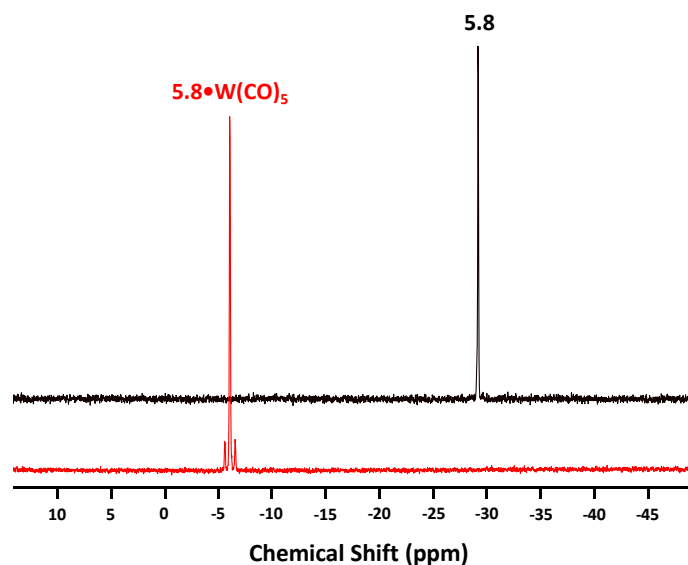


Figure 5.1. $^{31}\text{P}\{^1\text{H}\}$ NMR spectra of tertiary phosphine polymer **5.8** (black) and coordinated-tertiary phosphine polymer **5.8**• $\text{W}(\text{CO})_5$ (red) recorded in CDCl_3 .

5.2.2 FT-IR Spectroscopy

Comparison of the FT-IR spectra recorded for tertiary phosphine polymer **5.8** and coordinated-tertiary phosphine polymer **5.8**• $\text{W}(\text{CO})_5$ revealed that, aside from the observation of three absorption bands (2066, 1974, and 1909 cm^{-1}) from $\text{W}(\text{CO})_5$, the IR

spectra of tertiary phosphine polymer **5.8** and coordinated-tertiary phosphine polymer **5.8**•**W(CO)₅** match very well, further confirming that the polymer backbone remained intact during the post-polymerization reaction. The three diagnostic CO stretches observed in the FT-IR absorption spectrum of coordinated-tertiary phosphine polymer **5.8**•**W(CO)₅** were assigned based on theory proposed by Orgel⁴⁸ and Cotton⁴⁹ (Figure 5.2). The observed A_{1cis} and A_{1trans} stretching frequencies were very similar to those reported for complex **5.9**.⁵⁰ This implies that the σ donating ability of the phosphorous centres and the extent of π backbonding to CO ligands in coordinated-tertiary phosphine polymer **5.8**•**W(CO)₅** are similar to those of **5.9**. In addition, the observation of equal $^1J_{PW}$ coupling constants for coordinated-tertiary phosphine polymer **5.8**•**W(CO)₅** and **5.9** further supports the idea that the coordination behavior of phosphorous centres in **5.8**•**W(CO)₅** and **5.9** are similar because the strength of P-W bond is directly correlated with phosphorous-tungsten NMR coupling constants.⁵¹

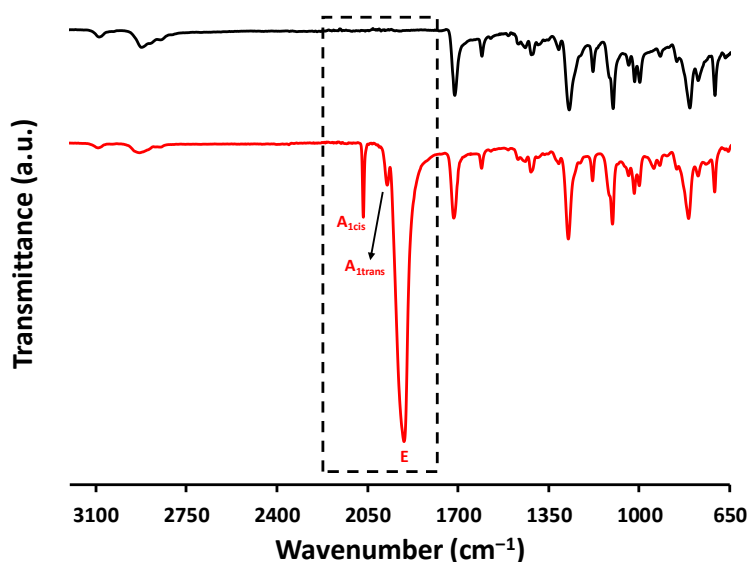


Figure 5.2. FT-IR spectra of tertiary phosphine polymer **5.8** (black) and coordinated-tertiary phosphine polymer **5.8**•**W(CO)₅** (red).

5.2.3 UV-vis Absorption Spectroscopy and Cyclic Voltammetry

The electronic structure of compounds **5.6–5.8** and **5.8**•**W(CO)₅** were studied by UV-vis absorption spectroscopy in CH_2Cl_2 . The recorded spectra revealed two absorption maxima

(λ_{max} : 322 and 440 nm) indicative of the presence of ferrocene and ruthenocene and were consistent with those recorded for related compounds (Figure A5.14, and Table 5.1).^{43, 50}

The electrochemical properties of secondary phosphine **5.5** has been described ($E_{1/2, \text{Fc}} = 0$, and $E_{\text{pa, Rc}} = 440$ mV).⁴³ The electrochemical behavior of **5.6–5.8**, and **5.8•W(CO)₅** were studied for THF solutions of the analytes in the presence of [*n*-Bu₄N][OTf] salt as supporting electrolyte. Cyclic voltammograms of **5.6–5.8** were comprised of three features (Figures 5.3, A5.15, and A5.16). A one-electron redox wave at -15 mV, which was slightly more negative compared to that of secondary phosphine **5.5**, corresponded to the reversible oxidation of ferrocene. The fact that these ferrocene moieties exhibited more negative potentials implies that the butyl substituents in **5.6–5.8** electronically enriched the phosphorous centres and ferrocene moieties. The second feature was attributed to the irreversible one-electron oxidation of ruthenocene (*ca.* 400 mV). This behavior was in accordance with reports describing electrochemical properties of ruthenocene, which can be oxidized to ruthenocenium cation and subsequently undergo a medium-related decomposition, dimerization, disproportion, bond activation, and/or ion scavenging processes.^{40, 52-56} The third feature was a prewave (*ca.* -150 mV), which was observed due to the adsorption/oxidation of the analytes on the surface of electrodes. Such behavior has been reported for several phosphines and it is likely that the lone pair of electrons on phosphorous promotes the adsorption.^{43, 57-58} However, such an oxidation event was not observed for coordinated-tertiary phosphine polymer **5.8•W(CO)₅**, due to the engagement of the electron pair of phosphorous centres in the P-W bond. The ferrocene units in coordinated-tertiary phosphine polymer **5.8•W(CO)₅** gave rise to a reversible one-electron oxidation wave at slightly more positive potential (0 mV) compared to those of recorded for **5.6–5.8**. This indicates that the coordination of phosphorous to W(CO)₅ inductively affected the ferrocene moieties and made them relatively electron poor and harder to oxidize. Similar to **5.6–5.8**, the ruthenocene groups in coordinated-tertiary phosphine polymer **5.8•W(CO)₅** gave rise to an irreversible oxidation half-wave (350 mV). In addition, the oxidation of W⁰ to W⁺¹ in W(CO)₅ complexes appeared as an irreversible one-electron oxidation half-wave at 750 mV in cyclic voltammogram of coordinated-tertiary phosphine polymer **5.8•W(CO)₅**. The latter electrochemical feature is consistent with

reports of the electrochemical properties of tungsten carbonyl metal complexes and further confirms the presence of $\text{W}(\text{CO})_5$ in the structure of $\mathbf{5.8}\cdot\text{W}(\text{CO})_5$.⁵⁹

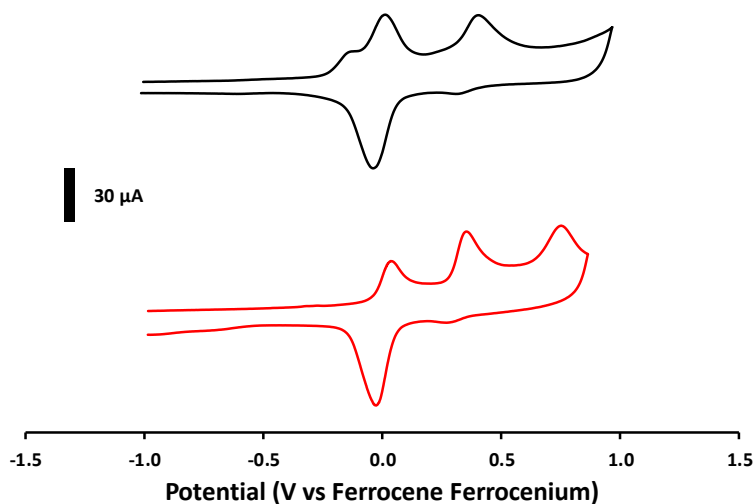


Figure 5.3. Cyclic voltammograms of tertiary phosphine polymer **5.8** (black) and coordinated-tertiary phosphine polymer $\mathbf{5.8}\cdot\text{W}(\text{CO})_5$ (red) recorded at 250 mV s^{-1} in solutions of THF containing $0.1 \text{ M } [n\text{-Bu}_4\text{N}][\text{OTf}]$ as supporting electrolyte.

Table 5.1. Selected characterization data for compounds **5.6–5.10**.

Compound	^{31}P NMR (δ)	ϵ , 322 nm ($\text{M}^{-1} \text{ cm}^{-1}$)	ϵ , 440 nm ($\text{M}^{-1} \text{ cm}^{-1}$)	$E_{1/2, \text{Fc}}$ (mV)	$E_{\text{pa}, \text{Rc}}^b$ (mV)	$E_{\text{pa}, \text{W}}^b$ (mV)
5.6	-28.8	300	100	-15 (-120) ^a	440	-
5.7	-29.0	300	100	-15 (-150) ^a	390	-
5.8	-29.2	300	100	-15 (-150) ^a	400	-
$\mathbf{5.8}\cdot\text{W}(\text{CO})_5$	-6.1	450	100	0	350	750

^aAnodic potential of prewave is reported in the bracket. ^bIrreversible process; anodic peak potential reported.

5.2.4 Gel Permeation Chromatography and Thermal Analysis

The molecular weights and molecular weight distribution of tertiary phosphine polymer **5.8** calculated from values recorded by GPC of the corresponding tertiary phosphine sulfide polymer $\mathbf{5.8}\cdot\text{S}$. The observation of a GPC trace with a shoulder at low molecular weight suggested that the growing chains stopped after reaching a certain size perhaps due to precipitation or high-molecular polymer chains were filtered out during the GPC sample preparation (Table 5.2). Coordinated-tertiary phosphine polymer $\mathbf{5.8}\cdot\text{W}(\text{CO})_5$ demonstrated a limited solubility in common GPC eluents and, even after 24 h stirring in THF, appeared as an orange solution containing some particulates. However, after filtration, the solution passed the GPC column without a problem. It is likely that

coordination of the phosphorous centres prevented the strong interaction of the phosphorous centres with the GPC column material. The GPC trace of $5.8 \cdot W(CO)_5$ appeared as a peak with an extremely broad feature toward high molecular weight direction. Since the characterization of coordinated-tertiary phosphine polymer $5.8 \cdot W(CO)_5$ by other methods confirmed its suggested structure, we postulate that the $W(CO)_5$ moieties caused $5.8 \cdot W(CO)_5$ molecules to self-aggregate in solution and lead to a broad distribution in its recorded GPC (Figure 5.4).

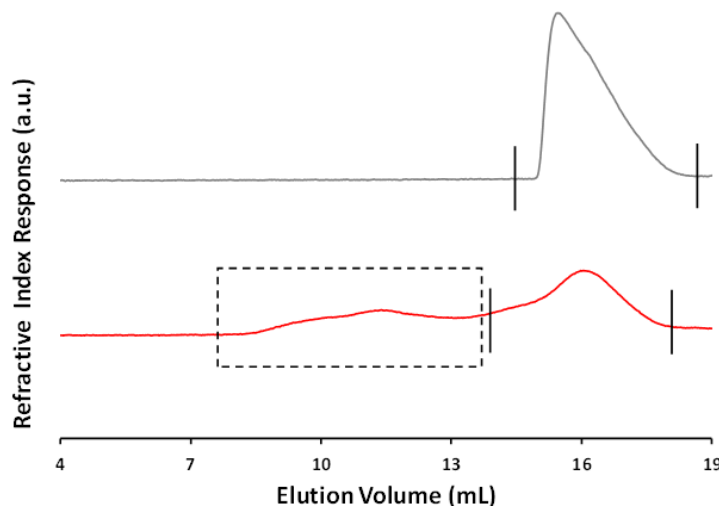


Figure 5.4. GPC traces recorded for polymers $5.8 \cdot S$ (grey) and $5.8 \cdot W(CO)_5$ (red) in THF. The limits used to estimate the molecular weights relative to monodisperse polystyrene standards are shown as black bars and the signal attributed to aggregates of $5.8 \cdot W(CO)_5$ in solution is shown in the dashed box.

The macromolecular nature of tertiary phosphine polymer 5.8 and coordinated-tertiary phosphine polymer $5.8 \cdot W(CO)_5$ were further confirmed by the observation of glass transition temperatures (T_g) in thermograms recorded by differential scanning calorimetry (DSC). Coordinated-tertiary phosphine polymer $5.8 \cdot W(CO)_5$ revealed a relatively higher T_g compared to that of 5.8 . This indicated that intramolecular interactions of polymer chains in $5.8 \cdot W(CO)_5$ are stronger than that of 5.8 and supports our interpretation of the GPC data.

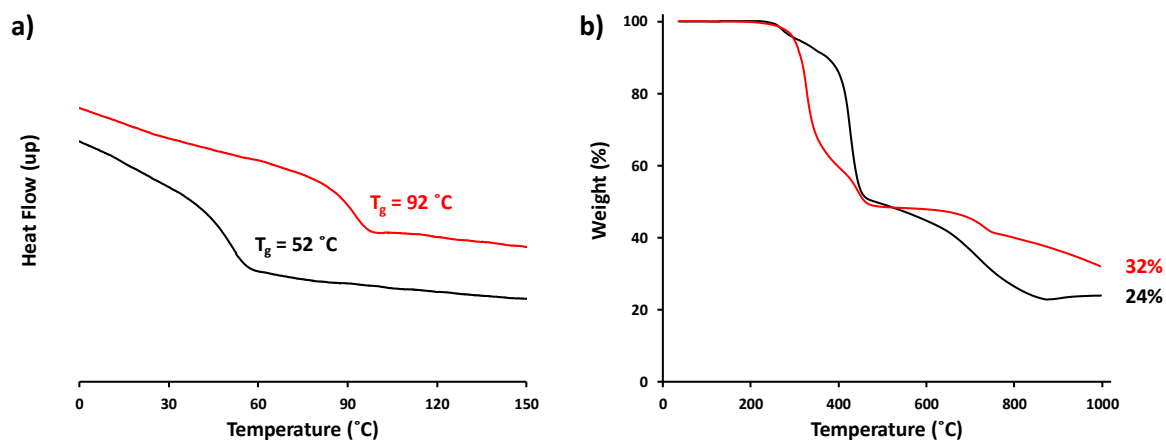


Figure 5.5. a) DSC thermograms of tertiary phosphine polymer **5.8** (black) and coordinated-tertiary phosphine polymer **5.8•W(CO)₅** (red) recorded at a scan rate of 10 °C min⁻¹ and b) TGA data obtained for tertiary phosphine polymer **5.8** (black) and coordinated-tertiary phosphine polymer **5.8•W(CO)₅** (red).

Thermogravimetric analysis (TGA) of tertiary phosphine polymer **5.8** and coordinated-tertiary phosphine polymer **5.8•W(CO)₅** showed they are stable up to a temperature of 220 °C. Comparison of the char yields with the metal content of the starting polymers (22.2% and 32.0% for **5.8** and **5.8•W(CO)₅**, respectively) suggests that the thermal degradation of these MCPs under an active flow of N₂ may have involved the loss of organic fractions.

Table 5.2. Selected characterization data for compounds tertiary phosphine polymer **5.8** and coordinated-tertiary phosphine polymer **5.8•W(CO)₅**.

Compound	M _n (g mol ⁻¹)	M _w (g mol ⁻¹)	<i>D</i>	T _g (°C)	Char Yield (%)	Polymer Metal Content (Mass %)
5.8	9,300 ^a	13,600 ^a	1.46 ^a	52	24.0	22.2
5.8•W(CO)₅	11,600	28,000	2.41	92	32.1	32.0

^aCalculated from the GPC data recorded for the corresponding sulfurized polymer **5.8•S**.

5.3 Conclusions

We have synthesized a heterobimetallic tertiary phosphine polymer and showed that all of its phosphorus centres are available for further chemistry. As an example, we reacted it with W(CO)₅•THF to synthesize the first example of a heterotrimetallic polymer. The structure and purity of the compounds synthesized were confirmed by methods such as multinuclear NMR, FT-IR, and UV-vis absorption spectroscopy, and elemental analysis. The presence of electroactive groups, including ferrocene, ruthenocene, and tungsten in the structure of the synthesized materials was confirmed by cyclic voltammetry wherein they gave rise to waves/half-waves consistent with those reported for related compounds. The macromolecular nature of coordinated-tertiary phosphine polymer/tertiary phosphine

polymer was confirmed by NMR spectroscopy, GPC, and the observation of glass transition temperature during DSC studies. The complete coordination of all phosphorous centres in the tertiary phosphine polymer to $W(CO)_5$ was confirmed by the observation of a downfield chemical shift in ^{31}P NMR spectrum and disappearance of phosphine signals. This conclusion was further supported by FT-IR studies, where the coordinated-tertiary phosphine polymer gave rise to three diagnostic absorption bands due to CO stretching from $W(CO)_5$ moieties. Thermal degradation of heterobimetallic tertiary phosphine polymer and heterotrimetallic coordinated-tertiary phosphine polymer resulted in the observation of char yields that were in close agreement with metal content of the corresponding polymers. We believe that our results have opened a new door to the design and synthesis of heterometallic materials and our future work will focus expanding the range of heterotrimetallic polymers known.

5.4 Experimental Section

5.4.1 General Considerations

Reactions and manipulations were carried out under a N_2 atmosphere using standard glove box or Schlenk techniques unless otherwise stated. Solvents were obtained from Caledon Laboratories and Fischer Scientific, dried using an Innovative Technologies Inc. solvent purification system, collected under vacuum, and stored under a nitrogen atmosphere over 4 Å molecular sieves. Reagents were purchased from Sigma-Aldrich or Alfa Aesar and used as received, aside from $W(CO)_6$, which was sublimed at 50 °C under vacuum and stored under N_2 . Secondary phosphine **5.5** was synthesized according to a reported protocol.⁴³ UV irradiation experiments were conducted using a custom built UV light source equipped with four high intensity light emitting diodes (LEDs) with irradiation peak centered at 350 nm. 1H , $^{13}C\{^1H\}$, and ^{31}P NMR spectra were recorded on a 600 MHz (1H : 599.5 MHz, $^{13}C\{^1H\}$: 150.8 MHz, ^{19}F : 563.9 MHz and ^{31}P : 242.6 MHz) Varian INOVA instrument. 1H NMR spectra were referenced to residual $CHCl_3$ (7.27 ppm) and $^{13}C\{^1H\}$ NMR spectra were referenced to $CDCl_3$ (77.0 ppm). gHSQCAD NMR spectra were used to support $^{13}C\{^1H\}$ NMR spectral assignments. Mass spectrometry data were recorded in positive-ion mode and using a high resolution Finnigan MAT 8400 or Micromass LCT electrospray ionization time-of-flight mass spectrometer. UV-vis absorption spectra were

recorded using a Cary 300 Scan instrument. FT-IR spectra were recorded using a PerkinElmer Spectrum Two FTIR spectrometer with an attenuated total reflectance (ATR) attachment and a single reflection diamond.

5.4.2 Cyclic Voltammetry

Cyclic voltammograms were collected using a Bioanalytical Systems Inc. (BASi) Epsilon potentiostat and analyzed using BASi Epsilon software. Typical electrochemical cells consisted of a three-electrode setup including a glassy carbon working electrode, platinum wire counter electrode, and silver wire *pseudo*-reference electrode. In a glovebox and away from light, 1 mM solutions of the analytes in dry and degassed THF were prepared and stirred overnight, before they were combined with supporting electrolyte (0.1 M [*n*-Bu₄N][OTf]) and run at a scan rate of 250 mV s⁻¹. Cyclic voltammograms were referenced relative to a decamethylferrocene internal standard (1 mM, -385 mV relative to ferrocene/ferrocenium under identical conditions) and corrected for internal cell resistance using the BASi Epsilon software.

5.4.3 Gel Permeation Chromatography

Polymer **5.8•S** and **5.8•W(CO)₅** were combined with chromatography-grade THF (5 mg mL⁻¹) and stirred for 24 h and filtered (Nylon membrane, 0.2 μm) before the gel permeation chromatography (GPC) experiments were conducted for the soluble portion using a Viscotek GPCmax VE 2001 GPC instrument equipped with an Agilent PolyPore guard column (PL1113-1500) and two sequential Agilent PolyPore GPC columns packed with porous poly(styrene-*co*-divinylbenzene) particles (MW range: 200–2,000,000 g mol⁻¹; PL1113-6500) regulated at a temperature of 30 °C. Signal responses were measured using a Viscotek VE 3580 RI detector, and molecular weights were determined by comparison of the maximum RI response with a calibration curve (10 points, 1500–786,000 g mol⁻¹) established using monodisperse polystyrene standards purchased from Viscotek.

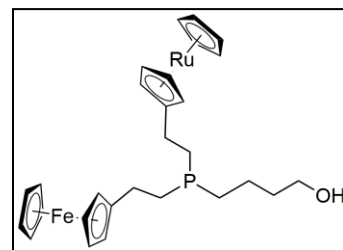
5.4.4 Thermal Analysis

Thermal degradation studies were performed using a TA Instruments Q50 TGA instrument under an atmosphere of N₂. Samples were placed in a platinum pan and heated at a rate of

10 °C min⁻¹ from 20 °C to 1000 °C under a flow of N₂ (60 mL min⁻¹). Glass transition temperatures were determined under an atmosphere of N₂ using differential scanning calorimetry (DSC) on a TA Instruments DSC Q20. The polymer samples were placed in an aluminum Tzero pan and heated from room temperature to the maximum temperature [200 °C for **5.8** and 180 °C for **5.8•W(CO)₅**] at 10 °C min⁻¹ under a flow of N₂ (50 mL min⁻¹) and cooled to -70 °C at 5 °C min⁻¹, before they underwent two more heat/cool cycles. The T_gs were determined from the second heat/cool cycle.

Preparation of Tertiary Phosphine **5.6** (1 × Fc, 1 × Rc)

In a sealed tube, secondary phosphine **5.5** (1.00 g, 1.99 mmol), 3-buten-1-ol (500 μL, 5.81 mmol, 2.9 equiv.), and AIBN (21 mg, 0.13 mmol, 0.065 equiv.) were combined with THF (5 mL) before the mixture was heated with stirring for 24 h at 75 °C. After cooling to room temperature, the resulting

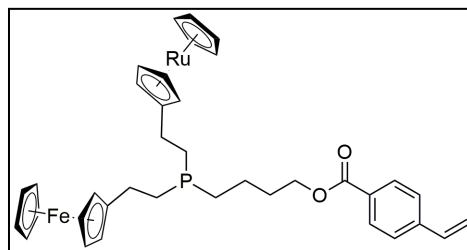


orange solution was concentrated *in vacuo*, dissolved in a minimum amount of CH₂Cl₂ and transferred to a silica/hexanes column (1" × 6"). Using N₂ pressure and a 5:1 hexanes:Et₂O solvent mixture as eluent, tertiary phosphine **5.6** (R_f = 0.22) was isolated from the column. The solution containing **5.6** was concentrated *in vacuo* to yield an orange solid that was dried overnight *in vacuo* at 80 °C in the presence of P₂O₅. Yield = 1.06 g, 93%. M.p. 64–66 °C. ¹H NMR: δ 4.54 [s, 2H, β-C₅H₄R(Ru)], 4.53 [s, 5H, C₅H₅(Ru)], 4.46 [s, 2H, α-C₅H₄R(Ru)], 4.12 [s, 5H, C₅H₅(Fe)], 4.10 [s, 2H, β-C₅H₄R(Fe)], 4.07 [s, 2H, α-C₅H₄R(Fe)], 3.68 (t, 2H, ³J_{HH} = 7 Hz, 2H, CH₂OH), 2.46 [m, 2H, (Fe)C₅H₄CH₂CH₂], 2.32 [m, 2H, (Ru)C₅H₄CH₂CH₂], 1.68 (m, 2H, CH₂CH₂OH), 1.64 [m, 2H, (Fe)C₅H₄CH₂], 1.59 [m, 2H, (Ru)C₅H₄CH₂], 1.39–1.47 (m, 2H, CH₂CH₂CH₂OH). ¹³C{¹H} NMR: δ 93.9 [d, ³J_{CP} = 13 Hz, *ipso*-C₅H₄R(Ru)], 89.8 [d, ³J_{CP} = 13 Hz, *ipso*-C₅H₄R(Fe)], 70.5 [s, β-C₅H₄R(Ru)], 70.4 [s, C₅H₅(Ru)], 69.4 [s, α-C₅H₅R(Ru)], 68.5 [s, C₅H₅(Fe)], 67.8 [s, β-C₅H₄R(Fe)], 67.2 [s, α-C₅H₅R(Fe)], 62.4 (s, CH₂OH), 34.3 (d, ³J_{CP} = 10 Hz, CH₂CH₂OH), 28.9 [d, ³J_{CP} = 13 Hz, (Ru)C₅H₄CH₂], 28.4 [d, ³J_{CP} = 13 Hz, (Fe)C₅H₄CH₂], 26.8 (d, ²J_{CP} = 13 Hz, CH₂CH₂CH₂OH), 26.0 [d, ²J_{CP} = 16 Hz, (Fe)C₅H₄CH₂CH₂], 25.5 [d, ²J_{CP} = 15 Hz, (Ru)C₅H₄CH₂CH₂], 22.2 (d, ¹J_{CP} = 13 Hz, CH₂CH₂CH₂CH₂OH). ³¹P{¹H} NMR: δ -28.8 (s). FT-IR: 3306 (br), 3082 (w), 2926 (w), 2878 (w), 2862 (w), 1638 (w), 1408 (w), 1315

(w), 1227 (w), 1099 (m), 1036 (m), 1022 (m), 998 (m), 922 (w), 806 (s), 666(w) cm^{-1} . UV-vis (CH_2Cl_2): λ_{max} 323 nm ($\epsilon = 300 \text{ M}^{-1} \text{ cm}^{-1}$) and 438 nm ($\epsilon = 100 \text{ M}^{-1} \text{ cm}^{-1}$). Mass Spec. (ESI, +ve mode): exact mass calculated for $[\text{C}_{28}\text{H}_{36}^{56}\text{FeOP}^{102}\text{Ru}]^+$: 577.0896; exact mass found: 577.0904; difference: +1.2 ppm. Anal. Calcd. (%) for $\text{C}_{28}\text{H}_{35}\text{OPFeRu}$: C, 58.44; H, 6.13. Found: C, 58.48; H, 6.14.

Preparation of Tertiary Phosphine Monomer **5.7** (1 \times Fc, 1 \times Rc)

In a sealed tube and in the absence of external light/heat sources, 4-vinylbenzoic acid (0.30 g, 2.0 mmol, 1.15 equiv.), 4-(dimethylamino)pyridine (0.25 g, 2.0 mmol, 1.15 equiv.), and *N,N'*-dicyclohexylcarbodiimide (0.43 g, 2.1 mmol, 1.2

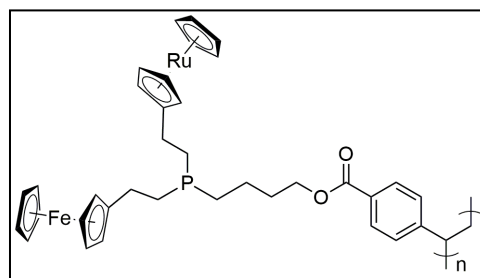


equiv.) were combined in dry CH_2Cl_2 (6 mL) and the resulting mixture was stirred for 15 min before tertiary phosphine **5.6** (1.00 g, 1.74 mmol) was added and the mixture stirred for an additional 90 min at room temperature. The resulting mixture was gravity filtered and the orange filtrate was concentrated *in vacuo*, before the resulting residue was dissolved in a minimum amount of CH_2Cl_2 and transferred to a silica/hexanes column (1" \times 6"). Using N_2 pressure and a 4:1 hexanes: Et_2O solvent mixture as eluent, tertiary phosphine monomer **5.7** ($R_f = 0.29$) was isolated from the column. The solution containing **5.7** was concentrated *in vacuo* to yield an orange oil. Yield = 1.15 g, 94%. ^1H NMR: δ 8.01 (d, 2H, $^3J_{\text{HH}} = 8 \text{ Hz}$, aryl CH), 7.46 (d, 2H, $^3J_{\text{HH}} = 8 \text{ Hz}$, aryl CH), 6.76 (dd, 1H, $^3J_{\text{HH},\text{cis}} = 11 \text{ Hz}$, $^3J_{\text{HH},\text{trans}} = 18 \text{ Hz}$, ArCH=CH₂), 5.87 (d, 1H, $^3J_{\text{HH},\text{trans}} = 18 \text{ Hz}$, ArCH=CH₂), 5.39 (d, 1H, $^3J_{\text{HH},\text{cis}} = 11 \text{ Hz}$, ArCH=CH₂), 4.53 [s, 7H, $\alpha\text{-C}_5\text{H}_4\text{R}(\text{Ru})$ and $\text{C}_5\text{H}_5(\text{Ru})$], 4.46 [s, 2H, $\beta\text{-C}_5\text{H}_4\text{R}(\text{Ru})$], 4.36 (t, 2H, $^3J_{\text{HH}} = 7 \text{ Hz}$, COOCH₂), 4.11 [s, 5H, $\text{C}_5\text{H}_5(\text{Fe})$], 4.08 [s, 4H, $\alpha\text{-C}_5\text{H}_5\text{R}(\text{Fe})$ and $\beta\text{-C}_5\text{H}_4\text{R}(\text{Fe})$], 2.47 [m, 2H, (Fe) $\text{C}_5\text{H}_4\text{CH}_2\text{CH}_2$], 2.32 [m, 2H, (Ru) $\text{C}_5\text{H}_4\text{CH}_2\text{CH}_2$], 1.89 (m, 2H, CH₂CH₂OOC), 1.69–1.55 [m, 6H, (Fe) $\text{C}_5\text{H}_4\text{CH}_2$, (Ru) $\text{C}_5\text{H}_4\text{CH}_2$, and PCH₂CH₂CH₂], 1.54–1.45 (m, 2H, CH₂CH₂CH₂OOC). $^{13}\text{C}\{^1\text{H}\}$ NMR: δ 166.3 (s, COO), 141.8 (s, CCHCH₂), 136.0 (s, CCHCH₂), 129.8 (s, COCCH), 129.4 (s, COC), 126.1 (s, COCCHCH), 116.4 (s, CCHCH₂), 93.8 [d, $^3J_{\text{CP}} = 12 \text{ Hz}$, *ipso*- $\text{C}_5\text{H}_4\text{R}(\text{Ru})$], 89.7 (d, $^3J_{\text{CP}} = 12 \text{ Hz}$, *ipso*- $\text{C}_5\text{H}_4\text{R}(\text{Fe})$], 70.5 [s, $\beta\text{-C}_5\text{H}_4\text{R}(\text{Ru})$], 70.4 [s, $\text{C}_5\text{H}_5(\text{Ru})$], 69.4 [s, $\alpha\text{-C}_5\text{H}_5\text{R}(\text{Ru})$], 68.4 [s, $\text{C}_5\text{H}_5(\text{Fe})$], 67.8 [s, $\beta\text{-C}_5\text{H}_4\text{R}(\text{Fe})$], 67.2 [s, $\alpha\text{-C}_5\text{H}_5\text{R}(\text{Fe})$], 64.4

(s, CH₂OOC), 30.3 (d, ³J_{CP} = 12 Hz, CH₂CH₂OOC), 28.9 [d, ³J_{CP} = 13 Hz, (Ru)C₅H₄CH₂], 28.4 [d, ³J_{CP} = 13 Hz, (Fe)C₅H₄CH₂], 26.6 (d, ²J_{CP} = 12 Hz, CH₂CH₂CH₂OOC), 26.0 [d, ²J_{CP} = 15 Hz, (Fe)C₅H₄CH₂CH₂], 25.5 [d, ²J_{CP} = 15 Hz, (Ru)C₅H₄CH₂CH₂], 22.5 (d, ¹J_{CP} = 14 Hz, PCH₂CH₂CH₂CH₂O). ³¹P{¹H} NMR: δ -29.0 (s). FT-IR: 3306 (br), 3088 (w), 2953 (m), 2922 (s), 2853 (m), 1710 (m), 1607 (w), 1461 (m), 1378 (w), 1270 (m), 1178 (w), 1101(m), 1016 (w), 995 (w), 914 (w), 804 (m), 781 (w), 711 (w) cm⁻¹. UV-vis (CH₂Cl₂): λ_{max} 322 nm (ε = 300 M⁻¹ cm⁻¹) and 440 nm (ε = 100 M⁻¹ cm⁻¹). Mass Spec. (EI, +ve mode): exact mass calculated for [C₃₇H₄₁⁵⁶FeO₂P⁹⁶Ru]⁺: 700.1271; exact mass found: 700.1244; difference: -3.8 ppm. Anal. Calcd. (%) for C₃₇H₄₁O₂PF₉₆Ru: C, 62.98; H, 5.86. Found: C, 62.29; H, 5.78.

Preparation of Tertiary Phosphine Polymer **5.8** (1 × Fc, 1 × Rc)

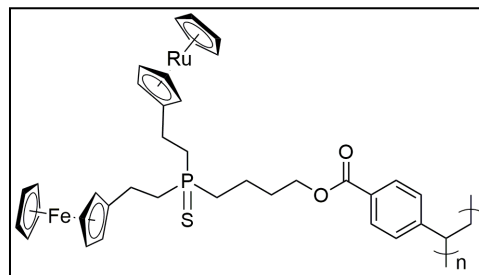
In a grease-free Schlenk flask, monomer **5.7** (0.40 g, 0.57 mmol) was dissolved in 2.00 mL of a THF stock solution containing AIBN (0.93 mg, 0.0057 mmol, 0.01 equiv.). The resulting solution was stirred at 75 °C for 16 h. After cooling to room temperature, the polymerization mixture was



poured into Et₂O and the solids were separated by centrifugation before they were collected, dissolved in a minimum amount of CHCl₃, and precipitated in Et₂O for twice more. The polymer **5.8** was dried *in vacuo*, and in the presence of P₂O₅, at 60 °C for 16 h to yield an orange powder. Yield = 0.24 g, 60%. ¹H NMR: δ 7.59 (s, br, 2H, aryl CH), 6.74–6.14 (m, br, 2H, aryl CH), 4.53 [s, 2H, β-C₅H₄R(Ru)], 4.51 [s, 5H, C₅H₅(Ru)], 4.43 [s, 2H, α-C₅H₅R(Ru)], 4.28 (s, 2H, CH₂OOC), 4.09 [s, 7H, β-C₅H₄R(Fe) and C₅H₅(Fe)], 4.04 [s, 2H, α-C₅H₄R(Fe)], 2.46 [s, 2H, (Fe)C₅H₄CH₂CH₂], 2.32 [s, 2H, (Ru)C₅H₄CH₂CH₂], 1.89 (s, 2H, CH₂CH₂OOC), 1.73–1.53 (m, 6H, (Fe)C₅H₄CH₂, (Ru)C₅H₄CH₂, PCH₂CH₂CH₂], 1.48 (s, 2H, CH₂CH₂CH₂OOC), 1.80–0.85 (m, br, 3H, ArCHCH₂, ArCHCH₂). ³¹P{¹H} NMR: δ -29.2 (s). FT-IR: 3086 (w), 2925 (w), 2850 (w), 1713 (s), 1608 (w), 1417 (w), 1312 (w), 1270 (s), 1178 (m), 1100 (s), 1040 (w), 1017 (m), 997 (m), 916 (w), 855 (w), 804 (s), 772 (m), 706 (s) cm⁻¹. UV-vis (CH₂Cl₂): λ_{max} 322 nm (ε = 300 M⁻¹ cm⁻¹) and 437 nm (ε = 100 M⁻¹ cm⁻¹).

Preparation of Tertiary Phosphine Sulfide Polymer **5.8•S** (1 × Fc, 1 × Rc)

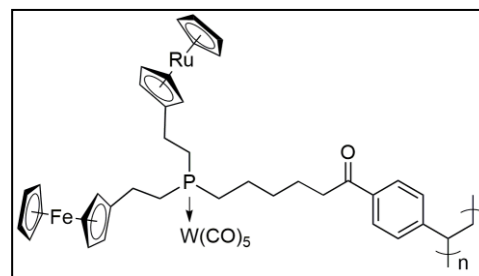
In air, tertiary phosphine polymer **5.8** (0.02 g, 0.03 mmol) and S₈ (0.02 g, 0.08 mmol, 2.7 equiv.) were combined in 2.00 mL of a CHCl₃ and stirred for 30 min at room temperature. The resulting mixture was gravity filtered and poured into Et₂O and the solids were separated by centrifugation before



they were collected, dissolved in a minimum amount of CHCl₃, and precipitated in Et₂O twice more. The tertiary phosphine sulfide polymer **5.8•S** was dried *in vacuo*, and in the presence of P₂O₅, at 60 °C for 16 h to yield a yellow powder. Yield = 0.14 g, 67%. ¹H NMR: δ 7.56 (s, br, 2H, aryl CH), 6.77–6.01 (m, br, 2H, aryl CH), 4.52 [s, 7H, β-C₅H₄R(Ru) and C₅H₅(Ru)], 4.44 [s, 2H, α-C₅H₅R(Ru)], 4.28 (s, 2H, CH₂OOC), 4.11 [s, 7H, β-C₅H₄R(Fe) and C₅H₅(Fe)], 4.06 [s, 2H, α-C₅H₄R(Fe)], 2.67 [s, 2H, (Fe)C₅H₄CH₂CH₂], 2.51 [s, 2H, (Ru)C₅H₄CH₂CH₂], 2.18–1.97 (m, 4H, CH₂CH₂OOC, PCH₂CH₂CH₂), 1.98–1.67 (m, 6H, (Fe)C₅H₄CH₂, (Ru)C₅H₄CH₂, CH₂CH₂CH₂OOC], 1.57 (s, br, 1H, ArCHCH₂), 1.34 (s, br, 2H, ArCHCH₂). ³¹P{¹H} NMR: δ 47.7 (s). GPC (THF, conventional calibration vs. PS standards): M_n = 9,700 g mol⁻¹, M_w = 14,200 g mol⁻¹, D = 1.46.

Preparation of Coordinated-Tertiary Phosphine Polymer **5.8•W(CO)₅** (1 × Fc, 1 × Rc, 1 × W(CO)₅)

In a glovebox, a quartz tube was charged with W(CO)₆ (0.15 g, 0.43 mmol, 6 equiv.) and THF (4 mL) capped with a rubber septum, and transferred to a fumehood before it was exposed to UV light for 45 min to produce a golden yellow solution. In a second flask, tertiary phosphine polymer **5.8**



(0.05 g, 0.07 mmol) was dissolved in THF (4 mL) and added to the W(CO)₅•THF solution in a dropwise manner before the resulting solution stirred for 60 min, concentrated, and

poured into dry Et₂O, and the solids were separated by centrifugation. The orange powder was collected, dissolved in a minimum amount of THF, and precipitated in Et₂O once more before the coordinated-tertiary phosphine polymer **5.8•W(CO)₅** was dried *in vacuo*, and in the presence of P₂O₅, at 60 °C for 16 h to yield a yellow powder. Yield = 0.05 g, 66%. ¹H NMR: δ 7.56 (s, br, 2H, aryl CH), 6.81–6.00 (m, br, 2H, aryl CH), 4.52 [s, 7H, β-C₅H₄R(Ru) and C₅H₅(Ru)], 4.44 [s, 2H, α-C₅H₅R(Ru)], 4.28 (s, 2H, CH₂OOC), 4.10 [s, 7H, β-C₅H₄R(Fe) and C₅H₅(Fe)], 4.07 [s, 2H, α-C₅H₄R(Fe)], 2.53 [s, 2H, (Fe)C₅H₄CH₂CH₂], 2.35 [s, 2H, (Ru)C₅H₄CH₂CH₂], 2.24–1.58 (m, 10H, CH₂CH₂OOC, PCH₂CH₂CH₂, (Fe)C₅H₄CH₂, (Ru)C₅H₄CH₂, CH₂CH₂CH₂OOC], 1.55 (s, br, 1H, ArCHCH₂), 1.30 (s, br, 2H, ArCHCH₂). ³¹P{¹H} NMR: δ –6.1 (s). FT-IR: 3088 (w), 2932 (w), 2848 (w), 2066 (m), 1974 (w), 1909 (s), 1717 (m), 1609 (w), 1418 (w), 1273 (m), 1180 (w), 1103 (m), 1018 (w), 809 (m), 708 (w), 600 (w) cm⁻¹. UV-vis (CH₂Cl₂): λ_{max} 325 nm (ε = 450 M⁻¹ cm⁻¹) and 430 nm (ε = 100 M⁻¹ cm⁻¹). GPC (THF, conventional calibration vs. PS standards): M_n = 11,600 g mol⁻¹, M_w = 28,000 g mol⁻¹, Đ = 2.41.

5.5 References

1. Liu, S.; Zhang, K.; Lu, J.; Zhang, J.; Yip, H.-L.; Huang, F.; Cao, Y. *J. Am. Chem. Soc.* **2013**, *135*, 15326–15329.
2. Deraedt, C.; Rapakousiou, A.; Wang, Y.; Salmon, L.; Bousquet, M.; Astruc, D. *Angew. Chem. Int. Ed.* **2014**, *53*, 8445–8449.
3. Gould, O. E. C.; Qiu, H.; Lunn, D. J.; Rowden, J.; Harniman, R. L.; Hudson, Z. M.; Winnik, M. A.; Miles, M. J.; Manners, I. *Nat. Commun.* **2015**, *6*, 10009.
4. Li, X.; Gao, Y.; Boott, C. E.; Winnik, M. A.; Manners, I. *Nat. Commun.* **2015**, *6*, 8127.
5. Braunschweig, H.; Damme, A.; Demeshko, S.; Dück, K.; Kramer, T.; Krummenacher, I.; Meyer, F.; Radacki, K.; Stellwag-Konertz, S.; Whittell, G. R. *J. Am. Chem. Soc.* **2015**, *137*, 1492–1500.
6. Chen, P.; Li, Q.; Grindy, S.; Holten-Andersen, N. *J. Am. Chem. Soc.* **2015**, *137*, 11590–11593.
7. Qiu, H.; Gao, Y.; Boott, C. E.; Gould, O. E. C.; Harniman, R. L.; Miles, M. J.; Webb, S. E. D.; Winnik, M. A.; Manners, I. *Science* **2016**, *352*, 697–701.
8. Winter, A.; Schubert, U. S. *Chem. Soc. Rev.* **2016**, *45*, 5311–5357.
9. Li, X.; Gao, Y.; Boott, C. E.; Hayward, D. W.; Harniman, R.; Whittell, G. R.; Richardson, R. M.; Winnik, M. A.; Manners, I. *J. Am. Chem. Soc.* **2016**, *138*, 4087–4095.
10. Abd-El-Aziz, A. S.; Kucukkaya, I.; Wagner, B. D., Advances in metal-containing macromolecules. In *Reference Module in Materials Science and Materials Engineering*, Elsevier: 2016.
11. Li, S.; Lin, M. M.; Toprak, M. S.; Kim, D. K.; Muhammed, M. *Nano Rev.* **2010**, *1*, 5214.

12. Whittell, G. R.; Hager, M. D.; Schubert, U. S.; Manners, I. *Nat. Mater.* **2011**, *10*, 176–188.
13. Astruc, D.; Chardac, F. *Chem. Rev.* **2001**, *101*, 2991–3023.
14. Buchmeiser, M. R. *Chem. Rev.* **2009**, *109*, 303–321.
15. McConnell, A. J.; Wood, C. S.; Neelakandan, P. P.; Nitschke, J. R. *Chem. Rev.* **2015**, *115*, 7729–7793.
16. Zhang, K. Y.; Liu, S.; Zhao, Q.; Huang, W. *Coord. Chem. Rev.* **2016**, *319*, 180–195.
17. Stanley, J. M.; Holliday, B. J. *Coord. Chem. Rev.* **2012**, *256*, 1520–1530.
18. Yan, Y.; Zhang, J.; Ren, L.; Tang, C. *Chem. Soc. Rev.* **2016**, *45*, 5232–5263.
19. Holliday, B. J.; Swager, T. M. *Chem. Commun.* **2005**, 23–36.
20. Wolf, M. O. *J. Inorg. Organomet. Polym.* **2006**, *16*, 189–199.
21. Liu, K.; Ho, C.-L.; Aouba, S.; Zhao, Y.-Q.; Lu, Z.-H.; Petrov, S.; Coombs, N.; Dube, P.; Ruda, H. E.; Wong, W.-Y.; Manners, I. *Angew. Chem. Int. Ed.* **2008**, *47*, 1255–1259.
22. Gilroy, J. B.; Patra, S. K.; Mitchels, J. M.; Winnik, M. A.; Manners, I. *Angew. Chem. Int. Ed.* **2011**, *50*, 5851–5855.
23. Dong, Q.; Li, G.; Ho, C.-L.; Faisal, M.; Leung, C.-W.; Pong, P. W.-T.; Liu, K.; Tang, B.-Z.; Manners, I.; Wong, W.-Y. *Adv. Mater.* **2012**, *24*, 1034–1040.
24. Zhang, J.; Ren, L.; Hardy, C. G.; Tang, C. *Macromolecules* **2012**, *45*, 6857–6863.
25. Zha, Y.; Thaker, H. D.; Maddikeri, R. R.; Gido, S. P.; Tuominen, M. T.; Tew, G. N. *J. Am. Chem. Soc.* **2012**, *134*, 14534–14541.
26. Zhang, J.; Yan, Y.; Chance, M. W.; Chen, J.; Hayat, J.; Ma, S.; Tang, C. *Angew. Chem. Int. Ed.* **2013**, *52*, 13387–13391.

27. Zhang, J.; Yan, Y.; Chen, J.; Chance, W. M.; Hayat, J.; Gai, Z.; Tang, C. *Chem. Mater.* **2014**, *26*, 3185–3190.
28. Dong, Q.; Li, G.; Wang, H.; Wing-Tat Pong, P.; Leung, C.-W.; Manners, I.; Ho, C.-L.; Li, H.; Wong, W.-Y. *J. Mater. Chem.* **2015**, *3*, 734–741.
29. Ciganda, R.; Gu, H.; Castel, P.; Zhao, P.; Ruiz, J.; Hernández, R.; Astruc, D. *Macromol. Rapid Commun.* **2016**, *37*, 105–111.
30. Meng, Z.; Sato, K.; Sukegawa, T.; Oyaizu, K.; Ho, C.-L.; Xiang, J.; Feng, Y.-H.; Lo, Y. H.; Nishide, H.; Wong, W.-Y. *J. Organomet. Chem.* **2016**, 51–55.
31. Cheng, A. Y.; Clendenning, S. B.; Yang, G.; Lu, Z.-H.; Yip, C. M.; Manners, I. *Chem. Commun.* **2004**, 780–781.
32. Clendenning, S. B.; Han, S.; Coombs, N.; Paquet, C.; Rayat, M. S.; Grozea, D.; Brodersen, P. M.; Sodhi, R. N. S.; Yip, C. M.; Lu, Z. H.; Manners, I. *Adv. Mater.* **2004**, *16*, 291–296.
33. Chan, W. Y.; Clendenning, S. B.; Berenbaum, A.; Lough, A. J.; Aouba, S.; Ruda, H. E.; Manners, I. *J. Am. Chem. Soc.* **2005**, *127*, 1765–1772.
34. Liu, K.; Clendenning, S. B.; Friebe, L.; Chan, W. Y.; Zhu; Freeman, M. R.; Yang, G. C.; Yip, C. M.; Grozea, D.; Lu, Z.-H.; Manners, I. *Chem. Mater.* **2006**, *18*, 2591–2601.
35. Chabanne, L.; Matas, I.; Patra, S. K.; Manners, I. *Polym. Chem.* **2011**, *2*, 2651–2660.
36. Zamora, M.; Bruña, S.; Alonso, B.; Cuadrado, I. *Macromolecules* **2011**, *44*, 7994–8007.
37. Paquette, J. A.; Gilroy, J. B. *J. Polym. Sci., Part A: Polym. Chem.* **2016**, *54*, 3257–3266.

38. Hailes, R. L. N.; Oliver, A. M.; Gwyther, J.; Whittell, G. R.; Manners, I. *Chem. Soc. Rev.* **2016**, *45*, 5358–5407.
39. Abd-El-Aziz, A. S.; Winram, D. J.; Shipman, P. O.; Bichler, L. *Macromol. Rapid Commun.* **2010**, *31*, 1992–1997.
40. Erhard, M.; Lam, K.; Haddow, M.; Whittell, G. R.; Geiger, W. E.; Manners, I. *Polymer. Chem.* **2014**, *5*, 1264–1274.
41. Rabiee Kenaree, A.; Berven, B. M.; Ragogna, P. J.; Gilroy, J. B. *Chem. Commun.* **2014**, *50*, 10714–10717.
42. Rabiee Kenaree, A.; Gilroy, J. B. *Dalton Trans.* **2016**, *45*, 18229–18240.
43. Rabiee Kenaree, A.; Cuthbert, T. J.; Barbon, S. M.; Boyle, P. D.; Gillies, E. R.; Ragogna, P. J.; Gilroy, J. B. *Organometallics* **2015**, *34*, 4272–4280.
44. Rauhut, M. M.; Currier, H. A.; Semsel, A. M.; Wystrach, V. P. *J. Org. Chem.* **1961**, *26*, 5138–5145.
45. Obata, T.; Kobayashi, E.; Aoshima, S.; Furukawa, J. *Polym. J.* **1993**, *25*, 1039–1048.
46. Patra, S. K.; Whittell, G. R.; Nagiah, S.; Ho, C.-L.; Wong, W.-Y.; Manners, I. *Chem. Eur. J.* **2010**, *16*, 3240–3250.
47. Lide, D. R. *CRC Handbook of Chemistry and Physics*. 89 ed.; CRC Press: Boca Raton, FL: 2008.
48. Orgel, L. E. *Inorg. Chem.* **1962**, *1*, 25–29.
49. Cotton, F. A.; Kraihanzel, C. S. *J. Am. Chem. Soc.* **1962**, *84*, 4432–4438.
50. Rabiee Kenaree, A.; Sauve, E. R.; Ragogna, P. J.; Gilroy, J. B. *Dalton Trans.* **2016**, *45*, 2859–2867.
51. Grim, S. O.; McAllister, P. R.; Singer, R. M. *Chem. Commun.* **1969**, 38–39.

52. Trupia, S.; Nafady, A.; Geiger, W. E. *Inorg. Chem.* **2003**, *42*, 5480–5482.
53. Swarts, J. C.; Nafady, A.; Roudebush, J. H.; Trupia, S.; Geiger, W. E. *Inorg. Chem.* **2009**, *48*, 2156–2165.
54. Geiger, W. E.; Barrière, F. *Acc. Chem. Res.* **2010**, *43*, 1030–1039.
55. Russell, A. D.; Gilroy, J. B.; Lam, K.; Haddow, M. F.; Harvey, J. N.; Geiger, W. E.; Manners, I. *Chem. Eur. J.* **2012**, *18*, 8000–8003.
56. Russell, A. D.; Gilroy, J. B.; Lam, K.; Haddow, M. F.; Harvey, J. N.; Geiger, W. E.; Manners, I. *Chem. Eur. J.* **2014**, *20*, 16216–16227.
57. Downard, A. J.; Goodwin, N. J.; Henderson, W. J. *Organomet. Chem.* **2003**, *676*, 62–72.
58. Seibert, A. R.; Cain, M. F.; Glueck, D. S.; Nataro, C. J. *Organomet. Chem.* **2011**, *696*, 2259–2262.
59. Abbott, A. P.; Malkov, A. V.; Zimmermann, N.; Raynor, J. B.; Ahmed, G.; Steele, J.; Kočovský, P. *Organometallics* **1997**, *16*, 3690–3695.

Chapter 6

6 Conclusions and Future Work

6.1 Conclusions

This dissertation presents our novel strategy involving the exploitation of hydrophosphination chemistry for the incorporation of transition metals into polymers. We have demonstrated that the radical-catalyzed hydrophosphination of vinylmetallocenes (metallocene: ferrocene and ruthenocene) is a straightforward method for the synthesis of primary, secondary, and tertiary ethylmetallocene phosphines that demonstrated exceptional stability toward air and moisture (Figure 6.1). This stability allowed for their facile purification in air as confirmed by several characterization techniques, including multinuclear NMR, FT-IR, and UV-vis absorption spectroscopy, mass spectrometry, elemental analysis, cyclic voltammetry, and X-ray crystallography.

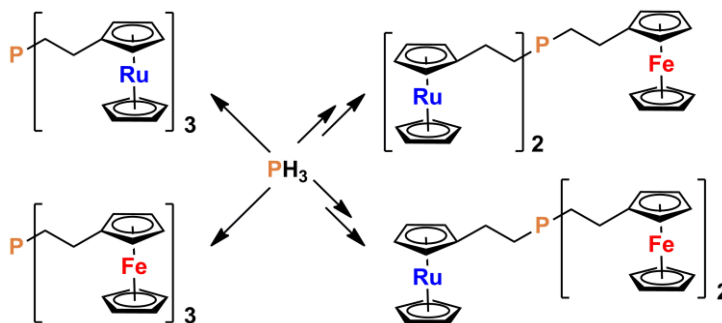


Figure 6.1. The synthesis of metal-containing phosphines from PH_3 gas.

To investigate the coordination behavior of this new family of phosphines and show that the ligand steric effects could be tuned by determination of number of ethylferrocene substituents on the phosphorous centre, we selected primary, secondary, and tertiary ethylferrocenephosphines, as representatives, and reacted them with photolytically produced $\text{M}(\text{CO})_5\cdot\text{THF}$ (M : Cr, Mo, W) (Figure 6.2). The successful coordination of all three ethylferrocenephosphines to the $\text{M}(\text{CO})_5$ moieties proved that the presence of bulky substituents in the phosphine structures didn't inhibit the phosphines from the ligation to

the metals. Analysis of FT-IR spectra for the benchmarking of the phosphines revealed that the σ donating ability of our primary, secondary, and tertiary ethylferrocenephosphines increased as ethylferrocene substituents were introduced and that the σ donating ability of our tertiary phosphine was higher than PPh_3 and lower compared to PEt_3 .

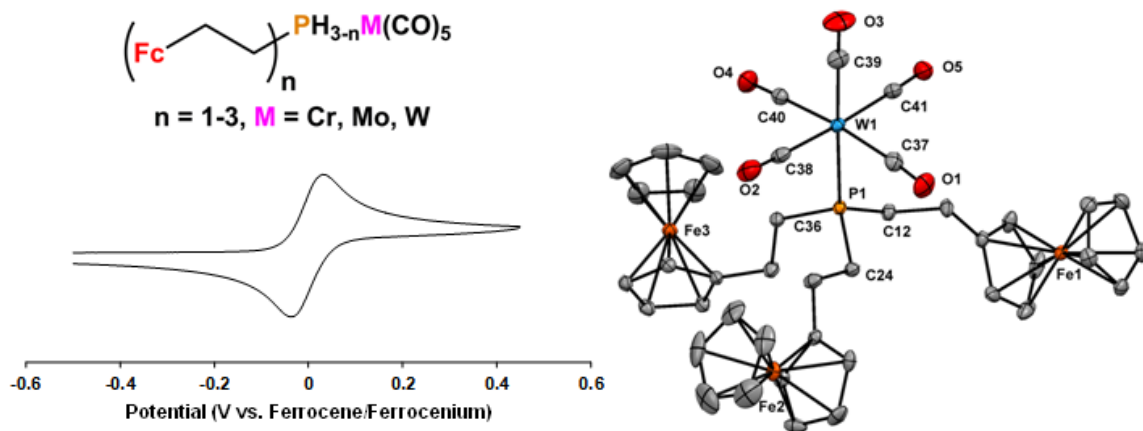


Figure 6.2. Solid-state structure and properties of $\text{W}(\text{CO})_5$ -phosphine metal complexes.

To test our design strategy for the synthesis of MCPs from metal-containing phosphine precursors, we synthesized a phosphonium triflate monomer by a three-step quaternization, esterification, and salt metathesis protocol. Free-radical polymerization of this monomer afforded phosphonium polyelectrolyte salts, and their macromolecular nature was confirmed by multinuclear NMR spectroscopy, GPC and DSC experiments. The full characterization of the monomer and polymers verified that their metal centres were preserved and that our strategy for the incorporation of metals into polymer structures was successful. In addition, the observation of high char yields during TGA experiments suggested the execution of pyrolysis studies which led to the formation of metal-containing nanoparticles (Figure 6.3).

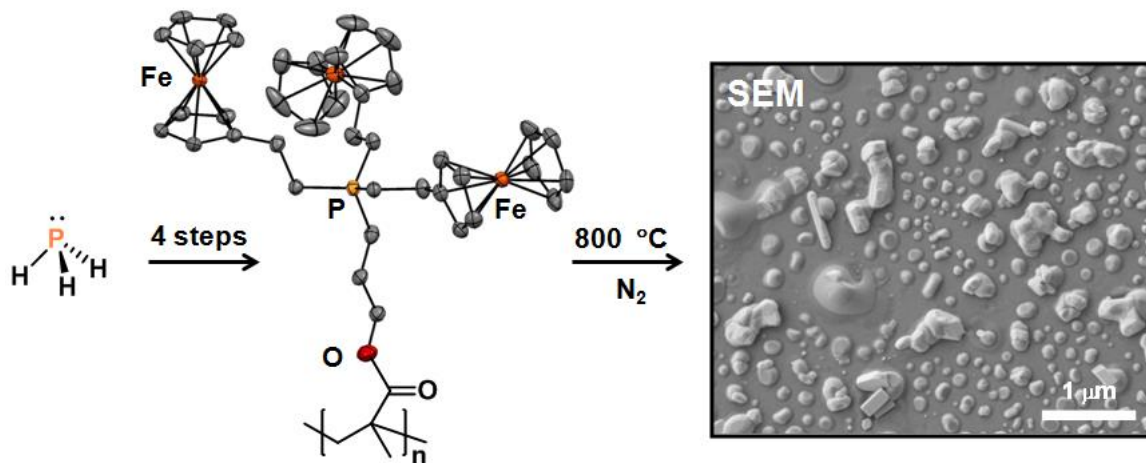


Figure 6.3. The production of nanomaterials from metal-containing polymers.

The fact that, in our strategy, the metal content/ratio of the monomers/polymers reflected that in the phosphine precursors motivated us to utilize this method for the synthesis of heterobimetallic phosphonium polyelectrolyte salts with precisely controlled metal content/ratio. By the quaternization reaction of four different tertiary ethylmetallocenophosphines (where ferrocene/ruthenocene: 3/0, 2/1, 1/2, and 0/3) with 4-vinylbenzylchloride and a salt metathesis reaction, we prepared four monomers that were successfully polymerized in the presence of AIBN. Extensive characterization of the monomers and polymers verified that all metallocene units in the structure of the monomers and polymers remained intact and that our strategy for the control of Fe/Ru ratios at both monomer and polymer levels were successful. Furthermore, analysis of the nanomaterials that resulted from the pyrolysis of these four phosphonium polyelectrolytes, demonstrated their potential for the production of highly metallized nanomaterials with metal ratios influenced by that of the corresponding phosphonium polyelectrolytes.

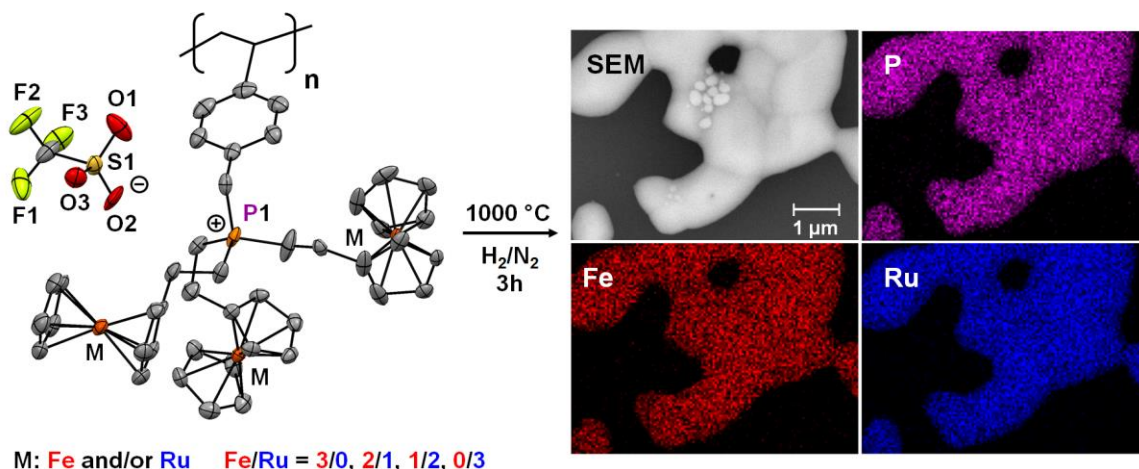
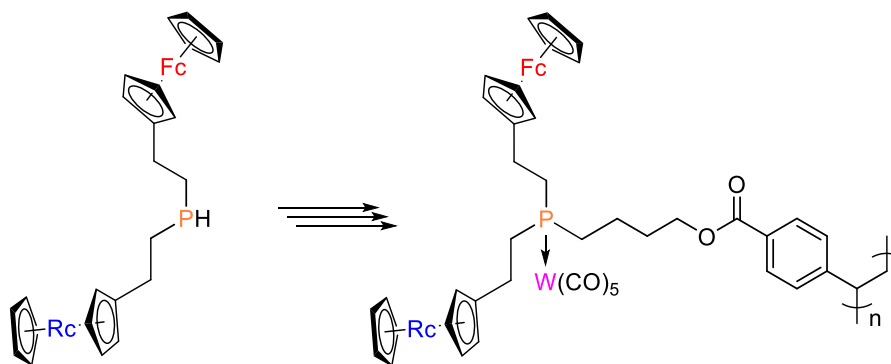


Figure 6.4. The synthesis of highly metallized nanomaterials from heterobimetallic phosphonium polyelectrolyte salts.

En route to a heterotrimetallic tertiary phosphine polymer, we took advantage of the reactivity of the P-H bond in the structure of a secondary ferrocene- and ruthenocene-containing phosphine and, in two steps, synthesized a styrene-based tertiary phosphine monomer that was polymerized by using a free-radical polymerization method. The resulting heterobimetallic tertiary phosphine polymer was coordinated to a photogenerated $W(CO)_5 \cdot THF$ metal complex in order to produce a novel heterotrimetallic polymer (Scheme 6.1). Extensive characterization of the monomer, tertiary phosphine polymer, and coordinated tertiary phosphine polymer showed that all of the phosphine centres in the tertiary phosphine polymer were coordinated to $W(CO)_5$ and that the metallocene moieties didn't degrade during the reactions. These results leave no doubt that we have successfully synthesized the first example of a heterotrimetallic polymers and again show the strength of our methodology for the synthesis of MCPs.



Scheme 6.1. Synthesis of a heterotrimetallic polymer.

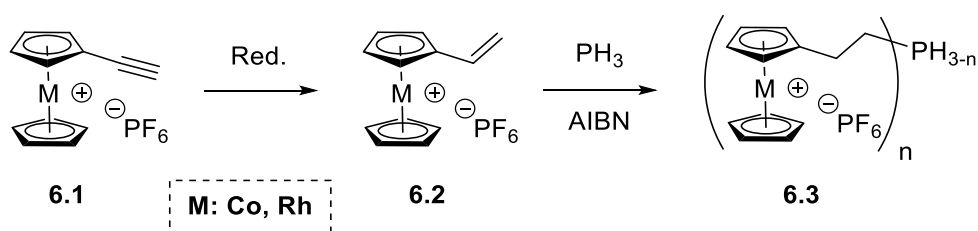
Overall, we have developed a new synthetic strategy for the preparation of stable metal-containing phosphines that can be utilized as ligands with tunable steric effects that also serve as precursors to heterometallic polymers with controlled metal ratios. In addition, we studied the pyrolysis behavior of our metal-containing polymers and proved their potential for the production of highly metallized nanomaterials. We believe that our results clearly demonstrate the success of our strategy and open a new door for materials scientists for the preparation of novel heterometallic polymers as well as nanomaterials.

6.2 Future Work

This work can be expanded in many different directions. Below, a few are described.

6.2.1 Novel MCP Designs: Based on New Stable Phosphines/Polymerizable Groups

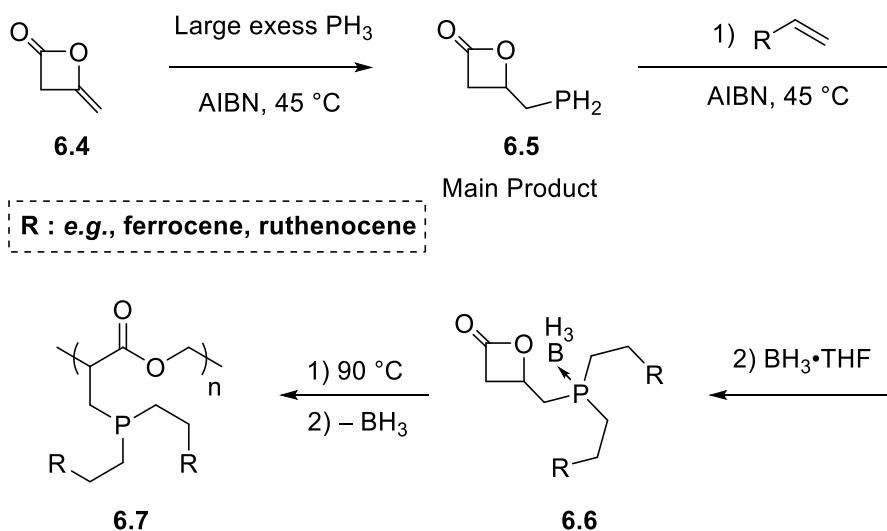
The hydrophosphination reaction of organometallic compounds bearing an olefin group can add several new members to this family of stable metal-containing phosphines. For example, alkyne substituted rhodocenium and cobaltocenium salts¹⁻² are good candidates for the synthesis of the corresponding vinylmetallocenes and following hydrophosphination reactions (Scheme 6.2). This approach can be beneficial for the realization of heterotrimetallic phosphines that combine the properties of three different transition metals.



Scheme 6.2. Synthesis of rhodocenium- and cobaltocenium-based phosphines.

The utilization of different polymerizable groups is another route that may afford novel MCPs. For instance, the hydrophosphination of **6.4** in the presence of catalytic amount of AIBN, large excess of PH_3 , and under a mild thermal condition can result in the production of **6.5**, which is likely to be stable toward air due to the presence of heteroatoms in close

proximity of the phosphorous. This PH_2 group can react with organometallic compounds bearing an olefin group to afford highly metallized monomers that can be protected by use of groups such as BH_3 and further undergo a ring-opening polymerization. The P centres in the structure of the resulting polymers can be later deprotected and be used as precursors to heterometallic polymers (Scheme 6.3).



Scheme 6.3. A novel MCP design based on a hydrophosphination reaction.

6.2.2 Block Copolymer Synthesis and Self-Assembly

In this dissertation, the free-radical polymerization of metal-containing phosphonium salts and a tertiary phosphine are described. Polymerization of these monomers with different comonomers via living methods such as reversible addition-fragmentation chain-transfer (RAFT) polymerization can afford diblock copolymers that can self-assemble into morphologies with metallic and non-metallic nano-sized domains. The pyrolysis of such materials in the solid-state can afford patterns of highly metallized nanomaterials (Figure 6.5).

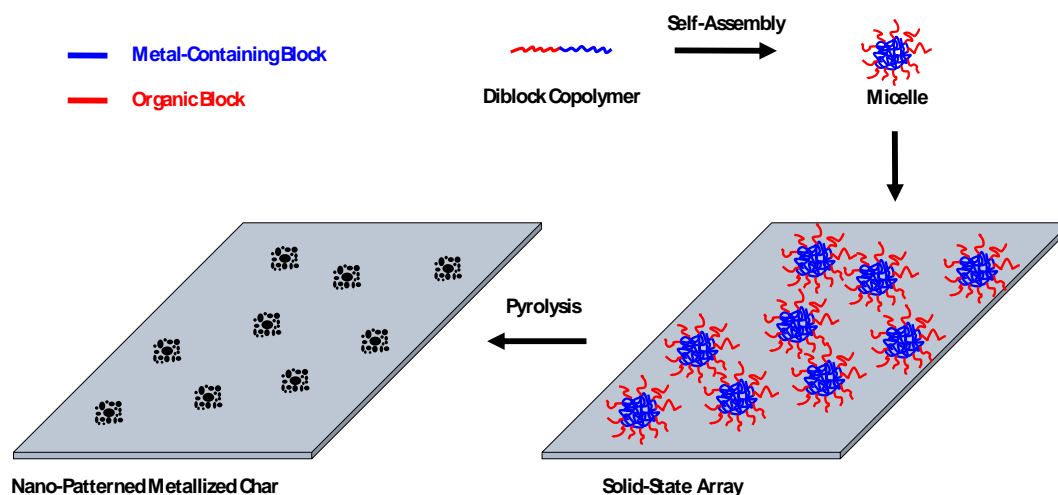


Figure 6.5. Self-assembly and nano-patterning of metallized nanomaterials.

6.2.3 Electron-Beam Lithography

Electron-beam lithography (EBL) is a method that can convert thin films of MCPs to patterns of metallized nanomaterials that may be used for data storage purposes or as templated nanocatalyst.³ The fact that pyrolysis of the phosphonium polyelectrolytes films yielded metal-containing nanomaterials is very encouraging for the use of our synthesized polymers as resists for EBL (Figure 6.6).

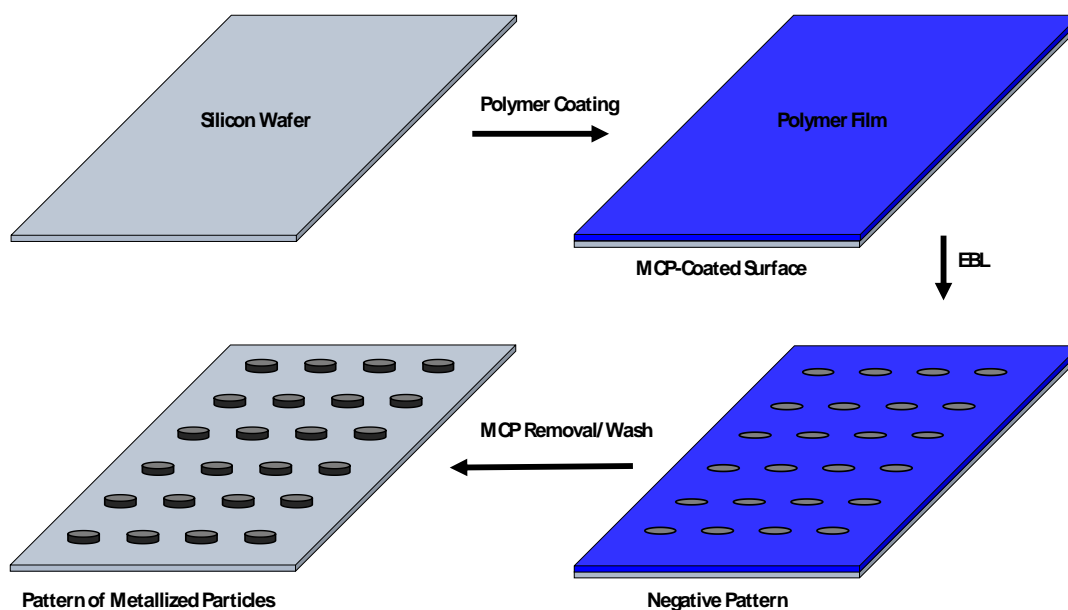


Figure 6.6. Fabrication of patterned nanomaterials by use of EBL.

6.2.4 Catalysis

Nano-sized transition metal phosphides comprised of FeP, Ni₂P, Co₂P, MoP, and WP have attracted great attention due to their activity toward H₂ production.⁴⁻⁵ As our preliminary characterization of the nanomaterials produced from the pyrolysis of phosphonium polyelectrolytes confirmed that they are enriched with Fe/Ru/P, investigation of their catalytic properties for the H₂ production may show that they have catalytic properties. In addition, since the pyrolysis of our coordinated tertiary phosphine polymers is likely to afford nanomaterials with new transition metal/phosphorous combinations, their pyrolysis and the study of the catalytic behavior of the pyrolytically-produced materials are also suggested. This work can be expanded by using our methodology for the synthesis of MCPs containing other transition metals and their pyrolysis.

6.3 References

1. Yan, Y.; Zhang, J.; Qiao, Y.; Tang, C. *Macromol. Rapid Commun.* **2014**, *35*, 254–259.
2. Wei, J.; Ren, L.; Tang, C.; Su, Z. *Polym. Chem.* **2014**, *5*, 6480–6488.
3. Chan, W. Y.; Clendenning, S. B.; Berenbaum, A.; Lough, A. J.; Aouba, S.; Ruda, H. E.; Manners, I. *J. Am. Chem. Soc.* **2005**, *127*, 1765–1772.
4. Callejas, J. F.; Read, C. G.; Roske, C. W.; Lewis, N. S.; Schaak, R. E. *Chem. Mater.* **2016**, *28*, 6017–6044.
5. Shi, Y.; Zhang, B. *Chem. Soc. Rev.* **2016**, *45*, 1529–1541.

Chapter 7

Appendices

Appendix 1 – Permission to Reuse Copyrighted Material



The screenshot shows the Copyright Clearance Center RightsLink interface. At the top left is the Copyright Clearance Center logo. To its right is the RightsLink logo. Further right are navigation buttons for Home, Create Account, Help, and an email icon. Below the Copyright Clearance Center logo is the ACS Publications logo with the tagline "Most Trusted. Most Cited. Most Read." The main content area displays the following information:

Title: Patchy Nanocapsules of Poly(vinylferrocene)-Based Block Copolymers for Redox-Responsive Release

Author: Roland H. Staff, Markus Gallei, Markus Mazurowski, et al

Publication: ACS Nano

Publisher: American Chemical Society

Date: Oct 1, 2012

Copyright © 2012, American Chemical Society

On the right side of the interface, there is a LOGIN button and a text box that reads: "If you're a copyright.com user, you can login to RightsLink using your copyright.com credentials. Already a RightsLink user or want to [learn more?](#)"

PERMISSION/LICENSE IS GRANTED FOR YOUR ORDER AT NO CHARGE

This type of permission/license, instead of the standard Terms & Conditions, is sent to you because no fee is being charged for your order. Please note the following:

- Permission is granted for your request in both print and electronic formats, and translations.
- If figures and/or tables were requested, they may be adapted or used in part.
- Please print this page for your records and send a copy of it to your publisher/graduate school.
- Appropriate credit for the requested material should be given as follows: "Reprinted (adapted) with permission from (COMPLETE REFERENCE CITATION). Copyright (YEAR) American Chemical Society." Insert appropriate information in place of the capitalized words.
- One-time permission is granted only for the use specified in your request. No additional uses are granted (such as derivative works or other editions). For any other uses, please submit a new request.

If credit is given to another source for the material you requested, permission must be obtained from that source.

BACK

CLOSE WINDOW



RightsLink®

[Home](#)
[Create Account](#)
[Help](#)


ACS Publications
Most Trusted. Most Cited. Most Read.

Title: Synthesis and Characterization of a Family of Air-Stable Ferrocene- and Ruthenocene-Containing Primary, Secondary, and Tertiary Phosphines

Author: Amir Rabiee Kenaree, Tyler J. Cuthbert, Stephanie M. Barbon, et al

Publication: Organometallics

Publisher: American Chemical Society

Date: Sep 1, 2015

Copyright © 2015, American Chemical Society

LOGIN

If you're a [copyright.com](#) user, you can login to RightsLink using your [copyright.com](#) credentials. Already a [RightsLink](#) user or want to [learn more?](#)

PERMISSION/LICENSE IS GRANTED FOR YOUR ORDER AT NO CHARGE

This type of permission/license, instead of the standard Terms & Conditions, is sent to you because no fee is being charged for your order. Please note the following:

- Permission is granted for your request in both print and electronic formats, and translations.
- If figures and/or tables were requested, they may be adapted or used in part.
- Please print this page for your records and send a copy of it to your publisher/graduate school.
- Appropriate credit for the requested material should be given as follows: "Reprinted (adapted) with permission from (COMPLETE REFERENCE CITATION). Copyright (YEAR) American Chemical Society." Insert appropriate information in place of the capitalized words.
- One-time permission is granted only for the use specified in your request. No additional uses are granted (such as derivative works or other editions). For any other uses, please submit a new request.

[BACK](#)
[CLOSE WINDOW](#)

Appendix 2 – Supporting Information for Chapter 2

NMR Spectra

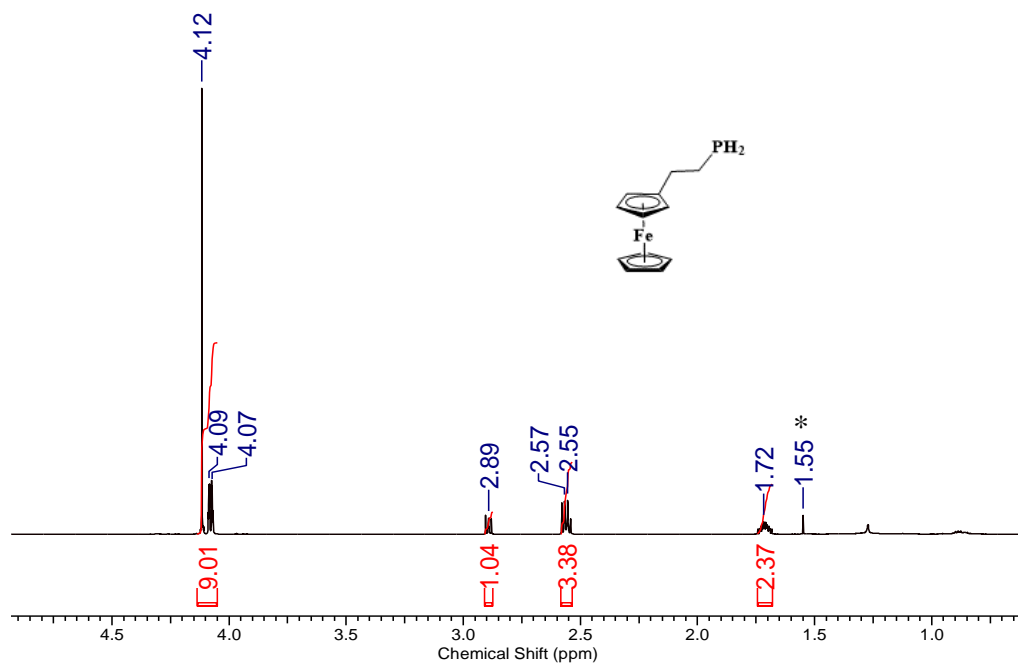


Figure A2.1. ^1H NMR spectrum of primary phosphine **2.7a** in CDCl_3 . The asterisk denotes residual H_2O signal.

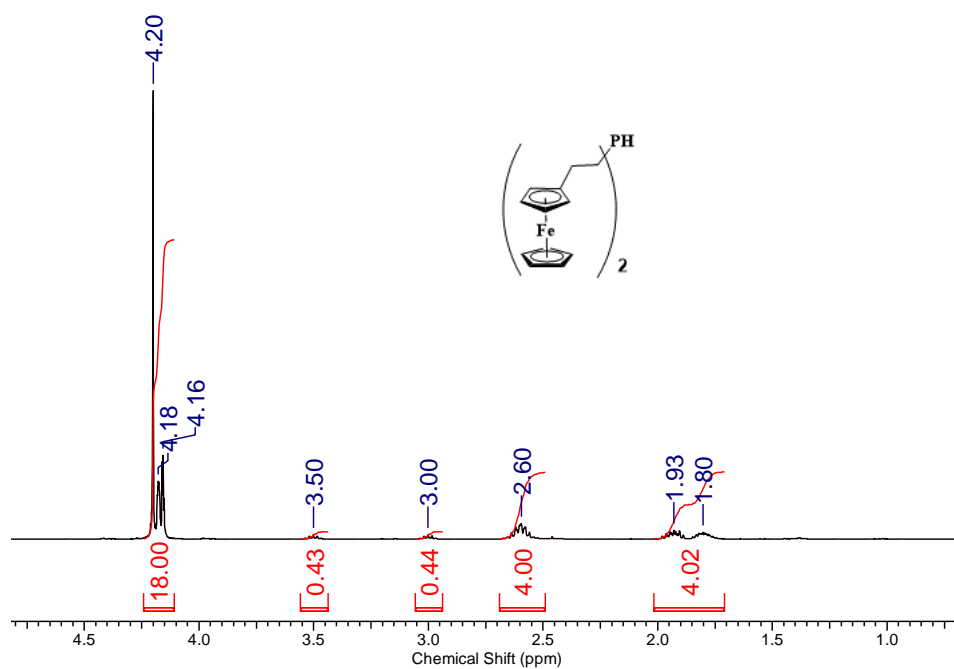


Figure A2.2. ^1H NMR spectrum of secondary phosphine **2.7b** in CDCl_3 .

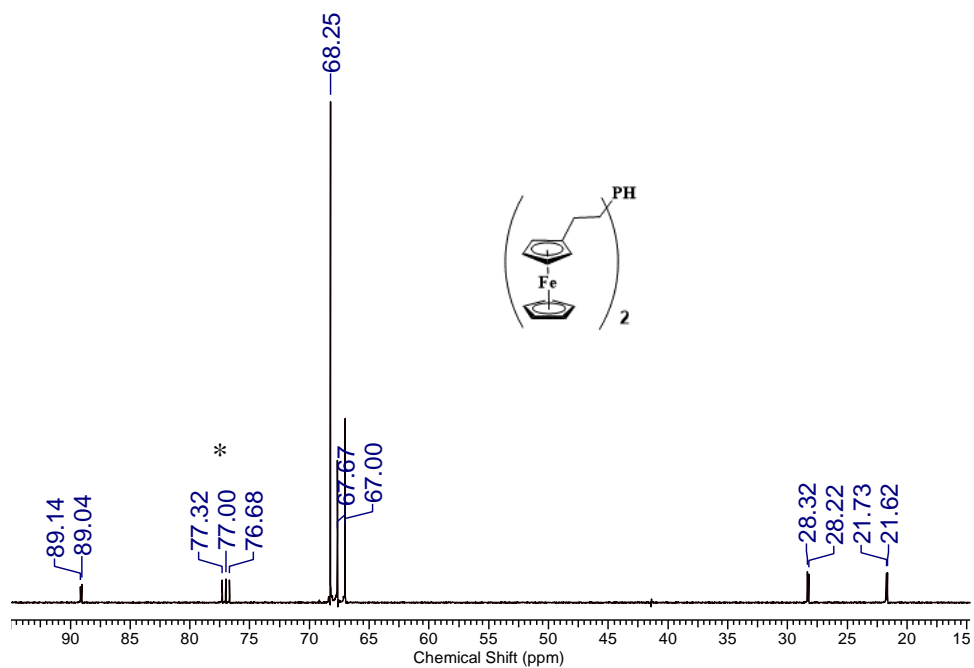


Figure A2.3. $^{13}\text{C}\{^1\text{H}\}$ NMR spectrum of secondary phosphine **2.7b** in CDCl_3 . The asterisk denotes the solvent signal.

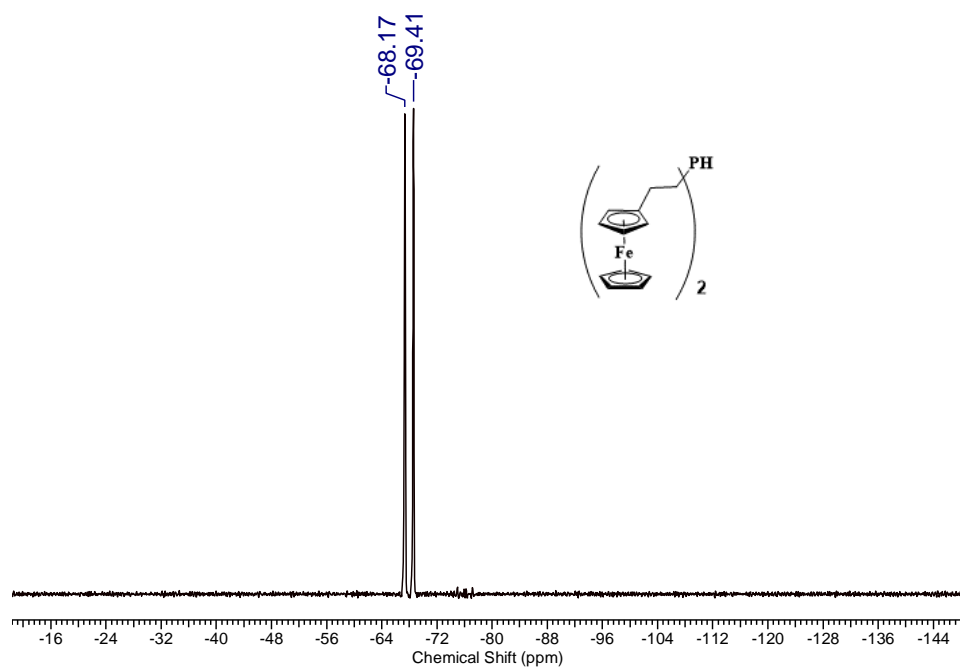


Figure A2.4. ^{31}P NMR spectrum of secondary phosphine **2.7b** in CDCl_3 .

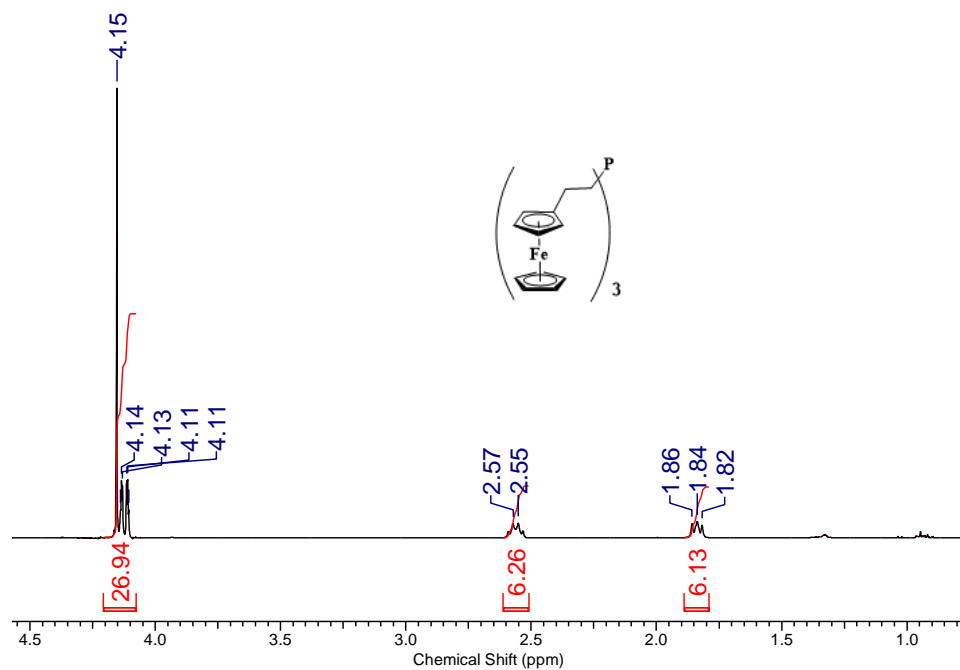


Figure A2.5. ^1H NMR spectrum of tertiary phosphine **2.7c** in CDCl_3 .

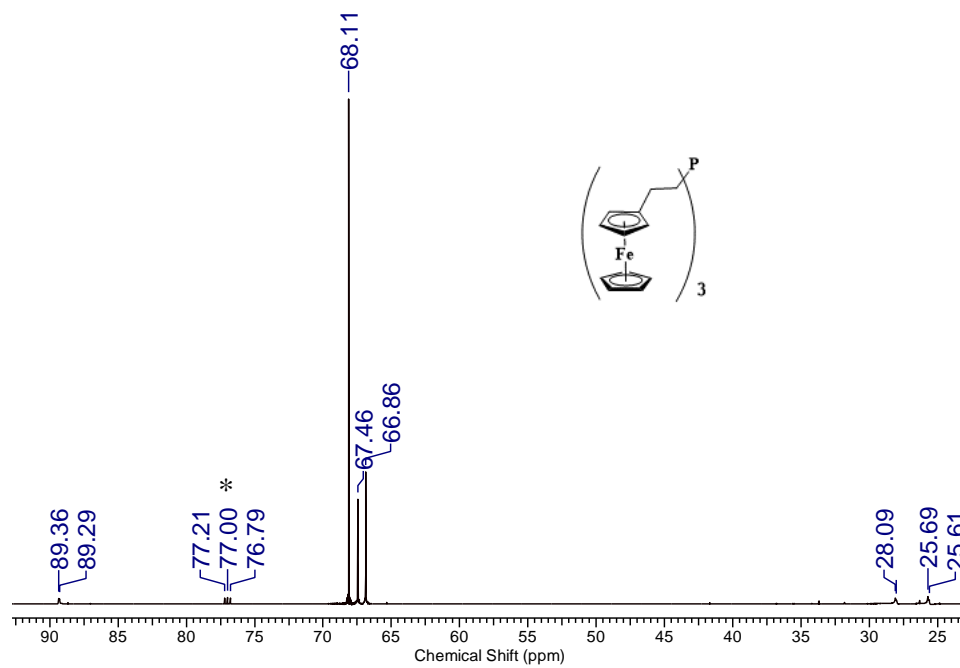


Figure A2.6. $^{13}\text{C}\{^1\text{H}\}$ NMR spectrum of tertiary phosphine **2.7c** in CDCl_3 . The asterisk denotes the solvent signal.

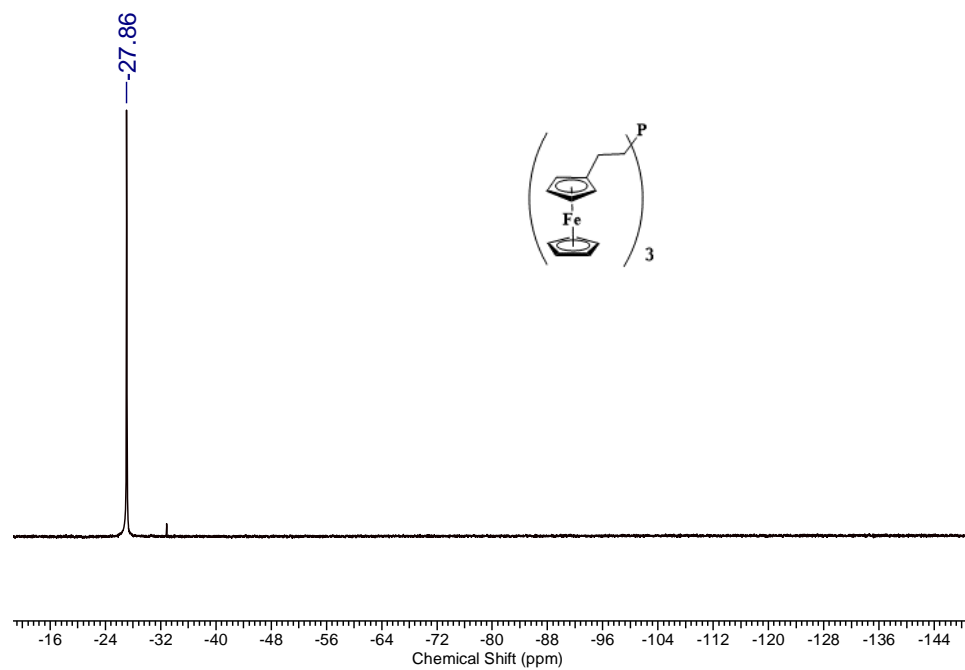


Figure A2.7. ³¹P{¹H} NMR spectrum of primary phosphine **2.7c** in CDCl₃.

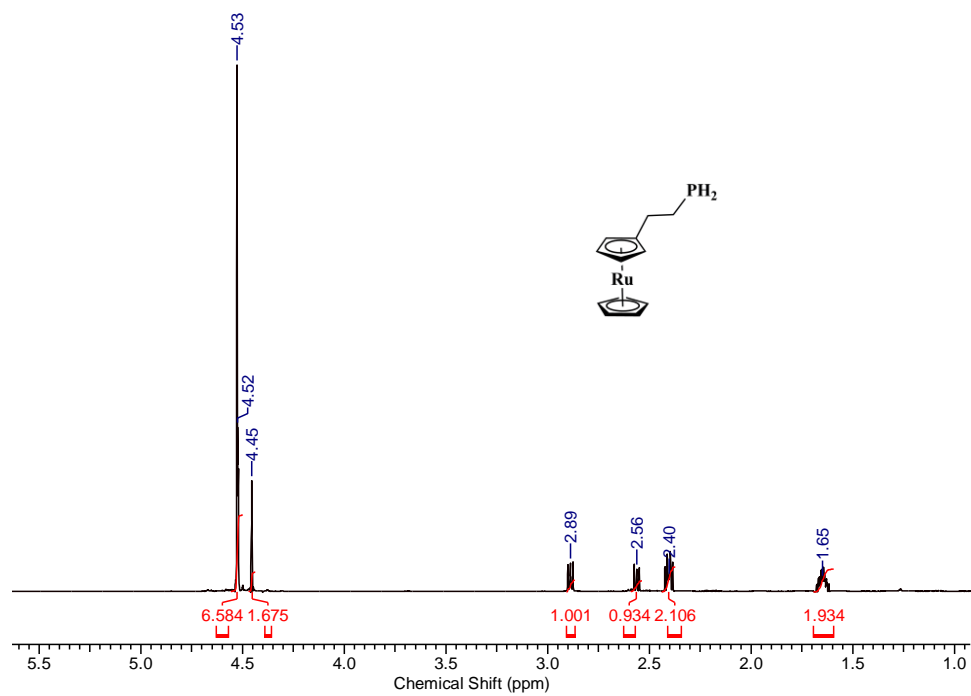


Figure A2.8. ¹H NMR spectrum of primary phosphine **2.8a** in CDCl₃.

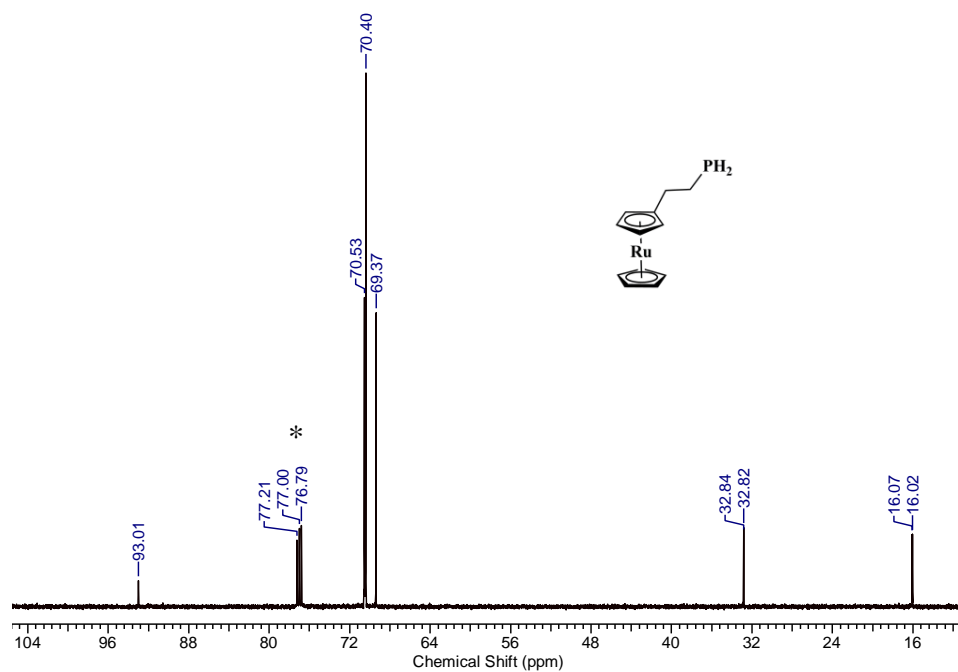


Figure A2.9. $^{13}\text{C}\{^1\text{H}\}$ NMR spectrum of primary phosphine **2.8a** in CDCl_3 . The asterisk denotes the solvent signal.

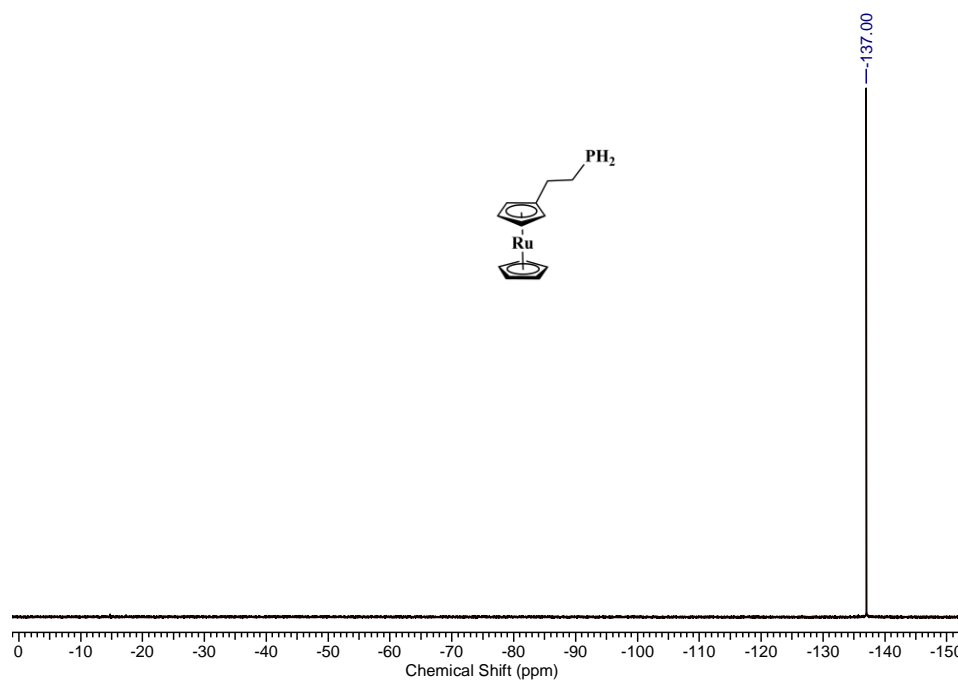


Figure A2.10. $^{31}\text{P}\{^1\text{H}\}$ NMR spectrum of primary phosphine **2.8a** in CDCl_3 .

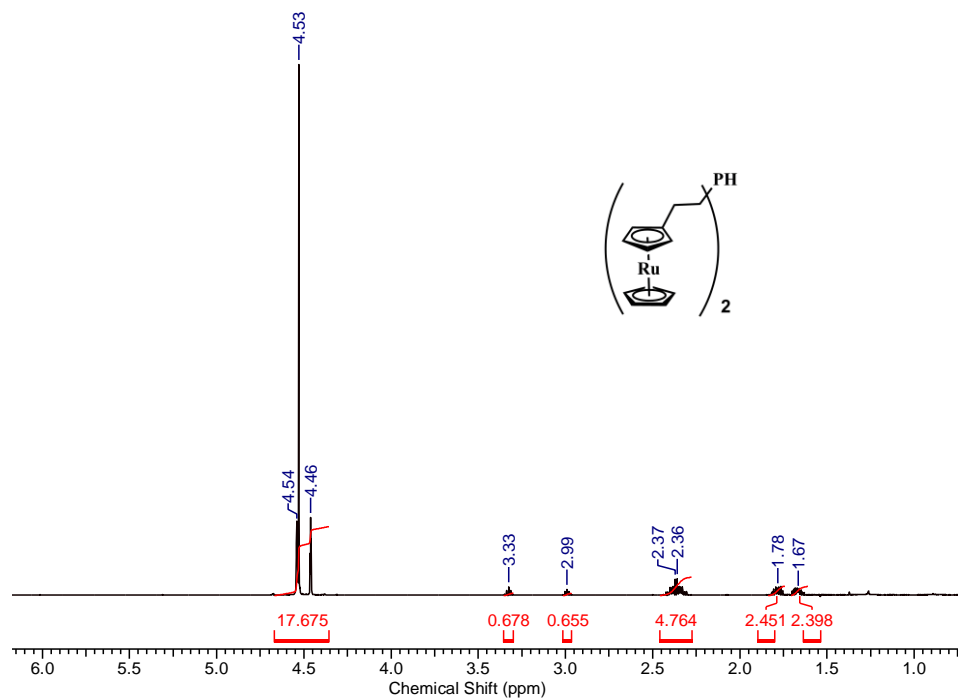


Figure A2.11. ^1H NMR spectrum of secondary phosphine **2.8b** in CDCl_3 .

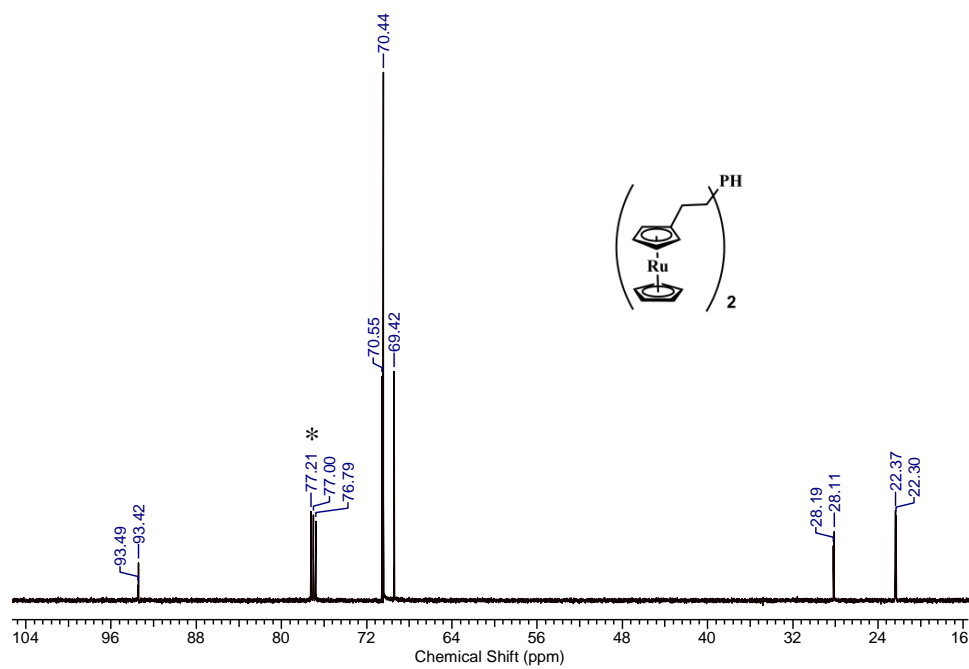


Figure A2.12. $^{13}\text{C}\{^1\text{H}\}$ NMR spectrum of secondary phosphine **2.8b** in CDCl_3 . The asterisk denotes the solvent signal.

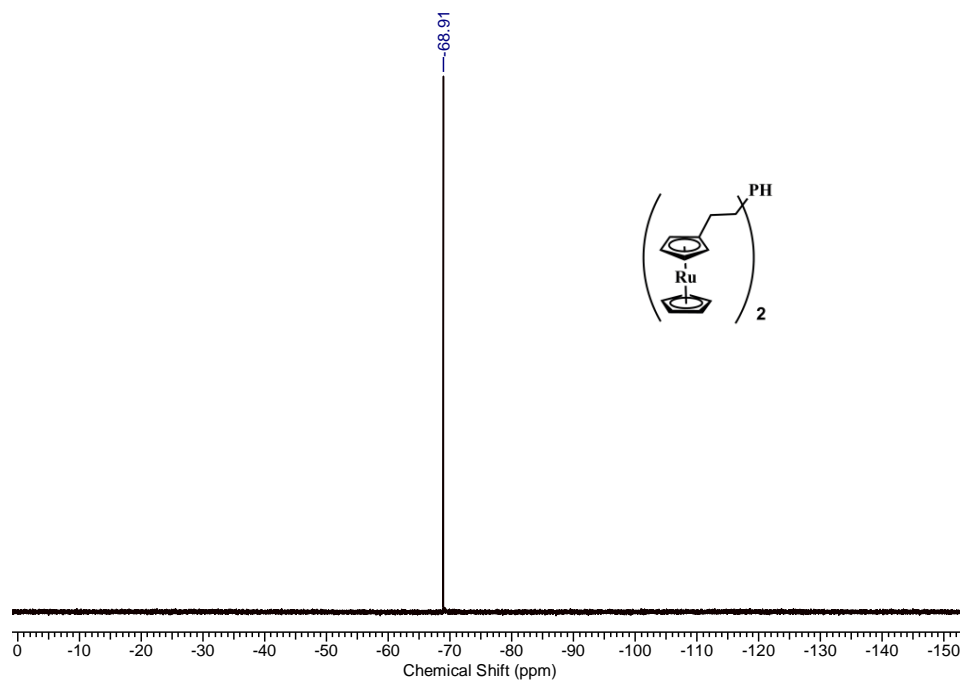


Figure A2.13. $^{31}\text{P}\{^1\text{H}\}$ NMR spectrum of secondary phosphine **2.8b** in CDCl_3 .

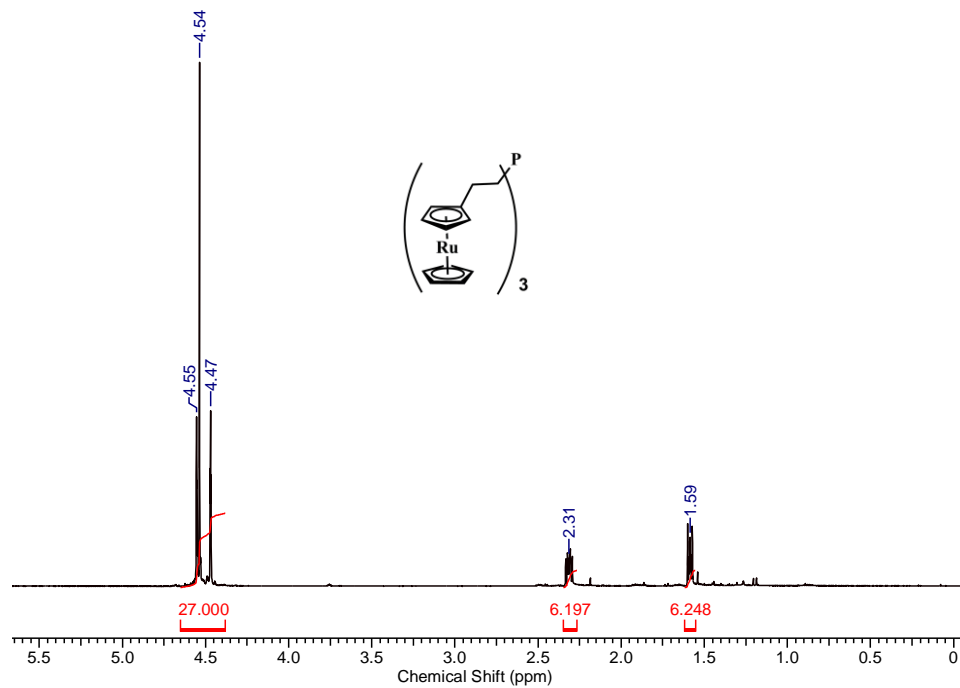


Figure A2.14. ^1H NMR spectrum of tertiary phosphine **2.8c** in CDCl_3 .

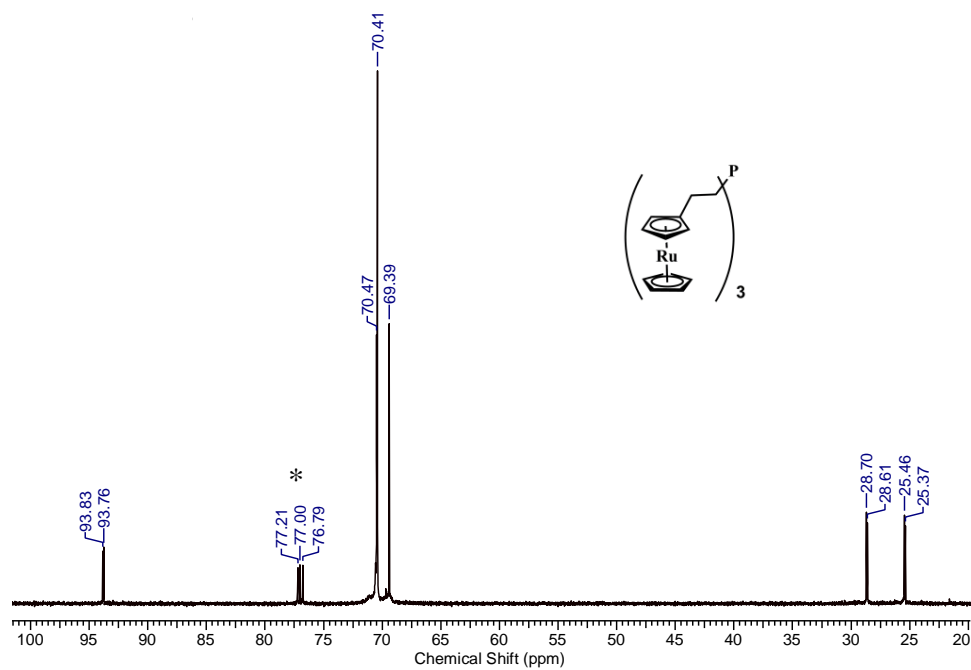


Figure A2.15. $^{13}\text{C}\{^1\text{H}\}$ NMR spectrum of tertiary phosphine **2.8c** in CDCl_3 . The asterisk denotes the solvent signal.

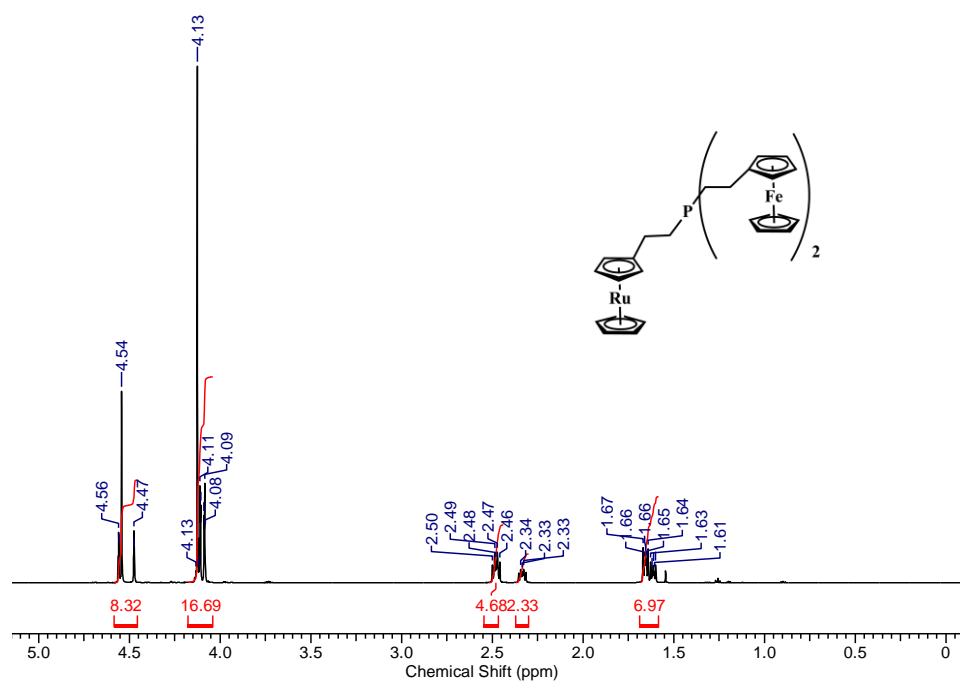


Figure A2.16. ^1H NMR spectrum of tertiary phosphine **2.10** in CDCl_3 .

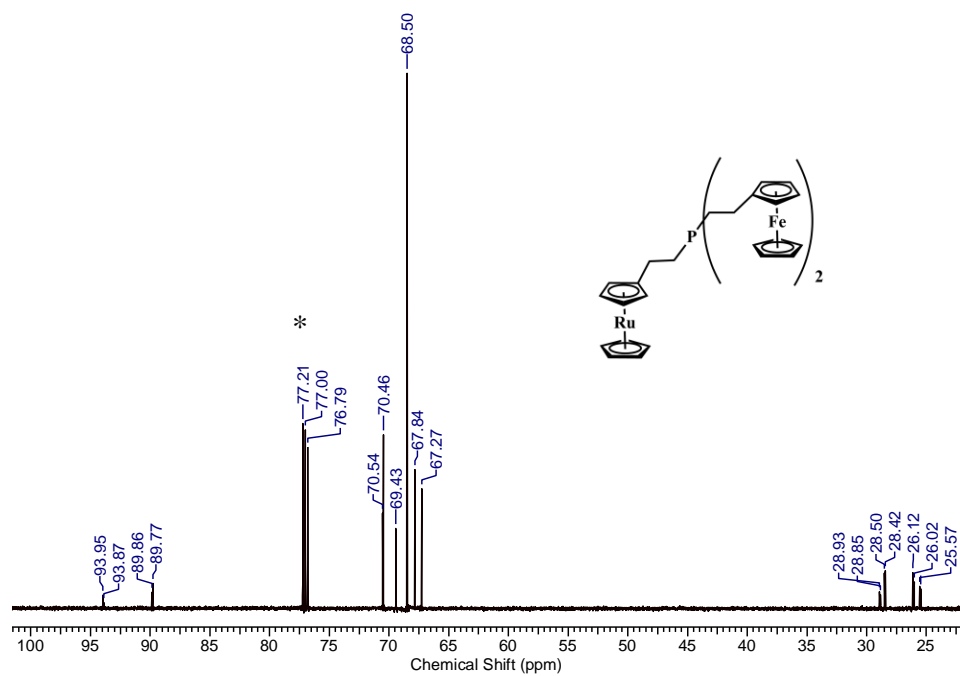


Figure A2.17. $^{13}\text{C}\{^1\text{H}\}$ NMR spectrum of tertiary phosphine **2.10** in CDCl_3 . The asterisk denotes the solvent signal.

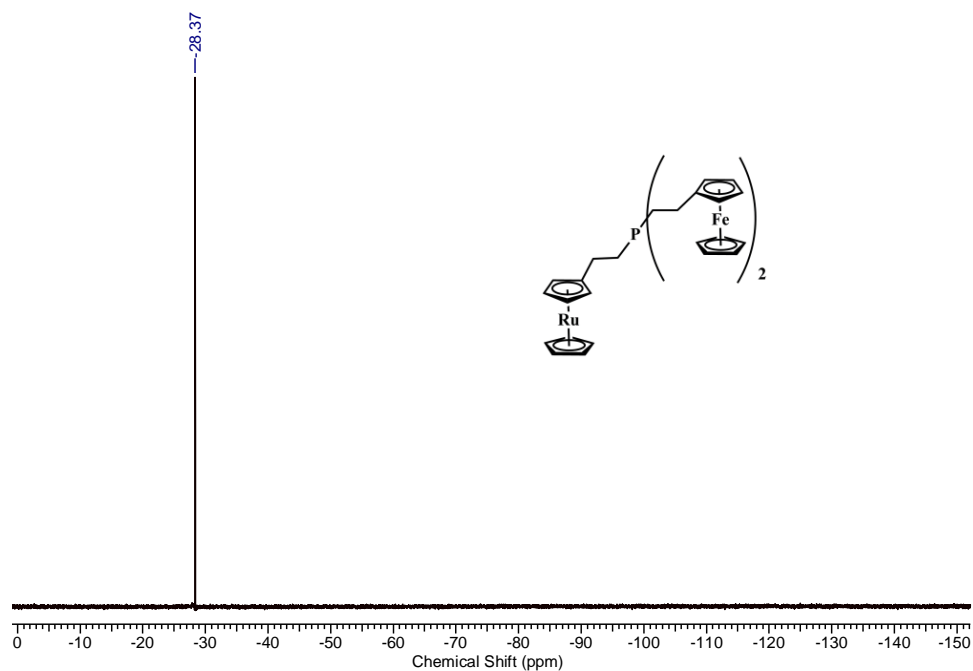


Figure A2.18. $^{31}\text{P}\{^1\text{H}\}$ NMR spectrum of tertiary phosphine **2.10** in CDCl_3 .

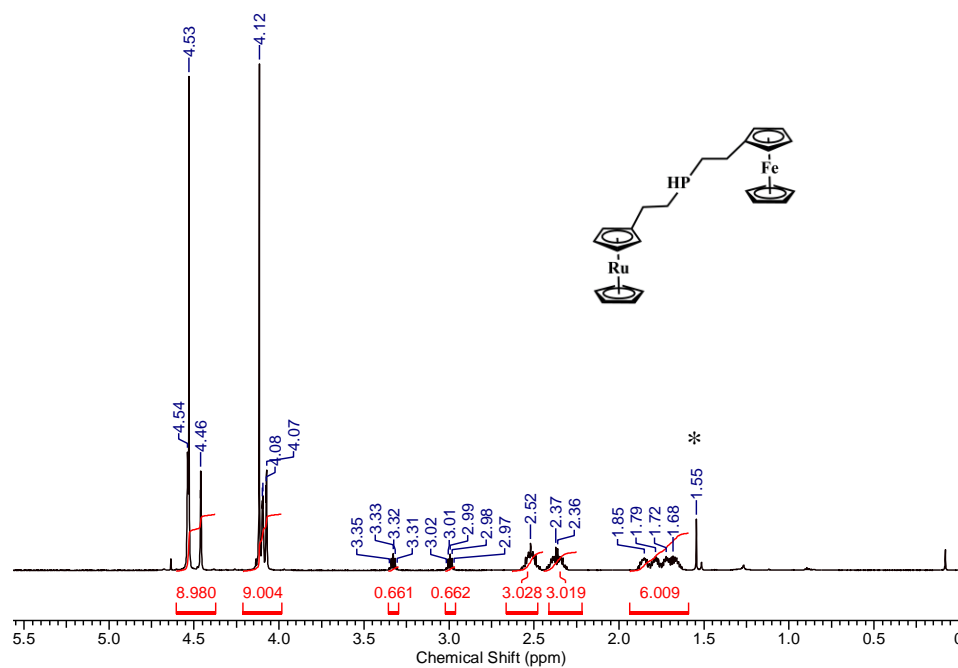


Figure A2.19. ^1H NMR spectrum of secondary phosphine **2.11** in CDCl_3 . The asterisk denotes residual H_2O signal.

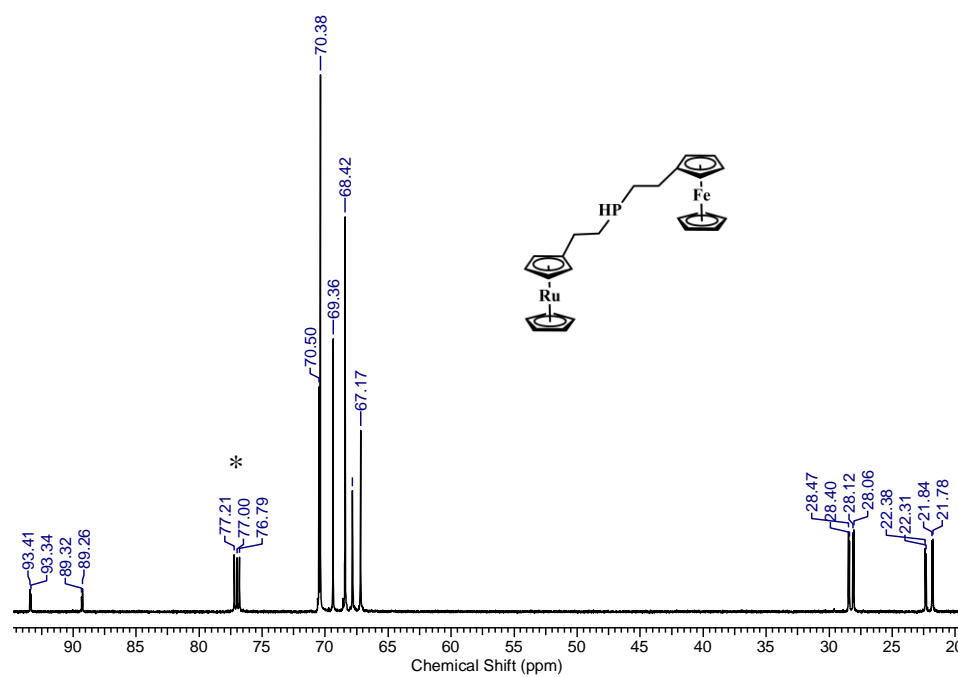


Figure A2.20. $^{13}\text{C}\{^1\text{H}\}$ NMR spectrum of secondary phosphine **2.11** in CDCl_3 . The asterisk denotes the solvent signal.

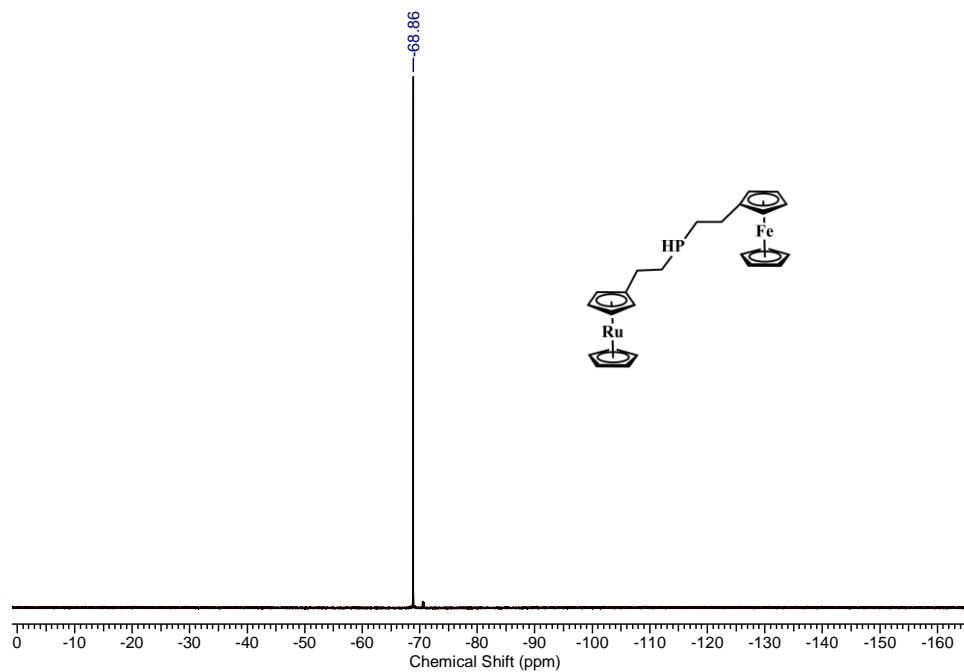


Figure A2.21. $^{31}\text{P}\{^1\text{H}\}$ NMR spectrum of secondary phosphine **2.11** in CDCl_3 .

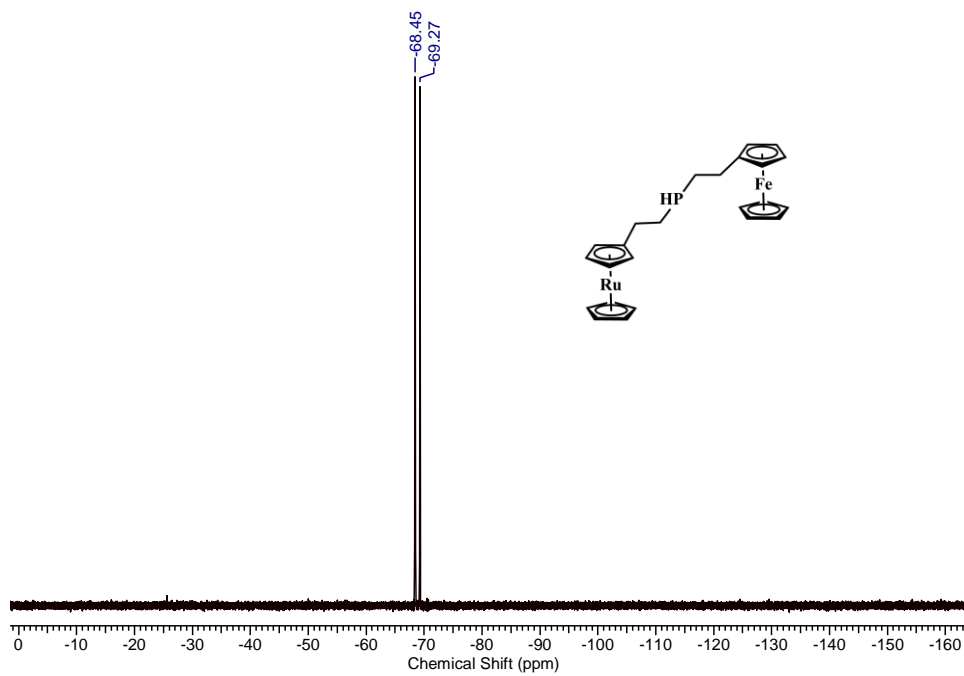


Figure A2.22. ^{31}P NMR spectrum of secondary phosphine **2.11** in CDCl_3 .

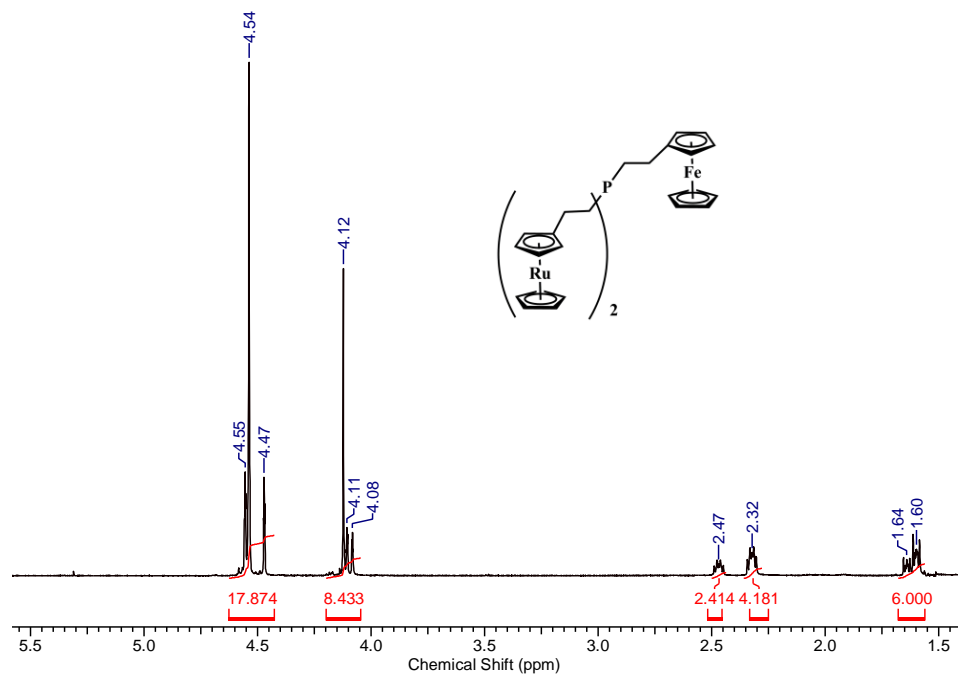


Figure A2.23. ^1H NMR spectrum of tertiary phosphine **2.12** in CDCl_3 .

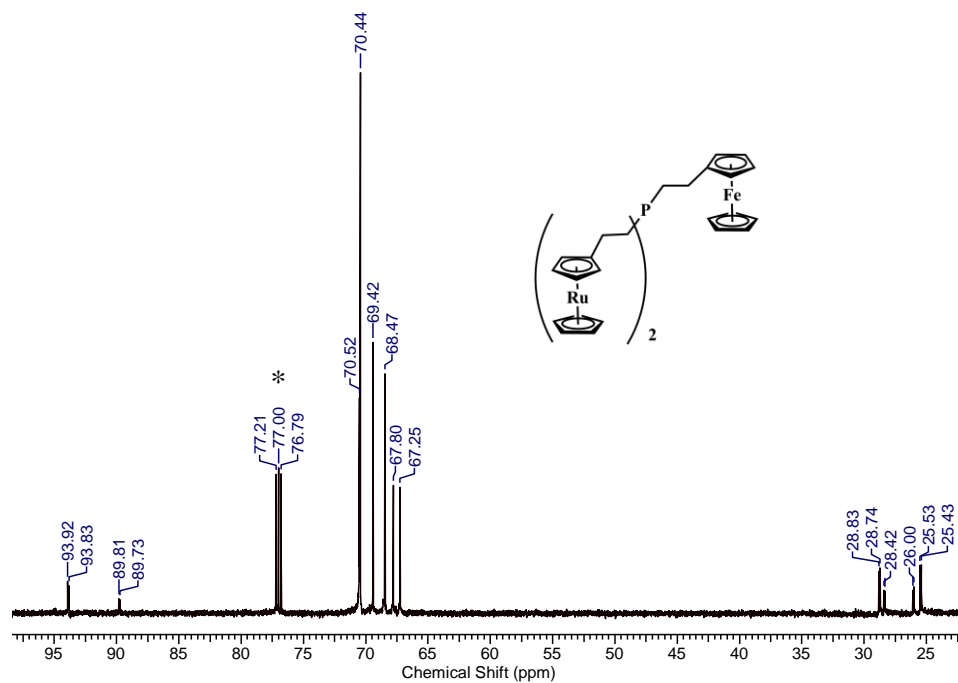


Figure A2.24. $^{13}\text{C}\{^1\text{H}\}$ NMR spectrum of tertiary phosphine **2.12** in CDCl_3 . The asterisk denotes the solvent signal.

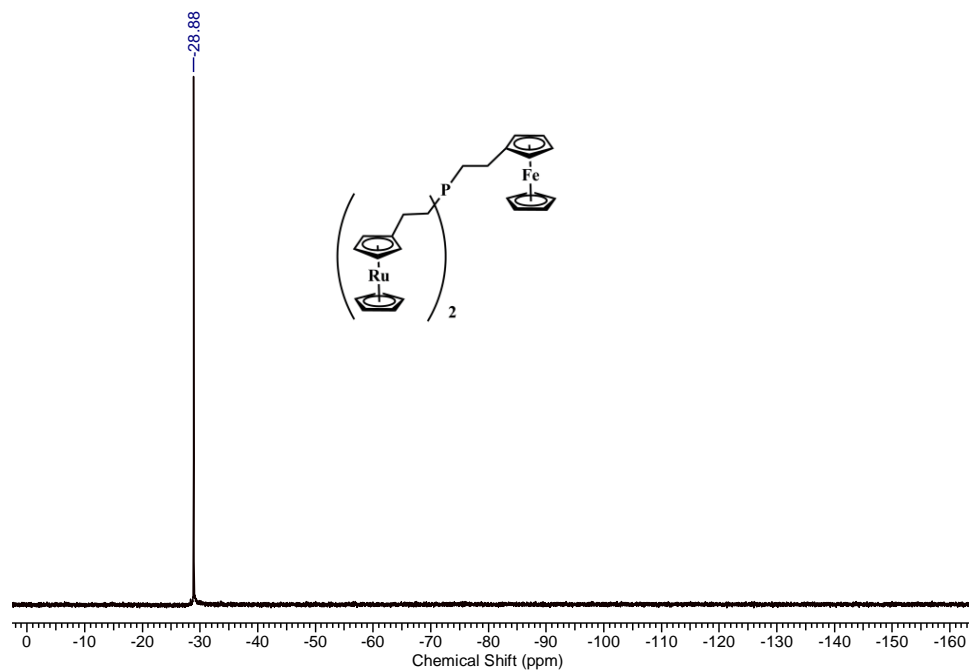


Figure A2.25. $^{31}\text{P}\{^1\text{H}\}$ NMR spectrum of tertiary phosphine **2.12** in CDCl_3 .

Solid-State Structures

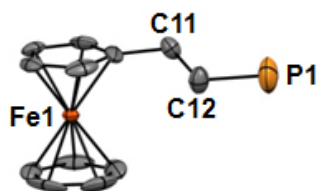


Figure A2.26. Solid-state structure of secondary phosphine **2.7a** ($1 \times \text{Fc}$). Thermal displacement ellipsoids are shown at 50% probability and hydrogen atoms have been omitted for clarity.

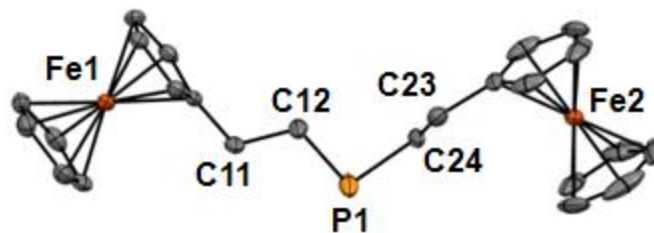


Figure A2.27. Solid-state structure of secondary phosphine **2.7b** ($2 \times \text{Fc}$). Thermal displacement ellipsoids are shown at 50% probability and hydrogen atoms have been omitted for clarity.

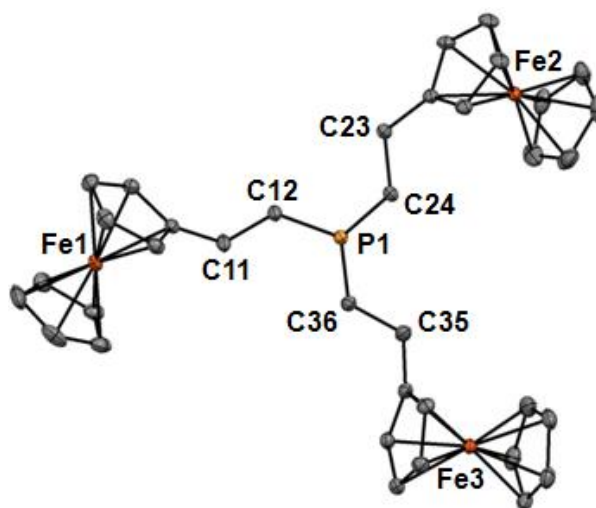


Figure A2.28. Solid-state structure of secondary phosphine **2.7c** ($3 \times \text{Fc}$). Thermal displacement ellipsoids are shown at 50% probability and hydrogen atoms have been omitted for clarity.

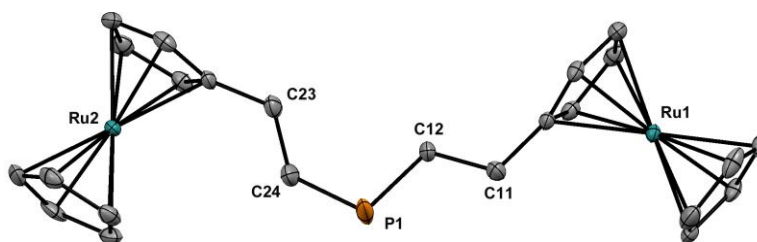


Figure A2.29. Solid-state structure of secondary phosphine **2.8b** ($2 \times \text{Rc}$). Thermal displacement ellipsoids are shown at 50% probability and hydrogen atoms have been omitted for clarity.

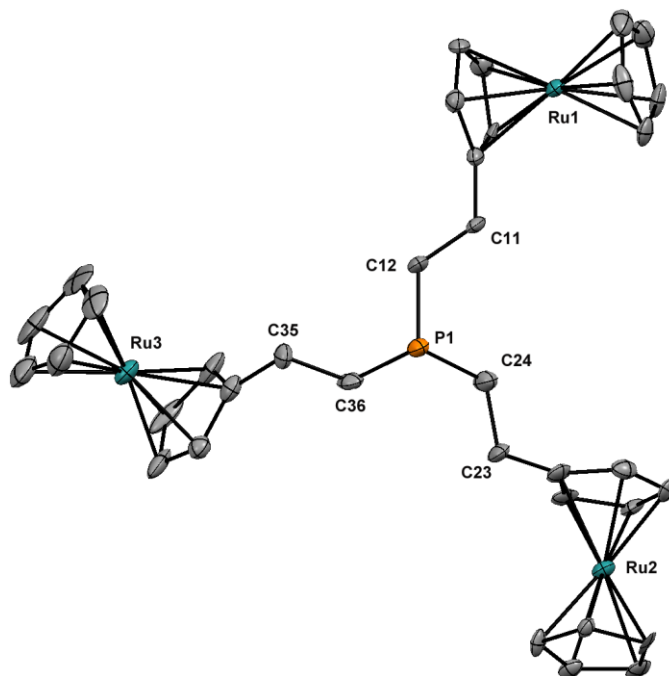


Figure A2.30. Solid-state structure of tertiary phosphine **2.8c** ($3 \times R_c$). Thermal displacement ellipsoids are shown at 50% probability and hydrogen atoms have been omitted for clarity.

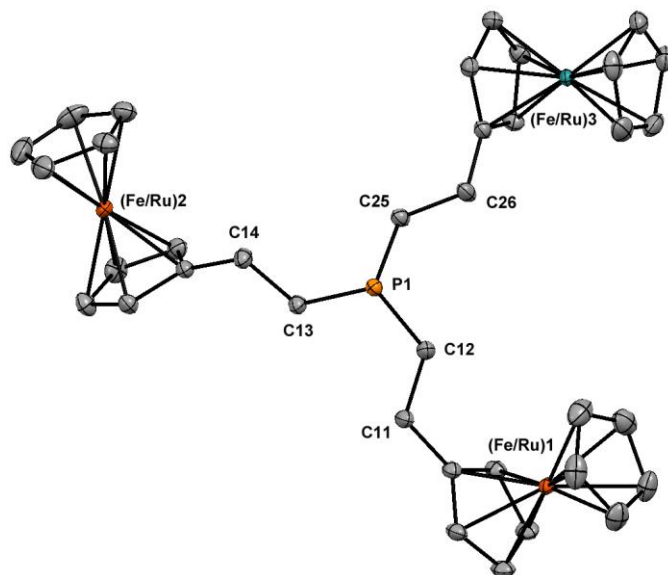


Figure A2.31. Solid-state structure of tertiary phosphine **2.10** ($1 \times R_c$, $2 \times F_c$). Thermal displacement ellipsoids are shown at 50% probability and hydrogen atoms have been omitted for clarity.

Analysis of Twinning for **2.8b**

The diffraction pattern was successfully indexed as a non-merohedral twin wherein the domains were related by an approximate 1 degree rotation about $[1\bar{1}\bar{1}]$. The twin fraction for the minor domain refined to a value of 0.4120(7). The twin law is given below:

Twin Law, Sample 1 of 1
 Transforms $h1.1(1)\rightarrow h1.2(2)$
 0.99989 -0.00134 0.73662
 -0.00009 -1.00000 0.00008
 0.00031 -0.00215 -0.99989

UV-vis Absorption Spectra

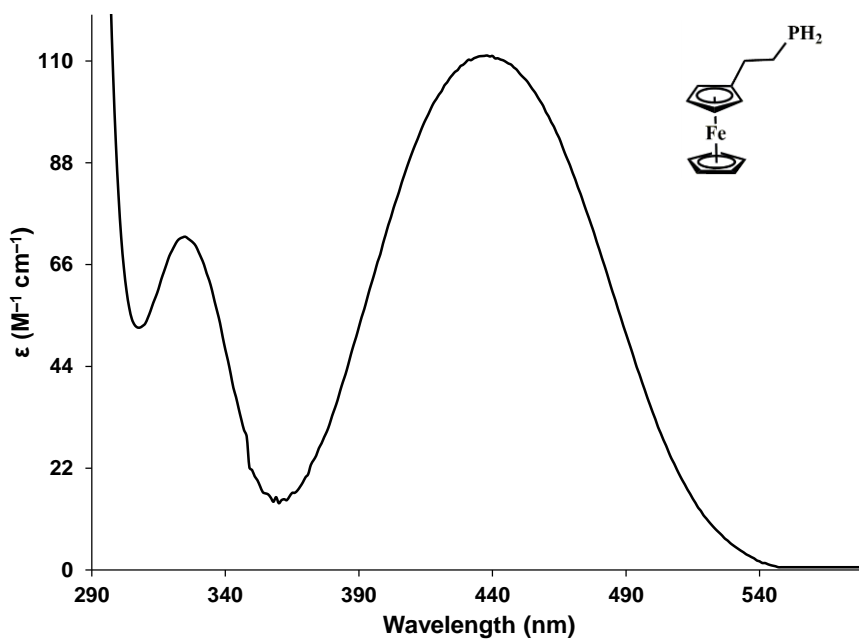


Figure A2.32. UV-vis absorption spectrum of primary phosphine **2.7a** ($1 \times \text{Fc}$) in THF.

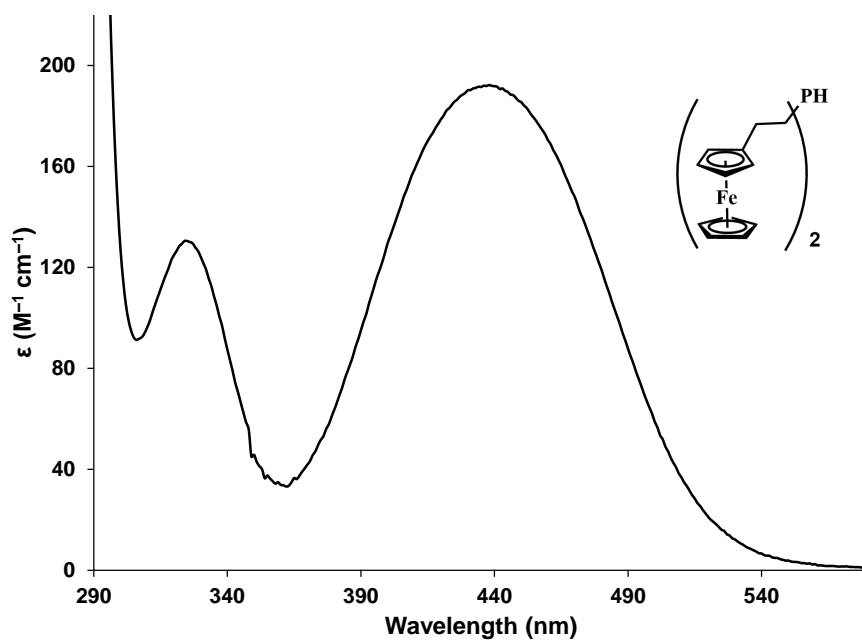


Figure A2.33. UV-vis absorption spectrum of secondary phosphine **2.7b** ($2 \times \text{Fc}$) in THF.

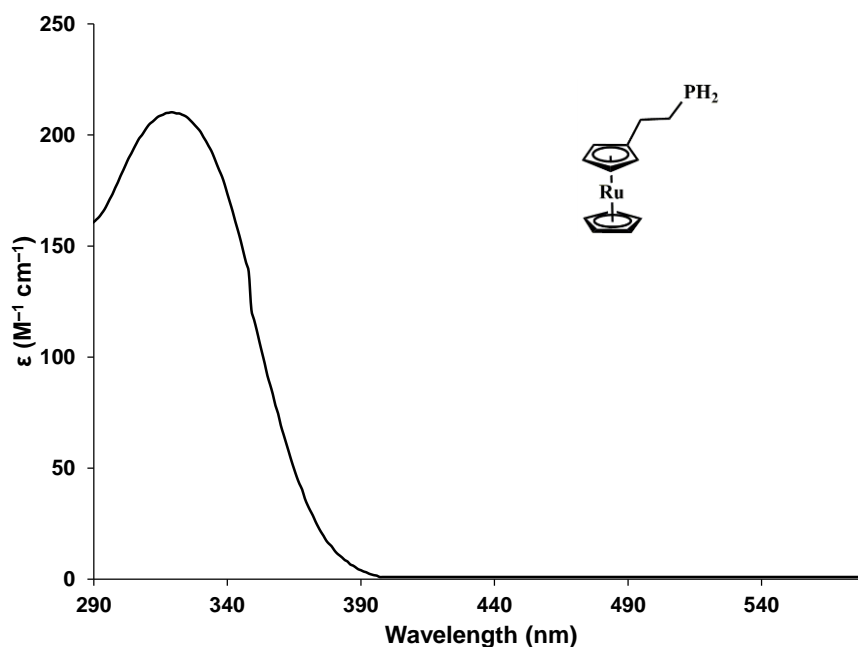


Figure A2.34. UV-vis absorption spectrum of primary phosphine **2.8a** ($1 \times \text{Rc}$) in THF.

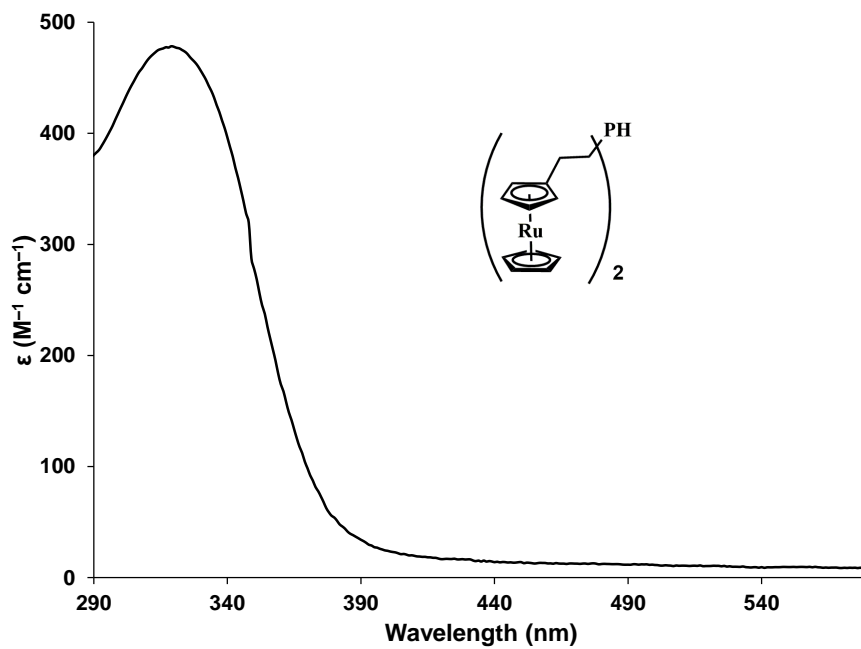


Figure A2.35. UV-vis absorption spectrum of secondary phosphine **2.8b** ($2 \times \text{Rc}$) in THF.

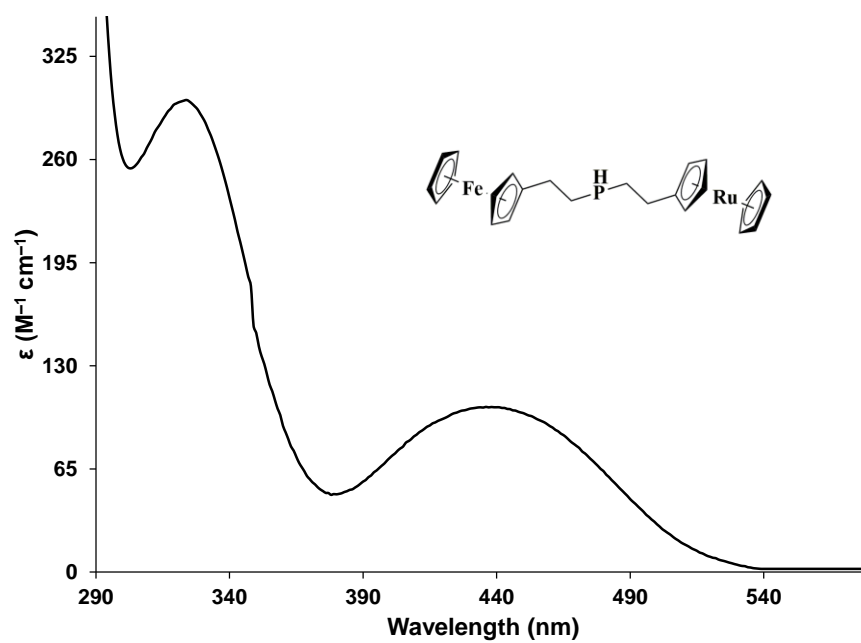


Figure A2.36. UV-vis absorption spectrum of secondary phosphine **2.11** ($1 \times \text{Rc}$, $1 \times \text{Fc}$) in THF.

Cyclic Voltammograms

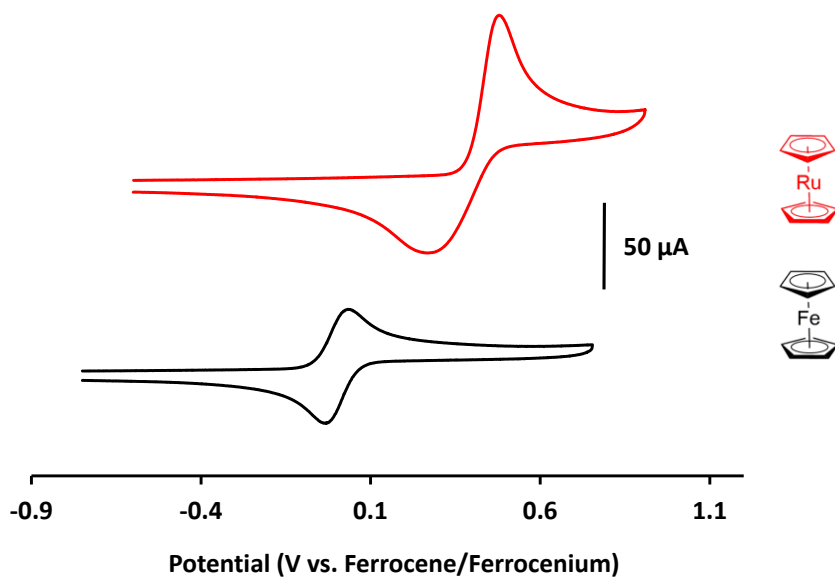


Figure A2.37. Cyclic voltammograms of ferrocene (black) and ruthenocene (red) recorded at 250 mV s^{-1} in 1 mM solutions of CH_2Cl_2 containing 0.1 M $[n\text{-Bu}_4\text{N}][\text{OTf}]$ as supporting electrolyte.

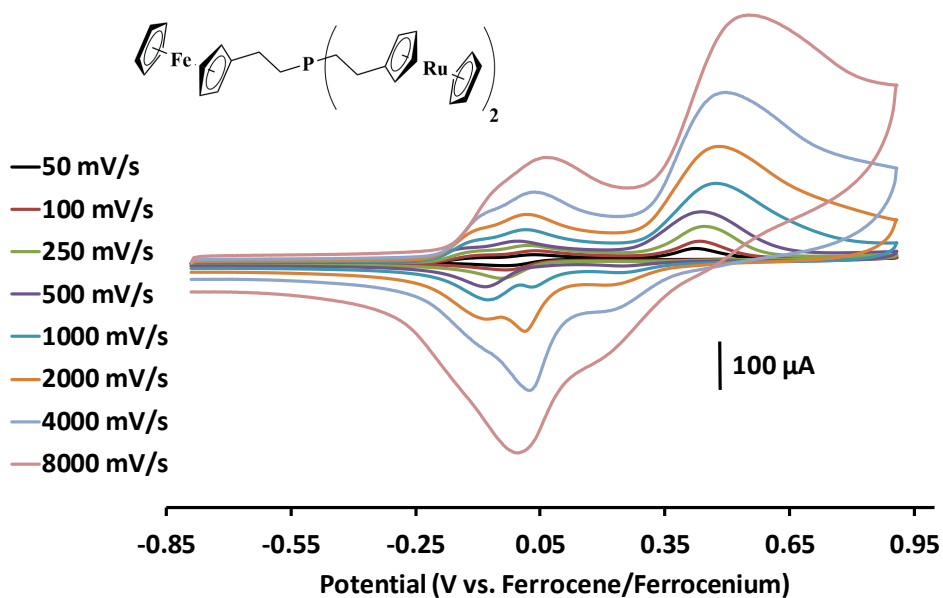


Figure A2.38. Cyclic voltammograms of tertiary phosphine **2.12** ($2 \times \text{Ru}$, $1 \times \text{Fc}$) at different scan rates in 1 mM solutions of CH_2Cl_2 containing 0.1 M $[n\text{-Bu}_4\text{N}][\text{OTf}]$ as supporting electrolyte.

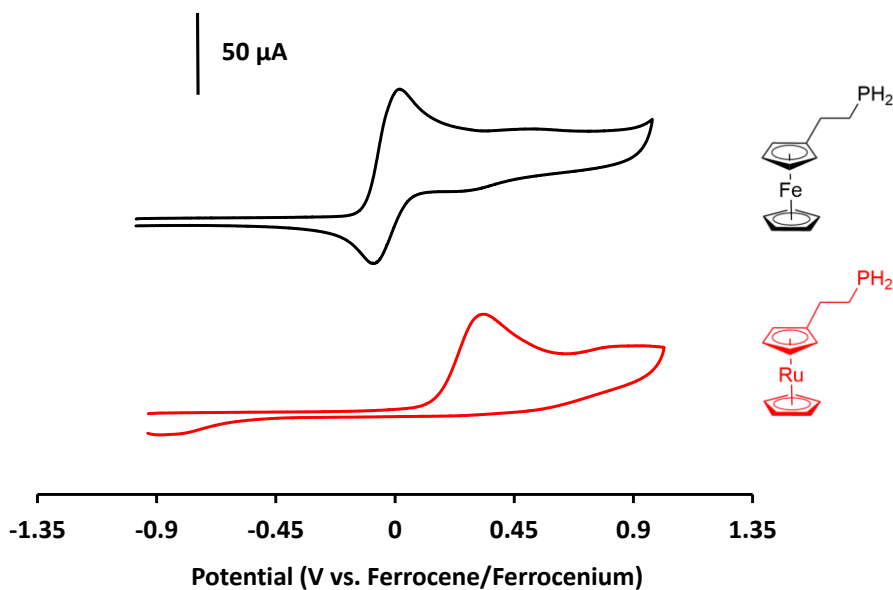


Figure A2.39. Cyclic voltammograms of **2.7a** ($1 \times \text{Fc}$, black) and **2.8a** ($1 \times \text{Rc}$, red) recorded at 250 mV s^{-1} in 1 mM solutions of CH_2Cl_2 containing 0.1 M $[n\text{-Bu}_4\text{N}][\text{OTf}]$ as supporting electrolyte.

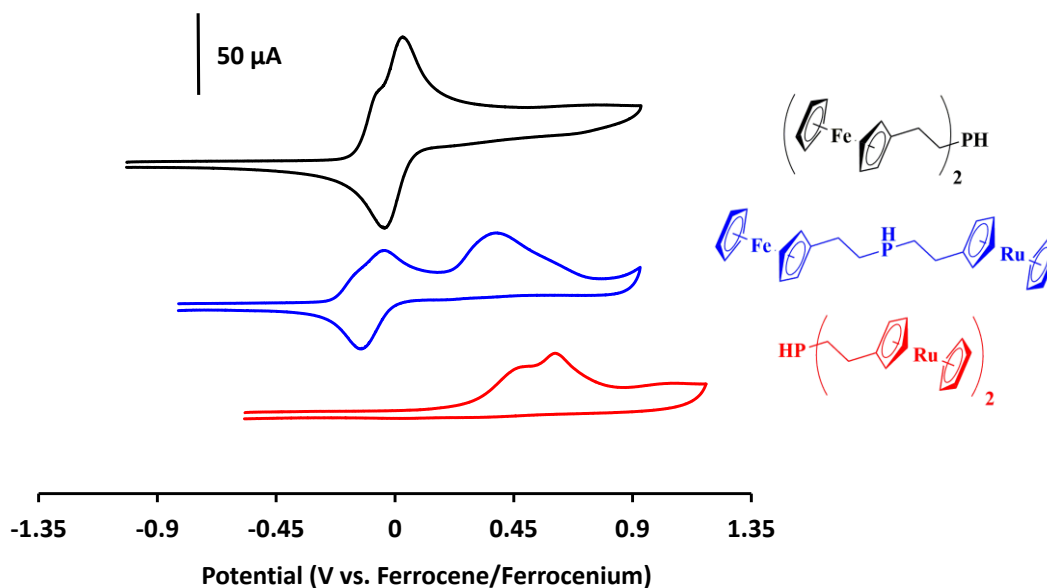


Figure A2.40. Cyclic voltammograms of secondary phosphines **2.7b** ($2 \times \text{Fc}$, black), **2.8b** ($2 \times \text{Rc}$, red), and **2.11** ($1 \times \text{Rc}$, $1 \times \text{Fc}$, blue) recorded at 250 mV s^{-1} in 1 mM solutions of CH_2Cl_2 containing 0.1 M $[n\text{-Bu}_4\text{N}][\text{OTf}]$ as supporting electrolyte.

Hydrophosphination Reaction Setup



Figure A2.41. Photographs of the reaction setup (top) and burn box (bottom) used for the safe handling and disposal of PH₃ gas during this study.

Appendix 3 – Supporting Information for Chapter 3

NMR Spectra

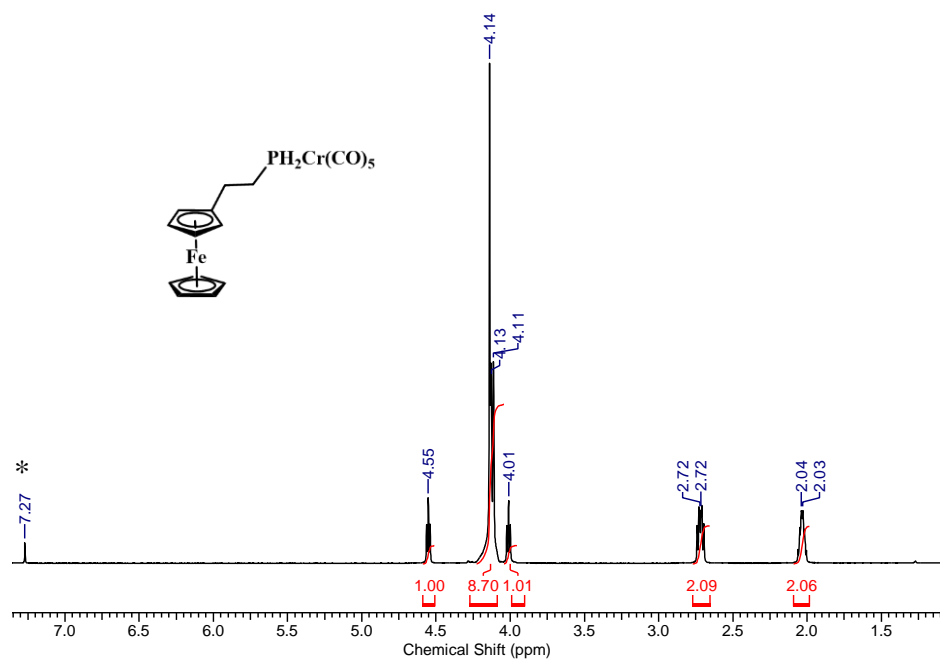


Figure A3.1. ^1H NMR spectrum of **3.5a** in CDCl_3 . The asterisk denotes residual CHCl_3 signal.

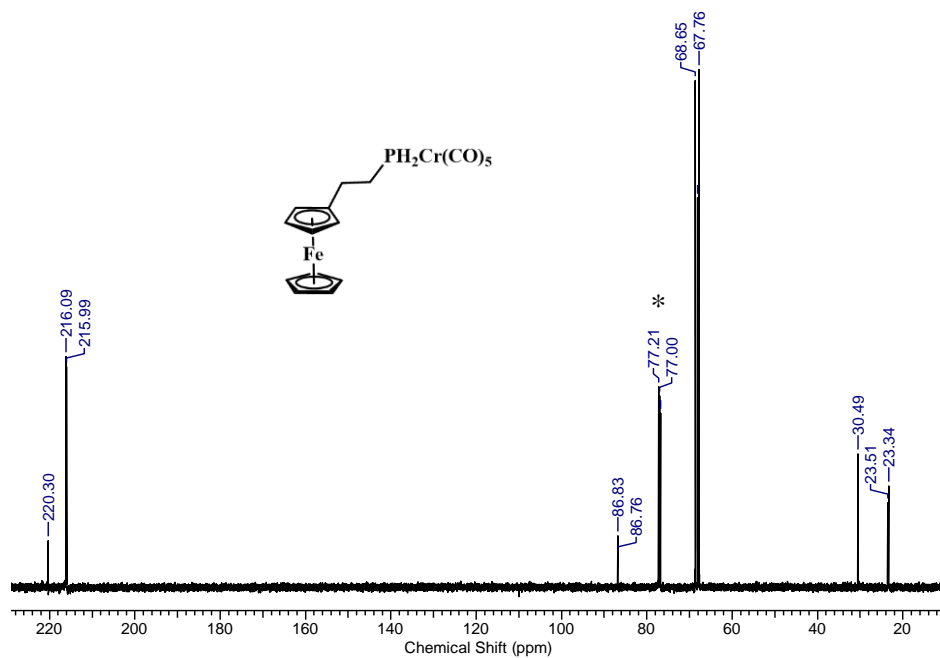


Figure A3.2. $^{13}\text{C}\{^1\text{H}\}$ NMR spectrum of **3.5a** in CDCl_3 . The asterisk denotes the solvent signal.

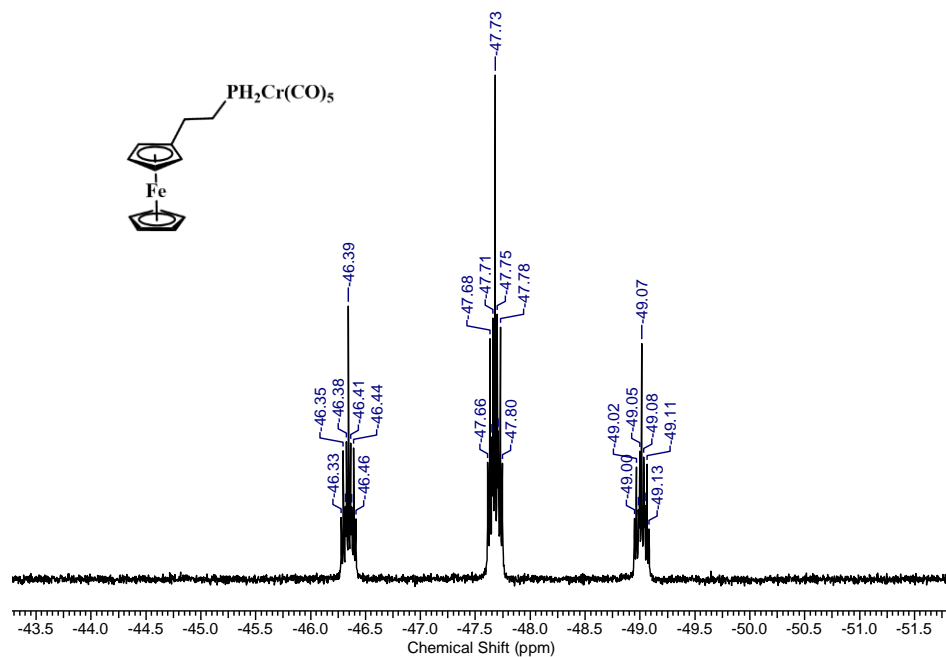


Figure A3.3. ^{31}P NMR spectrum of **3.5a** in CDCl_3 .

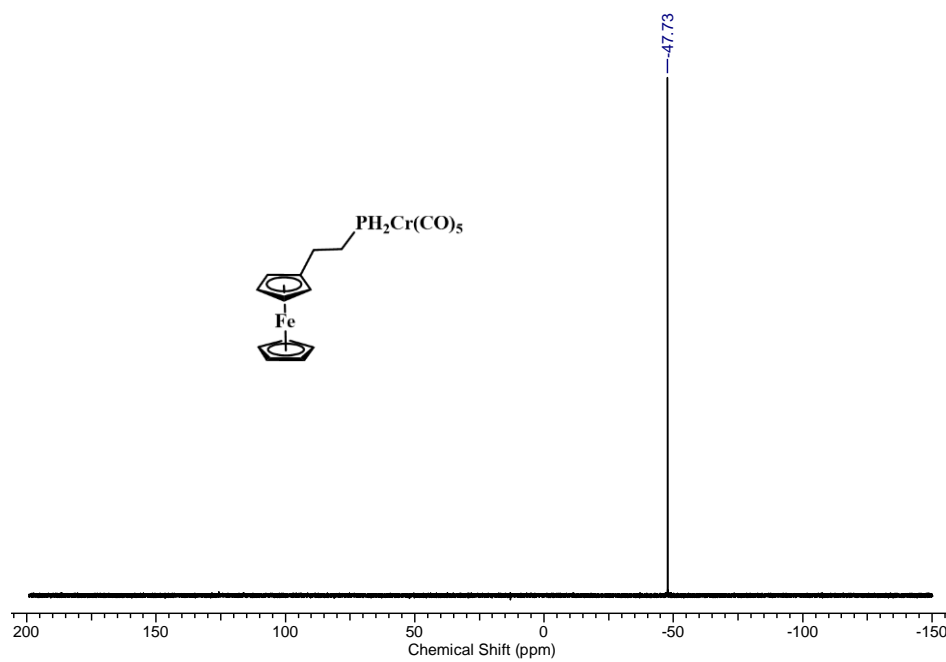


Figure A3.4. $^{31}\text{P}\{^1\text{H}\}$ NMR spectrum of **3.5a** in CDCl_3 .

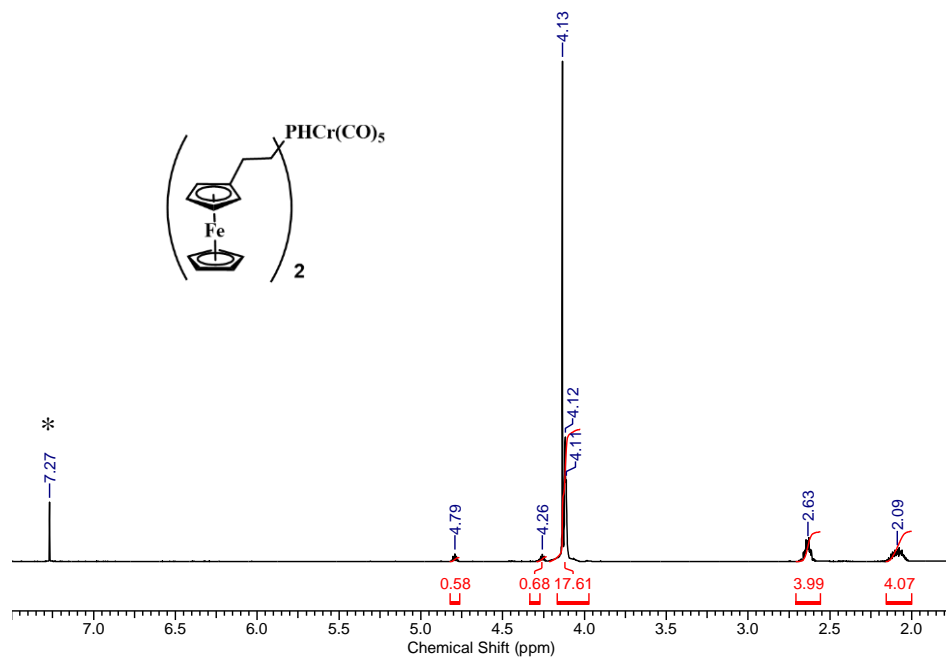


Figure A3.5. ^1H NMR spectrum of **3.5b** in CDCl_3 . The asterisk denotes residual CHCl_3 signal.

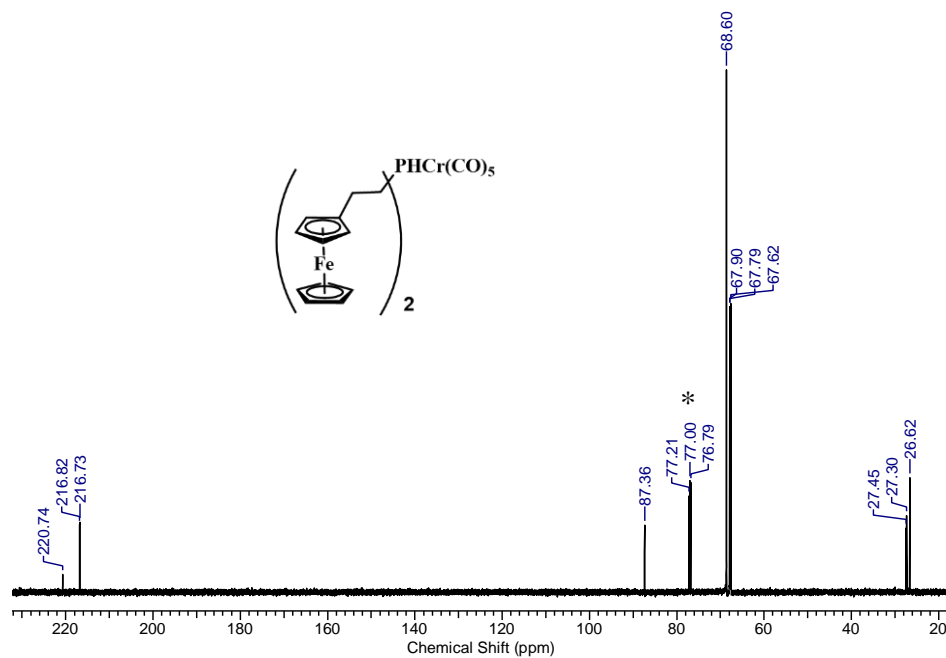


Figure A3.6. $^{13}\text{C}\{^1\text{H}\}$ NMR spectrum of **3.5b** in CDCl_3 . The asterisk denotes the solvent signal.

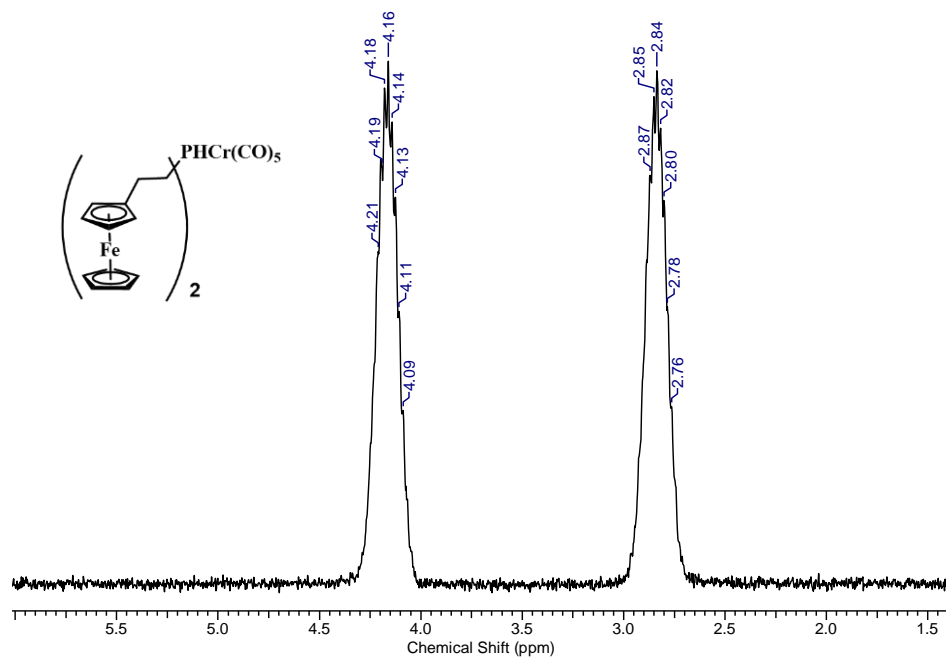


Figure A3.7. ^{31}P NMR spectrum of **3.5b** in CDCl_3 .

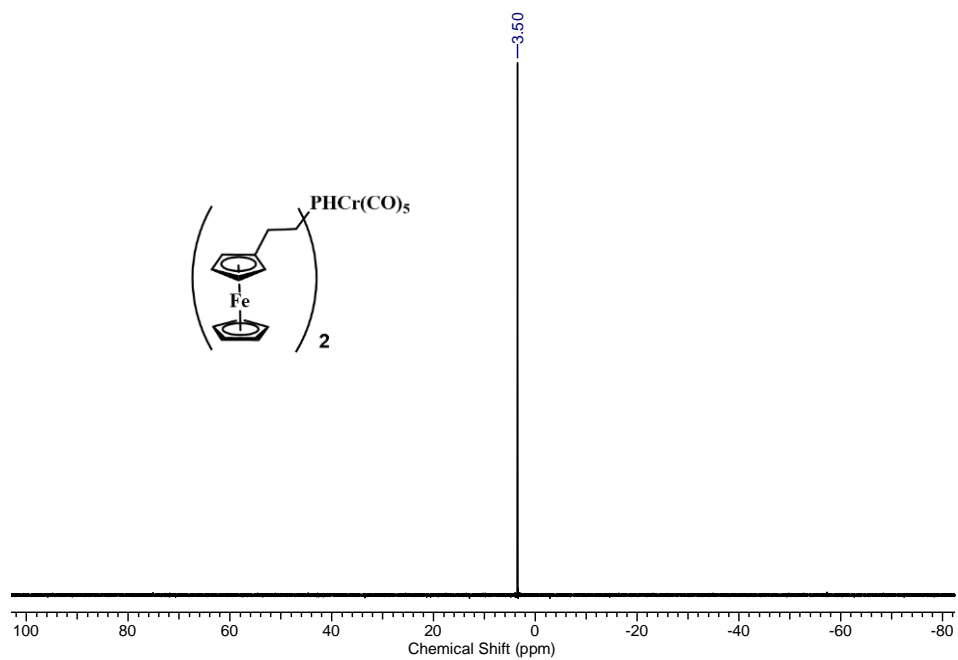


Figure A3.8. $^{31}\text{P}\{^1\text{H}\}$ NMR spectrum of **3.5b** in CDCl_3 .

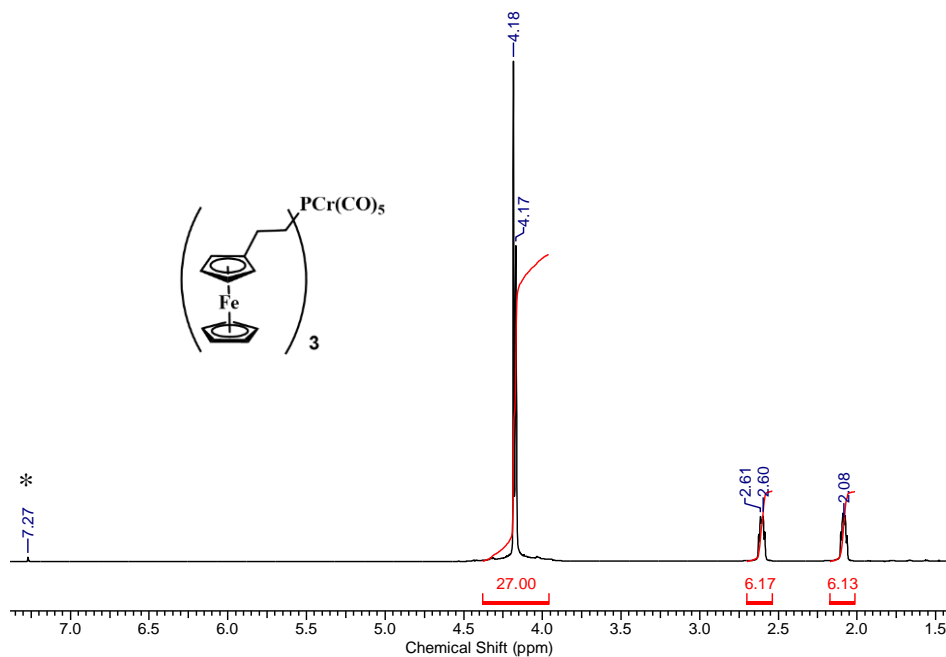


Figure A3.9. $^1\text{H NMR}$ spectrum of **3.5c** in CDCl_3 . The asterisk denotes residual CHCl_3 signal.

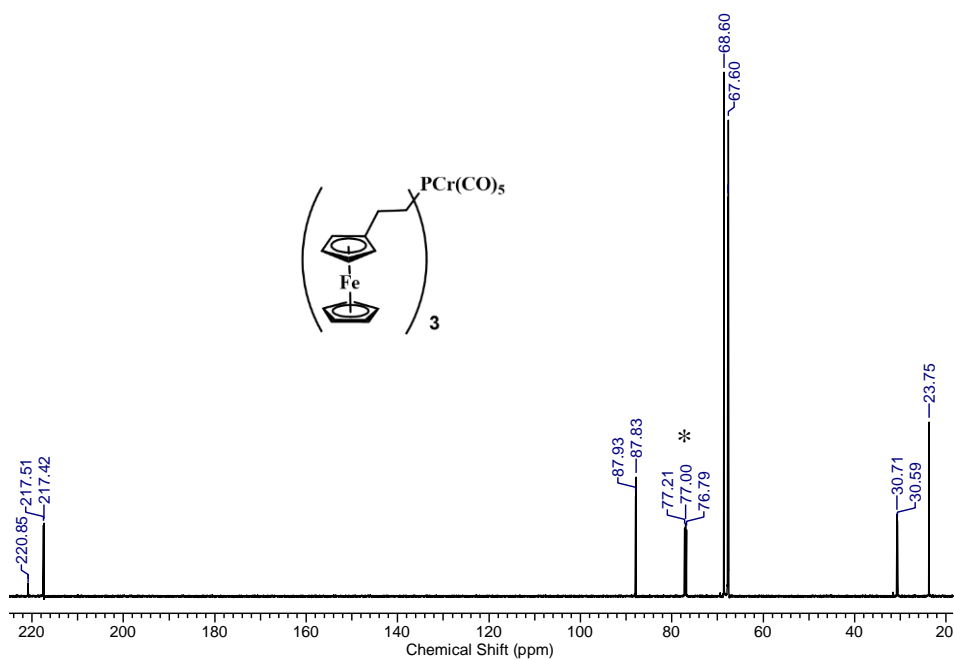


Figure A3.10. $^{13}\text{C}\{^1\text{H}\}$ NMR spectrum of **3.5c** in CDCl_3 . The asterisk denotes the solvent signal.

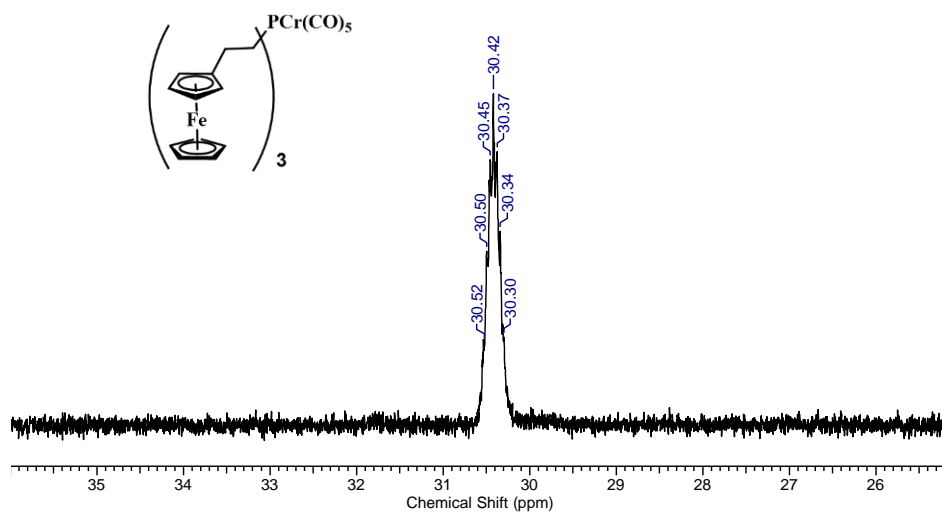


Figure A3.11. ^{31}P NMR spectrum of **3.5c** in CDCl_3 .

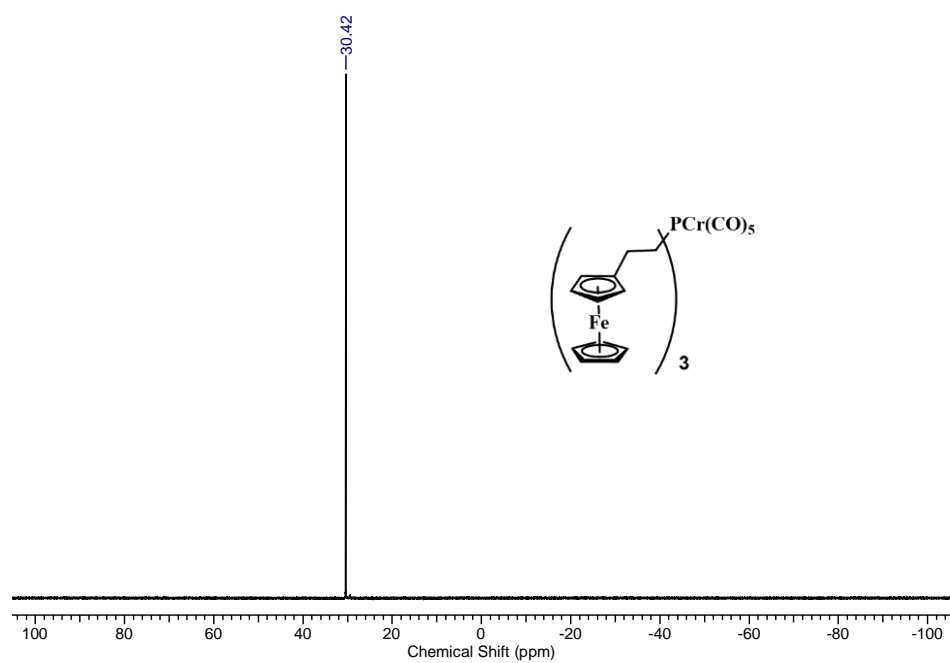


Figure A3.12. $^{31}\text{P}\{^1\text{H}\}$ NMR spectrum of **3.5c** in CDCl_3 .

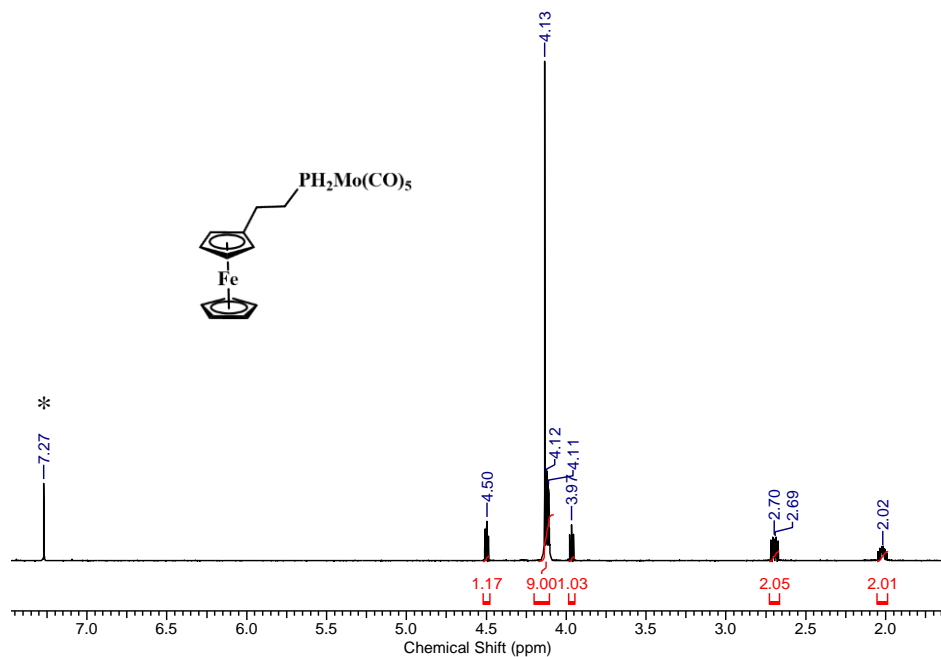


Figure A3.13. ^1H NMR spectrum of **3.6a** in CDCl_3 . The asterisk denotes residual CHCl_3 signal.

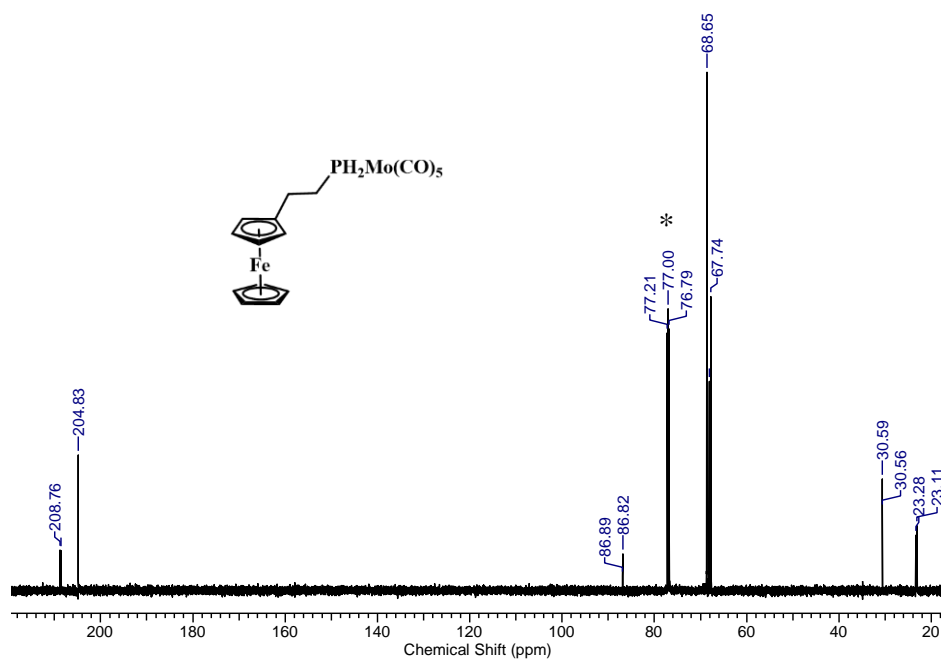


Figure A3.14. $^{13}\text{C}\{^1\text{H}\}$ NMR spectrum of **3.6a** in CDCl_3 . The asterisk denotes the solvent signal.

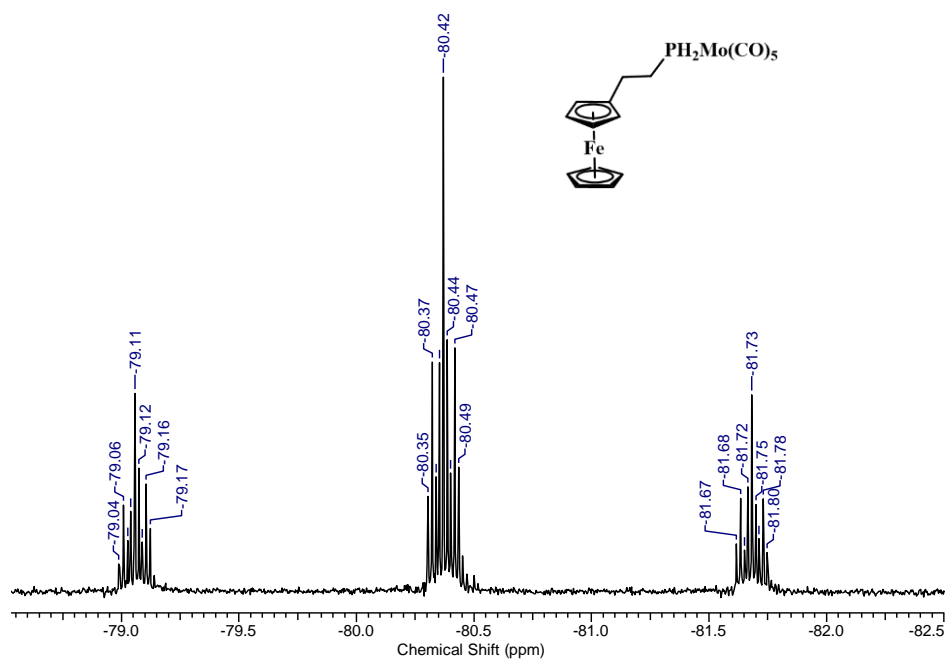


Figure A3.15. ^{31}P NMR spectrum of **3.6a** in CDCl_3 .

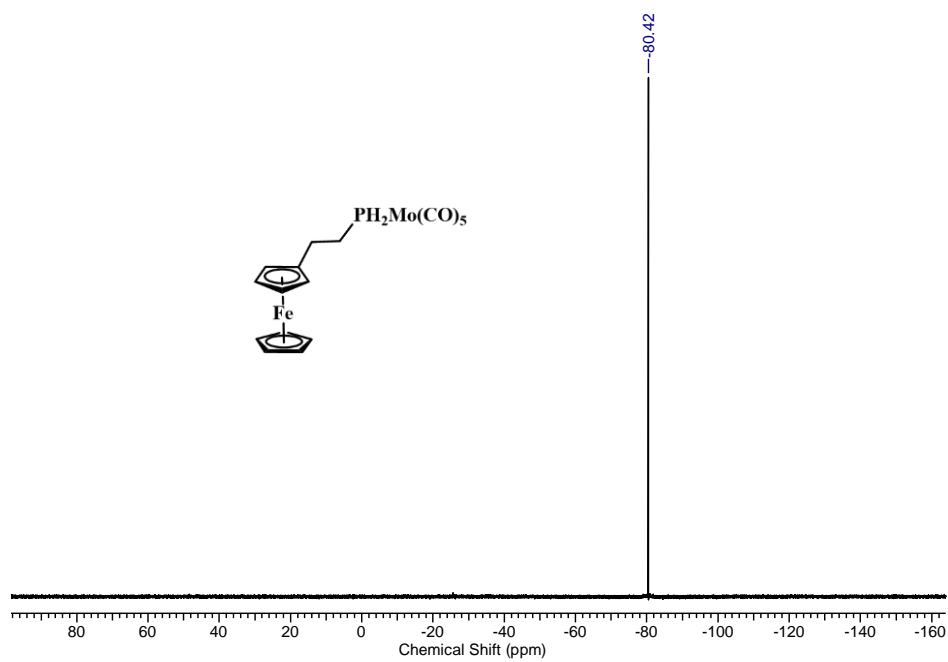


Figure A3.16. $^{31}\text{P}\{^1\text{H}\}$ NMR spectrum of **3.6a** in CDCl_3 .

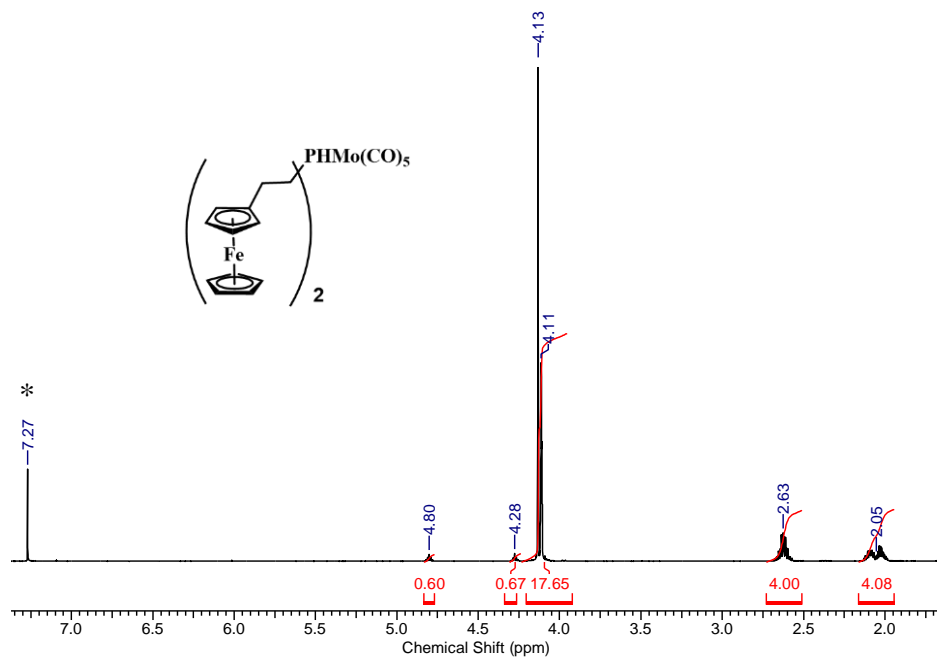


Figure A3.17. ^1H NMR spectrum of **3.6b** in CDCl_3 . The asterisk denotes residual CHCl_3 signal.

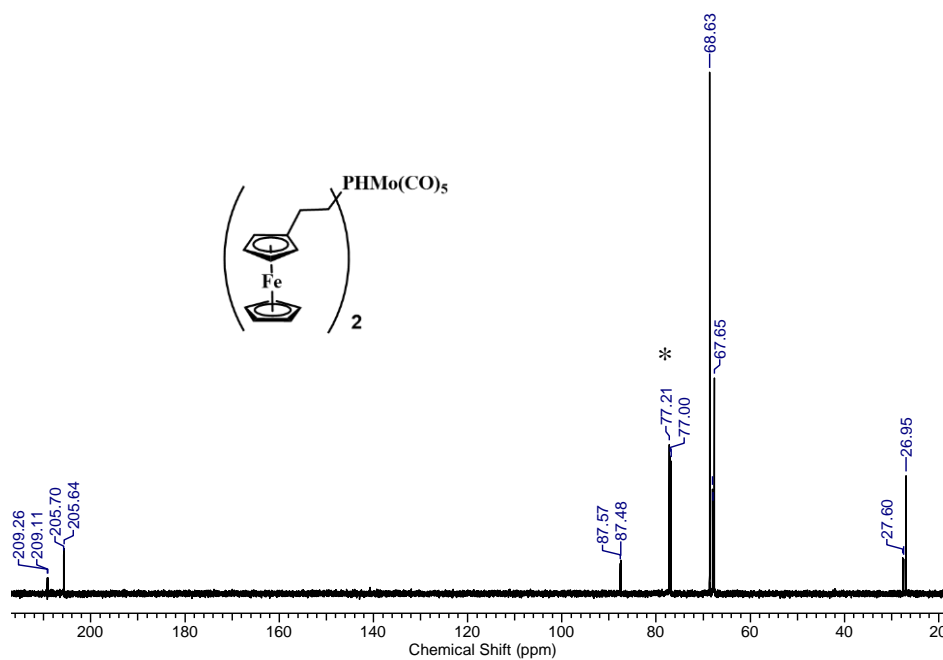


Figure A3.18. $^{13}\text{C}\{^1\text{H}\}$ NMR spectrum of **3.6b** in CDCl_3 . The asterisk denotes the solvent signal.

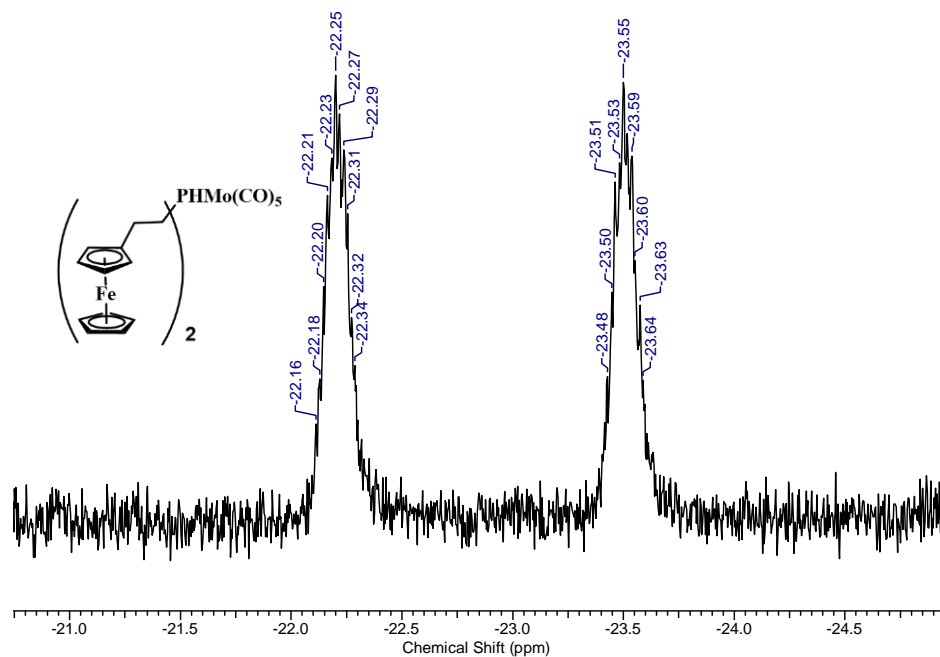


Figure A3.19. ^{31}P NMR spectrum of **3.6b** in CDCl_3 .

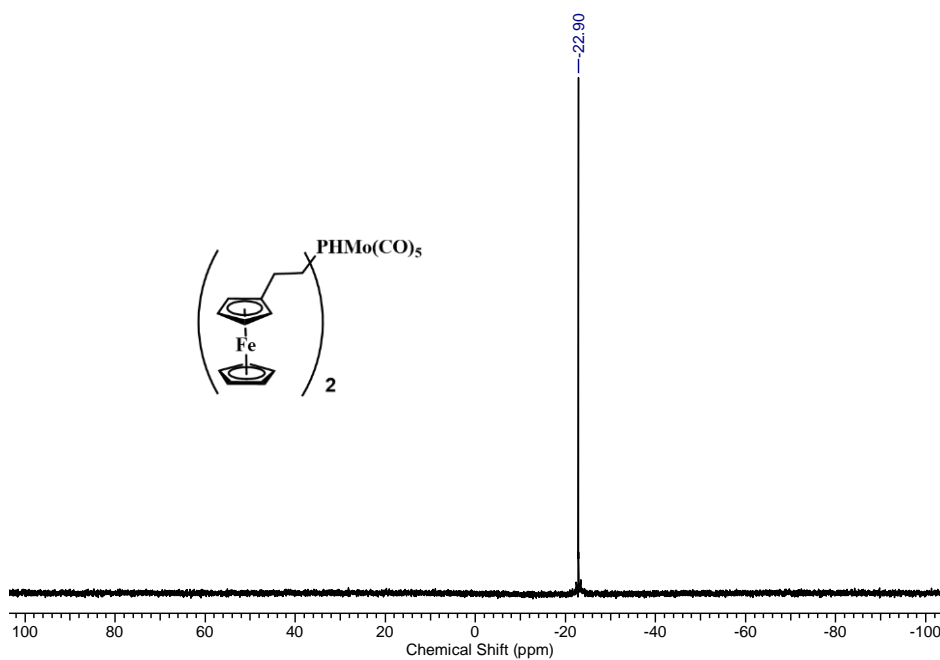


Figure A3.20. $^{31}\text{P}\{^1\text{H}\}$ NMR spectrum of **3.6b** in CDCl_3 .

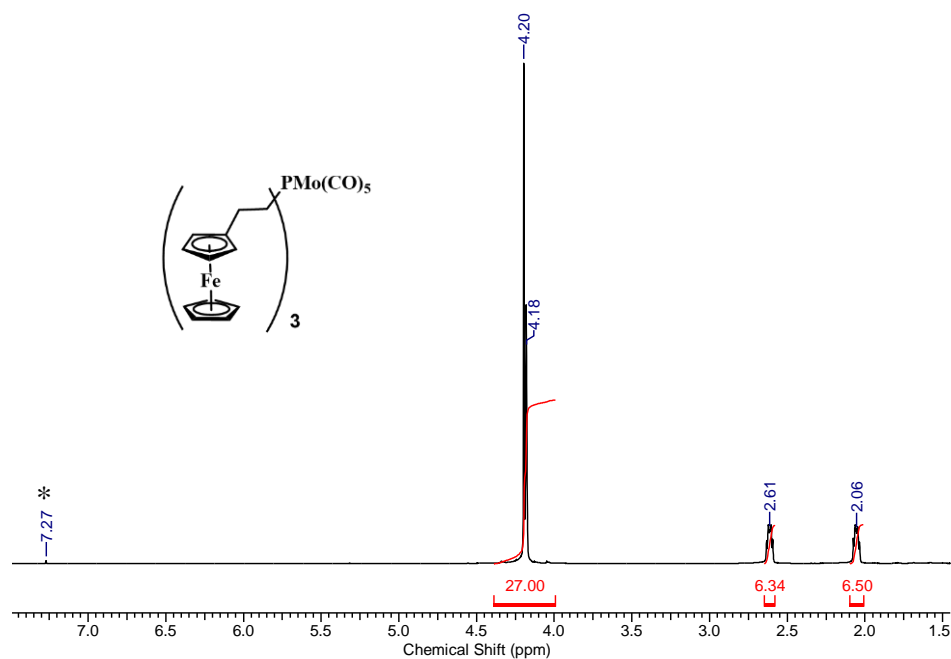


Figure A3.21. $^1\text{H NMR}$ spectrum of **3.6c** in CDCl_3 . The asterisk denotes residual CHCl_3 signal.

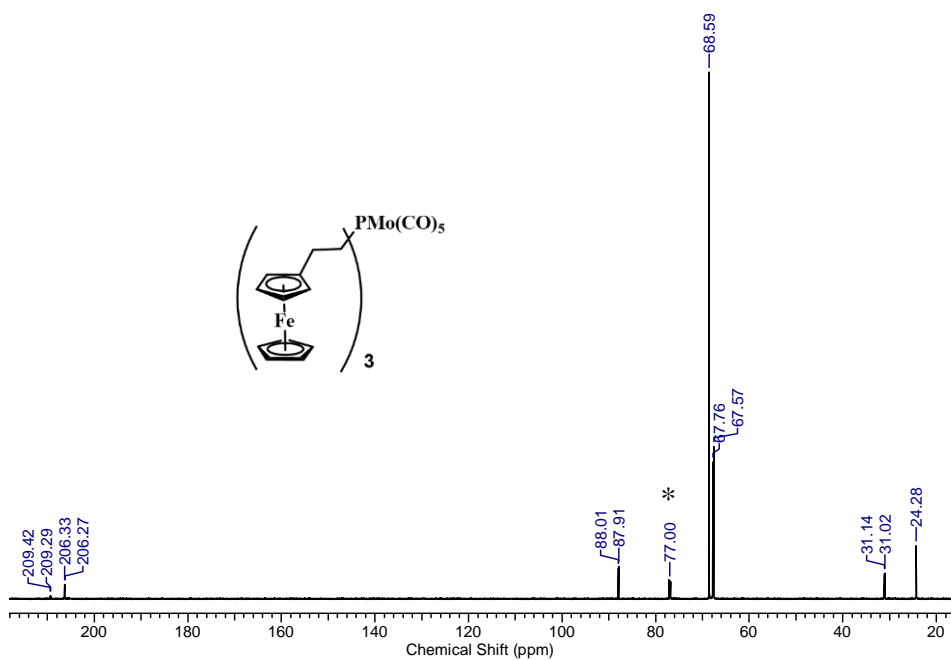


Figure A3.22. $^{13}\text{C}\{^1\text{H}\}$ NMR spectrum of **3.6c** in CDCl_3 . The asterisk denotes the solvent signal.

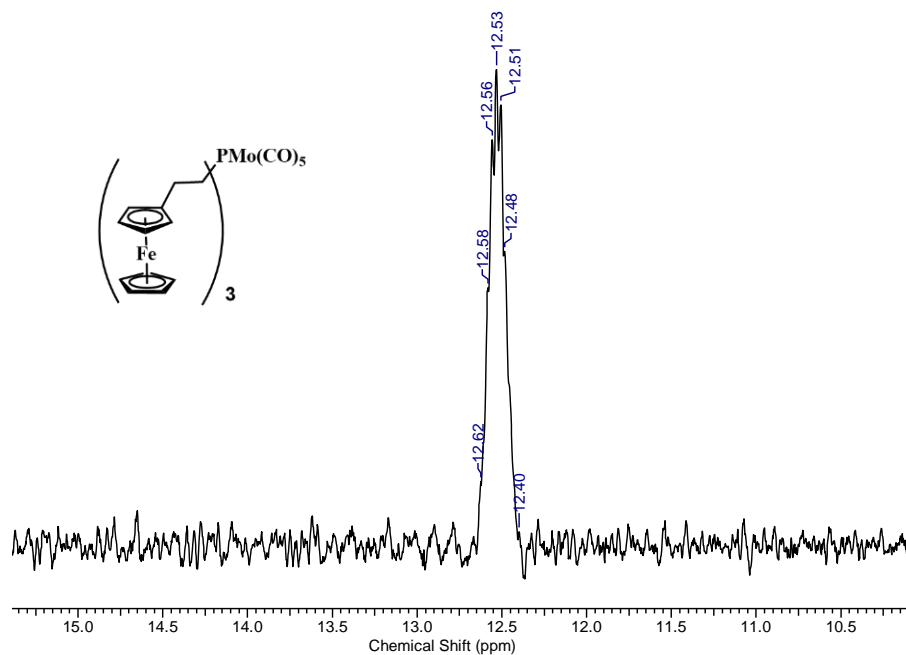


Figure A3.23. ^{31}P NMR spectrum of **3.6c** in CDCl_3 .

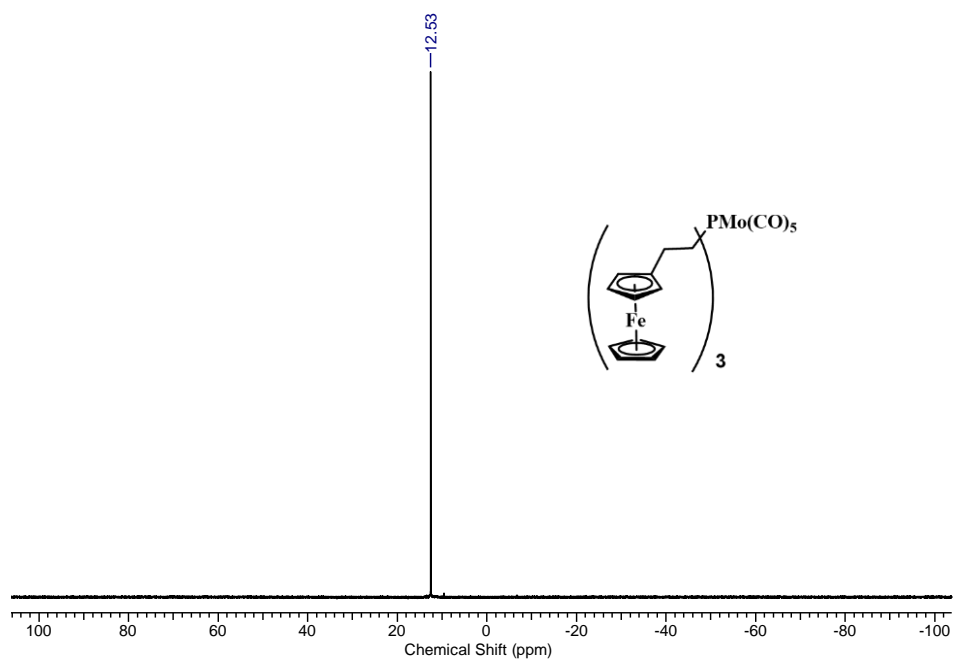


Figure A3.24. $^{31}\text{P}\{^1\text{H}\}$ NMR spectrum of **3.6c** in CDCl_3 .

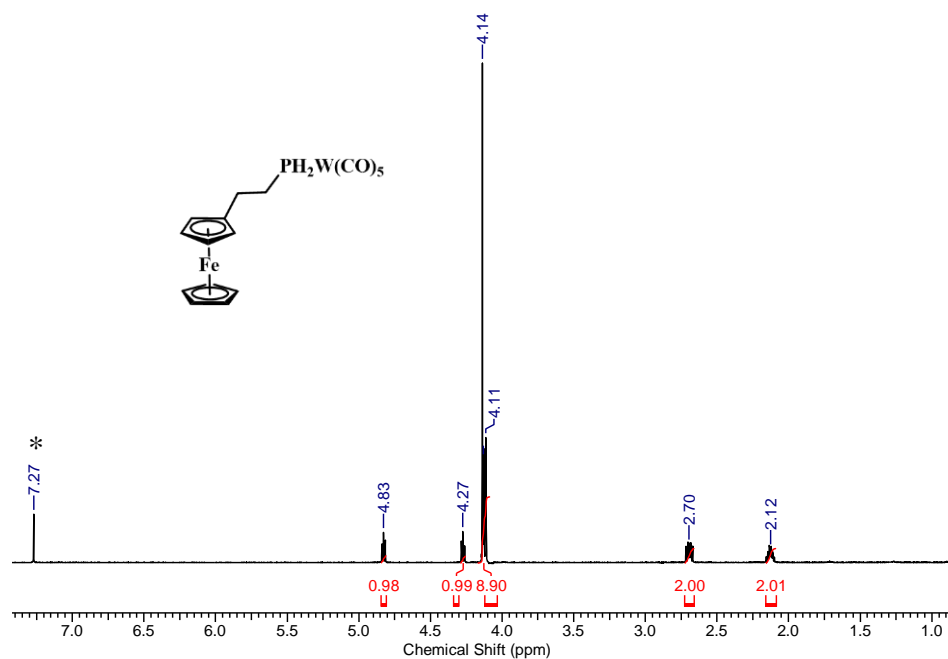


Figure A3.25. ^1H NMR spectrum of **3.7a** in CDCl_3 . The asterisk denotes residual CHCl_3 signal.

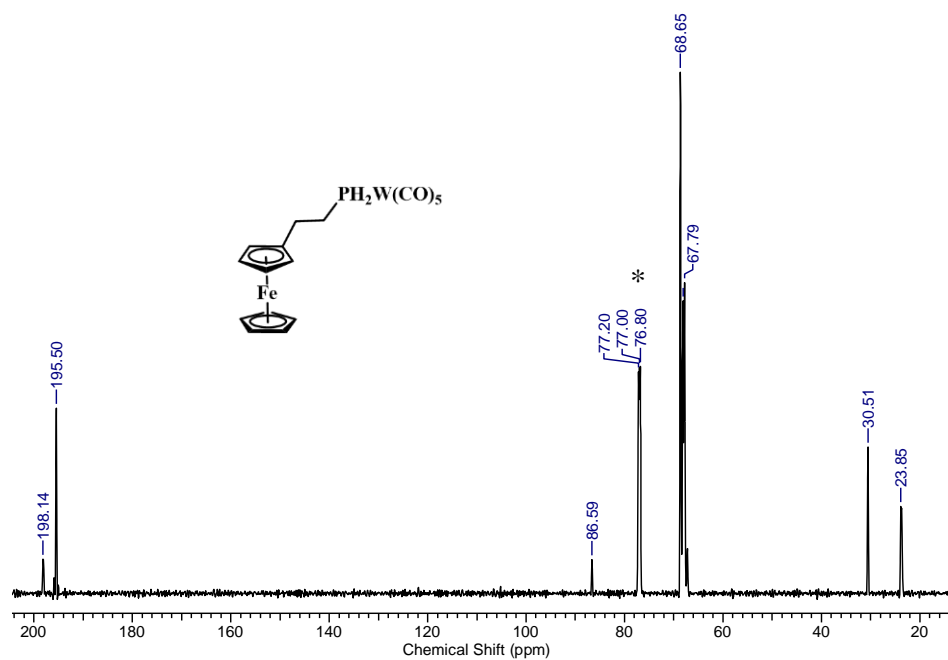


Figure A3.26. $^{13}\text{C}\{^1\text{H}\}$ NMR spectrum of **3.7a** in CDCl_3 . The asterisk denotes the solvent signal.

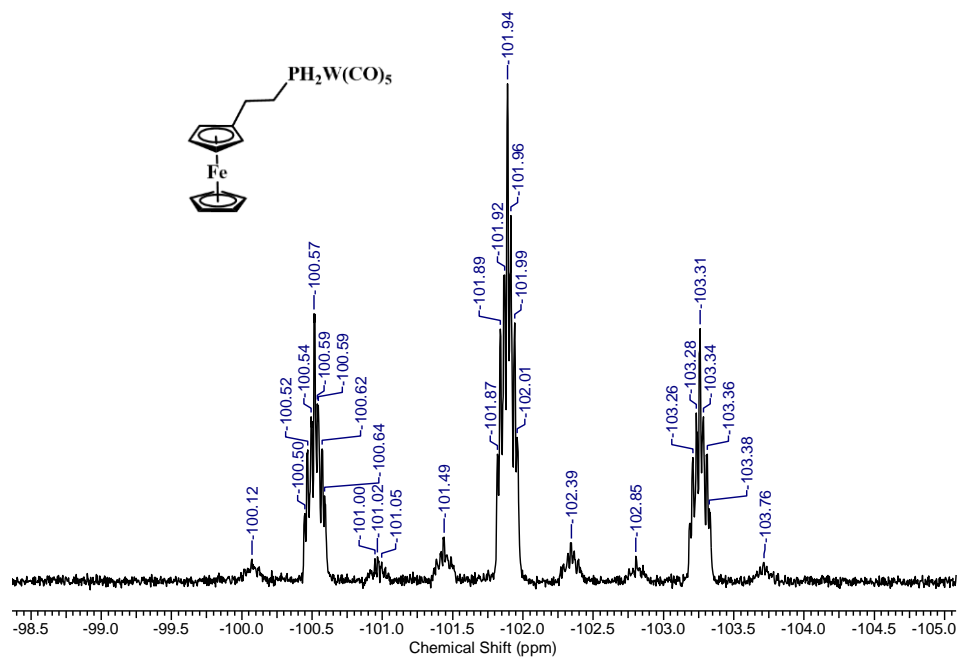


Figure A3.27. ^{31}P NMR spectrum of **3.7a** in CDCl_3 .

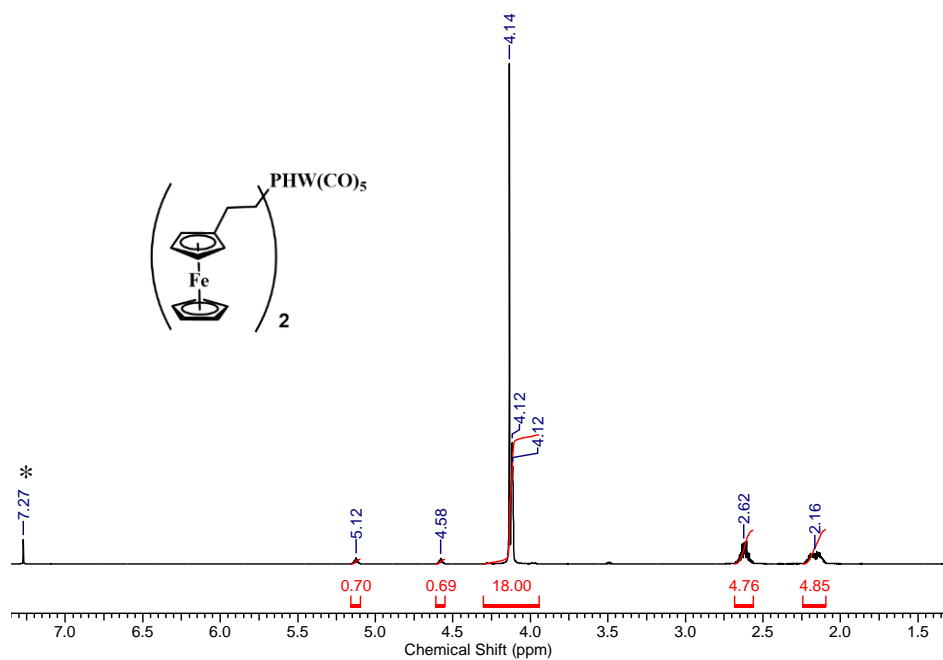


Figure A3.28. ^1H NMR spectrum of **3.7b** in CDCl_3 . The asterisk denotes residual CHCl_3 signal.

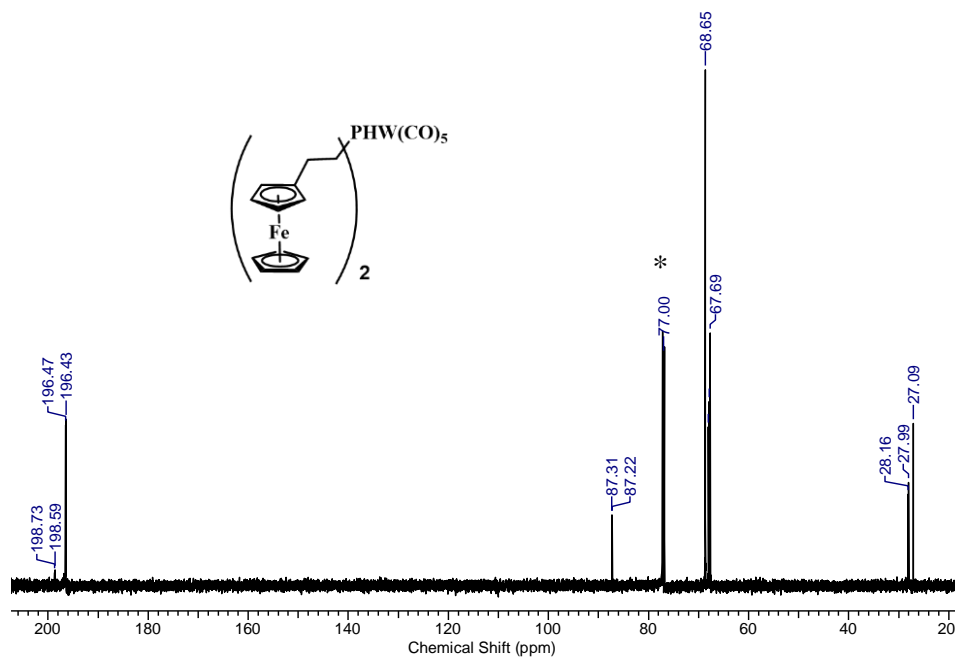


Figure A3.29. $^{13}\text{C}\{^1\text{H}\}$ NMR spectrum of **3.7b** in CDCl_3 . The asterisk denotes the solvent signal.

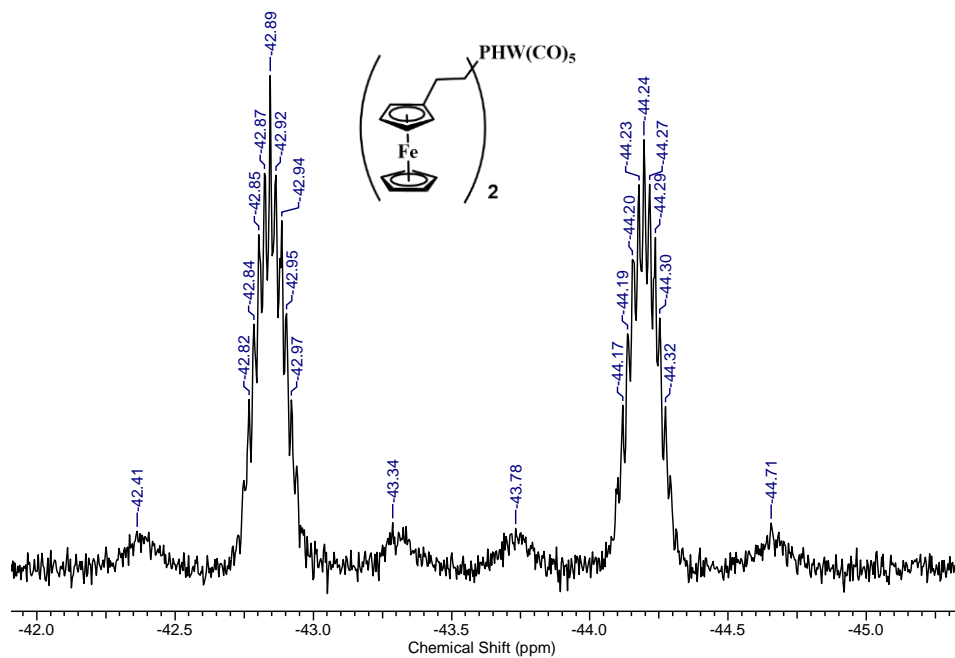


Figure A3.30. ^{31}P NMR spectrum of **3.7b** in CDCl_3 .

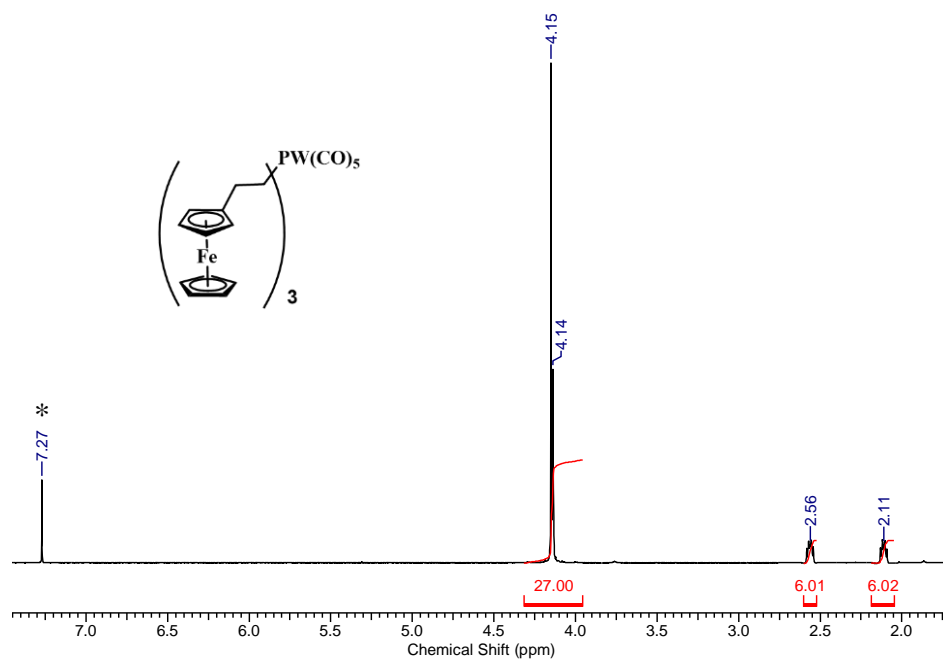


Figure A3.31. ^1H NMR spectrum of **3.7c** in CDCl_3 . The asterisk denotes residual CHCl_3 signal.

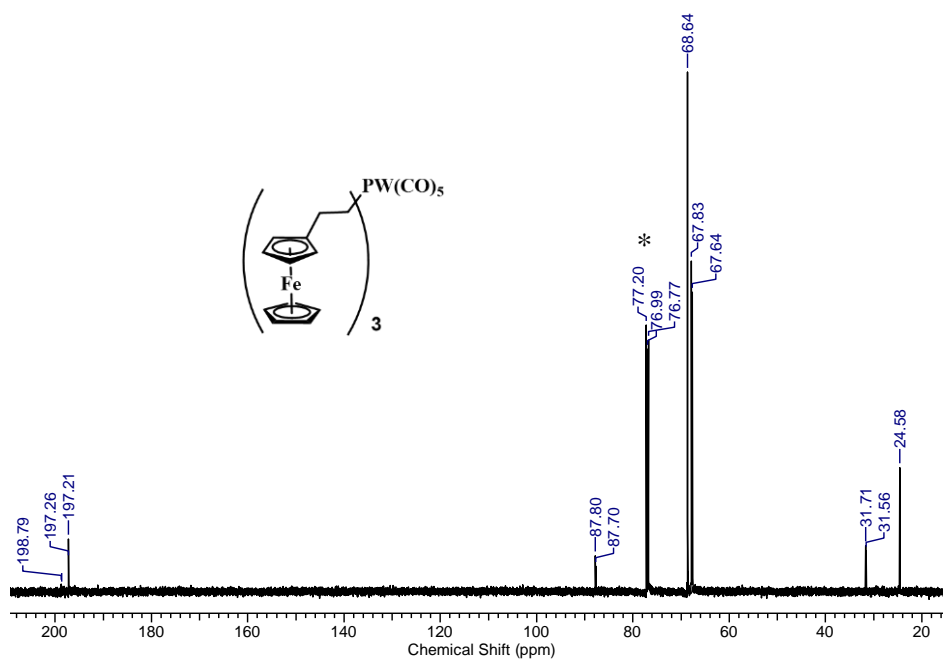


Figure A3.32. $^{13}\text{C}\{^1\text{H}\}$ NMR spectrum of **3.7c** in CDCl_3 . The asterisk denotes the solvent signal.

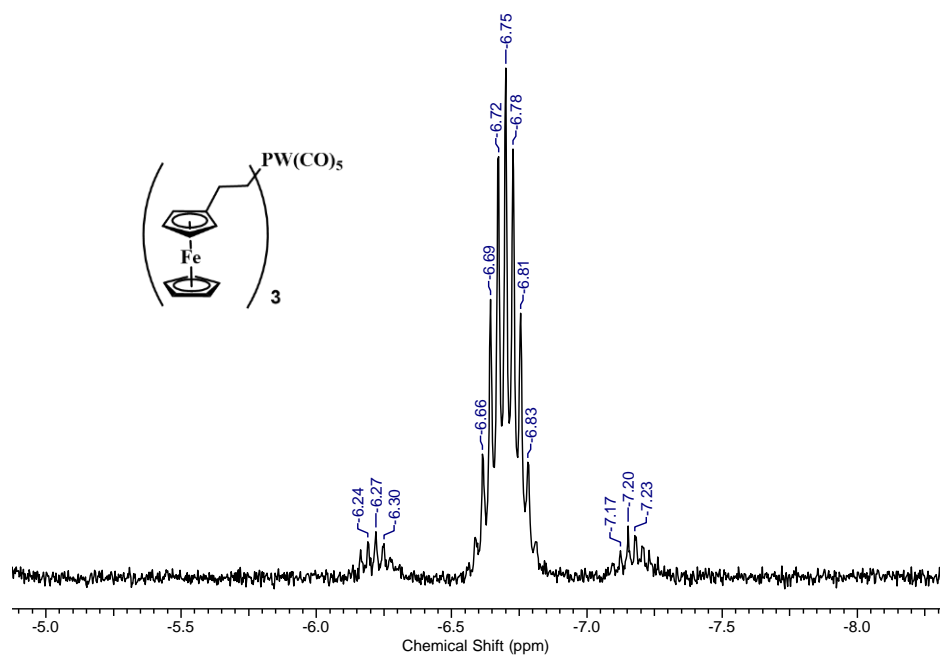


Figure A3.33. ^{31}P NMR spectrum of **3.7c** in CDCl_3 .

Solid-State Structures

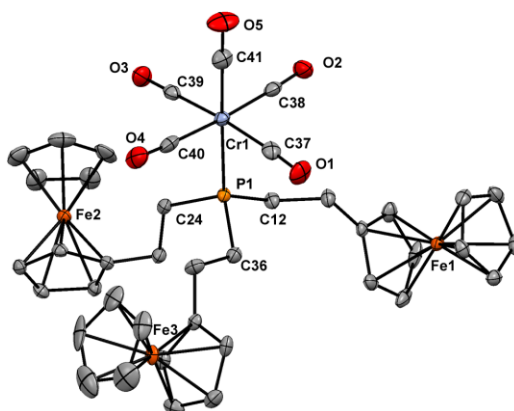


Figure A3.34. Solid-state structure of **3.5c**. Thermal displacement ellipsoids are shown at 50% probability and hydrogen atoms have been omitted for clarity.

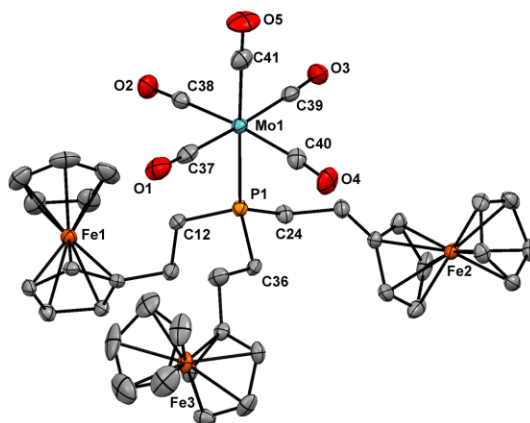


Figure A3.35. Solid-state structure of **3.6c**. Thermal displacement ellipsoids are shown at 50% probability and hydrogen atoms have been omitted for clarity.

FT-IR Absorption Spectra

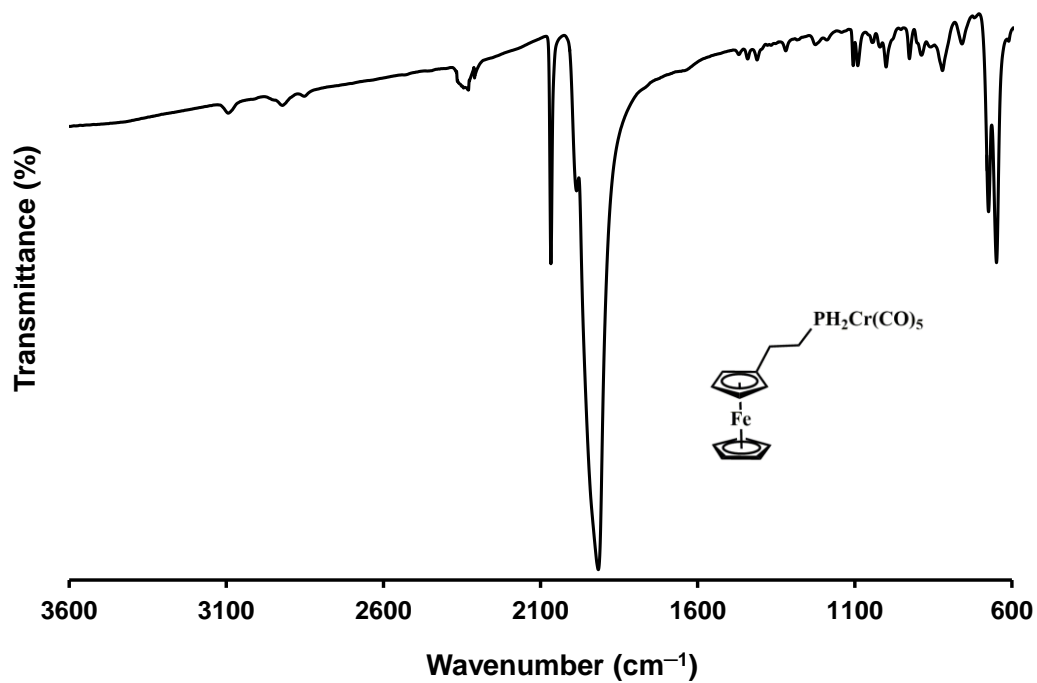


Figure A3.36. FT-IR absorption spectrum of **3.5a** recorded as a thin film on a KBr plate.

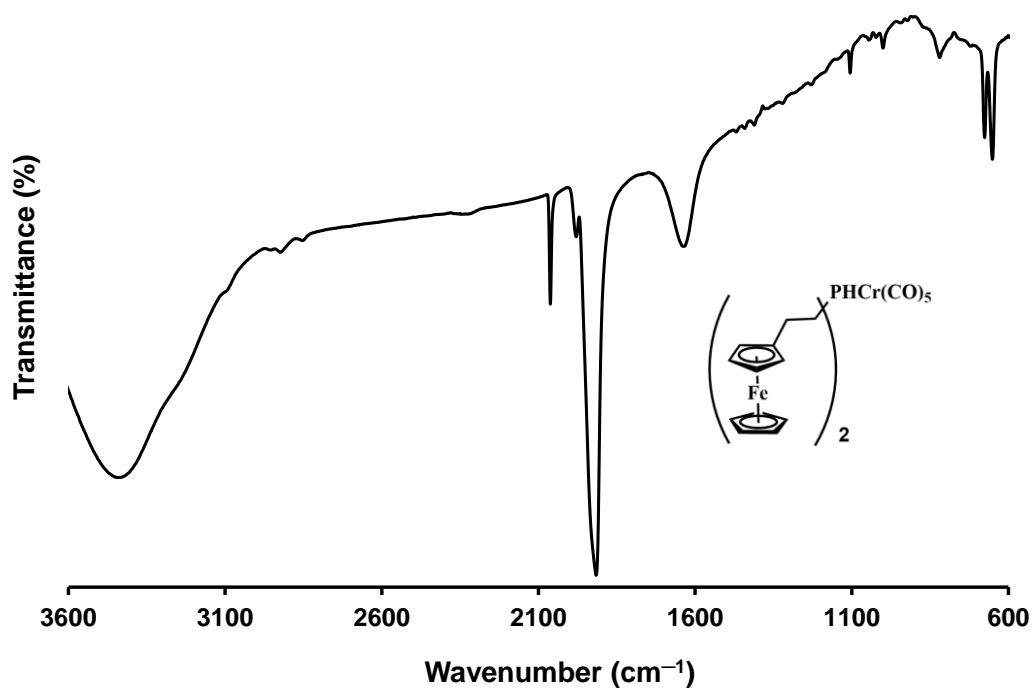


Figure A3.37. FT-IR absorption spectrum of **3.5b** recorded as a thin film on a KBr plate.

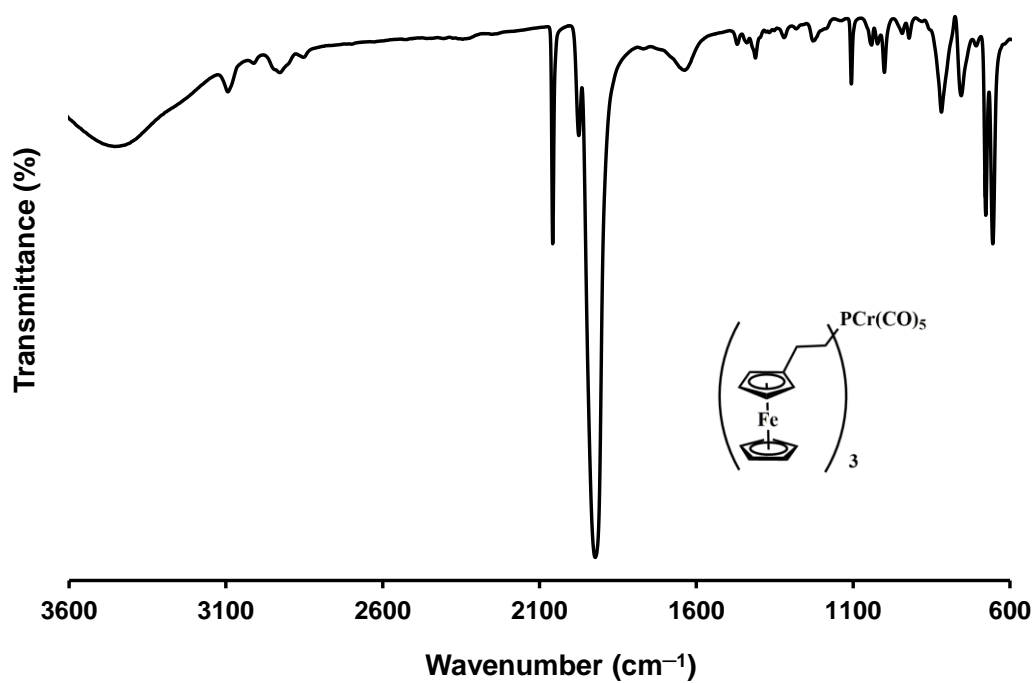


Figure A3.38. FT-IR absorption spectrum of **3.5c** recorded as a thin film on a KBr plate.

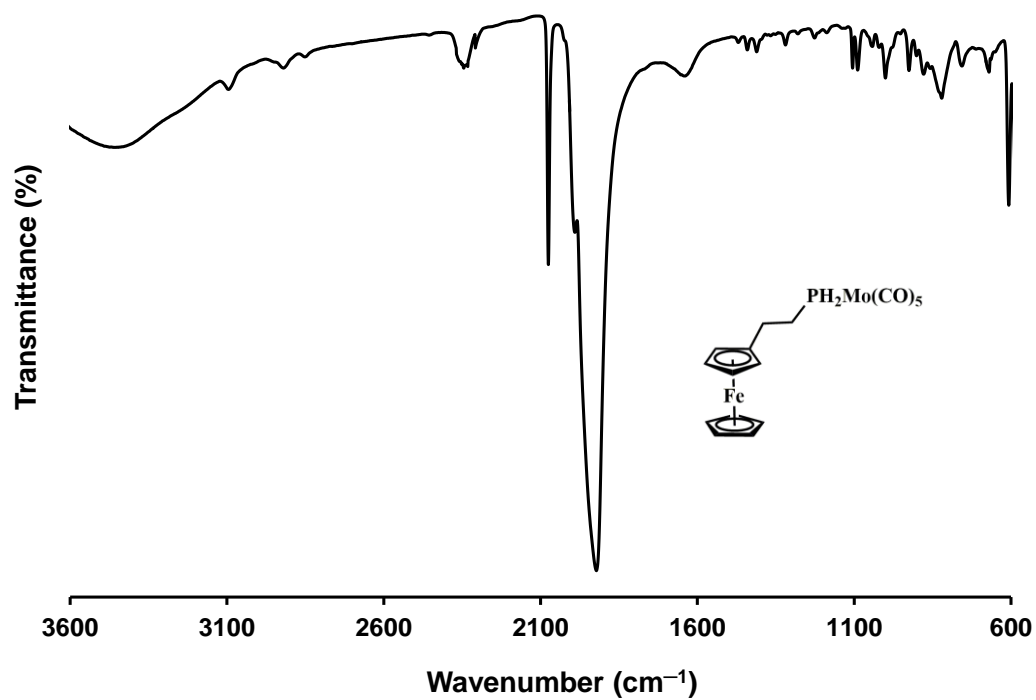


Figure A3.39. FT-IR absorption spectrum of **3.6a** recorded as a thin film on a KBr plate.

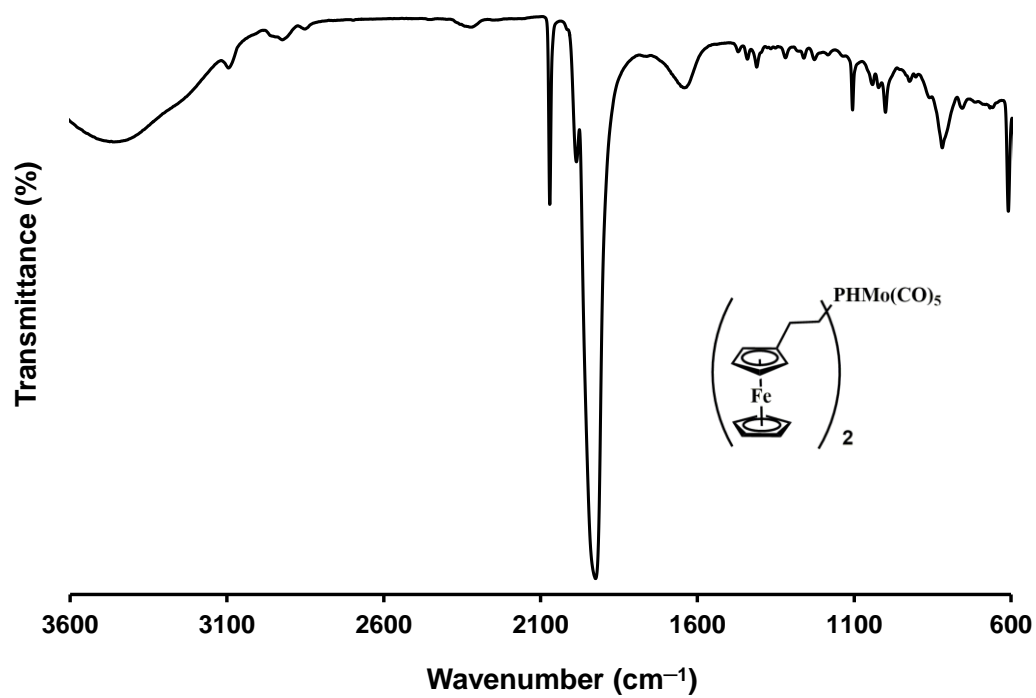


Figure A3.40. FT-IR absorption spectrum of **3.6b** recorded as a thin film on a KBr plate.

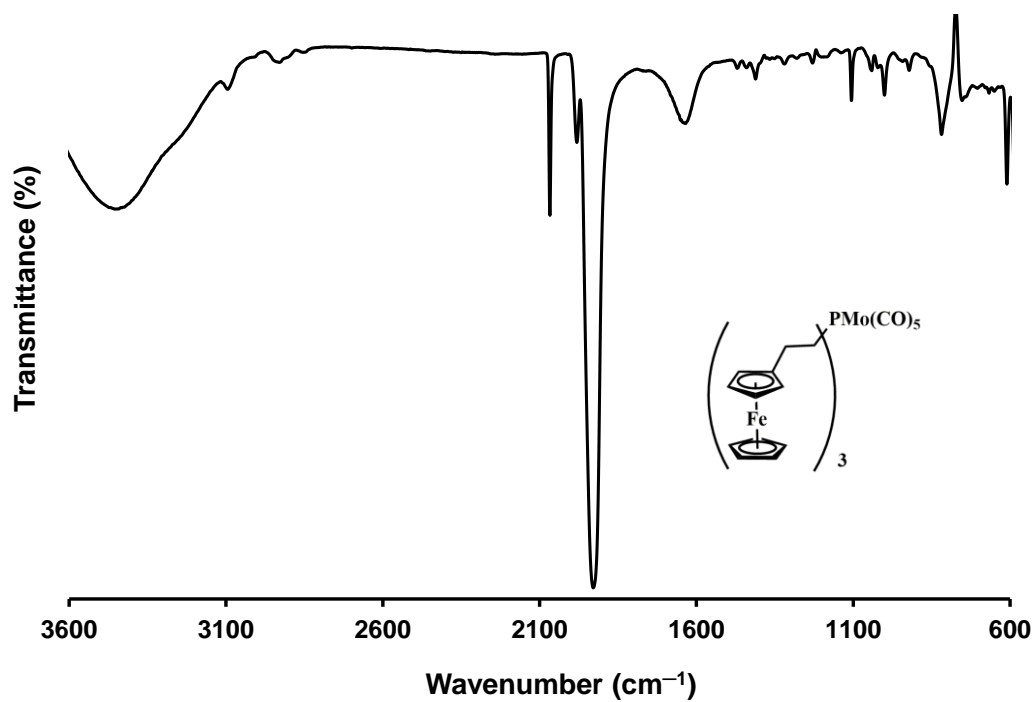


Figure A3.41. FT-IR absorption spectrum of 3.6c recorded as a thin film on a KBr plate.

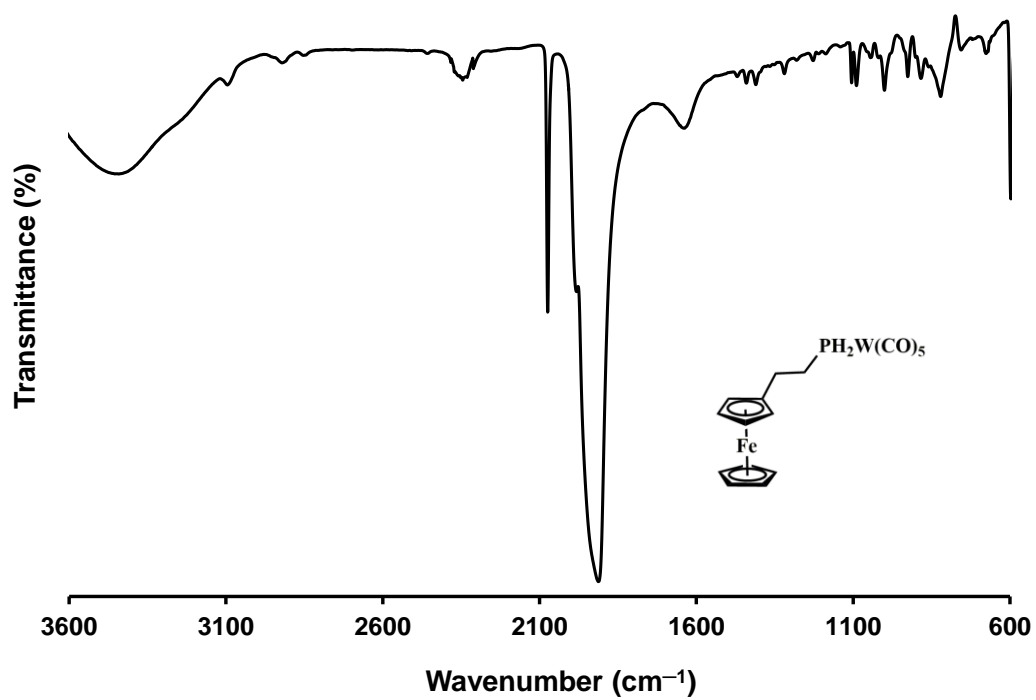


Figure A3.42. FT-IR absorption spectrum of 3.7a recorded as a thin film on a KBr plate.

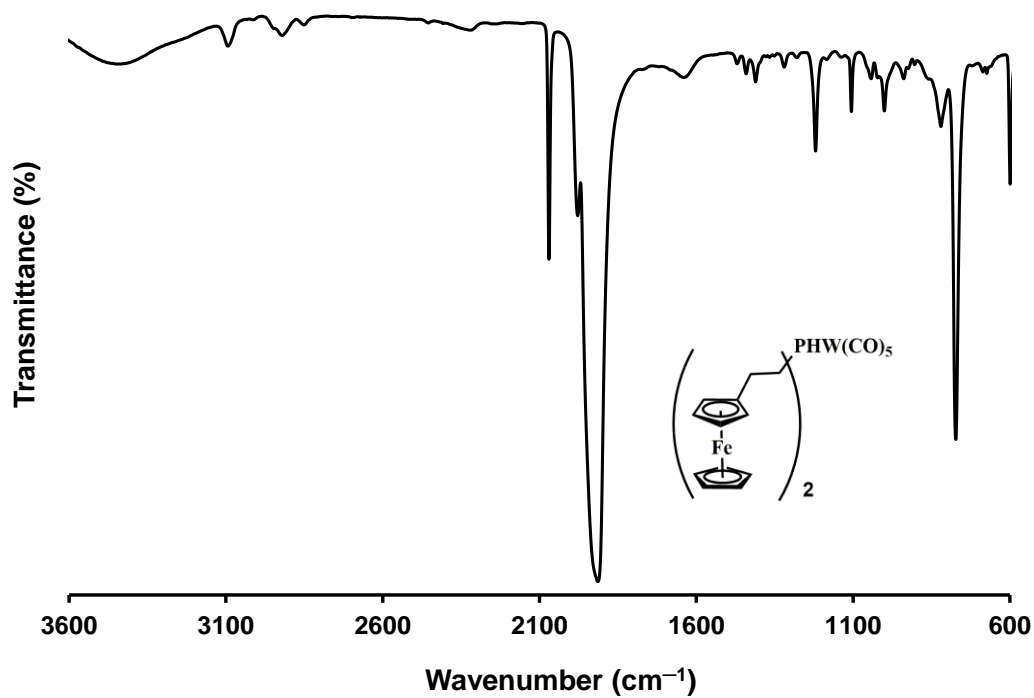


Figure A3.43. FT-IR absorption spectrum of **3.7b** recorded as a thin film on a KBr plate.

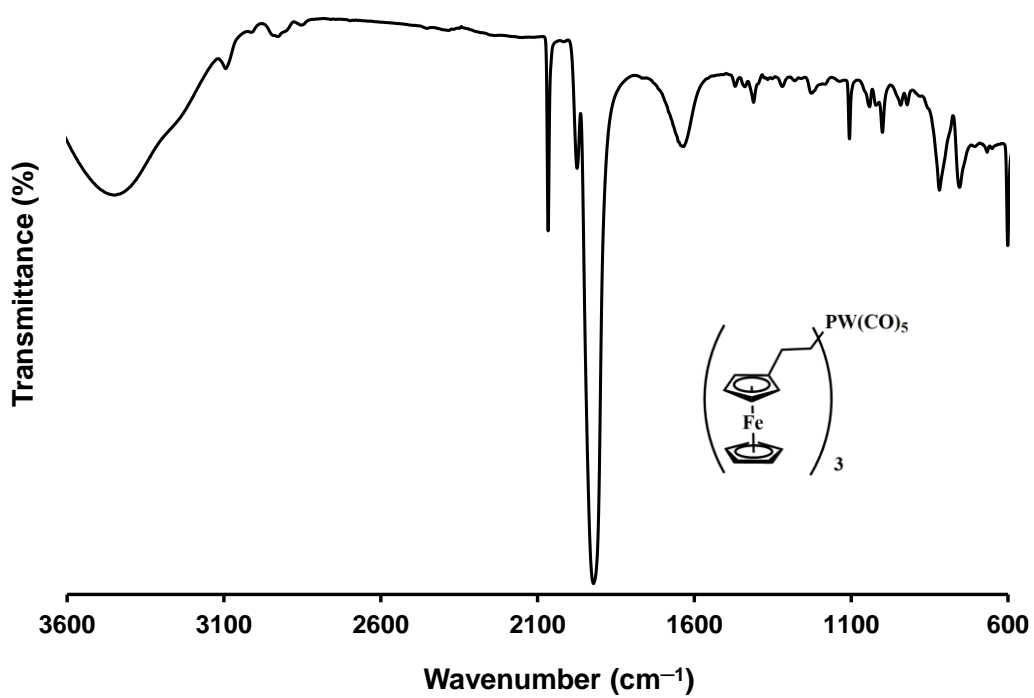


Figure A3.44. FT-IR absorption spectrum of **3.7c** recorded as a thin film on a KBr plate.

UV-Vis Absorption Spectra

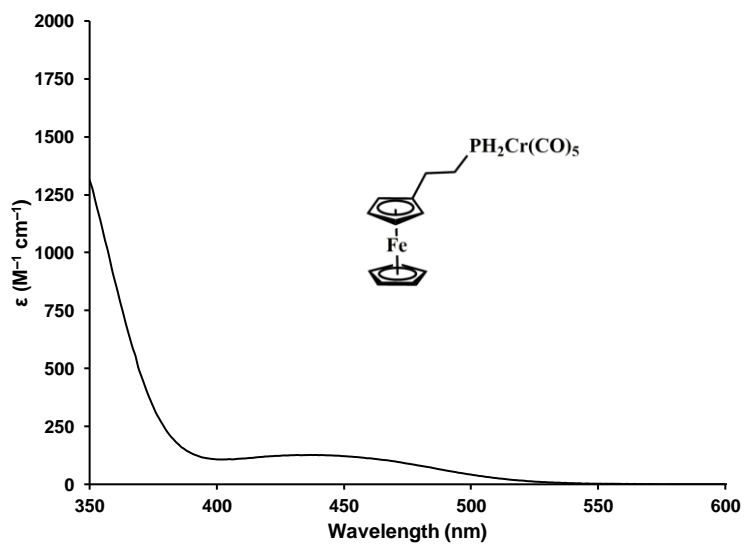


Figure A3.45. UV-Vis absorption spectrum of **3.5a** recorded in CH_2Cl_2 .

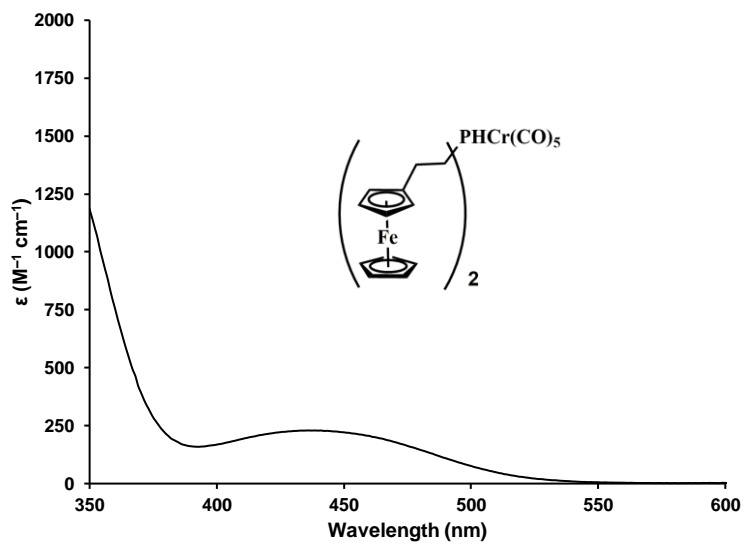


Figure A3.46. UV-Vis absorption spectrum of **3.5b** recorded in CH_2Cl_2 .

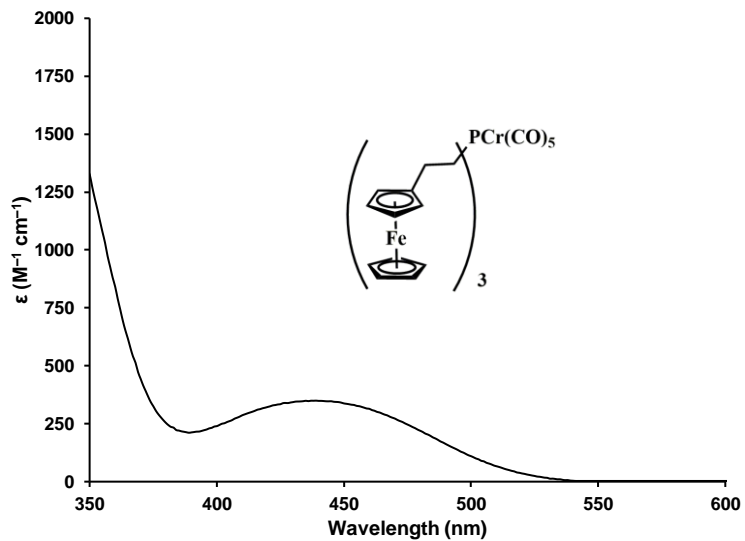


Figure A3.47. UV-Vis absorption spectrum of **3.5c** recorded in CH_2Cl_2 .

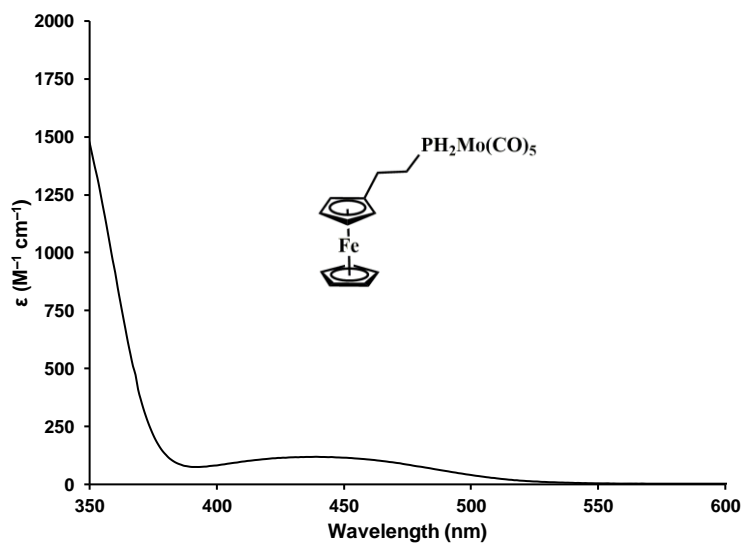


Figure A3.48. UV-Vis absorption spectrum of **3.6a** recorded in CH_2Cl_2 .

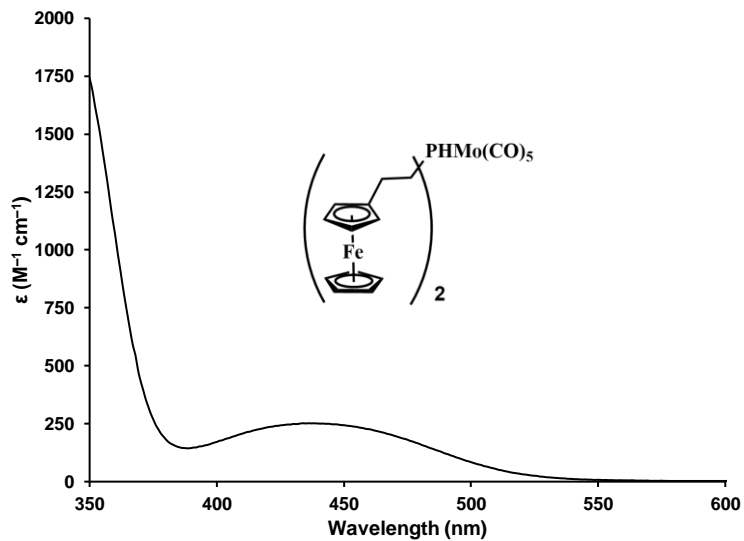


Figure A3.49. UV-Vis absorption spectrum of **3.6b** recorded in CH_2Cl_2 .

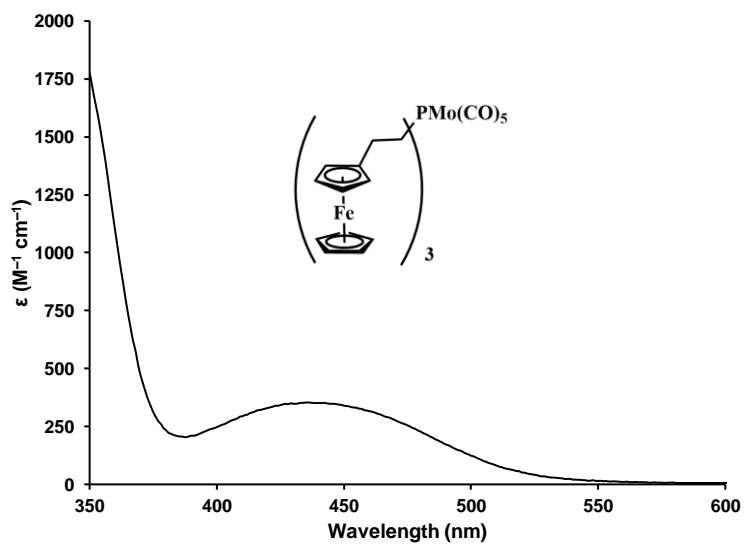


Figure A3.50. UV-Vis absorption spectrum of **3.6c** recorded in CH_2Cl_2 .

Cyclic Voltammograms

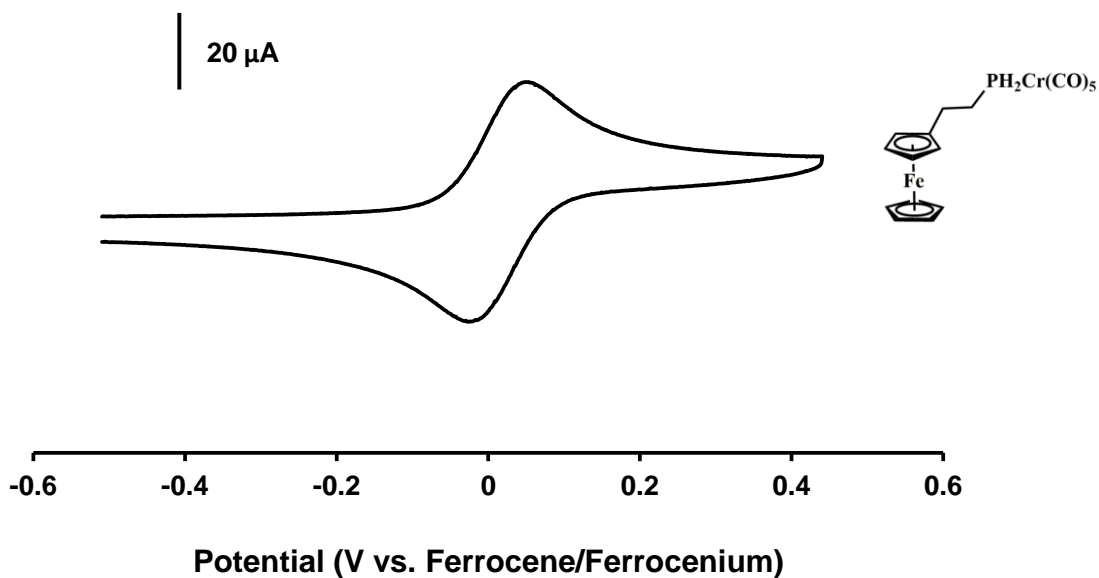


Figure A3.51. Cyclic voltammogram of **3.5a** recorded at 250 mV s^{-1} for a 1 mM degassed 2:1 $\text{CH}_2\text{Cl}_2:\text{CH}_3\text{CN}$ solution containing 0.1 M $[n\text{-Bu}_4\text{N}][\text{OTf}]$ as supporting electrolyte.

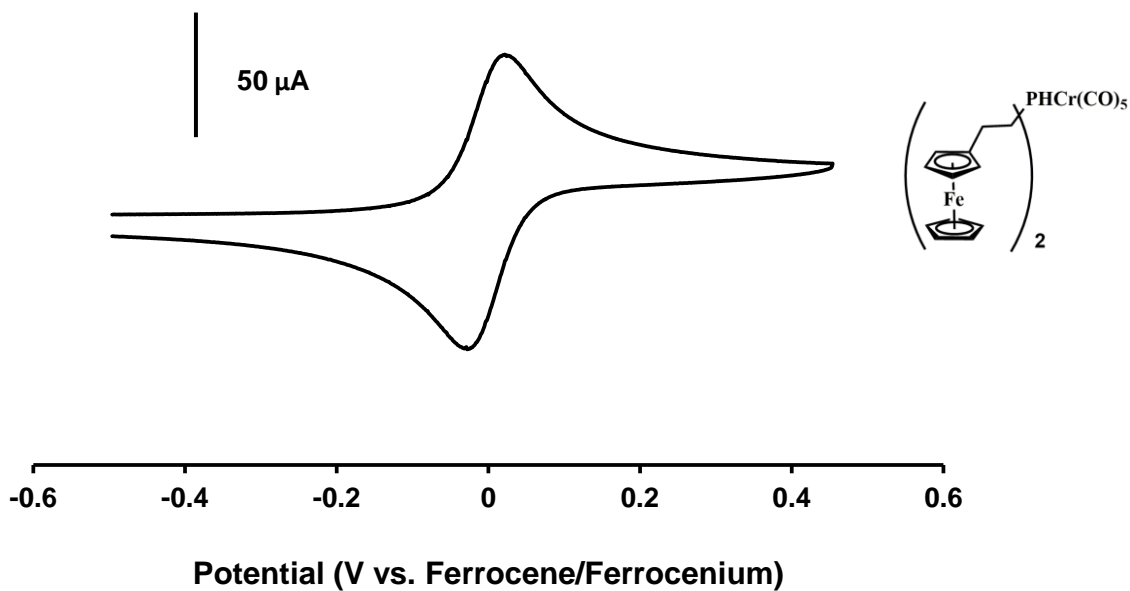


Figure A3.52. Cyclic voltammogram of **3.5b** recorded at 250 mV s^{-1} for a 1 mM degassed 2:1 $\text{CH}_2\text{Cl}_2:\text{CH}_3\text{CN}$ solution containing 0.1 M $[n\text{-Bu}_4\text{N}][\text{OTf}]$ as supporting electrolyte.

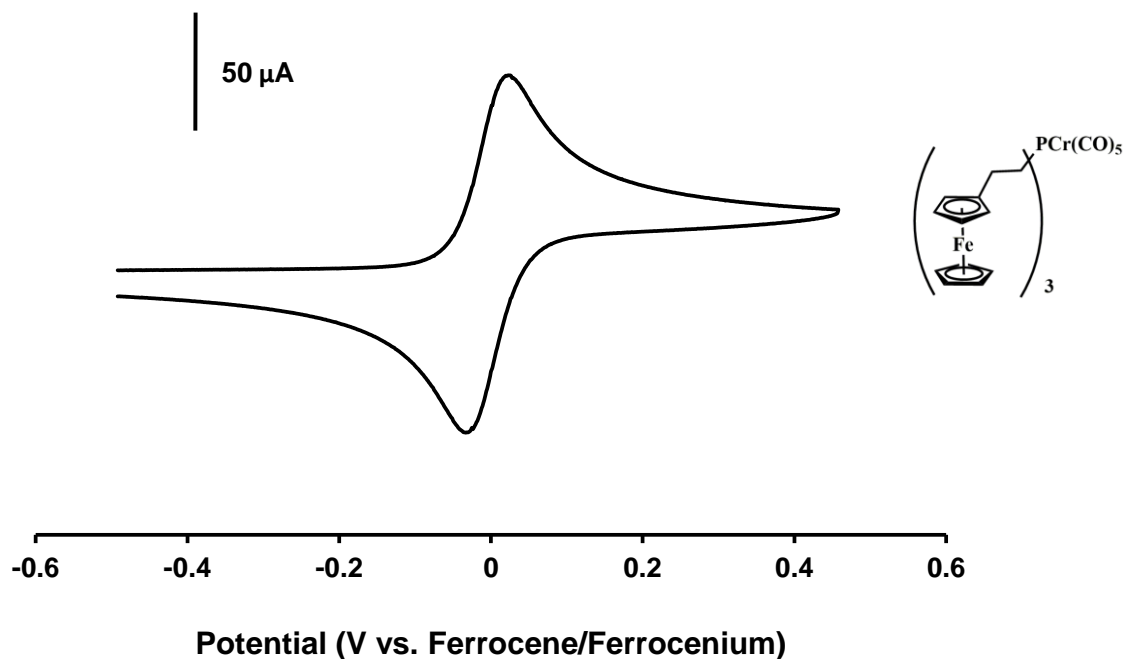


Figure A3.53. Cyclic voltammogram of **3.5c** recorded at 250 mV s^{-1} for a 1 mM degassed 2:1 $\text{CH}_2\text{Cl}_2:\text{CH}_3\text{CN}$ solution containing 0.1 M $[n\text{-Bu}_4\text{N}][\text{OTf}]$ as supporting electrolyte.

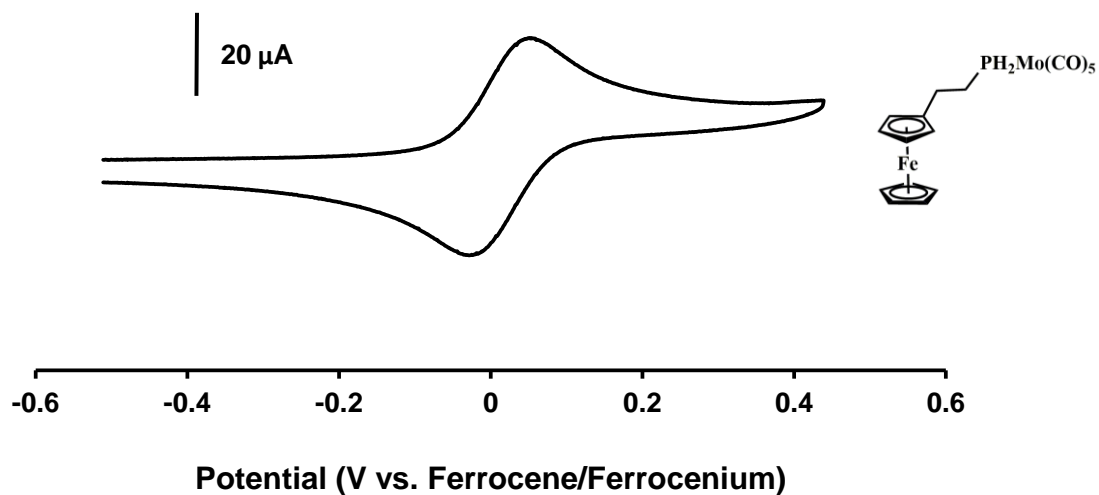


Figure A3.54. Cyclic voltammogram of **3.6a** recorded at 250 mV s^{-1} for a 1 mM degassed 2:1 $\text{CH}_2\text{Cl}_2:\text{CH}_3\text{CN}$ solution containing 0.1 M $[n\text{-Bu}_4\text{N}][\text{OTf}]$ as supporting electrolyte.

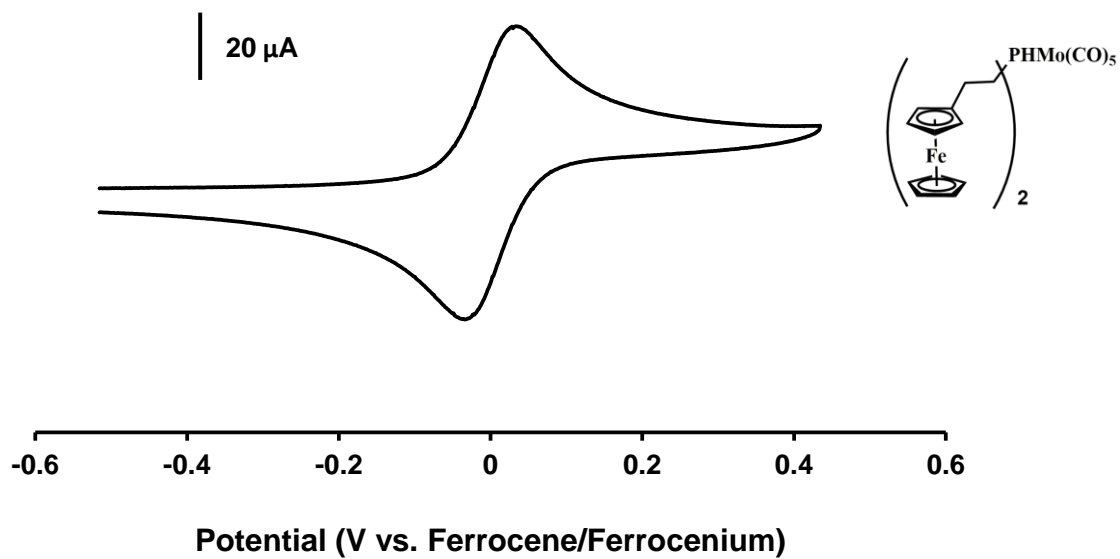


Figure A3.55. Cyclic voltammogram of **3.6b** recorded at 250 mV s^{-1} for a 1 mM degassed 2:1 $\text{CH}_2\text{Cl}_2:\text{CH}_3\text{CN}$ solution containing 0.1 M $[n\text{-Bu}_4\text{N}][\text{OTf}]$ as supporting electrolyte.

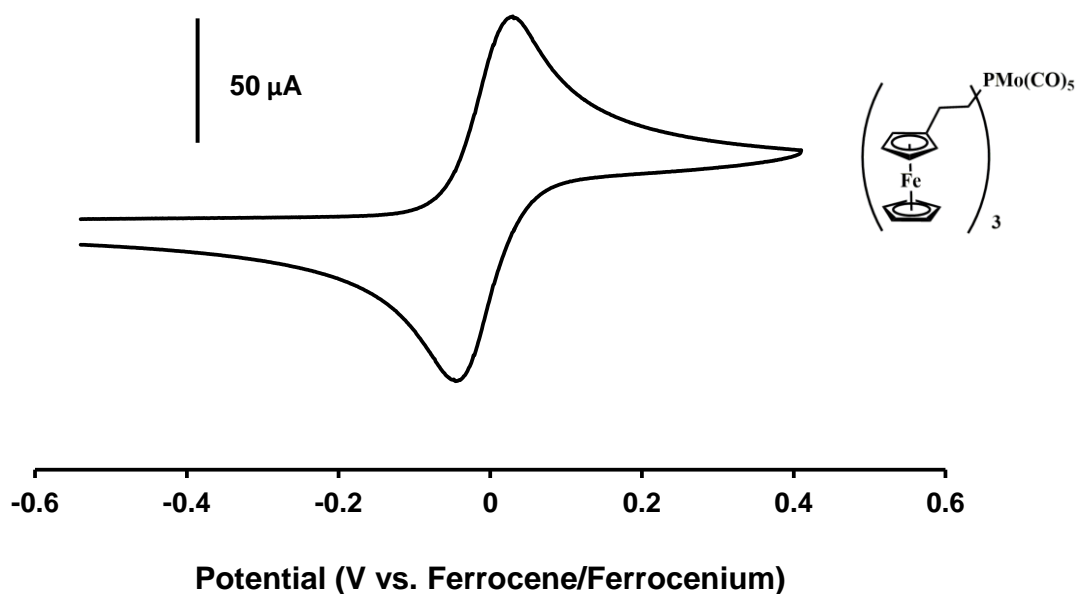


Figure A3.56. Cyclic voltammogram of **3.6c** recorded at 250 mV s^{-1} for a 1 mM degassed 2:1 $\text{CH}_2\text{Cl}_2:\text{CH}_3\text{CN}$ solution containing 0.1 M $[n\text{-Bu}_4\text{N}][\text{OTf}]$ as supporting electrolyte.

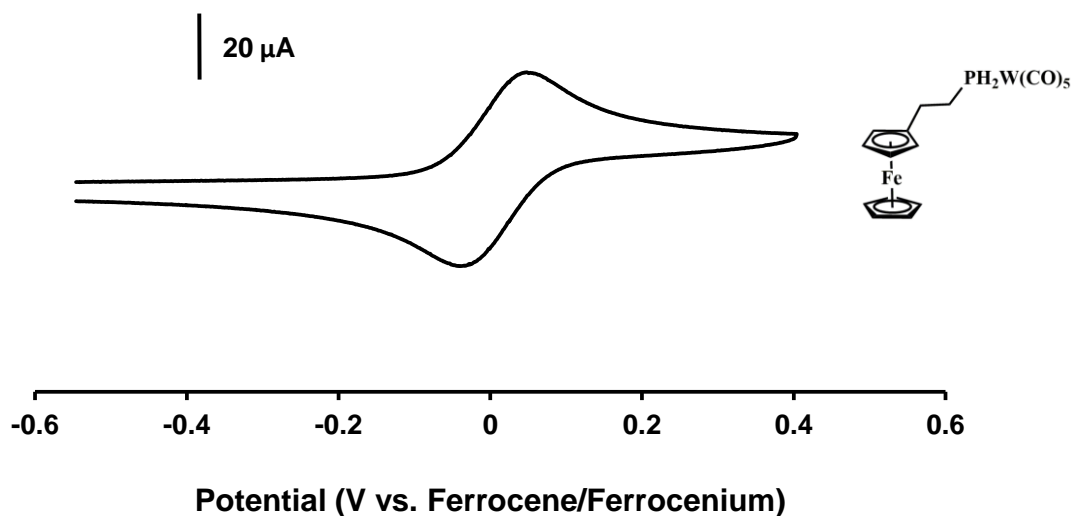


Figure A3.57. Cyclic voltammogram of **3.7a** recorded at 250 mV s^{-1} for a 1 mM degassed 2:1 $\text{CH}_2\text{Cl}_2:\text{CH}_3\text{CN}$ solution containing 0.1 M $[n\text{-Bu}_4\text{N}][\text{OTf}]$ as supporting electrolyte.

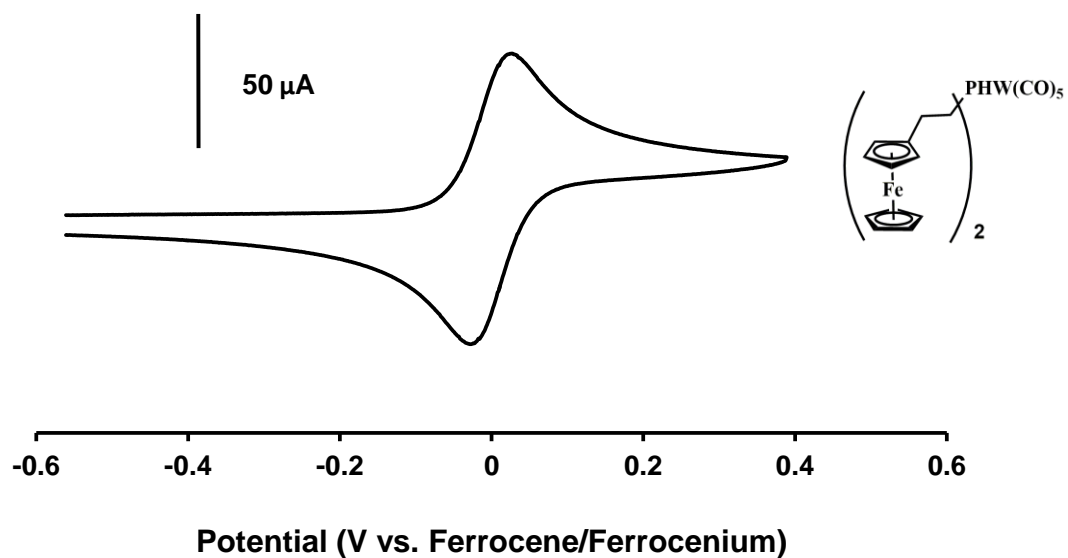


Figure A3.58. Cyclic voltammogram of **3.7b** recorded at 250 mV s^{-1} for a 1 mM degassed 2:1 $\text{CH}_2\text{Cl}_2:\text{CH}_3\text{CN}$ solution containing 0.1 M $[n\text{-Bu}_4\text{N}][\text{OTf}]$ as supporting electrolyte.

Appendix 4 – Supporting Information for Chapter 4

NMR Spectra

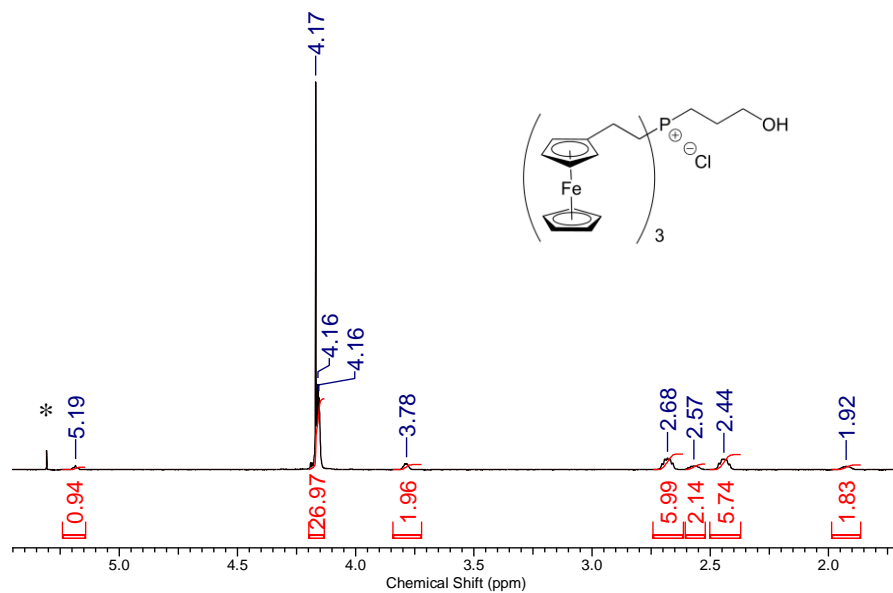


Figure A4.1. ^1H NMR spectrum of phosphonium chloride salt **4.8a** in CDCl_3 . The asterisk denotes residual CHCl_3 signal.

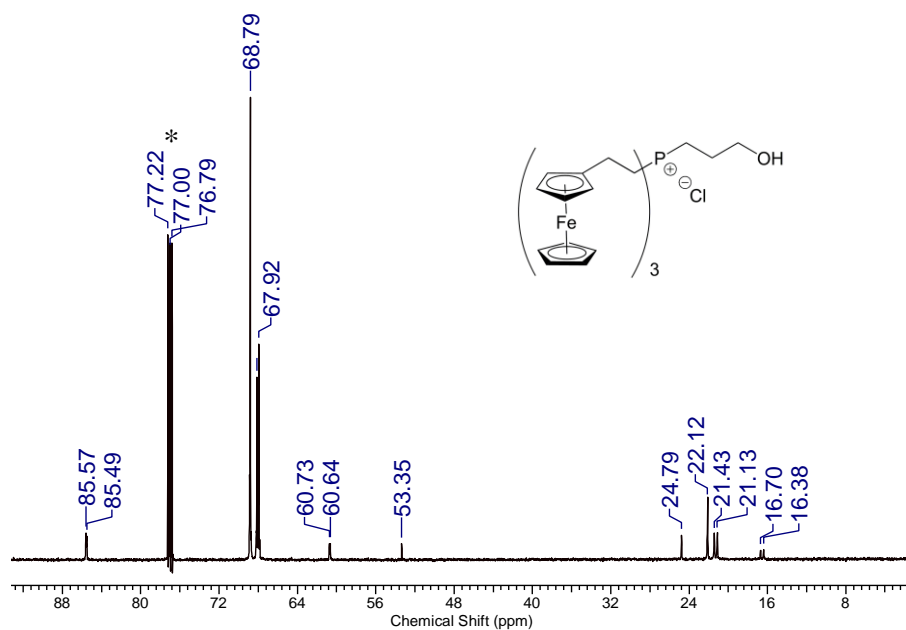


Figure A4.2. $^{13}\text{C}\{^1\text{H}\}$ NMR spectrum of phosphonium chloride salt **4.8a** in CDCl_3 . The asterisk denotes the solvent signal.

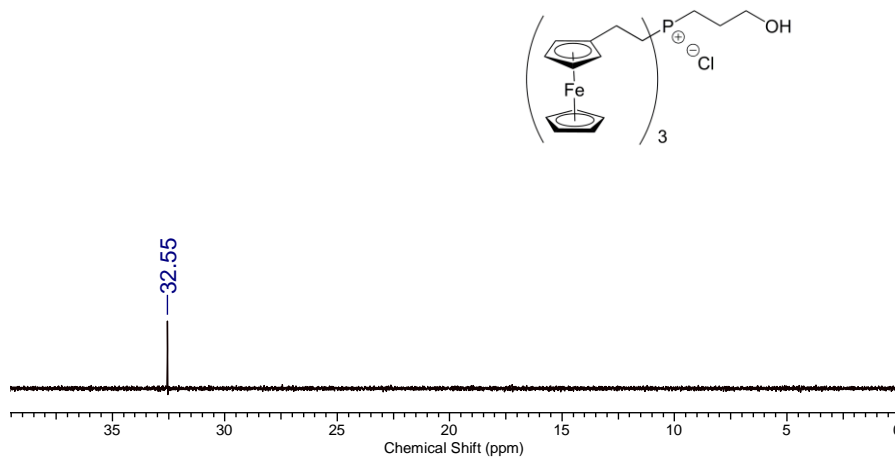


Figure A4.3. $^{31}\text{P}\{^1\text{H}\}$ NMR spectrum of phosphonium chloride salt **4.8a** in CDCl_3 .

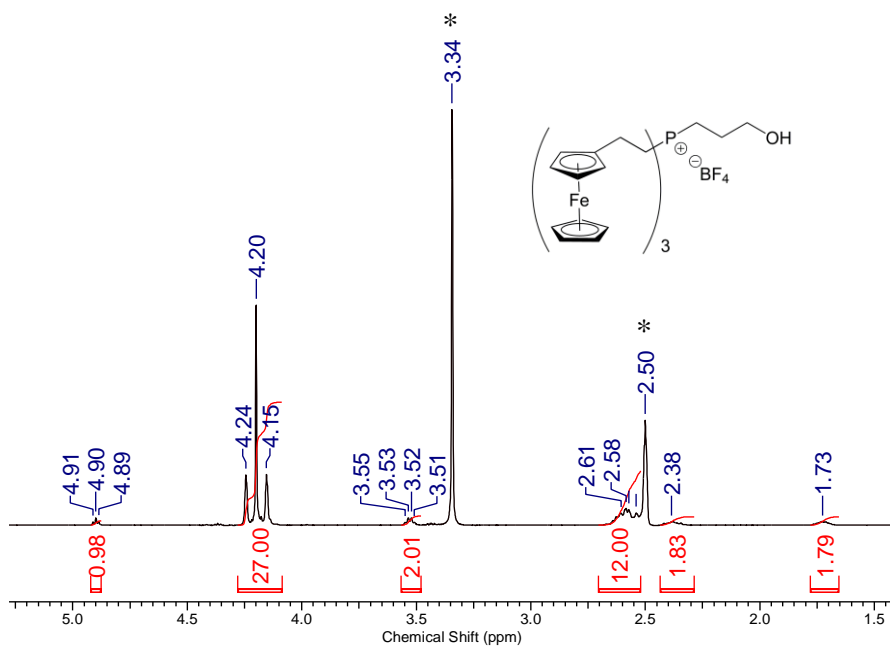


Figure A4.4. ^1H NMR spectrum of phosphonium tetrafluoroborate salt **4.8b** in d_6 -DMSO. The asterisks denote residual $(\text{CD}_3)(\text{CD}_2\text{H})\text{SO}$ and H_2O signals.

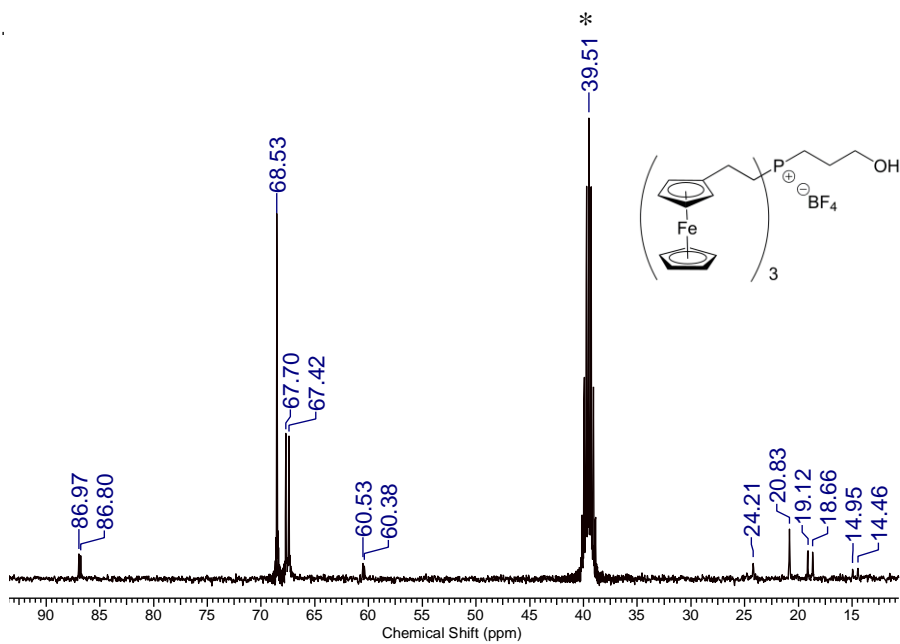


Figure A4.5. $^{13}\text{C}\{^1\text{H}\}$ NMR spectrum of phosphonium tetrafluoroborate salt **4.8b** in d_6 -DMSO. The asterisk denotes the solvent signal.

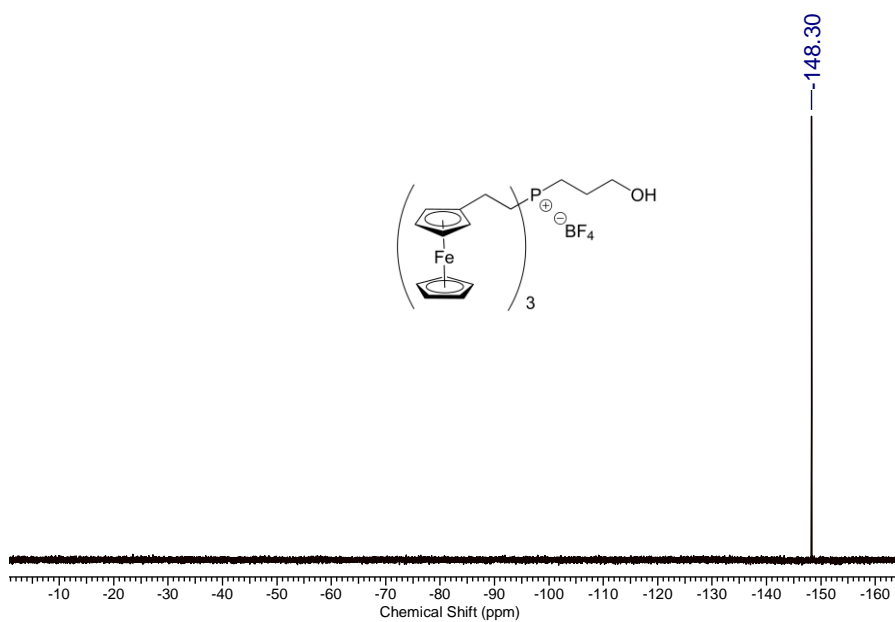


Figure A4.6. ^{19}F NMR spectrum of phosphonium tetrafluoroborate salt **4.8b** in d_6 -DMSO.

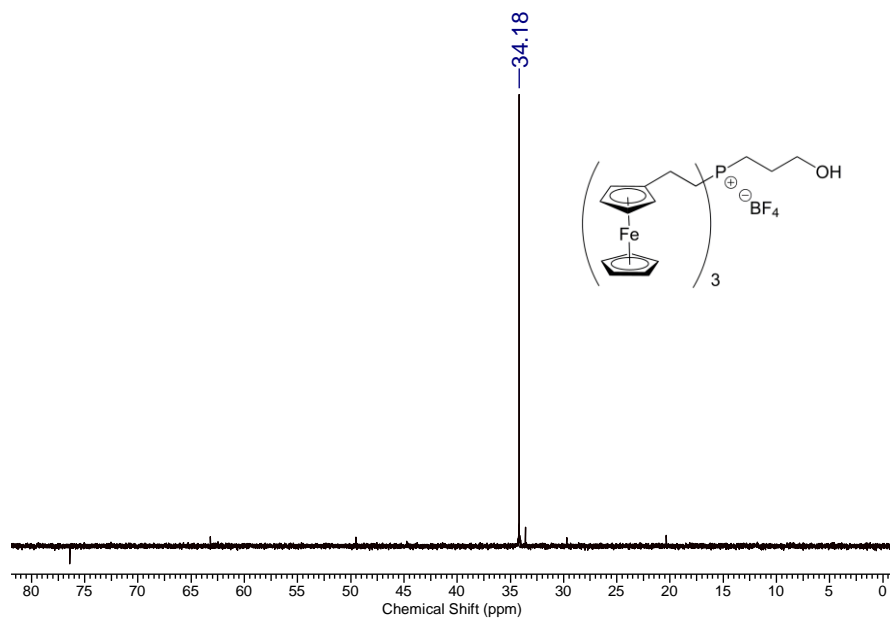


Figure A4.7. $^{31}\text{P}\{^1\text{H}\}$ NMR spectrum of phosphonium tetrafluoroborate salt **4.8b** in d_6 -DMSO.

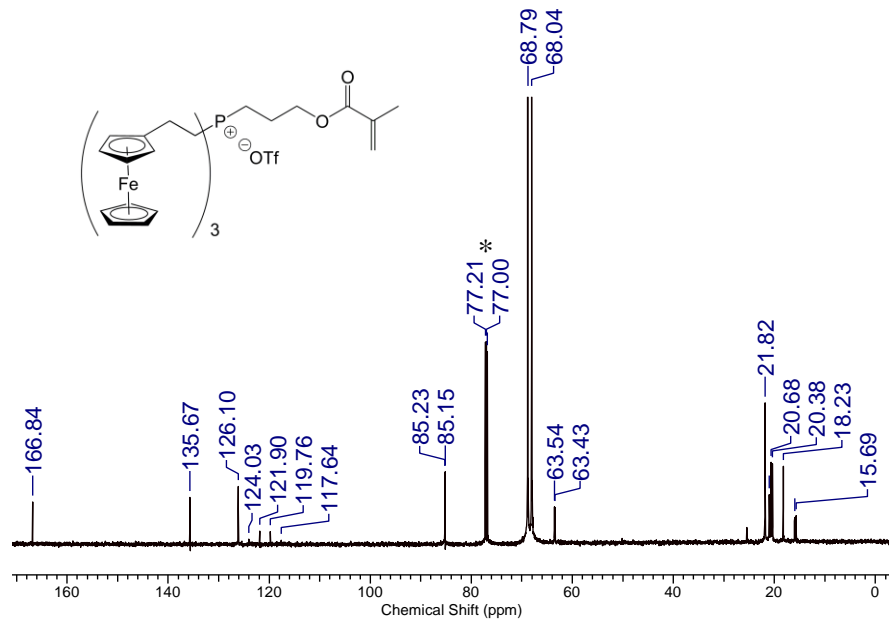


Figure A4.8. $^{13}\text{C}\{^1\text{H}\}$ NMR spectrum of phosphonium monomer **4.9** in CDCl_3 . The asterisk denotes the solvent signal.

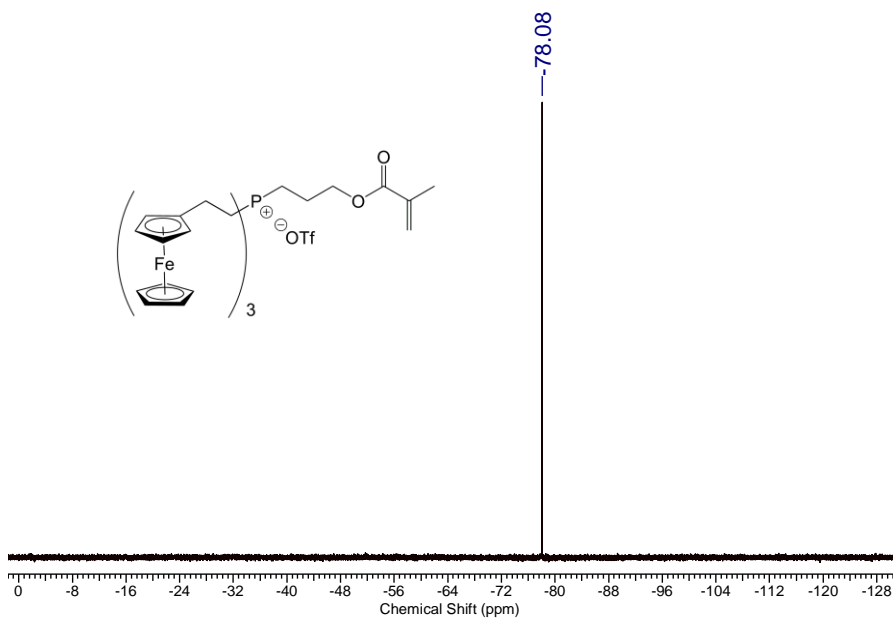


Figure A4.9. ^{19}F NMR spectrum of monomer **4.9** in CDCl_3 .

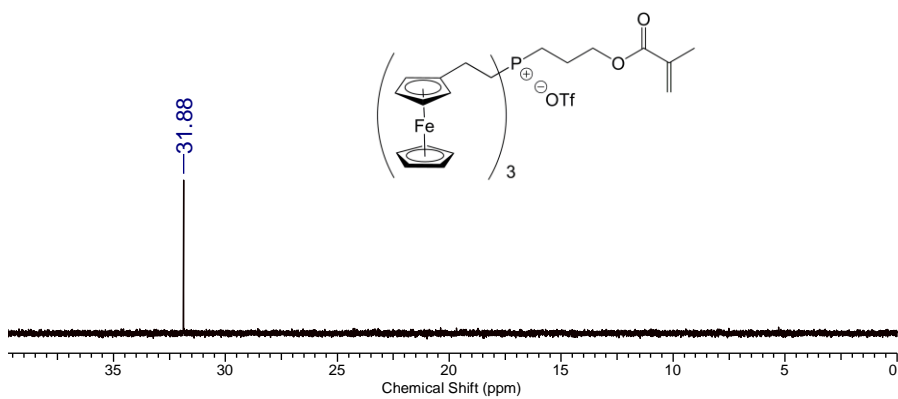


Figure A4.10. $^{31}\text{P}\{^1\text{H}\}$ NMR spectrum of monomer **4.9** in CDCl_3 .

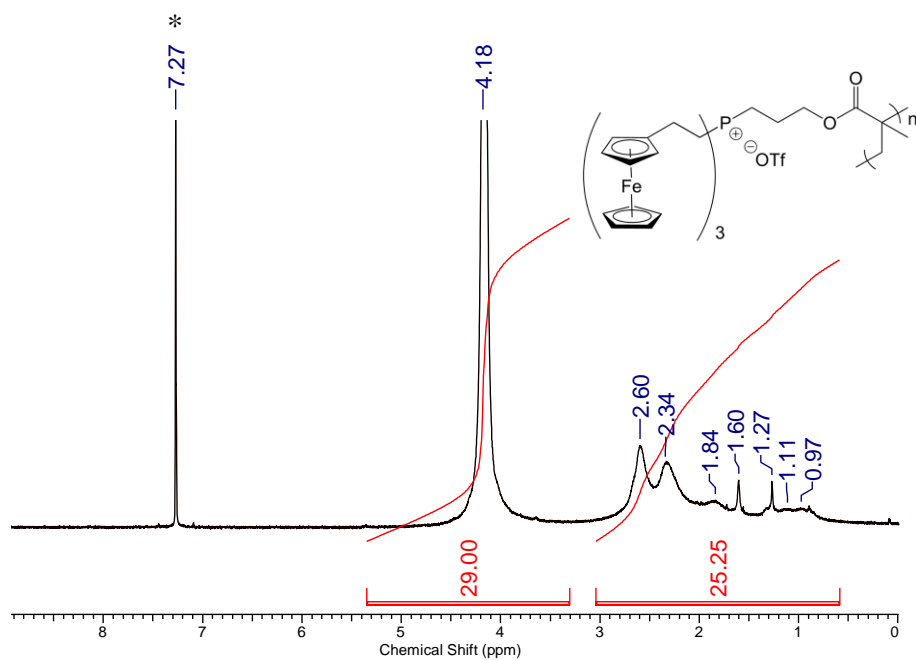


Figure A4.11. ^1H NMR spectrum of polyelectrolyte **4.10a** in CDCl_3 . The asterisk denotes residual CHCl_3 signal.

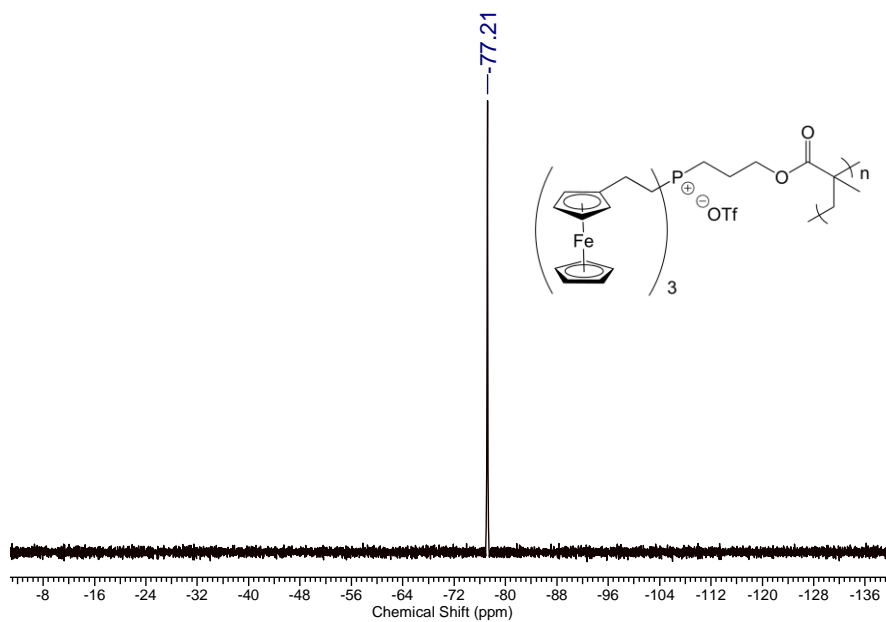


Figure A4.12. ^{19}F NMR spectrum of polyelectrolyte **4.10a** in CDCl_3 .

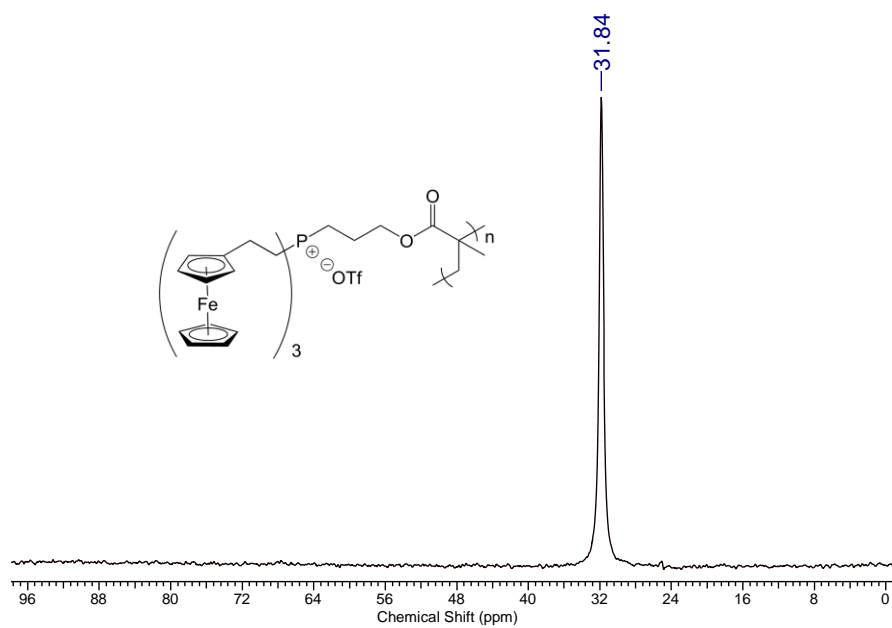


Figure A4.13. $^{31}\text{P}\{^1\text{H}\}$ NMR spectrum of polyelectrolyte **4.10a** in CDCl_3 .

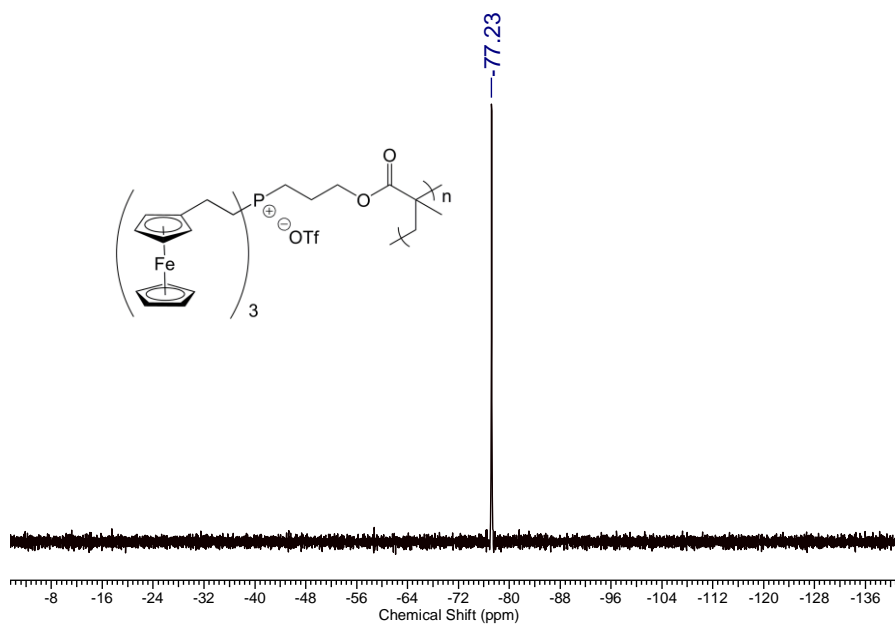


Figure A4.14. ^{19}F NMR spectrum of polyelectrolyte **4.10b** in CDCl_3 .

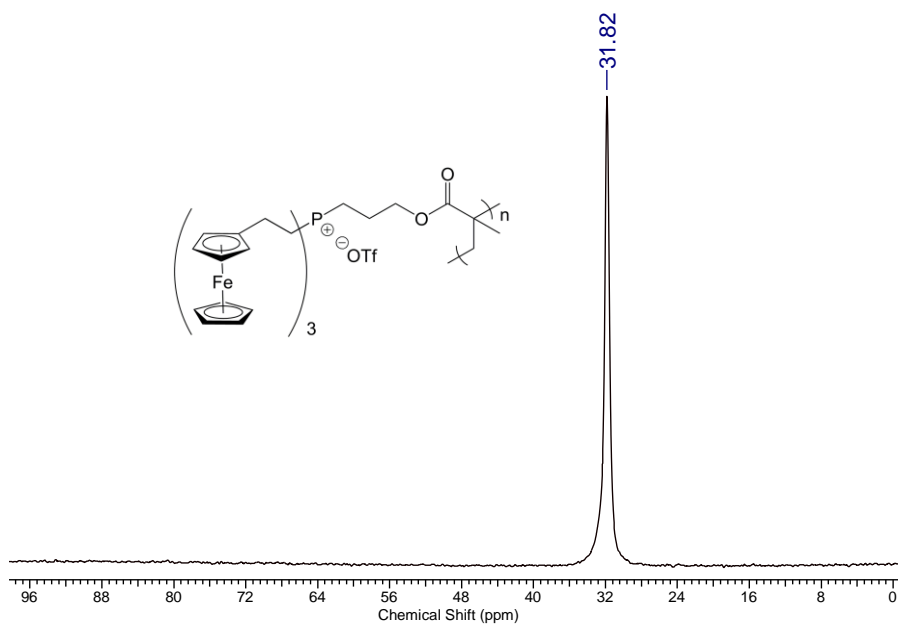


Figure A4.15. $^{31}\text{P}\{^1\text{H}\}$ NMR spectrum of polyelectrolyte **4.10b** in CDCl_3 .

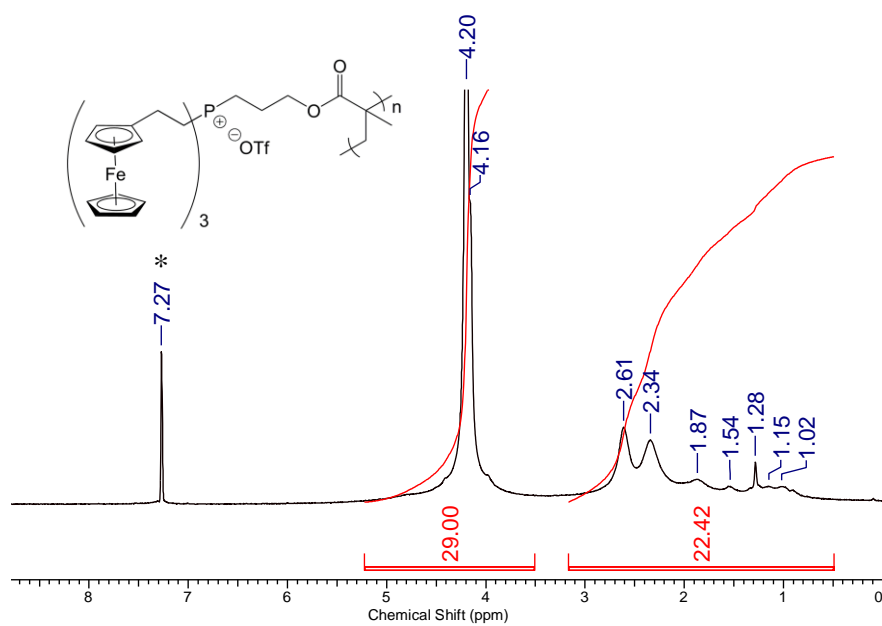


Figure A4.16. ^1H NMR spectrum of polyelectrolyte **4.10c** in CDCl_3 . The asterisk denotes residual CHCl_3 signal.

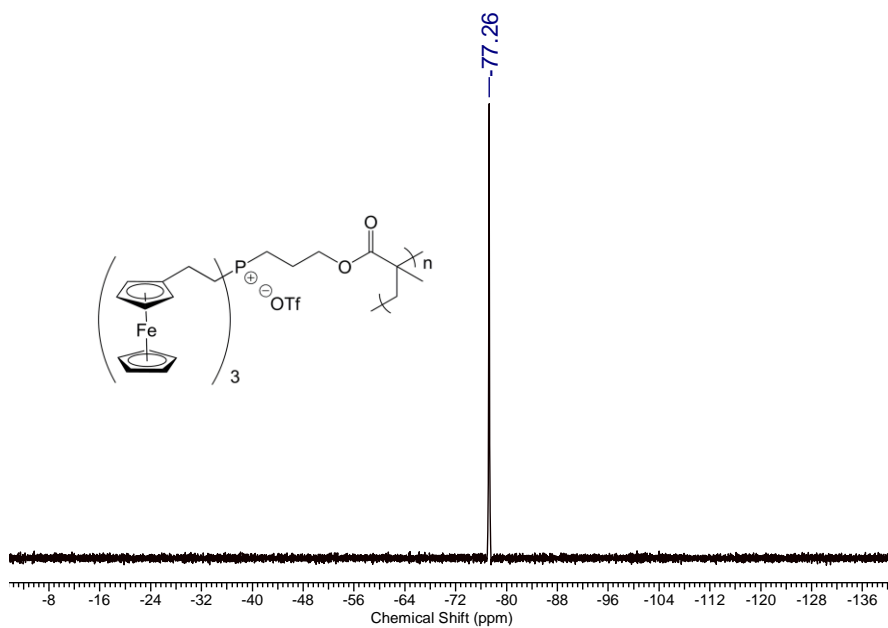


Figure A4.17. ^{19}F NMR spectrum of polyelectrolyte **4.10c** in CDCl_3 .

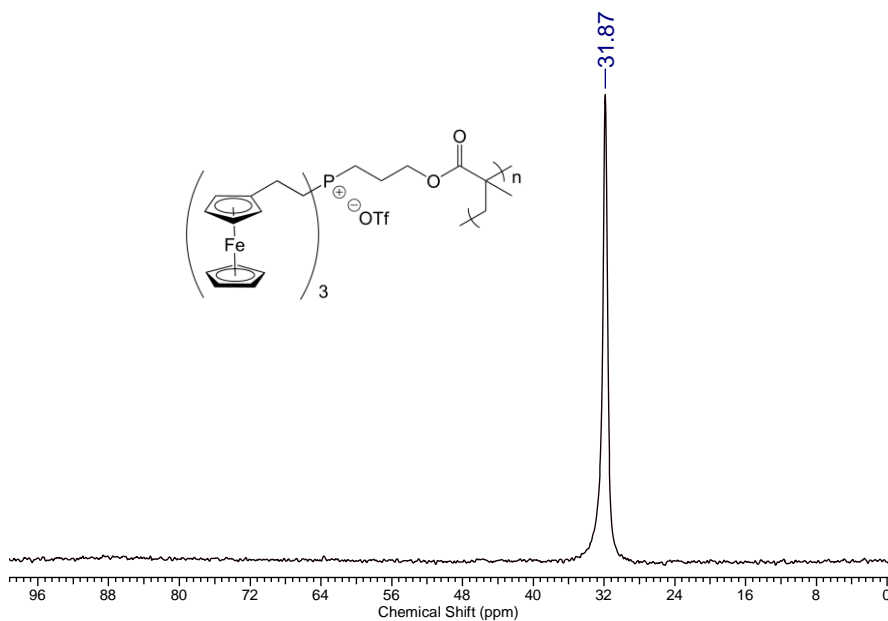


Figure A4.18. $^{31}\text{P}\{^1\text{H}\}$ NMR spectrum of polyelectrolyte **4.10c** in CDCl_3 .

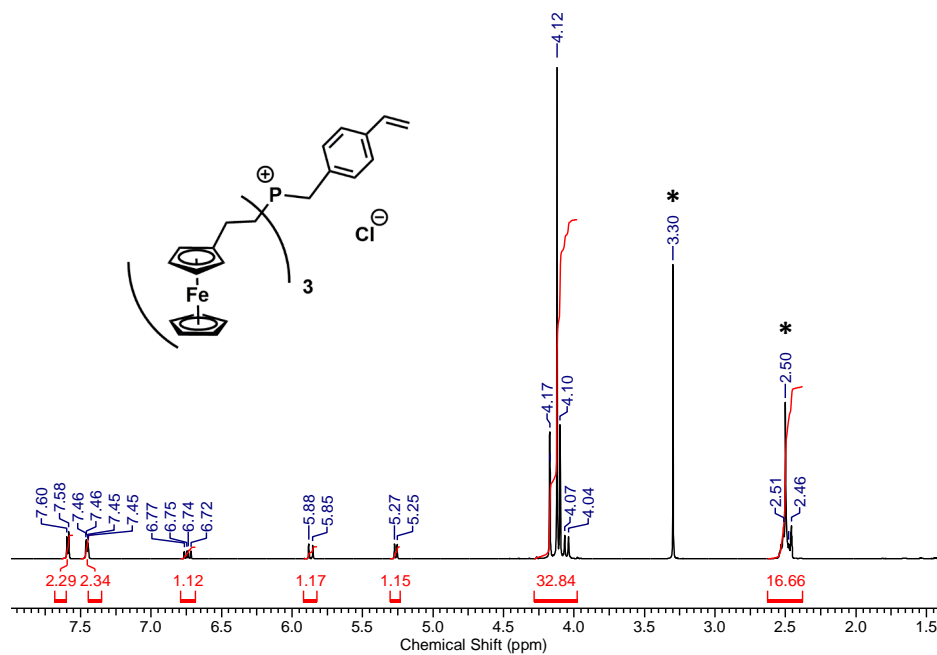


Figure A4.19. ^1H NMR spectrum of **4.12a** in $\text{DMSO-}d_6$. The asterisks denote residual $(\text{CD}_3)(\text{CD}_2\text{H})\text{SO}$ and H_2O signals.

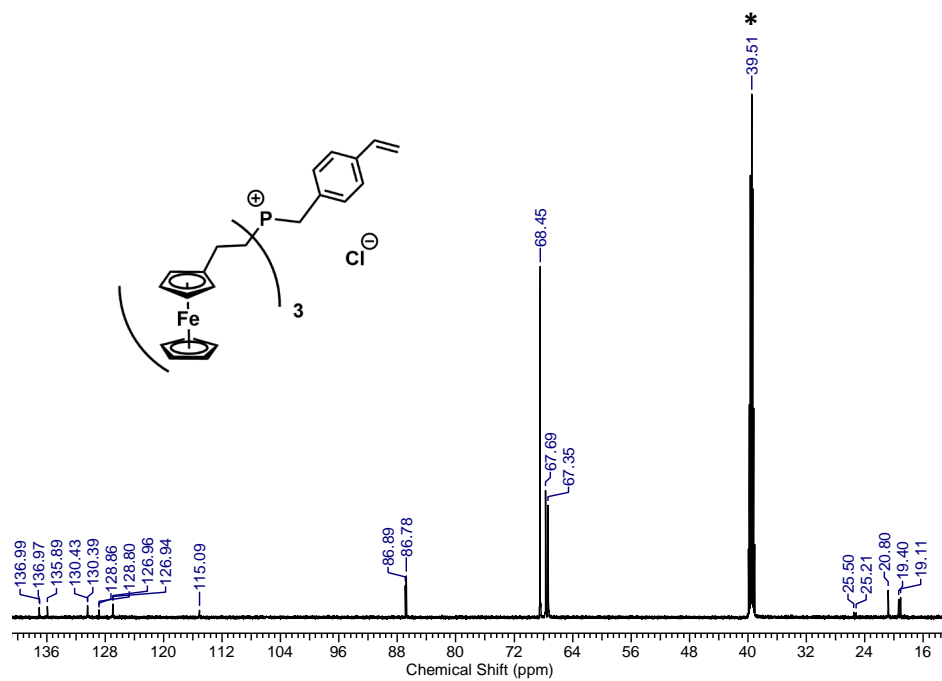


Figure A4.20. $^{13}\text{C}\{^1\text{H}\}$ NMR spectrum of **4.12a** in $\text{DMSO-}d_6$. The asterisk denotes the solvent signal.

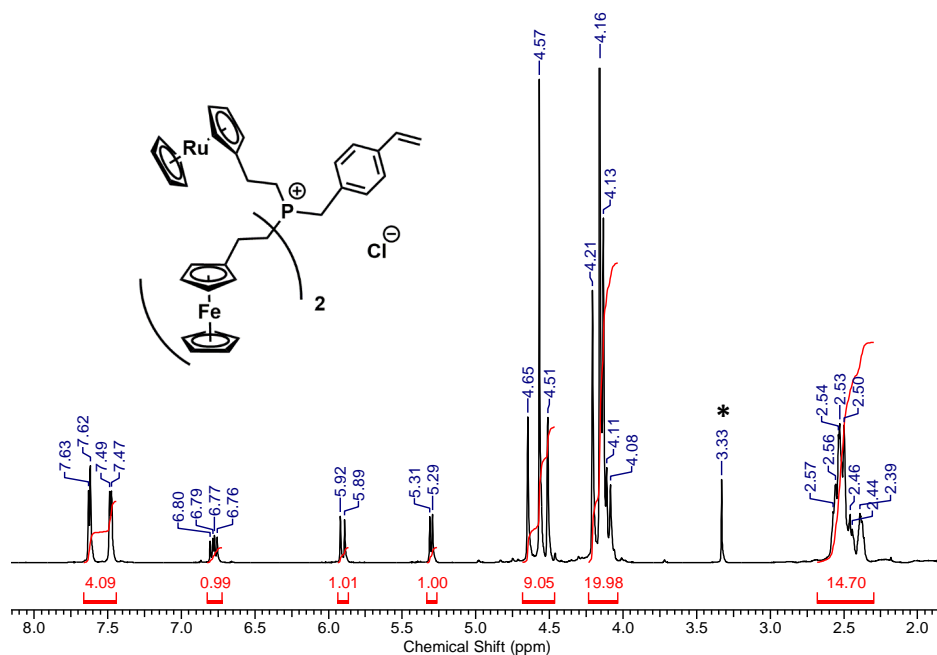


Figure A4.21. ^1H NMR spectrum of **4.12b** in DMSO- d_6 . The asterisk denotes residual $(\text{CD}_3)(\text{CD}_2\text{H})\text{O}$ signal.

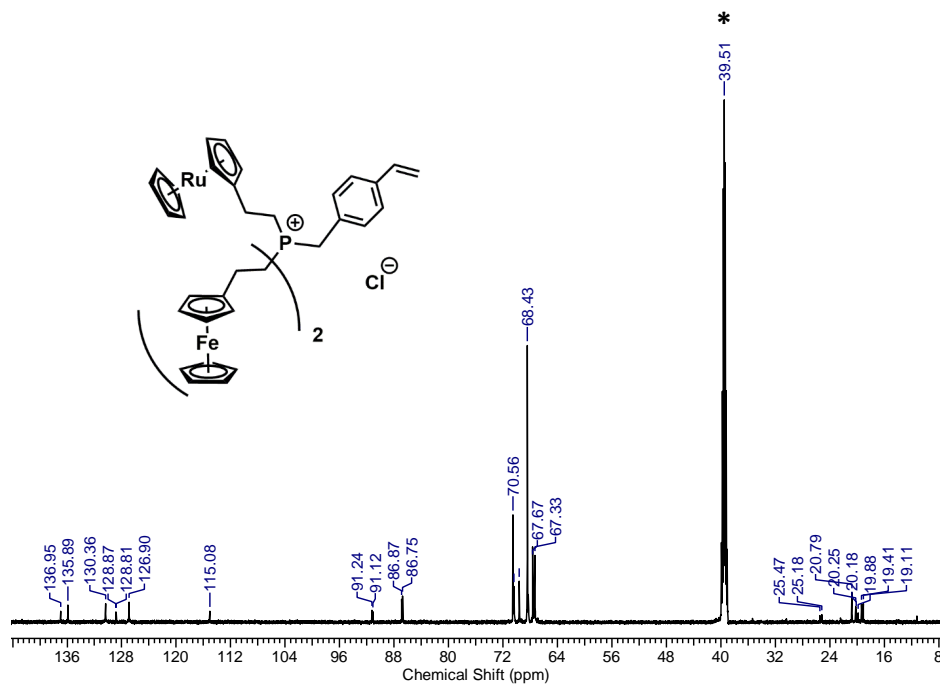


Figure A4.22. $^{13}\text{C}\{^1\text{H}\}$ NMR spectrum of **4.12b** in DMSO- d_6 . The asterisk denotes the solvent signal.

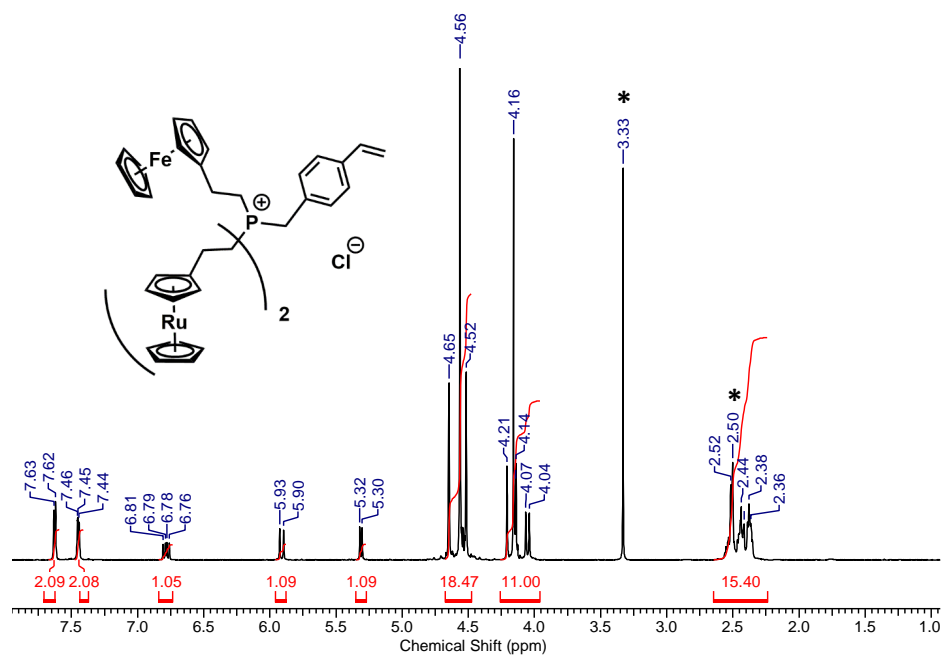


Figure A4.23. ^1H NMR spectrum of **4.12c** in $\text{DMSO-}d_6$. The asterisks denote residual $(\text{CD}_3)(\text{CD}_2\text{H})\text{SO}$ and H_2O signals.

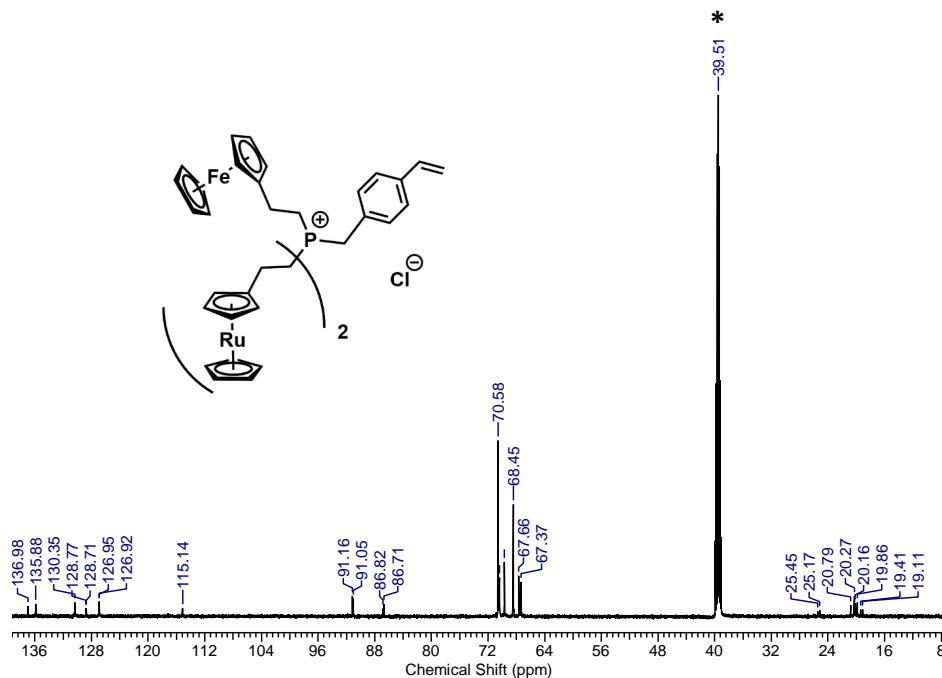


Figure A4.24. $^{13}\text{C}\{^1\text{H}\}$ NMR spectrum of **4.12c** in $\text{DMSO-}d_6$. The asterisk denotes the solvent signal.

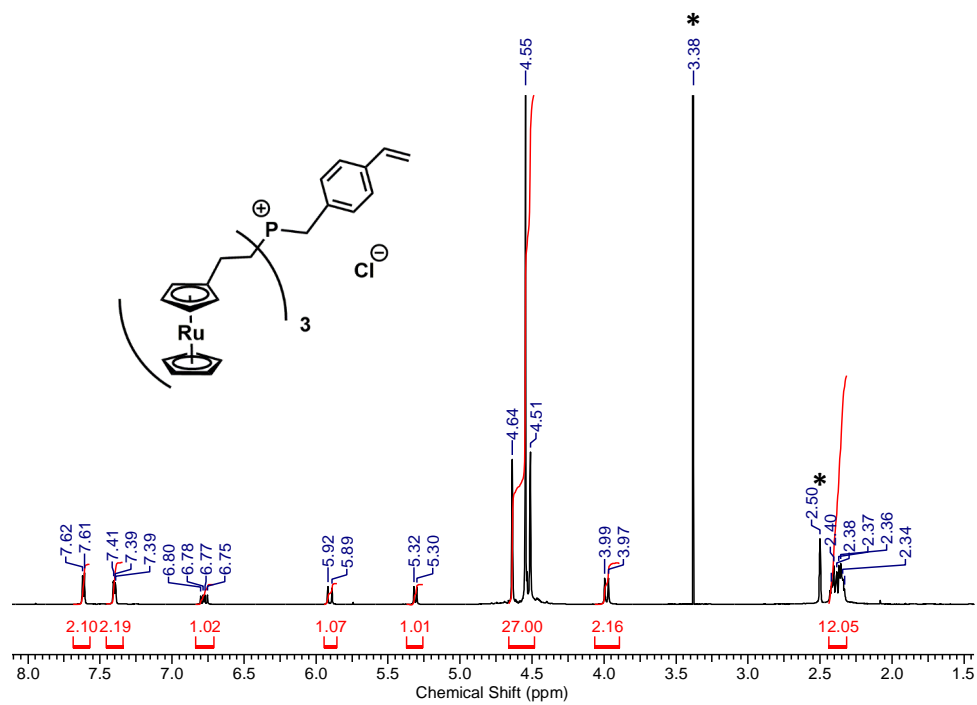


Figure A4.25. ^1H NMR spectra of **4.12d** in $\text{DMSO-}d_6$. The asterisks denote residual $(\text{CD}_3)(\text{CD}_2\text{H})\text{SO}$ and H_2O signals.

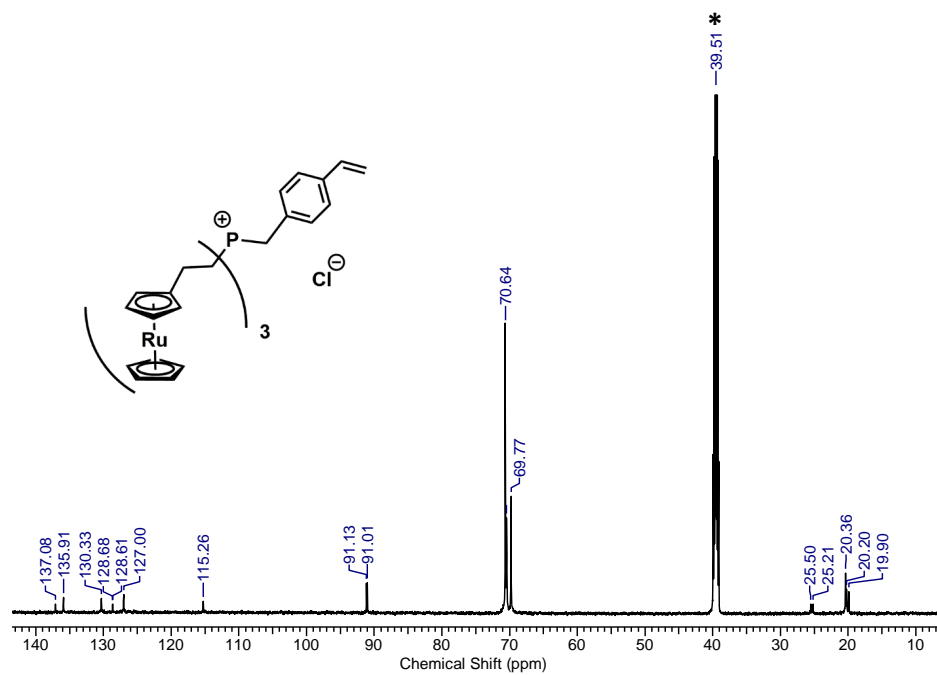


Figure A4.26. $^{13}\text{C}\{^1\text{H}\}$ NMR spectrum of **4.12d** in $\text{DMSO-}d_6$. The asterisk denotes the solvent signal.

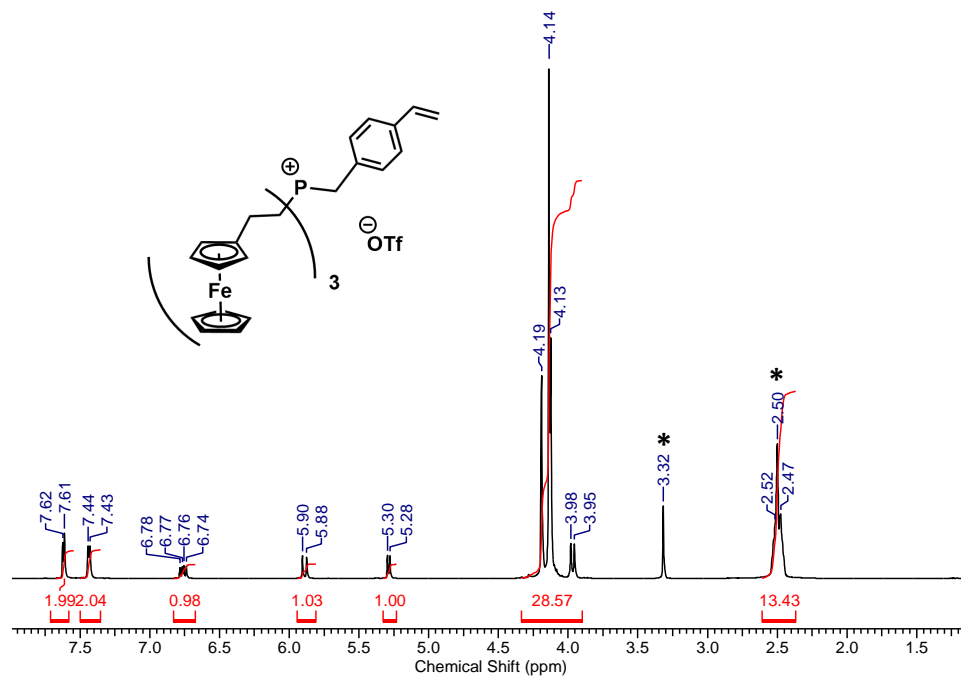


Figure A4.27. ^1H NMR spectrum of **4.13a** in $\text{DMSO-}d_6$. The asterisks denote the $(\text{CD}_3)(\text{CD}_2\text{H})\text{SO}$ and H_2O signals.

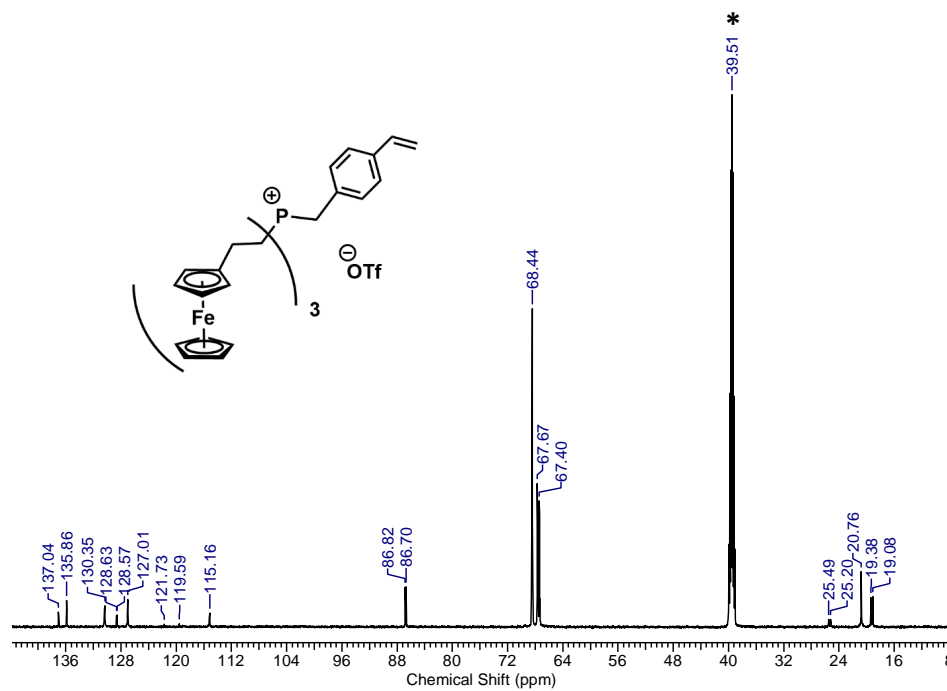


Figure A4.28. $^{13}\text{C}\{^1\text{H}\}$ NMR spectrum of **4.13a** in $\text{DMSO-}d_6$. The asterisk denotes the solvent signal.

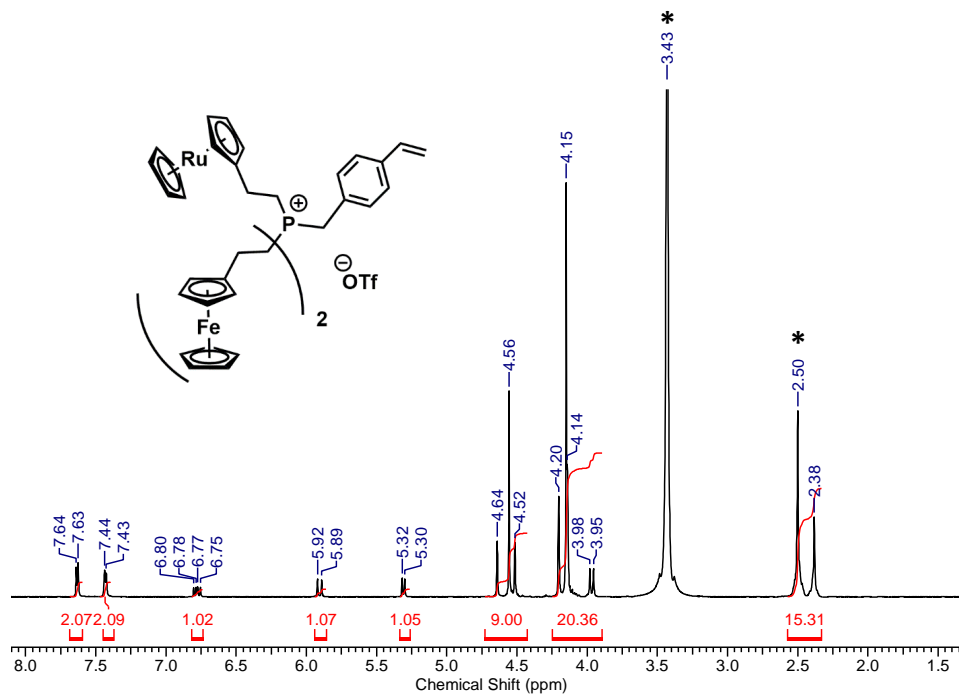


Figure A4.29. ^1H NMR spectrum of **4.13b** in $\text{DMSO-}d_6$. The asterisks denote the $(\text{CD}_3)(\text{CD}_2\text{H})\text{SO}$ and H_2O signals.

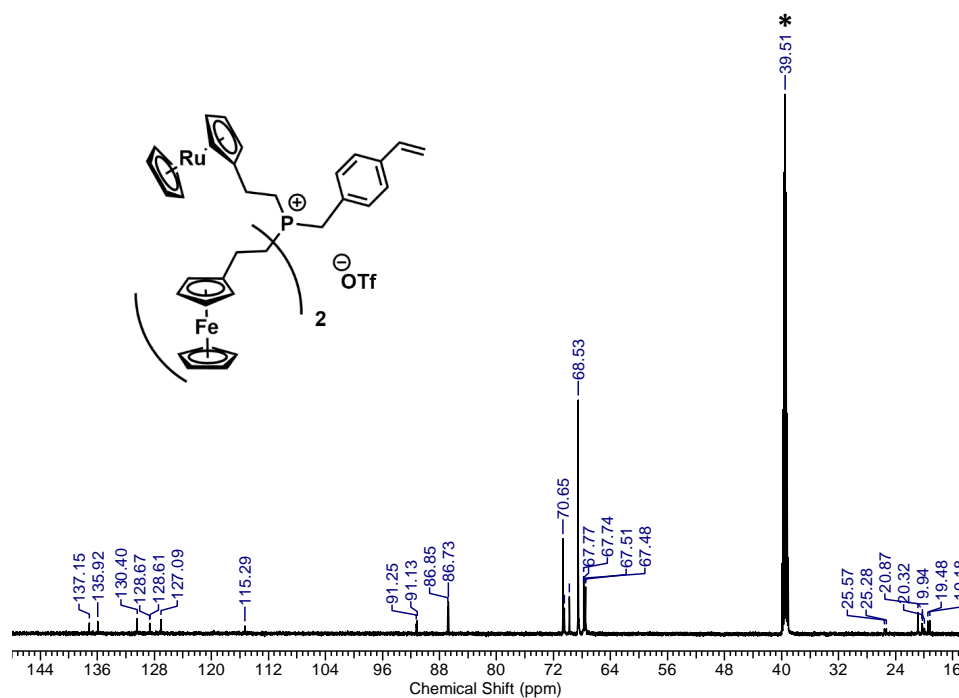


Figure A4.30. $^{13}\text{C}\{^1\text{H}\}$ NMR spectrum of **4.13b** in $\text{DMSO-}d_6$. The asterisk denotes the solvent signal.

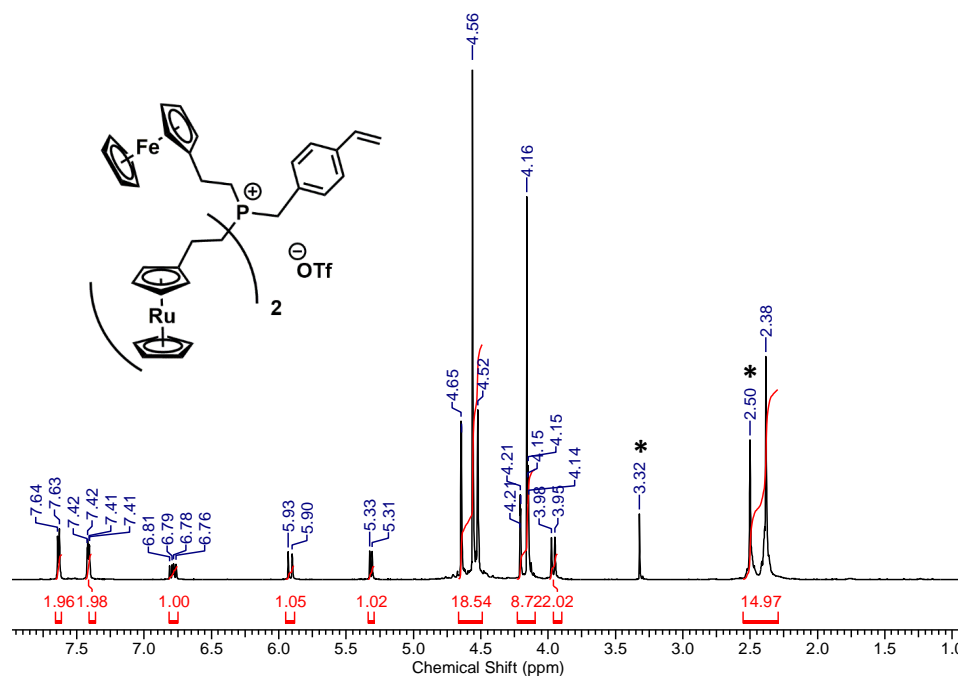


Figure A4.31. ¹H NMR spectrum of **4.13c** in DMSO-*d*₆. The asterisks denote the (CD₃)(CD₂H)SO and H₂O signals.

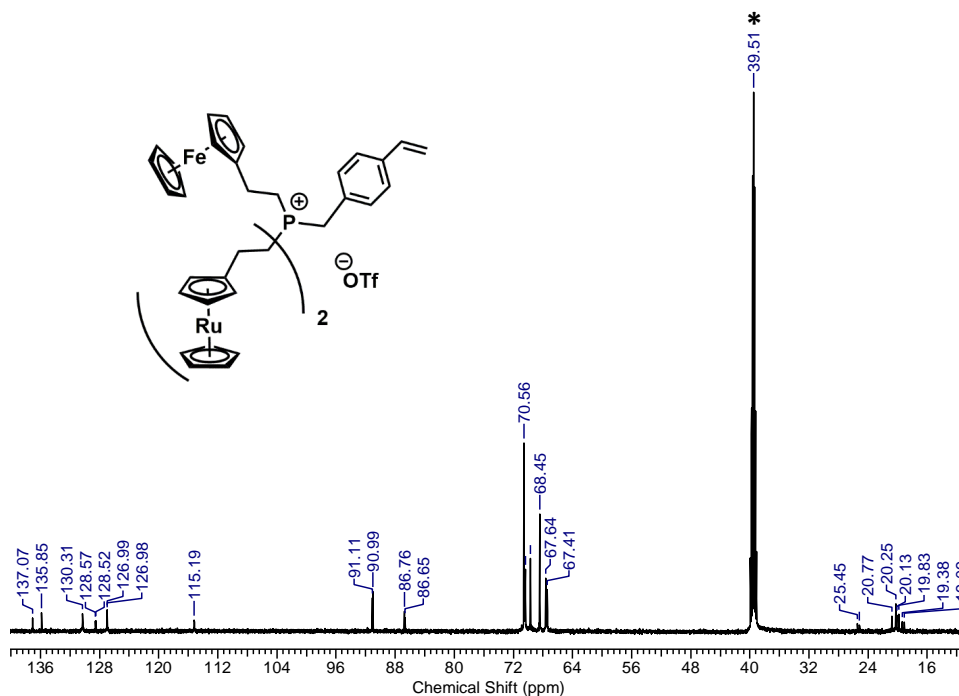


Figure A4.32. ¹³C{¹H} NMR spectrum of **4.13c** in DMSO-*d*₆. The quaternary carbon of the triflate anion was not detected. However, the purity of **4.13c** was confirmed by other methods such as ¹⁹F NMR spectroscopy and elemental analysis. The asterisk denotes the solvent signal.

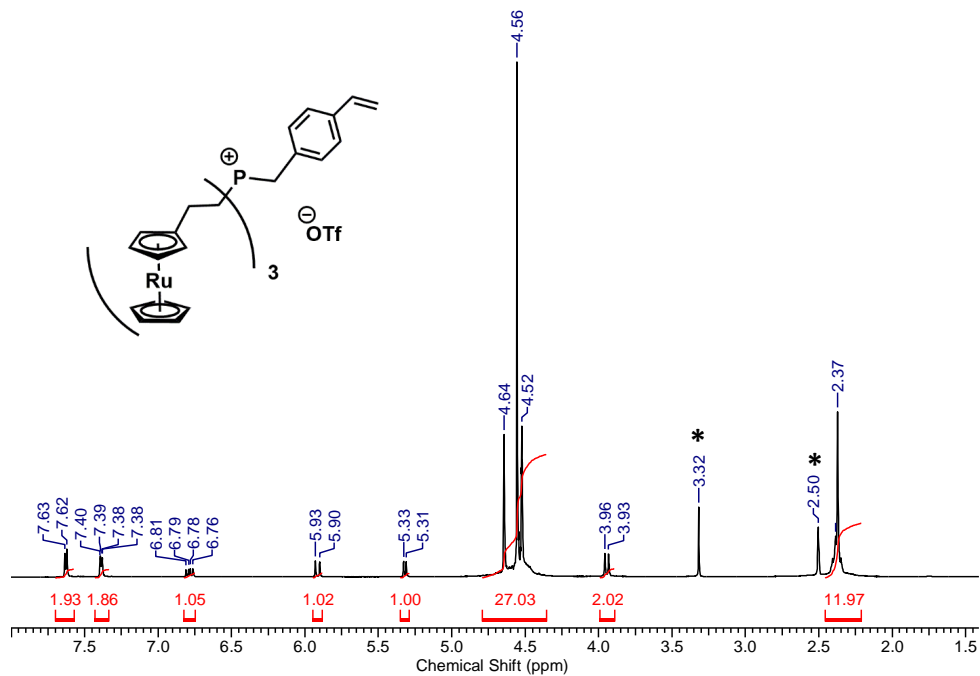


Figure A4.33. ^1H NMR spectrum of **4.13d** in $\text{DMSO-}d_6$. The asterisks denote residual $(\text{CD}_3)(\text{CD}_2\text{H})\text{SO}$ and H_2O signals.

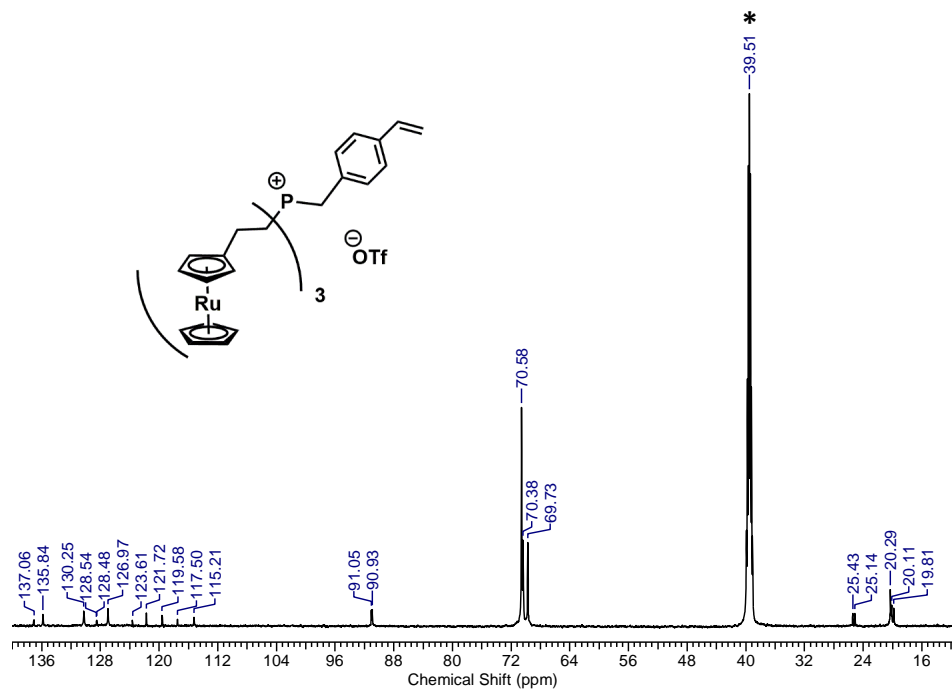


Figure A4.34. $^{13}\text{C}\{^1\text{H}\}$ NMR spectrum of **4.13d** in $\text{DMSO-}d_6$. The asterisk denotes the solvent signal.

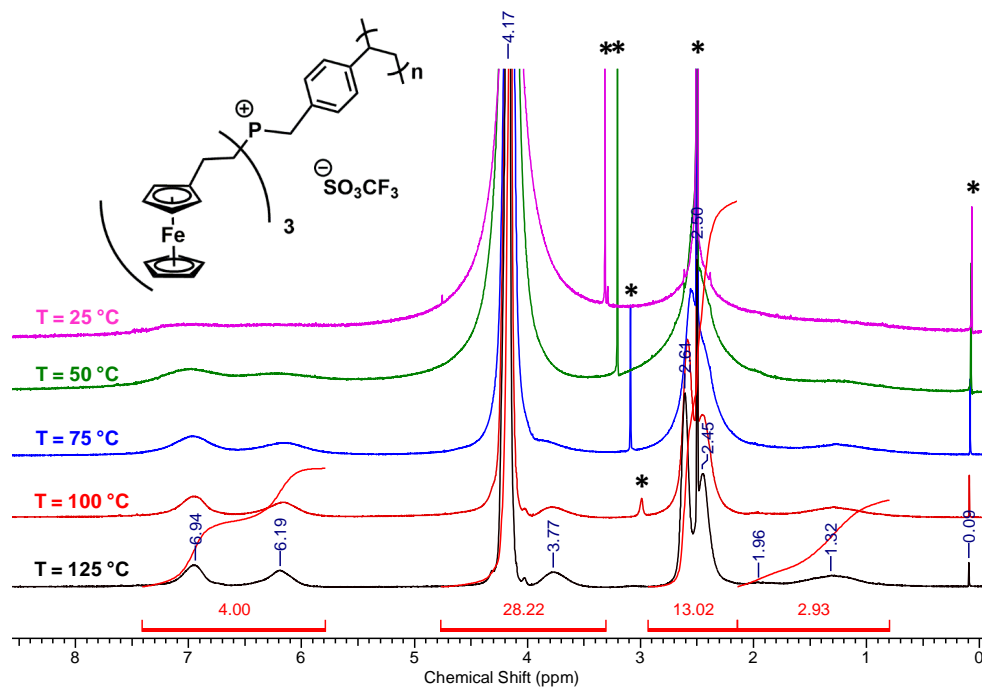


Figure A4.35. ^1H NMR spectra of **4.14a** recorded at different temperatures in $\text{DMSO-}d_6$. The asterisks denote residual $(\text{CD}_3)(\text{CD}_2\text{H})\text{SO}$ and H_2O signals and grease. Note – the residual H_2O signal shifts upfield as temperature increases.

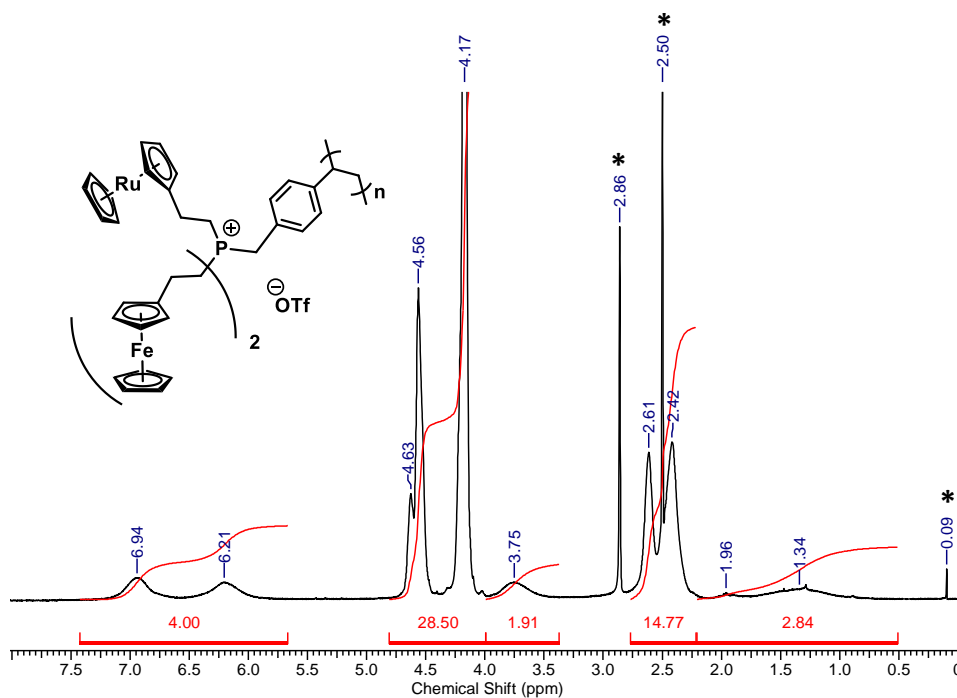


Figure A4.36. ^1H NMR spectrum of **4.14b** recorded in $\text{DMSO-}d_6$ at 125 °C. The asterisks denote residual $(\text{CD}_3)(\text{CD}_2\text{H})\text{SO}$ and H_2O signals and grease.

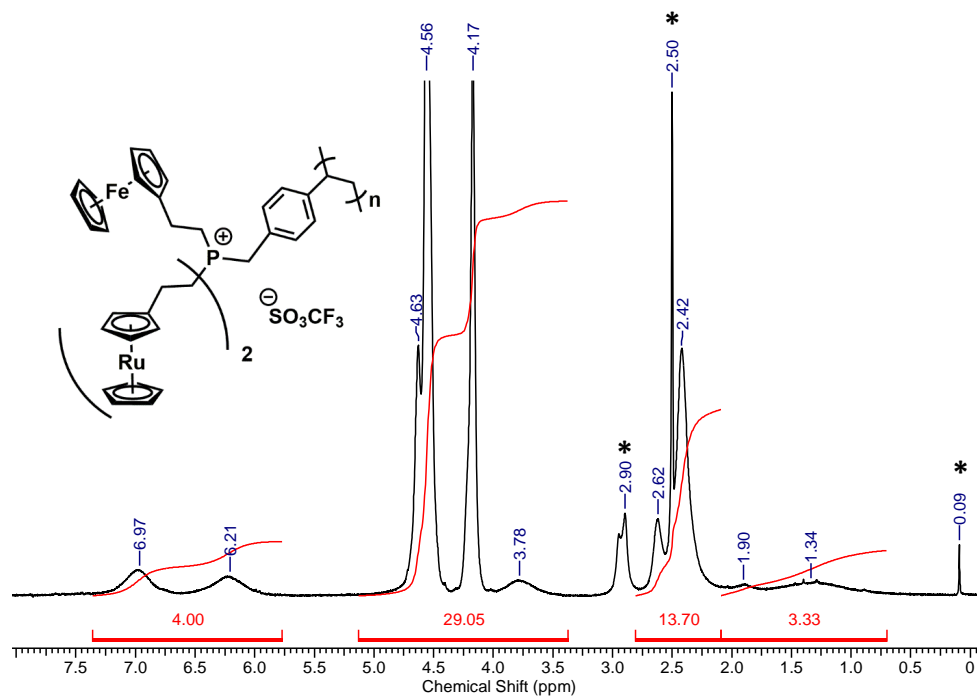


Figure A4.37. ¹H NMR spectrum of **4.14c** recorded in DMSO-*d*₆ at 125 °C. The asterisks denote residual (CD₃)(CD₂H)SO and H₂O signals and grease.

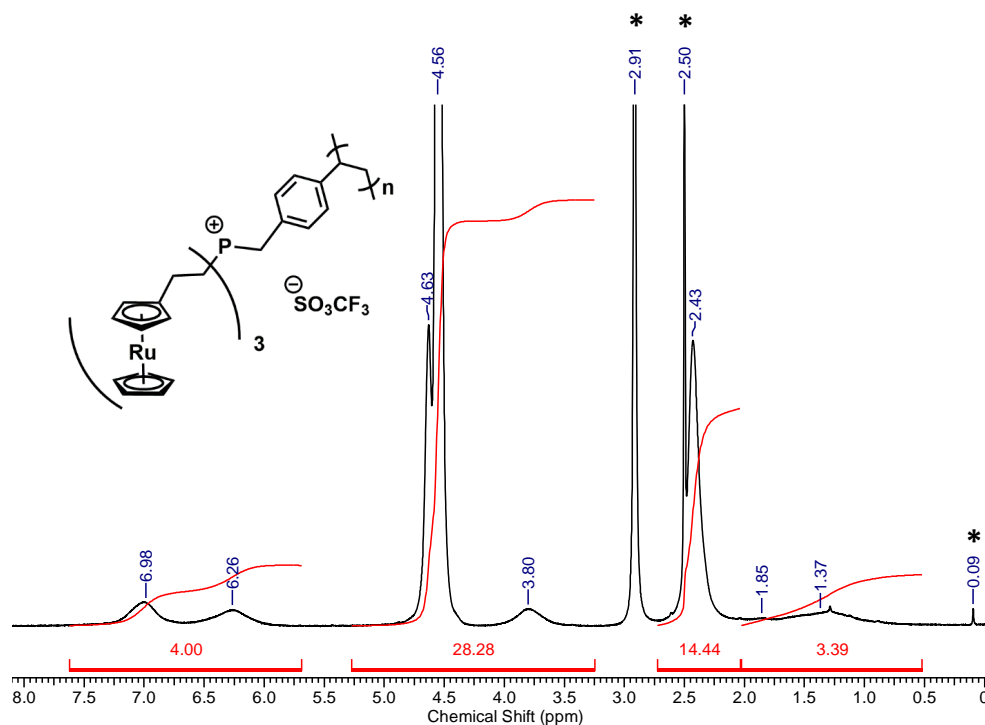


Figure A4.38. ¹H NMR spectrum of **4.14d** recorded in DMSO-*d*₆ at 125 °C. The asterisks denote residual (CD₃)(CD₂H)SO and H₂O signals and grease.

UV-Vis Absorption Spectra

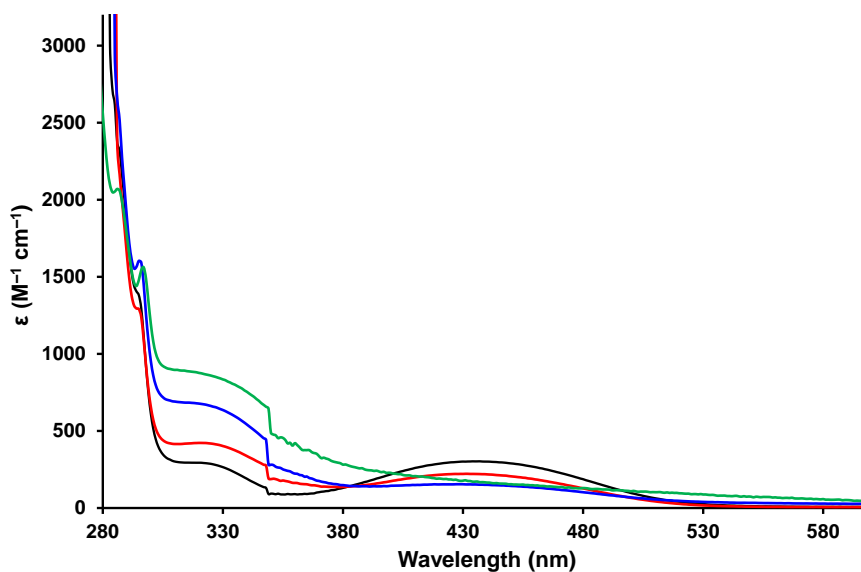


Figure A4.39. UV-vis absorption spectra recorded for **4.12a** ($3 \times Fc$; black), **4.12b** ($2 \times Fc$, $1 \times Rc$; red), **4.12c** ($1 \times Fc$, $2 \times Rc$; blue) and **4.12d** ($3 \times Rc$; green) in THF.

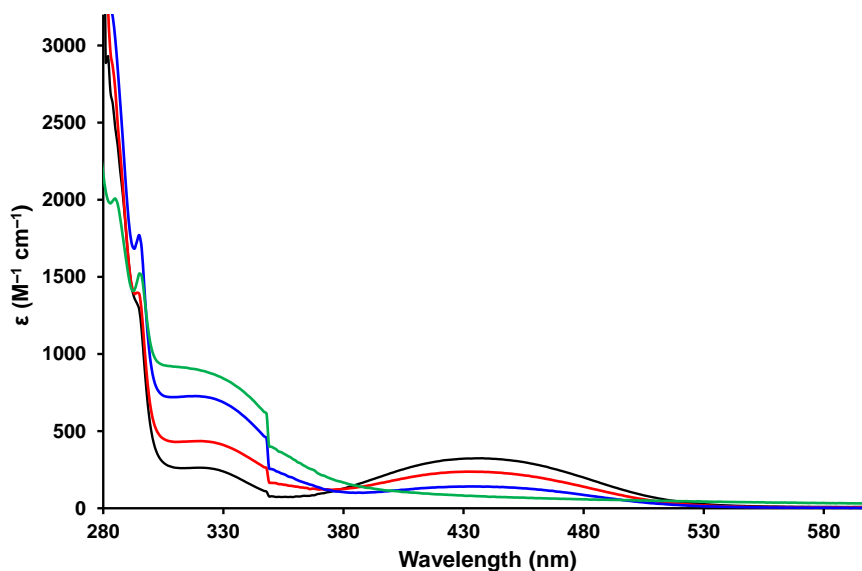


Figure A4.40. UV-vis absorption spectra recorded for **4.13a** ($3 \times Fc$; black), **4.13b** ($2 \times Fc$, $1 \times Rc$; red), **4.13c** ($1 \times Fc$, $2 \times Rc$; blue) and **4.13d** ($3 \times Rc$; green) in THF.

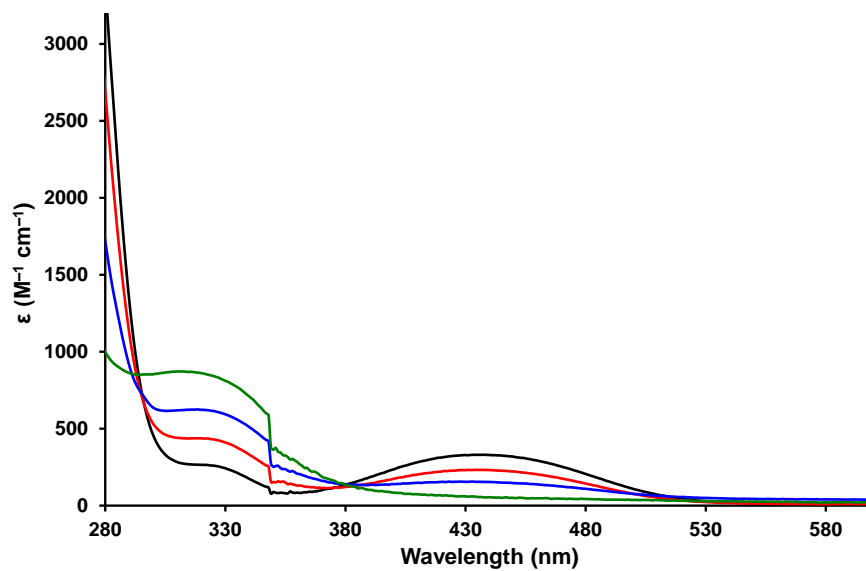


Figure A4.41. UV-vis absorption spectra recorded for **4.14a** ($3 \times \text{Fc}$; black), **4.14b** ($2 \times \text{Fc}$, $1 \times \text{Rc}$; red), **4.14c** ($1 \times \text{Fc}$, $2 \times \text{Rc}$; blue) and **4.14d** ($3 \times \text{Rc}$; green) in THF.

GPC Data

Table A4.1. Processed conventional calibration GPC data for phosphonium polyelectrolytes **4.10a–c**.

Sample	Injection	Max RI Response (mL)	M_n (g mol ⁻¹)	M_w (g mol ⁻¹)	\bar{D}
4.10a	1	19.45	43,050	117,400	2.73
	2	19.45	44,350	118,600	2.68
	3	19.44	42,000	118,650	2.83
	Average	19.45	43,100	118,200	2.74
	Std. Dev.	0.004	967	569	0.063
	%RSD	0.02%	2.24%	0.48%	2.28%
4.10b	1	19.79	31,200	76,750	2.46
	2	19.80	32,600	77,050	2.366
	3	19.74	33,300	83,150	2.50
	Average	19.78	32,050	79,000	2.44
	Std. Dev.	0.028	860	2,939	0.057
	%RSD	0.14%	2.66%	3.72%	2.32%
4.10c	1	19.51	45,000	104,750	2.33
	2	19.51	44,600	105,500	2.36
	3	19.50	45,750	106,800	2.33
	Average	19.51	45,150	105,700	2.34
	Std. Dev.	0.005	473	846	0.016
	%RSD	0.03%	1.05%	0.80%	0.69%

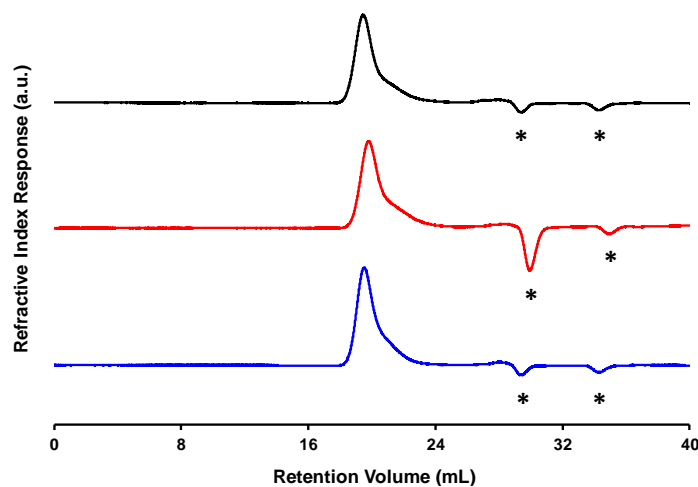
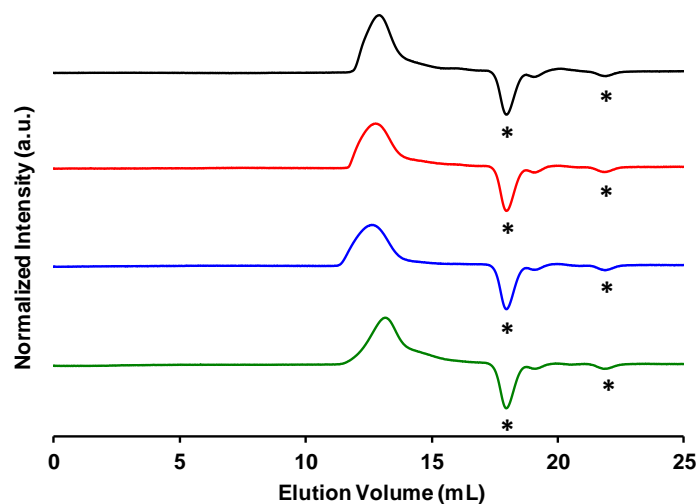
**Figure A4.42.** GPC traces of polyelectrolytes **4.10a** ($3 \times \text{Fc}$, black), **4.10b** ($3 \times \text{Fc}$, red), and **4.10c** ($3 \times \text{Fc}$, blue) recorded using a 60 °C DMF solution containing 0.02 M [*n*-Bu₄N][OTf]. The fluctuations from 27–37 mL arise due to changes in RI associated with sample injections. The asterisks denote system peaks.

Table A4.2. Processed conventional calibration GPC data for polyelectrolytes **4.14a–d**.

Sample	Injection	Max RI Response (mL)	M_n (g mol ⁻¹)	M_w (g mol ⁻¹)	\bar{D}
4.14a	1	12.91	45,850	148,250	3.23
	2	12.91	46,300	147,100	3.18
	3	12.92	48,500	148,750	3.07
	Average	12.91	46,900	148,000	3.16
	Std. Dev.	0.00	1,162	699	0.069
	%RSD	0.04%	2.48%	0.47%	2.19%
4.14b	1	12.77	44,000	176,800	4.02
	2	12.77	46,150	183,550	3.98
	3	12.77	45,150	194,400	4.31
	Average	12.77	45,100	184,900	4.10
	Std. Dev.	0.00	887	7,262	0.147
	%RSD	0.02%	1.97%	3.93%	3.60%
4.14c	1	12.64	68,100	256,850	3.77
	2	12.61	69,350	284,700	4.10
	3	12.60	69,850	292,750	4.19
	Average	12.61	69,100	278,100	4.02
	Std. Dev.	0.02	751	15,389	0.18
	%RSD	0.12%	1.09%	5.53%	4.48%
4.14d	1	13.16	37,250	137,300	3.68
	2	13.15	40,100	146,000	3.64
	3	13.15	38,650	147,150	3.81
	Average	13.15	38,650	143,450	3.71
	Std. Dev.	0.00	1,150	4,398	0.07
	%RSD	0.04%	2.97%	3.07%	1.89%

**Figure A4.43.** GPC traces of polyelectrolytes **4.14a** (3 × Fc, black), **4.14b** (2 × Fc, 1 × Rc; red), **4.14c** (1 × Fc, 2 × Rc; blue), and **4.14d** (3 × Rc, green) recorded using a 60 °C DMF solution containing 0.02 M [*n*-Bu₄N][OTf]. The asterisks denote system peaks.

Cyclic Voltammograms

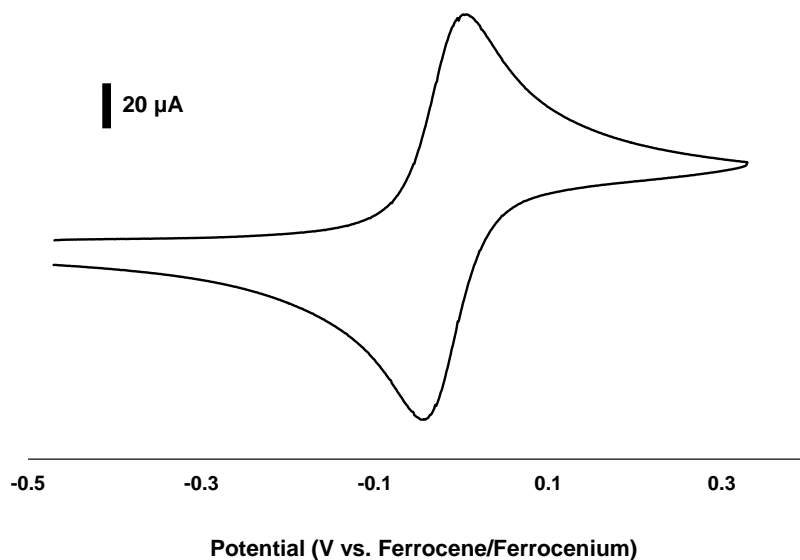


Figure A4.44. Cyclic voltammogram of monomers **4.8a** ($3 \times \text{Fc}$) recorded at 250 mV s^{-1} in solutions of 2/1 $\text{CH}_2\text{Cl}_2/\text{CH}_3\text{CN}$ containing 0.1 M $[\text{n-Bu}_4\text{N}][\text{OTf}]$ as supporting electrolyte.

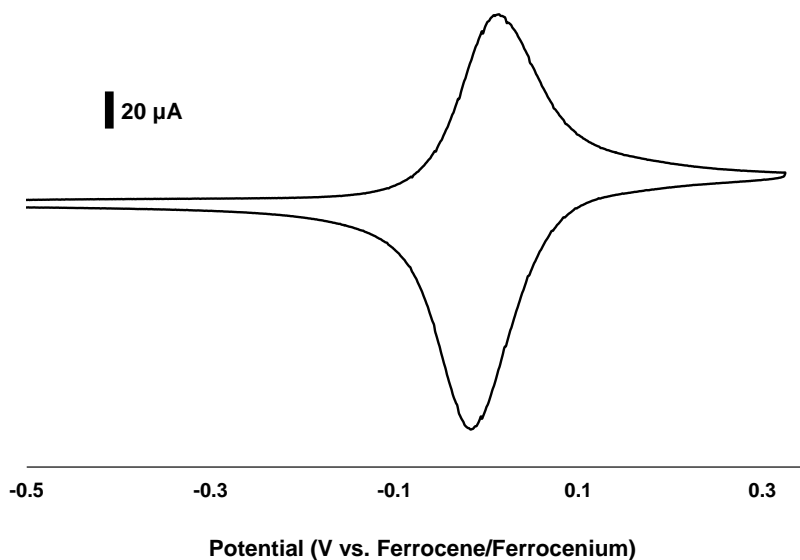


Figure A4.45. Cyclic Cyclic voltammogram of monomers **4.10a** ($3 \times \text{Fc}$) recorded at 250 mV s^{-1} in solutions of 2/1 $\text{CH}_2\text{Cl}_2/\text{CH}_3\text{CN}$ containing 0.1 M $[\text{n-Bu}_4\text{N}][\text{OTf}]$ as supporting electrolyte.

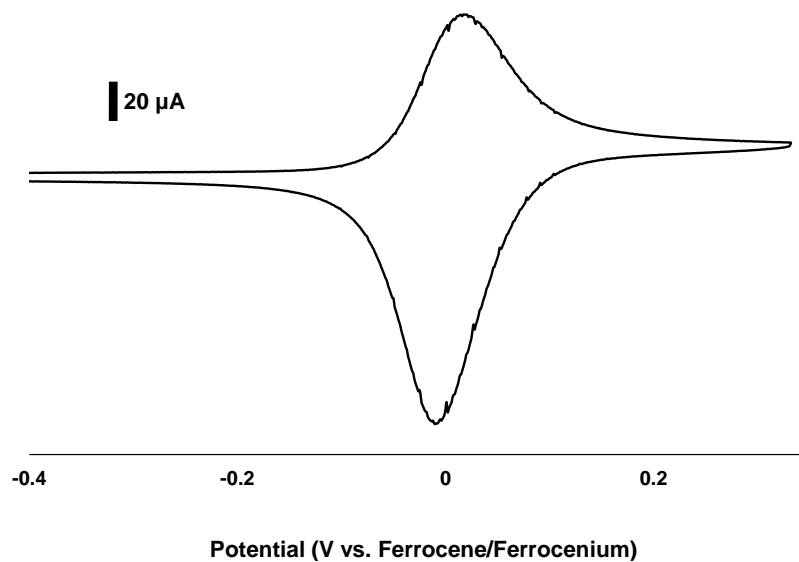


Figure A4.46. Cyclic voltammogram of monomers **4.10c** ($3 \times \text{Fc}$) recorded at 250 mV s^{-1} in solutions of 2/1 $\text{CH}_2\text{Cl}_2/\text{CH}_3\text{CN}$ containing 0.1 M $[\textit{n}\text{-Bu}_4\text{N}][\text{OTf}]$ as supporting electrolyte.

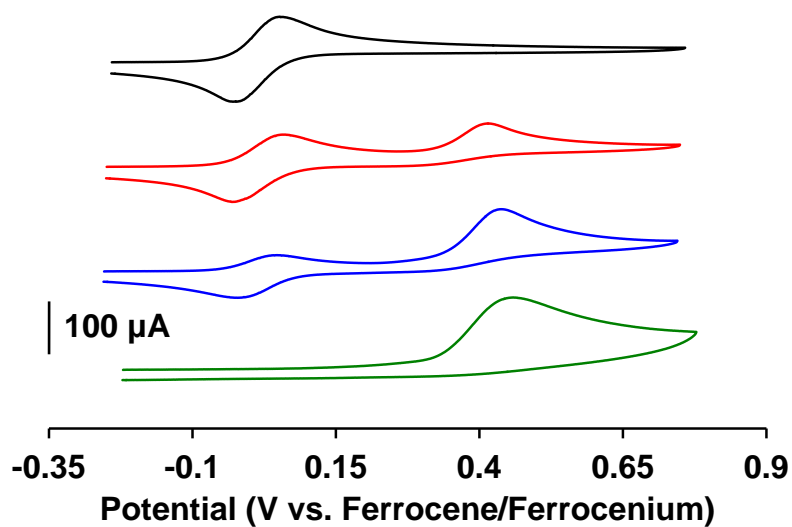


Figure A4.47. Cyclic voltammograms of monomers **4.13a** ($3 \times \text{Fc}$; black), **4.13b** ($2 \times \text{Fc}$, $1 \times \text{Rc}$; red), **4.13c** ($1 \times \text{Fc}$, $2 \times \text{Rc}$; blue), and **4.13d** ($3 \times \text{Rc}$; green) recorded at 250 mV s^{-1} in solutions of 2/1 $\text{CH}_2\text{Cl}_2/\text{CH}_3\text{CN}$ containing 0.1 M $[\textit{n}\text{-Bu}_4\text{N}][\text{OTf}]$ as supporting electrolyte.

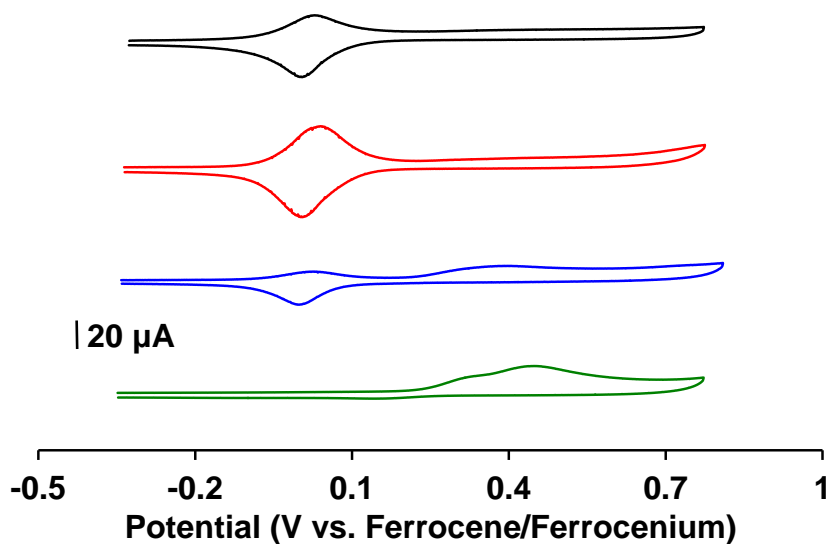
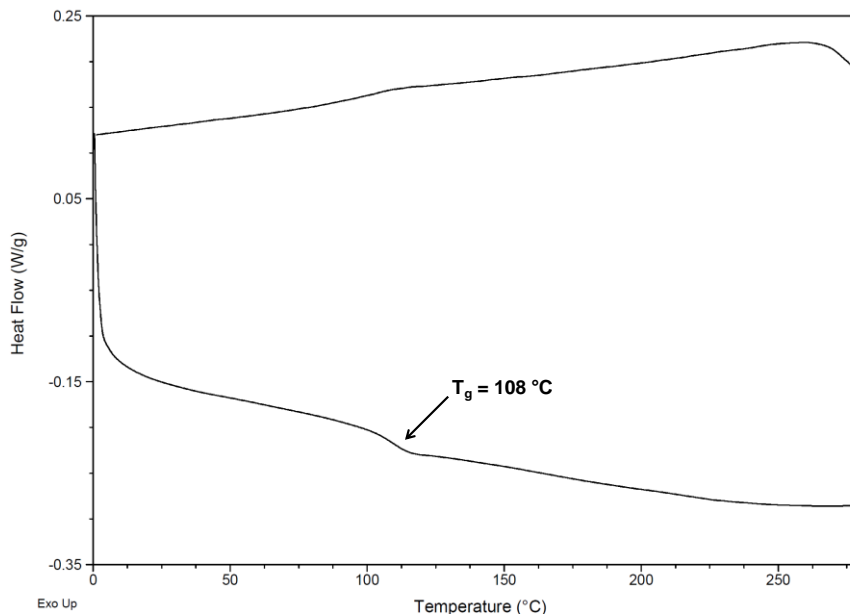
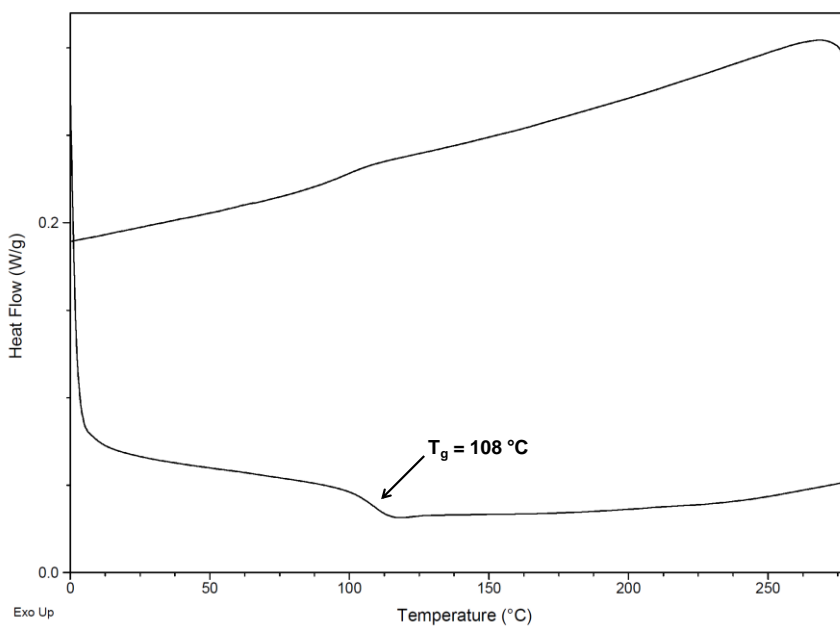


Figure A4.48. Cyclic voltammograms of polyelectrolytes: **4.14a** ($3 \times \text{Fc}$, black), **4.14b** ($2 \times \text{Fc}$, $1 \times \text{Rc}$; red), **4.14c** ($1 \times \text{Fc}$, $2 \times \text{Rc}$; blue), and **4.14d** ($3 \times \text{Rc}$, green) recorded at 250 mV s^{-1} in solutions of 2/1 $\text{CH}_2\text{Cl}_2/\text{CH}_3\text{CN}$ containing $0.1 \text{ M } [n\text{-Bu}_4\text{N}][\text{OTf}]$ as supporting electrolyte. Note – due to the limited and different solubilities of the polyelectrolytes in the solvent/electrolyte mixture, the intensities of the waves in the recorded cyclic voltammograms were lower compared to that of the corresponding monomers and also a clear trend was not observed when their cyclic voltammograms were compared. Furthermore, due to low concentration and extreme broadening, the irreversible oxidation wave of ruthenocene for **4.14b** was not observed.

Differential Scanning Calorimetry Thermograms

**Figure A4.49.** DSC thermogram of polyelectrolyte **4.10a**.**Figure A4.50.** DSC thermogram of polyelectrolyte **4.10b**.

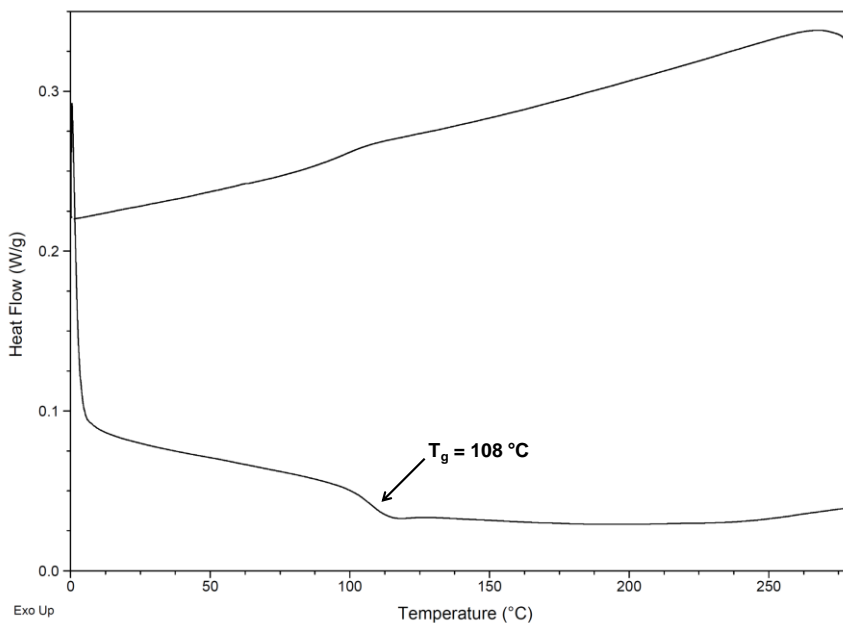


Figure A4.51. DSC thermogram of polyelectrolyte **4.10c**.

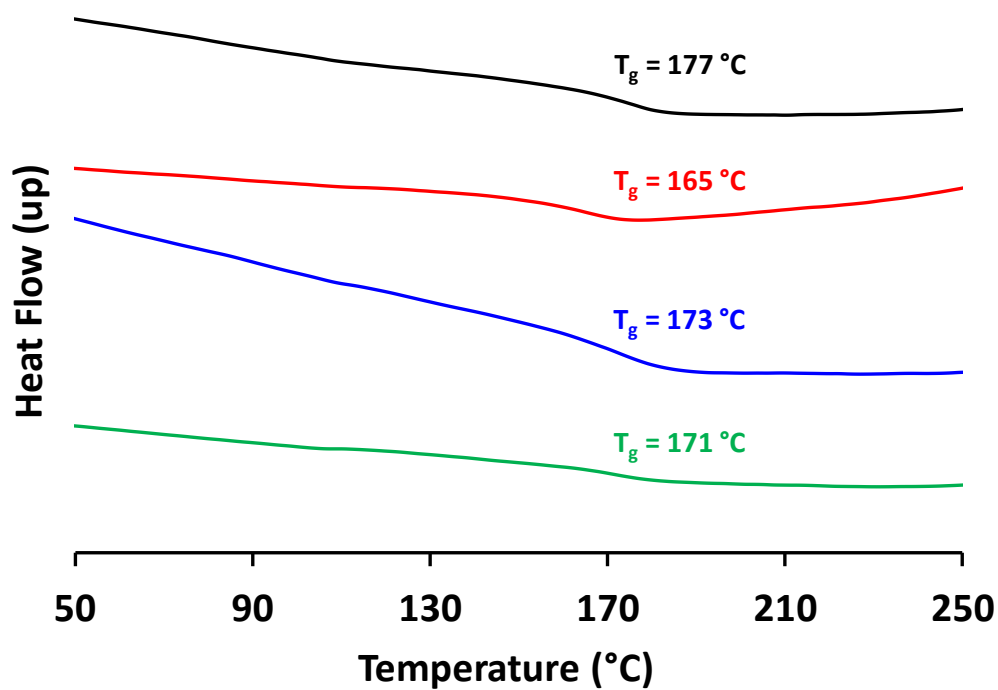


Figure A4.52. DSC thermograms of polyelectrolytes **4.14a** (3 × Fc, black), **4.14b** (2 × Fc, 1 × Rc; red), **4.14c** (1 × Fc, 2 × Rc; blue), and **4.14d** (3 × Rc, green) recorded at a scan rate of 10 °C min⁻¹.

Thermal Gravimetric Analysis

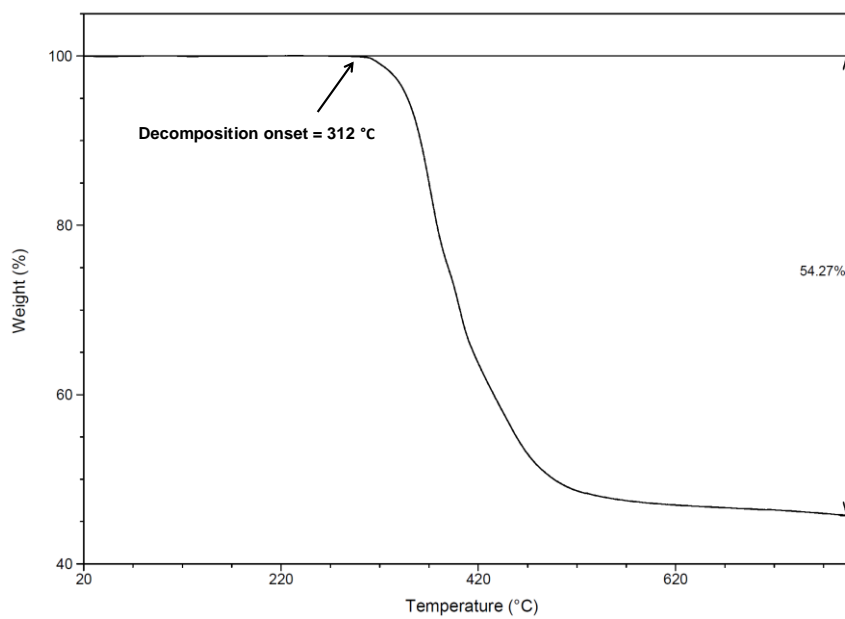


Figure A4.53. TGA trace for polyelectrolyte **4.10a**.

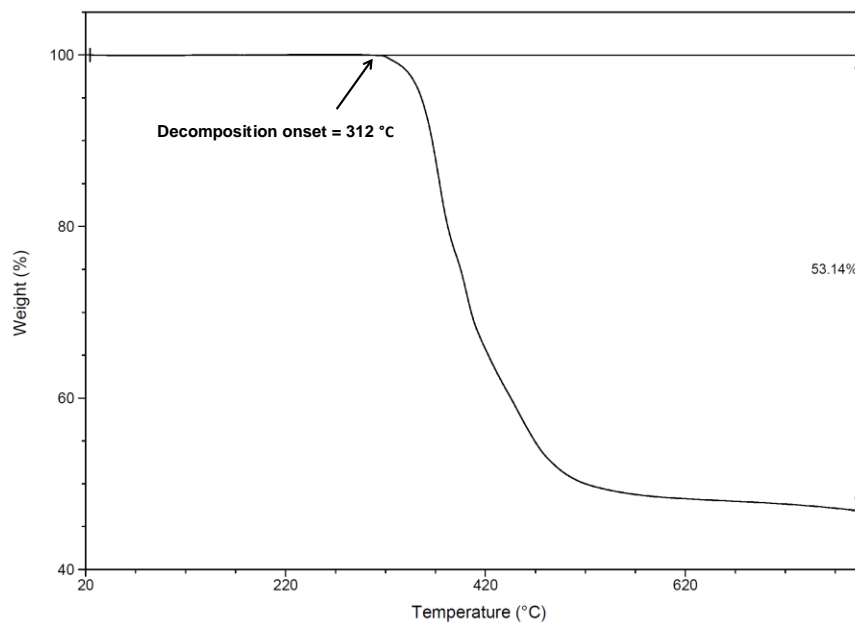


Figure A4.54. TGA trace for polyelectrolyte **4.10c**.

Scanning Electron Microscopy and Energy-Dispersive X-Ray Spectroscopy Results

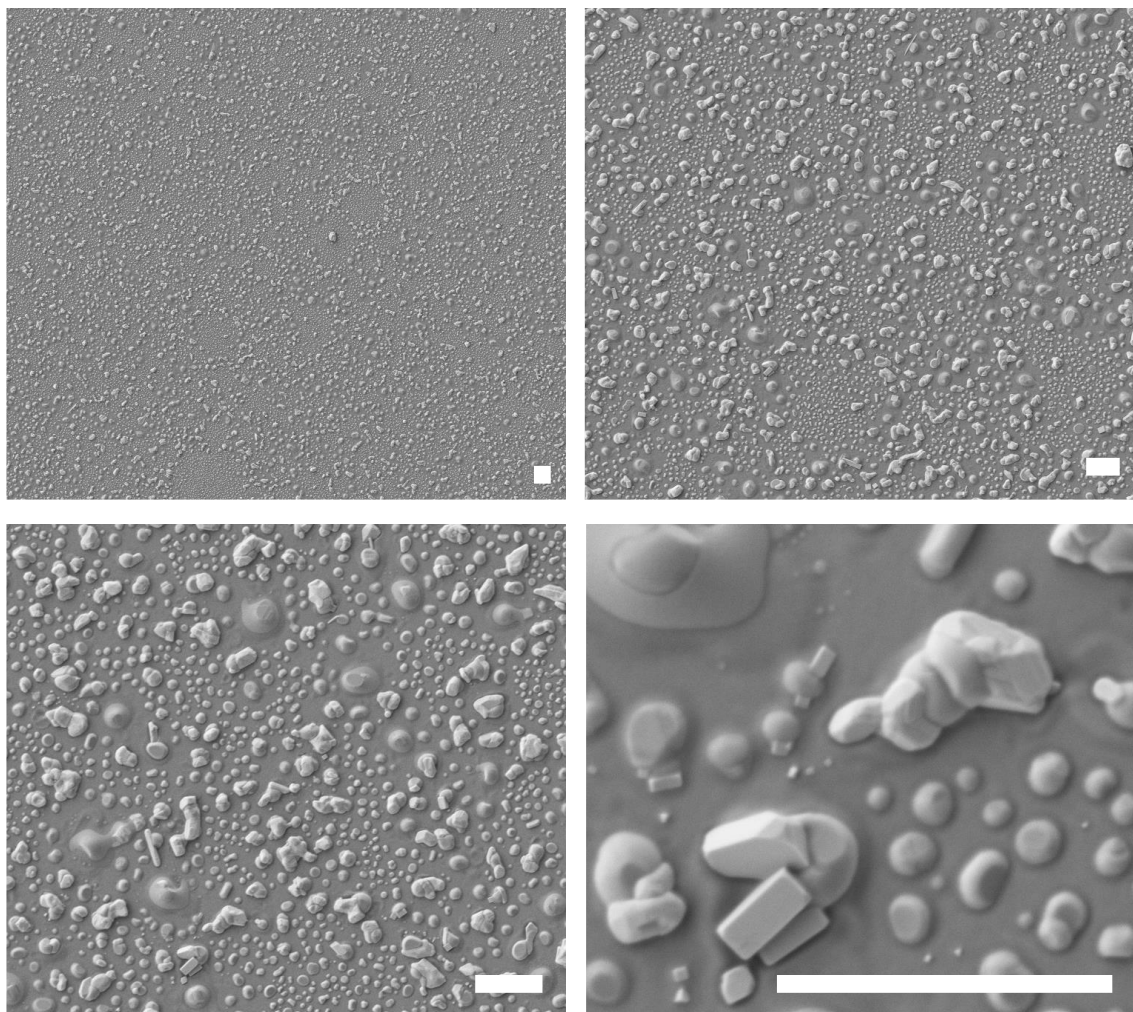


Figure A4.55. SEM images of the nanostructures produced by heating a thin film of polyelectrolyte **4.10b** at 800 °C for 2 h under a flow of N₂ gas. Scale bars = 1 μm.

Spectrum processing :

No peaks omitted

Processing option : All elements analyzed (Normalized)

Number of iterations = 4

Standard :

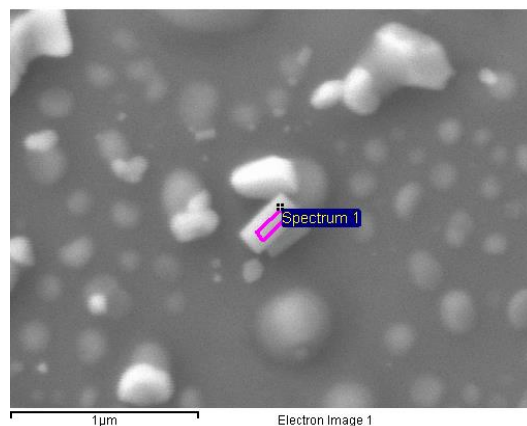
C CaCO₃ 1-Jun-1999 12:00 AM

O SiO₂ 1-Jun-1999 12:00 AM

Si SiO₂ 1-Jun-1999 12:00 AM

P GaP 1-Jun-1999 12:00 AM

Fe Fe 1-Jun-1999 12:00 AM



Element	Weight%	Atomic%
C K	1.74	4.53
O K	20.65	40.23
Si K	21.00	23.31
P K	0.75	0.75
Fe L	55.86	31.18
Totals	100.00	

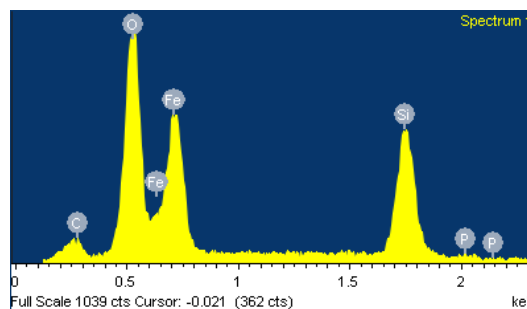


Figure A4.56. SEM image and elemental analysis for a crystallite produced by heating a thin film of polyelectrolyte **4.10b** at 800 °C for 2 h under a flow of N₂ gas. The analyzed area is indicated by the purple box and the ratio of Fe:O is consistent with formation of Fe₃O₄.

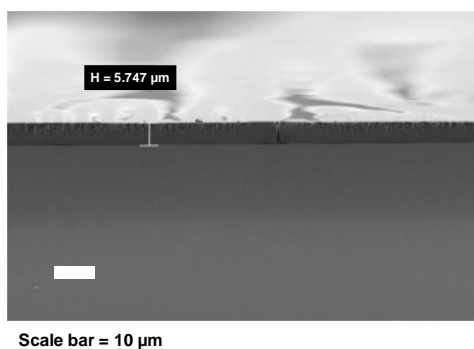


Figure A4.57. SEM of a cross section of a representative drop-cast film of polyelectrolyte **4.14a**.

Elemental Maps

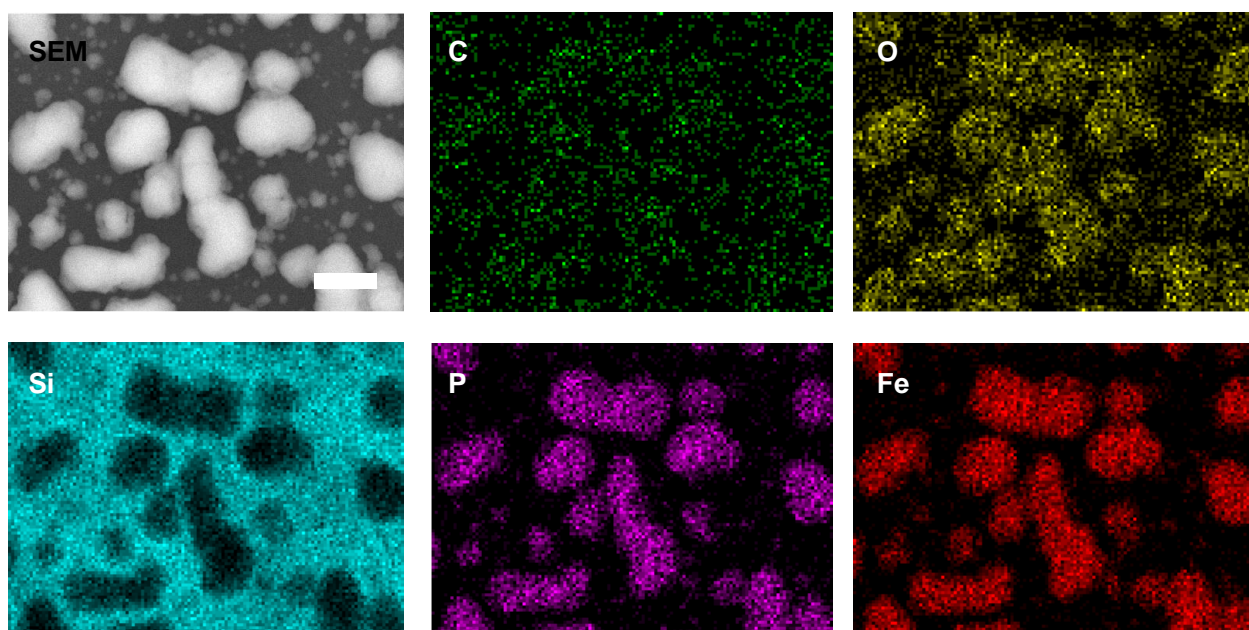


Figure A4.58. SEM image and elemental maps (C, O, Si, P, Fe) for the nanomaterials prepared via the pyrolysis of a film of polyelectrolyte **4.14a**. Scale bar = 1 μm .

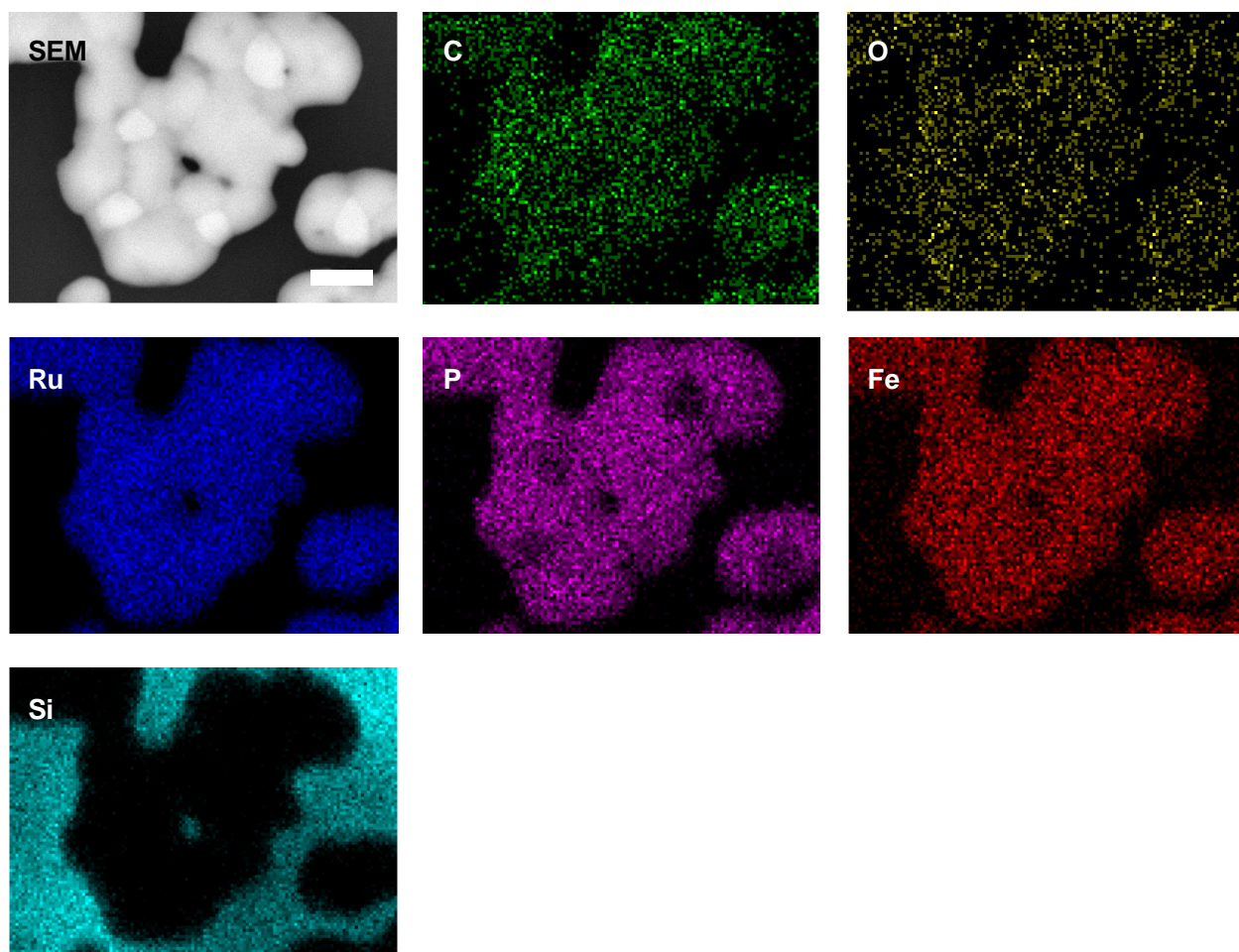


Figure A4.59. SEM image and elemental maps (C, O, Ru, P, Fe, Si) for the nanomaterials prepared via the pyrolysis of a film of polyelectrolyte **4.14c**. Scale bar = 1 μm .

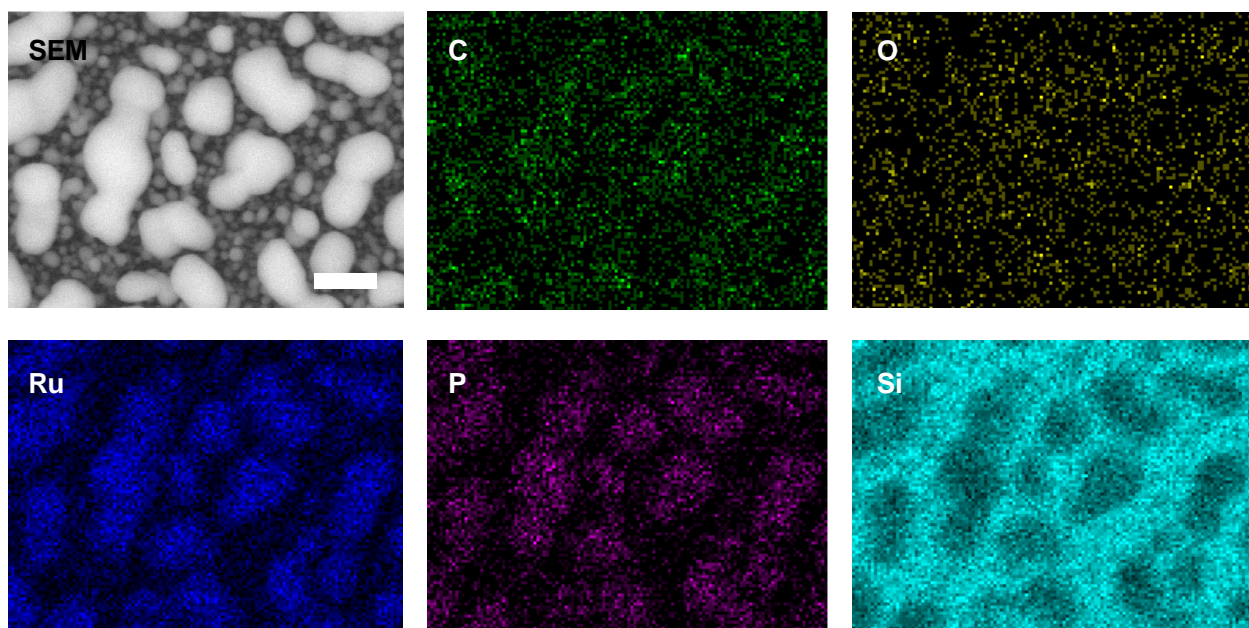
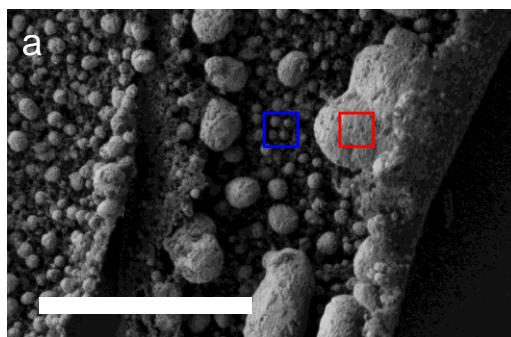


Figure A4.60. SEM image and elemental maps (C, O, Ru, P, Si) for the nanomaterials prepared via the pyrolysis of a film of polyelectrolyte **4.14d**. Scale bar = 350 nm.

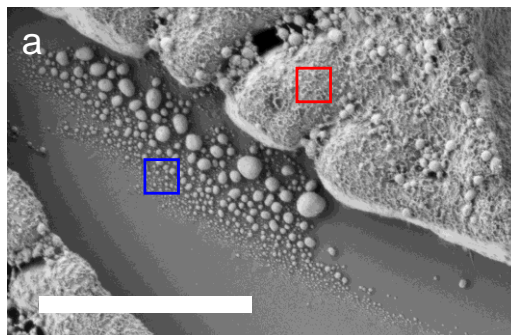
Scanning Electron Microscopy and Energy-Dispersive X-ray Spectroscopy Results



b	%^a	C	O	P	Fe
Bulk		20.6	18.6	21.3	39.4
		25.1	25.4	17.1	32.5
		25.3	28.8	16.3	29.5
		23.9	21.3	19.8	34.9
		20.2	29.2	14.3	36.4
	Average	23.0 ± 2.5	24.7 ± 4.6	17.7 ± 2.8	34.6 ± 3.8
Particles		36.9	27.1	11.1	24.9
		33.7	25.8	10.4	30.1
		46.3	26.9	8.2	18.6
		78.1	20.0	0.5	1.4
		79.5	18.6	0.7	1.3
		80.4	17.9	0.5	1.1
		48.6	33.0	7.5	10.9
		52.4	30.0	7.3	10.3
	Average	57.0 ± 19.5	24.9 ± 5.5	5.8 ± 4.5	12.3 ± 11.2

^aData normalized to exclude silicon detected from substrate.

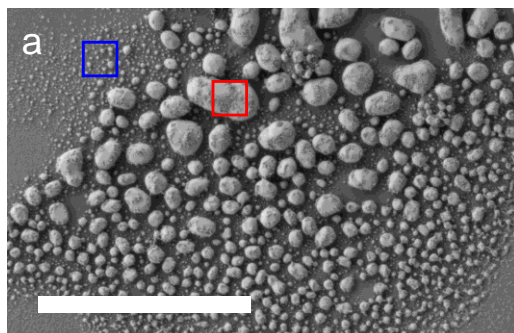
Figure A4.61. (a) Representative SEM image illustrating the areas analyzed to determine the elemental composition of dense regions of relatively large particles (*bulk*) and less dense regions of relatively small particles (*particles*) produced via the pyrolysis of a film of polyelectrolyte **4.14a**. (b) Data table summarizing the elemental composition of multiple areas of the silicon wafer determined using EDX spectroscopy. Scale bar = 5 μm .



b	% ^a	C	O	P	Fe	Ru
Bulk		14.1	25.9	16.3	26.8	16.9
		3.8	20.9	10.7	38.4	26.2
		10.9	44.7	11.8	23.6	8.9
		14.0	24.4	16.0	28.6	17.0
		13.2	27.3	16.2	26.1	17.1
		13.9	26.2	18.8	21.9	19.3
		16.6	25.4	18.8	20.5	18.7
		14.9	28.5	18.5	19.6	18.5
		13.2	27.4	19.4	20.5	19.4
		13.9	25.6	16.0	27.6	16.9
	12.3	26.6	15.9	28.5	16.8	
	Average	12.8 ± 3.3	27.5 ± 6.0	16.2 ± 2.8	25.6 ± 5.4	17.8 ± 4.0
Particles		16.2	30.7	14.9	24.0	14.2
		38.6	36.6	8.6	8.3	8.0
		26.7	34.2	12.1	16.5	10.4
		15.5	42.4	12.1	22.1	7.8
		21.2	28.6	14.3	22.3	13.7
	Average	23.6 ± 9.5	34.5 ± 5.4	12.4 ± 2.5	18.7 ± 6.4	10.8 ± 3.0

^aData normalized to exclude silicon detected from substrate.

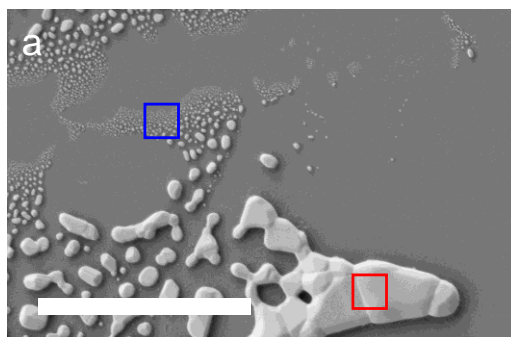
Figure A4.62. (a) Representative SEM image illustrating the areas analyzed to determine the elemental composition of dense regions of relatively large particles (*bulk*) and less dense regions of relatively small particles (*particles*) produced via the pyrolysis of a film of polyelectrolyte **4.14b**. (b) Data table summarizing the elemental composition of multiple areas of the silicon wafer determined using EDX spectroscopy. Scale bar = 5 μ m.



b	% ^a	C	O	P	Fe	Ru
Bulk		14.5	44.2	12.9	6.7	21.6
		14.6	46.5	12.0	6.6	20.2
		13.2	42.9	13.6	7.4	22.9
		13.7	42.0	13.7	7.3	23.3
		28.9	16.3	18.4	8.0	28.5
		22.1	14.9	20.3	9.6	33.2
		31.9	20.0	16.0	6.9	25.2
	Average	19.8 ± 7.8	32.4 ± 14.5	15.3 ± 3.1	7.5 ± 1.0	25.0 ± 4.5
Particles		16.0	48.9	9.4	6.6	19.1
		13.5	54.2	6.9	7.9	17.5
		70.6	19.5	2.8	1.6	5.4
		74.2	15.4	3.1	1.6	5.7
		64.7	26.1	2.6	1.5	5.0
		63.1	10.9	10.4	3.1	12.5
		62.8	11.6	9.8	3.3	12.6
	Average	52.1 ± 25.9	26.6 ± 17.8	6.4 ± 3.5	3.7 ± 2.6	11.1 ± 5.9

^aData normalized to exclude silicon detected from substrate.

Figure A4.63. (a) Representative SEM image illustrating the areas analyzed to determine the elemental composition of dense regions of relatively large particles (*bulk*) and less dense regions of relatively small particles (*particles*) produced via the pyrolysis of a film of polyelectrolyte **4.14c**. (b) Data table summarizing the elemental composition of multiple areas of the silicon wafer determined using EDX spectroscopy. Scale bar = 5 μm .



b	% ^a	C	O	P	Ru
Bulk		16.1	5.2	25.5	53.1
		17.8	5.2	25.1	51.9
		17.6	5.1	25.0	52.3
		18.3	5.0	25.0	51.7
		20.9	6.1	23.9	49.1
	Average	18.1 ± 1.8	5.3 ± 0.4	24.9 ± 0.6	51.6 ± 1.5
Particles		71.4	20.6	3.2	4.8
		76.0	16.4	3.1	4.6
		69.7	18.9	4.6	6.8
		72.1	15.4	5.1	7.4
		74.2	19.6	2.3	4.0
	Average	72.7 ± 2.4	18.2 ± 2.2	3.6 ± 1.2	5.5 ± 1.5

^aData normalized to exclude silicon detected from substrate.

Figure A4.64. (a) Representative SEM image illustrating the areas analyzed to determine the elemental composition of dense regions of relatively large particles (*bulk*) and less dense regions of relatively small particles (*particles*) produced via the pyrolysis of a film of polyelectrolyte **4.14d**. (b) Data table summarizing the elemental composition of multiple areas of the silicon wafer determined using EDX spectroscopy. Scale bar = 5 μm .

Powder X-ray Diffractograms

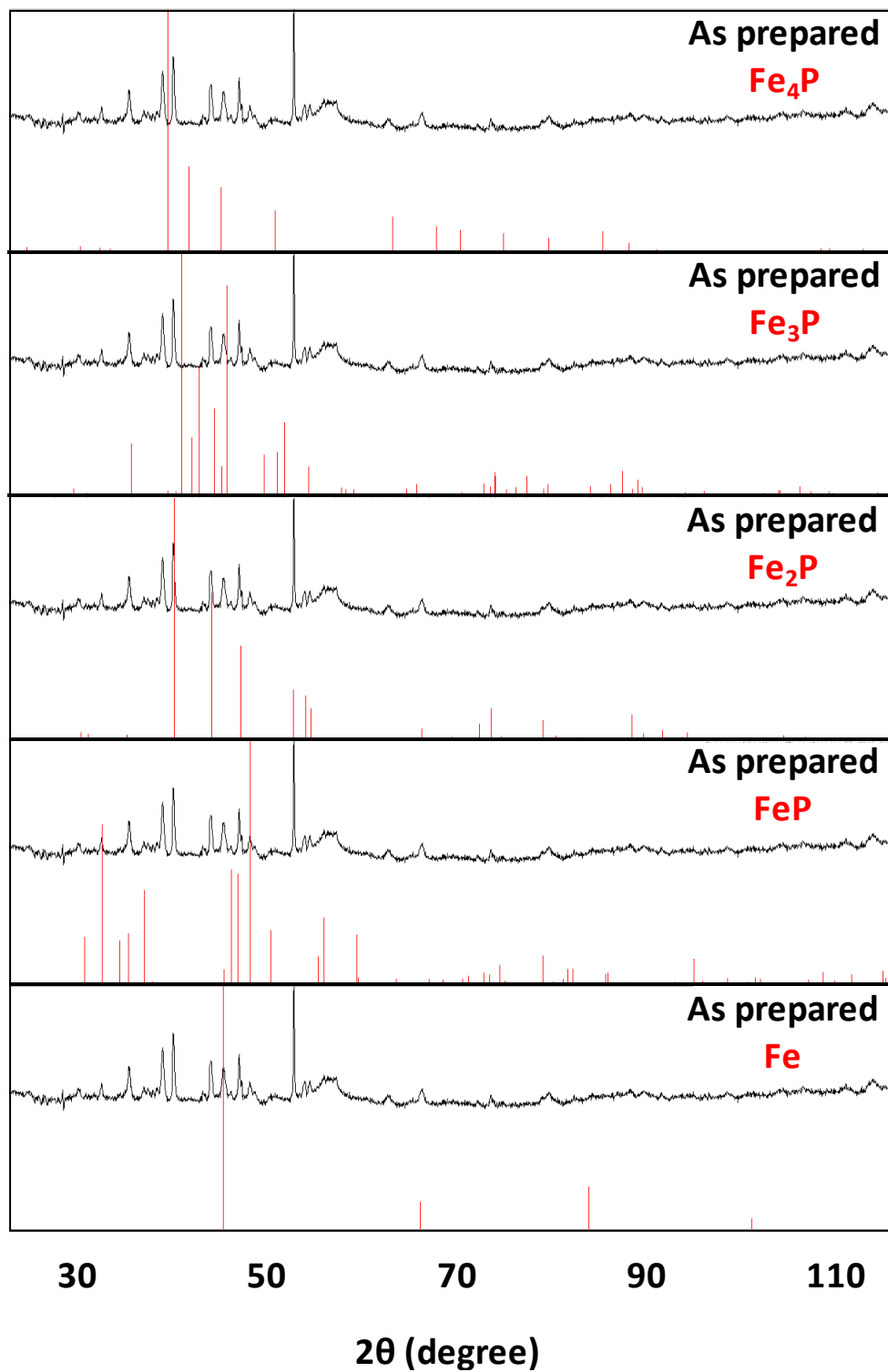


Figure A4.65. Powder X-ray diffractogram of the nanomaterials prepared via pyrolysis of a film of **4.14a** plotted vs. iron phosphides and iron.

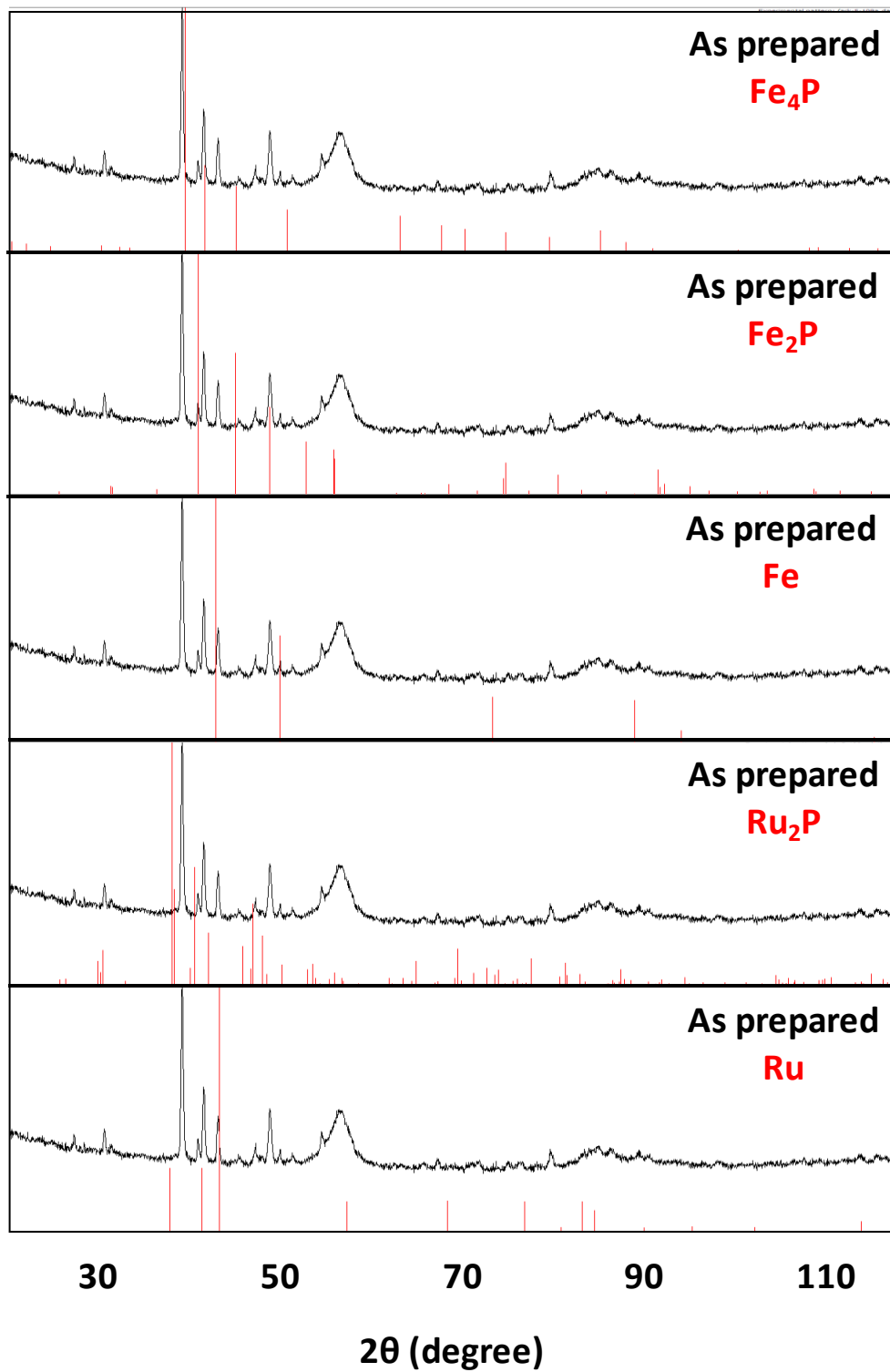


Figure A4.66. Powder X-ray diffractogram of the nanomaterials prepared via pyrolysis of a film of **4.14b** plotted vs. iron phosphides, iron, ruthenium phosphides and ruthenium.

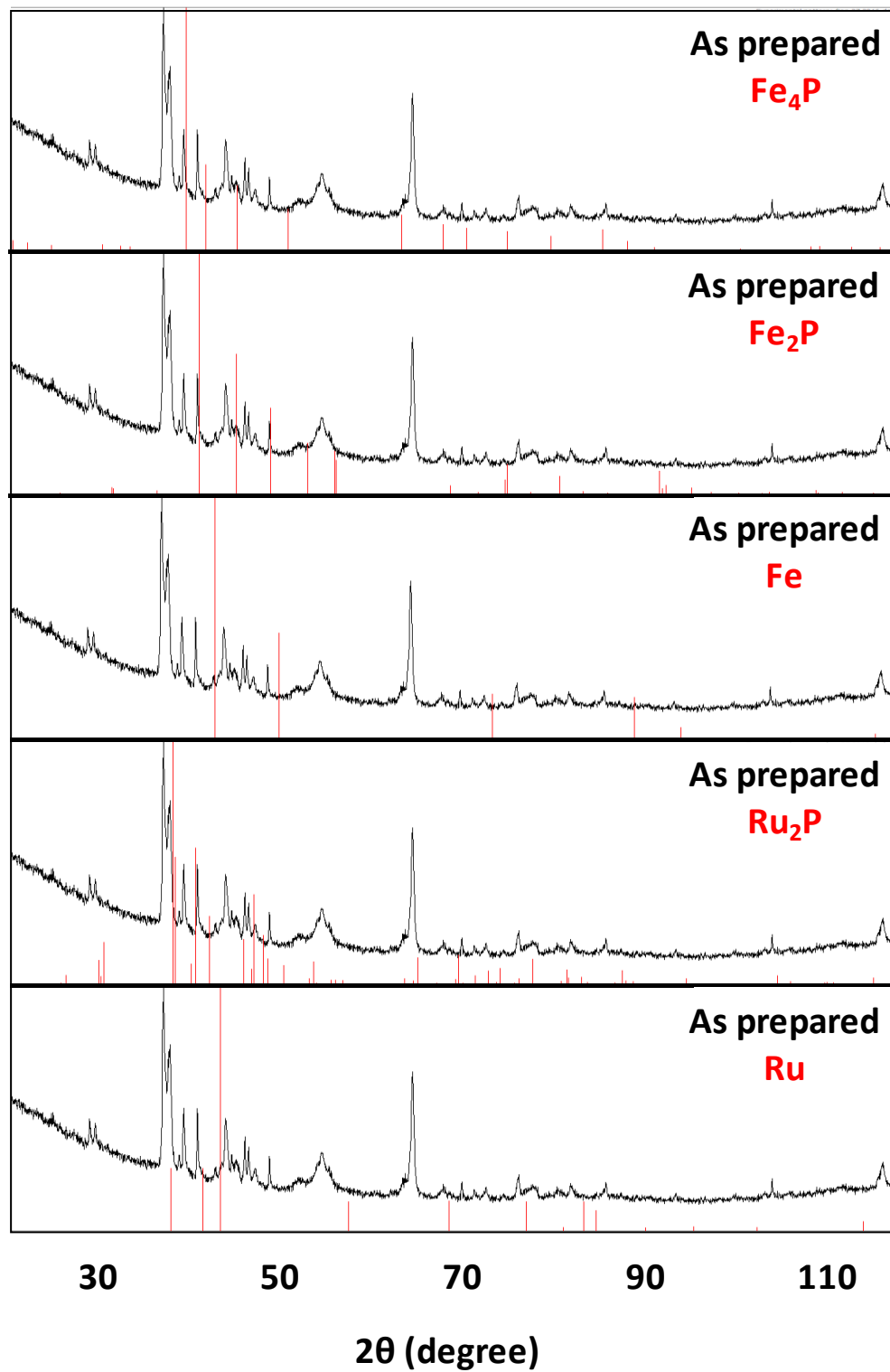


Figure A4.67. Powder X-ray diffractogram of the nanomaterials prepared via pyrolysis of a film of **4.14c** plotted vs. iron phosphides, iron, ruthenium phosphides and ruthenium.

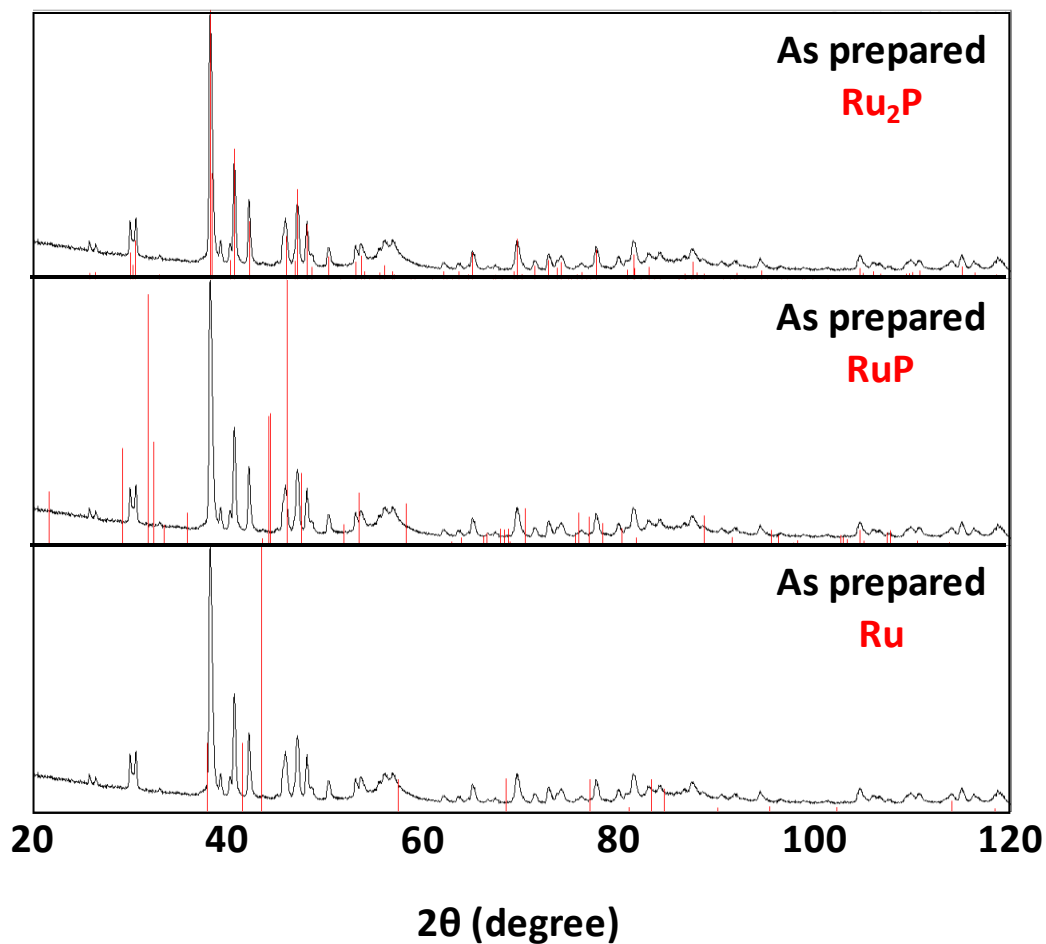


Figure A4.68. Powder X-ray diffractogram of the nanomaterials prepared via pyrolysis of a film of **4.14d** plotted vs. ruthenium phosphides and ruthenium.

Appendix 5 – Supporting Information for Chapter 5

NMR Spectra

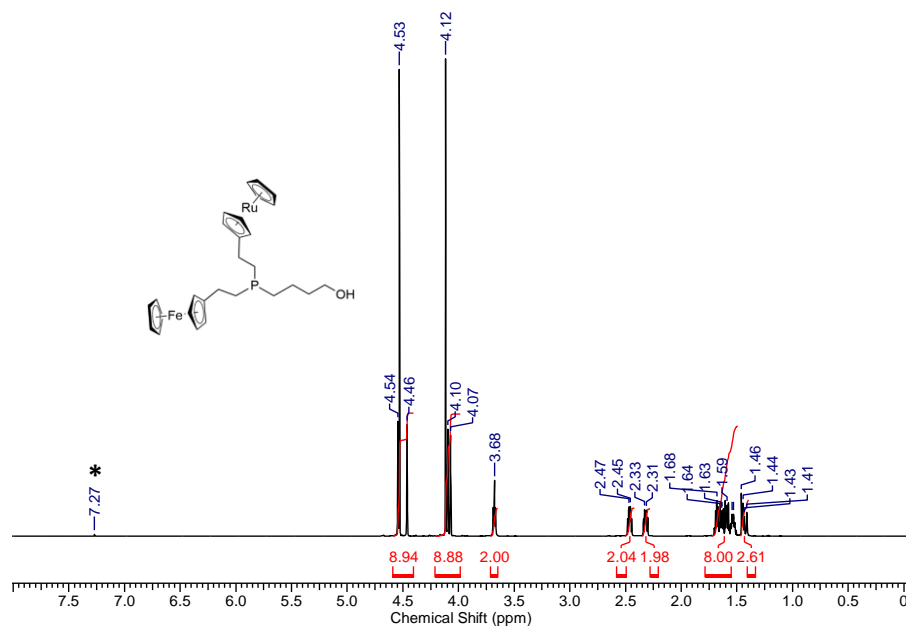


Figure A5.1. ^1H NMR spectrum of **5.6** in CDCl_3 . The asterisk denotes residual CHCl_3 signal.

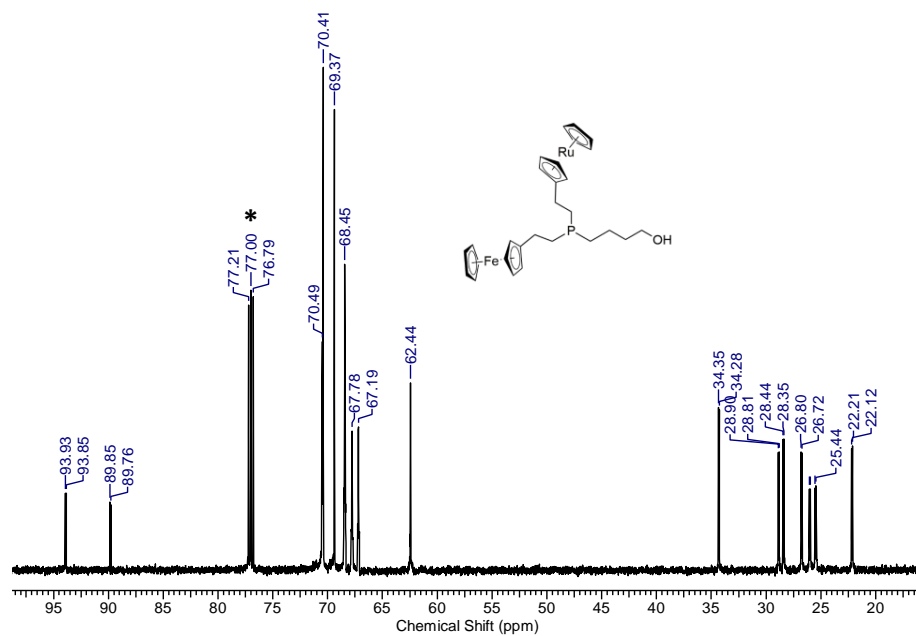


Figure A5.2. $^{13}\text{C}\{^1\text{H}\}$ NMR spectrum of **5.6** in CDCl_3 . The asterisk denotes the solvent signal.

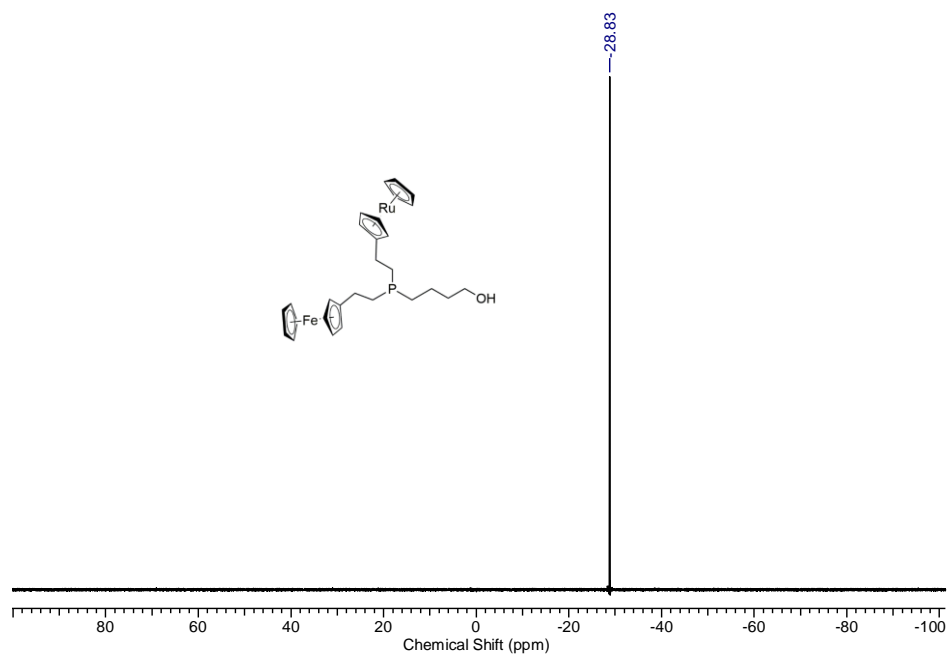


Figure A5.3. ^{31}P NMR{ ^1H } spectrum of **5.6** in CDCl_3 .

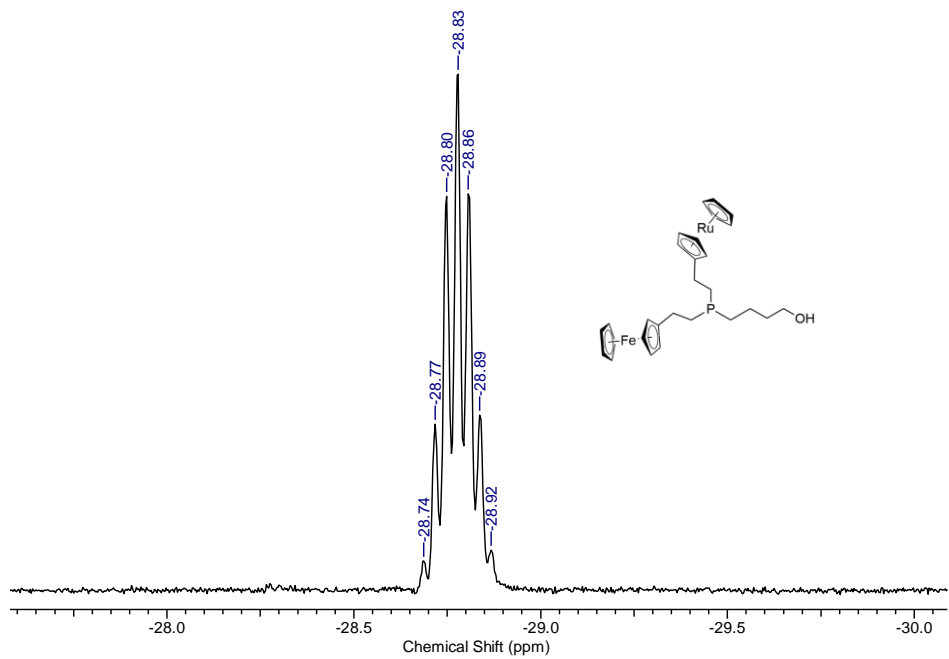


Figure A5.4. ^{31}P NMR spectrum of **5.6** in CDCl_3 .

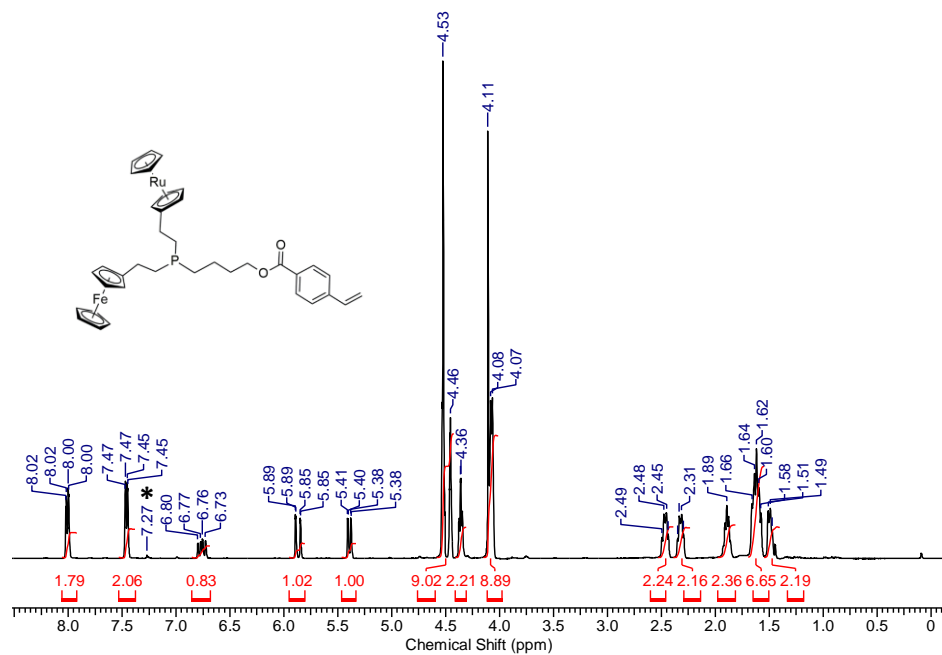


Figure A5.5. ^1H NMR spectrum of **5.7** in CDCl_3 . The asterisk denotes residual CHCl_3 signal.

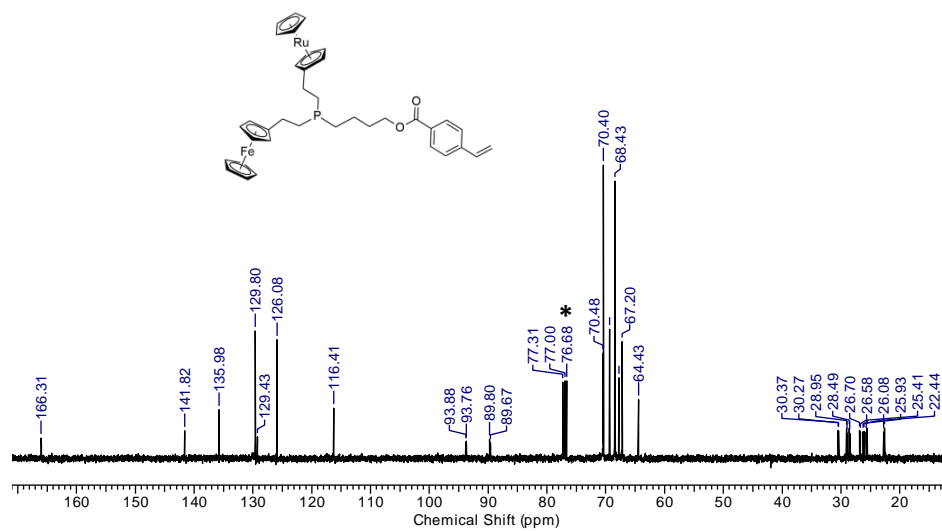


Figure A5.6. $^{13}\text{C}\{^1\text{H}\}$ NMR spectrum of **5.7** in CDCl_3 . The asterisk denotes the solvent signal.

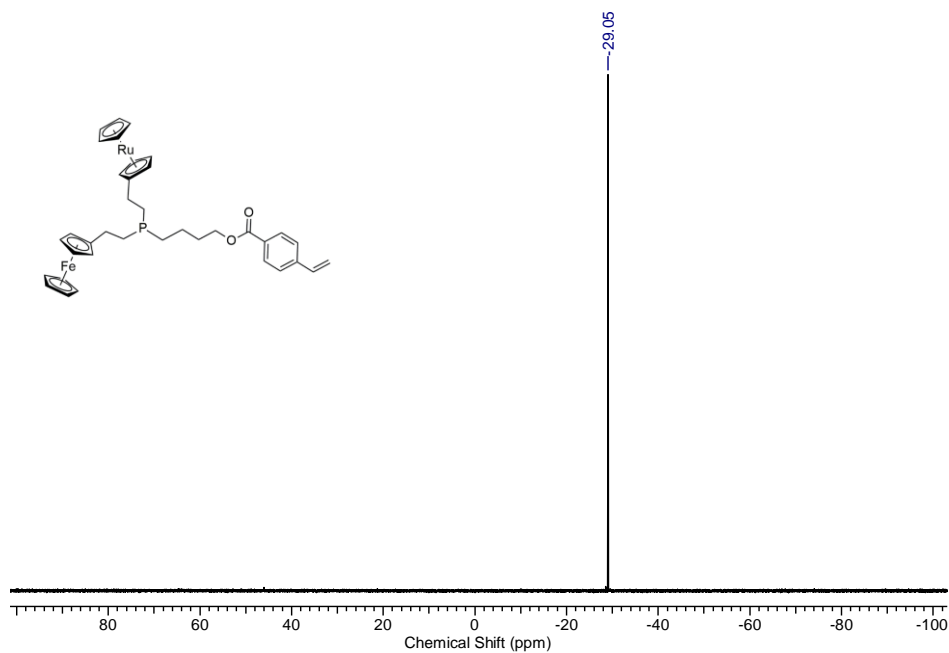


Figure A5.7. ^{31}P NMR $\{^1\text{H}\}$ spectrum of **5.7** in CDCl_3 .

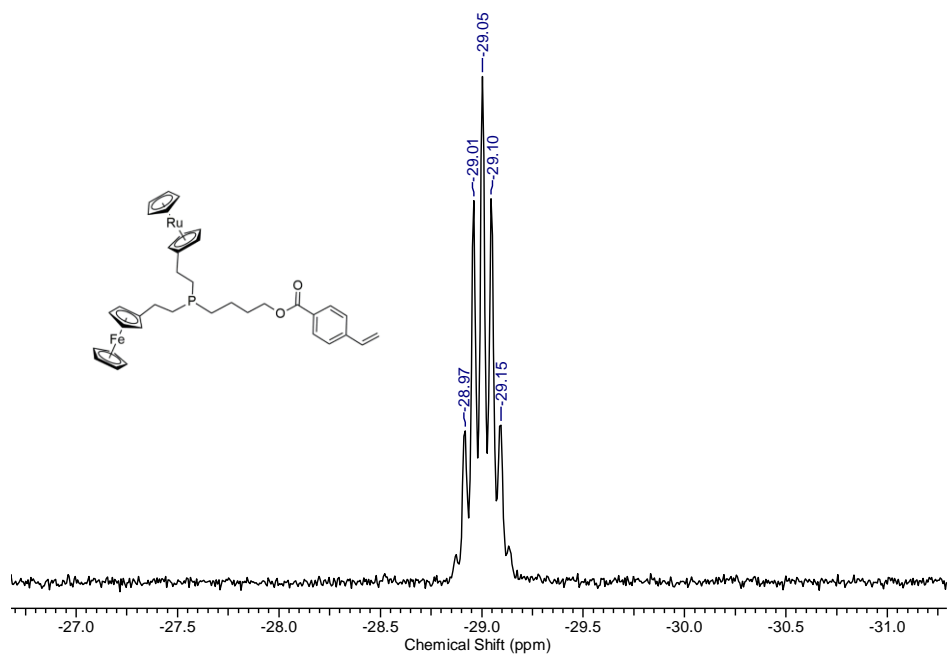


Figure A5.8. ^{31}P NMR spectrum of **5.7** in CDCl_3 .

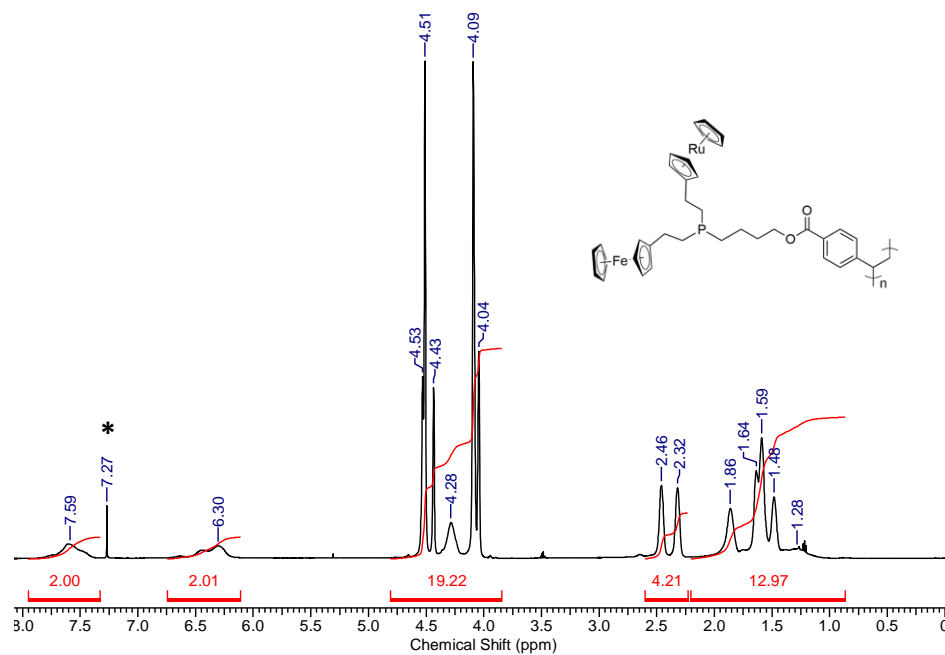


Figure A5.9. ^1H NMR spectrum of **5.8** in CDCl_3 . The asterisk denotes residual CHCl_3 signal.

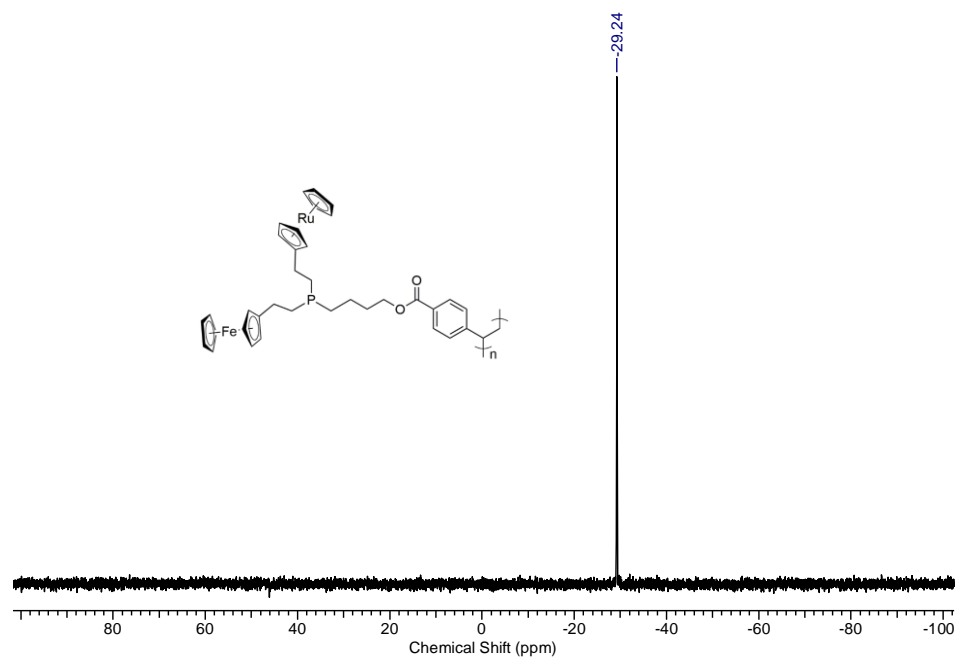


Figure A5.10. ^{31}P NMR $\{^1\text{H}\}$ spectrum of **5.8** in CDCl_3 .

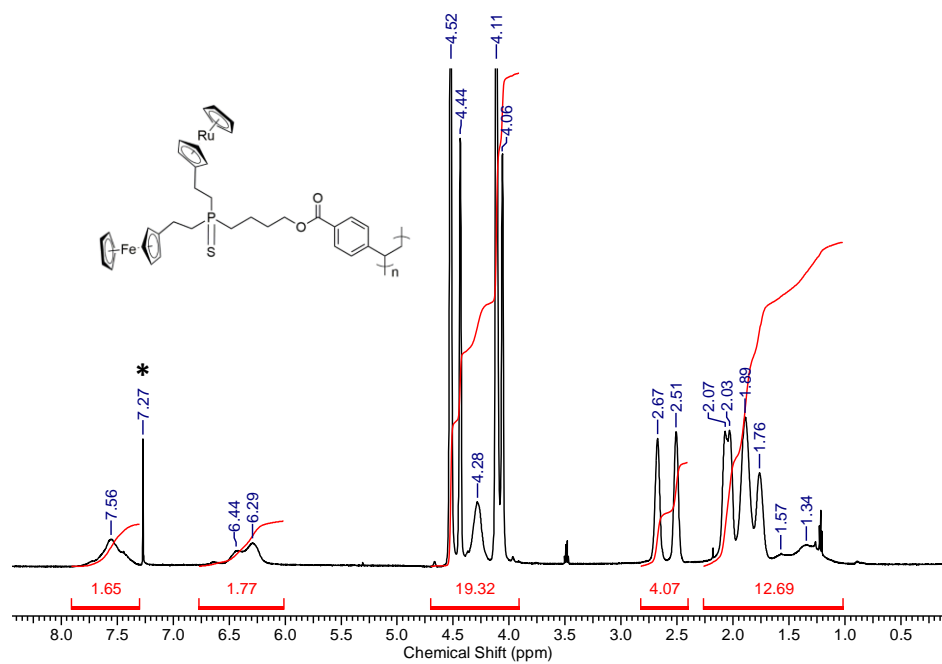


Figure A5.11. ^1H NMR spectrum of **5.8S** in CDCl_3 . The asterisk denotes residual CHCl_3 signal.

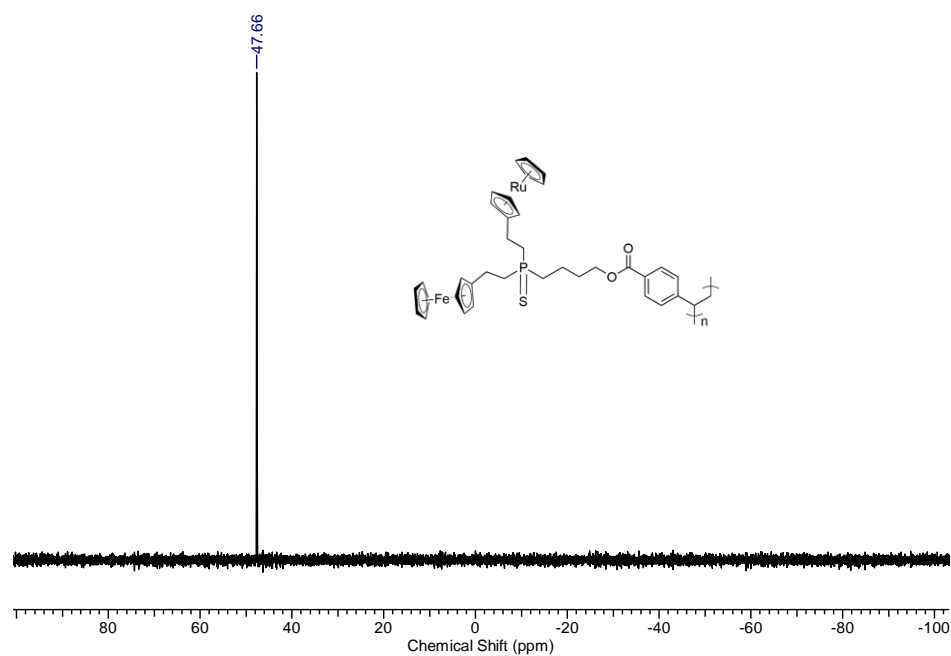


Figure A5.12. ^{31}P NMR $\{^1\text{H}\}$ spectrum of **5.8S** in CDCl_3 .

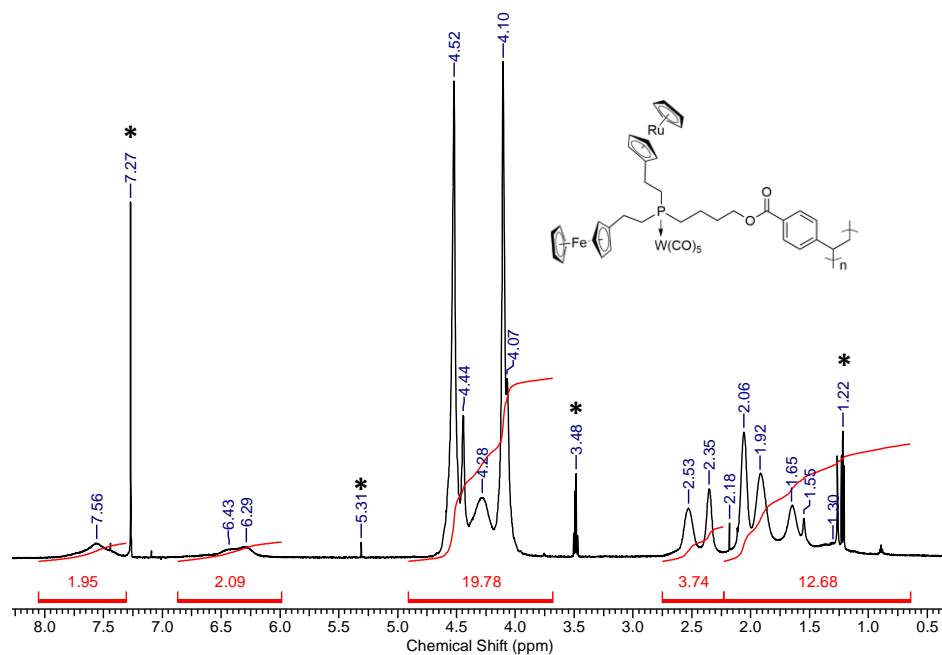


Figure A5.13. ^1H NMR spectrum of $5.8 \cdot \text{W}(\text{CO})_5$ in CDCl_3 . The asterisks denote residual CHCl_3 , Et_2O , and CH_2Cl_2 signals.

UV-Vis Absorption Spectra

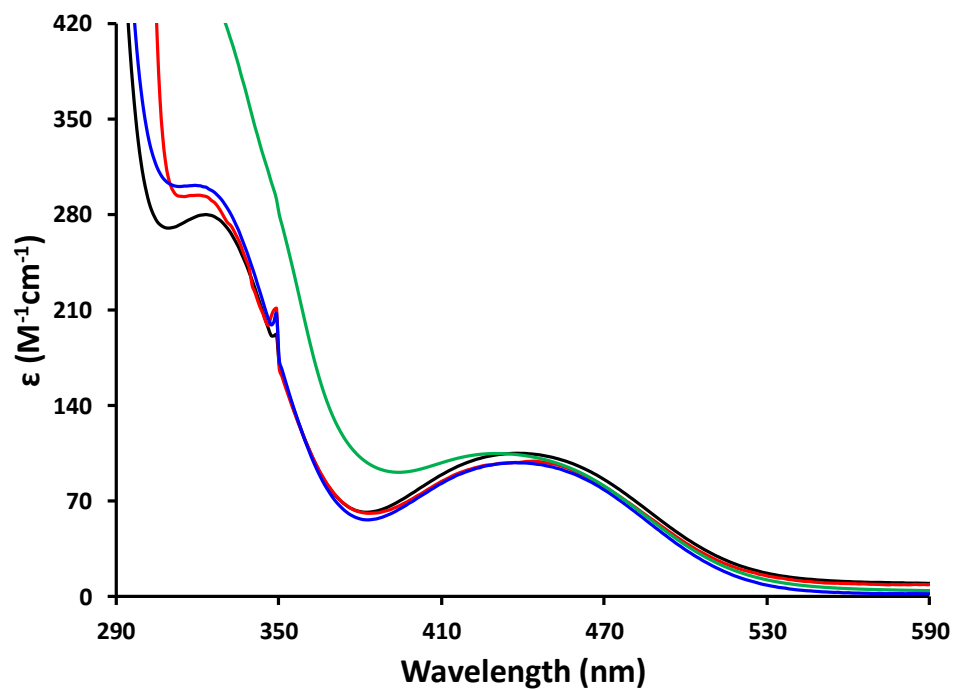


Figure A5.14. UV-vis absorption spectra recorded for **5.6** (black), **5.7** (red), **5.8** (blue), and **5.8**• $\text{W}(\text{CO})_5$ (green) in CH_2Cl_2 .

Cyclic Voltammograms

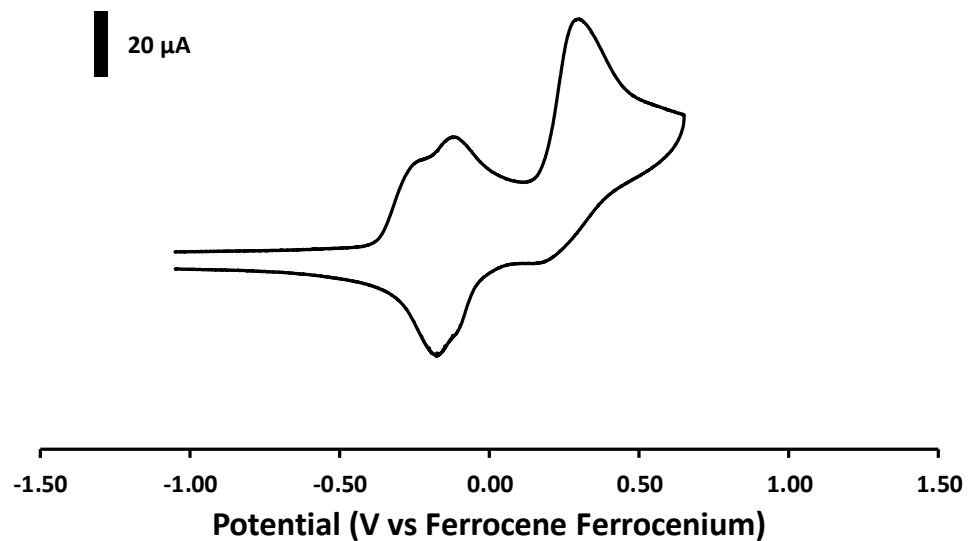


Figure A5.15. Cyclic voltammogram of **5.6** (1 × Fc, 1 × Rc) recorded at 250 mV s⁻¹ in solution of THF containing 0.1 M [*n*-Bu₄N][OTf] as supporting electrolyte.

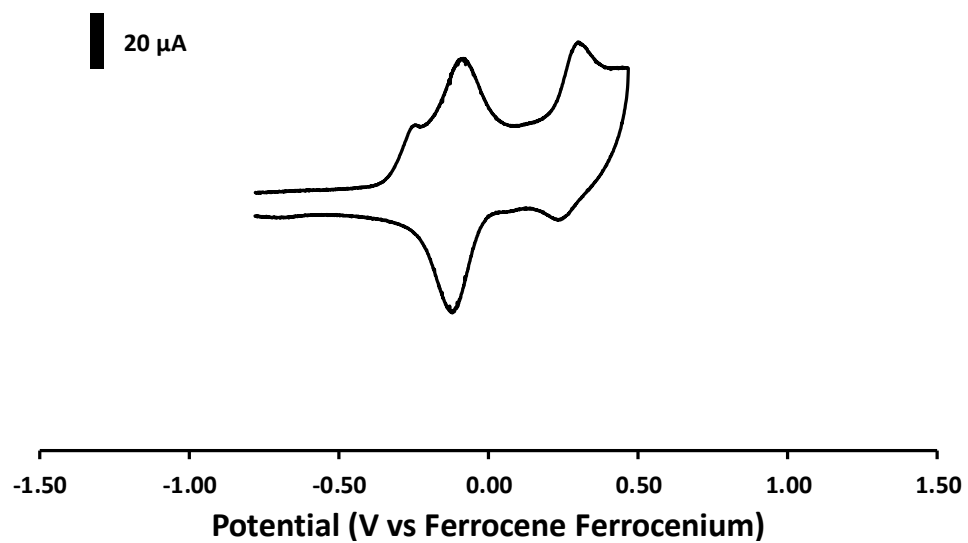


Figure A5.16. Cyclic voltammogram of monomer **5.7** (1 × Fc, 1 × Rc) recorded at 250 mV s⁻¹ in solution of THF containing 0.1 M [*n*-Bu₄N][OTf] as supporting electrolyte.

Curriculum Vitae

Name: Amir Rabiee Kenaree

Post-secondary Education and Degrees: The University of Western Ontario
London, Ontario, Canada
2013–2016 Ph.D.

The University of Tehran
Tehran, Tehran, Iran
2007–2010 M.Sc.

The University of Tehran
Tehran, Tehran, Iran
2002–2007 B.Sc.

Related Work Experience Teaching Assistant
The University of Western Ontario
2013–2016

Publications:

7. **Rabiee Kenaree, A.**; Gilroy, J.B.* Synthesis and Characterization of Metal-Rich Phosphonium Polyelectrolytes and Their Use as Precursors to Nanomaterials. *Dalton Trans.* **2016**, *45*, 18229–18240.
6. Azizipoor Fard, M.; **Rabiee Kenaree, A.**; Boyle, P.D.; Ragogna, P.J.; Gilroy, J.B.; Corrigan, J.F.* Coinage Metal Coordination Chemistry of Stable Primary, Secondary and Tertiary Ferrocenylethyl-Based Phosphines *Dalton Trans.* **2016**, *45*, 2868-2880.
5. **Rabiee Kenaree, A.**; Sauvé, E.R.; Ragogna, P.J.; Gilroy, J.B.* Coordination Complexes of Group 6 Metal Carbonyls and Primary, Secondary, and Tertiary Ethylferrocene Phosphines *Dalton Trans.* **2016**, *45*, 2859-2867.
4. **Rabiee Kenaree, A.**; Cuthbert, T.J.; Barbon, S.M.; Boyle, P.D.; Gillies, E.R.; Ragogna, P.J.; Gilroy, J.B.* Synthesis and Characterization of a Family of Air-Stable Ferrocene- and Ruthenocene-Containing Primary, Secondary, and Tertiary Phosphines. *Organometallics* **2015**, *34*, 4272-4280.
3. Guterman, R.; **Rabiee Kenaree, A.**; Gilroy, J.B.; Gillies, E.R.; Ragogna, P.J.* Polymer network formation using the phosphane-ene reaction: a thiol-ene analogue with diverse post-polymerization chemistry *Chem. Mater.* **2015**, *27*, 1412-1419.

2. **Rabiee Kenaree, A.**; Berven, B.M., Ragogna, P.J.*; Gilroy, J.B.* Highly-Metallized Phosphonium Polyelectrolytes *Chem. Commun.* **2014**, 50, 10714-10717.

1. **Rabiee Kenaree, A.**; Fatemi, S.* Application of Artificial Neural Network in Simulation of Supercritical Extraction of Valerenic Acid from *Valeriana officinalis* L *ISRN Chemical Engineering*, **2012**, 572421.

Presentations:

8. **Rabiee Kenaree, A.**; Gilroy, J.B.* Oral (National): Synthesis and Characterization of Highly-Metallized Phosphonium-Based Polyelectrolytes and Their Applications in Materials Science, 37th Canadian High Polymer Forum, Aug. 2016, Gananoque, ON.

7. **Rabiee Kenaree, A.**; Ragogna, P.J.; Gilroy, J.B.* Oral (International): Synthesis, Electrochemistry, Coordination Chemistry of Mixed-metallocene-containing Phosphines and their Application in Material Science, 98th CSC Conference, June 2015, Ottawa, ON.

6. **Rabiee Kenaree, A.**; Ragogna, P.J.; Gilroy, J.B.* Poster (Institutional): Highly-Metallized Phosphonium Polyelectrolytes, Interdisciplinary Research Showcase, Dec. 2014, London, ON.

5. **Rabiee Kenaree, A.**; Ragogna, P.J.; Gilroy, J.B.* Poster (National): Highly-Metallized Phosphonium Polyelectrolytes, Ontario Inorganic Discussion Weekend, York University, Nov. 2013, Toronto, ON.

4. **Rabiee Kenaree, A.**; Ragogna, P.J.; Gilroy, J.B.* Poster (Provincial): Highly-Metallized Phosphonium Polyelectrolytes, Center for Advanced Materials and Biomaterials Research Day, Nov. 2013, London, ON.

3. **Rabiee Kenaree, A.*** Lotfi, B. Poster Presentation (International): Simulation and Prediction of Nano-Particles' Diameters of Spray reaction Synthesis Process of c-ZrO₂ by Radial Basis Functions, 3rd Conference on Nanostructures, Mar. 2010, Kish Island, Iran.

2. **Rabiee Kenaree, A.**; Fatemi, S.; Lucas, C.* Poster (International): Computational Simulating of the Depletion of Dissolved Oxygen in Water Bodies, advances in wastewater treatment and reuse, Nov. 2009, Tehran, Iran

1. **Rabiee Kenaree, A.**; Fatemi, S.; Lucas, C.* Poster (National): Simulation and modeling of the oxygen depletion in ecological systems using SIMULINK software, first national conference on world environment day, May 2007, Tehran, Iran.